

IMFUFA **tekst**

- I, OM OG MED MATEMATIK OG FYSIK

Mathematical Modelling of the Dynamics of Pathological Hematopoiesis during Treatments

Zamra Sajid
IMFUFA, Roskilde University
PhD thesis

nr. 516 – 2021

Roskilde University,
Department of Science and Environment, IMFUFA
P.O. Box 260, DK - 4000 Roskilde
E-mail: imfufa@ruc.dk



Mathematical Modelling of the Dynamics of Pathological Hematopoiesis during Treatments

Zamra Sajid
IMFUFA, Roskilde University
PhD thesis

IMFUFA tekst nr. 516/2021 — 253 sider — ISSN: 0106-6242

Shortened abstract, full version available in main text.

The Philadelphia-negative myeloproliferative neoplasms (MPNs) are a group of hematopoietic stem-cell disorders, including essential thrombocythemia (ET), polycythemia vera (PV) and primary myelofibrosis (PMF). The excessive production in myeloid, erythroid or megakaryocytic cell lines characterizes the three classical MPNs. Furthermore, inflammation is thought to be a driver of MPNs and becomes a reason for developing other cancers in MPN patients. However, MPN patients may become alive for several years with a high risk of thrombosis, cardiovascular complications and chronic inflammatory diseases. Although many pathogenetic working mechanisms of MPNs are discovered, many of the therapeutic tools are still unexplored.

In this thesis, a series of mechanism-based mathematical models contribute to building further knowledge about the pathogenesis of MPNs. Inspired by the bio-medical literature, we address various research questions related to MPNs. In addition to the pathogenesis of MPNs, we propose a novel mathematical model describing the coupled mechanisms of thrombopoiesis and erythropoiesis.

Mathematical Modelling of the Dynamics of Pathological Hematopoiesis during Treatments

*This thesis has been submitted to the Doctoral School of Science and Environment,
Roskilde University,*

Ph.D. thesis

by

Zamra Sajid

Supervisors

Professor Johnny T. Ottesen

Associate Professor Morten Andersen



February, 2020

Abstract

The Philadelphia-negative myeloproliferative neoplasms (MPNs) are a group of hematopoietic stem-cell disorders, including essential thrombocythemia (ET), polycythemia vera (PV) and primary myelofibrosis (PMF). The excessive production in myeloid, erythroid or megakaryocytic cell lines characterizes the three classical MPNs. Furthermore, inflammation is thought to be a driver of MPNs and becomes a reason for developing other cancers in MPN patients. However, MPN patients may become alive for several years with a high risk of thrombosis, cardiovascular complications and chronic inflammatory diseases. Although many pathogenetic working mechanisms of MPNs are discovered, many of the therapeutic tools are still unexplored.

In this thesis, a series of mechanism-based mathematical models contribute to building further knowledge about the pathogenesis of MPNs. Inspired by the bio-medical literature, we address various research questions related to MPNs. In addition to the pathogenesis of MPNs, we propose a novel mathematical model describing the coupled mechanisms of thrombopoiesis and erythropoiesis.

The first mechanism-based Cancitis model describes the coupling between chronic inflammation and the development of MPNs. We perform a thorough mathematical investigation of the model and find the crucial parameters for the progression of the disease. Thereby we identify that the inflammatory stimuli and a few grouped parameters involved in the hematopoietic stem cell (HSC) dynamics are mainly responsible for governing the behavior of the model. Based on the Cancitis model, we further develop a range of mathematical models in the presented work.

A second model is a novel mathematical model proposed for PV dynamics. We zoom in on the excessive production of red blood cells and erythropoietin (EPO) feedbacks on healthy and malignant cells. A mathematical analysis of the model highlights HSC fitness and suggests that HSC dynamics govern disease progression. The model is capable of reproducing clinically observed dynamics before and during treatment.

A third novel mathematical model is proposed for ET dynamics where the excessive production of platelets is addressed. In addition, thrombopoietin (TPO) feedbacks mediates healthy and malignant cell lineage. The overall analysis reflects that targeted HSC therapy can control disease progression.

Finally, we develop a mathematical model combining the dynamics of erythrocytes and platelets. In contrast to previous models, this model does not contain malignant cells. It is known that erythrocytes and platelets share the same precursor megakaryocyte-erythroid progenitor (MEP). The purpose of the model is the investigation of the coupled mechanisms between erythrocytes and platelets. The model is validated and calibrated for various clinical experiments such as phlebotomy, body's reaction to EPO and TPO regimens.

Preface

This thesis has been submitted to the Doctoral School of Science and Environment, Roskilde University, Denmark partially fulfilled the requirements for obtaining the Ph.D. degree in Mathematics. The research was primarily carried out at the Department of Science and Environment, Roskilde University, Denmark under the supervision of Professor Johnny T. Ottesen and Associate Professor Morten Andersen.

The following articles are included in the chapters of thesis.

1. Mathematical analysis of the Cancitis model and the role of inflammation in blood cancer progression. Zamra Sajid, Morten Andersen and Johnny T. Ottesen. *Mathematical Biosciences and Engineering* 2019, Volume 16, Issue 6: 8268-8289.
<https://doi.org/10.3934/mbe.2019418>
2. System dynamics of cancer in erythropoiesis with multiple EPO feedbacks. Zamra Sajid, Morten Andersen and Johnny T. Ottesen. *System Dynamics Review*. *published*
3. Dynamics of erythropoiesis with multiple EPO feedbacks in blood cancer with stem cell competition. Zamra Sajid, Morten Andersen and Johnny T. Ottesen. *Journal of Theoretical Biology*, *Submitted*
4. Mathematical modelling of erythropoiesis and thrombopoiesis with multiple EPO and TPO feedbacks. Zamra Sajid, Morten Andersen and Johnny T. Ottesen. *Submitted*

I have contributed in the following published articles during my Ph.D., which are included in the appendix:

1. Bridging blood cancers and inflammation: The reduced Cancitis model. Johnny T. Ottesen, Rasmus Kristoffer Pedersen, Zamra Sajid, Johanne Gudmand-Høyer, Katrine O. Bangsgaard, Vibe Skov, Lasse Kjær, Trine A. Knudsen, Niels Pallisgaard, Hans Hasselbalch, Morten Wienecke Andersen. *Journal of Theoretical Biology* Volume 465, 21 March 2019, Pages 90-108.
<https://doi.org/10.1016/j.jtbi.2019.01.001>

2. Data-driven analysis of *JAK2V617F* kinetics during interferon-alpha2 treatment of patients with polycythemia vera and related neoplasms. Rasmus K Pedersen, Morten Andersen, Trine A Knudsen, Zamra Sajid, Johanne Gudmand-Hoeyer, Marc J B Dam, Vibe Skov, Lasse Kjaer, Christina Ellervik, Thomas S Larsen, Dennis Hansen, Niels Pallisgaard, Hans C Hasselbalch, Johnny T Ottesen. *Cancer Medicine* 2020 Mar; 9 (6): 2039-2051.

<https://doi.org/10.1002/cam4.2741>

3. Mathematical modelling as a proof of concept for MPNs as a human inflammation model for cancer development. Morten Andersen, Zamra Sajid, Rasmus K. Pedersen, Johanne Gudmand-Hoeyer, Christina Ellervik, Vibe Skov, Lasse Kjær, Niels Pallisgaard, Torben A. Kruse, Mads Thomassen, Jesper Troelsen, Hans Carl Hasselbalch, Johnny T. Ottesen. *Plos One*.

<https://doi.org/10.1371/journal.pone.0183620>

Acknowledgements

With immense pleasure and a deep sense of gratitude, I wish to express my sincere thanks to my supervisor Professor. Johnny T. Ottesen at Roskilde, University. Without his motivation and continuous encouragement, I can not accomplish this research successfully. In addition to his expertise in mathematical modeling of biological mechanisms, he is a very cooperative and supporting personality. I can never forget his words, 'Just come if you need any help.' During my Ph.D., Johnny never refused whenever I asked for his assistance. Furthermore, I wish to express my gratitude to my co-supervisor Associate Professor Morten Andersen for his amazing ideas and qualitative approach to present scientific results.

I am pleased to be a part of the collaborative team consists of our Cancitis group from Roskilde University and Hans C. Hasselbalch and his colleagues from Roskilde Hospital.

I wish to extend my profound sense of gratitude to my friends and colleagues at IM-FUFA, especially my group fellow Rasmus and office mate Raimundo for good company and a friendly atmosphere during my Ph.D.

Finally, I would like to thank my family and friends for all their encouragement and patience. I would especially like to express my gratitude to my parents, my husband Shoaib, and my sons Abdul and Abdullah for their moral support, along with patience and understanding.

Date: 12/02/2020

Zamra Sajid

Contents

Abstract	i
Preface	iv
Acknowledgements	vi
1 Introduction	1
1.1 Biological Background	1
1.2 Pathogenesis of MPNs and its types	3
1.3 Short Review of Existing Mathematical Models of Hematopoietic System and Hematological Diseases	9
1.4 Overview of Thesis	11
1.5 Concluding Remarks and Future Perspectives	23
2 Mathematical analysis of the Cancitis model and the role of inflam- mation in blood cancer progression	26
3 System dynamics of cancer in erythropoiesis with multiple EPO feed- backs	49
4 Dynamics of erythropoiesis with multiple EPO feedbacks in blood cancer with stem cell competition	73
5 Mathematical model of pathological dynamics of thrombopoiesis with multiple TPO feedbacks	117
5.1 Introduction	117
5.2 ET model	118
5.3 Results	122
5.3.1 Existence of steady states	122
5.3.2 Stability analysis	127

5.3.3	Sensitivity Analysis	131
5.3.4	Numerical Analysis and Treatment Scenarios	134
5.4	Conclusion	138
6	Mathematical modelling of erythropoiesis and thrombopoiesis with multiple EPO and TPO feedbacks	140
	Bibliography	189
Appendices		
Appendix A	Mathematical modelling as a proof of concept for MPNs as a human inflammation model for cancer development	190
Appendix B	Bridging blood cancers and inflammation: The reduced Cancitis model	209
Appendix C	Data-driven analysis of <i>JAK2V617F</i> kinetics during interferonalpha2 treatment of patients with polycythemia vera and related neoplasms	229

CHAPTER 1

Introduction

Mathematical modelling is a fast-growing research tool for exploring complex biological mechanisms. The potentials of mathematical models in medical research are significant to simulate medical outcomes. In vivo, clinical trials may be substituted with in vitro or in silico experiments combined with a mathematical model, hypothesized various physiological interventions for patients. The study of hematology using mathematical models has been continued for the past half-century leading to quality progress of forecasting optimal treatments. Moreover, mathematical oncology has gained much importance in recent years. Stepping forward, this thesis is devoted to mathematical modelling of hematological processes and focused on the development of blood cancer particularly, myeloproliferative neoplasms (MPNs). This thesis contains a series of mathematical models primarily concerned with hematopoiesis processes and the pathophysiology of blood disorders. The work may serve to the research in the pathogenesis, diagnosis and prognosis of MPN patients.

1.1 Biological Background

Hematopoiesis

Hematopoietic stem cells (HSCs) are multipotent cells that produce all blood cells required by the human body. Once an HSC differentiates, it undergoes a series of differentiation to become a mature cell. Such a process occurs in the bone marrow niche and is called hematopoiesis. In healthy individuals, approximately 10^{12} blood cells are produced every day in order to maintain the steady state levels of the peripheral blood. HSCs are capable of regenerating themselves, termed as self-renewal, meaning one HSC divides into two HSCs. In addition, one HSC may produce two daughters/progenitor cells, and it may differentiate into one HSC and one daughter cell. Hematopoietic stem cell niche is a particular environment where necessary signals

from the body carry out cells' differentiation. These differentiated cells are subdivided into myeloid and lymphoid groups of cells. The myeloid cells include red blood cells (erythrocytes), white blood cells (leukocytes), and platelets (thrombocytes), whereas T-cells, Natural killing cells and B-cells are included in the lymphoid group of cells. Specific associated growth hormone factors to different cell lineages are responsible for determining a cell type's fate when it differentiates from a stem cell. They stimulate growth, cell reproduction, and cell regeneration. For example, in some cases, such as bone marrow failure, the liver and spleen perform the hematopoietic function to increase these organs' size. Such a condition is called extramedullary hematopoiesis [70; 99].

Erythropoiesis

The process of production of red blood cells (erythrocytes) from a stem cell is called erythropoiesis. In the process of erythrocyte maturation, a cell undergoes several stages in the bone marrow. This stepwise differentiation includes a common myeloid progenitor, unipotent stem cell, proerythroblast, erythroblast, polychromatophilic, orthochromatic, and reticulocytes. A reticulocyte is an immature red blood cell that is finally released into the blood and becomes erythrocyte after a day. The average life span of the erythrocyte is about 120 days.

The hormone growth factor erythropoietin (EPO) is mainly responsible for stimulating early erythroid progenitor cells. The kidneys secrete EPO in response to low oxygen levels in the blood. Such a process usually occurs within the red bone marrow. In some diseases, this process can occur by the spleen or liver and is called extramedullary erythropoiesis. The erythropoietin regulates the erythropoiesis through a feedback loop; thus, the production and destruction of red blood cells are maintained in healthy states. Hence, low erythrocytes number leads to an elevated level of EPO. This growth hormone factor requires *JAK2*, a non-receptor tyrosine kinase for signal transduction. *JAK2* is implicated in signaling by members of the type II cytokine receptor family, e.g., interferon receptors, the single-chain receptors, e.g., EPO-R. It means that the loss of function of the erythropoietin receptor or *JAK2* may disrupt erythropoiesis [70; 99].

Thrombopoiesis

The process of production of thrombocytes/platelets from a stem cell is called thrombopoiesis. It starts with the differentiation of common myeloid progenitor into the high proliferative potential colony-forming unit megakaryocyte regulated by various cytokines. The next differentiation series include a formation of burst forming unit, megakaryocytic colony-forming units, megakaryoblasts, megakaryocytes, which then shed into thousands of platelets. The expected life span of platelets is about seven days.

The glycoprotein hormone thrombopoietin (TPO) is mainly responsible for regulating megakaryopoiesis (the production of megakaryocytes) but, the formation of platelets is known to be independent of TPO. This protein is a ligand for *MPL* (myeloproliferative leukemia). TPO is produced by the liver and is cleared by platelets. Thus, the decreased platelet mass subsequently decreases the degradation of TPO; hence, there is more TPO to stimulate thrombopoiesis. Therefore, it may conclude that plasma TPO concentration is inversely proportional to the platelet [70; 99].

Granulopoiesis

The production of granulocytes is referred to as granulopoiesis. The first stage involves the transformation of a common myeloid progenitor to a promyelocyte. This cell gives rise to a unique myelocyte, which can be classified as an eosinophil, basophil, or neutrophil progenitor.

The glycoprotein, granulocyte colony-stimulating factor (G-CSF) is the key to driving granulocytic development. In addition, G-CSF stimulates the survival, differentiation, and function of neutrophil precursors and mature neutrophils. The protein is produced by endothelium and immune cells like macrophages [70; 99].

In table 1.1, the reference range for hematological parameters are given [99],

Table 1.1 Reference range for hematological parameters in healthy humans

Category	Reference range [99]
Hematocrit	37% - 52%
Red blood cells	4.2 - 6.1 $\times 10^{12}$ / L
White blood cells	4.8 - 10.8 $\times 10^9$ /L
Platelets	150 - 400 $\times 10^9$ /L
EPO	6 - 16 IU/L
TPO	81.25 - 237.7 pg/ml

1.2 Pathogenesis of MPNs and its types

MPNs are a group of hematopoietic stem-cell disorders, including essential thrombocythemia (ET), polycythemia vera (PV) and primary myelofibrosis (PMF) [22; 45]. Since MPNs are a slowly developed disease, most patients remain alive with MPNs for several years. Although there is a high risk of thrombosis [6] with cardiovascular complications and an increased risk to develop autoimmune and chronic inflammatory diseases, including 40% increased risk of acute myelogenous leukemia [44; 64]. Clonal studies have been conducted in patients with ET where *JAK2V617F*, *CALR* (calreticulin) and *MPL* (myeloproliferative leukaemia protein) mutations are identified as clonal markers. *JAK2* gene is responsible for producing blood cells. *CALR* gene plays

an important role in immune system function, and the *MPL* gene is involved in thrombopoietin signal transduction and megakaryocytic differentiation. The three classical Philadelphia-negative myeloproliferative neoplasms are characterized by clonal expansion of hematopoietic progenitors, independence from cytokines and overproduction of mature erythroid and myeloid progeny.

Essential Thrombocythemia

ET is characterized by excessively produced megakaryocytes in the bone marrow resulting in the excessed amount of platelets in the blood. This condition may cause dizziness and headaches however, the worst is the increased risk of blood clots. The mutation *JAK2V617F* is identified in 50% cases of ET [44; 64]. Recently, mutations in *CALR* gene is found higher in patients with ET [69; 101]. Different clinical features of ET are explored after *CALR* mutations during in vivo experiments. For example, the mutant allele burden is lower in *JAK2*-mutated ET than in *CALR*-mutated ET, ET patients with *CALR* display higher platelet count, lower leukocyte count, and longer survival as compared to *JAK2* patients. ET may transform to the advanced myelofibrosis stage, associated with the allele burden in both ET types.

In addition, TPO related *MPL* mutations are found in 1-3% cases [14; 89] of ET. Despite a high number of platelets, ET patients show significantly increased TPO serum levels than normal subjects. The feedback loop between TPO and megakaryocyte/platelet is affected, resulting in reduced consumption and subsequent increase of TPO serum levels in ET [51; 69; 98]. However, many novel mechanisms relating to increased TPO levels and abnormal platelet production in ET are yet to be revealed.

ET patients have an excellent chance of living an average life span with proper monitoring and necessary treatment. However, for people older than 60, having a history of thrombosis or platelet counts greater than $1500 \times 10^9/L$ are high-risk patients [12]. In 2008, the WHO (World Health Organization) classified the diagnostic criteria for ET patients. According to WHO, a diagnosis must meet all four significant criteria or the first three primary and minor criteria (See Table 1.2).

Major Criteria	Minor Criteria
<p>Platelet count $\geq 450 \times 10^9/L$</p> <p>Bone marrow biopsy specimen showing proliferation mainly of the megakaryocytic lineage with increased number of enlarged, mature megakaryocytes. No significant increase of left-shift of neutrophil granulopoiesis or erythropoiesis</p> <p>Not meeting WHO criteria for BCR-ABL1+ CML, PV, PMF, myelodysplastic syndromes, or other myeloid neoplasms</p> <p>Presence of <i>JAK2V617F</i>, <i>CALR</i>, or <i>MPL</i> mutations</p>	<p>Presence of a clonal marker or absence of evidence for reactive thrombocytosis</p>

Table 1.2 Diagnostic criteria for ET according to WHO [10]

Polycythemia Vera

PV is characterized by the overabundance of red blood cells in the blood and elevated hemoglobin levels and hematocrit. In PV, the bone marrow becomes hypercellular and dominated by erythroid lineage; therefore, patients with PV are at a high risk of thrombotic complications. A subgroup of patients also suffers from elevated white blood cells and platelet count. The other PV characteristics include the presence of the *JAK2V617F* found in 95% of patients and a low level of EPO serum in the blood. The level of EPO serum helps in distinguishing between primary polycythemia and secondary polycythemia. In patients with PV, increased erythrocytes result in suppression of EPO levels. Although EPO therapy has been used in many diseases such as anemia, renal failure, etc., it is not yet been initiated for treatment in PV.

In [116], median survival for PV patients is recorded as 18.9 years depending on age and sex. Patients older than 60 years or having a previous thrombosis history are taken at high risk. In rare cases, while progressing to PMF, polycythemia vera may lead to other blood diseases, including acute myeloid leukemia (AML), if white blood cell counts are greater than $11 \times 10^9/L$. According to WHO, PV diagnosis is required to

meet all three significant criteria or the first two primary criteria and the minor criterion (See Table 1.3).

Table 1.3 Diagnostic criteria for PV according to WHO [10]

Major Criteria	Minor Criteria
<p>Hb > 16.5g/dL in men, > 16.0g/dL in women, or Hct > 49% in men, > 48% in women, or increased red cell mass greater than 25% above mean normal predicted value</p> <p>Bone marrow biopsy showing hypercellularity for age with trilineage growth (panmyelosis), including prominent erythroid, granulocytic, and megakaryocytic proliferation</p> <p>Presence of <i>JAK2</i>V617F mutation or <i>JAK2</i> exon 12 mutation</p>	<p>Subnormal EPO serum level</p>

Primary Myelofibrosis

Primary myelofibrosis (PMF) is a rare disease that occurs in approximately 1 in 500,000 people worldwide. PMF is characterized by bone marrow failure. The hematopoietic compartment is replaced with collagen fibers, and the bone marrow is unable to provide enough normal blood cells required by the human body. Approximately 90% of patients with PMF carry *JAK2*, *CALR* or *MPL* mutations. These mutations are not directly linked to PMF because the patients diagnosed with PMF have a history of ET or PV. Patients with PMF have a high score of transformation to (AML).

PMF patients may not show any symptoms at the early stage, but later fibrosis leads to a reduced amount of erythrocytes, leukocytes, and platelets. Due to bone marrow failure, other organs such as the spleen or liver may begin to produce blood cells. Such a process is called extramedullary hematopoiesis, leading to an enlarged spleen or an enlarged liver. Primary myelofibrosis is often diagnosed in people aged 50 to 80 years. According to WHO, diagnosis is required to meet all three significant criteria or at least one minor criterion confirmed in two consecutive determinations (See Table 1.4).

Table 1.4 Diagnostic criteria for PMF according to WHO [10]

Major Criteria	Minor Criteria
<p>Proliferation and atypia of megakaryocytes accompanied by either reticulin and/or collagen fibrosis grades 2 or 3 on a scale of 0 to 3</p> <p>Not meeting WHO criteria for ET, PV, BCR-ABL1+ CML, myelodysplastic syndromes, or other myeloid neoplasm</p> <p>Presence of <i>JAK2</i>, <i>CALR</i> or <i>MPL</i> mutation or in the absence of these mutations, presence of another clonal marker or absence of reactive myelofibrosis</p>	<p>Anemia not attributed to a comorbid condition</p> <p>Leukocytosis $\geq 11 \times 10^9/L$</p> <p>Palpable splenomegaly</p> <p>LDH increased to above upper normal limit of institutional reference range</p> <p>Leukoerythroblastosis</p>

Inflammation, an instigator of MPNs

Inflammation is triggered by inflammatory cytokines secreted from immune cells. Inflammation is a protective reaction in response to an injury, repairing damaged tissue during wound healing. The acute inflammatory response is an instantaneous response to injury. However, dysregulation of this process may result in chronic inflammation, as exemplified by MPNs. Generally, patients' chronic inflammatory state ends up in the overproduction of inflammatory cytokines by both the neoplastic clones and immune cells. Chronic inflammation is also a risk factor for developing atherosclerosis and thrombosis in patients with chronic inflammatory diseases. Similar mechanisms are operative in all types of MPNs destabilizing hematopoietic homeostasis [48]. The

JAK2V617F mutation leads to an alteration in the signaling of hematopoietic cells important in inflammation with evidence of elevated platelets and leukocytes, alteration in inflammatory cytokine levels, and reactivity to these cytokines [53; 92; 93]. In the association between inflammation and C-reactive protein (CRP), the elevated CRP level is observed in patients with ET and PV [13].

In brief, MPNs are associated with a chronic inflammatory state denoted as the "human inflammation model" with "inflamed bone marrow," "inflamed stem cell niche," and "inflamed circulation" [45]. Inflammation is partly responsible for the pathogenesis of MPNs. Therefore, it represents an important therapeutic target.

Treatment Strategies

Treatment for blood cancer depends on several factors. In clinics, the patient's overall health and type of blood cancer are determined to initiate the therapies. Similarly, the treatment of MPNs depends on the presence of symptoms. In general, the treatment aims to correct the abnormal blood counts after recognizing the type of MPNs. Chemotherapy is one of the standard forms of treatment for MPNs. It uses drugs to kill malignant blood cells in the body. It may be taken in a pill form or may be administered as IV (intravenous). In contrast to chemotherapy, radiation therapy uses high-energy X-rays to kill malignant cells. It may also be used to prepare for a stem cell transplant. A stem cell transplant is a procedure to replace the diseased bone marrow with healthy bone marrow where a patient may receive stem cells from healthy donors. Besides, several clinical experiences explore that stem cells are a proven candidate for therapies. Many drugs like interferon-alpha (IFN) arrest the progression of the disease targeting stem cells.

Specific treatments are applied depending on the type of MPNs. Phlebotomy is a first-line therapy specifically for patients with PV. It is useful to remove excess red blood cells from the body. For patients suffering from blood clotting, chemotherapy is used instead of phlebotomy utilizing the drug hydroxyurea. It limits the bone marrow's ability to produce blood cells in the body. Low-dose aspirin is an alternative medicine for PV patients unless contraindicated by significant bleeding [35; 109].

Moreover, platelet apheresis is often preferred for patients with ET, where platelets are removed from the blood using a particular machine [17]. Immune therapy works by using treatments that boost the immune system to recognize and attack malignant cells. IFN is thought to be one of the treatments that can be taken as immune therapy and reduce blood cell production. Furthermore, targeted therapies are used in the treatment of some cases of MPNs. They can block or regress the production of malignant cells by focusing on particular characteristics unique to MPN cells. One type of targeted therapy that may be used to treat MPNs is ruxolitinib, a drug that targets, for instance, the *JAK2V617F* and other associated mutations [88]. It is often observed that PMF

patients have anemia that can be treated with blood transfusions. In addition, there are a variety of ways to treat anemia, for example, the hormone erythropoietin [52].

Finally, the concept of chronic inflammation as a severe driver of disease progression in MPNs opens the avenue for clinical trials. Since IFN is expected to normalize the bone marrow and ruxolitinib activates the anti-inflammatory cytokines. Therefore, combining IFN and ruxolitinib therapies within MPNs is among the foremost promising new treatment strategies for patients with MPNs [16; 44; 45; 46; 47].

1.3 Short Review of Existing Mathematical Models of Hematopoietic System and Hematological Diseases

This section presents a review of the existing mathematical models regarding hematopoiesis and hematology. Since the blood and bone marrow sampling is easily accessible, the hematopoietic system and its diseases have been studied extensively, and different types of mathematical models have been developed. Many strategies are elaborated to get the appropriate answers to some problems, such as regulating red blood cells, the impact of cycle disorders on various pathologies such as anemia or leukemia, or optimal therapeutic strategies about blood diseases. In the following, we overview a few mathematical models of the hematopoietic system and their applications.

Compartmental models are popular to describe the time evolution of the different hematopoietic cell types. In this type of model, each cell type is identified with one compartment, and its dynamics are described by one ordinary differential equation (ODE). In [73], a two-compartment model investigated quiescent and mitotic stem cells with constant delay in aplastic anemia and periodic hematopoiesis. With a more complicated version, this model has been studied in [4] and [94]. The model given in [73] has been extended to account for the dynamics of stem cells, erythrocytes, platelets and leukocytes in [26; 95]. The extended model has been used to investigate oscillation for parameter ranges observed in periodic chronic myeloid leukemia, cyclical neutropenia and thrombocytopenia. Also, there are few mathematical models describing erythropoiesis, thrombopoiesis, or granulopoiesis independently. Many authors have formulated mathematical models describing the regulation and formation of red blood cells and their related regulated mechanisms, specifically EPO. Some of these models are based on hematological diseases [9; 11; 15; 27; 39; 87], and the others investigate the mechanisms in healthy human beings such as blood donation, erythropoiesis stimulating agents, etc. [38; 118]. In [67], a mathematical model of thrombopoiesis

is presented to understand the origin of cyclic thrombocytopenia, whereas in [107], an age-structured model with both normal and pathological platelet production is developed. Both models involve the hormone growth factor, TPO, for the regulation of platelets.

Furthermore, compartment models have been used as a tool to study the dynamics of cancer cell populations. In [81], an ODE model described the dynamics of chronic myeloid leukemia. The model from [81] is extended in [68] including the differentiation of progenitor cells into stem cells and in [61] describing T-cell dynamics to study the impact of immune response on CML treatment using delay differential equations. Mathematical models have been proposed describing the control networks for regulating the stem cell lineage [58; 59; 127]. The mathematical model presented in [66] shows that therapy targeting stem cell pool may eliminate tumor stem cells. In [110], a mathematical model of cancer stem cell dynamics is proposed, and the different scenarios of cancer initiation and possible treatment strategies have been discussed. The mathematical model given in [112] is useful for investigating the impact of cytokine dependence and independence of acute myeloid leukemic cells supported by patient data. A few modeling studies of myeloid malignancies were investigated in [43; 129] with MPNs as a particular example.

Cancitis Model

The Cancitis model is given special attention in this review since it becomes the foundation of this thesis. It was proposed in [7] (See Appendix A for details), where Andersen et al. aimed at building a mathematical model incorporating chronic inflammation as the trigger and driver of MPNs. The model consisted of a system of nonlinear ordinary differential equations describing the proliferation from stem cells to mature cells and healthy stem cells' mutations to become malignant stem cells. The model coupled the cell dynamics with an inflammatory response by introducing inflammatory feedback into the system. The model was used to describe interactions between macrophages, inflammatory and anti-inflammatory cytokines. The authors hypothesized that chronic inflammation is not triggered when the immune system is functioning properly. Hence, the model supported the concept of the "human inflammation model" [45] for MPNs development. Furthermore, the reduced Cancitis model consisting of two-dimensional equations was discussed in [86] (See Appendix B for details), including the effect of T-cells explicitly. The authors introduced a reproduction ratio of stem cells and concluded that the body might manage the initial stage of blood cancer when the self-renewal rate of malignant cells is not high. However, it fails to handle it if inflammation occurs.

Subsequently, a detailed mathematical analysis of the Cancitis model [7] is performed in [102], where Sajid et al. explore the interesting results showing the intricate

coupling between inflammation and MPNs. The classification of steady states is explicitly done in terms of inflammatory stimuli. Sajid et al. introduced a reproduction ratio similar in [86] and, besides, a ratio of inhibition of the hematopoietic relative to malignant stem cells is found. Moreover, it is demonstrated that by increasing inflammatory stimuli, a healthy state is transformed into a malignant state and reduces disease load for a co-existing steady state. The model provides an overview of the possible dynamics that may inform clinical practice, such as using inflammatory inhibitors during treatment.

Another reduction of the Cancitis model is presented in [8], where a two-dimensional model represents the *JAK2V617F* allele burden and white blood cell count as variables. The model suggests the treatment initiation at the early phase of the disease. The ratio of self-renewal of the hematopoietic and malignant stem cells is indicated as an important diagnostic marker. A further reduction to a one-dimensional model depends upon the allele burden suggested that exogenous inflammation develops blood cancer when malignant stem cells regenerate more than hematopoietic stem cells. Apart from a system of non-linear ODEs, the authors of [7] presented a data-driven analysis for the allele burden dynamics and argued early intervention strategy with interferon- α treatment. The empirical modeling approach to describe the behavior of the data was considered [90] (See Appendix C for details).

1.4 Overview of Thesis

The questions that form the basis of this thesis result from combining information from many publications. Besides Chapter 1 and Chapter 5 each of the chapters constitutes a stand-alone scientific contribution. In this section, we present a brief summary of our results. Note, to avoid unnecessary repetition, the description of parameters is not given in this section. We refer the reader to see the definition of parameters in their related chapters. In each mathematical model, HSC denotes the hematopoietic stem cells and MSC denotes the malignant stem cells.

Chapter 1 contains introductory and concluding remarks.

Chapter 2 consists of the published research [102]. In Chapter 2, we analyse Cancitis model [7] mathematically and numerically. MPNs are commonly known as inflammatory diseases, and it is believed that chronic inflammation triggers MPNs progression. Also, a number of evidences indicate that hematopoietic stem cell is the MPN-initiating cell and MPN is found to derive by the outgrowth of a single stem cell. Based on these perceptions, the first two research question addressed in Chapter 2 are,

- When is it suitable to give anti-inflammatory agents in clinical practice?
- What are the key features of the stem cells, contributed in the progression of

MPNs?

The Cancitis model includes one lineage of healthy cells and one lineage of malignant cells. We retain the possibility that a stem cell may self renew, die, or differentiate into a mature cell. A mature cell does not differentiate but dies. Moreover, the debris of dead cells is common for both lineages, and the model is coupled with the inflammatory system. The model incorporates a possible mode of interaction between healthy and malignant cells such as niche feedback inhibiting factors. Thus, the Cancitis model consists of six ordinary non-linear differential equations, the number of HSC (x_0), the number of MSC (y_0), the number of healthy mature cells (HMC- x_1), the number of malignant mature cells (MMC- y_1), the debris of dead cells (a) and the immune response i.e. the inflammatory level (s).

We conduct a mathematical investigation of the Cancitis model and establish the criteria for existence of physiological steady states. These steady states include a trivial steady state, a healthy steady state without malignancy, a full-blown diseased steady state and a co-existence steady state where both healthy and malignant cells exist. We explore the coupling between MPN progression and increased inflammation. Furthermore, a stability analysis enables us to have a range of parameters for which the treatment becomes successful and hematopoietic state becomes stable. The model has been investigated for various choices of parameter values. In figure 1.4.1 (Figure 2 in [102]), clusters of five important parameters are considered to investigate the number of steady states and their stability, $\mathcal{C} = \frac{c_{xx}}{c_{yy}}$, $\mathcal{R} = \frac{\zeta_{H2}}{\zeta_{L2}} = \frac{\alpha_x}{\alpha_y}$ and I where,

$$\alpha_x = \frac{d_{x0} + a_x}{r_x} \quad \text{and} \quad \alpha_y = \frac{d_{y0} + a_y}{r_y}. \quad (1.4.1)$$

We may interpret that \mathcal{R} denotes the fitness of stem cells. \mathcal{R} represents if malignant stem cells have better fitness than hematopoietic stem cells, the situation becomes worse. \mathcal{C} interprets the inhibition of hematopoietic relative to malignant cells. Generally, in blood cancer, $c_{yy} \leq c_{xx}$ is assumed since malignant cells are insensitive to environmental effects. The parameter I represents the external inflammatory effects and is assumed to depend on external factors such as smoking.

In Fig. 1.4.1, we can observe that for $\mathcal{R} > 1$, the hematopoietic and co-existing steady states are either unstable or do not exist (See Fig. 1.4.1a-1.4.1b). However, for $\mathcal{R} < 1$, several possibilities of obtaining the unique stable hematopoietic or co-existing steady states emerge in a specific parameter regime. The bi-stability of the hematopoietic and malignant steady states is also illustrated for a range of parameter values. Moreover, Fig. 1.4.1a and Fig. 1.4.1b illustrate that for $\mathcal{R} > 1$, reducing inflammatory stimuli may worsen the situation since it vanishes the hematopoietic steady state. In contrast, when hematopoietic stem cells have better fitness than malignant stem cells, i.e., $\mathcal{R} < 1$, increasing inflammation does not have adverse effects (See Fig.

1.4.1f).

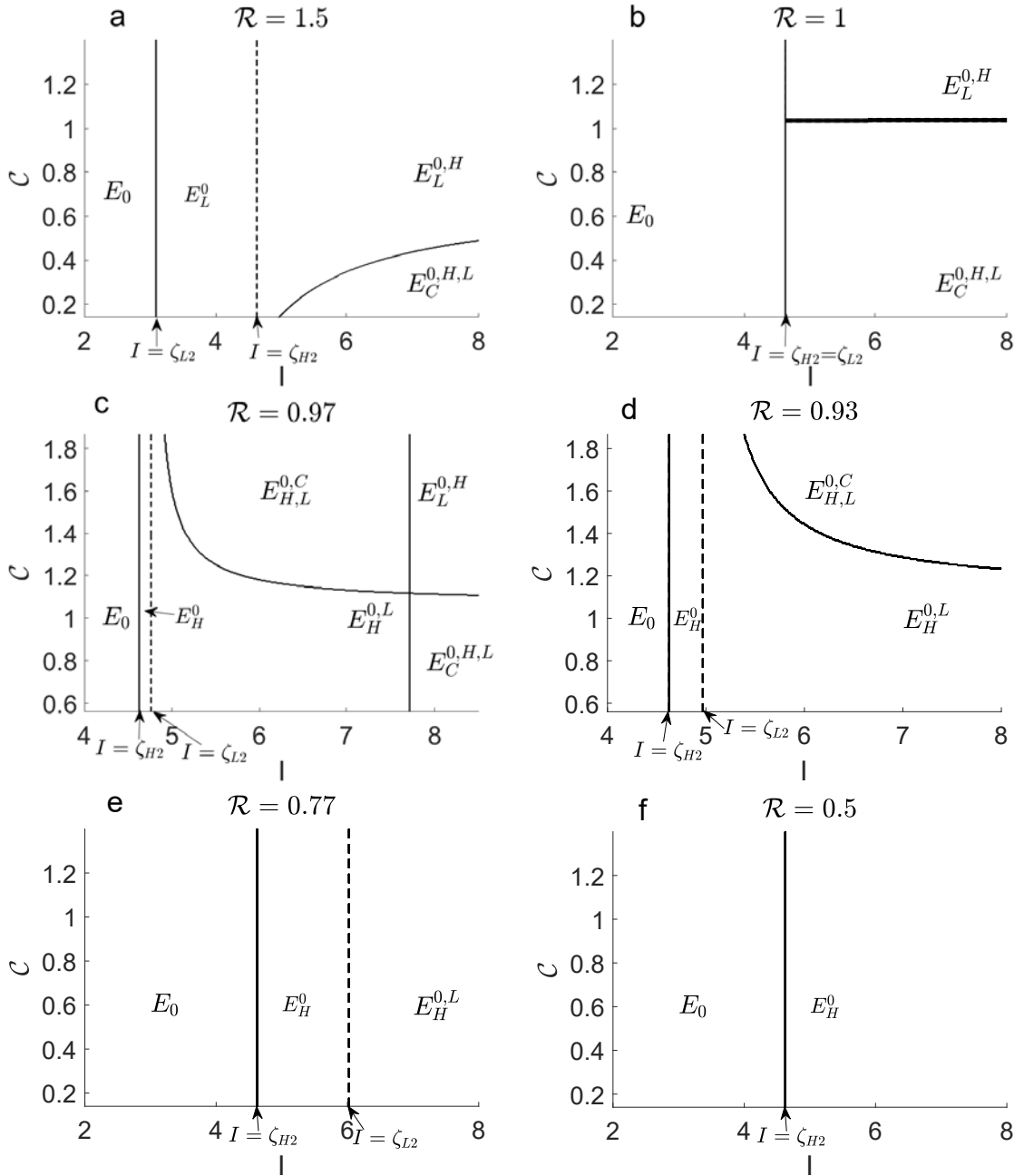


Fig. 1.4.1 Admissibility and stability of the steady states depending on the parameters I and C for different values of \mathcal{R} . Crossing a solid curve implies a change in which type of stable steady state exists i.e. trivial, malignant, hematopoietic or coexistence. Crossing a dotted curves implies the same steady state is stable in both regions but the number of steady states is changed. The stable steady states are written as subscript of E and unstable steady states are written as superscript of E .

The Cancitis model generally focused on the progression of MPNs and not on any specific type of MPNs. Motivated by the Cancitis model, we now narrow our research towards types of MPNs. Chapter 3 and Chapter 4 consist of [103] and [104] (submitted for publication). In these chapters, we address PV and important factors involved in

the progression of PV. In Chapter 3, a system dynamic approach is used to simulate the model outcome and dynamics, whereas in Chapter 4 a complete mathematical investigation is covered. These two different styles of chapters presenting the same model help facilitate a wide range of readers. Following, we briefly describe the results of both chapters.

As mentioned above, in detail, PV is characterized by the excessive production of red blood cells, and EPO is primarily responsible for erythropoiesis. The other characteristics of PV is a high load of the *JAK2V617F* allele burden [44; 45; 64] and low EPO plasma levels [23]. Moreover, thrombosis is the most prevalent complication for patients with PV [41] and the development of second cancer is the high risk factor. Several authors hypothesize that origin of MPN, including all its types, is the hematopoietic stem cells. Also, we have explored the importance of stem cell parameters in Chapter 2. The development of stem cell therapies for myeloid malignancies like PV and ET is getting attention in recent years [57; 61; 72; 83; 91; 106; 123]. Furthermore, in clinical trials, EPO is the popular erythropoiesis-stimulating agent used in several hematological diseases such as anemia, PMF, etc. However, EPO therapy is not yet been initiated in PV. In our mathematical model, it is possible to evaluate the influence of both EPO and stem cell dynamics on the progression and regression of the disease. Thus, we post a set of questions in [103] and [104],

- How do stem cells control erythropoiesis in the development of PV?
- Which parameters are crucial for the abnormal growth of erythrocytes in PV?
- Which mechanisms are mainly responsible for the development of disease?
- How does EPO associate with the *JAK2V617F* allele burden?

Concerning PV, we formulate a novel mathematical **PV model**. Based on the concept of the Cancitis model, we consider one lineage of healthy cells and one lineage of malignant cells. We specify that the stem cells may self renew and die but differentiate only into the erythroid lineage. A mature red blood cell does not differentiate but dies. Moreover, we include multiple EPO feedback on healthy and malignant cells. We consider that EPO inhibits the death rate and stimulates the differentiation rate of mature cells. In addition, EPO production is taken as a Hill function of mature cells. Thus, the PV model consists of five ordinary non-linear differential equations, the number of HSC (x_0), the number of erythrocytes (RBC- x_r), the number of MSC (y_0), the number of malignant erythrocytes (MMC- y_r) and the concentration of EPO (E).

A thorough analytical and numerical investigation has been done for PV model. The number of parameters is reduced from 23 to 15 due to dimensional analysis, and the sensitivity analysis is performed to explore the relationship between the input parameters and the PV dynamics outcome. In addition, the trapping region \mathcal{T}_R of the resulting dimensionless PV model is constructed for non-negative initial conditions.

The interesting feature of the model is that the stem cell dynamics can be independently analyzed as a two-dimensional system. The possible steady states of the **stem cell submodel** depend on four parameters. The parameter p_{x1} describes the inhibition of Y_0 on X_0 (hematopoietic stem cell count), p_{y1} describes the inhibition of X_0 on Y_0 (malignant stem cell count), whereas p_{x2} and p_{y2} are the degradation rates of X_0 and Y_0 respectively. Following proposition 1.4.1 (Proposition 1 in [104]) describes the possible steady states of the two-dimensional stem cell submodel.

Proposition 1.4.1. Conditions allowing existence and stability of feasible steady states of two-dimensional stem cell submodel are,

1. A trivial stem cell steady state, D_0 , always exists and is stable for $p_{x2} > 1$ and $p_{y2} > 1$.
2. A feasible hematopoietic stem cell steady state, D_H , exists and is unique if and only if $p_{x2} < 1$ with $\bar{X}_{0H} = \frac{1}{p_{x2}} - 1$. D_H is stable for $p_{y1} > \gamma^{-1}$ and unstable for $p_{y1} < \gamma^{-1}$.
3. A feasible malignant stem cell steady state, D_L , exists and is unique if and only if $p_{y2} < 1$ with $\bar{Y}_{0L} = \frac{1}{p_{y2}} - 1$. D_L is stable for $p_{x1} > \gamma$ and unstable for $p_{x1} < \gamma$.
4. A feasible co-existing stem cell steady state, D_C , exists and is unique if $p_{x2} < 1$ and $p_{y2} < 1$ and either (a) or (b) is fulfilled, where
 - (a) $p_{x1} < \gamma$ and $p_{y1} < \gamma^{-1}$. In this case D_C is stable.
 - (b) $p_{x1} > \gamma$ and $p_{y1} > \gamma^{-1}$. In this case D_C is an unstable (saddle).

D_C is only feasible, when D_H and D_L exist. The coordinates of D_C are $\bar{X}_{0C} = \frac{\bar{X}_{0H} - p_{x1}\bar{Y}_{0L}}{1 - p_{x1}p_{y1}}$ and $\bar{Y}_{0C} = \frac{\bar{Y}_{0L} - p_{y1}\bar{X}_{0H}}{1 - p_{x1}p_{y1}}$.

Proof. See Chapter 4 for details. □

Interestingly, the dynamics of the PV model and the stem cell submodel are uniform. (See corollary 1.4.1) (Corollary 1 in [104]).

Corollary 1.4.1. *The existence of the steady states of the PV model is guaranteed by the stem cell PV submodel given in proposition (1.4.1), i.e.,*

- A trivial steady state $S_0 = (0, 0, 0, 0, 10^4)$ always exists.
- A feasible hematopoietic steady state $S_H = (\bar{X}_{0H}, 0, \bar{X}_{rH}, 0, \bar{E}_{qH})$ exists if and only if a feasible D_H exists in the stem cell PV submodel.
- A feasible malignant steady state $S_L = (0, \bar{Y}_{0L}, 0, \bar{Y}_{rL}, \bar{E}_{qL})$ exists if and only if is a feasible D_L exists in the stem cell PV submodel.
- A feasible co-existing steady state $S_C = (\bar{X}_{0C}, \bar{Y}_{0C}, \bar{X}_{rC}, \bar{Y}_{rC}, \bar{E}_{qC})$ exists if and only if a feasible D_C exists in the stem cell PV submodel.

The quasi steady state approximation for EPO concentration allows reduction of the five-dimensional PV model into a four-dimensional system (**the reduced PV model**) where both models have identical steady states.

Using the reduced PV model, we have performed a few *in silico* experiments by perturbing parameters involved in stem cells, mature cells, and EPO for the prognosis of a virtual subject. In Fig. 1.4.2 (Fig.7 in [104]), we perturb stem cells inhibiting factors p_{x1} and p_{y1} for treatment. To obtain a co-existing steady state, we choose $p_{x1} = 1.3$, $p_{x2} = 0.25$ $p_{y1} = 0.1$ and $p_{y2} = 0.4$ while all other parameters are fixed at their default values (See details in Chapter 4).

In Figures 1.4.2a-1.4.2b the solution to the reduced PV model is projected on the (X_0, Y_0) plane. In Figure 1.4.2a by simulating a drug increasing p_{y1} and decreasing p_{x1} , a co-existing steady state with high malignant cell count $(X_0, Y_0) = (1.21, 1.38)$ switches to a co-existing steady state with low malignant cell counts $(X_0, Y_0) = (2.95, 0.47)$. It takes approximately two years for this simulated treatment to reduce the disease load. Thereafter, treatment is set on pause by resetting p_{x1} and p_{y1} at their previous values. During almost half a year, the trajectory moves significantly back towards the co-existing steady state with high malignant cell counts (see Figure 1.4.2b).

Thus, perturbing inhibiting factors normalizes the HSC and RBC count (See Figure 1.4.2c, Figure 1.4.2d). In order to reduce the risk of blood clots, the RBC count is recommended to be in a normal range. Furthermore, Figure 1.4.2e shows that the concentration of EPO is increased, whereas Figure 1.4.2f illustrates that adjusting inhibiting factors reduces the *JAK2V617F* allele burden from 53% to 16%, which is an excellent prognosis. In conclusion, it may suggest that future PV therapy should focus on targeted, personalized treatment addressing specific alterations within the bone marrow niche.

In the model, we implement the idea of EPO therapy. We increase the parameters (the factor affecting the production of EPO) and observe that the EPO concentration and the number of mature cells are decreased. In the second case, when EPO dose is given. It increases the mature cell count while the *JAK2V617F* allele burden remains unchanged. Using EPO as a prognostic tool may reduce the risk of thrombosis in PV patients, for the short time, it may not reduce the disease load, which eventually can trigger the chances of relapse. Validation of the proposed model is attained by comparing the model simulations to clinical data, which contains the number of erythrocytes and measurement of the *JAK2V617F* allele burden. However, we do not have available EPO data of PV patients.

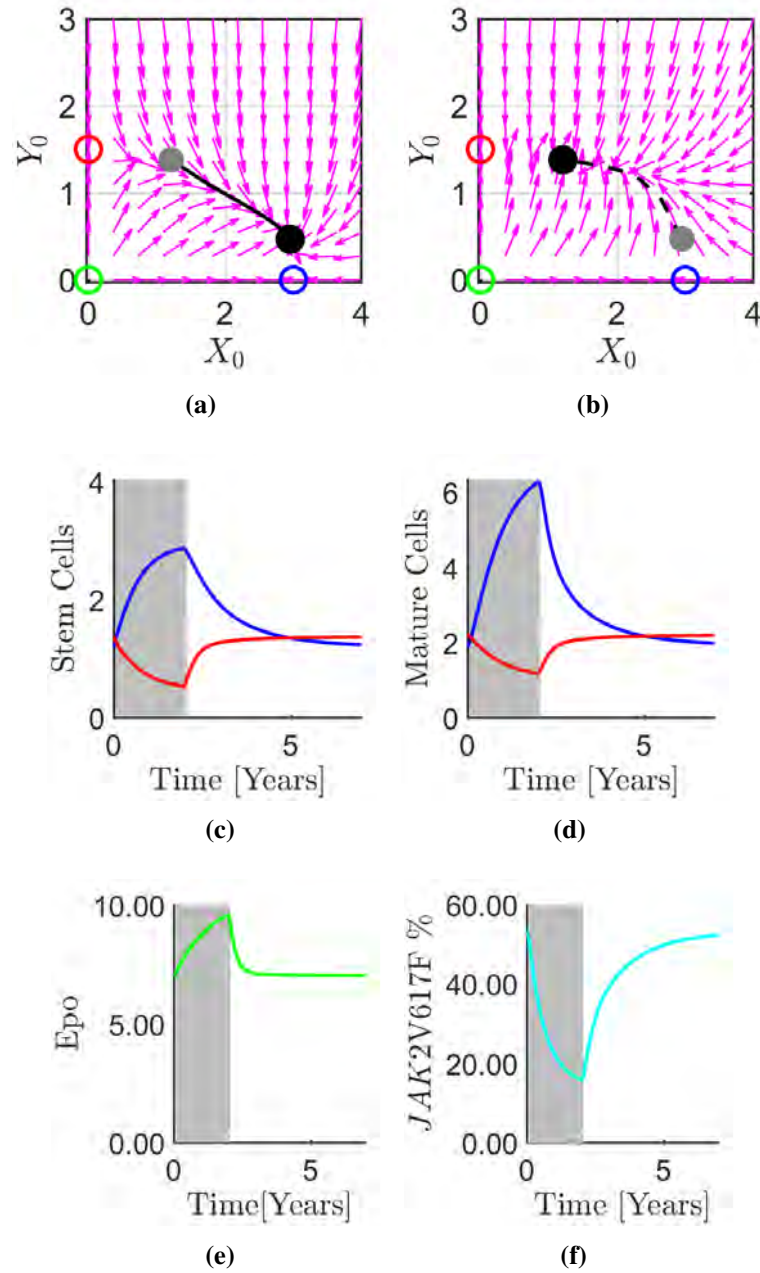


Fig. 1.4.2 An example of the disease dynamics from the reduced PV model is shown. The filled grey circle in panel (a) is obtained using $p_{x1} = 1.3$, $p_{x2} = 0.25$, $p_{y1} = 0.1$ and $p_{y2} = 0.4$. Decreasing p_{x1} and increasing p_{y1} in panel (a) shows that a patient is moved from a co-existing steady state (upper grey circle) with high malignant cell count towards a co-existing steady state (lower black circle) with low malignant cell count and normalized hematopoietic cell count at $p_{x1} = 0.1$, $p_{x2} = 0.25$, $p_{y1} = 0.35$ and $p_{y2} = 0.4$. In panel (b), setting back p_{x1} and p_{y1} , the patient moves back toward the original co-existing steady state (upper black circle) following the stipulated black curve. Panels (c), (d), (e) and (f) demonstrate the dynamics during treatment period (grey) and dynamics after treatment. Red, blue, green and cyan curves show malignant cells, hematopoietic cells, the concentration of EPO, and the JAK2V617F allele burden respectively. Note, the time scale is converted into real time.

The encouraging results obtained by the PV model further motivate us to discover the mechanism in patients with ET. As mentioned, ET is characterized by the excessive production of platelets. The precursor of platelets are megakaryocytes, and each

megakaryocyte sheds into thousand of platelets. The production of megakaryocytes is called megakaryopoiesis, and TPO is principally responsible for this process. Since all types of MPNs share common features, ET is also thought to be triggered by a stem cell disorder like PV. Thus, it will be captivating to investigate the role of stem cell dynamics and TPO in the **ET model**. Chapter 5 discusses a set of questions as follows,

- What is the role of stem cell dynamics in the development of ET?
- Which parameters are crucial for the progression, relapse and cure of the disease?
- By which mechanism does TPO concentration affect the pathogenesis of ET?

Concerning ET, we formulate a novel mathematical **ET model**. Based on the concept of the previous two models, we consider one lineage of healthy cells and one lineage of malignant cells. However, this model does not consist of symmetrical properties for both cell lineages like the Cancitis model and PV model. We specify that stem cells may self renew and die but differentiate only into the megakaryocytic lineage. A megakaryocyte may die or shed into platelets. Moreover, we include multiple TPO feedback on healthy and malignant cells. We consider that TPO inhibits the death rate of healthy megakaryocytes and malignant platelets. Furthermore, TPO stimulates the differentiation rate of megakaryocytes and the self-renewal rate of stem cells in both lineages. TPO is either eliminated naturally or degraded by platelets. Thus, the ET model consists of seven ordinary non-linear ODEs, the number of HSC (x_0), the number of megakaryocytes (MEG- x_m), the number of platelets (x_p) the number of MSC (y_0), the number of malignant megakaryocytes (MMEG- y_m), the number of malignant platelets (MPLT- y_p) and the concentration of TPO (T).

We perform an analytical investigation of steady states and their stability wherever is possible. However, a numerical investigation has been given much attention to describe behavior of the system. We characterize the steady states and their stability. A set of bifurcation diagrams capture the interesting dynamics of the model. Various approaches to numerical investigation reveal that stem cell parameters describe the possible topologies. For instance, Fig. 5.3.3 illustrates different types of stable and unstable steady states when the death rates of stem cells d_{x_0} and d_{y_0} are varied.

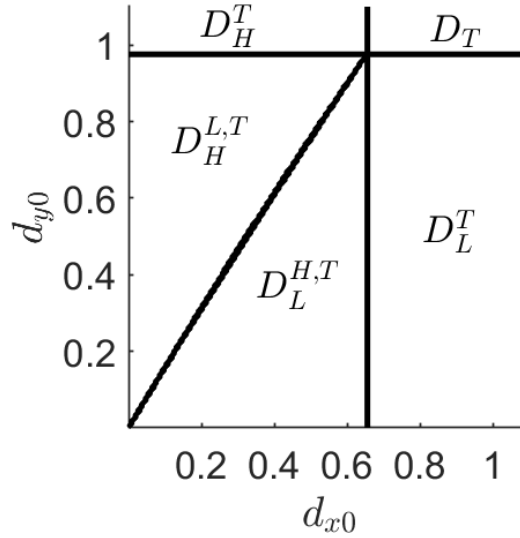


Fig. 1.4.3 The stability of the steady states, i.e. trivial, malignant, hematopoietic or coexistence, depending on the parameters d_{x0} and d_{y0} . The stable steady states are written as a subscript of D and unstable steady states are written as a superscript of D.

The derived results by sensitivity analysis further support the importance of stem cell parameters. We found that the self-renewal and death rates of the stem cells influence all the included variables. However, we may not ignore the significance of niche inhibiting factors of the stem cells. We may obtain a stable or unstable co-existing steady state by perturbing niche inhibiting parameters. The excellent fits of clinical data during treatment are obtained by perturbing d_{x0} and d_{y0} . For the available data before and during treatment, we identify a set of parameters for pre-treatment data-fit and perturb d_{x0} and d_{y0} while fitting data of treatment period for the same subject. Apart from data fitting, we conduct an in silico analysis of TPO in patients with ET. Our model indicates that reducing TPO concentration may reduce the blood counts in bone marrow and bloodstream, but it might not reduce the disease load. In general, ET does not shorten the life expectancy of a patient. However, patients having a history of thrombosis are considered to be at intermediate risk. TPO serum levels may be administered, preventing the risk of thrombosis. The TPO mechanisms in the pathogenesis of ET are yet to be revealed. In short, we need more clinical data containing TPO measurements for ET patients to validate our results.

In previous chapters, we have performed a series of investigations for myeloid malignancies. The contributions further motivate us to extend our mathematical model and study the combined dynamics of erythrocytes and platelets. However, in the first step, we do not include malignant cells because the mathematical model setting requires calibration and validation for healthy individuals. Thus, a few set of interesting questions arise for investigation,

- Which subsets of parameters are important for the independent mechanisms of

erythropoiesis and thrombopoiesis?

- How do EPO and TPO affect different cell populations?
- Which parameters are sensitive for the model outcome?
- How does the study contribute to understand the clinically observed dynamics?

In Chapter 6, we propose a framework for a novel mathematical model [105] describing a coupled mechanism of erythropoiesis and thrombopoiesis to address the questions mentioned above. The seven-dimensional mathematical model consists of non-linear ODEs. The three ODEs describe the dynamics of HSC (x_0), megakaryocyte-erythroid progenitor (MEP- x_c) and megakaryocytes (MEG- x_m) in the bone marrow, whereas four ODEs are considered for the erythrocytes (RBC- x_r), platelets (PLT- x_p), EPO (E) and TPO (T). Furthermore, we incorporate multiple feedback regulated by EPO and TPO for the production of cell populations.

We assume that HSC differentiates into MEP cells where MEP cells have potential to give rise to both erythroid and megakaryocytic cells and megakaryocytes shed into platelets [32]. Reviewing literature discloses various physiological processes relating EPO and TPO with different types of cells from where we capture a few necessary mechanisms. For instance, TPO stimulates HSC by affecting the self-renewal of HSC, EPO stimulates RBC differentiation and inhibits their death rate. Moreover, TPO stimulates RBC and PLT count and PLT stimulates the degradation of TPO while TPO inhibits the death rate of MEG and EPO inhibits megakaryopoiesis.

Interestingly, erythropoiesis and thrombopoiesis subsystems can be independently analyzed apart from the full model. These subsystems are useful for estimating important subsets of the full model parameters involved in the various clinical experiments. In addition, the subsystems are prioritized in clinical trials where the physicians are interested in observing hematological parameters specific to erythroid or megakaryocyte lineage. However, the drawback of subsystems is that they are unable to represent the coupled mechanisms between erythropoiesis and thrombopoiesis. The simplified structures of subsystems allow us to perform mathematical investigations and find their steady states. These subsystems have a unique positive steady state and stability conditions of these steady states are stated.

A sensitivity analysis shown in Fig. 1.4.4 (Fig. S6 in [105]) identifies the sensitive parameters for variables involved in the model. We choose a 10% variation in the parameter values to observe the changes in cell count and concentration of EPO and TPO. Fig. 1.4.4a shows -10% variation, whereas Fig. 1.4.4b shows +10% variation in parameter values.

1. **HSC parameters:** The self-renewal rate r_x , death rate d_{x0} and inhibiting factor c_{xx} involved in HSC do not affect erythrocytes and EPO. However, increasing r_x increases the other cell population (HSC, MEP, MEG) and decreases the TPO

levels or vice versa. In contrast to r_x , increasing d_{x0} and c_{xx} reduces the HSC, MEP, MEG and PLT count while increases the TPO level. Notice, HSC, MEP, MEG and PLT count is equivalently increased or decreased.

2. **MEP parameters:** The differentiate rate a_x , amplification factor A_x , a fraction of MEP b_x and death rate of MEP d_{xc} are involved in MEP dynamics. Decreasing A_x and b_x shows a little increase in HSC and MEP count however, MEG and PLT count is reduced by 10%, whereas the TPO levels are increased or vice versa. The change in EPO level and RBC count is not noticeable compared to b_x when A_x is decreased. d_{xc} is the least sensitive parameter involved in the MEP equation.
3. **Subsystem 1 (Erythropoiesis):** The production of RBC is affected by δ_{xr1} and δ_{xr2} and the death rate of RBC is affected by η_{xr1} and η_{xr2} . Moreover, EPO production involves p_E and k_0 whereas, the degradation of EPO is denoted by k_E . The influence of parameters on HSC and MEP involved in subsystem 1 is not notable. Decreasing δ_{xr1} and η_{xr2} decreases the RBC and PLT count while EPO and TPO levels are increased or vice versa. Similarly, reducing δ_{xr2} and η_{xr1} increases the RBC and PLT count and decreasing the EPO and TPO levels or vice versa. Reducing p_E and increasing k_0 and k_E , increases the MEG and PLT count, and reduces the RBC count, EPO and TPO levels or vice versa.
4. **Subsystem 2 (Thrombopoiesis):** The production of MEG involves δ_{xm1} and δ_{xm2} and the death rate of MEG is affected by η_{xm1} and η_{xm2} . PLT are produced with the rate $b_{xp}a_{xp}$ and d_{xp} is the death rate of PLT. The production of TPO is represented by p_T , whereas k_{T1} and k_{T2} show the degradation of TPO. Decreasing (increasing) δ_{xm1} , a_{xp} and k_{T2} increases (decreases) the HSC and MEP count, whereas decreasing (increasing) δ_{xm2} , d_{xp} and p_T decreases (increases) the HSC and MEP count. Decreasing δ_{xm1} and η_{xm2} , and increasing δ_{xm2} and η_{xm1} decreases EPO levels and the number of MEG and PLT, while increases the RBC count and TPO concentration or vice versa. Moreover, reducing b_{xp} and a_{xp} , and increasing d_{xp} increases the number of MEG and RBC and TPO levels while the PLT count and EPO levels are reduced. Furthermore, decreasing p_T and increasing k_{T1} and k_{T2} decreases the TPO levels and the number of MEG, PLT and RBC, whereas increasing the EPO concentration.

For accurate results, we calculate the numerical values of variables involved in the model after perturbing the parameter values by $\pm 10\%$ and conclude that the parameters involved in HSC dynamics are the most sensitive for HSC and MEP count. Notice, HSC and MEP are increased and decreased simultaneously with equal percentage. The parameters A_x and b_{xp} vary MEG count by 8% and we may say that they are inversely related to each other, i.e., if A_x increases the number, b_{xp} decreases the MEG count. Analyzing the PLT count, the parameters A_x and d_{xp} differ PLT count by 8% and 6%

respectively. Considering RBC count and EPO, we notice that p_E , k_E and k_0 perturb the variables by 5%. Note, k_E and k_0 have the same effect, i.e., either decreases or increases the number of RBC and EPO levels, whereas p_E has an opposite effect compared to k_E and k_0 . Finally, TPO concentration is sensitive to A_x and p_T and we observe a 6% variation in TPO levels when these parameters are changed. However, A_x and p_T have inverse effects on TPO levels. If one induces the increase, the other decreases the levels.

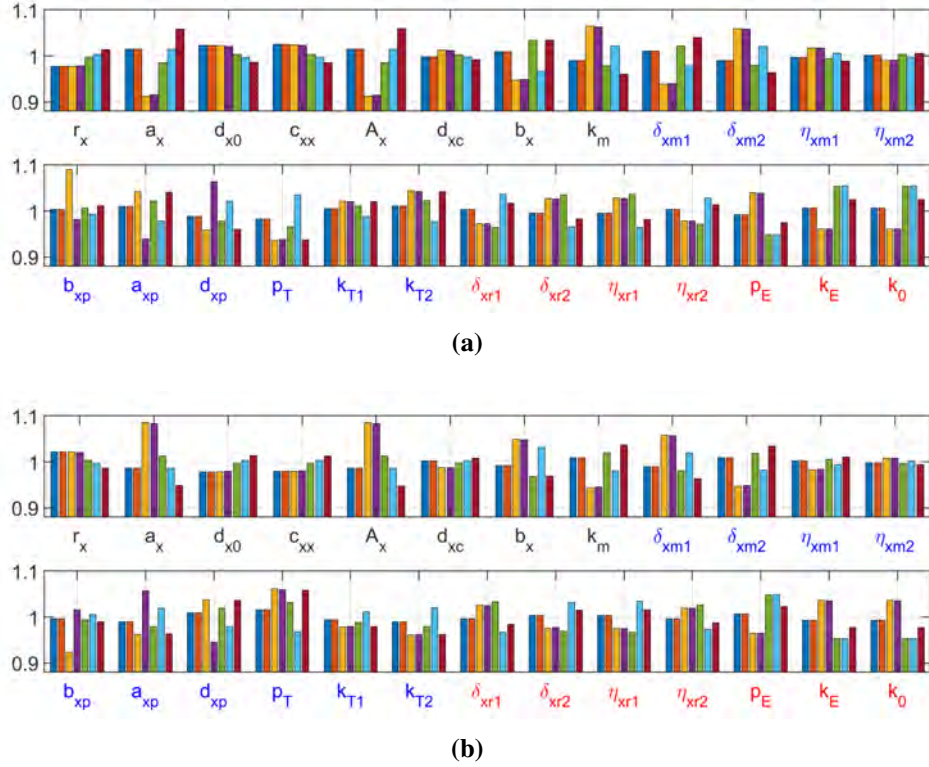


Fig. 1.4.4 Panels (a) and (b) show the effect when parameters are decreased and increased by 10% respectively. For each parameter, seven columns are shown; blue, red, mustard, purple, green, light blue and maroon correspond to the average of x_0 , x_c , x_m , x_p , x_r , E and T . Parameters in red represent the subsystem 1 and parameters in blue represent the subsystem 2.

Furthermore, we calibrate the model by fitting to various experimental data set. The appropriate fitting of data is an appealing feature of the model. The model and its subsystems stipulate excellent results which adequately describe many critical situations such as recovery of the blood cells after phlebotomy, body's reaction to different administration regimens of EPO and TPO. For the default values of parameters, we are able to fit a few data sets for of phlebotomy. Furthermore, the subsystems are in excellent agreement with the data. These subsystems help us estimate parameters of the full model in many situations where coupling between the two subsystems is of no interest. For instance, the parameters η_{xr1} , p_E and k_E are estimated in subsystem 1, used for data fitting in the full model in case where EPO dose stimulates the RBC count.

Similarly, in another scenario, where TPO dose stimulates the platelet count, we use the same parameters values from subsystem 2 for data fitting in the full model. However, a drawback of these nested models is their inability to explain the coupled mechanisms of full model. For example, in [50], the authors were interested in investigating PLT count when EPO injection is given. In such situations, our full model may interpret the outcomes of clinical trials.

Besides data fitting, we conduct several other *in silico* experiments for a virtual subject. For example, the transfusion of red blood cells and platelets. These procedures are primarily preferred for hematological diseases because such *in vivo* experiments are critical for healthy individuals. Our model indicates that HSC remains unaffected after blood transfusion and apheresis. During these treatments, the mechanism affecting HSC are not yet well understood. Therefore, we might not interpret this effect accurately in a physiological sense. In our model, we are able to investigate the synergy between EPO and TPO and simulate the combined effect of EPO and TPO dose. The analysis shows that HSC, MEP and RBC count are increased, whereas the MEG and PLT count is first decreased, and then after a few days, the number of MEG and PLT is increased. However, when the TPO dose is given alone, we have not seen this sudden drop in MEG and PLT count. According to our perception, this sudden drop can be eliminated by decreasing inhibiting effect of EPO on MEG.

In summary, the presented model has the novel feature of simulating and replicating the coupled dynamics of erythropoiesis and thrombopoiesis. The adaptations necessary to combine them are discussed in detail. We demonstrate how the proposed model and its subsystems can develop clinically meaningful predictions regarding EPO and TPO applications. The overall analysis strengthens the argument that our model is a valid candidate in clinical settings for various experiments. As a future perspective, the model can be extended for multiple hematological diseases where we may include the different pathological aspects for the novel intervention strategies.

1.5 Concluding Remarks and Future Perspectives

In this thesis, a series of mathematical models describing the physiology and pathology of cells have been discussed with various feedback loops. We briefly explain the similarities and differences between the models. In each proposed model, a mechanism-based approach is employed however, only the essential mechanisms are captured. The models consist of one HSC compartment with a common structure in all models, i.e., HSC may self-renew, die or differentiate into the progenitor cells. The niche feedback inhibits HSC self-renewal and is implemented as Michaelis-Menten like expression.

HSC differentiates into the mature blood cells, which are distinct in the models. For instance, in Chapter 2 (Cancit model), the mature blood cell type is not distinguished. In Chapter 3 and Chapter 4 (PV model), red blood cells are specific. In Chapter 5 (ET model), platelets are considered, and in the last Chapter 6, combined dynamics of red blood cells and platelets are introduced.

The Cancit model, PV model and ET model, except the model proposed in Chapter 6, contain malignant cell lineage where malignant stem cells have a similar structure to HSC. Another common feature is considering the progenitor cells as intermediate steps between stem cells and mature blood cells. Unlike the ET model, the Cancit model and PV model have a symmetrical structure of healthy and malignant cells. The Cancit model entails the debris of the dead cells and immune system influenced by inflammatory stimuli. These mechanisms are not considered in the remaining models since the remaining models focus on the inclusion of principal growth factors for mature blood cells. The Cancit model, PV model and ET model revolve around the importance of stem cell dynamics. The models reveal that HSCs contribute to the initiation and pathogenesis of MPNs. Therefore an efficacious treatment should act on stem cell level. In addition, EPO and TPO therapies may refer as preventive therapies for thrombosis. However, they cannot reduce the disease load and reverse a malignant state to a healthy state. Its possible explanation may be the inappropriate interpretation of *JAK2* allele burden. However, we need clinical data to advocate our results and draw any conclusion. Above all, each model can regenerate clinically observed dynamics and suggest novel intervention strategies. Finally, in Chapter 6, we integrate the healthy hematopoiesis part of the PV and ET model. Based on existing clinical information, we decide which mechanisms are essential to include. We calibrate the model by comparing different simulation settings to existing experimental results from the literature.

A motivating application of the proposed model in Chapter 6 is to observe the evolution from ET to PV. However, a shortage of time does not enable us to complete the ongoing work in this thesis. TPO related *MPL* mutations are found in 1-3% cases of ET [14; 89] and increased TPO serum levels are observed in many patients with ET [51; 69; 98]. However, many novel mechanisms relating to high TPO levels and abnormal platelet production in ET are still hidden and waiting for uncovering. Similarly, EPO serum levels help in distinguishing between primary polycythemia (PV) and secondary polycythemia. In patients with PV, increased erythrocytes result in suppression of EPO levels. Although EPO therapy has been used in many diseases, it is not yet been initiated for treatment in PV.

In clinical practice, the treatment of MPNs aims to correct the abnormal blood counts, and in some cases, specific treatments are applied depending on the type of MPNs. Phlebotomy is also considered as first-line therapy for PV to remove excess red blood cells from the body. In [2] relations between hematocrit and EPO is investigated

in normal adults and PV patients. The EPO concentration is increased each time after phlebotomy is performed [3; 130]. Moreover, platelet apheresis is often preferred for patients with ET, where platelets are removed from the blood [17]. PMF patients having anemia can be treated with blood transfusions. In addition, there are a variety of ways to treat anemia, for example, the EPO therapy [52].

Based on estimates of parameters for a typical healthy individual, the proposed model, in Chapter 6, is used to explore the changes in some of these parameters necessary to account for the dynamics of hematological diseases as done by several authors [26; 39; 67; 73; 95]. The model may also be extended from the healthy subjects to patients of MPNs by coupling the model to malignant cells using a similar approach by [7; 110]. It may help physicians initiate therapy and observe patient's hematological parameters during treatment. However, a few particular challenges need to be addressed. For example, valid data of MPNs patients is required, including those who develop PV from ET over time. The underlying pathological dynamics have to be modeled, such as the feedback mechanisms of EPO and TPO in disease progression.

Many mathematical models are developed with the specific purpose of knowledge discovery of biological systems. Alternatively, models can be used to test hypotheses, estimate important parameters by fitting a model to data, or determine which variables or interactions are the most essential to a biological process. Using mathematical methods, we can interpret and uncover many mechanisms. For instance, bifurcation analysis and sensitivity analysis are two different methods used to describe how small changes in an input parameter can cause a qualitative change in the system's behavior. We can also isolate parts of the mathematical system based on fast-slow dynamics (quasi steady state assumption) and observe an impact on the qualitative behavior of the system. Given values for which such changes occur are expected to be within a realistic range, this can indicate the reasons for heterogeneity in patients. If the model structure and behavior reflect the biological system and produce reliable results, it is intended to improve the model in collaboration with professionals in the field. Mathematical models also have the advantage that a range of *in silico* experiments can be performed, which are not possible or quite expensive in medical practice, even with animal experimentation.

Apart from advantages, we can not ignore the limitations and challenges of research in this field. The major problem is achieving enough data that has measurements over time. Determining the parameters on limited data results in uncertain parameter-values. In order to retain simplicity, the modelers prefer to model the biological mechanisms by considering the minimum range of important processes, which results in leaving out many mechanisms. However, the modelers should aim not to produce blue-sky research but be directed towards a definite goal.

CHAPTER 2

Mathematical analysis of the Cancitis model and the role of inflammation in blood cancer progression



Research article

Mathematical analysis of the Cancitis model and the role of inflammation in blood cancer progression

Zamra Sajid, Morten Andersen* and Johnny T. Ottesen

IMFUFA, Department of Science and Environment, Roskilde University, Denmark

* **Correspondence:** Email: moan@ruc.dk; Tel: +4546743936.

Abstract: Recently, a tight coupling has been observed between inflammation and blood cancer such as the Myeloproliferative Neoplasms (MPNs). A mechanism based six-dimensional model - the Cancitis model - describing the progression of blood cancer coupled to the inflammatory system is analyzed. An analytical investigation provides criteria for the existence of physiological steady states, trivial, hematopoietic, malignant and co-existing steady states. The classification of steady states is explicitly done in terms of the inflammatory stimuli. Several parameters are crucial in determining the attracting steady state(s). In particular, increasing inflammatory stimuli may transform a healthy state into a malignant state under certain circumstances. In contrast for the co-existing steady state, increasing inflammatory stimuli may reduce the malignant cell burden. The model provides an overview of the possible dynamics which may inform clinical practice such as whether to use inflammatory inhibitors during treatment.

Keywords: cancer; inflammation; mathematical modelling; steady states; stability

1. Introduction

Myeloproliferative Neoplasms (MPNs) is a group of hematopoietic stem cell disorders, including essential thrombocytosis (ET), polycythemia vera (PV) and primary myelofibrosis (PMF) [1, 2]. The pathogenesis of these neoplasms is yet to be fully discovered. For patients with MPNs, the mutation *JAK2V617F* is found present in the most cases of ET (50%) and in 95% of the cases with PV and PMF ultimately leading to acute myeloid leukemia (AML) [3,4]. This suggests a biological continuum where the diseases evolve from early cancers (ET and PV) into the advanced myelofibrosis stage, with an increasing load of *JAK2V617F* mutations from a low burden at ET and PV to a high load [2, 5]. MPNs imply an increased risk for the development of other cancers [1, 4].

Recent research supports that MPNs can be regarded as chronic inflammatory diseases and MPNs has been described as a "human inflammation model", which leads to premature atherosclerosis, clonal

evolution and an increased risk of second cancers. [2, 3, 6]. This is based on evidence from clinical observations, experiments and molecular studies [3].

Several insightful theoretical studies have been published on control dynamics of biological networks. Mathematical models have been proposed [7–9] describing the control networks for regulation of stem cell lineage. Mathematical modelling of cancer is useful for understanding of cancer initiation, progression [10, 11], to confirm or dismiss biological/medical hypotheses, and to study effects of single or multi modality treatments *in silico*. The mathematical model presented in [12] shows that successful therapy may eliminate tumour stem cells. A five-dimensional model given in [13] includes active and quiescent stem cells, progenitor cells, mature cells and one immune compartment describing chronic myelogenous leukemia. In [14] a mathematical model of cancer stem cell dynamics is proposed and the different scenarios of cancer initiation and possible treatments strategies have been discussed. The mathematical model given in [15] is useful for investigating the impact of cytokine-dependence of acute myeloid leukemic cells. In addition, the model allows distinguishing between cytokine-dependent and cytokine-independent acute myeloid leukemia (AML) and both scenarios are supported by patient data.

However, only a few mathematical models of MPNs exist. Some work includes investigation of the origin of myeloid malignancies with MPNs as a particular example [16]. In [17], a two dimensional model of MPNs is investigated without including the immune response dynamically. The Cancitis model including chronic inflammation as the trigger and driver of MPNs was proposed in [5]. In [5], T-cells are not explicitly considered whereas, in [18], the effect of these cells has been included specifically. The analysis of a two dimensional mathematical model [18] is used to discuss *in silico* effect of existing and novel treatments. The model presented here is identical to the model presented in [5] except for the simpler functional form of the stem cells niche interaction used here and in [18].

In the present paper we conduct a thorough mathematical investigation of the Cancitis model and explore the intricate coupling between inflammation and MPNs. We address the following questions which have not been systematically investigated previously: Which steady states of the system are feasible and which trajectories are attracted to the steady states? How do the number and stability of the steady states change when varying the parameters, in particular, the exogenous inflammatory stimuli, self-renewal and death rates of stem cells, and inhibitory strength of the stem cell niche interaction? Which set of clustered parameters control the dynamics of the system? Does the analysis suggest correlated parameters? The bio-medical applications of the model analysis are discussed, e.g. how the inflammation influences the transition between healthy and diseased states. In addition, the analysis predicts effects of ongoing and potential combination therapies.

2. The Cancitis model

The Cancitis model stated in [5] is illustrated in Figure 1, with the system of differential equations shown in system (2.1). In this section the details of the model and the reasoning behind it is presented.

The model describes the proliferation of hematopoietic stem cells (HSC) into hematopoietic mature cells (HMC) and likewise malignant stem cells (MSC) into malignant mature cells (MMC). Additionally, the model considers the number of dead cells and the level of inflammation. The debris from the dead cells stimulates the immune response, which in turn affects the self-renewal rate of both HSCs and MSCs.

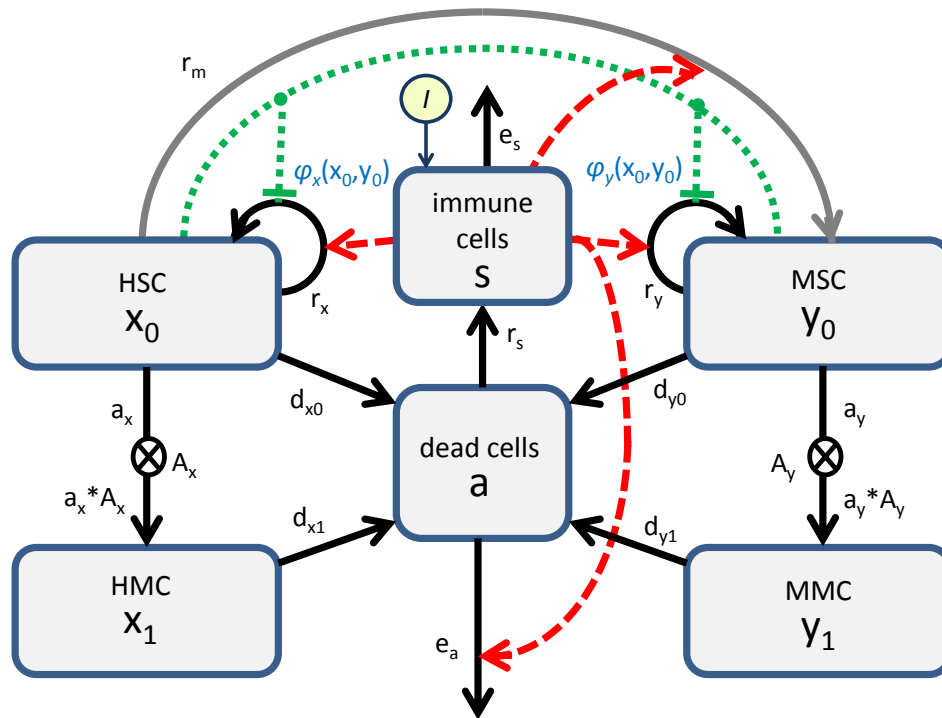


Figure 1. The boxes illustrate the compartments of the Cancitis model. The arrows represent the rates of the flows between and out of these compartments. Red stipulated arrows represent the effect of inflammation which is stimulated by exogenous inflammatory stimuli, I . Green stipulated lines represent the bone marrow niches interaction with a 'crowding' competition between HSC and MSC. Stem cells (HSC and MSC) may self-renew, die or differentiate, while mature cells die after a while (MMC, HMC). Dead cells (a) are engulfed by the immune cells (s), that stimulate production of stem cells, increase risk of mutation and increase the removal of dead cells (For more details, see main text).

The model consists of six ordinary differential equations one for each compartment; the number of HSC (x_0), the number of HMC (x_1), the number of MSC (y_0), the number of MMC (y_1), the number of dead cells (a), and the level of inflammation (s).

The equations are of the general form,

$$\left\{ \begin{array}{l} \text{Change in amount of a} \\ \text{compartment per time} \end{array} \right\} = \left\{ \begin{array}{l} \text{rate of production times} \\ \text{the producing source} \end{array} \right\} - \left\{ \begin{array}{l} \text{rate of elimination times the} \\ \text{amount in the compartment} \end{array} \right\}.$$

and read specifically,

$$\dot{x}_0 = r_x(\phi_x s - \alpha_x)x_0 - r_m s x_0, \quad (2.1a)$$

$$\dot{x}_1 = a_x A_x x_0 - d_{x1} x_1, \quad (2.1b)$$

$$\dot{y}_0 = r_y(\phi_y s - \alpha_y)y_0 + r_m s x_0, \quad (2.1c)$$

$$\dot{y}_1 = a_y A_y y_0 - d_{y1} y_1, \quad (2.1d)$$

$$\dot{a} = d_{x0} x_0 + d_{y0} y_0 + d_{x1} x_1 + d_{y1} y_1 - e_a a s, \quad (2.1e)$$

$$\dot{s} = r_s a - e_s s + I, \quad (2.1f)$$

with

$$\alpha_x = \frac{d_{x0} + a_x}{r_x} \quad \text{and} \quad \alpha_y = \frac{d_{y0} + a_y}{r_y}. \quad (2.2)$$

The expressions for the inhibitory niche feedback are chosen as Michaelis-Menten-like functions in contrast to [5],

$$\phi_x \equiv \phi_x(x_0, y_0) = \frac{1}{1 + c_{xx}x_0 + c_{xy}y_0}, \quad (2.3a)$$

$$\phi_y \equiv \phi_y(x_0, y_0) = \frac{1}{1 + c_{yx}x_0 + c_{yy}y_0}. \quad (2.3b)$$

A stem cell can proliferate in three ways; symmetric self-renewal (resulting in two new stem cells), asymmetric self-renewal (resulting in one stem cell and one progenitor cell) and symmetric differentiation (resulting in two progenitor cells). The rate of self-renewal is denoted as r_x and r_y for HSC and MSC respectively. The self-renewal of stem cells is known to be inhibited by self-regulating niche feedback [19], resulting in decreased self-renewal when the level of stem cells in the bone marrow is high. Adopting the approach taken in [12], [20] and [21], this is implemented by Michaelis-Menten-like functions $\phi_x(x_0, y_0)$ and $\phi_y(x_0, y_0)$, shown in Eq (2.3b). Allowing the feedback to be different for HSC and MSC, the constants c_{xx} and c_{xy} capture the effects of HSC and MSC on the self-renewal of HSC, while c_{yx} and c_{yy} capture the corresponding effects on the self-renewal of MSC. Additionally, the inflammatory level also affects the self-renewal [22, 23]. This leads a to self-renewal term per cell of $r_x \phi_x s$ and $r_y \phi_y s$ for HSC and MSC respectively. The parameter c_{ij} describes the inhibitory strength of the signalling bone marrow niche feedback from cell type j onto cell type i . It is generally assumed that $c_{yy} \leq c_{yx} \leq c_{xy} \leq c_{xx}$, since malignant cells are less sensitive to inhibitive niche feedback than hematopoietic cells [22, 24].

In [25], a multi compartmental model is proposed relying on a single external feedback mechanism. It is shown that the equilibrium level of mature cells depends only on the self-renewal parameters for the HSC and it is independent of the other compartments. Therefore, the progenitor cells are considered as intermediate steps between stem cells and mature cells, and are implicitly accounted for by multiplication factors A_x and A_y for HSC and MSC respectively. The rate at which the HSC reduces in transforming to HMC is denoted by a_x while the similar rate for MSC transforming to MMC is denoted by a_y . As such, the HMC and MMC accordingly increase with rates $a_x A_x$ and $a_y A_y$ respectively. To account for the cell apoptosis, the four types of cells are removed with rates d_{x0} , d_{x1} , d_{y0} and d_{y1} , for the corresponding cell types.

Genetic mutations are by nature to be described as Poisson processes [26–29]. However, not all mutations are malignant; only mutation which happens on a particular location of the DNA, i.e. at specific amino acids causes a specific mutation, e.g. the JAK2V617F mutation. The probability for hitting a specific location is about 1/30000. In [30] the average mutation probability is estimated to 0.0035 per year, which corresponds to a specific mutation probability of $0.0035/30000 = 1.210^{-7}$

per year. Thus, the probability for one specific malignant mutation is about 10^{-7} per cell per year. Moreover, the mutation is affected by the inflammation, s [31, 32], which is explicitly stated, and resulting in the effective mutation rate $r_m s$. Assuming three sequential mutations are needed to generate a specific malignant stem cell the resulting probability becomes much higher (10^{-25} per year per cell if the mutations are assumed independent). This could be implemented in the otherwise deterministic model but it would increase the computational cost, since it depends on both the probability of a single cell mutation and the number of potential mutating cells at a given time, which itself is determined by the preceding mutational history. To avoid such complications we initialize by having a single MSC and none MMC, and put the mutation rate to zero. This is justified by the fact that the probability of a single cell mutating is small compared to the self-renewal of the MSCs. Thus, the first mutation drives the development leaving a later identical mutation insignificant to the dynamics, which is confirmed by numerical simulations.

The number of dead cells has an up-regulatory effect on the immune response denoted r_s . External environmental factors also influence the inflammatory level. This is captured in the model by the term I . Throughout we take $I > 0$, as a perfect sterile environment is an utopic idealization. This term may vary over time due to environmental changes, but in our mathematical analysis we will consider I as piecewise constant. The inflammation, s , is down-regulated naturally by the eliminating rate e_s .

Additionally, the change in the amount of dead cells per time is given by the death rate times the number of cells minus the clearance by the immune system. As given in [33] clearance is described by a second order equation $-e_a a s$ since the engulfed immune cells have to meet the dead cells debris to mediate endocytosis. Thus, clearance is bilinear in both a and s representing the activity of the immune system, eliminating the dead cells with an elimination rate e_a .

Initial conditions for the Cancitis model in equations are needed for the given system of differential equations (2.1–2.3b). Here, we mainly focus on the model after the first mutation, i.e. with $y_0(0) = 1$, $y_1(0) = 0$, $r_m = 0$, and the remaining variables as those in the healthy steady state (see below). All other parameter values are assumed to be positive.

2.1. Steady states of the model

The stable steady states are attractors in the six dimensional phase space. This motivates systematic study of the existence and location of steady states and how this is affected by perturbing parameter values.

Motivated by the biology where the number of cells and concentrations are required to be non-negative numbers, we will use the terminology that a steady state is admissible if and only if all the components are non-negative, i.e. if and only if a steady state is in the non-negative octahedron.

Consider the system of Eqs (2.1–2.3b). For steady state solutions, $\dot{x}_0 = \dot{x}_1 = \dot{y}_0 = \dot{y}_1 = \dot{a} = \dot{s} = 0$,

$$\left(\frac{\bar{s}}{\alpha_x} - (1 + c_{xx}\bar{x}_0 + c_{xy}\bar{y}_0) \right) \bar{x}_0 = 0, \quad (2.4a)$$

$$\left(\frac{\bar{s}}{\alpha_y} - (1 + c_{yx}\bar{x}_0 + c_{yy}\bar{y}_0) \right) \bar{y}_0 = 0, \quad (2.4b)$$

$$\bar{x}_1 = \frac{a_x A_x \bar{x}_0}{d_{x1}}, \quad (2.4c)$$

$$\bar{y}_1 = \frac{a_y A_y \bar{y}_0}{d_{y1}}, \quad (2.4d)$$

$$d_{x0} \bar{x}_1 + d_{x1} \bar{x}_1 + d_{y0} \bar{y}_0 + d_{y1} \bar{y}_1 - e_a \bar{a} \bar{s} = 0, \quad (2.4e)$$

$$\bar{a} = \frac{e_s}{r_s} \left(\bar{s} - \frac{I}{e_s} \right). \quad (2.4f)$$

The values of x_0 , x_1 , y_0 , y_1 , a and s at steady state are denoted as \bar{x}_0 , \bar{x}_1 , \bar{y}_0 , \bar{y}_1 , \bar{a} and \bar{s} respectively. The admissible steady states can be classified as,

- a trivial steady state if and only if $\bar{x}_0 = \bar{y}_0 = 0$,
- a (purely) hematopoietic steady state if and only if $\bar{y}_0 = 0$ and $\bar{x}_0 > 0$,
- a (purely) malignant steady state if and only if $\bar{x}_0 = 0$ and $\bar{y}_0 > 0$, or
- a co-existing steady state if and only if $\bar{x}_0 > 0$ and $\bar{y}_0 > 0$.

The admissibility of steady states necessitates certain inequalities to be fulfilled, which leads to restriction on the parameters, e.g. from Eq (2.4f), non-negativity of \bar{a} requires $\bar{s} \geq \frac{I}{e_s}$. I is assumed to be positive thus $\frac{I}{e_s} > 0$. Hence

$$\bar{s} \geq \frac{I}{e_s} > 0, \quad (2.5)$$

for any admissible steady state. Note that, \bar{x}_1 and \bar{y}_1 are non-negative if and only if \bar{x}_0 and \bar{y}_0 are non-negative, respectively. Substituting expressions of \bar{x}_1 and \bar{y}_1 in Eq (2.4e) gives,

$$e_a \bar{a} \bar{s} = \beta_x \bar{x}_0 + \beta_y \bar{y}_0, \quad (2.6)$$

where $\beta_x = a_x A_x + d_{x0}$ and $\beta_y = a_y A_y + d_{y0}$. Thus, Eqs (2.4e–2.4f) and (2.6) result in a second order equation in \bar{s} having the general solution,

$$\bar{s}_{\pm} = \frac{I}{2e_s} \left(1 \pm \sqrt{1 + \zeta(\beta_x \bar{x}_0 + \beta_y \bar{y}_0)} \right), \quad (2.7)$$

where $\zeta = \frac{4r_s e_s}{e_a I^2} > 0$. \bar{s}_- is negative for positive \bar{x}_0 or \bar{y}_0 . In case, $(\bar{x}_0, \bar{y}_0) = (0, 0)$, Eq (2.7) leads to $\bar{s}_- = 0$ contradicting $\bar{s} > 0$. Thus, $s = \bar{s}_-$ is not biologically realizable and we therefore put $\bar{s} = \bar{s}_+$ in the further analysis. Note that, for non-trivial steady states, $\bar{s} > \frac{I}{e_s}$. In addition, non-negativity of \bar{x}_0 and \bar{y}_0 implies non-negativity of \bar{x}_1 , \bar{y}_1 , \bar{s} and \bar{a} .

Hence, the existence of admissible steady states \bar{x}_0 , \bar{y}_0 , \bar{x}_1 , \bar{y}_1 , \bar{s} and \bar{a} follows from Eqs (2.4a), (2.4b) and (2.7).

Below we make a complete analysis of the existence of various steady states depending on how I relates to the remaining parameters. This choice is due to the fact that the external inflammatory stimuli I is of great interest in health care and to elucidate consequences of using inflammation inhibitors as part of treatment.

Proposition 1. *A trivial steady state E_0 always exists,*

$$E_0 = \left(0, 0, 0, 0, 0, \frac{I}{e_s} \right). \quad (2.8)$$

Proof. Follow directly from Eqs (2.4e) and (2.5). \square

Hematopoietic steady states may exist depending on the rest of the parameter values. As above we chose the inflammatory stimuli I as the leading parameter and make a complete analysis of possible hematopoietic steady states. The analysis of the existence of the hematopoietic steady states depends crucially on the following lumped parameters,

$$I_H = 2\sqrt{\frac{e_s r_s \beta_x}{e_a c_{xx}} - \frac{r_s \beta_x}{e_a c_{xx} \alpha_x}}, \quad (2.9)$$

$$\zeta_{H1} = 2e_s \alpha_x - \frac{r_s \beta_x}{e_a c_{xx} \alpha_x}, \quad (2.10)$$

$$\zeta_{H2} = e_s \alpha_x, \quad (2.11)$$

$$\zeta_{H3} = \frac{r_s \beta_x}{e_s e_a c_{xx}}, \quad (2.12)$$

the last two always being positive.

Proposition 2. *Two hematopoietic steady states $E_{H\pm}$ may exist in the following cases,*

- If $\alpha_x^2 \leq \frac{\zeta_{H3}}{4}$ then E_{H+} exists if and only if $I > 0$.
- If $\frac{\zeta_{H3}}{4} < \alpha_x^2 \leq \zeta_{H3}$ then E_{H+} exists if and only if $I \geq I_H$.
- If $\zeta_{H3} < \alpha_x^2$ then E_{H+} exists if and only if $I > \zeta_{H2}$.
- If $\alpha_x^2 \leq \frac{\zeta_{H3}}{4}$ then E_{H-} exists if and only if $I \leq \zeta_{H2}$.
- If $\frac{\zeta_{H3}}{4} < \alpha_x^2 \leq \zeta_{H3}$ then E_{H-} exists if and only if $I_H \leq I \leq \zeta_{H2}$.
- If $\zeta_{H3} < \alpha_x^2$ then E_{H-} does not exist.

In case of existence, $E_{H+} = (\bar{x}_{0H+}, \bar{x}_{1H+}, 0, 0, \bar{a}_{H+}, \bar{s}_{H+})$ is given by $\bar{x}_{0H+} = \frac{1}{2e_s c_{xx} \alpha_x} (I - \zeta_{H1} + \sqrt{(\zeta_{H1} - I)^2 - 4e_s \alpha_x (\zeta_{H2} - I)})$, $\bar{s}_{H+} = \alpha_x (1 + c_{xx} \bar{x}_{0H+})$, $\bar{a}_{H+} = \frac{\beta_x \bar{x}_{0H+}}{e_a \bar{s}_{H+}}$, and $\bar{x}_{1H+} = \frac{a_x A_x \bar{x}_{0H+}}{d_{x1}}$ whereas $E_{H-} = (\bar{x}_{0H-}, \bar{x}_{1H-}, 0, 0, \bar{a}_{H-}, \bar{s}_{H-})$ is given by $\bar{x}_{0H-} = \frac{1}{2e_s c_{xx} \alpha_x} (I - \zeta_{H1} - \sqrt{(\zeta_{H1} - I)^2 - 4e_s \alpha_x (\zeta_{H2} - I)})$, $\bar{s}_{H-} = \alpha_x (1 + c_{xx} \bar{x}_{0H-})$, $\bar{a}_{H-} = \frac{\beta_x \bar{x}_{0H-}}{e_a \bar{s}_{H-}}$, and $\bar{x}_{1H-} = \frac{a_x A_x \bar{x}_{0H-}}{d_{x1}}$.

Proof. A hematopoietic steady state E_H follows from Eqs (2.4a) and (2.7) with $y_0 = y_1 = 0$ as possible positive solutions to

$$\bar{x}_{0H}^2 + \frac{1}{e_s c_{xx} \alpha_x} (\zeta_{H1} - I) \bar{x}_{0H} + \frac{1}{e_s c_{xx}^2 \alpha_x} (\zeta_{H2} - I) = 0. \quad (2.13)$$

For the solutions to (2.13) to be real,

$$(\zeta_{H1} - I)^2 \geq 4\zeta_{H2}(\zeta_{H2} - I). \quad (2.14)$$

In case $I \geq \zeta_{H2}$, (2.14) is always fulfilled. In case $I < \zeta_{H2}$, (2.14) is equivalent to

$$I^2 + \frac{2r_s \beta_x}{e_a c_{xx} \alpha_x} I + \frac{r_s \beta_x}{e_a c_{xx} \alpha_x} \left(\frac{r_s \beta_x}{e_a c_{xx} \alpha_x} - 4e_s \alpha_x \right) \geq 0. \quad (2.15)$$

Solving for I we get,

$$I \geq I_H = \gamma_x \left(\alpha_x^2 - \frac{\zeta_{H3}}{4} \right), \quad (2.16)$$

with

$$\gamma_x = \frac{\frac{4e_s r_s \beta_x}{e_a c_{xx} \alpha_x^2}}{\frac{r_s \beta_x}{e_a c_{xx} \alpha_x} + 2 \sqrt{\frac{e_s r_s \beta_x}{e_a c_{xx}}}} > 0. \quad (2.17)$$

From Eqs (2.14) and (2.16) it follows that the solutions to Eq (2.13) are real for $I \geq \zeta_{H2}$ or $I_H \leq I < \zeta_{H2}$ in case $I_H < \zeta_{H2}$.

Whenever the solutions to (2.13) are real, they are given by

$$\bar{x}_{0H\pm} := \frac{1}{2e_s c_{xx} \alpha_x} \left(I - \zeta_{H1} \pm \sqrt{(\zeta_{H1} - I)^2 - 4e_s \alpha_x (\zeta_{H2} - I)} \right), \quad (2.18)$$

which depends on the sign of the following five quantities,

$$\zeta_{H1} = 2 \frac{e_s}{\alpha_x} \left(\alpha_x^2 - \frac{\zeta_{H3}}{2} \right), \quad (2.19)$$

$$I_H = \gamma_x \left(\alpha_x^2 - \frac{\zeta_{H3}}{4} \right), \quad (2.20)$$

$$\Delta_{12} = \zeta_{H1} - \zeta_{H2} = \frac{e_s}{\alpha_x} \left(\alpha_x^2 - \zeta_{H3} \right), \quad (2.21)$$

$$\Delta_{H1} = \zeta_{H1} - I_H = \frac{e_s}{\alpha_x + \sqrt{\zeta_{H3}}} \left(\alpha_x^2 - \zeta_{H3} \right), \text{ and} \quad (2.22)$$

$$\Delta_{H2} = I_H - \zeta_{H2} = -\frac{e_s}{\alpha_x (\alpha_x + \sqrt{\zeta_{H3}})^2} \left(\alpha_x^2 - \zeta_{H3} \right)^2 \leq 0, \quad (2.23)$$

where the last one immediately implies that the criteria for real solutions of Eq (2.13) is $I \geq I_H$. If the solutions, $\bar{x}_{0H\pm}$, are positive and real, then the formulas for the remaining variables easily follow from Eqs (2.4a–2.4f).

To continue we first consider \bar{x}_{0H+} and afterwards \bar{x}_{0H-} .

For $\alpha_x^2 \leq \frac{\zeta_{H3}}{4}$, it follows from Eqs (2.19)–(2.22) that $\zeta_{H1} < 0$, $\zeta_{H1} < \zeta_{H2}$, $I_H \leq 0$, and $\zeta_{H1} < I_H$. Thus, $\bar{x}_{0H+} > 0$ if and only if $I > 0$.

For $\frac{\zeta_{H3}}{4} < \alpha_x^2 \leq \frac{\zeta_{H3}}{2}$, it follows from Eqs (2.19)–(2.22) that $\zeta_{H1} \leq 0$, $\zeta_{H1} < \zeta_{H2}$, $I_H > 0$, and $\zeta_{H1} < I_H$. Thus, $\bar{x}_{0H+} > 0$ if and only if $I > I_H$.

For $\frac{\zeta_{H3}}{2} < \alpha_x^2 \leq \zeta_{H3}$, it follows from Eqs (2.19)–(2.22) that $\zeta_{H1} > 0$, $\zeta_{H1} \leq \zeta_{H2}$, $I_H > 0$, $\zeta_{H1} < I_H$, and $I_H \leq \zeta_{H2}$. Thus, $\bar{x}_{0H+} > 0$ if and only if $I > I_H$.

For $\zeta_{H3} < \alpha_x^2$ are $\zeta_{H1} > 0$, it follows from Eqs (2.19)–(2.23) that $\zeta_{H1} > \zeta_{H2}$, $I_H > 0$, $\zeta_{H1} > I_H$, and $I_H \leq \zeta_{H2}$. Thus, $\bar{x}_{0H+} > 0$ if and only if $I > \zeta_{H2}$.

Similar, \bar{x}_{0H-} is real if and only if $I \geq I_H$ and $\zeta_{H1} < I < \zeta_{H2}$.

For $\alpha_x^2 \leq \frac{\zeta_{H3}}{4}$, it follows from Eqs (2.19) and (2.20) that $\zeta_{H1} < 0 < \zeta_{H2}$, and $I_H \leq 0$. Thus, $\bar{x}_{0H-} > 0$ if and only if $I < \zeta_{H2}$.

For $\frac{\zeta_{H3}}{4} < \alpha_x^2 \leq \frac{\zeta_{H3}}{2}$, it follows from Eqs (2.19), (2.20) and (2.23) that $\zeta_{H1} \leq 0 < \zeta_{H2}$, $I_H > 0$, and $I_H < \zeta_{H2}$. Thus, $\bar{x}_{0H-} > 0$ if and only if $I_H \leq I < \zeta_{H2}$.

For $\frac{\zeta_{H3}}{2} < \alpha_x^2 \leq \zeta_{H3}$, it follows from Eqs (2.19)–(2.21) and (2.23) that $0 < \zeta_{H1} < \zeta_{H2}$, $I_H > 0$, and

$I_H < \zeta_{H2}$. Thus, $\bar{x}_{0H-} > 0$ if and only if $I_H \leq I < \zeta_{H2}$.

For $\zeta_{H3} < \alpha_x^2$, it follows from Eqs (2.20) and (2.21) that $\zeta_{H1} > \zeta_{H2}$ and $I_H > 0$. Thus, $\bar{x}_{0H-} > 0$ if and only if $\zeta_{H1} < I < \zeta_{H2}$, which is a contradiction. \square

The conditions for the existence of the **hematopoietic steady states** are summarized in Table 1.

Table 1. Summarizing necessary and sufficient criteria for admissibility of E_H . The first column conditions how α_x is related to ζ_{H3} , the middle column shows the existence conditions for E_{H+} and the last column shows the existence conditions for $E_{H\pm}$ explicitly in terms of I .

For	Only E_{H+} if	Both E_{H+} and E_{H-} if
$\alpha_x^2 < \frac{\zeta_{H3}}{4}$	$I > \zeta_{H2}$	$I \leq \zeta_{H2}$
$\frac{\zeta_{H3}}{4} < \alpha_x^2 < \zeta_{H3}$	$I > \zeta_{H2}$	$I_H \leq I \leq \zeta_{H2}$
$\zeta_{H3} < \alpha_x^2$	$I > \zeta_{H2}$	\emptyset

Malignant steady states may exist depending on the range of the parameters. As above we chose the inflammatory stimuli I as our leading parameter and make a complete analysis of possible malignant steady states. The analysis of the existence of the malignant steady states depends crucially on the following lumped parameters,

$$I_H = 2\sqrt{\frac{e_s r_s \beta_y}{e_a c_{yy}}} - \frac{r_s \beta_y}{e_a c_{yy} \alpha_y}, \quad (2.24)$$

$$\zeta_{L1} = 2e_s \alpha_y - \frac{r_s \beta_y}{e_a c_{yy} \alpha_y}, \quad (2.25)$$

$$\zeta_{L2} = e_s \alpha_y, \quad (2.26)$$

$$\zeta_{L3} = \frac{r_s \beta_y}{e_s e_a c_{yy}}, \quad (2.27)$$

the last two being positive.

Proposition 3. *Two malignant steady states $E_{L\pm}$ may exist in the following cases,*

- If $\alpha_y^2 \leq \frac{\zeta_{L3}}{4}$ then E_{L+} exists if and only if $I > 0$.
- If $\frac{\zeta_{L3}}{4} < \alpha_y^2 \leq \zeta_{L3}$ then E_{L+} exists if and only if $I \geq I_L$.
- If $\zeta_{L3} < \alpha_y^2$ then E_{L+} exists if and only if $I > \zeta_{L2}$.
- If $\alpha_y^2 \leq \frac{\zeta_{L3}}{4}$ then E_{L-} exists if and only if $I \leq \zeta_{L2}$.
- If $\frac{\zeta_{L3}}{4} < \alpha_y^2 \leq \zeta_{L3}$ then E_{L-} exists if and only if $I_L \leq I \leq \zeta_{L2}$.
- If $\zeta_{L3} < \alpha_y^2$ then E_{L-} does not exist.

In case of existence, $E_{L+} = (0, 0, \bar{y}_{0L+}, \bar{y}_{1L+}, \bar{a}_{L+}, \bar{s}_{L+})$ is given by $\bar{y}_{0L+} = \frac{1}{2e_s c_{yy} \alpha_y} (I - \zeta_{L1} + \sqrt{(\zeta_{L1} - I)^2 - 4e_s \alpha_y (\zeta_{L2} - I)})$, $\bar{s}_{L+} = \alpha_y (1 + c_{yy} \bar{y}_{0L+})$, $\bar{a}_{L+} = \frac{\beta_y \bar{y}_{0L+}}{e_a \bar{s}_{L+}}$,

and $\bar{y}_{1L+} = \frac{a_x A_x \bar{y}_{0L+}}{d_{y1}}$ whereas $E_{L-} = (0, 0, \bar{y}_{0L-}, \bar{y}_{0L-}, \bar{a}_{L-}, \bar{s}_{L-})$ is given by $\bar{y}_{0L-} = \frac{1}{2e_s c_{yy} \alpha_y} \left(I - \zeta_{L1} - \sqrt{(\zeta_{L1} - I)^2 - 4e_s \alpha_y (\zeta_{L2} - I)} \right)$, $\bar{s}_{L-} = \alpha_y (1 + c_{yy} \bar{y}_{0L-})$, $\bar{a}_{L-} = \frac{\beta_y \bar{y}_{0L-}}{e_a \bar{s}_{L-}}$, and $\bar{y}_{1L-} = \frac{a_x A_x \bar{y}_{0L-}}{d_{y1}}$.

Proof. Due to symmetry in indices x and y , the proof for the malignant case is equivalent to that for the hematopoietic case except index H has to be substituted by L . \square

The result is summarized in Table 2.

Table 2. Summarizing necessary and sufficient criteria for admissibility of E_L . The first column conditions how α_y is related to ζ_{L3} , the middle column shows the existence conditions for E_{L+} and the last column shows the existence conditions for $E_{L\pm}$ explicitly formulated in terms of I .

For	Only E_{L+} if	Both E_{L+} and E_{L-} if
$\alpha_y^2 < \frac{\zeta_{L3}}{4}$	$I > \zeta_{L2}$	$I \leq \zeta_{L2}$
$\frac{\zeta_{L3}}{4} < \alpha_y^2 < \zeta_{L3}$	$I > \zeta_{L2}$	$I_L \leq I \leq \zeta_{L2}$
$\zeta_{L3} < \alpha_y^2$	$I > \zeta_{L2}$	\emptyset

The existence of a **co-existing steady state**

$$E_C = (\bar{x}_{0C}, \bar{x}_{1C}, \bar{y}_{0C}, \bar{y}_{1C}, \bar{a}_C, \bar{s}_C),$$

is far more cumbersome to deal with, since a wealth of sub-cases may arrive depending on various inequality-relations between the parameters. To avoid many tedious but straight forward calculations we limit ourself to the non-degenerate cases where $\zeta_{C1} = \alpha_y c_{yx} - \alpha_x c_{xx} \neq 0$ and $\zeta_{C2} = \alpha_y c_{yy} - \alpha_x c_{xy} \neq 0$.

From Eqs (2.4a and 2.4b), a linear relation between \bar{x}_0 and \bar{y}_0 directly follows,

$$\zeta_{C1} \bar{x}_{0C} + \zeta_{C2} \bar{y}_{0C} - \zeta_{C3} = 0, \quad (2.28)$$

where $\zeta_{C3} = \alpha_x - \alpha_y$. Thus, for the non-degenerate cases,

$$\bar{y}_{0C} = \frac{\zeta_{C1}}{\zeta_{C2}} \left(\frac{\zeta_{C3}}{\zeta_{C1}} - \bar{x}_{0C} \right), \quad (2.29)$$

which geometrically corresponds to a straight line through $(0, \frac{\zeta_{C3}}{\zeta_{C2}})$ and $(\frac{\zeta_{C3}}{\zeta_{C1}}, 0)$. Hence, two generic cases arrive, for $(0, \frac{\zeta_{C3}}{\zeta_{C2}})$ corresponding to positive slope, $\frac{\zeta_{C1}}{\zeta_{C2}} < 0$ corresponding to negative slope, $\frac{\zeta_{C1}}{\zeta_{C2}} > 0$. The first case defines a half line in the positive octahedron and in this case $\bar{x}_{0C} \in (\max\{0, \frac{\zeta_{C3}}{\zeta_{C1}}\}; \infty)$ and $\bar{y}_{0C} \in (\max\{0, \frac{\zeta_{C3}}{\zeta_{C2}}\}; \infty)$. The second case corresponds to either no admissible solution (if and only if $\frac{\zeta_{C3}}{\zeta_{C2}} < 0$ and $\frac{\zeta_{C3}}{\zeta_{C1}} < 0$) or a line segment in the positive octahedron which requires that $\frac{\zeta_{C3}}{\zeta_{C2}} > 0$ and $\frac{\zeta_{C3}}{\zeta_{C1}} > 0$ and in that case are $\bar{x}_{0C} \in (0, \frac{\zeta_{C3}}{\zeta_{C1}})$ and $\bar{y}_{0C} \in (0, \frac{\zeta_{C3}}{\zeta_{C2}})$. From Eq (2.4a) and (2.29),

$$\bar{s}_C = m_1 \bar{x}_{0C} + m_0, \quad (2.30)$$

with $m_0 = \alpha_x(c_{xy} \frac{\zeta_{C3}}{\zeta_{C2}} + 1)$ and $m_1 = \alpha_x(c_{xx} - c_{xy} \frac{\zeta_{C1}}{\zeta_{C2}})$. Before continuing, it is emphasized that $\zeta_1, \zeta_2, \zeta_3, m_0,$ and m_1 all are independent of I but may be positive, negative or in case of m_0 and m_1 zero. From Eq (2.7) it follows that a real and positive \bar{s} exist for $(\bar{x}_{0C}, \bar{y}_{0C}) \in \mathbb{R}_+ \times \mathbb{R}_+$,

$$\bar{s}_C = \frac{I}{2e_s} \left(1 + \sqrt{1 + \frac{\zeta_0}{I^2} (\beta_x \bar{x}_{0C} + \beta_y \bar{y}_{0C})} \right) \quad (2.31)$$

where $\zeta_0 = \frac{4r_s e_s}{e_a} > 0$. Similarly, a negative real root exists. Substituting (2.29) into (2.31) give,

$$\bar{s}_C = \frac{I}{2e_s} + \sqrt{\left(\frac{I}{2e_s}\right)^2 + \frac{\zeta_0 \beta_y \zeta_{C3}}{4e_s^2 \zeta_{C2}} + \frac{\zeta_0}{4e_s^2} \left(\beta_x - \beta_y \frac{\zeta_{C3}}{\zeta_{C2}}\right) \bar{x}_{0C}}. \quad (2.32)$$

Combining Eq (2.30) and (2.32) results in,

$$n_0 - I + n_1 \bar{x}_{0C} = \sqrt{I^2 + n_2 + n_3 \bar{x}_{0C}}, \quad (2.33)$$

where $n_0 = 2e_s m_0, n_1 = 2e_s m_1, n_2 = \frac{\zeta_0 \beta_y \zeta_{C3}}{\zeta_{C2}}$ and $n_3 = \zeta_0 \left(\beta_x - \beta_y \frac{\zeta_{C1}}{\zeta_{C2}}\right)$.

Note that Eq (2.33) has no real solution if either of $f(x) = n_0 - I + n_1 x$ and $g(x) = I^2 + n_2 + n_3 x$ are negative. Thus, if both $f(x)$ and $g(x)$ are positive, Eq (2.33) is equivalent to,

$$n_1^2 x^2 + (2n_1(n_0 - I) - n_3)x + (n_0^2 - n_2 - 2n_0 I) = 0, \quad (2.34)$$

which may have up to two real positive solutions. Hence, there can be at most two coexistence steady states. More specifically,

$$x_{0C+} = -\frac{2n_1(n_0 - I) - n_3}{2n_1^2} + \sqrt{\left(\frac{2n_1(n_0 - I) - n_3}{2n_1^2}\right)^2 - \frac{n_0^2 - n_2 - 2n_0 I}{n_1}}, \quad (2.35)$$

is positive if and only if $f(x_{0C+}) > 0, g(x_{0C+}) > 0,$ and

$$\frac{n_0^2 - n_2 - 2n_0 I}{n_1} < 0 \quad \text{or} \quad \frac{2n_1(n_0 - I) - n_3}{n_1^2} < 0. \quad (2.36)$$

Similar,

$$x_{0C-} = -\frac{2n_1(n_0 - I) - n_3}{2n_1^2} - \sqrt{\left(\frac{2n_1(n_0 - I) - n_3}{2n_1^2}\right)^2 - \frac{n_0^2 - n_2 - 2n_0 I}{n_1}}, \quad (2.37)$$

is positive if and only if $f(x_{0C-}) > 0, g(x_{0C-}) > 0,$ and

$$\frac{2n_1(n_0 - I) - n_3}{2n_1^2} > \frac{n_0^2 - n_2 - 2n_0 I}{n_1} > 0 \quad \text{and} \quad \frac{2n_1(n_0 - I) - n_3}{2n_1^2} < 0. \quad (2.38)$$

Note, some possibilities of equality signs in the inequalities are left out for simplification reasons. Equality may occur on a set of measure zero which is unlikely for a noisy biological system and including these possibilities makes the analysis much more messy. For practical purposes one may first calculate the two (possibly complex) roots x of Eq (2.34) and afterwards examine whether these are real and positive, whether $f(x) > 0$ and $g(x) > 0,$ and whether the corresponding \bar{y}_{0C} calculated from Eq (2.29) is positive, thus the remaining component of E_C will be positive too and the steady state admissible.

Continuing analytically is possible but becomes somehow cumbersome and instead we point out that for any choice of parameter values, there can be at most two coexistence steady states, their existence and value depending on the admissibility of x_{0C+} (Eq (2.35)) and x_{0C-} (Eq (2.37)).

3. Stability and bifurcation analysis

In this section we analytically and numerically examine the stability properties of the various admissible steady states of Eq (2.1) in terms of selected parameters.

3.1. Stability properties of the trivial steady state

The Jacobian of the trivial steady states E_0 is a triangular matrix and four of the six eigenvalues, $-d_{x1}$, $-d_{y1}$, $-e_s$ and $\frac{-Ie_a}{e_s}$, are negative but the two, $\frac{r_x}{e_s}(I - e_s\alpha_x)$ and $\frac{r_y}{e_s}(I - e_s\alpha_y)$, may be positive, negative, zero. Thus, by the Hartman-Grobman Theorem [34]

Lemma 1. E_0 is asymptotically stable if $I < e_s \min\{\alpha_x, \alpha_y\}$, whereas it is unstable if $I > e_s \min\{\alpha_x, \alpha_y\}$.

At $E_{H\pm}$ the Jacobian for the hematopoietic states can be calculated (see Supplementary) and the resulting sixth order characteristic equation shows that $E_{H\pm}$ are stable for

$$\bar{s}_H < \alpha_y(1 + c_{yx}\bar{x}_{0H}). \quad (3.1)$$

However, this is not the generic case, since $\alpha_y < \alpha_x$ (and $c_{yx} \leq c_{xx}$), which contradicts $\bar{s}_H = \alpha_x(1 + c_{xx}\bar{x}_{0H})$. Intensive numerical investigations shows that $E_{H\pm}$ are unstable.

The stability of E_L is similar to that for the hematopoietic steady state except that it is stable if

$$\bar{s}_L < \alpha_x(1 + c_{xy}\bar{y}_{0L}), \quad (3.2)$$

which is fulfilled in the generic case, since $\alpha_x < \alpha_y$ (and $c_{xy} \leq c_{yy}$). This follows from $\bar{s}_L = \alpha_y(1 + c_{yy}\bar{y}_{0L})$. The Jacobian may be found in supplementary.

Lastly, consider the **co-existing steady state**. The Jacobian at E_C may be found in supplementary. However, it is hard to prove any result analytically and we therefore do the stability investigation numerically the in next section.

3.1.1. Numerical Simulations and treatment scenarios

In this section, we focus on numerical results. The default values of parameters used in Figure 2 are given in Table 3. The values are the same as given in [18].

Table 3. Default parameter values and their lumped counterpart.

Parameter	Value	Unit	Parameter	Value	Unit
r_x	$8.7 \cdot 10^{-4}$	day ⁻¹	r_y	$1.3 \cdot 10^{-3}$	day ⁻¹
a_x	$1.1 \cdot 10^{-5}$	day ⁻¹	a_y	$1.1 \cdot 10^{-5}$	day ⁻¹
A_x	$4.7 \cdot 10^{13}$	-	A_y	$4.7 \cdot 10^{13}$	-
d_{x_0}	$2 \cdot 10^{-3}$	day ⁻¹	d_{y_0}	$2 \cdot 10^{-3}$	day ⁻¹
d_{x_1}	129	day ⁻¹	d_{y_1}	129	day ⁻¹
c_{xx}	$5.6 \cdot 10^{-5}$	-	c_{yx}	$5.2 \cdot 10^{-5}$	-
c_{xy}	$5.4 \cdot 10^{-5}$	-	c_{yy}	$5.0 \cdot 10^{-5}$	-
e_s	2	day ⁻¹	r_s	$3 \cdot 10^{-4}$	day ⁻¹
e_a	$2 \cdot 10^9$	day ⁻¹	I	7	day
α_x	2.31	-	α_y	1.54	-
β_x	$5.17 \cdot 10^8$	-	β_y	$5.17 \cdot 10^8$	-
ζ_0	$1.2 \cdot 10^{-12}$	-	ζ_{C1}	$-4.9 \cdot 10^{-5}$	-
ζ_{C2}	$7.4146 \cdot 10^{-4}$	-	ζ_{C3}	0.7646	-
n_0	9.76	-	n_1	-0.51	-
n_2	0.64	-	n_3	$6.61 \cdot 10^{-4}$	-
ζ_{H1}	8.65	-	ζ_{H2}	4.62	-
ζ_{L1}	5.18	-	ζ_{L2}	3.09	-
ζ_{H3}	0.69	-	ζ_{L3}	0.7646	-

The model has been investigated for various choices of parameter values. In Figure 2, clusters of five important parameters, $C = \frac{c_{xx}}{c_{yy}}$, $\mathcal{R} = \frac{\zeta_{H2}}{\zeta_{L2}} = \frac{\alpha_x}{\alpha_y}$ and I are considered to investigate the number of steady states and their stability. In the default case $\mathcal{R} > 1$ (Figure 2a), a trivial steady state always exists, and for low inflammation, i.e., $I < \zeta_{L2}$ it is stable otherwise it is unstable. For $I > \zeta_{L2}$, a purely malignant steady state becomes admissible. For values of I where the trivial and the malignant steady states are admissible, the malignant steady state is stable whereas the trivial steady state is unstable. An unstable hematopoietic steady state becomes admissible as I becomes larger than the threshold value ζ_{H2} , and increasing I further causes emergence of a stable co-existing steady state while the malignant steady state becomes unstable. Thus, for $I > \zeta_{H2}$ and C sufficiently small, four steady states appear namely the trivial, the hematopoietic, the malignant and the co-existing steady states where the co-existing steady state is stable and the rest are unstable. This illustrates that the co-existing steady state depends on I , C and \mathcal{R} . Increasing C from a small, initial value makes the co-existing steady state vanish and the malignant steady state becomes stable whereas the trivial and the hematopoietic steady states remain unstable.

Secondly, consider the second case where $\mathcal{R} = 1$ implying that $\zeta_{H2} = \zeta_{L2}$ (Figure 2b). Increasing I across this value generates an unstable hematopoietic steady state and a malignant steady state simultaneously. For $C < 1$ the malignant steady state is unstable, and a stable coexistence steady state is created as I increase past ζ_{H2} . For $C > 1$ no coexistence steady state is created, instead the malignant steady state is stable. Hence, for $\mathcal{R} = 1$, decreasing C may change the topology from a stable malignant steady state to a stable coexistence steady state i.e. improving the prognosis from disease escape to disease equilibrium. The stable co-existing steady state bifurcates from the trivial steady state and re-

mains stable until $C = 1$. As C exceeds 1, the co-existing steady state disappears, the malignant steady state becomes stable and the trivial and the hematopoietic steady state become unstable.

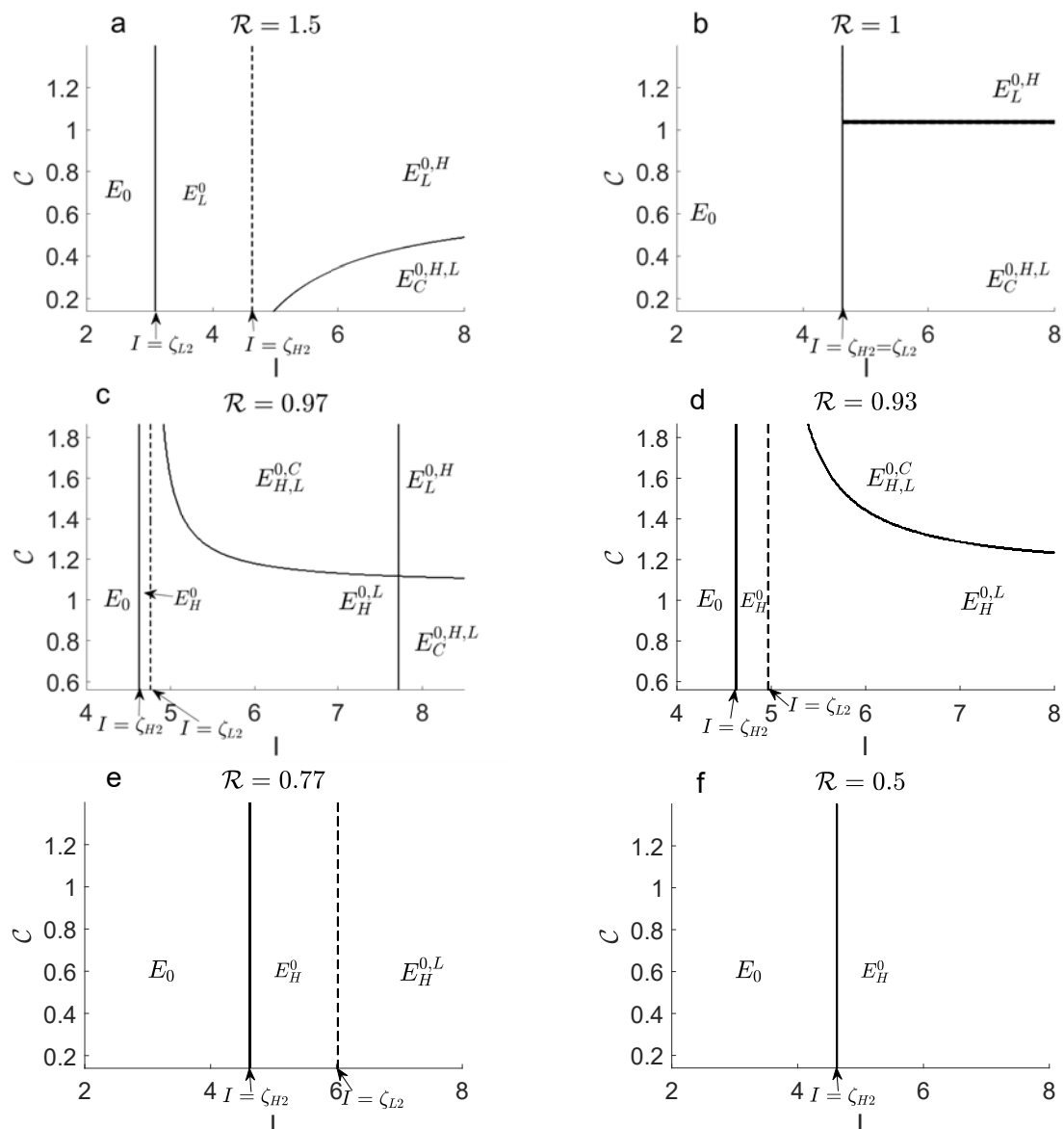


Figure 2. Admissibility and stability of the steady states depending on the parameters I and C for different values of \mathcal{R} . Crossing a solid curve implies a change in which type of stable steady state exists i.e. trivial, malignant, hematopoietic or coexistence. Crossing a dotted curves implies the same steady state is stable in both regions but the number of steady states is changed. The stable steady states are written as subscript of E and unstable steady states are written as superscript of E .

In the remaining panels, $\mathcal{R} < 1$, which implies that a stable hematopoietic steady state is created as the first transition to appear when increasing I from low values past the threshold value ζ_{H2} . Simultaneously, the trivial steady state becomes unstable. In Figure 2c where $\mathcal{R} = 0.97$ the hematopoietic steady

state remains stable for low values of C until I passes a threshold value where a stable coexistence steady state is created leaving the hematopoietic steady state unstable.

For larger values of C there is no coexistence steady state. Instead, as I is increased, a region of bistability appears with a stable hematopoietic steady state and a stable malignant steady state. Increasing I further the hematopoietic steady state becomes unstable. Hence, to reduce disease load, in the case of $\mathcal{R} < 1$, and large values of C and I , it may be optimal treatment to reduce the C value prior to reducing the inflammatory level to avoid being stuck in the basin of attraction of the malignant steady state.

In Figure 2d where $\mathcal{R} = 0.93$, the coexistence steady state no longer appears, the region of bistability has shrunk and a hematopoietic stable steady state is more dominant.

In Figure 2e and f, \mathcal{R} is decreased to 0.77 and 0.5 respectively, and the bistability region is no longer visible. For $I > \zeta_{H2}$ a hematopoietic steady state is the only stable steady state. Figure 2 indicates that reducing C and \mathcal{R} should be targets of intervention. A reduction of I may improve prognosis as well, for example for parameter values as in 2c.

4. Discussion and conclusion

A mechanism-based model published in [5] - the Cancitis model - describing the interaction of the hematopoietic cells, malignant cells and inflammation is analysed here. A thorough mathematical investigation of the model is presented in this paper which did not appear previously. We conducted an analytical analysis of the steady states and showed that four kinds of steady states may exist i.e. trivial, hematopoietic, malignant and co-existing steady states. We characterized the stability of each of these steady states and identified transitions conditions in the number of steady states and in their stability. Trivial, hematopoietic, malignant and coexistence steady states all appear for some parameter values. The steady states are highly relevant as all trajectories appear to approach a steady state after some time - see Figure 3. The case of bistability is visualized in the bottom right panel of Figure 3, with the basin of attraction shown in the (x_0, y_0) -plane using initial condition $(x_1, y_1, a, s) = (4 \times 10^{11}, 4 \times 10^{11}, 600, 2)$. The initial conditions for x_0 and y_0 are varied in a range $1 - 10^5$. The malignant steady state has a large basin of attraction (region (i)), while region (ii) marks the basin of attraction for the hematopoietic steady state.

The intuitive interpretation in most bio-medical literature attributes the main cause for cancer development to the frequency of stem cell division. Another main cause is the regulatory feedback that allows stem cells residing in niche to further divide into blood cell required in blood stream. Our investigation is in agreement with this perception and quantifies this intuitive concept. Furthermore, it shows that stem cell population is important to target in treatment to prevent disease progression.

In [14] and [15] a model without immune interaction is presented. The authors discuss a fraction similar to \mathcal{R} and show that it is important for the dynamics of the system. It has been shown [15] that the leukemic cell load can be temporarily reduced if the growth of HSC is larger than that of leukemic cells for cytokine-dependent AML.

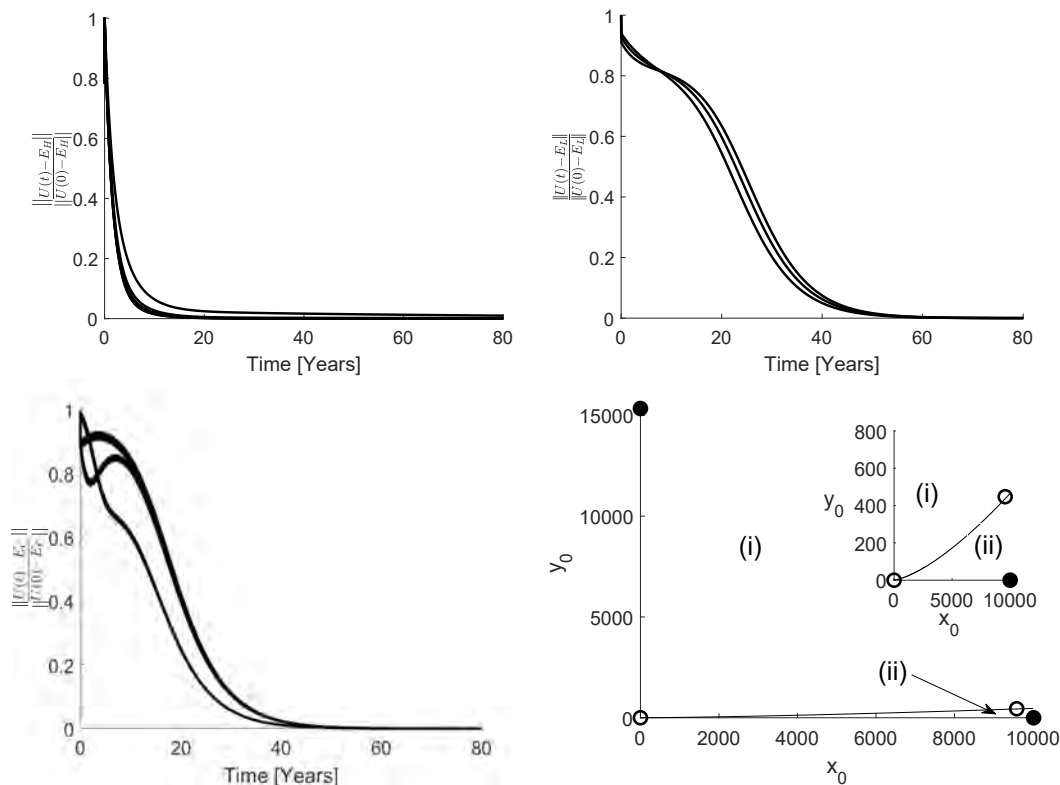


Figure 3. The first three panels illustrate that when a unique, stable steady state exists, it is globally attracting (based on a numerical argument). $U(t)$ denotes the solution of the six-dimensional model 2.1. In the top left panel, $\frac{\|U(t)-E_H\|}{\|U(0)-E_H\|}$ is plotted against time for three different initial conditions. It corresponds to the region where E_H is stable with $C = 0.8$, $\mathcal{R} = 0.97$ and $I = 6$. $\frac{\|U(t)-E_H\|}{\|U(0)-E_H\|}$ tending to zero for large time implies that $U(t)$ is close to E_H for large time. The top right panel shows the stability of E_L with $C = 0.2$, $\mathcal{R} = 1.5$ and $I = 4$. The bottom left panel shows the stability of E_C with $C = 0.1$, $\mathcal{R} = 1.5$ and $I = 7$. The bottom right panel corresponds to bi-stability of E_H and E_L with $C = 1.4$, $\mathcal{R} = 0.97$. The solution to the 6D model is projected onto the x_0 and y_0 plane. Region (i) denotes the set of initial conditions with trajectories converging to E_L whereas region (ii) denotes that trajectories converge to E_H . Black circles show four steady states, E_0 , E_H , E_L and E_C , where filled circle shows stable steady states and empty circle shows unstable steady states.

It is generally assumed that $c_{yy} \leq c_{xx}$ since malignant cells might be less sensitive to environmental crowding [22] and [24]. The ratio C of inhibition of the hematopoietic relative to malignant cells is one of several important prognostic markers. For large values of I , bi-stable and mono-stable regions depend upon C . It can be observed in Figure 2 that for small values of C , i.e., $c_{yy} \geq c_{xx}$, either the hematopoietic steady state is stable or the co-existing steady state is stable which can be interpreted as a good prognosis. However, large values of C may lead to a worse situation, e.g. in one case, the malignant steady state is stable or there exists bi-stability of the hematopoietic and the malignant steady states (see Figure 2c). In addition to the ratio of inhibitive niche feedback, the ratio \mathcal{R} is also important to consider, since it determines how robust the hematopoietic condition may be and how disastrously a

potential blood cancer disease will develop. Thus for $\mathcal{R} > 1$ we have a more serious situation than for $\mathcal{R} < 1$ showing that if this reproduction ratio exceeds the threshold $\mathcal{R}_0 = 1$, it is more disastrous than if it is below \mathcal{R}_0 .

The *JAK2V617F* allele burden is expected to increase due to the expansion of malignant cells. The *JAK2V617F* allele burden is interpreted as the ratio of malignant cells to the total number of mature cells. The model predicted *JAK2V617F* allele burden is shown in Figure 4 for the region where E_C is stable. Perturbation of a parameter may improve or impair prognosis when the coexistence point is the stable attractor. The top panel of Figure 4, shows that decreasing C and \mathcal{R} improve prognosis by lowering the allele burden. Contrarily, increasing I , causes a decay in allele burden. This suggests that inflammatory inhibitors could counteract treatments in this case. In other cases, increasing I typically leads to a worse prognosis, considering Figure 2.

The model presented here may inform clinical practice to make group specific treatment protocols with particular focus on the inflammatory components which may accelerate or dampen the disease progression. Interventions should address decreasing C and \mathcal{R} and potentially I but the latter depends on the remaining parameter values as adverse effects may be observed.

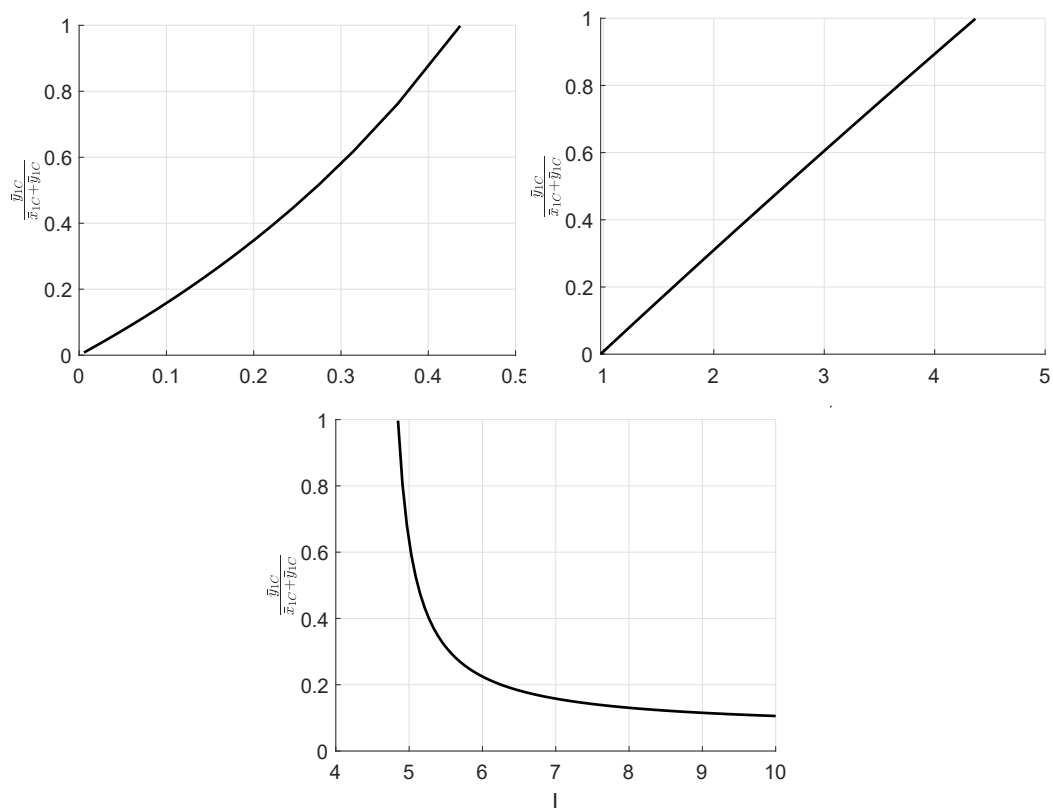


Figure 4. Allele burden (the ratio of \bar{y}_{1c} to the total number of \bar{x}_{1c} and \bar{y}_{1c}) at the steady state for the region where the co-existing steady state is stable. On the top, left and right panels show that by increasing C and \mathcal{R} , allele burden also increases. On the contrary, increasing I reduces the allele burden. In the top panel $\mathcal{R} = 1.5$ and $I = 7$, in the top right, $C = 0.1$ and $I = 7$ and in the bottom panel, $\mathcal{R} = 1.5$ and $C = 0.1$.

Conflict of interest

No conflict of interest.

References

1. P. J. Campbell and A. R. Green, The myeloproliferative disorders, *N. Engl. J. Med.*, **355** (2006), 2452–2466.
2. H. C. Hasselbalch, Chronic inflammation as a promotor of mutagenesis in essential thrombocythemia , polycythemia vera and myelofibrosis. A human inflammation model for cancer development?, *Leukemia Res.*, **37** (2013), 214–220.
3. H. C. Hasselbalch, Perspectives on chronic inflammation in essential thrombocythemia , polycythemia vera , and myelofibrosis: is chronic inflammation a trigger and driver of clonal evolution and development of accelerated atherosclerosis and second cancer?, *Blood*, **119** (2012), 3219–3226.
4. S. Y. Kristinsson, O. Landgren, J. Samuelsson, et al., Autoimmunity and the risk of myeloproliferative neoplasms, *Haematologica*, **95** (2010), 1216–1220.
5. M. Andersen, Z. Sajid, R. K. Pedersen, et al., Mathematical modelling as a proof of concept for MPNs as a human inflammation model for cancer development, *Plos One*, **12** (2017), 1–18.
6. T. Barbui, A. Carobbio, G. Finazzi, et al., Inflammation and thrombosis in essential thrombocythemia and polycythemia vera : different role of C-reactive protein and pentraxin 3, *Haematologica*, **96** (2011), 315–318.
7. N. L. Komarova, Principles of regulation of self-renewing cell lineages, *Plos One*, **8** (2013).
8. N. L. Komarova and P. van den Driessche, Stability of control networks in autonomous homeostatic regulation of stem cell lineages, *B. Math. Biol.*, **80** (2015), 1345–1365.
9. J. Yang, D. E. Axelrod and N. L. Komarova, Determining the control networks regulating stem cell lineages in colonic crypts, *J. Theor. Biol.*, **429** (2017), 190–203 .
10. F. Michor, Y. Iwasa and M. A. Nowak, Dynamics of cancer progression, *Nature Rev. Cancer*, **4** (2004), 197–205.
11. F. Michor, T. P. Hughes, Y. Iwasa, et al., Dynamics of chronic myeloid leukaemia, *Nature*, **435** (2005), 1267–1270.
12. D. Dingli and F. Michor, Successful Therapy Must Eradicate Cancer Stem Cells, *Stem Cells*, **24** (2006), 2603–2610.
13. G. Clapp, T. Lepoutre, R. El Cheikh, et al., Implication of autologous immune system in bcr-abl transcript variations in chronic myelogenous leukemia patients treated with imatinib, *Cancer Res.*, **75** (2015), 4053–4062.
14. T. Stiehl and A. Marciniak-Czochra, Mathematical modelling of leukemogenesis and cancer stem cell dynamics, *Math. Model. Nat. Phenom.*, **7** (2012), 166–202.
15. T. Stiehl, A. D. Ho and A. Marciniak-Czochra, Mathematical modelling of the impact of cytokine response of acute myeloid leukemia cells on patient prognosis, *Sci. Rep.*, **2809** (2018).

16. H. Haeno, R. L. Levine, D. G. Gilliland, et al., A progenitor cell origin of myeloid malignancies, *Proc. Natl. Acad. Sci. USA*, **106** (2009), 16616–16621.
17. J. Zhang, A. G. Fleischman, D. Wodarz, et al., Determining the role of inflammation in the selection of JAK2 mutant cells in myeloproliferative neoplasms, *J. Theor. Biol.*, **425** (2017), 43–52.
18. J. T. Ottesen, Z. Sajid, R. K. Pedersen, et al., Bridging blood cancers and inflammation: The reduced Cancitis model, *J. Theor. Biol.*, **465** (2019), 90–108.
19. C. Walkley, J. Shea, N. Sims, et al., Rb regulates interactions between hematopoietic stem cells and their bone marrow microenvironment, *Cell*, **129** (2007), 1081–1095.
20. T. Stiehl, N. Baran, A. D. Ho, et al., Cell division patterns in acute myeloid leukemia stem-like cells determine clinical course: A model to predict patient survival, *Cancer Res.*, **75** (2015), 940–949.
21. T. Walenda, T. Stiehl, H. Braun, et al., Feedback Signals in Myelodysplastic Syndromes: Increased Self-Renewal of the Malignant Clone Suppresses Normal Hematopoiesis, *PLoS Comput. Biol.*, **10** (2014), e1003599.
22. Y. W. Kim, B. K. Koo, H. W. Jeong, et al., Defective Notch activation in microenvironment leads to myeloproliferative disease, *Blood*, **112** (2008), 4628–4638.
23. K. Y. King and M. A. Goodell, Inflammatory modulation of hematopoietic stem cells: viewing the hematopoietic stem cell as a foundation for the immune response, *Nat. Rev. Immunol.*, **11** (2014), 685–692.
24. E. Rovida, I. Marzi, M. G. Cipolleschi, et al., One more stem cell niche: how the sensitivity of chronic myeloid leukemia cells to imatinib mesylate is modulated within a “hypoxic” environment, *Hypoxia*, (2014), 1–10.
25. A. Marciniak-Czochra, T. Stiehl, A. D. Ho, et al., Modeling of asymmetric cell division in hematopoietic stem cells—regulation of self-renewal is essential for efficient repopulation, *Stem Cells Dev.*, **18** (2009), 377–385.
26. A. L. Jackson and L. A. Loeb, The mutation rate and cancer, *Eur. J. Haematol.*, **97** (2016), 63–69.
27. A. Knutson, Mutation and Cancer: Statistical study of retinoblastoma, *Proc. Natl. Acad. Sci. USA*, **68** (1971), 820–823.
28. F. Michor, Y. Iwasa and N. MA, The age incidence of chronic myeloid leukemia can be explained by a one-mutation model, *Proc. Natl. Acad. Sci. USA*, **103** (2006), 14931–14934.
29. F. Michor, Mathematical models of cancer stem cells, *J. Clin. Oncol.*, **26** (2008), 2854–2861.
30. E. Voit, A first course in system biology, *Garland Science, Taylor & Francis Group, New York and London*, **68** (2013).
31. A. L. Sørensen and H. C. Hasselbalch, Smoking and Philadelphia-negative chronic myeloproliferative neoplasms, *Genetics*, **148** (1998), 1483–1490.
32. H. C. Hasselbalch, Smoking as a contributing factor for development of polycythemia vera and related neoplasms, *Leukemia Res.*, **015** (2015).
33. V. A. Kuznetsov and G. D. Knott, Modeling tumor regrowth and immunotherapy, *Math. Comput. Model.*, **33** (2001), 1275–1287.

34. C. Robinson, Dynamical Systems, Stability, Symbolic Dynamics, and Chaos, in *Second CRC Press, Boca Raton, Fla., 1999.*

Supplementary

Stability analysis of Steady states:

At $E_{H\pm}$ the Jacobian of the **purely hematopoietic steady state** becomes,

$$J_{E_H} = \begin{bmatrix} a_{11} & 0 & a_{13} & 0 & 0 & a_{16} \\ a_{21} & a_{22} & 0 & 0 & 0 & 0 \\ 0 & 0 & a_{33} & 0 & 0 & 0 \\ 0 & 0 & a_{43} & a_{44} & 0 & 0 \\ a_{51} & a_{52} & a_{53} & a_{54} & a_{55} & a_{56} \\ 0 & 0 & 0 & 0 & a_{65} & a_{66} \end{bmatrix} \quad (\text{S.1})$$

where

$$a_{11} = r_x \left(\frac{\bar{s}_H}{(1+c_{xx}\bar{x}_{0H})^2} - \alpha_x \right),$$

$$a_{13} = -\frac{r_x c_{xy} \bar{s}_H \bar{x}_{0H}}{(1+c_{xx}\bar{x}_{0H})^2},$$

$$a_{16} = \frac{r_x \bar{x}_{0H}}{(1+c_{xx}\bar{x}_{0H})},$$

$$a_{21} = a_x A_x,$$

$$a_{22} = -d_{x1},$$

$$a_{33} = r_y \left(\frac{\bar{s}_H}{1+c_{yy}\bar{x}_{0H}} - \alpha_y \right),$$

$$a_{43} = a_y A_y,$$

$$a_{44} = -d_{y1},$$

$$a_{51} = d_{x0},$$

$$a_{52} = d_{x1},$$

$$a_{53} = d_{y0},$$

$$a_{54} = d_{y1},$$

$$a_{55} = -e_a \bar{s}_H,$$

$$a_{56} = -e_a \bar{a}_H,$$

$$a_{65} = r_s,$$

$$a_{66} = -e_s,$$

and rest of the elements of J_{E_H} are zero.

At $E_{L\pm}$ the Jacobian of the **purely malignant steady state**.

$$J_{E_L} = \begin{bmatrix} a_{11} & 0 & 0 & 0 & 0 & 0 \\ a_{21} & a_{22} & 0 & 0 & 0 & 0 \\ a_{31} & 0 & a_{33} & 0 & 0 & a_{36} \\ 0 & 0 & a_{43} & a_{44} & 0 & 0 \\ a_{51} & a_{52} & a_{53} & a_{54} & a_{55} & a_{56} \\ 0 & 0 & 0 & 0 & a_{65} & a_{66} \end{bmatrix} \quad (\text{S.2})$$

where

$$\begin{aligned}
 a_{11} &= r_x \left(\frac{\bar{s}_L}{1+c_{xy}\bar{y}_{0L}} - \alpha_x \right), \\
 a_{21} &= a_x A_x, \\
 a_{22} &= -d_{x1}, \\
 a_{31} &= -\frac{r_y c_{yx} \bar{s}_L \bar{y}_{0L}}{(1+c_{yy}\bar{y}_{0L})^2}, \\
 a_{33} &= r_y \left(\frac{\bar{s}_L}{(1+c_{yy}\bar{y}_{0L})^2} - \alpha_y \right), \\
 a_{36} &= \frac{r_y \bar{y}_{0L}}{1+c_{yy}\bar{y}_{0L}}, \\
 a_{43} &= a_y A_y, \\
 a_{44} &= -d_{y1}, \\
 a_{51} &= d_{x0}, \\
 a_{52} &= d_{x1}, \\
 a_{53} &= d_{y0}, \\
 a_{54} &= d_{y1}, \\
 a_{55} &= -e_a \bar{s}_L, \\
 a_{56} &= -e_a \bar{a}_L, \\
 a_{65} &= r_s, \\
 a_{66} &= -e_s
 \end{aligned}$$

and rest of the elements of array are zero.

At $E_{C\pm}$ the Jacobian of the **co-existing steady state** becomes,

$$J_{EC} = \begin{bmatrix} a_{11} & 0 & a_{13} & 0 & 0 & a_{16} \\ a_{21} & a_{22} & 0 & 0 & 0 & 0 \\ a_{31} & 0 & a_{33} & 0 & 0 & a_{36} \\ 0 & 0 & a_{43} & a_{44} & 0 & 0 \\ a_{51} & a_{52} & a_{53} & a_{54} & a_{55} & a_{56} \\ 0 & 0 & 0 & 0 & a_{65} & a_{66} \end{bmatrix} \quad (\text{S.3})$$

where

$$\begin{aligned}
 a_{11} &= r_x \left(\frac{\bar{s}_C}{(1+c_{xx}\bar{x}_{0C}+c_{xy}\bar{y}_{0C})^2} - \alpha_x \right), \\
 a_{13} &= -\frac{r_x c_{xy} \bar{s}_C \bar{x}_{0C}}{(1+c_{xx}\bar{x}_{0C}+c_{xy}\bar{y}_{0C})^2}, \\
 a_{16} &= \frac{r_x \bar{x}_{0C}}{(1+c_{xx}\bar{x}_{0C}+c_{xy}\bar{y}_{0C})}, \\
 a_{21} &= a_x A_x, \\
 a_{22} &= -d_{x1}, \\
 a_{31} &= -\frac{r_y c_{yx} \bar{s}_C \bar{y}_{0C}}{(1+c_{yx}\bar{x}_{0C}+c_{yy}\bar{y}_{0C})^2}, \\
 a_{33} &= r_y \left(\frac{\bar{s}_C}{(1+c_{yx}\bar{x}_{0C}+c_{yy}\bar{y}_{0C})^2} - \alpha_y \right), \\
 a_{36} &= \frac{r_y \bar{y}_{0C}}{(1+c_{yx}\bar{x}_{0C}+c_{yy}\bar{y}_{0C})}, \\
 a_{43} &= a_y A_y, \\
 a_{44} &= -d_{y1}, \\
 a_{51} &= d_{x0}, \\
 a_{52} &= d_{x1}, \\
 a_{53} &= d_{y0},
 \end{aligned}$$

$$a_{54} = d_{y1},$$

$$a_{55} = -e_a \bar{s}_C,$$

$$a_{56} = -e_a \bar{a}_C,$$

$$a_{65} = r_s,$$

$$a_{66} = -e_s$$

and rest of the elements of the J_{E_C} are zero.



AIMS Press

©2019 the Author(s), licensee AIMS Press. This is an open access article distributed under the terms of the Creative Commons Attribution License (<http://creativecommons.org/licenses/by/4.0>)

CHAPTER 3

System dynamics of cancer in erythropoiesis with multiple EPO feedbacks

System dynamics of cancer in erythropoiesis with multiple EPO feedbacks

Keywords: Polycythemia vera, hematological diseases, system dynamics modelling, EPO, steady states, stability, erythrocytes

Abstract

Blood production is a tightly regulated process, and disturbances can pose a severe risk to human health. Polycythemia vera (PV) is an example of such a disorder characterized by excessive production of erythrocytes and the presence of the *JAK2V617F* mutation. A 5D PV model with competing healthy and malignant cells, including erythropoietin (EPO), is proposed and analyzed. The production of EPO is governed by the number of erythrocytes, while EPO influences the proliferation and death rate of erythrocytes. Stem cell dynamics can be independently analyzed as a two-dimensional system. A numerical analysis shows that steady states and their stability of the 2D stem cell PV submodel are in agreement with the PV model. Combining the model with data of PV patients, we demonstrate the model's prognostic significance. It follows that an efficient treatment must target stem cell properties such as the bone marrow microenvironment and stem cell death rates.

1 Introduction

Blood formation known as hematopoiesis is a complex and tightly regulated process. Different types of blood cells are produced in the bone marrow from hematopoietic stem cells (HSCs). A hematopoietic stem cell can divide into two HSCs, and it can produce one stem cell and one progenitor cell or produce two progenitor cells. The progenitor cells then differentiate in a chain of steps and produce different types of mature blood cells, mainly red blood cells, white blood cells and platelets.

In the present work, we will focus on the red blood cells (erythrocytes) and the growth factors that contribute to red blood cells' production. In the bone marrow, stem cells differentiate into various progenitor cells, and finally, reticulocytes are released into the bloodstream, which matures into erythrocytes within about three days. The whole process is called erythropoiesis. Figure 1 illustrates the development of erythrocytes from stem cells. In healthy individuals, the life span of an erythrocyte is 120 days, and then the erythrocytes are engulfed by macrophages in the spleen (Rodak et al., 2008; Litchman et al., 2006). This process is controlled by the growth hormone EPO. A high concentration of EPO increases the number of BFU-Es recruited into CFU-E and ultimately leads to an increased production rate of erythrocytes (Adamson, 1974; Granziero et al., 2001; Iiyama et al., 2006; Jelkmann, 2013; Krantz, 1991; Silva et al., 1996). The kidneys secrete EPO into the blood with a half-life of 6 hours (Mahaffy et al., 1998).

The homeostasis of erythropoiesis requires an appropriate balance between the rate of erythrocyte production and erythrocyte destruction. EPO is thought to control the number of mature cells in the blood by interrupting the apoptotic mechanism (Granziero et al., 2001; Jelkmann, 2013; Silva et al., 1996; Testa, 2004; Weitzman et al., 2000).

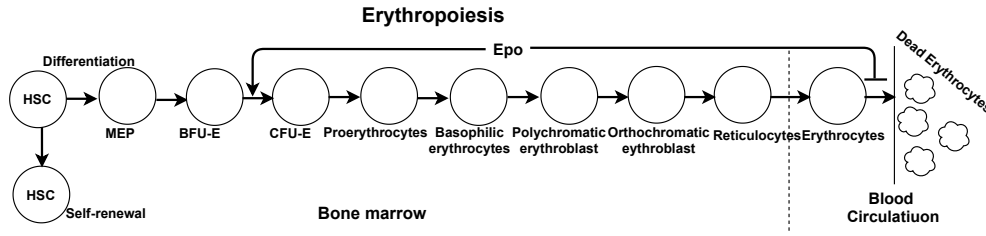


Figure 1: Different stages are involved in the development of erythrocytes (erythropoiesis). EPO increases the differentiation from BFU-E to CFU-E, whereas it inhibits the death rate of erythrocytes.

PV is a hematological disease and a subcategory of myeloproliferative neoplasms (MPNs) (Campbell and Green, 2006; Hasselbalch, 2012; Hasselbalch, 2013). The characteristics of PV are excessive production of erythrocytes, the presence of the *JAK2V617F* mutation and low EPO plasma levels in the blood (Carnesko et al., 1998). The *JAK2* gene is responsible for producing proteins that control cell growth and production. The mutation *JAK2V617F* is a disruption of the *JAK2* gene and occurs in 95% of patients with PV. Possible PV development is a transformation to acute myeloid leukemia (AML) with an increasing load of *JAK2V617F* mutations (Hasselbalch, 2012; Kristinsson et al., 2010; Hasselbalch, 2013). EPO also plays an important role in the progression of PV. In 2016, the World Health Organization (WHO) declared that subnormal serum EPO levels are considered a secondary criterion in the diagnosis of PV.

In system dynamics (SD), several models describe the behavior of the non-linear dynamic structures present in the human body (Abdel-Hamid, 2002; Hossainichimeh et al., 2015; Hsieh et al., 1990; Karanfil and Barlas, 2008; Lee et al., 2016; Mehrjerdi, 2013). In (Rogers et al., 2018), a SD model of erythropoiesis was developed and calibrated in renal patients with anemia by establishing a personalized EPO dosage to stabilize hemoglobin levels. In (Senturk et al. 2020) a biomedical model was introduced to study the effects of recombinant human erythropoietin (rHuEPO) as a doping agent. None of the previous work has addressed these issues, including multiple EPO feedback on healthy and malignant cells, the importance of stem cell dynamics in controlling erythropoiesis, and the importance of stem cell parameters for efficient treatments in PV.

In this paper, we present and investigate a PV model that considers the competition between healthy and malignant cells and the EPO feedback on both cell lines. In section 2, we formulate the model and explain the physiological relevance of the parameters. In addition, we simplify the model using dimensional analysis. In section 3 we identify the physiological steady states determined by the stem cell dynamics. Furthermore, we perform sensitivity analysis and identify the sensitive parameters for cancer development. Finally, in silico treatment strategies targeting stem cell dynamics are shown. In section 4 final remarks, including model trajectories, are given in comparison to data for PV patients treated with interferon- α (IFN).

2 Description of the PV (Polycythemia vera) models

2.1 PV model

The SD *PV model* describes the proliferation of hematopoietic stem cells (HSC) to erythrocytes (RBC) and malignant stem cells (MSC) carrying the *JAK2V617F* mutation to malignant mature cells (MMC). In addition, the model takes into account that EPO stimulates the production of RBCs. A stock-flow diagram for the PV model appears in Figure 2. There are five variables (stocks) that describe the number of HSCs (x_0), the number of RBCs (x_r), the number of MSCs (y_0), the number of MMCs (y_r), and the concentration of EPO (E). The PV model is inspired by mathematical models in (Andersen et al., 2017; Ottesen et al., 2019; Colijn and Mackey, 2005) and reads

$$\frac{dx_0}{dt} = (r_x \phi_x - d_{x_0} - a_x)x_0, \quad (1a)$$

$$\frac{dy_0}{dt} = (r_y \phi_y - d_{y_0} - a_y)y_0, \quad (1b)$$

$$\frac{dx_r}{dt} = a_x A_x(E)x_0 - d_{x_r}(E)x_r, \quad (1c)$$

$$\frac{dy_r}{dt} = a_y A_y(E)y_0 - d_{y_r}(E)y_r, \quad (1d)$$

$$\frac{dE}{dt} = f(x_r, y_r) - kE. \quad (1e)$$

with

$$\phi_x = \frac{1}{1 + c_{xx}x_0 + c_{xy}y_0} \quad \text{and} \quad \phi_y = \frac{1}{1 + c_{yx}x_0 + c_{yy}y_0}. \quad (2)$$

Hence, the general form of the equations is,

$$\frac{d(\text{Stock})}{dt} = \text{Inflow} - \text{Outflow}$$

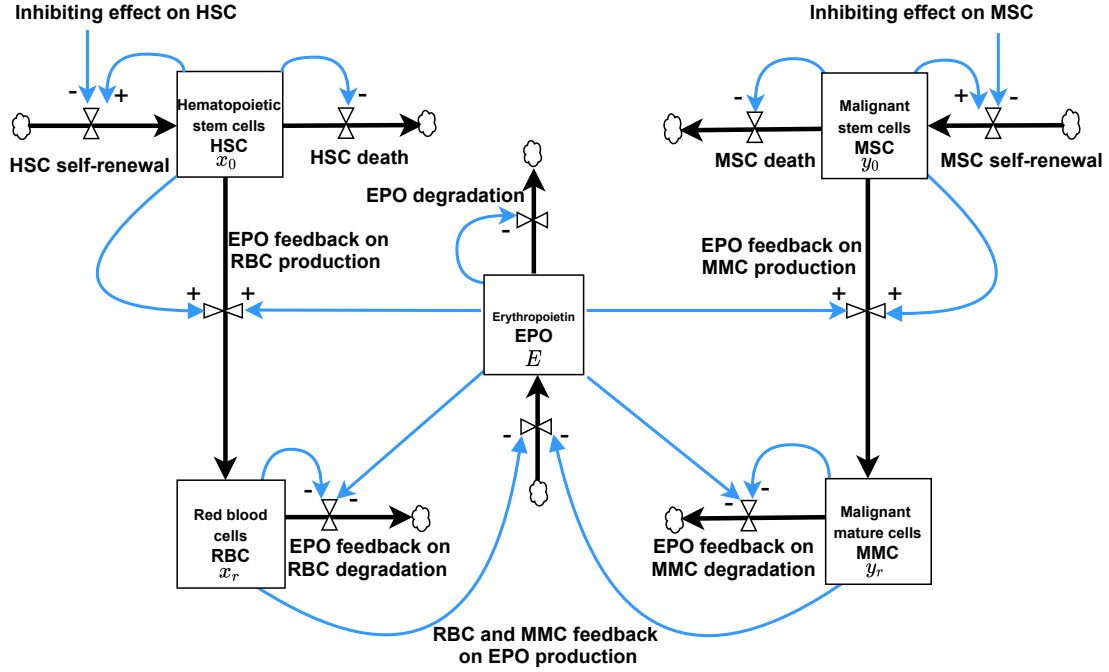


Figure 2: Black arrows represent flows, blue arrows show relationship between variables and boxes denote stock variables.

The self-renewal rate for HSC and MSC are denoted as r_x and r_y , respectively. Since the self-renewal of stem cells is inhibited by niche feedback (Walkley et al., 2007), the production of stem cells in the bone marrow decreases when the amount of stem cells exceeds the normal level. We implement this inhibition by Michaelis-Menten-like functions $\phi_x(x_0, y_0)$ and $\phi_y(x_0, y_0)$, which is also adopted in (Dingli and Michor, 2006; Stiehl et al., 2015; Walenda et al., 2014). Feedback strengths c_{xx} and c_{xy} show an inhibitory effect on the self-renewal of HSC similarly, c_{yx} and c_{yy} capture the corresponding effects on the self-renewal of MSC. We assume $c_{yy} \leq c_{yx} \leq c_{xy} \leq c_{xx}$, since malignant cells are less sensitive to stem cell microenvironment as compared to hematopoietic cells (Kim et al., 2008; Rovida et al., 2014).

HSC differentiates towards RBC with rate a_x while the similar rate for MSC differentiation towards MMC is denoted by a_y . The progenitor cells are not considered explicitly however, they are implicitly accounted for by multiplication factors A_x and A_y such that the resulting production rates of HSC and MSC become $a_x A_x$ and $a_y A_y$ respectively. For further details see (Andersen et al., 2017).

Since EPO stimulates the production of mature red cells (Adamson, 1974; Granziero et al., 2001; Iiyama et al., 2006; Jelkmann, 2013; Krantz, 1991; Silva et al., 1996) we choose to write the EPO-dependent amplification

factors,

$$A_x(E) = \delta_x \frac{E}{1 + \alpha_x E}, \quad (3)$$

$$A_y(E) = \delta_y \frac{E}{1 + \alpha_y E}, \quad (4)$$

where δ_x and δ_y are positive constants and α_x and α_y , are non-negative constants.

To account for the death rates, the stem cells are removed with rates d_{x_0} and d_{y_0} . Furthermore, EPO has been shown to inhibit erythrocytes apoptosis (Granziero et al., 2001; Jelkmann, 2013; Silva et al., 1996; Testa, 2004; Weitzman et al., 2000). Thus, an increase in EPO leads to a decrease in the apoptosis rate of erythrocytes. Assuming $d_{xr}(E)$ and $d_{yr}(E)$ are decreasing functions of E , we choose

$$d_{xr}(E) = \eta_x \frac{1}{1 + \beta_x E}, \quad (5)$$

$$d_{yr}(E) = \eta_y \frac{1}{1 + \beta_y E}, \quad (6)$$

where η_x , η_y , β_x and β_y are non-negative constants.

The negative feedback function $f(x_r, y_r)$ is a monotone decreasing function of x_r and y_r (Belair et al., 1995; Bradford et al., 1997), it is assumed to have the form,

$$f(x_r, y_r) = \frac{p}{1 + k_0(x_r + y_r)^m},$$

which is a Hill function in $x_r + y_r$ with Hill constants p , k_0 and m . Hence, an increase in the number of x_r and y_r decreases the production of EPO. For simplicity, we consider $m = 1$ in the subsequent analysis.

The default parameter values are summarized in table 1, and an illustration of the PV model, including stem cells, RBC counts, and EPO based on the default values is shown in Figure 3.

Parameter	Explanation	Value	Unit	Reference
r_x	Self-renewal rate of HSC	$5 \cdot 10^{-3}$	day ⁻¹	Dingli and Michor, 2006
r_y	Self-renewal rate of MSC	$1.15 \cdot 10^{-2}$	day ⁻¹	*
a_x	Differentiation rate of HSC	$3.58 \cdot 10^{-5}$	day ⁻¹	*
a_y	Differentiation rate of MSC	$3.58 \cdot 10^{-5}$	day ⁻¹	*
d_{x_0}	Death rate of HSC	$2 \cdot 10^{-3}$	day ⁻¹	Andersen et al., 2017
d_{y_0}	Death rate of MSC	$2 \cdot 10^{-3}$	day ⁻¹	Ottesen et al., 2019 Andersen et al., 2017
c_{xx}	Inhibition by HSC on HSC	$5.6 \cdot 10^{-5}$	-	Ottesen et al., 2019
c_{yx}	Inhibition by HSC on MSC	$5.2 \cdot 10^{-5}$	-	Ottesen et al., 2019
c_{xy}	Inhibition by MSC on HSC	$5.4 \cdot 10^{-5}$	-	Ottesen et al., 2019
c_{yy}	Inhibition by MSC on MSC	$5.0 \cdot 10^{-5}$	-	Ottesen et al., 2019
p	Production rate of EPO	$1.56 \cdot 10^4$	day ⁻¹	Belair et al., 1995
k_0	Factor affecting production of EPO	$8.9 \cdot 10^{-11}$	-	*
α_x	Factor affecting production of RBC	$5 \cdot 10^{-3}$	-	*
α_y	Factor affecting production of MMC	$5 \cdot 10^{-3}$	-	Assumed
β_x	Factor affecting removal of RBC	$9 \cdot 10^{-3}$	-	*
β_y	Factor affecting removal of MMC	$9 \cdot 10^{-3}$	-	Assumed
δ_x	Stimulation rate of RBC	$3 \cdot 10^9$	-	*
δ_y	Stimulation rate of MMC	$3 \cdot 10^{10}$	-	Assumed
η_x	Death rate of RBC	$8 \cdot 10^{-3}$	day ⁻¹	Belair et al., 1995 Colijn and Mackey, 2005
η_y	Death rate of MMC	$8 \cdot 10^{-3}$	day ⁻¹	Assumed
k	Degradation rate of EPO	2.8	day ⁻¹	Belair et al., 1995

Table 1: Default parameter values of the PV model. *Calculated using steady state equations.

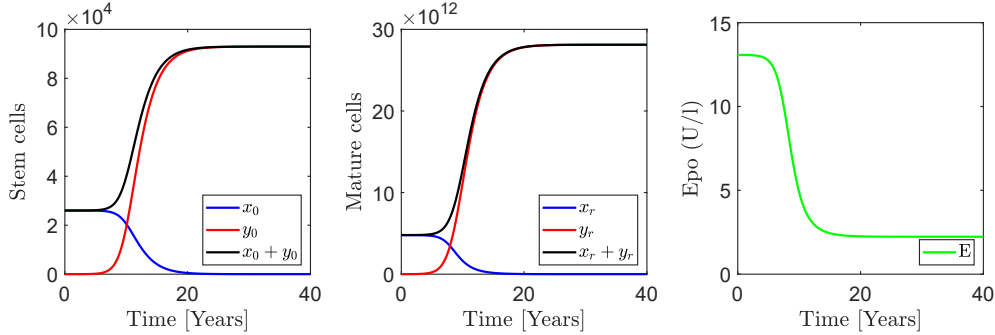


Figure 3: A typical PV model based on the development of stem cells, RBC counts and EPO in case of a *JAK2V617F* positive myeloid neoplasm for default parameters. Red curves are malignant cells, blue shows healthy hematopoietic cells and black denotes the sum of the cells. Initial conditions are $(x_0, y_0, x_r, y_r, E) = (2.6 \cdot 10^4, 1, 4.8 \cdot 10^{12}, 0, 13.1)$ at $t = 0$. Time is plotted on the x -axis. The left panel shows the growth of malignant stem cell count and the middle panel shows the evolution of mature malignant cell count. Hematopoietic stem cells are higher in number as compared to malignant cells in the early years. However, after some years, the malignant stem cells overcome the hematopoietic stem cells leading to the extinction of the healthy cell population. The right panel shows that the concentration of EPO decreases over time.

2.2 Dimensionless PV model

We non-dimensionalize and scale the model, transforming the variables and parameters such that simplified equations are obtained. Another advantage is that the parameters cluster together thus the resulting number of governing parameters becomes minimal. We non-dimensionalize the equations of the system (1) using the following scales,

$$x_0 = \hat{x}_0 X_0, y_0 = \hat{y}_0 Y_0, x_r = \hat{x}_r X_r, y_r = \hat{y}_r Y_r, E = \hat{e} E_q, t = \hat{t} \tau$$

where small letters with hat are scaling constants, capital letters on the right side are dimensionless variables and τ is dimensionless time.

$$\frac{dX_0}{d\tau} = \zeta_x \left(\frac{1}{1 + X_0 + p_{x1} Y_0} - p_{x2} \right) X_0, \quad (7a)$$

$$\frac{dY_0}{d\tau} = \zeta_y \left(\frac{1}{1 + p_{y1} X_0 + Y_0} - p_{y2} \right) Y_0, \quad (7b)$$

$$\frac{dX_r}{d\tau} = \left(\frac{E_q}{1 + q_{x1} E_q} X_0 - \frac{q_{x2}}{1 + q_{x3} E_q} X_r \right), \quad (7c)$$

$$\frac{dY_r}{d\tau} = \left(\frac{E_q}{1 + q_{y1} E_q} Y_0 - \frac{q_{y2}}{1 + q_{y3} E_q} Y_r \right), \quad (7d)$$

$$\frac{dE_q}{d\tau} = \frac{1}{\epsilon} \left(\frac{10^4}{1 + r_{e1} X_r + r_{e2} Y_r} - E_q \right). \quad (7e)$$

The selection for scaling constants and the grouped parameters is given in table (2). Note, the *dimensionless PV model* given in equations (7a)-(7e) involves 15 parameters and the actual values of dimensionless parameters are given in table 3 computed using the values in table 1.

$\hat{x}_0 = c_{xx}^{-1}$	$\hat{y}_0 = c_{yy}^{-1}$
$\hat{x}_r = p a_x \delta_x (10^4 r_x c_{xx})^{-1}$	$\hat{y}_r = p a_y \delta_y (10^4 r_x c_{yy})^{-1}$
$\hat{e} = p (10^4 k)^{-1}$	$\hat{t} = k (r_x)^{-1}$
$p_{x1} = c_{xy} (c_{yy})^{-1}$	$p_{x2} = (d_{x0} + a_x) r_x^{-1}$
$p_{y1} = c_{yx} (c_{xx})^{-1}$	$p_{y2} = (d_{y0} + a_y) r_y^{-1}$
$q_{x1} = \alpha_x p (10^4 k)^{-1}$	$q_{y1} = \alpha_y p (10^4 k)^{-1}$
$q_{x2} = \eta_x k (r_x)^{-1}$	$q_{y2} = \eta_y k (r_x)^{-1}$
$q_{x3} = \beta_x p (10^4)^{-1}$	$q_{y3} = \beta_y p (10^4)^{-1}$
$r_{e1} = k_0 p a_x \delta_x (10^4 r_x c_{xx})^{-1}$	$r_{e2} = k_0 p a_y \delta_y (10^4 r_x c_{yy})^{-1}$
$\zeta_x = k$	$\zeta_y = k r_y (r_x)^{-1}$
$\epsilon = r_x (k^2)^{-1}$	

Table 2: Definition of variables and parameters of the dimensionless PV model.

Parameter	Explanation	Value
p_{x1}	Inhibition by MSC on HSC	1.08
p_{x2}	Death rate of HSC	0.40
p_{y1}	Inhibition by HSC on MSC	0.93
p_{y2}	Death rate of MSC	0.17
q_{x1}	Factor affecting production of RBC	0.002
q_{x2}	Death rate of RBC	4.48
q_{x3}	Factor affecting removal of RBC	0.005
q_{y1}	Factor affecting production of MMC	0.002
q_{y2}	Death rate of MMC	4.48
q_{y3}	Factor affecting removal of MMC	0.005
r_{e1}	Factor affecting production of EPO	53.07
r_{e2}	Factor affecting production of EPO	594
ζ_x	Factor affecting self-renewal and death rates of HSC	2.80
ζ_y	Factor affecting self-renewal and death rates of MSC	6.44
ϵ	Factor affecting production and degradation of EPO	$6.37 \cdot 10^{-4}$

Table 3: Default dimensionless (no unit) parameter values of the dimensionless PV model.

The stem cell dynamic in equations (7a) and (7b) is independent of the remaining model thus, we refer it to the *stem cell PV submodel*.

3 Results

Below we present the numerical investigation for the dimensionless PV model and the stem cell PV submodel, including steady states of the model, sensitivity analysis, and an in silico approach for treatment.

3.1 Steady states analysis

In this section, we identify the unstable and stable steady states. Since a non-negative number of cells and concentrations is of physiological interest, the feasible steady states can be classified as follows,

- a trivial steady state always exists $S_0 = (0, 0, 0, 0, E_q)$,
- a hematopoietic steady state exists if and only if the malignant cell count is zero, whereas the hematopoietic cell count is positive $S_H = (X_0, 0, X_r, 0, E_q)$,
- a malignant steady state exists if and only if the hematopoietic cell count is zero, whereas the malignant cell count is positive $S_L = (0, Y_0, 0, Y_r, E_q)$,
- a co-existing steady state exists if and only if both hematopoietic and malignant cell count is positive $S_C = (X_0, Y_0, X_r, Y_r, E_q)$.

In Figure 4, we identify the various steady states of the stem cell PV submodel. We use MATLAB to perform simulations and numerical analysis. The possible steady states depend on the inhibiting strengths p_{x1} and p_{y1} and the death rates p_{x2} and p_{y2} . Figure 4a illustrates that the trivial steady state is stable for p_{x2} and p_{y2} greater than 1. At this point, we observe two scenarios. Decreasing p_{x2} below 1, the stable hematopoietic steady state emerges and the trivial steady state becomes unstable as illustrated in Figure 4b. This state is hematopoietic corresponds to the healthy state. Instead of p_{x2} , if we decrease p_{y2} below 1, the stable malignant steady state is shown while the trivial steady state becomes unstable as illustrated in Figure 4c. Hence, this investigation reveals the importance of death rates p_{x2} and p_{y2} to obtain stable hematopoietic and malignant steady states.

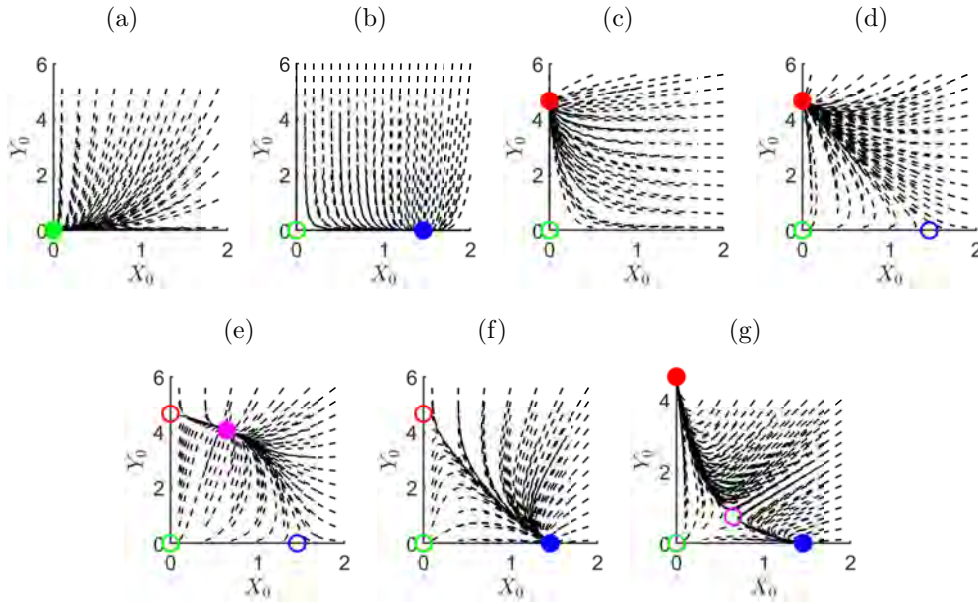


Figure 4: The stem cell PV submodel illustrates that the trajectories for different initial conditions ultimately approach the stable steady states. Full circles are stable steady states and open circles are unstable steady states. Green, blue, red and magenta correspond to trivial, hematopoietic, malignant and co-existing steady states respectively. The trajectories are shown as black dotted lines. The panels are as follows, (a) $p_{x2} = 1.1$, $p_{y2} = 1.1$, (b) $p_{x2} = 0.40$, $p_{y2} = 1.1$, (c) $p_{x2} = 1.1$, $p_{y2} = 0.17$, (d) default values (e) $p_{x1} = 0.20$, $p_{y1} = 0.93$, (f) $p_{x1} = 0.20$, $p_{y1} = 4.0$, (g) $p_{x1} = 1.08$, $p_{y1} = 6.0$.

Next, we examine the impact of parameters involved in the hematopoietic and malignant stem cell niche. For the default parameter values, the inhibitory effect on the hematopoietic stem cells by the malignant stem cells dominates ($p_{x1} > p_{y1}$). In this case, the malignant steady state is stable, whereas the trivial and hematopoietic steady states are unstable (See Figure 4d). Decreasing p_{x1} from the default value, a co-existing steady

state appears at $p_{x1} = 0.2$ and takes over the stability of malignant steady state (See Figure 4e). At this stage, we can re-establish the hematopoietic steady state by perturbing parameters in favor of a healthy cell population. For example, fix $p_{x1} = 0.2$ and increase p_{y1} , the co-existing steady state approaches the unstable hematopoietic steady state. When a co-existing steady state merges with the hematopoietic steady state, the hematopoietic steady state becomes stable as illustrated in Figure 4f. The special case of bistability obtained by increasing p_{y1} from the default value to $p_{y1} = 6$ gives both stable malignant and hematopoietic steady states whereas the co-existing steady state is unstable. The stable co-existing steady state is obtained when two cell populations are equally fit. This state can persist for several years, especially in slowly developing diseases like PV without major blood function impairment. However, the transformation to a malignant or hematopoietic steady state is possible from a stable co-existing steady state. Therefore, the right treatment approach is essential to achieve favorable outcomes in a co-existing state. In case of bi-stability of healthy and malignant cells, the impact of the initial number of cells determines the fate of cell populations. For example, some initial values converge to the hematopoietic steady state while the others converge to the malignant steady state. We may also observe the transient time towards the hematopoietic and malignant states. Furthermore, the regions exhibiting bistability can be potentially targeted during the treatment to delay or prevent disease progression. For instance, in our model, increasing the inhibiting factor of malignant stem cells, i.e., p_{y1} increases the basin of attraction for the hematopoietic steady state. Hence, this investigation reveals the importance of inhibiting factors for stem cells of both types concerning the successful therapy of the disease.

We can understand the dynamics of the PV model through the stem cell PV submodel. Figure 5 illustrates a few cases where a unique steady state is stable. It shows that all trajectories in the dimensionless PV model approach a steady state determined by the stem cell PV submodel for various initial conditions. We convert the time scale to real time for the remaining figures.

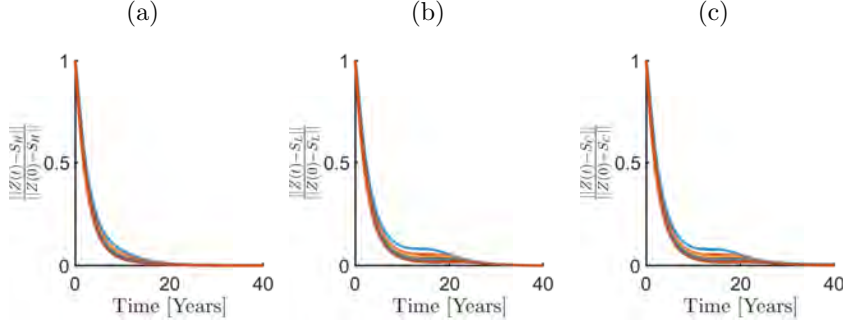


Figure 5: Panels (a), (b) and (c) illustrate a unique stable steady state is attracting. $Z(t)$ denotes the solution of the dimensionless PV model where time is converted to real time. S_H , S_L and S_C correspond to the hematopoietic, malignant and co-existing steady states. In panel (a) $\frac{\|Z(t) - S_H\|}{\|Z(0) - S_H\|}$ is plotted against time for five sets of initial conditions for the stem cells, corresponding to Figure 4f. Since $\frac{\|Z(t) - S_H\|}{\|Z(0) - S_H\|}$ approaches zero for large time, $Z(t)$ approaches S_H . Similarly panels (b) and (c) correspond to Figure 4d and Figure 4e showing stability of S_L and S_C respectively.

3.2 Sensitivity Analysis

Sensitivity analysis of the dimensionless PV model is performed to explore the relationship between the input parameters and the PV dynamics outcome. In clinical trials and practice, the total cell count and the *JAK2V617F* allele burden are measured in blood samples from PV patients therefore, we consider these two criteria for sensitivity analysis. For $p_{x1} = 0.2$ and all other parameters are fixed at their default values (See Table 3) leads to a stable co-existing steady state. We choose 10% variation in the values of the parameters and calculate the total count of erythrocytes as $X_r + Y_r$ and the *JAK2V617F* allele burden as $\frac{Y_r}{X_r + Y_r}$ at steady state. First, we consider the parameters involved in the stem cell PV submodel. Figure 6 illustrates that p_{x1} , p_{y1} , p_{x2} and p_{y2} are sensitive parameters for the mature cell count and the *JAK2V617F* allele burden. Hence, perturbing these four parameters involved in the stem cell dynamics are important for the evolution of PV.

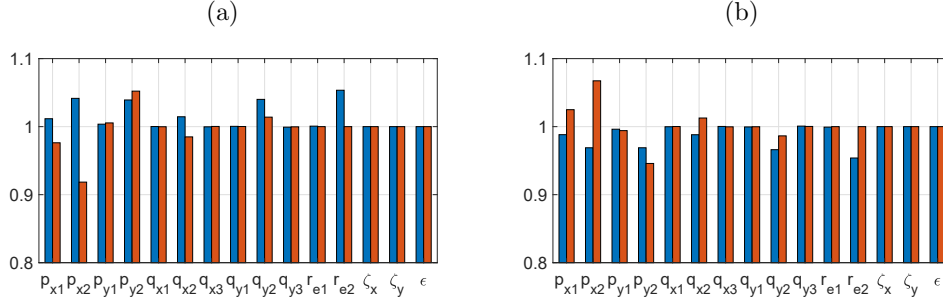


Figure 6: Panels (a) and (b) show the effect when parameters are decreased (below 1) and increased (above) by 10%, respectively. For each parameter two columns are shown; the first (blue) shows the effect on the total number of erythrocytes, $X_r + Y_r$ and the second (maroon) shows the effect on the $JAK2V617F$ allele burden, $\frac{Y_r}{X_r + Y_r}$.

Next, we observe that the death rates of mature cells q_{x2} and q_{y2} are also sensitive for cell count and allele burden. Finally, r_{e2} a factor affecting the production of EPO, is also a sensitive parameter to the erythrocyte count. Concluding, this investigation shows that stem cell dynamics govern the PV progression.

3.3 In silico treatment strategies

IFN is known to induce hematological remission in various hematological diseases like polycythemia vera, essential thrombocytosis, etc. (Kildajian et al., 2006; Samuelsson et al., 2006; Stauffer et al., 2013; Lindgren et al., 2018). Despite its use in clinical practice, the mechanisms by which IFN affects hematopoietic stem and progenitor cells in blood cancer is still under discussion.

In (Lu et al., 2010) the authors reported the increased death rate in hematopoietic stem and progenitor cells in vitro after IFN therapy. Similarly, (Mullally et al., 2013) states that IFN reduces the $JAK2V617F$ allele burden by targeting malignant stem cells. In addition, the increased death rate in erythroid progenitor cells is noticed after IFN treatment, resulting in normalized red blood cell count. In contrast to previous studies, it is reported in (King et al., 2015) that IFN arrests the disease progression by increasing cell division and differentiation with no evidence of affecting the death rate of the stem cells.

Several clinical experiences explore that cancer development during different treatment phases occur in patients, e.g., complete recovery, relapse, or entering a co-existing state where malignant and hematopoietic cells co-exist. Since stem cell dynamics govern the entire system we focus on the parameters involved in stem cell dynamics. First, we take the death rate of the malignant stem cell as our treatment parameter. In Figure 7 we

assume that a virtual patient is in a co-existing state. Simulating a drug by increasing the death rate of malignant stem cells p_{y2} by a factor 2, a high malignant cell count co-existing steady state (white area) switches to a low malignant cell count co-existing steady state (grey area). Figures 7a and 7b show that a high value of p_{y2} normalizes the hematopoietic stem cells count as well as the erythrocyte count, hence reducing the *JAK2V617F* allele burden. In addition, the EPO level is increased as shown in Figure 7d. Figure 7 is taken as an example of IFN therapy.

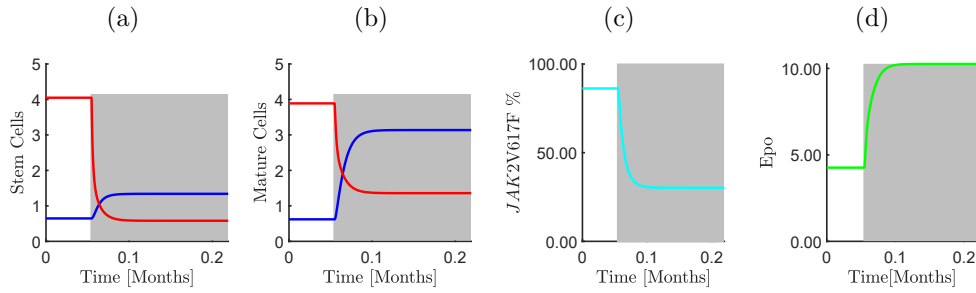


Figure 7: An example of in silico treatment by increasing the death rate of malignant stem cells. Blue, red, cyan and green correspond to the healthy cells, malignant cells, the *JAK2V617F* allele burden and EPO respectively. Panels (a), (b), (c) and (d) demonstrate dynamics before treatment and after treatment (grey area). A co-existing state of low hematopoietic cells and high malignant cells ($p_{x1} = 0.2$ from Figure 4e) before treatment, switches to co-existing state with high level of hematopoietic cells and low level of malignant cells by increasing p_{y2} from 0.17 to 0.34 and keep all other fixed at default values.

The bone marrow niche regulates the proliferative capacity of stem cells and blood cancer is associated with the bone marrow niche (Santar et al., 2015). It is an ongoing discussion how hematopoietic and malignant stem cells compete in the bone marrow niche. The microenvironment controls such competition in the niches, which may be affected by therapies. In a second scenario (considering a virtual subject being in a co-existing state), we take the treatment parameter p_{y1} , which captures the inhibitory effect for malignant stem cells. Before perturbing p_{y1} , a co-existing steady state exists with high malignant and low hematopoietic cell count. Increasing p_{y1} by a factor three, a co-existing steady state moves towards another co-existing state (shown in the grey area) where the malignant cell count is lower and the hematopoietic cell level is higher as shown in Figure 7. In addition, the *JAK2V617F* allele burden is reduced from 86 % to approximately 50 %, and the EPO level is increased. Hence, the microenvironment for stem cells may be a good target for therapies.

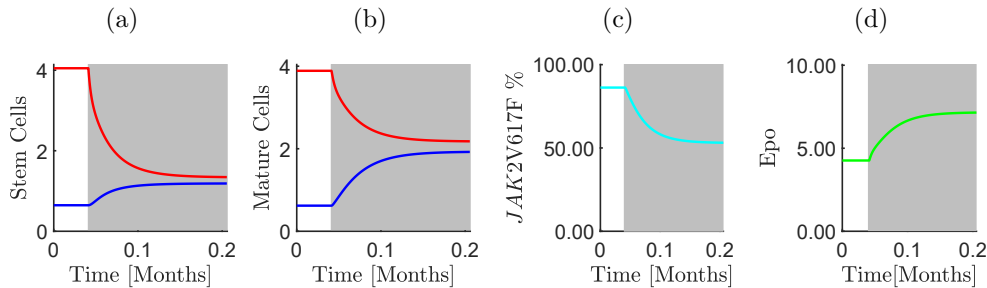


Figure 8: An example of in silico treatment targets inhibitory effect for malignant stem cells. Blue, red, cyan and green correspond to the healthy cells, malignant cells, the *JAK2V617F* allele burden and EPO respectively. Panels (a), (b), (c) and (d) demonstrate dynamics before treatment and after treatment (grey area). A co-existing state of low hematopoietic cells and high malignant cells ($p_{x1} = 0.2$ from Figure 4e) before treatment, switches to a co-existing state of high hematopoietic cells and low malignant cells by increasing p_{y1} from 0.93 to 2.79 and keep all other fixed at default values.

4 Discussion and conclusions

In this work, a PV model is proposed and analyzed that incorporates both hematopoietic and malignant cells. In addition, the interaction of EPO with healthy and malignant mature red blood cells is considered. A dimensional analysis reduced the number of parameters from 23 to 15. A 2D stem cell PV submodel facilitates the observation of model dynamics. The existence and stability of all steady states (trivial, hematopoietic, malignant, co-existing) in the stem cell PV submodel are visualized in Figure 4. It is further emphasized that the dynamics of the PV model and the stem cell PV submodel are similar. Finally, the sensitivity analysis identifies the most effective parameters for disease progression. We conclude that it is important to target the stem cells during treatment to prevent the development of the disease as the main contribution of the overall analysis. This investigation aligns with the view that the development of blood cancer is linked to stem cell division and the regulatory feedback mechanism in the niche. Figure 7 is an example of controlling the division of malignant stem cells by increasing their death rate p_{y2} . Figure 8 is an example of regulating the feedback mechanism in the niche by increasing the inhibitory effect on malignant stem cells p_{y1} . The comparison of both figures shows that the death rate of malignant stem cells may be a good candidate to consider during treatment, as a small perturbation of the parameter leads to rapid remission.

Figure 9 compares the PV model trajectories with data from PV patients receiving IFN treatment. Figure 9a and Figure 9b are good examples of fitting the data for total erythrocyte count to a disease and treatment course. Figure 9c illustrates data fitting to both erythrocyte count and the

$JAK2V617F$ allele burden during treatment for the same parameter set. Comparison of simulation of the PV model with patient data shows that the proposed model can reproduce both pre-treatment and treatment data and is consistent with the dynamics observed in clinics.

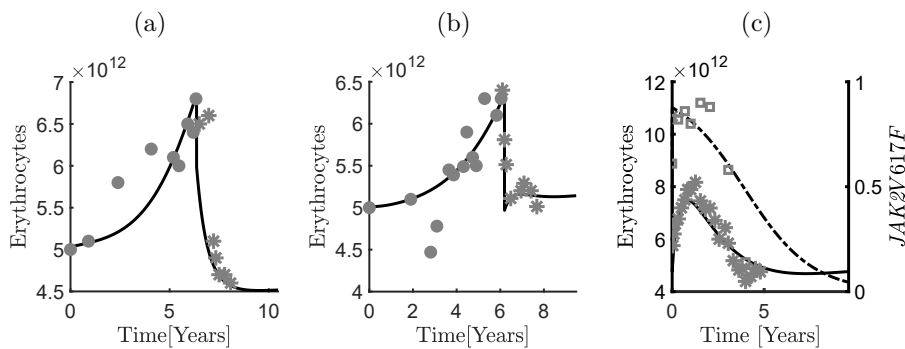


Figure 9: Three PV patients treated with IFN are compared with the PV model. The data for the total number of erythrocytes ($X_r + Y_r$) are displayed as filled circles for the periods without treatment (before the 6th year) and as stars during treatment (after the 6th year) in the two leftmost panels. In the rightmost panel data of a third patient during treatment is displayed. The asterisks represent the total number of erythrocytes, whereas the boxes represent the $JAK2V617F$ allele burden $\frac{Y_r}{X_r + Y_r}$. The model predictions are shown as full curves for the erythrocyte count and as dashed curves for the $JAK2V617F$ allele burden decay. The data shown in the first two panels are from (Michiels et al., 2014). The data shown in the last panel is from the clinical trial “DALIAH” (EudraCT number: 2011-001919-31).

In summary, the presented model has the novel feature of incorporating both healthy and malignant cells with different feedback mechanisms depending on both EPO and erythrocytes. The stem cell submodel pinpoints the governing parameters as well as suggesting novel treatment strategies. Furthermore, the model indicates that PV is a stem cell-driven disease. It is supported by the idea that a small population of stem cells, sharing self-renewal and differentiation properties, balancing homeostasis, and allowing cancer growth was first introduced in (Makino et al., 1959) and has been given more attention in recent years. Therefore, it stands to reason that treatments focusing on the elimination of malignant stem cells reduce disease load and improve outcomes for patients. A stem cell transplant, or a bone marrow transplant, is an example of such a promising treatment for blood cancer where the malignant cells are replaced with the healthy stem cells, preventing a relapse. As an alternative to stem cell transplant, a few drugs have been used that selectively target malignant stem cells and induce their apoptosis rate (Lu et al., 2010; Mullally et al., 2013). Another medical perspective is that malignant stem cells interact with stem cell niches and outcompete hematopoietic stem cells. Our model simulations interpret that

targeting the death rate and the inhibitory factor of malignant stem cells helps in disease regression. The PV model is able to explain various existing treatments and suggest novel intervention strategies.

Glossary

AML Acute Myeloid Leukemia, a cancer of the myeloid blood cells.

EPO A hormone release into the blood stream by the kidney and stimulates red blood cells.

Erythrocytes Red blood cells.

Erythropoiesis The process of making erythrocytes in the bone marrow.

HSC Hematopoietic stem cell, develop into different type of blood cells.

Hydroxyurea therapy A medication used in sickle-cell disease.

IFN Interferon α , a medication used for an auto immune disorder and for some cancers.

JAK2 gene The JAK2 gene is responsible for making a protein that promotes production of blood cells from the hematopoietic cells.

JAK2V617F A somatic mutation in the JAK2 gene which is responsible for overproduction of blood cells in PV.

MPNs Myeloproliferative Neoplasms, characterized by the uncontrolled growth of blood cells.

PV Polycythemia vera, characterized by the excessive production of red blood cells.

RBC Red blood cells.

References

- Abdel-Hamid TK. 2002. Modelling the dynamics of human energy regulation and its implications for obesity treatment. *System Dynamics Review* Vol. 18, No. 4, 431–471.
- Adamson J. 1974 The relationship of erythropoietin and iron metabolism to red blood cell production in humans. *Semin. Oncol.* 21, 9-15.
- Andersen M, Sajid Z, Pedersen RK, Gudmand-Hoeyer J, Ellervik C, Skov V, Kjær L, Pallisgaard N, Kruse TA, Thomassen M, Troelsen J, Hasselbalch HC, Ottesen JT. 2017. Mathematical modelling as a proof of concept for MPNs as a human inflammation model for cancer development. *PLoS ONE* 12(8): e0183620.
- Belair J, Mackey MC, Mahaffy JM. 1995. Age-structured and two delay models for erythropoiesis. *Math. Biosci.* 128, 317-346.
- Bradford G, Williams B, Rossi R, Bertonecello I. 1997. Quiescence, cycling and turnover in the primitive haematopoietic stem cell compartment. *Exper. Hematol.* 25. 445-453.
- Campbell PJ, Green AR. 2006. The myeloproliferative disorders. *N. Engl. J. Med.* 355: 2452-2466.
- Carneskog J, Kutti J, Wadenvik H, Lundberg PA, Lindstedt G. 1998. Plasma erythropoietin by high-detectability immune-radiometric assay in untreated and treated patients with Polycythemia vera and essential thrombocythemia. *Eur J Haematol*, 60: 278-82.
- Colijn C, Mackey MC. 2005. A mathematical model of hematopoiesis—I. Periodic chronic myelogenous leukemia. *Journal of Theoretical Biology.* 237: 117-132.
- Dingli D, Michor F. 2006. Successful Therapy Must Eradicate Cancer. *Stem Cells*, 24(12): 2603.
- Santar CG, Desmond R, Feng X, Bat T, Chen J, Heuston E, Mizukawa B, Mulloy JC, Bodine DM, Larochelle A, Dunbar CE. 2015. Functional Niche Competition Between Normal Hematopoietic Stem and Progenitor Cells and Myeloid Leukemia Cells. *Stem Cells*, 33(12): 3635-42.
- Granziero L, Ghia P, Circosta P, Gottardi D, Strola G, Geuna M, Montagna L, Piccoli P, Chilosi M, Caligaris-Cappio F. 2001. Survivin is expressed on CD40 stimulation and interfaces proliferation and apoptosis in B-cell chronic lymphocytic leukemia. *Blood* 97, 9: 2777-2783.

- Hasselbalch HC. 2012. Perspectives on chronic inflammation in essential thrombocythemia , polycythemia vera , and myelofibrosis: is chronic inflammation a trigger and driver of clonal evolution and development of accelerated atherosclerosis and second cancer? *Blood*, 119: 3219–3226.
- Hasselbalch HC. 2013. Chronic inflammation as a promotor of mutagenesis in essential thrombocythemia, polycythemia vera and myelofibrosis. A human inflammation model for cancer development? *Leukemia Research*, 37: 214–220.
- Hosseini N, Rahmandad H, Wittenborn AK. 2015. Modelling the hypothalamus–pituitary–adrenal axis: A review and extension. *Mathematical Biosciences* 268, 52–65.
- Hsieh BS, Chen YM, Wu KD, Kuo YM, Hsieh CH, Lee PW. 1990. A simulation study on renin and aldosterone secretions in primary aldosteronism. *Journal of Formosan Medical Association* 89(5): 346–349.
- Iiyama M, Kakihana K, Kurosu T, Miura O. 2006. Reactive oxygen species generated by hematopoietic cytokines play roles in activation of receptor-mediated signaling and in cell cycle progression. *Cellular Signalling* 18 , 2: 174-182.
- Jelkmann W. 2013. Physiology and pharmacology of erythropoietin. *Transfus Med Hemother*, 40:302–309.
- Karanfil Ö, Barlas Y. 2008. A dynamic simulator for the management of disorders of the body water homeostasis. *Operations Research* 56(6): 1474–1492.
- Kiladjian JJ, Cassinat B, Turlure P, Cambier N, Roussel M, Bellucci S, Menot ML, Massonnet G, Dutel JL, Ghomari K, Rousselot P, Grange MJ, Chait Y, Vainchenker W, Parquet N, Abdelkader-Aljassem L, Bernard JF, Rain JD, Chevret S, Chomienne C, Fenaux P. 2006. High molecular response rate of polycythemia vera patients treated with pegylated interferon alpha-2a. *Blood*. 108(6): 2037-40.
- Kim YM, Koo BK, Jeong HW, Yoon MJ, Song R, Shin J, Jeong DC, Kim SH, Kong YY. 2008. Defective Notch activation in micro-environment leads to myeloproliferative disease, *Blood*. 112(12): 4628-38 .
- King KY, Matatall KA, Shen CC, Goodell MA, Swierczek SI, Prchal JT. 2015. Comparative long-term effects of interferon α and hydroxyurea on human hematopoietic progenitor cells, *International Society for Experimental Hematology*. 43: 912–918.

- Krantz SB. 1991. Erythropoietin. *Blood*. 77(3): 419–434.
- Kristinsson SY, Landgren O, Samuelsson J. 2010. Autoimmunity and the risk of myeloproliferative neoplasms. *Haematologica* 95: 1216–1220.
- Lee L, Heffernan M, McDonnell G, Short SD, Naganathan V. 2016. A system dynamics modelling approach to studying the increasing prevalence of people with intellectual developmental disorders in New South Wales. *Australian Health Review* 40(3): 235–243.
- Lichtman MA, Beutler E, Kipps TJ, Seligsohn U, Kaushansky K, Prchal JT. 2006. *Williams Hematology*. McGraw-Hill: New York, NY, USA.
- Lindgren M, Samuelsson J, Nilsson L, Knutsen H, Ghanima W, Westin J, Johansson PL, Andréasson B. 2018. Genetic variation in IL28B (IFNL3) and response to interferon-alpha treatment in myeloproliferative neoplasms. *Eur J Haematol*. 100(5): 419-425.
- Lu M, Zhang W, Li Y. 2010. Interferon-alpha targets JAK2V617F positive hematopoietic progenitor cells and acts through the p38 MAPK pathway. *Exp Hematol*. 38: 472–480.
- Mahaffy JM, Belair J, Mackey MC. 1998. Hematopoietic model with moving boundary condition and state dependent delay: Applications in Erthropoeisis. *J. Theor. Biol.* 190: 135-146.
- Makino S. 1959. The role of tumor stem-cells in regrowth of the tumor following drastic applications. *Acta Unio Int Contra Cancrum*. 15(Suppl 1): 196-8.
- Mehrjerdi YZ. 2013. A dynamic systems approach to weight related health problems. *International Journal of Quality and Reliability Management* 30(5): 571–589.
- Michiels JJ, Schroyens W, Lindemans J, Kate FWJT, Lam KH, De Raeve H. 2014. The erythrocyte count on top of bone marrow histology discriminates essential thrombocythemia and polycythemia vera in *JAK2V617F* mutated prefibrotic myeloproliferative neoplasm with no or minor splenomegaly. *Journal of Haematology and Thromboembolic Diseases*, 2:4.
- Mullally A, Bruedigam C, Poveromo L, Heidel FH, Purdon A, Vu T, Austin R, Heckl D, Breyfogle LJ, Kuhn CP, Kalaitzidis D, Armstrong SA, Williams DA, Hill GR, Ebert BL, Lane SW. 2013. Depletion of Jak2V617F myeloproliferative neoplasm-propagating stem cells by interferon- α in a murine model of polycythemia vera. *Blood* 121 (18): 3692–3702.

- Ottesen JT, Sajid Z, Pedersen RK, Gudmand-Hoeyer J, Bangsgaard KO, Skov V, Kjær L, Knudsen TA, Pallisgaard N, Kruse TA, Thomassen M, Troelsen J, Hasselbalch HC, Andersen M. 2019. Bridging blood cancers and inflammation: The reduced Cancitis model. *Journal of Theoretical Biology* 465: 90-108.
- Rodak BF, Fritsma GA, Doig K. 2008. *Hematology: Clinical principles and applications*.
- Rogers J, Gallaher EJ, Dingli D. 2018. Personalized ESA doses for anemia management in hemodialysis patients with end-stage renal disease. *System Dynamics Review*. 34, 121–153.
- Rovida E, Marzi I, Cipolleschi MG, Sbarba PD. 2014. One more stem cell niche: how the sensitivity of chronic myeloid leukemia cells to imatinib mesylate is modulated within a “hypoxic” environment, *Hypoxia*, 1-10.
- Sajid Z, Andersen M, Ottesen JT. 2019. Mathematical analysis of the Cancitis model and the role of inflammation in blood cancer progression. *MBE*, 16(6): 8268–8289.
- Samuelsson J, Hasselbalch H, Bruserud O, Temerinac S, Brandberg Y, Merup M, Linder O, Bjorkholm M, Pahl HL, Birgegard G, Nordic Study Group for Myeloproliferative Disorders. 2006. A phase II trial of pegylated interferon alpha-2b therapy for polycythemia vera and essential thrombocythemia: feasibility, clinical and biologic effects, and impact on quality of life. *Cancer*. 106(11): 2397-405.
- Senturk F, Barlas Y, Yasarcan H. 2020. Modelling the pharmacodynamics of rHuEPO, a blood doping drug.
- Silva M, Grillot D, Benito, Richard C, Nunez G, Fernandez- Luna J. 1996. Erythropoietin can promote erythroid progenitor survival by repressing apoptosis through bcl-1 and bcl-2. *Blood* 88, 1576-1582.
- Stauffer Larsen T, Iversen KF, Hansen E, Mathiasen AB, Marcher C, Frederiksen M, Larsen H, Helleberg I, Riley CH, Bjerrum OW, Rønnov-Jessen D, Møller MB, de Stricker K, Vestergaard H, Hasselbalch HC. 2013. Long term molecular responses in a cohort of Danish patients with essential thrombocythemia, polycythemia vera and myelofibrosis treated with recombinant interferon alpha. *Leuk Res*. 37(9): 1041-5.
- Stiehl T, Baran N, Ho AD, Marciniak-Czochra A. 2015. Cell division patterns in acute myeloid leukemia stem-like cells determine clinical course: A model to predict patient survival. *Cancer Research*. 75(6): 940-949.

- Testa U. 2004. Apoptotic mechanism in the control of erythropoiesis. *Leukemia* 18, 7: 1176-1199.
- Walenda T, Stiehl T, Braun H, Frobel J, Ho AH, Schroeder T, Goecke TW, Rath B, Germing U, Marciniak-Czochra A, Wagner W. 2014. Feedback signals in myelodysplastic syndromes: Increased self-renewal of the malignant clone suppresses normal hematopoiesis. *PLoS Computational Biology*, **10**(4).
- Walkley C, Shea J, Sims N, Purton L, Orkin S. 2007. Rb regulates interactions between hematopoietic stem cells and their bone marrow micro-environment, *Cell*, 129: 1081-95.
- Weitzman JB, Fiette L, Matsuo K, Yaniv M. 2000. JunD protects cells from p53- dependent senescence and apoptosis. *Mol Cell* 6, 5: 1109-1119.

CHAPTER 4

Dynamics of erythropoiesis with multiple EPO feedbacks in blood cancer with stem cell competition

Dynamics of erythropoiesis with multiple EPO feedbacks in blood cancer with stem cell competition

Zamra Sajid^{1*}, Morten Andersen¹ and Johnny T. Ottesen¹

¹IMFUFA, Dep. of Science and Environment, Roskilde University

*zamra@ruc.dk

Abstract

Hematological diseases are pathological conditions primarily affecting the blood production or blood-producing organs. Polycythemia vera (PV) is an example of such disease characterized by clonal stem-cell proliferation of erythrocytes and the presence of the *JAK2V617F* mutation. A five-dimensional PV model incorporating healthy and malignant cells with multiple erythropoietin (EPO) feedbacks is proposed, analyzed and validated. The governing parameters are identified and their impact on the dynamic especially during treatments is described. A complete classification of steady states and their stability is obtained, showing that a two-dimensional stem cell PV submodel is in one-to-one correspondence with the PV model. Finally, the model can reproduce clinically observed dynamics reflecting existing treatments and suggest novel intervention strategies. It follows that an effective therapy should target stem cell properties such as the stem cell competition in the micro-environment. The model shows that a therapy increasing EPO is unfavorable since the total mature cell count is increased in response to EPO dose. However, decreasing the EPO concentration decreases the total cell count preventing thrombotic complications.

Keywords: Polycythemia vera, mathematical modelling, EPO, dimensionless model, steady states, stability, erythrocytes

1 Introduction

Hematopoiesis is the formation of blood cells required by the human body. Different types of blood cells are derived from the hematopoietic stem cells (HSCs), located in the bone marrow. A subset of these cells differentiates and classifies into mature

blood cells, mainly red blood cells (erythrocytes), white blood cells (leukocytes) and platelets.

In the present work we focus on erythrocytes. Erythrocytes are produced from stem cells in the bone marrow. A stem cell differentiates into myeloid-erythroid progenitor cells (MEP), and then to early progenitors stage committed to the erythroid lineage, i.e., burst-forming unit erythroid (BFU-E) and colony-forming unit erythroid (CFU-E). The later stages are pro-erythroblast, basophilic erythroblast, polychromatic erythroblast, orthochromatic erythroblast, and finally, reticulocytes. The reticulocytes mature into erythrocytes in about 1 to 3 days [48]. This full process of producing erythrocytes is called erythropoiesis. In healthy individuals, erythrocytes are enveloped by macrophages in the spleen after 120 days [48, 35]. This process is controlled by the growth hormone factor EPO. EPO is released to the bloodstream by the kidneys with a half-life of 6 hours [38]. The hormone EPO stimulates the production of new red blood cells. Furthermore, a high EPO concentration may accelerate the differentiation of BFU-E recruited into CFU-E, increasing the number of erythrocytes in the bloodstream [2, 24, 28, 29, 33, 52]. In general, an appropriate balance is necessary between the rate of cell production and destruction in maintaining normal homeostasis. It is believed that EPO inhibits the cell death to control the number of cells [24, 29, 52, 54, 59].

Polycythemia vera (PV), a subcategory of myeloproliferative neoplasms (MPNs), is a clonal disorder of hematopoiesis thought to originate from hematopoietic stem cells [11, 26, 27]. Characteristics of PV are the excessive production of erythrocytes, presence of the driver mutation *JAK2V617F* and low production of erythropoietin (EPO) [12]. Patients older than 60 years or having a history of thrombosis are at high risk. The prospective fatal complication in PV includes the disease transformation into myelofibrosis or acute myeloid leukemia [6, 27] due to the *JAK2V617F* allele burden which is found in 95% of patients with PV [26, 34]. The subnormal serum EPO levels are a part of PV diagnostic criteria declared by the World Health Organisation in 2016. Hydroxyurea (HU) is a widely used drug against PV. In [30], the increased EPO concentration in plasma after initiation of HU has been addressed. However, the mechanism behind the increased plasma EPO concentration is unknown. One possibility is that HU decreases the erythroid cells. The authors concluded that the measurement of EPO serum should be carried out before initiation of treatment if the diagnostic or prognostic procedures includes EPO.

In the present paper, we introduce and investigate a mathematical model of PV that incorporates the competition between healthy and malignant cells (characterized by the *JAK2V617F* mutation) and EPO feedbacks on both cell lines. We conduct a thorough mathematical investigation and address the following questions: Which physiological steady states does the model allow, and how do these vary as parameter values are perturbed? Which group of parameters controls the dynamics of the system and how? What is the role of stem cell dynamics concerning the dynamics of the entire system? In particular, how does the competition of stem cells impact the full system dynamics? Which parameters can usefully be targeted in interventions?

A few mathematical models of erythropoiesis exist in the literature. In [47], the focus was primarily observing the dose-response relationship between bone marrow and spleen micro-environments for erythropoiesis building on work described in [37, 60, 61]. In [9], the model consisted of two partial differential equations, describing the cells in the bone marrow and erythrocytes in the blood. Belair et al. [9] described the physiological processes leading to the production of erythrocytes. This model was modified and analyzed by different authors and fitted to experimental data for phlebotomy [39, 40]. Mahaffy et al. [39, 40] concluded that both models provided an insight into disease state centered around stem cells. Further, the death rate of progenitor cells depending on EPO was added with a moving boundary condition for erythrocytes [3]. This work captured the dynamics involved in periodic hematological diseases. The author showed that growth factor (EPO) and destabilization of the feedback loop from red blood cells to EPO may be responsible for such oscillations. In [14] and [16], the mechanism of self-renewal of progenitor cells was included in the erythropoiesis model. Both models were used to simulate anemia and parametrized with mice data. A detailed model was presented in [20] concerning the differentiation series from a stem cell to an erythrocyte. The authors accounted for a mechanism triggering the active destruction of young red blood cells called neocytolysis. The model simulated blood donation and administration of erythropoiesis stimulating agents. The same group of authors did parameter estimation with patients' data through a mathematical model of erythropoiesis [21]. The model given in [7] was based on work [14] where the authors considered growth factor EPO dynamics, and feedback control functions describing immature cell self-renewal and differentiation. One of the mathematical model presented in [8] incorporated iron and evaluated the effects of inflammation and neocytolysis. In [55], a three compartment model was applied to blood loss dynamics in healthy subjects having a negative feedback mechanism for erythropoiesis. Recently, the same group of authors extended the model to optimize personalized phlebotomy schedules for patients with PV [36].

The pioneering work of erythropoiesis [9, 38, 39, 40] dynamics laid the ground for hematological disease modelling. A few modelling studies of myeloid malignancies were investigated in [25, 62]. The Cancitis model included inflammatory factor dynamically as the driver and trigger of MPNs [6, 50]. The reduction of the Cancitis model is given in [5, 45] where [45] included the effect of T-cells and [5] represented the model in terms of *JAK2V617F* and white blood cell count. In the next section, we present our novel mathematical PV model.

2 The PV Model

In the *PV model*, the hematopoietic stem cells (HSC) proliferate into healthy erythrocytes (RBC) and malignant stem cells (MSC) proliferate into mature malignant cells (MMC). In addition, different feedbacks between erythrocytes and EPO are considered. The malignant cells are characterized by the *JAK2V617F* mutation. Here, we do not explicitly model the first mutational hit but consider expanding or suppressing existing populations of malignant cells.

The PV model consists of five ordinary non-linear differential equations, the number of HSC (x_0), the number of RBC (x_r), the number of MSC (y_0), the number of MMC (y_r) and the concentration of EPO (E). The conceptual model is illustrated in Figure 1. The PV model is inspired by mathematical models given in [6, 13] and reads

$$\frac{dx_0}{dt} = (r_x \phi_x - d_{x_0} - a_x)x_0, \quad (1a)$$

$$\frac{dy_0}{dt} = (r_y \phi_y - d_{y_0} - a_y)y_0, \quad (1b)$$

$$\frac{dx_r}{dt} = a_x A_x(E)x_0 - d_{xr}(E)x_r, \quad (1c)$$

$$\frac{dy_r}{dt} = a_y A_y(E)y_0 - d_{yr}(E)y_r, \quad (1d)$$

$$\frac{dE}{dt} = f(x_r, y_r) - kE. \quad (1e)$$

with

$$\phi_x = \frac{1}{1 + c_{xx}x_0 + c_{xy}y_0} \quad \text{and} \quad \phi_y = \frac{1}{1 + c_{yx}x_0 + c_{yy}y_0}. \quad (2)$$

The rate of self-renewal is denoted as r_x and r_y for HSC and MSC respectively. It is believed that the self-renewal is inhibited by regulatory niche feedback [57], this inhibition is implemented here through Michaelis-Menten-like functions $\phi_x(x_0, y_0)$ and $\phi_y(x_0, y_0)$ [17, 53, 56]. Feedback constants c_{xx} and c_{xy} represents the inhibitory effect on the self-renewal of HSC, while the corresponding effect on the self-renewal of MSC is captured by c_{yx} and c_{yy} . The stem cells die with rates d_{x_0} and d_{y_0} .

The parameter a_x denotes the rate at which the HSC differentiates into RBC, while a_y represents the rate for MSC transforming to MMC. The progenitor cells are considered stages between stem cells and mature cells and are accounted for by amplification factors A_x and A_y for HSC and MSC, respectively. These amplification factors are dependent on EPO as EPO is thought to stimulate the production of mature red cells [2, 24, 28, 29, 33, 52],

$$A_x(E) = \delta_x \frac{E}{1 + \alpha_x E}, \quad (3)$$

$$A_y(E) = \delta_y \frac{E}{1 + \alpha_y E}, \quad (4)$$

where δ_x and δ_y are positive constants and α_x and α_y , are positive constants.

It is hypothesized that an increase in the growth factor concentration EPO leads to a decrease in the apoptosis rate [24, 29, 52, 54, 59]. Therefore, we assume that $d_{xr}(E)$ and $d_{yr}(E)$ are decreasing function of E s.t $\lim_{E \rightarrow \infty} d_{xr}(E) = 0$ and $\lim_{E \rightarrow \infty} d_{yr}(E) = 0$, by choosing

$$d_{xr}(E) = \eta_x \frac{1}{1 + \beta_x E}, \quad (5)$$

$$d_{yr}(E) = \eta_y \frac{1}{1 + \beta_y E}, \quad (6)$$

where η_x , η_y , β_x and β_y are non-negative constants. For $E = 0$, $d_{xr} = \eta_x$ and $d_{yr} = \eta_y$.

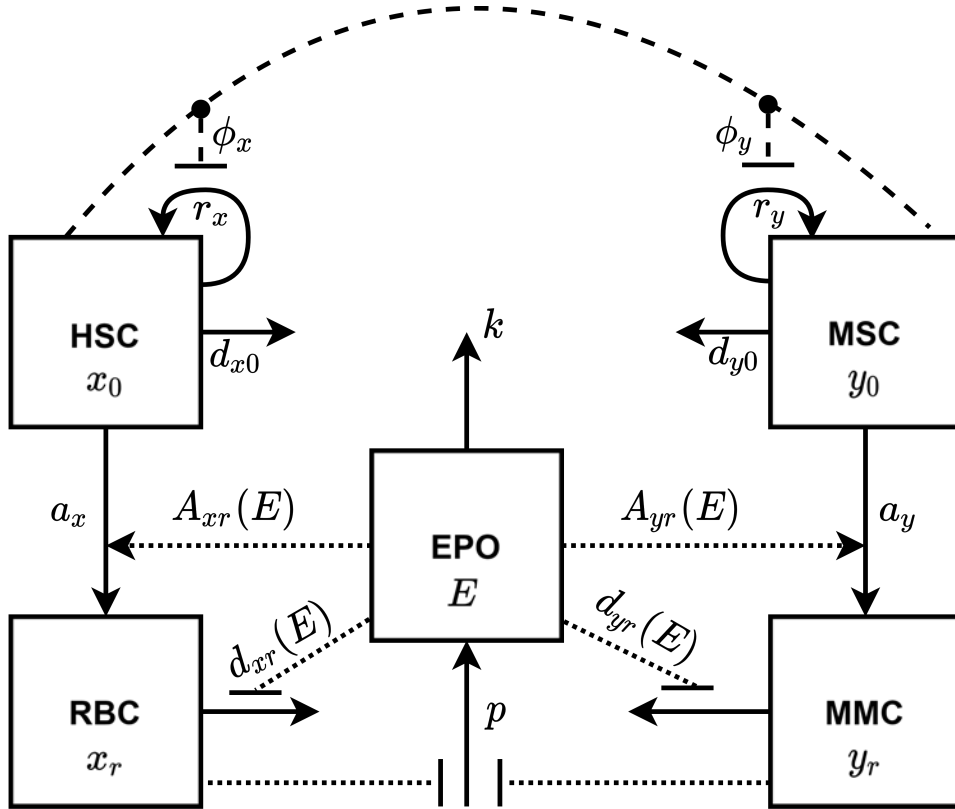


Figure 1: The boxes illustrate the compartments of the PV model. The full arrows represent the rates of the flows between and out of these compartments. Black stipulated lines (labeled ϕ_x and ϕ_y , respectively) represent the interaction between bone marrow niches and stem cells. Stem cells (HSC and MSC) may self renew (r_x and r_y), die (d_{x0} and d_{y0}) or differentiate (a_x , a_y), while mature cells (RBC, MMC) are produced (with rates $a_x A_{xr}(E)$ and $a_y A_{yr}(E)$) due to multiplication by the progenitor cells. Mature cells do not differentiate but die with rates $d_{xr}(E)$ and $d_{yr}(E)$. EPO stimulates the proliferation rates and inhibits the death rates of both RBC and MMC, while the amount of mature cells inhibits the production of EPO. Black dotted lines present the interaction of EPO with the remaining model.

We assume a negative feedback function $f(x_r, y_r)$ depending on x_r and y_r for EPO production. This function is a monotone decreasing in x_r and y_r and of the form of Hill function [9, 10],

$$f(x_r, y_r) = \frac{p}{1 + k_0(x_r + y_r)^m},$$

where p , k_0 and m are Hill constants. We consider $m = 1$ in the subsequent analysis.

2.1 Parameter Estimation

The differential equations system (1) has 5 variables and 23 parameters, which are assumed to be positive. Here we identify the parameter values for typical steady state of the variables. Some of the parameter values are taken from the literature to make a first educated guess. Some of them can be found by using steady-state conditions, whereas the rest are assumed.

In the stable hematopoietic steady state the numbers of stem cells are approximately 10^4 to 10^6 [13, 17, 25, 41, 53] and the number of erythrocytes is 10^{11} to 10^{13} [18, 48]. Moreover, the steady state value of EPO is within (6 – 16) [U/L] [20, 39, 48]. Thus, based on literature, we choose hematopoietic steady state values to be $(\bar{x}_0, \bar{y}_0, \bar{x}_r, \bar{y}_r, \bar{E}) = (2.6 \cdot 10^4, 0, 4.8 \cdot 10^{12}, 0, 13.1)$ for the normal healthy individual.

Hematopoietic stem cells divide approximately once per year [1, 19]. We take $r_x = 5 \cdot 10^{-3}$ per day as [17]. In addition, elimination from the stem cell compartment is approximately 0.002 cells per day, $d_{x0} = 2 \cdot 10^{-3}$ per day [6, 17, 45, 50]. Malignant stem cells have an advantage as compared with hematopoietic stem cells that their self renewal rate is higher thus, $r_y > r_x$. For simplicity we assume $d_{y0} = d_{x0}$ and $a_y = a_x$ [6, 19, 45, 50] since otherwise is not known. We consider that $r_x > d_{x0} + a_x$ thereby equation (1a) in steady state gives $a_x = 3.58 \cdot 10^{-5}$. Since malignant cells are less sensitive to micro-environment niche feedback as compared to hematopoietic cells [31, 49], we assume $c_{yy} \leq c_{yx} \leq c_{xy} \leq c_{xx}$. The values are taken from [45, 50].

The life span of RBC for healthy humans is about 120 days [9, 13, 20, 38], we choose the removal rate from the erythrocyte compartment dependent on EPO to be $d_{xr}(\bar{E}) = 1/120$ per day. We choose $\eta_x = 8 \cdot 10^{-3}$ per day such that for $\bar{E} = 0$, $d_{xr}(0) \approx \eta_x$. Using $d_{xr}(\bar{E})$ and \bar{E} in equation (5), $\beta_x = 9 \cdot 10^{-3}$ is obtained.

In addition, equation (1c) at steady state gives, $A_x(\bar{E}) = 3 \cdot 10^9$. We choose $\delta_x = 8.6 \cdot 10^8$ such that the model is in a steady state at $t = 0$. With the help of equation (3), $\alpha_x = 5 \cdot 10^{-3}$. In contrast, parameters for malignant red blood cells are not considered in existing literature. Therefore, we choose $\eta_y = \eta_x$, $\beta_y = \beta_x$, $\alpha_y = \alpha_x$ for simplicity. To give the advantage to MMC, we choose amplification factor $\delta_y = 3 \cdot 10^{10}$ which is greater than δ_x .

For EPO, we need to estimate the degradation rate k of EPO and Hill function parameters, p and k_0 . In [20, 38, 40], the half life of EPO is reported about 4 to 24 hours and in [7, 9, 20, 38, 39] the decay constant of EPO varies between 2 and 7 per day thus, we suppose that the half-life of EPO is 6 hours, $k = \frac{\ln(2)}{T_{1/2}} \approx 2.8 \text{ day}^{-1}$. The parameter $p = 1.56 \cdot 10^4$ is estimated in [9, 39], thereby equation (1e) in steady state gives $k_0 = 8.9 \cdot 10^{-11}$. See details in Appendix (A).

The default parameter values are summarized in table 1 and a typical PV model outcome is shown in Figure 2.

Parameter	Value	Unit	Explanation
r_x	$5 \cdot 10^{-3}$	day^{-1}	Self-renewal rate of HSC
r_y	$1.15 \cdot 10^{-2}$	day^{-1}	Self-renewal rate of MSC
a_x	$3.58 \cdot 10^{-5}$	day^{-1}	Differentiation rate of HSC
a_y	$3.58 \cdot 10^{-5}$	day^{-1}	Differentiation rate of MSC
d_{x_0}	$2 \cdot 10^{-3}$	day^{-1}	Death rate of HSC
d_{y_0}	$2 \cdot 10^{-3}$	day^{-1}	Death rate of MSC
c_{xx}	$5.6 \cdot 10^{-5}$	-	Inhibition by HSC on HSC
c_{yx}	$5.2 \cdot 10^{-5}$	-	Inhibition by HSC on MSC
c_{xy}	$5.4 \cdot 10^{-5}$	-	Inhibition by HSC on MSC
c_{yy}	$5.0 \cdot 10^{-5}$	-	Inhibition by MSC on MSC
p	$1.56 \cdot 10^4$	day^{-1}	Production rate of EPO
k_0	$8.9 \cdot 10^{-11}$	-	Factor affecting production of EPO
α_x	$5 \cdot 10^{-3}$	-	Factor affecting production of RBC
α_y	$5 \cdot 10^{-3}$	-	Factor affecting production of MMC
β_x	$9 \cdot 10^{-3}$	-	Factor affecting production of MMC
β_y	$9 \cdot 10^{-3}$	-	Factor affecting removal of MMC
δ_x	$3 \cdot 10^9$	-	Stimulation rate of RBC
δ_y	$3 \cdot 10^{10}$	-	Stimulation rate of MMC
η_x	$8 \cdot 10^{-3}$	day^{-1}	Death rate of RBC
η_y	$8 \cdot 10^{-3}$	day^{-1}	Death rate of MMC
k	2.8	day^{-1}	Degradation rate of EPO

Table 1: Default parameter values of the PV model.

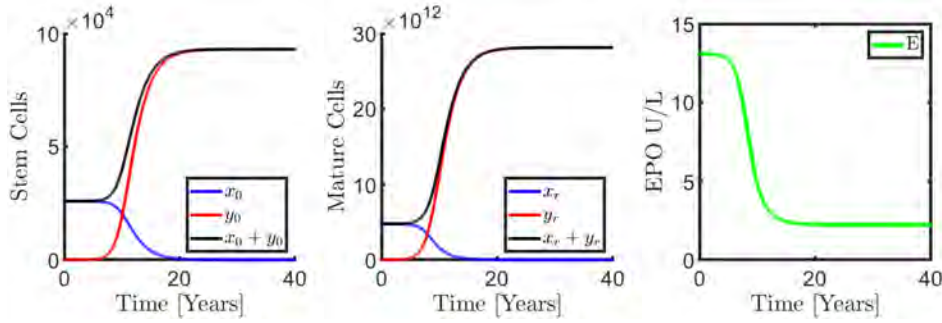


Figure 2: A PV model shows the progression of disease with initial conditions, $(x_0, y_0, x_r, y_r, E) = (2.6 \cdot 10^4, 1, 4.8 \cdot 10^{12}, 0, 13.1)$ at $t = 0$. Red curves denote malignant cells, blue are healthy hematopoietic cells and black curves are sum of the cells. Time is plotted on the x -axis. The left panel shows the evolution of malignant stem cells count and the middle panel shows the evolution of mature malignant cell count. In the early phase, HSCs are large in number than MSCs. However, after some years, when disease evolves, MSCs become dominant leading to the destruction of HSCs. The right panel shows the degradation of EPO over time.

3 Dimensional Analysis

A dimensionless form of the PV model is obtained by clustered parameters and scaling the variables of the model to facilitate the analysis. We non-dimensionalise the equations of system (1) using the following scales,

$$x_0 = \tilde{x}_0 X_0, y_0 = \tilde{y}_0 Y_0, x_r = \tilde{x}_r X_r, y_r = \tilde{y}_r Y_r, E = \tilde{e} E_q, t = \tilde{t} \tau$$

where small letters with tilde are scaling constants, capital letters are dimensionless variables and τ is dimensionless time. (See details in Appendix B). The new system of equations consists of 15 parameters. The *dimensionless PV model* is as follows,

$$\frac{dX_0}{d\tau} = \zeta_x \left(\frac{1}{1 + X_0 + p_{x1} Y_0} - p_{x2} \right) X_0, \quad (7a)$$

$$\frac{dY_0}{d\tau} = \zeta_y \left(\frac{1}{1 + p_{y1} X_0 + Y_0} - p_{y2} \right) Y_0, \quad (7b)$$

$$\frac{dX_r}{d\tau} = \frac{E_q}{1 + q_{x1} E_q} X_0 - \frac{q_{x2}}{1 + q_{x3} E_q} X_r, \quad (7c)$$

$$\frac{dY_r}{d\tau} = \frac{E_q}{1 + q_{y1} E_q} Y_0 - \frac{q_{y2}}{1 + q_{y3} E_q} Y_r, \quad (7d)$$

$$\epsilon \frac{dE_q}{d\tau} = \frac{10^4}{1 + r_{e1} X_r + r_{e2} Y_r} - E_q. \quad (7e)$$

where, $\epsilon = \frac{r_x}{k^2}$, $\zeta_x = k$, $\zeta_y = k \frac{r_y}{r_x}$, $p_{x1} = \frac{c_{xy}}{c_{yy}}$, $p_{x2} = \frac{d_{x0} + a_x}{r_x}$, $p_{y1} = \frac{c_{yx}}{c_{xx}}$, $p_{y2} = \frac{d_{y0} + a_y}{r_y}$, $q_{x1} = \frac{\alpha_x p}{10^4 k}$, $q_{x2} = \frac{\eta_x k}{r_x}$, $q_{x3} = \frac{\beta_x p}{10^4 k}$, $q_{y1} = \frac{\alpha_y p}{10^4 k}$, $q_{y2} = \frac{\eta_y k}{r_x}$, $q_{y3} = \frac{\beta_y p}{10^4 k}$, $r_{e1} = \frac{k_0 p a_x \delta_x}{10^4 r_x c_{xx}}$, $r_{e2} = \frac{k_0 p a_y \delta_y}{10^4 r_x c_{yy}}$. Default values of the dimensionless PV model are computed from the default parameter values of the PV model.

By singular perturbation theory, the equation (7e) involve small epsilon terms $\epsilon = 6.37 \cdot 10^{-4}$ that may be taken in the limit of vanishing left hand sides and thereby we obtain the *PV reduced model*. Using the values in table 1, the values of dimensionless parameters are computed in table 2.

The stem cell dynamics given by equations (7a) and (7b) is referred to the *stem cell PV submodel*, since the stem cell dynamics is independent of the remaining system.

Parameter	Value	Explanation
p_{x1}	1.08	Inhibition by MSC on HSC
p_{x2}	0.40	Death rate of HSC
p_{y1}	0.93	Inhibition by HSC on MSC
p_{y2}	0.17	Death rate of MSC
q_{x1}	0.002	Factor affecting production of RBC
q_{x2}	4.48	Death rate of RBC
q_{x3}	0.005	Factor affecting removal of RBC
q_{y1}	0.002	Factor affecting production of MMC
q_{y2}	4.48	Death rate of MMC
q_{y3}	0.005	Factor affecting removal of MMC
r_{e1}	53.07	Factor affecting production of EPO
r_{e2}	594	Factor affecting production of EPO
ζ_x	2.80	Factor affecting self-renewal and death rates of HSC
ζ_y	6.44	Factor affecting self-renewal and death rates of MSC
ϵ	6.37×10^{-4}	Factor affecting self-renewal and death rates of MSC

Table 2: Default dimensionless parameter values of the dimensionless PV model.

3.1 Positivity and Boundedness of Solutions

Consider the dimensionless PV model (7) for non negative initial conditions. The system (7) is Lipschitz continuous in $(\mathbb{R}_+ \cup \{0\})^5$, since all expressions on the right hand side have continuous partial derivatives in the domain which guarantee local existence and uniqueness of the solution to the system (7) [42].

In the following, we demonstrate the positivity of solutions. From equation (7a), if $\frac{dX_0(\tau_0)}{d\tau} = 0$ for any $\tau = \tau_0$, then $X_0(\tau) = 0$ for all $\tau \geq \tau_0$. Similar argument holds for $Y_0(\tau)$. From equation (7c), it is easily observed that $\frac{dX_r}{d\tau} \geq 0$ for $X_r = 0$. Similar reasoning applies for equation (7d) and (7e). Hence the flow will remain in the non-negative octant.

A trapping region \mathcal{T}_R exists, having the property that trajectories initially inside \mathcal{T}_R can not escape it. Let $\mathcal{T}_R = [0, M_{X_0}] \times [0, M_{Y_0}] \times [0, M_{X_r}] \times [0, M_{Y_r}] \times [0, M_{E_q}]$, where M denotes a trapping boundary for the corresponding variables. In the following we will find such trapping boundary.

First, consider equation (7a),

$$\begin{aligned} \frac{dX_0}{d\tau} &= \zeta_x \left(\frac{1}{1 + X_0 + p_{x1}Y_0} - p_{x2} \right) X_0, \\ &\leq \zeta_x \left(\frac{1}{X_0} - p_{x2} \right) X_0. \end{aligned}$$

Thus, a trapping region bound for X_0 may be defined, $M_{X_0} \equiv \frac{1}{p_{x2}}$ such that, $\frac{dX_0}{d\tau} < 0$ for $X_0 > \frac{1}{p_{x2}}$. Similar argument can be constructed for equation (7b) with upper bound $M_{Y_0} \equiv \frac{1}{p_{y2}}$.

Next consider equation (7e),

$$\begin{aligned}\epsilon \frac{dE_q}{d\tau} &= \frac{10^4}{1 + r_{e1}X_r + r_{e2}Y_r} - E_q, \\ &\leq 10^4 - E_q.\end{aligned}$$

Thus,

$$\frac{dE_q}{d\tau} < 0 \text{ for } E_q > 10^4 \equiv M_{E_q}.$$

Finally, consider equations (7c)

$$\begin{aligned}\frac{dX_r}{d\tau} &= \frac{E_q}{1 + q_{x1}E_q}X_0 - \frac{q_{x2}}{1 + q_{x3}E_q}X_r, \\ &\leq M_{E_q}M_{X_0} - \frac{q_{x2}}{1 + q_{x3}M_{E_q}}X_r.\end{aligned}$$

Thus,

$$\frac{dX_r}{d\tau} < 0 \text{ for } X_r > \frac{M_{E_q}M_{X_0}(1 + q_{x3}M_{E_q})}{q_{x2}} \equiv M_{X_r},$$

and similarly for (7d)

$$\frac{dY_r}{d\tau} < 0 \text{ for } Y_r > \frac{M_{E_q}M_{Y_0}(1 + q_{y3}M_{E_q})}{q_{y2}} \equiv M_{Y_r}.$$

Hence, there exists a forward invariant trapping region \mathcal{T}_R such that the solutions starting outside \mathcal{T}_R are attracted into the region. Hence, the trajectories exist globally in forward time [42].

4 Analysis of the Stem Cell PV Submodel

4.1 Existence and Stability Criteria of the Steady States

First, we make a complete analysis of the existence of various steady states and state their stability conditions regarding the stem cell PV submodel. Afterward, we use this information for the dimensionless PV model.

The steady states (\bar{X}_0, \bar{Y}_0) for the stem cell PV submodel, Eqs (7a) and (7b) fulfil,

$$\zeta_x \left(\frac{1}{1 + \bar{X}_0 + p_{x1}\bar{Y}_0} - p_{x2} \right) \bar{X}_0 = 0, \quad (8a)$$

$$\zeta_y \left(\frac{1}{1 + p_{y1}\bar{X}_0 + \bar{Y}_0} - p_{y2} \right) \bar{Y}_0 = 0. \quad (8b)$$

Since the number of cells and concentrations are required to be non-negative, the feasible steady states can be classified w.r.t their stem cells as

- a trivial stem cell steady state, D_0 , if and only if $\bar{X}_0 = \bar{Y}_0 = 0$,
- a hematopoietic stem cell steady state, D_H , if and only if $(\bar{X}_0, \bar{Y}_0) = (\bar{X}_{0H}, 0)$ with $\bar{X}_{0H} > 0$,
- a malignant stem cell steady state, D_L , if and only if $(\bar{X}_0, \bar{Y}_0) = (0, \bar{Y}_{0L})$ with $\bar{Y}_{0L} > 0$,
- a co-existing stem cell steady state, D_C , if and only if $(\bar{X}_0, \bar{Y}_0) = (\bar{X}_{0C}, \bar{Y}_{0C})$ with $\bar{X}_{0C} > 0$ and $\bar{Y}_{0C} > 0$.

The possible steady states depend on the stem cell parameters. The parameter p_{x1} describes the inhibition of Y_0 on X_0 , p_{y1} describes the inhibition of X_0 on Y_0 whereas p_{x2} and p_{y2} are the degradation rates of X_0 and Y_0 respectively.

We limit ourselves to studying $p_{x2} \neq 1$ and $p_{y2} \neq 1$ and define $\gamma = \frac{\frac{1}{p_{x2}} - 1}{\frac{1}{p_{y2}} - 1}$.

Proposition 1. *Conditions allowing existence and stability of feasible steady states are,*

1. A **trivial stem cell steady state**, D_0 , always exists and is stable for $p_{x2} > 1$ and $p_{y2} > 1$ and unstable for $p_{x2} < 1$ and $p_{y2} < 1$.
2. A feasible **hematopoietic stem cell steady state**, D_H , exists and is unique if and only if $p_{x2} < 1$ with $\bar{X}_{0H} = \frac{1}{p_{x2}} - 1$. D_H is stable for $p_{y1} > \gamma^{-1}$ and unstable for $p_{y1} < \gamma^{-1}$.
3. A feasible **malignant stem cell steady state**, D_L , exists and is unique if and only if $p_{y2} < 1$ with $\bar{Y}_{0L} = \frac{1}{p_{y2}} - 1$. D_L is stable for $p_{x1} > \gamma$ and unstable for $p_{x1} < \gamma$.
4. A feasible **co-existing stem cell steady state**, D_C , exists and is unique if $p_{x2} < 1$ and $p_{y2} < 1$ and either (a) or (b) is fulfilled, where

(a) $p_{x1} < \gamma$ and $p_{y1} < \gamma^{-1}$. In this case D_C is stable.

(b) $p_{x1} > \gamma$ and $p_{y1} > \gamma^{-1}$. In this case D_C is unstable (a saddle).

D_C is only feasible, when D_H and D_L exist. The coordinates of D_C are $\bar{X}_{0C} = \frac{\bar{X}_{0H} - p_{x1}\bar{Y}_{0L}}{1 - p_{x1}p_{y1}}$ and $\bar{Y}_{0C} = \frac{\bar{Y}_{0L} - p_{y1}\bar{X}_{0H}}{1 - p_{x1}p_{y1}}$.

Proof. A **trivial stem cell steady state** D_0 always exists. For stability, we compute the Jacobian of the stem cell PV submodel,

$$J = \begin{bmatrix} \zeta_x \left(\frac{1 + p_{x1}Y_0}{(1 + X_0 + p_{x1}Y_0)^2} - p_{x2} \right) & -\frac{\zeta_x p_{x1} X_0}{(1 + X_0 + p_{x1}Y_0)^2} \\ -\frac{\zeta_y p_{y1} Y_0}{(1 + p_{y1}X_0 + Y_0)^2} & \zeta_y \left(\frac{1 + p_{y1}X_0}{(1 + p_{y1}X_0 + Y_0)^2} - p_{y2} \right) \end{bmatrix} \quad (9a)$$

The determinant of the Jacobian J_{D_0} at D_0 is,

$$\det(J_{D_0}) = \zeta_x \zeta_y (1 - p_{x2})(1 - p_{y2}).$$

$\det(J_{D_0})$ is positive either if $p_{x2} < 1$ and $p_{y2} < 1$ or if $p_{x2} > 1$ and $p_{y2} > 1$, and it is negative if either $p_{x2} > 1$ or $p_{y2} > 1$.

The trace of the Jacobian J_{D_0} at D_0 ,

$$\text{tr}(J_{D_0}) = \zeta_x(1 - p_{x2}) + \zeta_y(1 - p_{y2}),$$

is negative if $p_{x2} > 1$ and $p_{y2} > 1$. Hence, D_0 is a stable steady state for $p_{x2} > 1$ and $p_{y2} > 1$ and unstable for $p_{x2} < 1$ and $p_{y2} < 1$.

A hematopoietic stem cell steady state, D_H , follows from equation (8a),

$$\bar{X}_{0H} = \frac{1}{p_{x2}} - 1, \quad (10)$$

Hence, \bar{X}_{0H} is unique and feasible if and only if $p_{x2} < 1$. Let $h_1 = \zeta_x p_{x2}(1 - p_{x2})$ and $h_2 = \frac{\zeta_y p_{y2} \left(\frac{1}{p_{x2}} - 1\right)}{1 + p_{y1} \left(\frac{1}{p_{x2}} - 1\right)} (\gamma^{-1} - p_{y1})$. Thus, $h_1 > 0$ for $p_{x2} < 1$ and $h_2 < 0$ for $p_{y1} > \gamma^{-1}$ while $h_2 > 0$ for $p_{y1} < \gamma^{-1}$. Hence, the determinant of the Jacobian J_{D_H} at D_H is, $\det(J_{D_H}) = -h_1 h_2$, is positive for $p_{y1} > \gamma^{-1}$ and negative for $p_{y1} < \gamma^{-1}$. Likewise, the trace of the Jacobian J_{D_H} at D_H is, $\text{tr}(J_{D_H}) = -h_1 + h_2$ which is negative for $h_2 < 0$. Hence, D_H is stable for $p_{y1} > \gamma^{-1}$ and unstable for $p_{y1} < \gamma^{-1}$.

A malignant stem cell steady state, D_L , follows from equations (8b),

$$\bar{Y}_{0L} = \frac{1}{p_{y2}} - 1. \quad (11)$$

Hence \bar{Y}_{0L} is unique and feasible if and only if $p_{y2} < 1$. Let $l_1 = \zeta_y p_{y2}(1 - p_{y2})$ and $l_2 = \frac{\zeta_x p_{x2} \left(\frac{1}{p_{y2}} - 1\right)}{1 + p_{x1} \left(\frac{1}{p_{y2}} - 1\right)} (\gamma - p_{x1})$. Thus, $l_1 > 0$ for $p_{y2} < 1$ and $l_2 < 0$ for $p_{x1} > \gamma$ while $l_2 > 0$ for $p_{x1} < \gamma$. Hence, the determinant of the Jacobian J_{D_L} at D_L is, $\det(J_{D_L}) = -l_1 l_2$, is positive for $p_{x1} > \gamma$ and negative for $p_{x1} < \gamma$. Likewise, the trace of the Jacobian J_{D_L} at D_L is, $\text{tr}(J_{D_L}) = -l_1 + l_2$ which is negative for $l_2 < 0$. Hence, D_L is stable for $p_{x1} > \gamma$ and unstable for $p_{x1} < \gamma$.

A co-existing stem cell steady state D_C , follows from the equations (8a) and (8b),

$$\bar{X}_{0C} + p_{x1} \bar{Y}_{0C} = \frac{1}{p_{x2}} - 1, \quad (12a)$$

$$p_{y1} \bar{X}_{0C} + \bar{Y}_{0C} = \frac{1}{p_{y2}} - 1. \quad (12b)$$

The left hand side is positive for feasible D_C and the right hand sides equals D_H and D_L , respectively. Hence, feasible D_H and D_L are necessary for feasible D_C .

In case $p_{x1} p_{y1} \neq 1$ there is at most one co-existing steady state i.e.,

$$\bar{X}_{0C} = \frac{\bar{X}_{0H} - p_{x1} \bar{Y}_{0L}}{1 - p_{x1} p_{y1}} \quad (13a)$$

$$\bar{Y}_{0C} = \frac{\bar{Y}_{0L} - p_{y1} \bar{X}_{0H}}{1 - p_{x1} p_{y1}}, \quad (13b)$$

or equivalently

$$\bar{X}_{0C} = \frac{\frac{1}{p_{y2}} - 1}{1 - p_{x1}p_{y1}} (\gamma - p_{x1}), \quad (14a)$$

$$\bar{Y}_{0C} = \frac{\frac{1}{p_{x2}} - 1}{1 - p_{x1}p_{y1}} (\gamma^{-1} - p_{y1}). \quad (14b)$$

\bar{X}_{0C} and \bar{Y}_{0C} are feasible either for $p_{x2} < 1$, $p_{y2} < 1$, $p_{x1} < \gamma$ and $p_{y1} < \gamma^{-1}$ or for $p_{x2} < 1$, $p_{y2} < 1$, $p_{x1} > \gamma$ and $p_{y1} > \gamma^{-1}$.

The entries of the Jacobian at D_C by using the expressions for steady states, $\frac{1}{1 + \bar{X}_{0C} + p_{x1}\bar{Y}_{0C}} = p_{x2}$ and $\frac{1}{1 + p_{y1}\bar{X}_{0C} + \bar{Y}_{0C}} = p_{y2}$,

$$J_{D_C(1,1)}(\bar{X}_{0C}, \bar{Y}_{0C}) = -\zeta_x p_{x2}^2 \bar{X}_{0C}, \quad (15a)$$

$$J_{D_C(1,2)}(\bar{X}_{0C}, \bar{Y}_{0C}) = -\zeta_x p_{x1} p_{x2}^2 \bar{X}_{0C}, \quad (15b)$$

$$J_{D_C(2,1)}(\bar{X}_{0C}, \bar{Y}_{0C}) = -\zeta_y p_{y1} p_{y2}^2 \bar{Y}_{0C}, \quad (15c)$$

$$J_{D_C(2,2)}(\bar{X}_{0C}, \bar{Y}_{0C}) = -\zeta_y p_{y2}^2 \bar{Y}_{0C}. \quad (15d)$$

Thus, the trace of the Jacobian becomes,

$$\text{tr}(J_{D_C}) = -\zeta_x p_{x2}^2 \bar{X}_{0C} - \zeta_y p_{y2}^2 \bar{Y}_{0C},$$

which is always negative, since all the parameters are positive.

The determinant of the Jacobian,

$$\det(J_{D_C}) = \zeta_x p_{x2}^2 \zeta_y p_{y2}^2 \bar{X}_{0C} \bar{Y}_{0C} (1 - p_{x1}p_{y1}),$$

is positive if and only if $p_{x1}p_{y1} < 1$ and D_C is stable, if $p_{x1}p_{y1} > 1$, D_C is a saddle steady state.

Note that $p_{y1} < \gamma^{-1}$ and $p_{x1} < \gamma$ implies $p_{x1}p_{y1} < 1$ whereas $p_{y1} > \gamma^{-1}$ and $p_{x1} > \gamma$ implies $p_{x1}p_{y1} > 1$. Note, in case $p_{x1}p_{y1} = 1$, $\frac{p_{y1}}{p_{x2}} = \frac{1}{p_{y2}}$ and a line of equilibria exists. However, this degenerated case will not be considered. \square

In Figure 3, all the possible topologies from Proposition (1) are displayed for positive p_{x1} , p_{y1} , p_{x2} and p_{y2} except $p_{x2} \neq 1$ and $p_{y2} \neq 1$.

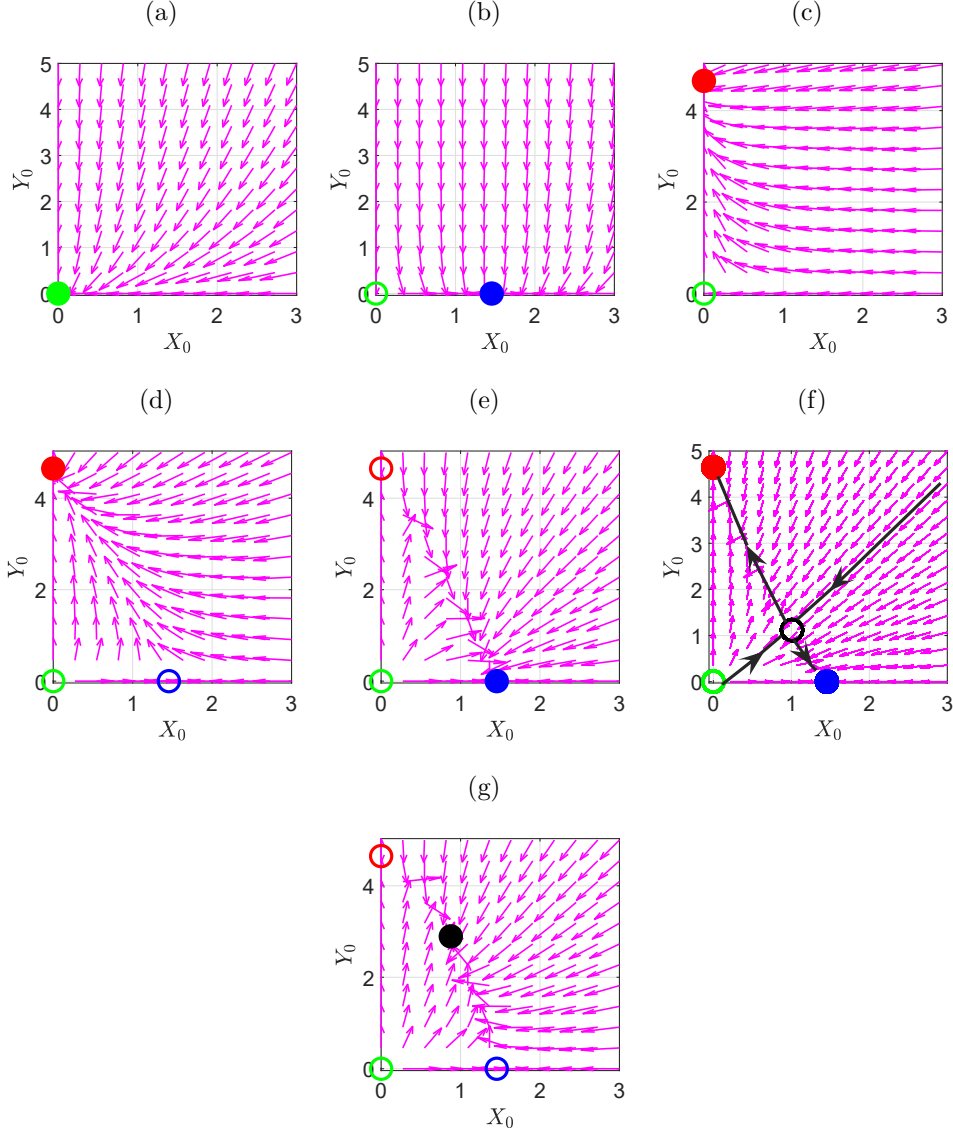


Figure 3: Phase plane diagrams of the stem cell PV submodel illustrate the various cases in proposition 1. Full circles are stable steady states and open circles are unstable steady states. Green, blue, red and black colors correspond to trivial, hematopoietic, malignant and co-existing steady states respectively. Stable and unstable manifolds are shown where a saddle co-existing steady state exists (panel (f)). The panels are as follows, (a) $p_{x2} > 1$ and $p_{y2} > 1$, (b) $p_{x2} < 1, p_{y2} > 1$ and $p_{y1} > \gamma^{-1}$, (c) $p_{x2} > 1, p_{y2} < 1$ and $p_{x1} > \gamma$, (d) $p_{x2} < 1, p_{y2} < 1, p_{x1} > \gamma$ and $p_{y1} < \gamma^{-1}$, (e) $p_{x2} < 1, p_{y2} < 1, p_{x1} < \gamma$ and $p_{y1} > \gamma^{-1}$ (f) $p_{x2} < 1, p_{y2} < 1, p_{x1} > \gamma$ and $p_{y1} > \gamma^{-1}$ (g) $p_{x2} < 1, p_{y2} < 1, p_{x1} < \gamma$ and $p_{y1} < \gamma^{-1}$.

The analysis can be extended from a local analysis to a global analysis as done in another two-dimensional model [5] relying on the Poincaré-Bendixson theorem. Hence, for criteria corresponding to Figure 3f, bistability appears.

In all other panels, the unique, locally stable steady state is attracting solutions with initial condition.

4.2 Bifurcation Analysis

In this section, we illustrate that the model trajectories tend to a stable malignant state D_L , to a stable healthy state D_H , or to a stable co-existing steady state D_C , as $t \rightarrow \infty$ depending on inhibiting factors p_{x1} and p_{y1} and death rates of the stem cells p_{x2} and p_{y2} . The parameters p_{x1} , p_{x2} , p_{y1} and p_{y2} become the bifurcation parameters, where γ serves as a threshold between healthy and malignant states. p_{x1} and p_{y1} denote the inhibiting strengths and, p_{x2} and p_{y2} are the death rates for the stem cells. Bifurcation diagrams are constructed relying on Proposition (1) and topologies shown in Figure 3.

In Figure 4, p_{x2} and p_{y2} are used as bifurcation parameters with fixed values of p_{x1} and p_{y1} . In Figure 4(i), we let $p_{x1} > \gamma$ and $p_{y1} < \gamma^{-1}$ therefore, the co-existing steady state does not exist. An important transition line is $p_{x2} = p_{y2}$ separating malignant and healthy cases. In region e, the hematopoietic steady state is stable, and the malignant steady state is unstable, revealing the importance of death rates.

In Figure 4(ii), p_{x1} is decreased by 50% and fixed. This allows for a region with topology (g) i.e. a stable co-existing steady state appears. A similar figure may appear by increasing the value of p_{y1} .

In another scenario shown in Figure 4(iii), p_{x1} is increased compared to panel (i), where bi-stability (f) appears satisfying $p_{x1} > \gamma$ and $p_{y1} > \gamma^{-1}$. In this region, the co-existing steady state is a saddle fixed point (see Figure 3f). A similar figure emerges by decreasing p_{y1} .

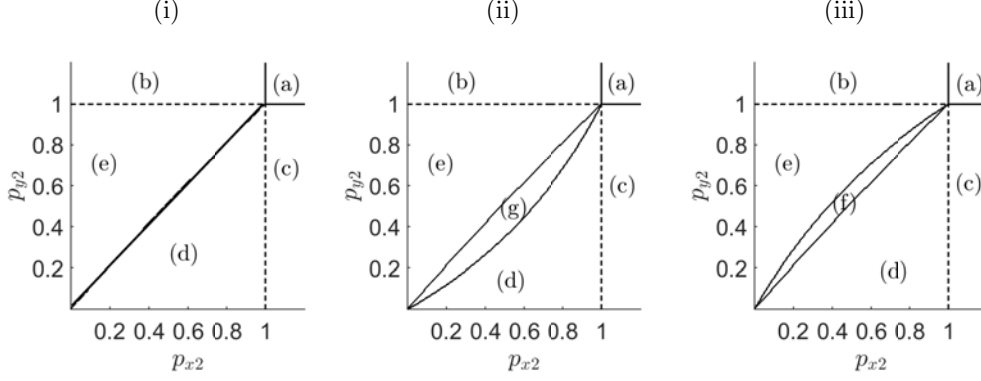


Figure 4: A bifurcation diagram for different values of p_{x1} , p_{x2} , p_{y1} and p_{y2} . Various regions are denoted by letters referring to topologies in Figure 3. In panel (i), p_{x1} and p_{y1} are fixed at default values. Figure (ii) and (iii) are similar to (i) but with decrease and increase in p_{x1} by 50% compared to the default value, respectively. Crossing a solid curve implies a change in type of stable steady state. Crossing a dotted curve indicates the identical stable steady state in both regions, but the number of steady states is changed. The letters (a), (b), (c), (d), (e), (f) and (g) refer to the sub-figures of Figure 3.

The competitive effect of hematopoietic and malignant stem cell niche parameters p_{x1} and p_{y1} are now investigated in greater detail. Particularly, we investigate the hypothetical treatment affecting the relative stem cell competition $\frac{p_{x1}}{p_{y1}}$ by setting

$$p_{x1} = (1 - \sigma)\gamma, \quad (16a)$$

$$p_{y1} = \sigma\gamma^{-1}, \quad (16b)$$

where $\sigma \in [0, 1]$. Hence, for small σ , $p_{x1} \gg p_{y1}$ and for σ close to 1 $p_{y1} \gg p_{x1}$.

Equation (16) is substituted in equation (13)

$$\bar{X}_{0C} = \frac{\bar{X}_{0H} - (1 - \sigma)\gamma\bar{Y}_{0L}}{1 - \sigma(1 - \sigma)}, \quad (17a)$$

$$\bar{Y}_{0C} = \frac{\bar{Y}_{0L} - \sigma\gamma^{-1}\bar{X}_{0H}}{1 - \sigma(1 - \sigma)}. \quad (17b)$$

The co-existing steady state goes continuously from D_L for $\sigma = 0$ to D_H for $\sigma = 1$. Hence, intervention solely addressing $\frac{p_{x1}}{p_{y1}}$ is sufficient to revert a stable D_L situation, to D_C being stable and finally reach a stable D_H thus, leading to cure (See Figure 5).

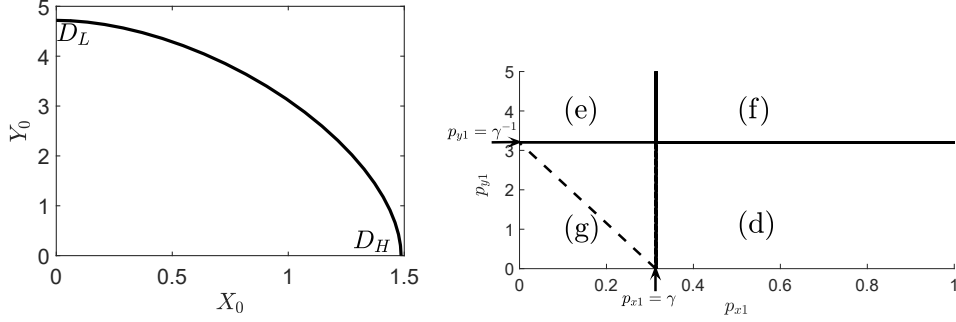


Figure 5: The left panel shows a one-parameter curve that connects the malignant steady state to the hematopoietic steady state given by the equation (17) by changing the value of $\frac{p_{x1}}{p_{y1}}$. In the right panel, the corresponding bifurcation diagram is shown with stability regions denoted by letters referring to Figure 3 whereas the stipulated line is the one-parameter curve given by equation (16).

5 Steady states of the Dimensionless PV Model

After a complete classification of the topologies for the stem cell PV submodel, we return to study the dimensionless PV model. The steady states $(\bar{X}_0, \bar{Y}_0, \bar{X}_r, \bar{Y}_r, \bar{E}_q)$ for Eqs (7) fulfil,

$$\zeta_x \left(\frac{1}{1 + \bar{X}_0 + p_{x1}\bar{Y}_0} - p_{x2} \right) \bar{X}_0 = 0, \quad (18a)$$

$$\zeta_y \left(\frac{1}{1 + p_{y1}\bar{X}_0 + \bar{Y}_0} - p_{y2} \right) \bar{Y}_0 = 0, \quad (18b)$$

$$\bar{X}_r = \frac{\bar{E}_q(1 + q_{x3}\bar{E}_q)}{q_{x2}(1 + q_{x1}\bar{E}_q)} \bar{X}_0, \quad (18c)$$

$$\bar{Y}_r = \frac{\bar{E}_q(1 + q_{y3}\bar{E}_q)}{q_{y2}(1 + q_{y1}\bar{E}_q)} \bar{Y}_0, \quad (18d)$$

$$\bar{E}_q = \frac{10^4}{1 + r_{e1}\bar{X}_r + r_{e2}\bar{Y}_r}. \quad (18e)$$

Corollary 1. *The existence of the steady states of the PV model given in equation (7) is guaranteed by the stem cell PV submodel given in proposition (1), i.e.,*

- A **trivial steady state** $S_0 = (0, 0, 0, 0, 10^4)$ always exists.
- A feasible **hematopoietic steady state** $S_H = (\bar{X}_{0H}, 0, \bar{X}_{rH}, 0, \bar{E}_{qH})$ exists if and only if a feasible D_H exists in the stem cell PV submodel.
- A feasible **malignant steady state** $S_L = (0, \bar{Y}_{0L}, 0, \bar{Y}_{rL}, \bar{E}_{qL})$ exists if and only if a feasible D_L exists in the stem cell PV submodel.

- A feasible **co-existing steady state** $S_C = (\bar{X}_{0C}, \bar{Y}_{0C}, \bar{X}_{rC}, \bar{Y}_{rC}, \bar{E}_{qC})$ exists if and only if a feasible D_C exists in the stem cell PV submodel.

See Appendix (C) for proof.

6 The Reduced PV Model

From the dimensionless form, it follows that ϵ in equation (7e) of order 10^{-4} may be considered as smaller than compared to 1. Thus, we may use a quasi steady state approximation for the concentration of EPO. Thus, we substitute the expression of \bar{E}_q into the remaining equations (7a-7d) providing *the reduced PV model*,

$$\frac{dX_0}{d\tau} = \zeta_x \left(\frac{1}{1 + X_0 + p_{x1}Y_0} - p_{x2} \right) X_0, \quad (19a)$$

$$\frac{dY_0}{d\tau} = \zeta_y \left(\frac{1}{1 + p_{y1}X_0 + Y_0} - p_{y2} \right) Y_0, \quad (19b)$$

$$\frac{dX_r}{d\tau} = \frac{\bar{E}_q}{1 + q_{x1}\bar{E}_q} X_0 - \frac{q_{x2}}{1 + q_{x3}\bar{E}_q} X_r, \quad (19c)$$

$$\frac{dY_r}{d\tau} = \frac{\bar{E}_q}{1 + q_{y1}\bar{E}_q} Y_0 - \frac{q_{y2}}{1 + q_{y3}\bar{E}_q} Y_r. \quad (19d)$$

with

$$\bar{E}_q = \frac{10^4}{1 + r_{e1}X_r + r_{e2}Y_r} \quad (20)$$

The quasi steady state approximation shows an excellent agreement with the PV model during disease progression as illustrated in Figure 6.

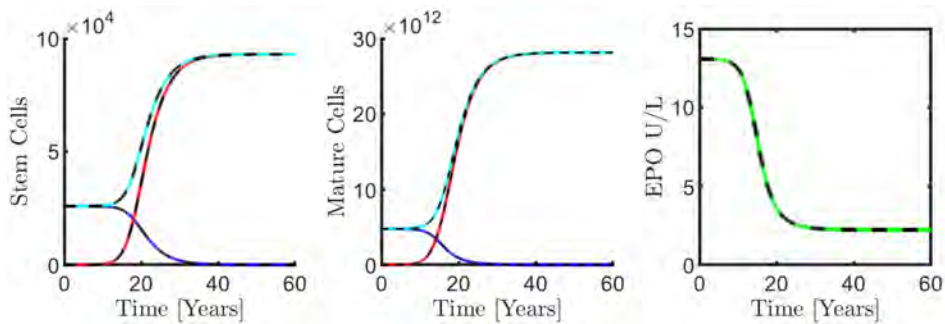


Figure 6: Comparison of the reduced PV model (stipulated curves) and the PV model (full curves) for default parameter values. Red curves are malignant cells, blue shows healthy hematopoietic cells, cyan denotes the sum of the cells and, the right panel shows the concentration of EPO. All variables are converted into variables with units.

The dimensionless PV model and the reduced PV model have identical steady states. The stability of the steady states in the reduced PV model

(19) is analytically tractable and addressed in the following, showing a complete agreement with the stem cell PV submodel. We consider $p_{x2} \neq 1$ and $p_{y2} \neq 1$.

Proposition 2. $R_0 = (0, 0, 0, 0)$ is a stable steady state for $p_{x2} > 1$ and $p_{y2} > 1$ whereas it is unstable for $p_{x2} < 1$ and $p_{y2} < 1$.

Proof. The Jacobian of the trivial steady states R_0 (see Appendix D) is a triangular matrix and two of the four eigenvalues, $\frac{-q_{y2}}{(1+10^4 q_{y1})}$ and $\frac{-q_{x2}}{(1+10^4 q_{x1})}$ are negative but the remaining two $\zeta_x(1 - p_{x2})$ and $\zeta_y(1 - p_{y2})$ may be positive, negative or zero. Hence, R_0 is stable for $p_{x2} > 1$ and $p_{y2} > 1$ and unstable for $p_{x2} < 1$ and $p_{y2} < 1$. \square

Proposition 3. When a feasible hematopoietic steady state $R_H = (\bar{X}_{0H}, 0, \bar{X}_{rH}, 0)$ exists, it is stable for $p_{y1} > \gamma^{-1}$ and unstable for $p_{y1} < \gamma^{-1}$.

Proof. At R_H , the Jacobian for the hematopoietic steady state can be calculated. Three of the four eigenvalues, $\zeta_x p_{x2}(p_{x2} - 1)$, $-q_{y2} \frac{r_{e1} \bar{X}_{rH} + 1}{1 + r_{e1} \bar{X}_{rH} + 10^4 q_{y1}}$ and $\frac{A_{33}}{(1 + r_{e1} \bar{X}_{rH} + 10^4 q_{x1})^2 (1 + r_{e1} \bar{X}_{rH} + 10^4 q_{x3})^2}$ where $A_{33} < 0$ (see Appendix D) are always negative for $p_{x2} < 1$ whereas the last $\frac{\frac{1}{p_{y2}} - 1}{\frac{1}{p_{x2}} - 1} - p_{y1} = \gamma^{-1} - p_{y1}$ may be positive, negative or zero depending on whether p_{y1} is less than, greater than or equal to γ^{-1} . Hence, R_H is stable for $p_{y1} > \gamma^{-1}$ and unstable for $p_{y1} < \gamma^{-1}$. \square

Proposition 4. When a feasible malignant steady state $R_L = (0, \bar{Y}_{0L}, 0, \bar{Y}_{rL})$ exists, it is stable for $p_{x1} > \gamma$ and unstable for $p_{x1} < \gamma$.

Proof. The Jacobian for the malignant steady state R_L is a triangular matrix. Three of the four eigenvalues, $\zeta_y p_{y2}(p_{y2} - 1)$, $-q_{x2} \frac{r_{e2} \bar{Y}_{rL} + 1}{1 + r_{e2} \bar{Y}_{rL} + 10^4 q_{x1}}$ and $\frac{A_{44}}{(1 + r_{e2} \bar{Y}_{rL} + 10^4 q_{y1})^2 (1 + r_{e2} \bar{Y}_{rL} + 10^4 q_{y3})^2}$ where $A_{44} < 0$ (see Appendix D) are always negative for $p_{y2} < 1$ however the last $\frac{\frac{1}{p_{x2}} - 1}{\frac{1}{p_{y2}} - 1} - p_{x1} = \gamma - p_{x1}$ may be positive, negative or zero depending on whether p_{x1} is less than, greater than or equal to γ . Hence, R_L is stable for $p_{x1} > \gamma$ and unstable for $p_{x1} < \gamma$. \square

Proposition 5. When a feasible co-existing steady state R_C exists, it is stable for $p_{x1} < \gamma$ and $p_{y1} < \gamma^{-1}$ and unstable for $p_{x1} > \gamma$ and $p_{y1} > \gamma^{-1}$.

Proof. The Jacobian for the co-existing steady state can be calculated (See Appendix D). Two of the four eigenvalues are always negative but the other two may be positive, negative or zero. It is shown that R_C is stable for $p_{x1} < \gamma$ and $p_{y1} < \gamma^{-1}$ and unstable for $p_{x1} > \gamma$ and $p_{y1} > \gamma^{-1}$. \square

In conclusion, the existence and stability of the steady states in the reduced PV model is a one-to-one correspondence with those of the stem cell PV submodel.

7 Results

This section demonstrates various *in silico* treatments and the role of parameters in the prognosis of a virtual patient using the dimensionless PV model.

In Silico Analysis of Stem Cells

The bone marrow niche influences the biological behavior of hematopoietic stem cells via different signaling cascades and maintains normal hematopoiesis. More efforts have been put into understanding the regulatory mechanisms of niche, which ensures hematopoietic homeostasis by controlling the self-renewal and differentiation of HSCs. The development of therapies targeting the interaction of the stem cells with a niche for myeloid malignancies like PV is getting attention in recent years [31, 46, 51, 58]. Here, we perturb stem cells inhibiting factors p_{x1} and p_{y1} for treatment. To obtain a co-existing steady state, we choose $p_{x1} = 1.3$, $p_{x2} = 0.25$, $p_{y1} = 0.1$ and $p_{y2} = 0.4$ while all other parameters are fixed at their default values.

In Figures 7a-7b the solution of the PV model is projected on the (X_0, Y_0) plane. The parameters involved in the stem cell PV submodel affect the dynamics of erythrocytes and EPO (see Figures 7c, 7d, 7e). In Figure 7a by simulating a drug increasing p_{y1} and decreasing p_{x1} , a co-existing steady state with high malignant cell count $(X_0, Y_0) = (1.21, 1.38)$ switches to a co-existing steady state with low malignant cell counts $(X_0, Y_0) = (2.95, 0.47)$. It takes approximately two years for this simulated treatment to reduce the disease load. Thereafter, treatment is set on pause by resetting p_{x1} and p_{y1} at their previous values. During almost half a year, the trajectory moves significantly back towards the co-existing steady state with high malignant cell counts (see Figure 7b).

Thrombosis is the most prevalent complication for patients with PV [23]. Therefore, it is important to control the excessive production of erythrocytes to reduce the risk of blood clots. It is achieved by perturbing inhibiting factors resulting in the normalized number of hematopoietic stem cells and erythrocytes (Figures 7c and 7d).

The other characteristics of PV is a high load of the *JAK2V617F* allele burden [26, 27, 34] and low EPO plasma levels [12]. Figure 7e shows that the concentration of EPO is increased by changing inhibiting factors in favor of hematopoietic stem cells. In addition, Figure 7f illustrates that adjusting inhibiting factors reduces the *JAK2V617F* allele burden from 53% to 16%, which is favorable. In conclusion, it may suggest that future PV therapy should focus on targeted treatments, which can affect the bone marrow micro-environment.

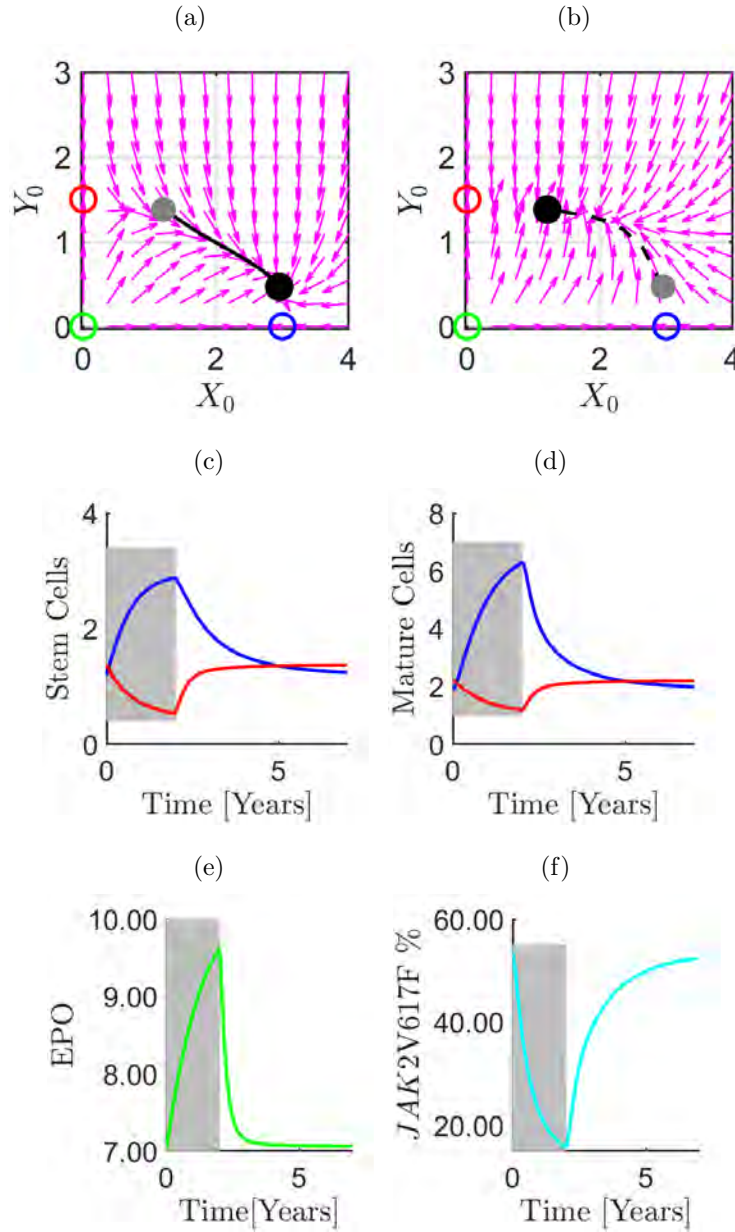


Figure 7: An example of the disease dynamics from the PV model is shown. The filled grey circle in panel (a) is obtained using $p_{x1} = 1.3$, $p_{x2} = 0.25$, $p_{y1} = 0.1$ and $p_{y2} = 0.4$. Decreasing p_{x1} and increasing p_{y1} in panel (a) shows that a patient is moved from a co-existing steady state (upper grey circle) with high malignant cell count towards a co-existing steady state (lower black circle) with low malignant cell count and normalized hematopoietic cell count at $p_{x1} = 0.1$, $p_{x2} = 0.25$, $p_{y1} = 0.35$ and $p_{y2} = 0.4$. In panel (b), setting back p_{x1} and p_{y1} to their original values, the patient moves back toward the original co-existing steady state (upper black circle) following the stipulated black curve. Panels (c), (d), (e) and (f) demonstrate the dynamics during the treatment period (grey) and dynamics after treatment. Red, blue, green and cyan curves show malignant cells, hematopoietic cells, the concentration of EPO, and the $JAK2V617F$ allele burden respectively. Note, the time scale is converted into real time.

In clinical practice, the *JAK2*V617F allele burden, $\frac{Y_r}{X_r+Y_r}$, is measured and is expected to increase due to the expansion of malignant cells for untreated PV. Many authors advocate that the potential influencing therapeutic choices should target the bone marrow niche since the bone marrow niche homeostasis is disrupted, which promotes the survival of malignant stem cells [15, 44]. Figure 8 shows that perturbation of inhibiting factors, p_{x1} and p_{y1} , may improve or worsen prognosis by affecting the allele burden whenever the co-existence steady state is stable. The left panel of Figure 8 shows that decreasing p_{x1} improves prognosis by reducing the *JAK2*V617F allele burden. Similarly, the right panel of Figure 8 shows that increasing the p_{y1} value reduces the co-existence steady state allele burden.

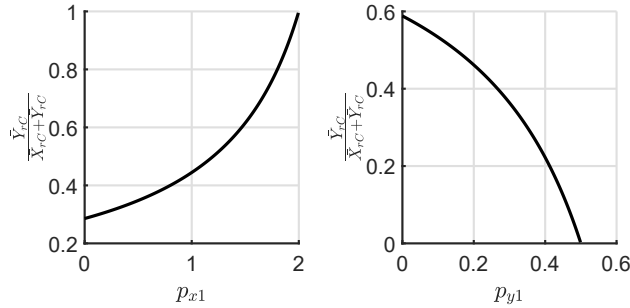


Figure 8: Allele burden at the steady state for a parameter regime where the co-existing steady state is stable. The left panel shows that by increasing p_{x1} , the allele burden also increases, whereas the right panel shows that increasing p_{y1} decreases the allele burden. In the left panel, $p_{y1} = 0.1$ and in the right panel $p_{x1} = 1.3$ whereas $p_{x2} = 0.25$ and $p_{y2} = 0.4$ in both panels.

In Silico Analysis of Erythrocytes

Several treatments aim to lower the number of erythrocytes to prevent blood clots and other complications in patients with PV. Figure 9 shows that increasing the q_{y1} -value has a positive effect on the mature cell dynamics. The *JAK2*V617F allele burden at steady state is reduced to 9% (stipulated curves) from 53% (full curves). In general, the influence of IFN on EPO is still poorly understood, but we may observe in Figure 9 that the concentration of EPO is increased by increasing q_{y1} .

Phlebotomy is applied as first-line therapy to PV patients with a dose of aspirin. It normalizes the erythrocyte count and decreases the thrombotic complications. In [43], the case of a PV patient is studied where the onset of the disease is controlled by phlebotomy alone. In our model, we perform phlebotomy by removing 10% mature cells count as illustrated in Figure 10. It is shown that phlebotomy increases the EPO concentration and decreases the mature cell count for a short period. After two months, the cell count

and EPO level return to the baseline value without altering *JAK2V617F* allele burden.

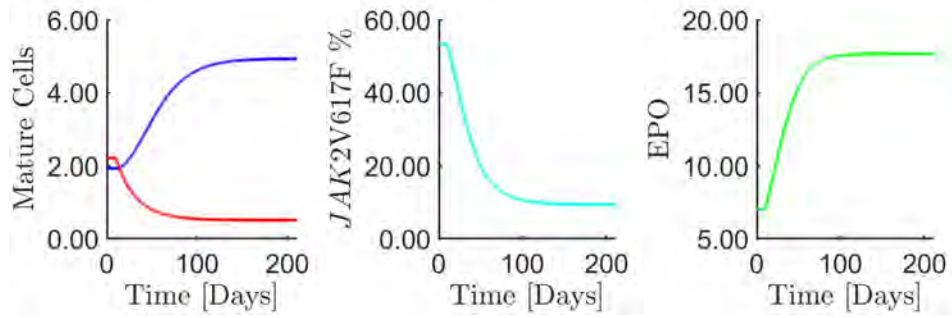


Figure 9: An example of in silico treatment by decreasing the differentiation rate of malignant mature cells. Blue, red, cyan and green represent the healthy cells, malignant cells, the *JAK2V617F* allele burden and EPO respectively. For a co-existing steady state we set $p_{x1} = 1.3$, $p_{x2} = 0.25$, $p_{y1} = 0.1$, $p_{y2} = 0.4$. Before treatment a co-existing state containing low hematopoietic cells and high malignant cells switches to a co-existing state consists of high hematopoietic cells and low malignant cells by increasing q_{y1} from 0.002 to 0.6. Note, the time scale is converted to real time.

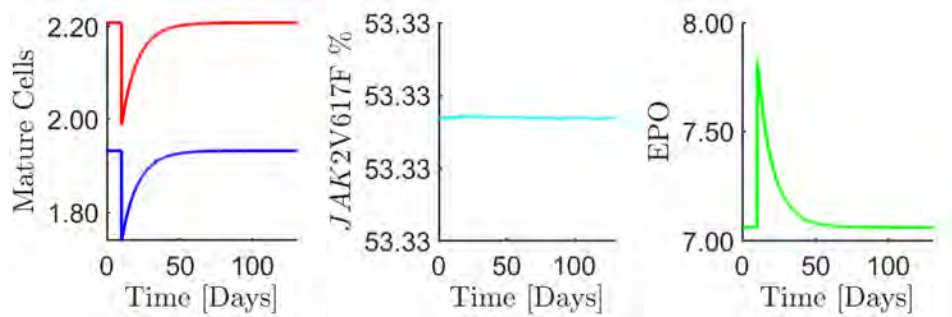


Figure 10: An example of in silico treatment by phlebotomy. Blue, red, cyan and green represent the healthy cells, malignant cells, the *JAK2V617F* allele burden and EPO respectively. For a co-existing steady state we set $p_{x1} = 1.3$, $p_{x2} = 0.25$, $p_{y1} = 0.1$, $p_{y2} = 0.4$. After phlebotomy at day ten, the mature cells and the EPO level returns to the baseline value in two months. The *JAK2V617F* allele burden remains unchanged. Note, the time scale is converted to real time.

In Silico Analysis of EPO

In clinical trials, EPO is the famous erythropoiesis-stimulating agent stimulating erythrocytes. EPO dose is used in several hematological diseases such as anemia, PMF, etc. However, any medication regarding EPO has not yet been initiated in PV. We perform a few in silico trials to observe the effect of EPO concentration on the mature cell count and the *JAK2V617F* allele burden. Figure 11 illustrates that by increasing r_{e2} decreases the EPO

concentration and the number of total mature cells. In contrast, initiating EPO therapy by injecting EPO dose increases the mature cell count as illustrated in Figure 12 whereas the *JAK2V617F* allele burden remains unchanged.

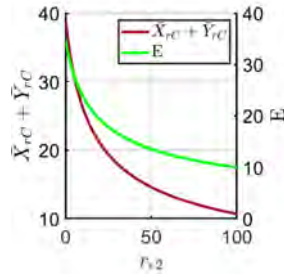


Figure 11: The total erythrocyte count ($\bar{X}_{rC} + \bar{Y}_{rC}$) and EPO concentration E at the steady state for a parameter regime where the co-existing steady state is stable ($p_{x1} = 0.2$). The figure shows decrease in $\bar{X}_{rC} + \bar{Y}_{rC}$ and E by increasing r_{e2} .

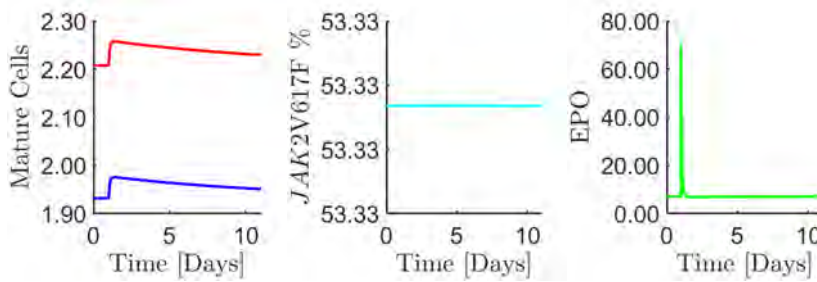


Figure 12: An example of in silico EPO therapy. Blue, red, cyan and green represent the healthy cells, malignant cells, the *JAK2V617F* allele burden and EPO respectively. For a co-existing steady state we set $p_{x1} = 1.3$, $p_{x2} = 0.25$, $p_{y1} = 0.1$, $p_{y2} = 0.4$. EPO dose is given at day one, which increases the healthy and malignant red blood cells whereas the *JAK2V617F* remains unchanged. Note, the time scale is converted to real time.

Fitting of Data

The model trajectories compared to three data sets of individual PV patients receiving IFN treatment are illustrated in Figure 13. Comparing simulation results to patient data validates the proposed model and shows its capability to reproduce data before and after treatment. We identify a set of parameters for three subjects and report values in tables 3, 4 and 5. The remaining parameters are fixed at their default values.

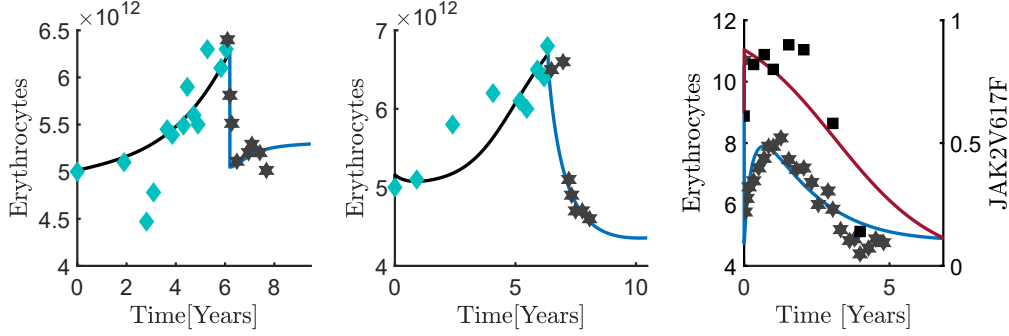


Figure 13: The three panels correspond to patients having PV and treated with IFN are compared to the PV model. In the left two panels, data for the total erythrocyte counts ($X_r + Y_r$) are shown in green diamonds before six years without treatments whereas, after six years, data for cell count are shown in dark grey stars curve during treatment. In the rightmost panel, stars represent the total erythrocyte counts, whereas squares denote the $JAK2V617F$ allele burden $\frac{Y_r}{X_r + Y_r}$ data from a patient during treatment. Model predictions are shown as full curves for erythrocyte counts (black untreated and blue treated) and for the $JAK2V617F$ allele burden (maroon). The data shown in the first two panels is from [43]. The data shown in the last panel is from the clinical trial “DALIAH” (EudraCT number: 2011-001919-31).

Before treatment		After treatment	
Parameter	Value	Parameter	Value
r_y	$9 \cdot 10^{-3}$	r_y	$9 \cdot 10^{-3}$
a_y	$3.7 \cdot 10^{-4}$	a_y	$3.7 \cdot 10^{-4}$
d_{x0}	$2 \cdot 10^{-3}$	d_{x0}	$3 \cdot 10^{-4}$
d_{y0}	$2 \cdot 10^{-3}$	d_{y0}	$7 \cdot 10^{-3}$
δ_x	$2.07 \cdot 10^8$	δ_x	$2.4 \cdot 10^8$
δ_y	$2.19 \cdot 10^8$	δ_y	$5 \cdot 10^7$
η_x	$8.57 \cdot 10^{-4}$	η_x	$8.57 \cdot 10^{-4}$
η_y	$3.2 \cdot 10^{-3}$	η_y	$3.2 \cdot 10^{-3}$
k_0	$5.22 \cdot 10^{-11}$	k_0	$5.22 \cdot 10^{-11}$

Table 3: Parameter values for the left panel in Figure 13. The parameters in red are calibrated by fitting data during treatment.

Before treatment		After treatment	
Parameter	Value	Parameter	Value
r_y	$1.2 \cdot 10^{-2}$	r_y	$1.2 \cdot 10^{-2}$
a_y	$8 \cdot 10^{-5}$	a_y	$8 \cdot 10^{-5}$
d_{x0}	$2 \cdot 10^{-3}$	d_{x0}	$3 \cdot 10^{-4}$
d_{y0}	$2.4 \cdot 10^{-3}$	d_{y0}	$7 \cdot 10^{-3}$
δ_x	$2.07 \cdot 10^8$	δ_x	$3.3 \cdot 10^8$
δ_y	$2.19 \cdot 10^8$	δ_y	$2 \cdot 10^8$
η_x	$8.57 \cdot 10^{-4}$	η_x	$8.57 \cdot 10^{-4}$
η_y	$3.2 \cdot 10^{-3}$	η_y	$3.2 \cdot 10^{-3}$
k_0	$5.22 \cdot 10^{-11}$	k_0	$5.22 \cdot 10^{-11}$

Table 4: Parameter values for the middle Figure 13. The parameters in red are calibrated while fitting data during treatment.

Parameter	Value	Parameter	Value
r_y	$1 \cdot 10^{-3}$	a_y	$1 \cdot 10^{-4}$
d_{x0}	$6 \cdot 10^{-4}$	d_{y0}	$2 \cdot 10^{-3}$
k_0	$5.22 \cdot 10^{-11}$	p	$3 \cdot 10^5$
δ_x	$2.1 \cdot 10^8$	δ_y	$2 \cdot 10^8$
η_x	$2.6 \cdot 10^{-3}$	η_y	$1.5 \cdot 10^{-3}$

Table 5: Parameter values deviated from the default for the right Figure 13. All other values are set at their default.

8 Discussion and Conclusions

In this article, a PV model integrating both hematopoietic and malignant cells with multiple EPO feedback is analyzed. A thorough mathematical investigation of the model is presented. The number of parameters is reduced from 23 to 15 as a result of dimensional analysis. Stem cell dynamics can be investigated from a two-dimensional stem cell PV submodel, and four kinds of steady states may exist, i.e., trivial, hematopoietic, malignant and co-existing steady states. The existence and stability of all steady states in the stem cell PV submodel are identified, analyzed and visualized in a phase plane Figure 3. With a quasi steady state approximation, the PV model consisting of a system of non-linear ordinary differential equation is approximated by a four dimensional system, the reduced PV model. Finally, it is demonstrated that the steady states of the stem cell PV submodel and the steady states of the reduced PV model are in correspondence. Thus, stem cell properties determine the qualitative outcome of the PV model. Other authors have previously supported the crucial importance of stem cell dynamics for the behavior of full system. In [41], a compartmental

model is proposed and it is shown that a feasible and stable steady state is obtained by modulating the self-renewal rate of HSC. Another important work [13] indicates that differentiation and apoptosis rates related to the stem cell compartment are essential parameters to simulate patient data. The parameter changes in the stem cell and leukocyte compartments are sufficient to destabilize the steady state.

In biomedical literature, the irregular stem cell division and the bone marrow niche's regulatory feedback are drivers for blood cancer development which are incorporated in our model. According to these perceptions, our investigation shows that the stem cell population is a good candidate for therapy to prevent disease progression. The death rates, p_{x2} and p_{y2} are related to the fitness of stem cell type whereas p_{x1} and p_{y1} describes niche feedback. Decreasing p_{x1} and increasing p_{y1} may turn a stable full blown malignant steady state into a stable hematopoietic steady state, as illustrated in Figure 5 and Figure 7. The similar concept is discussed in [50] where the relation between niche feedback, stem cell fitness and inflammatory stimuli is well explored for a good prognosis. Moreover, stem cell therapy is useful to normalize the blood count and EPO level in the blood.

Besides stem cell therapy, many clinical experts focus on reducing the erythrocyte count in the peripheral blood, preventing thromboembolic events. Phlebotomy is a standard therapy implemented in PV patients for removing an excessive amount of blood cells. Some investigations address that intervention with interferon- α (IFN) increases the differentiation of progenitor cells in the myeloid cell line [32]. We implement a similar idea where we reduce the differentiation of mature malignant cells by increasing q_{y1} in Figure 9. It increases the healthy cell count and decreases the malignant cell count in the blood, and the *JAK2V617F* allele burden is reduced. Before any drug therapy, phlebotomy is initiated when the patient is diagnosed with PV. It reduces the chances of thrombotic events for a short time. Figure 10 shows the reduction in mature cell count after phlebotomy, whereas the EPO concentration is increased.

It is an interesting discussion whether EPO should be taken into account as a diagnostic or prognostic tool in PV patients. We perform simulations to investigate the effect of EPO dose on the mature cells and the *JAK2V617F* allele burden (See Figure 12). Our model reveals that EPO dose might increase the mature cell count with no effect on *JAK2V617F*. However, decreasing EPO concentration decreases the total erythrocyte count and stop the risk of thrombosis. In the case of available data of EPO for PV patients, the proposed model can be validated, and we may acquire a better knowledge of EPO mechanism in PV patients.

Appendix

A Parameter Estimation

The steady state of the full model (1) has the following form, where bars indicate steady state values

$$(r_x \phi_x - d_{x0} - a_x) \bar{x}_0 = 0, \quad (\text{A.1a})$$

$$a_x A_x(\bar{E}) \bar{x}_0 - d_{xr}(\bar{E}) \bar{x}_r = 0, \quad (\text{A.1b})$$

$$\frac{p}{1 + k_0 \bar{x}_r} - k \bar{E} = 0, \quad (\text{A.1c})$$

with $\bar{y}_0 = \bar{y}_r = 0$ and

$$\phi_x = \frac{1}{1 + c_{xx} \bar{x}_0}, \quad (\text{A.2})$$

$$A_x(\bar{E}) = \delta_x \frac{\bar{E}}{1 + \alpha_x \bar{E}}, \quad (\text{A.3})$$

$$d_{xr}(\bar{E}) = \eta_x \frac{1}{1 + \beta_x \bar{E}}. \quad (\text{A.4})$$

Based on literature, we choose hematopoietic steady state values such as $(\bar{x}_0, \bar{y}_0, \bar{x}_r, \bar{y}_r, \bar{E}) = (2.6 \cdot 10^4, 0, 4.52 \cdot 10^{12}, 0, 13.9)$.

Hematopoietic stem cells divide approximately once per year [1, 19]. We let $r_x = 5 \cdot 10^{-3}$ per day [17]. In addition, elimination from the stem cell compartment is approximately 0.002 cells per day, $d_{x0} = 2 \cdot 10^{-3}$ per day [17, 45, 6, 50]. $c_{xx} = 5.6 \cdot 10^{-5}$ is taken from [45, 50] based on reasoning that hematopoietic cells are more sensitive to inhibitive niche feedback than malignant cells. From equation (A.1a),

$$a_x = r_x \phi_x - d_{x0},$$

gives $a_x = 3.58 \cdot 10^{-5}$.

Since the life span of RBC for healthy humans is about 120 days [9, 13, 38, 20], we choose the removal rate dependent on EPO from the erythrocyte compartment to be, $d_{xr}(\bar{E}) = 1/120$ per day. We choose $\eta_x = 8 \cdot 10^{-3}$ per day such that for $\bar{E} = 0$, $d_{xr}(0) \approx \eta_x$. Thereafter, from equation (A.4),

$$\beta_x = \frac{1}{\bar{E}} \left(\frac{\eta_x}{d_{xr}(\bar{E})} - 1 \right).$$

Thus, $\beta_x = 9 \cdot 10^{-3}$ is obtained.

From equation (A.1b),

$$A_x(\bar{E}) = \frac{d_{xr}(\bar{E}) \bar{x}_r}{a_x \bar{x}_0}$$

gives $A_x(\bar{E}) = 3 \cdot 10^9$. We make a first guess for $\delta_x = 8.6 \cdot 10^8$. With the help of equation (A.3),

$$\alpha_x = \frac{1}{\bar{E}} \left(\frac{\delta_x \bar{E}}{A_x(\bar{E})} - 1 \right)$$

providing $\alpha_x = 5 \cdot 10^{-3}$.

In [20, 38, 40], the half life of EPO is reported to be about 4 to 24 hours and in [7, 9, 20, 38, 39] the decay constant of EPO varies between 2 and 7 per day. Thus, we suppose that the half-life of EPO to be 6 hours as default value, $k = \frac{\ln(2)}{T_{1/2}} \approx 2.8 \text{day}^{-1}$. The parameter $p = 1.56 \cdot 10^4$ is estimated in [39, 9], thereby from equation (A.1c),

$$k_0 = \frac{1}{\bar{x}_r} \left(\frac{p}{k\bar{E}} - 1 \right)$$

we obtain $k_0 = 8.9 \cdot 10^{-11}$.

B Dimensional analysis

Formulating differential equations in dimensionless form may reduce the number of free parameters by collecting the original parameters into clusters of parameters. All variable in system (1) are scaled by a constant having the unit of the variable and denoted with same symbol as the variables but with a tilde above. Thus, we non-dimensionalise the equations of system (1) using following scales,

$$x_0 = \tilde{x}_0 X_0, y_0 = \tilde{y}_0 Y_0, x_r = \tilde{x}_r X_r, y_r = \tilde{y}_r Y_r, E = \tilde{e} E_q, t = \tilde{t} \tau$$

where small letters with tilde are scaling constants, capital letters are dimensionless variables and τ is dimensionless time. Hence, system (1) in dimensionless variables reads,

$$\frac{dX_0}{d\tau} = \frac{\tilde{t}}{\tilde{x}_0} \left(\frac{r_x}{1 + c_{xx}\tilde{x}_0 X_0 + c_{xy}\tilde{y}_0 Y_0} - d_{x0} - a_x \right) \tilde{x}_0 X_0, \quad (\text{B.1a})$$

$$\frac{dY_0}{d\tau} = \frac{\tilde{t}}{\tilde{y}_0} \left(\frac{r_y}{1 + c_{yx}\tilde{x}_0 X_0 + c_{yy}\tilde{y}_0 Y_0} - d_{y0} - a_y \right) \tilde{y}_0 Y_0, \quad (\text{B.1b})$$

$$\frac{dX_r}{d\tau} = \frac{\tilde{t}}{\tilde{x}_r} \left(\frac{a_x \delta_1 \tilde{e} E_q}{1 + \alpha_1 \tilde{e} E_q} \tilde{x}_0 X_0 - \frac{\eta_1}{1 + \beta_1 \tilde{e} E_q} \tilde{x}_r X_r \right), \quad (\text{B.1c})$$

$$\frac{dY_r}{d\tau} = \frac{\tilde{t}}{\tilde{y}_r} \left(\frac{a_y \delta_2 \tilde{e} E_q}{1 + \alpha_2 \tilde{e} E_q} \tilde{y}_0 Y_0 - \frac{\eta_2}{1 + \beta_2 \tilde{e} E_q} \tilde{y}_r Y_r \right), \quad (\text{B.1d})$$

$$\frac{dE_q}{d\tau} = \frac{\tilde{t}}{\tilde{e}} \left(\frac{p}{(1 + k_0(\tilde{x}_r X_r + \tilde{y}_r Y_r))} - k \tilde{e} E_q \right). \quad (\text{B.1e})$$

i.e.

$$\frac{dX_0}{d\tau} = r_x \tilde{t} \left(\frac{1}{1 + c_{xx} \tilde{x}_0 X_0 + c_{xy} \tilde{y}_0 Y_0} - \frac{d_{x0} + a_x}{r_x} \right) X_0, \quad (\text{B.2a})$$

$$\frac{dY_0}{d\tau} = r_y \tilde{t} \left(\frac{1}{1 + c_{yx} \tilde{x}_0 X_0 + c_{yy} \tilde{y}_0 Y_0} - \frac{d_{y0} + a_y}{r_y} \right) Y_0, \quad (\text{B.2b})$$

$$\frac{dX_r}{d\tau} = \tilde{t} \frac{a_x \delta_1 \tilde{e} E_q}{\tilde{x}_r (1 + \alpha_1 \tilde{e} E_q)} \tilde{x}_0 X_0 - \tilde{t} \frac{\eta_1}{1 + \beta_1 \tilde{e} E_q} X_r, \quad (\text{B.2c})$$

$$\frac{dY_r}{d\tau} = \tilde{t} \frac{a_y \delta_2 \tilde{e} E_q}{\tilde{y}_r (1 + \alpha_2 \tilde{e} E_q)} \tilde{y}_0 Y_0 - \tilde{t} \frac{\eta_2}{1 + \beta_2 \tilde{e} E_q} Y_r, \quad (\text{B.2d})$$

$$\frac{dE_q}{d\tau} = \tilde{t} \frac{p}{\tilde{e} (1 + k_0 (\tilde{x}_r X_r + \tilde{y}_r Y_r))} - \tilde{t} k E_q. \quad (\text{B.2e})$$

We may choose

$$\tilde{x}_0 = \frac{1}{c_{xx}} \approx 10^4, \quad (\text{B.3a})$$

$$\tilde{y}_0 = \frac{1}{c_{yy}} \approx 10^4, \quad (\text{B.3b})$$

$$\tilde{x}_r = \frac{p a_x \delta_1}{10^4 r_x c_{xx}} \approx 10^{11}, \quad (\text{B.3c})$$

$$\tilde{y}_r = \frac{p a_y \delta_2}{10^4 r_x c_{yy}} \approx 10^{12}, \quad (\text{B.3d})$$

$$\tilde{e} = \frac{p}{10^4 k} \approx 10^1, \quad (\text{B.3e})$$

$$\tilde{t} = \frac{k}{r_x} \approx 10^3. \quad (\text{B.3f})$$

and the system (B.2) becomes

$$\frac{dX_0}{d\tau} = k \left(\frac{1}{1 + X_0 + \frac{c_{xy}}{c_{yy}} Y_0} - \frac{d_{x0} + a_x}{r_x} \right) X_0, \quad (\text{B.4a})$$

$$\frac{dY_0}{d\tau} = k \frac{r_y}{r_x} \left(\frac{1}{1 + \frac{c_{yx}}{c_{xx}} X_0 + Y_0} - \frac{d_{y0} + a_y}{r_y} \right) Y_0, \quad (\text{B.4b})$$

$$\frac{dX_r}{d\tau} = \frac{E_q}{1 + \frac{\alpha_1 p}{10^4 k} E_q} X_0 - \frac{\eta_1 k}{r_x} \frac{1}{1 + \frac{\beta_1 p}{10^4 k} E_q} X_r, \quad (\text{B.4c})$$

$$\frac{dY_r}{d\tau} = \frac{E_q}{1 + \frac{\alpha_2 p}{10^4 k} E_q} Y_0 - \frac{\eta_2 k}{r_x} \frac{1}{1 + \frac{\beta_2 p}{10^4 k} E_q} Y_r, \quad (\text{B.4d})$$

$$\epsilon \frac{dE_q}{d\tau} = \frac{1}{10^{-4} \left(1 + k_0 \left(\frac{p a_x \delta_1}{10^4 r_x c_{xx}} X_r + \frac{p a_y \delta_2}{10^4 r_x c_{yy}} Y_r \right) \right)} - E_q. \quad (\text{B.4e})$$

Set $\epsilon = \frac{r_x}{k^2} \approx 10^{-4}$, $\zeta_x = k \approx 1$, $\zeta_y = k \frac{r_y}{r_x} \approx 1$, $p_{x1} = \frac{c_{xy}}{c_{yy}} \approx 1$, $p_{x2} = \frac{d_{x0} + a_x}{r_x} \approx 10^{-1}$, $p_{y1} = \frac{c_{yx}}{c_{xx}} \approx 10^{-1}$, $p_{y2} = \frac{d_{y0} + a_y}{r_y} \approx 10^{-1}$, $q_{x1} = \frac{\alpha_x p}{10^4 k} \approx 10^{-3}$, $q_{x2} =$

$\frac{\eta_x k}{r_x} \approx 1, q_{x3} = \frac{\beta_x p}{10^4 k} \approx 10^{-3}, q_{y1} = \frac{\alpha_y p}{10^4 k} \approx 10^{-3}, q_{y2} = \frac{\eta_y k}{r_x} \approx 1, q_{y3} = \frac{\beta_y p}{10^4 k} \approx 10^{-3}, r_{e1} = \frac{k_0 p \alpha_x \delta_x}{10^4 r_x c_{xx}} \approx 10^2, r_{e2} = \frac{k_0 p \alpha_y \delta_y}{10^4 r_x c_{yy}} \approx 10^3$, gives

$$\frac{dX_0}{d\tau} = \zeta_x \left(\frac{1}{1 + X_0 + p_{x1} Y_0} - p_{x2} \right) X_0, \quad (\text{B.5a})$$

$$\frac{dY_0}{d\tau} = \zeta_y \left(\frac{1}{1 + p_{y1} X_0 + Y_0} - p_{y2} \right) Y_0, \quad (\text{B.5b})$$

$$\frac{dX_r}{d\tau} = \left(\frac{E_q}{1 + q_{x1} E_q} X_0 - \frac{q_{x2}}{1 + q_{x3} E_q} X_r \right), \quad (\text{B.5c})$$

$$\frac{dY_r}{d\tau} = \left(\frac{E_q}{1 + q_{y1} E_q} Y_0 - \frac{q_{y2}}{1 + q_{y3} E_q} Y_r \right), \quad (\text{B.5d})$$

$$\epsilon \frac{dE_q}{d\tau} = \left(\frac{10^4}{1 + r_{e1} X_r + r_{e2} Y_r} - E_q \right). \quad (\text{B.5e})$$

C Existence of steady states of the full model

Consider the system of Eqs (B.5). Expressions for steady state solutions are,

$$\zeta_x \left(\frac{1}{1 + \bar{X}_0 + p_{x1} \bar{Y}_0} - p_{x2} \right) \bar{X}_0 = 0, \quad (\text{C.1a})$$

$$\zeta_y \left(\frac{1}{1 + p_{y1} \bar{X}_0 + \bar{Y}_0} - p_{y2} \right) \bar{Y}_0 = 0, \quad (\text{C.1b})$$

$$\bar{X}_r = \frac{\bar{E}_q (1 + q_{x3} \bar{E}_q)}{q_{x2} (1 + q_{x1} \bar{E}_q)} \bar{X}_0, \quad (\text{C.1c})$$

$$\bar{Y}_r = \frac{\bar{E}_q (1 + q_{y3} \bar{E}_q)}{q_{y2} (1 + q_{y1} \bar{E}_q)} \bar{Y}_0, \quad (\text{C.1d})$$

$$\bar{E}_q = \left(\frac{10^4}{1 + r_{e1} \bar{X}_r + r_{e2} \bar{Y}_r} \right). \quad (\text{C.1e})$$

Following, we will show that the existence of feasible steady states of the full model is guaranteed by steady states of the stem cell submodel. We consider $p_{x2} \neq 1$ and $p_{y2} \neq 1$.

A **trivial steady state** exists always i.e. $S_0 = (0, 0, 0, 0, 10^4)$.

For **hematopoietic steady state**, $S_H = (\bar{X}_{0H}, 0, \bar{X}_{rH}, 0, \bar{E}_{qH})$, substitute equation (C.1e) in equation (C.1c),

$$q_{x2}r_{e1}^2\bar{X}_{rH}^3 + q_{x2}r_{e1}(10^4q_{x1} + 2)\bar{X}_{rH}^2 + (-10^4r_{e1}\bar{X}_{0H} + q_{x2}(1 + 10^4q_{x1}))\bar{X}_{rH} - 10^4(10^4q_{x3} + 1)\bar{X}_{0H} = 0. \quad (\text{C.2})$$

Since the coefficients with the first two terms i.e. $q_{x2}r_{e1}^2$ and $q_{x2}r_{e1}(10^4q_{x1} + 2)$ are always positive whereas the last term $-10^4(10^4q_{x3} + 1)\bar{X}_{0H}$ remains always negative for positive \bar{X}_{0H} i.e. $p_{x2} < 1$. Thus, by using Descartes' rule of sign, there exists exactly one positive root of equation (C.2) i.e. \bar{X}_{rH+} thus, a unique \bar{E}_{qH} also exists. Hence, a feasible S_H exists if and only if D_H exists in the stem cell submodel.

For **malignant steady state**, $S_L = (0, \bar{Y}_{0L}, 0, \bar{Y}_{rL}, \bar{E}_{qL})$, substitute equation (C.1e) in equation (C.1d),

$$q_{y2}r_{e2}^2\bar{Y}_{rL}^3 + q_{y2}r_{e2}(10^4q_{y1} + 2)\bar{Y}_{rL}^2 + (-10^4r_{e2}\bar{Y}_{0L} + q_{y2}(1 + 10^4q_{x1}))\bar{Y}_{rL} - 10^4(10^4q_{y3} + 1)\bar{Y}_{0L} = 0 \quad (\text{C.3})$$

Since the first two terms remain positive whereas the last term remains negative for positive \bar{Y}_{0L} i.e. $p_{y2} < 1$. Thus, by using Descartes' rule of sign, there exists exactly one positive root of equation (C.3) i.e. \bar{Y}_{rL+} thus, a unique \bar{E}_{qL} also exists. Hence, a feasible S_L exists if and only if D_L exists in the stem cell submodel.

For **co-existing steady state** $S_C = (\bar{X}_{0C}, \bar{Y}_{0C}, \bar{X}_{rC}, \bar{Y}_{rC}, \bar{E}_{qC})$, substituting expressions (C.1c) and (C.1d) in (C.1e),

$$\epsilon_4\bar{E}_q^4 + \epsilon_3\bar{E}_q^3 + \epsilon_2\bar{E}_q^2 - \epsilon_1\bar{E}_q^1 - \epsilon_0\bar{E}_q^0 = 0. \quad (\text{C.4})$$

where $\epsilon_4 = q_{x3}q_{y1}q_{y2}r_{e1}\bar{X}_{0C} + q_{x1}q_{x2}q_{y3}r_{e2}\bar{Y}_{0C}$,
 $\epsilon_3 = (q_{x1}q_{y1}q_{y2} + r_{e2}(q_{x1} + q_{y3})\bar{Y}_{0C})q_{x2} + (q_{x3} + q_{y1})q_{y2}r_{e1}\bar{X}_{0C}$,
 $\epsilon_2 = (((1 - 10^4q_{y1})q_{x1} + q_{y1})q_{y2} + r_{e2}\bar{Y}_{0C})q_{x2} + q_{y2}r_{e1}\bar{X}_{0C}$,
 $\epsilon_1 = 10^4q_{x2}q_{y2}(q_{x1} + q_{y1} - 10^{-4})$ and $\epsilon_0 = q_{x2}q_{y2}10^4$. For positive \bar{X}_{0C} and \bar{Y}_{0C} , coefficients ϵ_4 and ϵ_3 are always positive and ϵ_0 remains negative. The coefficients ϵ_2 is negative for

$$10^4 > \frac{1}{q_{x1}q_{y1}} \left(\frac{r_{e1}\bar{X}_{0C}}{q_{x2}} + \frac{r_{e2}\bar{Y}_{0C}}{q_{y2}} + q_{x1} + q_{y1} \right)$$

positive for

$$10^4 < \frac{1}{q_{x1}q_{y1}} \left(\frac{r_{e1}\bar{X}_{0C}}{q_{x2}} + \frac{r_{e2}\bar{Y}_{0C}}{q_{y2}} + q_{x1} + q_{y1} \right).$$

and zero for

$$10^4 = \frac{1}{q_{x1}q_{y1}} \left(\frac{r_{e1}\bar{X}_{0C}}{q_{x2}} + \frac{r_{e2}\bar{Y}_{0C}}{q_{y2}} + q_{x1} + q_{y1} \right).$$

The coefficient ϵ_1 is negative for $q_{x1} + q_{y1} > 10^{-4}$, positive for $q_{x1} + q_{y1} < 10^{-4}$ and zero for $q_{x1} + q_{y1} = 10^{-4}$.

Cases	ϵ_4	ϵ_3	ϵ_2	ϵ_1	ϵ_0	Roots
1 st	+	+	+	+	-	1 pos real root
2 nd	+	+	-	-	-	1 pos real root
3 rd	+	+	+	-	-	1 pos real root
4 th	+	+	-	+	-	3 or 1 pos real roots
5 th	+	+	-/+	0	-	1 pos real roots
6 th	+	+	0	+/-	-	1 pos real roots

Table 6: Descartes Rule of sign

Let us analyse the 4th case, where $\epsilon_1 > 0$ and $\epsilon_2 < 0$.

$\epsilon_2 = 10^{-4} \left(\frac{r_{e1}\bar{X}_{0C}}{q_{x2}} + \frac{r_{e2}\bar{Y}_{0C}}{q_{y2}} \right) + 10^{-4}(q_{x1} + q_{y1}) - q_{x1}q_{y1}$. Since $q_{x1} \geq 0$, $q_{y1} \geq 0$ and $q_{x1} + q_{y1} < 10^{-4}$, we may say, $q_{x1} < 10^{-4}$ and $q_{y1} < 10^{-4}$, thus, $\epsilon_2 > \left(10^{-4} \left(\frac{r_{e1}\bar{X}_{0C}}{q_{x2}} + \frac{r_{e2}\bar{Y}_{0C}}{q_{y2}} \right) + 10^{-4}(q_{x1} + q_{y1}) - 10^{-4}q_{y1} \right)$ or $\epsilon_2 > \left(10^{-4} \left(\frac{r_{e1}\bar{X}_{0C}}{q_{x2}} + \frac{r_{e2}\bar{Y}_{0C}}{q_{y2}} \right) + 10^{-4}q_{x1} \right)$ which is always positive. It excludes the possibility of three positive roots. Hence, there exists a unique positive root of \bar{E}_q . From equations (C.1c) and (C.1d), we obtain a unique $(\bar{X}_{rC}, \bar{Y}_{rC})$. Hence, a feasible S_C exists if and only if D_C exists in the stem cell submodel.

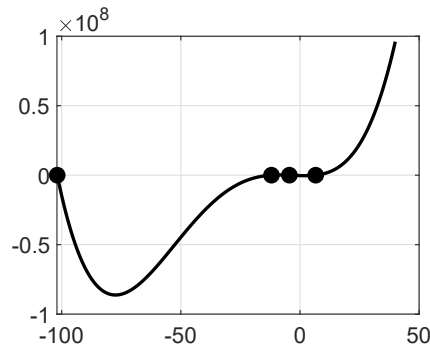


Figure C.1: Graph for polynomial equation (C.4) related to Case 3, for $p_{x1} = 0.2$ and $p_{y1} = 2$ (co-existing steady state does not exist for default values of p_{x1} and p_{y1}). Roots are denoted by filled black circles.

D Stability of the reduced model:

In this section, we evaluate the Jacobian at various steady states.

At R_0 the Jacobian of a **trivial steady state** is

$$J_{R_0} = \begin{bmatrix} a_{11} & 0 & 0 & 0 \\ 0 & a_{22} & 0 & 0 \\ a_{31} & 0 & a_{33} & 0 \\ 0 & a_{42} & 0 & a_{44} \end{bmatrix} \quad (\text{D.1})$$

where

$$\begin{aligned} a_{11} &= \zeta_x (1 - p_{x2}), \\ a_{22} &= \zeta_y (1 - p_{y2}), \\ a_{31} &= \frac{10^4}{1+10^4 q_{x1}}, \\ a_{33} &= -\frac{q_{x2}}{1+10^4 q_{x1}}, \\ a_{42} &= \frac{10^4}{1+10^4 q_{y1}}, \\ a_{44} &= -\frac{q_{y2}}{1+10^4 q_{y1}}. \end{aligned}$$

At R_H the Jacobian of the **hematopoietic steady state** is

$$J_{R_H} = \begin{bmatrix} a_{11} & a_{12} & 0 & 0 \\ 0 & a_{22} & 0 & 0 \\ a_{31} & 0 & a_{33} & a_{34} \\ 0 & a_{42} & 0 & a_{44} \end{bmatrix} \quad (\text{D.2})$$

where

$$\begin{aligned} a_{11} &= \zeta_x p_{x2} (p_{x2} - 1), \\ a_{12} &= \zeta_x p_{x1} p_{x2} (p_{x2} - 1), \\ a_{22} &= \zeta_y \left(\frac{1}{\left(p_{y1} \left(\frac{1}{p_{x2}} - 1 \right) + 1 \right)} - p_{y2} \right), \\ a_{31} &= \frac{10^4}{1+r_{e1} \bar{X}_{rH} + 10^4 q_{x1}}, \\ a_{33} &= \frac{A_{33}}{(1+r_{e1} \bar{X}_{rH} + 10^4 q_{x1})^2 (1+r_{e1} \bar{X}_{rH} + 10^4 q_{x3})^2}, \\ a_{34} &= \frac{10^{12} r_{e2} A_{34}}{(1+r_{e1} \bar{X}_{rH} + 10^4 q_{x1})^2 (1+r_{e1} \bar{X}_{rH} + 10^4 q_{x3})^2}, \\ a_{42} &= \frac{10^4}{1+r_{e1} \bar{X}_{rH} + 10^4 q_{y1}}, \\ a_{44} &= -\frac{q_{y2} (1+r_{e1} \bar{X}_{rH})}{1+r_{e1} \bar{X}_{rH} + 10^4 q_{y1}}. \end{aligned}$$

$$\begin{aligned} A_{33} &= \left(-q_{x2} r_{e1}^4 \bar{X}_{rH}^4 - 2 \cdot 10^4 \left(q_{x2} (q_{x3} + q_{x1} + \frac{1}{5 \cdot 10^3}) \bar{X}_{rH} + \frac{\bar{X}_{0H}}{2} \right) r_{e1}^3 \bar{X}_{rH}^2 \right) + \\ &\left(-10^8 \left((q_{x1}^2 + (4q_{x3} + \frac{3}{5 \cdot 10^3}) q_{x1} + \frac{q_{x3}}{2 \cdot 10^3} + \frac{3}{5 \cdot 10^7}) q_{x2} \bar{X}_{rH} + 2q_{x3} \bar{X}_{0H} + \frac{\bar{X}_{0H}}{5 \cdot 10^3} \right) r_{e1}^2 \bar{X}_{rH} \right) + \\ &\left(-2 \cdot 10^{11} r_{e1} (q_{x3} + \frac{1}{10^4}) \left((q_{x1} + \frac{1}{5 \cdot 10^3}) (q_{x1} + \frac{1}{10^4}) q_{x2} \bar{X}_{rH} + \frac{(q_{x3} + \frac{1}{10^4}) \bar{X}_{0H}}{2} \right) \right) + \\ &\left(-10^{12} q_{x2} (q_{x3} + \frac{1}{10^4}) (q_{x1} + \frac{1}{10^4})^2 \right). \end{aligned}$$

$$A_{34} = \frac{r_{e1}^2 q_{x2} q_{x3} \bar{X}_{rH}^3}{10^8} + \frac{r_{e1}}{5 \cdot 10^3} \left(q_{x2} q_{x3} \left(q_{x1} + \frac{1}{10^4} \right) + \frac{r_{e1}}{2 \cdot 10^4} \bar{X}_{0H} \right) \bar{X}_{rH}^2 + \left(q_{x3} \left(\frac{r_{e1} \bar{X}_{0H}}{5 \cdot 10^3} + q_{x2} \left(q_{x1} + \frac{1}{10^4} \right) \right) + \frac{r_{e1} \bar{X}_{0H}}{5 \cdot 10^7} \right) \bar{X}_{rH} + \left(q_{x3} + \frac{1}{10^4} \right)^2 \bar{X}_{0H}.$$

At R_L the Jacobian of the **malignant steady state** is

$$J_{R_L} = \begin{bmatrix} a_{11} & 0 & 0 & 0 \\ a_{21} & a_{22} & 0 & 0 \\ a_{31} & 0 & a_{33} & 0 \\ 0 & a_{42} & a_{43} & a_{44} \end{bmatrix} \quad (\text{D.3})$$

where

$$\begin{aligned} a_{11} &= \zeta_x \left(\frac{1}{\left(p_{x1} \left(\frac{1}{p_{y2}} - 1 \right) + 1 \right)} - p_{x2} \right), \\ a_{21} &= \zeta_y p_{y2} p_{y1} (p_{y2} - 1), \\ a_{22} &= \zeta_y p_{y2} (p_{y2} - 1), \\ a_{31} &= \frac{10^4}{1 + r_{e2} \bar{Y}_{rL} + 10^4 q_{x1}}, \\ a_{33} &= -\frac{q_{x2} (1 + r_{e2} \bar{Y}_{rL})}{1 + r_{e2} \bar{Y}_{rL} + 10^4 q_{x1}}, \\ a_{42} &= \frac{10^4}{1 + r_{e2} \bar{Y}_{rL} + 10^4 q_{y1}}, \\ a_{43} &= \frac{10^{12} r_{e1} A_{43}}{(1 + r_{e2} \bar{Y}_{rL} + 10^4 q_{y1})^2 (1 + r_{e2} \bar{Y}_{rL} + 10^4 q_{y3})^2}, \\ a_{44} &= \frac{A_{44}}{(1 + r_{e2} \bar{Y}_{rL} + 10^4 q_{y1})^2 (1 + r_{e2} \bar{Y}_{rL} + 10^4 q_{y3})^2}, \\ A_{43} &= \frac{r_{e2}^2 q_{y2} q_{y3} \bar{Y}_{rL}^3}{10^8} + \frac{r_{e2}}{5 \cdot 10^3} \left(q_{y2} q_{y3} \left(q_{y1} + \frac{1}{10^4} \right) + \frac{r_{e2}}{2 \cdot 10^4} \bar{Y}_{0L} \right) \bar{Y}_{rL}^2 + \left(q_{y3} \left(\frac{r_{e2} \bar{Y}_{0L}}{5 \cdot 10^3} + q_{y2} \left(q_{y1} + \frac{1}{10^4} \right) \right) + \frac{r_{e2} \bar{Y}_{0L}}{5 \cdot 10^7} \right) \bar{Y}_{rL} + \left(q_{y3} + \frac{1}{10^4} \right)^2 \bar{Y}_{0L}. \\ A_{44} &= \left(-q_{y2} r_{e2}^4 \bar{Y}_{rL}^4 - 2 \cdot 10^4 \left(q_{y2} (q_{y3} + q_{y1} + \frac{1}{5 \cdot 10^3}) \bar{Y}_{rL} + \frac{\bar{Y}_{0L}}{2} \right) r_{e2}^3 \bar{Y}_{rL}^2 \right) + \left(-10^8 \left((q_{y1}^2 + (4q_{y3} + \frac{3}{5 \cdot 10^3}) q_{y1} + \frac{q_{y3}}{2 \cdot 10^3} + \frac{3}{5 \cdot 10^7}) q_{y2} \bar{Y}_{rL} + 2q_{y3} \bar{Y}_{0L} + \frac{\bar{Y}_{0L}}{5 \cdot 10^3} \right) r_{e2}^2 \bar{Y}_{rL} \right) + \left(-2 \cdot 10^{11} r_{e2} \left(q_{y3} + \frac{1}{10^4} \right) \left((q_{y1} + \frac{1}{5 \cdot 10^3}) (q_{y1} + \frac{1}{10^4}) q_{y2} \bar{Y}_{rL} + \frac{(q_{y3} + \frac{1}{10^4}) \bar{Y}_{0L}}{2} \right) \right) + \left(-10^{12} q_{y2} \left(q_{y3} + \frac{1}{10^4} \right) \left(q_{y1} + \frac{1}{10^4} \right)^2 \right). \end{aligned}$$

At R_C the Jacobian of the **co-existing steady state**.

$$J_{R_C} = \begin{bmatrix} a_{11} & a_{12} & 0 & 0 \\ a_{21} & a_{22} & 0 & 0 \\ a_{31} & 0 & a_{33} & a_{34} \\ 0 & a_{42} & a_{43} & a_{44} \end{bmatrix} \quad (\text{D.4})$$

where

$$\begin{aligned} a_{11} &= \zeta_x \left(\frac{p_{x1} \bar{Y}_{0C} + 1}{(\bar{X}_{0C} + p_{x1} \bar{Y}_{0C} + 1)^2} - p_{x2} \right) = -\zeta_x p_{x2}^2 \bar{X}_{0C}, \\ a_{12} &= -\zeta_x p_{x1} \frac{\bar{X}_{0C}}{(\bar{X}_{0C} + p_{x1} \bar{Y}_{0C} + 1)^2} = -\zeta_x p_{x1} p_{x2}^2 \bar{X}_{0C}, \\ a_{21} &= -\zeta_y p_{y1} \frac{\bar{Y}_{0C}}{(p_{y1} \bar{X}_{0C} + \bar{Y}_{0C} + 1)^2} = -\zeta_y p_{y1} p_{y2}^2 \bar{Y}_{0C}, \\ a_{22} &= \zeta_y \left(\frac{p_{y1} \bar{X}_{0C} + 1}{(p_{y1} \bar{X}_{0C} + \bar{Y}_{0C} + 1)^2} - p_{y2} \right) = -\zeta_y p_{y2}^2 \bar{Y}_{0C}, \end{aligned}$$

$$\begin{aligned}
a_{31} &= \frac{10^4}{(1+r_{e1}\bar{X}_{rC}+r_{e2}\bar{Y}_{rC})\left(\frac{10^4q_{x1}}{1+r_{e1}\bar{X}_{rC}+r_{e2}\bar{Y}_{rC}}+1\right)}, \\
a_{33} &= -\frac{10^4r_{e1}\bar{X}_{0C}}{(1+r_{e1}\bar{X}_{rC}+r_{e2}\bar{Y}_{rC})^2\left(\frac{10^4q_{x1}}{1+r_{e1}\bar{X}_{rC}+r_{e2}\bar{Y}_{rC}}+1\right)} + \frac{10^8q_{x1}r_{e1}\bar{X}_{0C}}{(1+r_{e1}\bar{X}_{rC}+r_{e2}\bar{Y}_{rC})^3\left(\frac{10^4q_{x1}}{1+r_{e1}\bar{X}_{rC}+r_{e2}\bar{Y}_{rC}}+1\right)^2} \\
&\quad - \frac{10^4q_{x2}q_{x3}r_{e1}\bar{X}_{rC}}{(1+r_{e1}\bar{X}_{rC}+r_{e2}\bar{Y}_{rC})^2\left(\frac{10^4q_{x3}}{1+r_{e1}\bar{X}_{rC}+r_{e2}\bar{Y}_{rC}}+1\right)^2} - \frac{q_{x2}}{(1+r_{e1}\bar{X}_{rC}+r_{e2}\bar{Y}_{rC})+1} \\
a_{42} &= \frac{10^4}{(1+r_{e1}\bar{X}_{rC}+r_{e2}\bar{Y}_{rC})\left(\frac{10^4q_{y1}}{1+r_{e1}\bar{X}_{rC}+r_{e2}\bar{Y}_{rC}}+1\right)}, \\
a_{34} &= -\frac{10^4r_{e2}\bar{X}_{0C}}{(1+r_{e1}\bar{X}_{rC}+r_{e2}\bar{Y}_{rC})^2\left(\frac{10^4q_{x1}}{1+r_{e1}\bar{X}_{rC}+r_{e2}\bar{Y}_{rC}}+1\right)} + \frac{10^8q_{x1}r_{e2}\bar{X}_{0C}}{(1+r_{e1}\bar{X}_{rC}+r_{e2}\bar{Y}_{rC})^3\left(\frac{10^4q_{x1}}{1+r_{e1}\bar{X}_{rC}+r_{e2}\bar{Y}_{rC}}+1\right)^2} \\
&\quad - \frac{10^4q_{x2}q_{x3}r_{e2}\bar{X}_{rC}}{(1+r_{e1}\bar{X}_{rC}+r_{e2}\bar{Y}_{rC})^2\left(\frac{10^4q_{x3}}{1+r_{e1}\bar{X}_{rC}+r_{e2}\bar{Y}_{rC}}+1\right)^2} \\
a_{42} &= \frac{10^4}{(1+r_{e1}\bar{X}_{rC}+r_{e2}\bar{Y}_{rC})\left(\frac{10^4q_{y1}}{1+r_{e1}\bar{X}_{rC}+r_{e2}\bar{Y}_{rC}}+1\right)}, \\
a_{43} &= -\frac{10^4r_{e1}\bar{Y}_{0C}}{(1+r_{e1}\bar{X}_{rC}+r_{e2}\bar{Y}_{rC})^2\left(\frac{10^4q_{y1}}{1+r_{e1}\bar{X}_{rC}+r_{e2}\bar{Y}_{rC}}+1\right)} + \frac{10^8q_{y1}r_{e1}\bar{Y}_{0C}}{(1+r_{e1}\bar{X}_{rC}+r_{e2}\bar{Y}_{rC})^3\left(\frac{10^4q_{y1}}{1+r_{e1}\bar{X}_{rC}+r_{e2}\bar{Y}_{rC}}+1\right)^2} \\
&\quad - \frac{10^4q_{y2}q_{y3}r_{e1}\bar{Y}_{rC}}{(1+r_{e1}\bar{X}_{rC}+r_{e2}\bar{Y}_{rC})^2\left(\frac{10^4q_{y3}}{1+r_{e1}\bar{X}_{rC}+r_{e2}\bar{Y}_{rC}}+1\right)^2} \\
a_{44} &= -\frac{10^4r_{e2}\bar{Y}_{0C}}{(1+r_{e1}\bar{X}_{rC}+r_{e2}\bar{Y}_{rC})^2\left(\frac{10^4q_{y1}}{1+r_{e1}\bar{X}_{rC}+r_{e2}\bar{Y}_{rC}}+1\right)} + \frac{10^8q_{y1}r_{e2}\bar{Y}_{0C}}{(1+r_{e1}\bar{X}_{rC}+r_{e2}\bar{Y}_{rC})^3\left(\frac{10^4q_{y1}}{1+r_{e1}\bar{X}_{rC}+r_{e2}\bar{Y}_{rC}}+1\right)^2} \\
&\quad - \frac{10^4q_{y2}q_{y3}r_{e2}\bar{Y}_{rC}}{(1+r_{e1}\bar{X}_{rC}+r_{e2}\bar{Y}_{rC})^2\left(\frac{10^4q_{y3}}{1+r_{e1}\bar{X}_{rC}+r_{e2}\bar{Y}_{rC}}+1\right)^2} - \frac{q_{y2}}{(1+r_{e1}\bar{X}_{rC}+r_{e2}\bar{Y}_{rC})+1}.
\end{aligned}$$

The elements of array given above are negative except a_{31} .

The characteristic polynomial at J_{R_C} is,

$$(\lambda_C^2 - (a_{11} + a_{22})\lambda_C + a_{11}a_{22} - a_{21}a_{12})(\lambda_C^2 - (a_{33} + a_{44})\lambda_C + a_{33}a_{44} - a_{34}a_{43}) = 0$$

The eigenvalues are,

$$\lambda_{1,2}^{\pm} = \frac{1}{2} \left(a_{11} + a_{22} \pm \sqrt{(a_{11} - a_{22})^2 - 4(a_{11}a_{22} - a_{21}a_{12})} \right)$$

and

$$\lambda_{3,4}^{\pm} = \frac{1}{2} \left(a_{33} + a_{44} \pm \sqrt{(a_{33} - a_{44})^2 - 4(a_{33}a_{44} - a_{34}a_{43})} \right)$$

Let us investigate the type of eigenvalues. In case $a_{11}a_{22} > a_{21}a_{12}$ and $a_{33}a_{44} > a_{34}a_{43}$, all four eigenvalues are negative and R_C is stable.

$$a_{11}a_{22} > a_{21}a_{12} \iff p_{x1}p_{y1} < 1$$

and $a_{33}a_{44} - a_{34}a_{43} = \frac{A_1A_2}{A_3}$ is positive

where

$$A_1 = 10^{20} (r_{e1}\bar{X}_{rC} + r_{e2}\bar{Y}_{rC} + 1),$$

$$A_2 = \frac{1}{10^{12}} (a_1 (a_2 + a_3 + a_4) q_{y2}) (a_6 + a_7),$$

$$\begin{aligned}
A_3 &= (r_{e1}\bar{X}_{rC} + r_{e2}\bar{Y}_{rC} + 10^4 q_{y3} + 1)^2 (r_{e1}\bar{X}_{rC} + r_{e2}\bar{Y}_{rC} + 10^4 q_{y1} + 1)^2 (r_{e1}\bar{X}_{rC} + r_{e2}\bar{Y}_{rC} + 10^4 q_{x3} + 1)^2 (r_{e1}\bar{X}_{rC} + r_{e2}\bar{Y}_{rC} + 10^4 q_{x1} + 1)^2, \\
a_1 &= \frac{(r_{e1}\bar{X}_{rC} + r_{e2}\bar{Y}_{rC} + 10^4 q_{y1} + 1)^2 q_{y2}}{10^8}, \\
a_2 &= \frac{r_{e1}^3 \bar{X}_{rC}^3}{10^4} + \bar{X}_{rC}^2 \left(q_{y3} + 2q_{x3} + \frac{3}{10^4} + \frac{3r_{e2}\bar{Y}_{rC}}{10^4} \right) r_{e1}^2, \\
a_3 &= 3\bar{X}_{rC} \left(\frac{r_{e2}^2 \bar{Y}_{rC}^2}{10^4} + \bar{Y}_{rC} \left(q_{y3} + q_{x3} + \frac{1}{5 \cdot 10^3} \right) r_{e2} + \frac{(2 \cdot 10^4 q_{x3} + 2)(q_{y3} + \frac{3}{2 \cdot 10^4})}{3} \right) r_{e1}, \\
a_4 &= (2r_{e2}\bar{Y}_{rC} + 2 \cdot 10^4 q_{x3} + 2) \left(\frac{r_{e2}^2 \bar{Y}_{rC}^2}{2 \cdot 10^4} + \bar{Y}_{rC} \left(q_{y3} + \frac{1}{10^4} \right) r_{e2} + \frac{q_{y3}}{2} + \frac{1}{2 \cdot 10^4} \right), \\
a_5 &= \bar{Y}_{0C} \left(\frac{r_{e1}\bar{X}_{rC}}{10^4} + \frac{r_{e2}\bar{Y}_{rC}}{10^4} + q_{y3} + \frac{1}{10^4} \right)^2 r_{e2} (r_{e1}\bar{X}_{rC} + r_{e2}\bar{Y}_{rC} + 10^4 q_{x3} + 1), \\
a_6 &= \left(\frac{r_{e1}\bar{X}_{rC}}{10^4} + \frac{r_{e2}\bar{Y}_{rC}}{10^4} + q_{x1} + \frac{1}{10^4} \right)^2 q_{x2}, \\
a_7 &= \frac{q_{y2} r_{e1} \bar{X}_{0C} (r_{e1}\bar{X}_{rC} + r_{e2}\bar{Y}_{rC} + 10^4 q_{y1} + 1)^2 (r_{e1}\bar{X}_{rC} + r_{e2}\bar{Y}_{rC} + 10^4 q_{x3} + 1)^2 \left(\frac{r_{e1}\bar{X}_{rC}}{10^4} + \frac{r_{e2}\bar{Y}_{rC}}{10^4} + q_{y3} + \frac{1}{10^4} \right)}{10^{12}}.
\end{aligned}$$

Hence, R_C is stable for $p_{x1}p_{y1} < 1$ i.e. $p_{x1} < \gamma$ and $p_{y1} < \gamma^{-1}$.

In conclusion, the stability of the steady states in the reduced model is one-to-one correspondence with those of the stem cell submodel.

References

- [1] Abkowitz JL, Catlin SN, McCallie MT, Gutterop P Evidence that the number of hematopoietic stem cells per animal is conserved in mammals. *Blood*, 03-0822.
- [2] Adamson J. 1974 The relationship of erythropoietin and iron metabolism to red blood cell production in humans. *Semin. Oncol.* 21, 9-15.
- [3] Adimy M, Crauste F, Ruan S. 2006. Modelling hematopoiesis mediated by growth factors with applications to periodic haematological diseases. *Bull Math Biol* 68:2321–2351.
- [4] Adimy M, Crauste F. 2007. Modelling and asymptotic stability of a growth factor-dependent stem cells dynamics model with distributed delay. *Discrete and Continuous Dynamical Systems* 1(1).
- [5] Andersen M, Hasselbalch H, Kjaer L, Skov V and Ottesen JT. 2020. Global dynamics of healthy and cancer cells competing in the hematopoietic system, *Mathematical Biosciences* 626, 1-15.
- [6] Andersen M, Sajid Z, Pedersen RK, Gudmand-Hoeyer J, Ellervik C, Skov V, Kjær L, Pallisgaard N, Kruse TA, Thomassen M, Troelsen J, Hasselbalch HC , Ottesen JT. 2017. Mathematical modelling as a proof of concept for MPNs as a human inflammation model for cancer development.
- [7] Angulo O, Crauste F, López-Marcos JC. 2018. Numerical integration of an erythropoiesis model with explicit growth factor dynamics. *Journal of Computational and Applied Mathematics*, 330: 770-782.
- [8] Banks HT, Bliss KM, Tran H. 2012. Modelling Red Blood Cell and Iron Dynamics in Patients with Chronic Kidney Disease. North Carolina State University. Center for Research in Scientific Computation.
- [9] Belair J, Mackey MC, Mahaffy JM. 1995. Age- structured and two delay models for erythropoiesis. *Math. Biosci.* 128, 317-346.
- [10] Bradford G, Williams B, Rossi R, Bertoncetto I. 1997. Quiescence, cycling and turnover in the primitive haematopoietic stem cell compartment. *Exper. Hematol.* 25. 445-453.
- [11] Campbell PJ, Green AR. 2006. The myeloproliferative disorders. *N. Engl. J. Med.* 355: 2452–2466.

- [12] Carneskog J, Kutti J, Wadenvik H, Lundberg PA, Lindstedt G. 1998. Plasma erythropoietin by high-detectability immune-radiometric assay in untreated and treated patients with Polycythemia vera and essential thrombocythemia. *Eur J Haematol*, 60: 278-82.
- [13] Colijn C, Mackey MC. 2005. A mathematical model of hematopoiesis—I. Periodic chronic myelogenous leukemia. *Journal of Theoretical Biology*. 237: 117-132.
- [14] Crauste F, Pujo-Menjouet L, Genieys S, Molina C, Gandrillon O. 2008. Adding self-renewal in committed erythroid progenitors improves the biological relevance of a mathematical model of erythropoiesis. *Journal of Theoretical Biology*. 250: 322–338.
- [15] Curto-Garcia N, Harrison C and McLornan DP. 2000. Bone marrow niche dysregulation in myeloproliferative neoplasms. *Haematologica*, Volume 105(5): 1189-1200.
- [16] Demin I, Crauste F, Gandrillon O, Volpert V. 2010. A multi-scale model of erythropoiesis. *Journal of Biological Dynamics*. 4:1, 59-70.
- [17] Dingli D, Michor F. 2006. Successful Therapy Must Eradicate Cancer. *Stem Cells*, 24(12): 2603.
- [18] Erslev AJ. 1990. Production of erythrocytes. *Haematology*, pages 389–397.
- [19] Foo J, Drummond MW, Clarkson B, Holyoake T, Michor F. 2009. Eradication of Chronic Myeloid Leukemia Stem Cells: A Novel Mathematical Model predicts no therapeutic benefit of adding G-CSF to Imatinib. *PLoS Comput Biol* 5(9).
- [20] Fuerterer DH, Kappel F, Thijssen S, Levin N, Kotanko P. 2013. A model of erythropoiesis in adults with sufficient iron availability. *J. Math. Biol.* 66: 1209–1240.
- [21] Fuerterer DH, Kappel F, Zhang H, Thijssen S, Kotanko P. 2017. Prediction of hemoglobin levels in individual hemodialysis patients by means of a mathematical model of erythropoiesis. *Plos One*.
- [22] Giesl P and Hafstein S. 2015. Review on computational methods for Lyapunov functions. *textitDiscrete and continuous dynamical systems*, vol 20.
- [23] Griesshammer M, Kiladjian JJ, Besses C. 2019 Thromboembolic events in polycythemia vera. *Annals of Hematology* 98:1071–1082.

- [24] Granziero L, Ghia P, Circosta P, Gottardi D, Strola G, Geuna M, Montagna L, Piccoli P, Chilosi M, Caligaris-Cappio F. 2001. Survivin is expressed on CD40 stimulation and interfaces proliferation and apoptosis in B-cell chronic lymphocytic leukemia. *Blood* 97, 9: 2777-2783.
- [25] Haeno H, Levine RL, Gilliland DG, Michor F. 2009. A progenitor cell origin of myeloid malignancies. *Proceedings of the National Academy of Sciences of the United States of America*, 106(39): 16616-16621.
- [26] Hasselbalch HC. 2012. Perspectives on chronic inflammation in essential thrombocythemia , polycythemia vera , and myelofibrosis: is chronic inflammation a trigger and driver of clonal evolution and development of accelerated atherosclerosis and second cancer? *Blood*, **119**: 3219–3226.
- [27] Hasselbalch HC. 2013. Chronic inflammation as a promotor of mutagenesis in essential thrombocythemia, polycythemia vera and myelofibrosis. A human inflammation model for cancer development? *Leukemia Research*, 37: 214–220.
- [28] Iiyama M, Kakihana K, Kurosu T, Miura O. 2006. Reactive oxygen species generated by hematopoietic cytokines play roles in activation of receptor- mediated signaling and in cell cycle progression. *Cellular Signalling* 18 , 2: 174-182.
- [29] Jelkmann W. 2013. Physiology and pharmacology of erythropoietin. *Transfus Med Hemother*, 40: 302–309.
- [30] Johansson P, Andreasson B. 2006. Hydroxyurea therapy increases plasma erythropoietin in patients with essential thrombocythaemia or polycythaemia vera. *Clin. Lab. Haem.* 28: 233-236.
- [31] Kim YM, Koo BK, Jeong HW, Yoon MJ, Song R, Shin J, Jeong DC, Kim SH, Kong YY. 2008. Defective Notch activation in micro-environment leads to myeloproliferative disease, *Blood*. 112(12): 4628-38 .
- [32] King KY, Matatall KA, Shen CC, Goodell MA, Swierczek SI, Prchal JT. 2015. Comparative long-term effects of interferon α and hydroxyurea on human hematopoietic progenitor cells, *International Society for Experimental Hematology*. 43: 912–918.
- [33] Krantz SB. 1991. Erythropoietin. *Blood*. 77(3): 419–434.
- [34] Kristinsson SY, Landgren O, Samuelsson J. 2010. Autoimmunity and the risk of myeloproliferative neoplasms. *Haematologica* 95: 1216–1220.
- [35] Lichtman MA, Beutler E, Kipps TJ, Seligsohn U, Kaushansky K, Prchal JT. 2006. *Williams Hematology*. McGraw-Hill: New York, NY, USA.

- [36] Lilienthal P, Tetschke P, Schalk E, Fischer T, Sager S. 2020 Optimized and Personalized Phlebotomy Schedules for Patients Suffering From Polycythemia Vera. *Frontiers in physiology*. *Frontiers in Physiology*.
- [37] Loeffler M, Pantel K, Wulff H, Wichmann HE. 1989. A mathematical model of erythropoiesis in mice and rats. Part 1. Structure of the model. *Cell Tissue Kinetics* 22: 13–30.
- [38] Mahaffy JM, Belair J, Mackey MC. 1998. Hematopoietic model with moving boundary condition and state dependent delay: Applications in Erthropoiesis. *J. theor. Biol.* 190: 135-146.
- [39] Mahaffy JM. 1999. Age-structured modelling of haematopoiesis. San Diego State University.
- [40] Mahaffy JM, Polk SW, Roeder RK. 1999. An age-structured model for erythropoiesis following a phlebotomy. Tech. Rep. CRM-2598, Department of Mathematical Sciences, San Diego State University, San Diego, CA 92182-0314.
- [41] Marciniak-Czochra A, Stiehl T, Ho AD, Jäger W, Wagner W. 2009. Modelling of asymmetric cell division in hematopoietic stem cells—regulation of self-renewal is essential for efficient repopulation, *Stem Cells Dev*, 18(3) (2009), 377-85.
- [42] Meiss JD. 2007. *Differential Dynamical Systems*.
- [43] Michiels JJ, Schroyens W, Lindemans J, Kate FWJT, Lam KH, De Raeve H. 2014. The Erythrocyte count on top of bone marrow histology discriminates Essential Thrombocythemia and Polycythemia Vera in *JAK2V617F* mutated prefibrotic Myeloproliferative Neoplasm with no or minor splenomegaly. *Journal of Haematology and Thromboembolic Diseases*, 2:4.
- [44] Mullally A, Poveromo L, Schneider RK, Al- Shahrour F, Lane SW, Ebert BL. 2012. Distinct roles for long-term hematopoietic stem cells and erythroid precursor cells in a murine model of *Jak2V617F*-mediated polycythemia vera. *Blood*, 120(1): 166-172.
- [45] Ottesen JT, Sajid Z, Pedersen RK, Gudmand-Hoeyer J, Bangsgaard KO, Skov V, Kjær L, Knudsen TA, Pallisgaard N, Kruse TA, Thomassen M, Troelsen J, Hasselbalch HC, Andersen M. 2019. Bridging blood cancers and inflammation: The reduced Cancitis model. *Journal of Theoretical Biology* 465: 90-108.
- [46] Pinho S, Frenette PS. 2019 Haematopoietic stem cell activity and interactions with the niche. *Molecular Cell Biology*. Volume 20.

- [47] Pantel, K, Loeffler M, Bungart B, Wichmann HE. 1990. A mathematical model of erythropoiesis in mice and rats. Part 4: Differences between bone marrow and spleen Cell Proliferation, July 1990, **23**(4):283-297.
- [48] Rodak BF, Fritsma GA, Doig K. 2008. Hematology: Clinical principles and applications.
- [49] Rovida E, Marzi I, Cipolleschi MG, Sbarba PD. 2014. One more stem cell niche: how the sensitivity of chronic myeloid leukemia cells to imatinib mesylate is modulated within a “hypoxic” environment, *Hypoxia*, 1-10.
- [50] Sajid Z, Andersen M, Ottesen JT. 2019. Mathematical analysis of the Cancitis model and the role of inflammation in blood cancer progression. *MBE*, 16(6): 8268–8289.
- [51] Santar CG, Desmond R, Feng X, Bat T, Chen J, Heuston E, Mizukawa B, Mulloy JC, Bodine DM, Larochelle A, Dunbar CE. 2015. Functional Niche Competition Between Normal Hematopoietic Stem and Progenitor Cells and Myeloid Leukemia Cells. *Stem Cells*, 33(12): 3635-42.
- [52] Silva M, Grillot D, Benito, Richard C, Nunez G, Fernandez- Luna J. 1996. Erythropoietin can promote erythroid progenitor survival by repressing apoptosis through bcl-1 and bcl-2. *Blood* 88, 1576-1582.
- [53] Stiehl T, Baran N, Ho AD, Marciniak-Czochra A. 2015. Cell division patterns in acute myeloid leukemia stem-like cells determine clinical course: A model to predict patient survival. *Cancer Research*. 75(6):940-949.
- [54] Testa U. 2004. Apoptotic mechanism in the control of erythropoiesis. *Leukemia* 18, 7: 1176-1199.
- [55] Tetschke M, Lilienthal P, Pottgiesser T, Fischer T, Schalk E, Sager S. 2018. Mathematical Modeling of RBC Count Dynamics after Blood Loss. *Processes* 6, 157.
- [56] Walenda T, Stiehl T, Braun H, Frobel J, Ho AH, Schroeder T, Goecke TW, Rath B, Germing U, Marciniak-Czochra A, Wagner W. 2014 Feedback signals in Myelodysplastic Syndromes: Increased Self-Renewal of the Malignant Clone Suppresses Normal Hematopoiesis. *PLoS Computational Biology*, 10(4).
- [57] Walkley C, Shea J, Sims N, Purton L, Orkin S. 2007. Rb regulates interactions between hematopoietic stem cells and their bone marrow micro-environment, *Cell*, 129: 1081-95.

- [58] Wan PX, Wang BW, Wang ZC. 2015 Importance of the stem cell microenvironment for ophthalmological cell-based therapy. *World J Stem Cells* 7(2): 448-460.
- [59] Weitzman JB, Fiette L, Matsuo K, Yaniv M. 2000. JunD protects cells from p53- dependent senescence and apoptosis. *Mol Cell* 6, 5: 1109-1119.
- [60] Wichmann HE, Loeffler M, Pantel K, Wulff HH. 1989. A mathematical model of erythropoiesis in mice and rats. Part 2. Stimulated erythropoiesis. *Cell Tissue Kinetics* 22:31–49.
- [61] Wulff H, Wichmann HE, Pantel K, Loeffler M. 1989. A mathematical model of erythropoiesis in mice and rats. Part 3: suppressed erythropoiesis. *Cell Tissue Kinetics* 22:51–61.
- [62] Zhang J, Fleischman AG, Wodarz D. 2017. Determining the role of inflammation in the selection of *JAK2* mutant cells in myeloproliferative neoplasms. *J. Theor. Biol.*, 425: 43–52.
- [63] Zauli G, Vitale M, Falcieri E, Gibellini D, Bassini A, Celeghini C, Columbaro M, Capitani S. 1997. In vitro senescence and apoptotic cell death of human megakaryocytes. *Blood* 90, 2234-2243.

CHAPTER 5

Mathematical model of pathological dynamics of thrombopoiesis with multiple TPO feedbacks

5.1 Introduction

In this chapter, we present a mechanism-based mathematical model of essential thrombocythemia (ET). ET is characterized by the excessive production of platelets. There are several arguments behind the pathophysiological dynamics of platelets in ET patients. One of them is that the thrombopoietin (TPO) serum levels are significantly increased compared with normal subjects despite a high number of platelets. TPO is the principal growth hormone that regulates megakaryocyte and platelet development. It stimulates the differentiation and maturation of megakaryocytes, inhibits their death rate, and stimulates the release of platelets via fragmentation of megakaryocytes. Recent studies show that TPO receptors increase the self-renewal of hematopoietic stem cells, especially under stress and inflammation. [32]. TPO is internalized, degraded and removed from the peripheral blood primarily by platelets [70; 99]. The relation between TPO and platelets is not yet been investigated in ET patients.

In case of pathological conditions, TPO is reported to have a significant effect. In [66; 113], TPO is investigated as a stimulating agent of megakaryocytes, which ultimately increases platelet production in thrombocytopenia. It may hypothesize that the feedback loop between TPO and megakaryocytes is disturbed in patients with ET [98]. An inadequate binding of TPO to its defective receptor may increase TPO serum levels in ET compared to a healthy individual [51; 69]. Hence, the increased TPO levels might be the consequence of an abnormal platelet population and disease progression in ET. Moreover, a few pieces of evidence show that TPO stimulates blast colony formation

in samples from approximately 50% of patients with acute myeloid leukemia (AML) [82], and enhanced proliferation of a megakaryocytic leukemic cell line [84]. It is also investigated that TPO induces cell cycle activation and may protect AML blasts from programmed cell death [114]. However, there are some contradiction, for instance, in [37], the argument that TPO affects tumor cells is not supported [37].

We develop a novel mathematical model based on the following biologically motivated assumption,

Assumptions:

1. A1: TPO stimulates both healthy and malignant megakaryocyte.
2. A2: TPO inhibits the death rate of healthy megakaryocytes and malignant platelets.
3. A3: TPO stimulates the self-renewal of hematopoietic and malignant stem cells.
4. A4: TPO is degraded by the platelet receptors, in addition to natural degradation.

The other included biological assumptions are already described in previous chapters, for example, niche feedback etc.

Like the previous models, the ET model incorporates the competition between healthy and malignant stem cells with multiple TPO feedback on both cell lines. In contrast to Cancitis and ET models, this novel model consists of three cell types, i.e., stem cells, megakaryocytes and platelets. Moreover, the model contains asymmetrical structure, i.e., TPO affects on healthy and malignant cells through different mechanisms. We have investigated a set of interesting questions: Which parameters govern the dynamics of the system? How does TPO involve in the progression of ET? How does the stem cell dynamic control the disease onset? What are the possible novel intervention strategies for ET patients? Which parameters can be targeted for a good prognosis of disease?

5.2 ET model

In this section, we present our novel mathematical ET model. In the ET model, the hematopoietic stem cells (HSC) proliferate into healthy megakaryocytes (MEG) and malignant stem cells (MSC) proliferate into malignant megakaryocytes (MMEG). MEG further differentiates into platelets (PLT), whereas MMEG differentiates into malignant platelets (MPLT). In addition, the multiple feedback of TPO with the rest of the dynamics is considered.

ET model consists of seven ordinary non-linear differential equations, the number of HSC (x_0), the number of MEG (x_m), the number of platelets (x_p) the number of MSC (y_0), the number of MMEG (y_m), the number of MPLT (y_p) and the concentration of TPO (T). The conceptual model is illustrated in Fig. 5.2.1. The ET model is inspired by mathematical models given in [7; 67] and reads

$$\frac{dx_0}{dt} = (r_x T \phi_x - d_{x0} - a_x)x_0, \quad (5.2.1a)$$

$$\frac{dy_0}{dt} = (r_y T \phi_y - d_{y0} - a_y)y_0, \quad (5.2.1b)$$

$$\frac{dx_m}{dt} = a_x A_x(T)x_0 - b_{xp}x_m - d_{xm}(T)x_m, \quad (5.2.1c)$$

$$\frac{dy_m}{dt} = a_y A_y(T)y_0 - b_{yp}y_m - d_{ym}y_m, \quad (5.2.1d)$$

$$\frac{dx_p}{dt} = a_{xp}b_{xp}x_m - d_{xp}x_p, \quad (5.2.1e)$$

$$\frac{dy_p}{dt} = a_{yp}b_{yp}y_m - d_{yp}(T)y_p, \quad (5.2.1f)$$

$$\frac{dT}{dt} = p - k_1 T - k_2 x_p T, \quad (5.2.1g)$$

The rate of self-renewal is denoted as r_x and r_y for HSC and MSC respectively. It is believed that the self-renewal is inhibited by regulatory niche feedback [122], this inhibition is implemented here through Michaelis-Menten-like functions $\phi_x(x_0, y_0)$ and $\phi_y(x_0, y_0)$ [66; 111; 121]. The inhibitory effect on the self-renewal of HSC is captured by feedback constants c_{xx} and c_{xy} , while the corresponding effect on the self-renewal of MSC is captured by c_{yx} and c_{yy} . Thus, we define

$$\phi_x = \frac{1}{1 + c_{xx}x_0 + c_{xy}y_0}, \quad \phi_y = \frac{1}{1 + c_{yx}x_0 + c_{yy}y_0}, \quad (5.2.2)$$

Further, we assume that TPO stimulates the self-renewal of the stem cells (assumption 3). The stem cells die with rates d_{x0} and d_{y0} .

The parameter a_x denotes the rate at which the HSC differentiates into MEG, while a_y represents the rate for MSC transforming to MMEG. The progenitor cells are considered stages between stem cells and mature cells and are accounted for by amplification factors A_x and A_y for HSC and MSC, respectively. Considering assumption 1, we take these amplification factors dependent on TPO as TPO is thought to stimulate the production of megakaryocytes

$$A_x(T) = \delta_{x1} \frac{T}{1 + \delta_{x2}T}, \quad A_y(T) = \delta_{y1} \frac{T}{1 + \delta_{y2}T}, \quad (5.2.3)$$

The parameters $a_{xp}b_{xp}$ and $a_{yp}b_{yp}$ denotes the production of platelets from megakaryocytes. It is hypothesized that an increase in the growth factor concentration TPO leads to a decrease in the apoptosis rate of MEG and MPLT. Therefore, according to assumption 2, we assume that $d_{xm}(T)$ and $d_{yp}(T)$ are decreasing function of T , by choosing

$$d_{xm}(T) = \eta_{x1} \frac{1}{1 + \eta_{x2}T}, \quad d_{yp}(T) = \eta_{y1} \frac{1}{1 + \eta_{y2}T}. \quad (5.2.4)$$

The death rate of PLT is denoted by d_{xp} . The parameters p is the baseline production for TPO, whereas k_1 denotes the natural degradation of TPO. Considering assumption 4, we take the parameter k_2 eliminating TPO through platelet receptors.

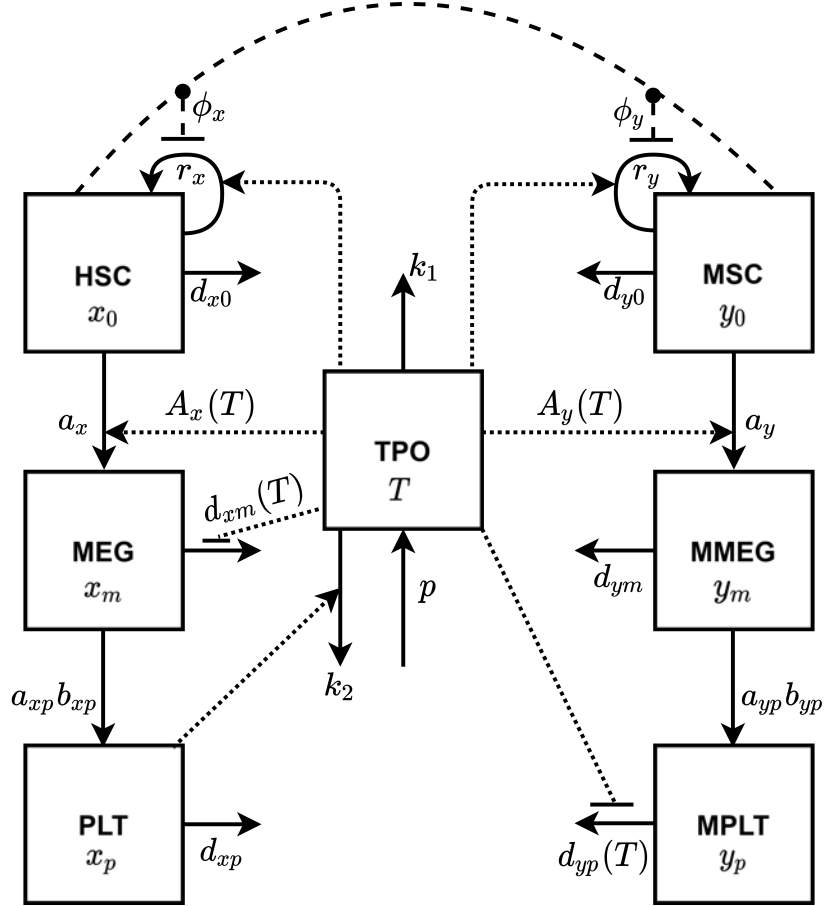


Fig. 5.2.1 The boxes illustrate the compartments of the ET model. Solid arrows represent the rates of the flows between and out of these compartments. The boxes illustrate the compartments of the PV model. The full arrows represent the rates of the flows between and out of these compartments. Black stipulated lines (ϕ_x and ϕ_y , respectively) represent the interaction between bone marrow niches and stem cells. Stem cells (HSC and MSC) may self renew (r_x and r_y), die (d_{x0} and d_{y0}) or differentiate (a_x , a_y), and megakaryocytes (x_m , y_m) are produced (with rates $a_x A_x(T)$ and $a_y A_y(T)$). The megakaryocytes may die with rates d_{xm} and d_{ym} or shed into platelets x_p and y_p with rate $a_{xp} b_{xp}$ and $a_{yp} b_{yp}$. Platelets die with rates d_{xp} and $d_{yp}(T)$. T stimulates the proliferation rates of megakaryocytes and inhibits the death rate of x_m . Black dotted lines present the interaction of TPO with the remaining model. TPO is produced with rate p and degraded with rate k_1 in addition, x_p stimulates the degradation of TPO with k_2 . TPO stimulates the self-renewal of stem cells while inhibiting d_{yp} .

The default parameter values are summarized in table 5.1 and a typical ET model is shown in Figure 5.2.2.

Table 5.1 Default parameter values of the ET model.

Parameter	Value	Unit	Explanation
r_x	$8.7 \cdot 10^{-4}$	day ⁻¹	Self-renewal rate of HSC
r_y	$1.3 \cdot 10^{-3}$	day ⁻¹	Self-renewal rate of MSC
a_x	$1.1 \cdot 10^{-5}$	day ⁻¹	Differentiation rate of HSC
a_y	$1.1 \cdot 10^{-5}$	day ⁻¹	Differentiation rate of MSC
d_{x_0}	$2 \cdot 10^{-3}$	day ⁻¹	Death rate of HSC
d_{y_0}	$2 \cdot 10^{-3}$	day ⁻¹	Death rate of MSC
c_{xx}	$5.6 \cdot 10^{-5}$	-	Inhibition by HSC on HSC
c_{yx}	$5.2 \cdot 10^{-5}$	-	Inhibition by HSC on MSC
c_{xy}	$5.4 \cdot 10^{-5}$	-	Inhibition by HSC on MSC
c_{yy}	$5.0 \cdot 10^{-5}$	-	Inhibition by MSC on MSC
δ_{x1}	$9 \cdot 10^4$	-	Factor stimulating production of MEG
δ_{x2}	$1 \cdot 10^{-2}$	-	Factor affecting production of MEG
η_{x1}	$2 \cdot 10^{-2}$	-	Factor affecting removal of HMEG
η_{x2}	$9.4 \cdot 10^{-3}$	-	Factor affecting removal of MEG
d_{xp}	$1.15 \cdot 10^{-1}$	day ⁻¹	Death rate of PLT
b_{xp}	$1 \cdot 10^{-1}$	day ⁻¹	Differentiation rate of PLT
a_{xp}	$3 \cdot 10^3$	-	Number of fragmented PLT per MEG
δ_{y1}	$9 \cdot 10^4$	-	Factor stimulating production of MMEG
δ_{y2}	$1 \cdot 10^{-1}$	-	Factor affecting production of MMEG
η_{y1}	$1 \cdot 10^{-1}$	-	Factor affecting removal of MPLT
η_{y2}	$9.9 \cdot 10^{-3}$	-	Factor affecting removal of MPLT
d_{ym}	$5 \cdot 10^{-2}$	day ⁻¹	Death rate of MMEG
b_{yp}	$5 \cdot 10^{-2}$	day ⁻¹	Differentiation rate of MPLT
a_{yp}	$8 \cdot 10^2$	-	Number of fragmented MPLT per MMEG
p	300	day ⁻¹	Production rate of TPO
k_1	0.4	day ⁻¹	Degradation rate of TPO
k_2	10^{-11}	day ⁻¹	Degradation rate of TPO by platelets

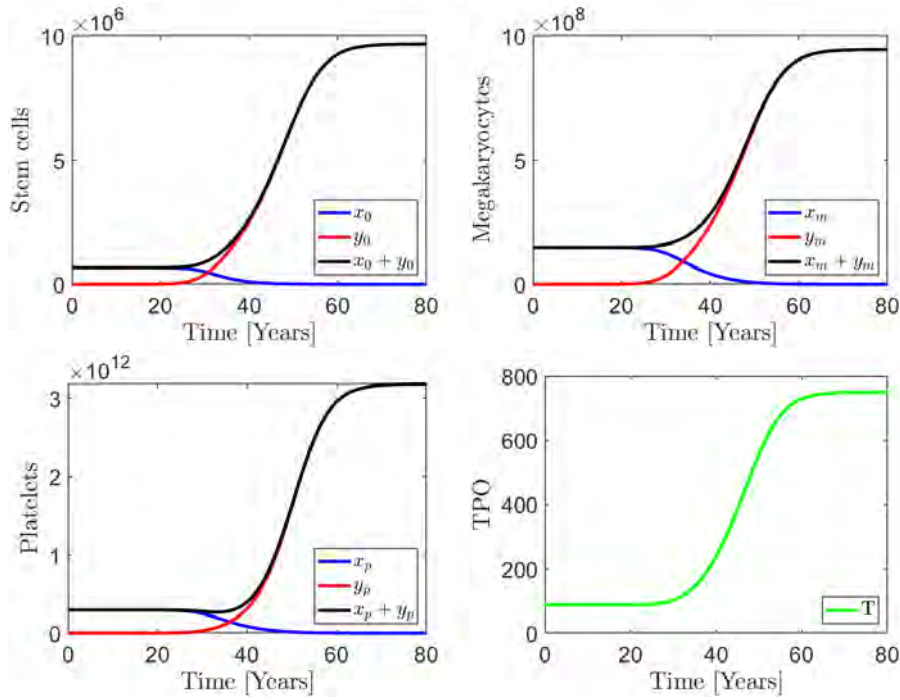


Fig. 5.2.2 An ET model shows the progression of the disease with initial conditions, $(x_0, y_0, x_m, y_m, x_p, y_p, T) = (6.68 \cdot 10^5, 1, 1.48 \cdot 10^8, 0, 2.97 \cdot 10^{11}, 0, 88.81)$ at $t = 0$. Red curves denote malignant cells, blue are healthy hematopoietic cells and black curves are the sum of the cells. Time is plotted on the x -axis. In the above-left panel, the evolution of malignant stem cell count is shown, whereas in the above-right panel, the development of mature malignant megakaryocyte cell count is shown. The below-left panel shows the evolution of malignant platelet count. In the early phase, healthy cells are large in number than malignant cells. However, after some years, when disease evolves, malignant cells become dominant, leading to the destruction of healthy cells. The below right panel shows the increase in TPO concentration over time.

5.3 Results

This section presents an analytical investigation of the model. Furthermore, we perform sensitivity analysis and produce a set of bifurcation diagrams. ET model is validated using clinical data. The section also suggests a few *in silico* trials showing novel intervention strategies.

5.3.1 Existence of steady states

Based on physiology, we consider the number of cells and concentrations to be non-negative. The parameters are assumed to be positive. The steady states $(\bar{x}_0, \bar{y}_0, \bar{x}_m, \bar{y}_m, \bar{x}_p, \bar{y}_p, \bar{T})$ for system of Eqs 5.2.1 fulfil,

$$(r_x \phi_x \bar{T} - d_{x0} - a_x) \bar{x}_0 = 0, \quad (5.3.1a)$$

$$(r_y \phi_y \bar{T} - d_{y0} - a_y) \bar{y}_0 = 0, \quad (5.3.1b)$$

$$\bar{x}_m = \frac{a_x A_x(\bar{T})}{b_{xp} + d_{xm}(\bar{T})} \bar{x}_0, \quad (5.3.1c)$$

$$\bar{y}_m = \frac{a_y A_y(\bar{T})}{b_{yp} + d_{ym}} \bar{y}_0, \quad (5.3.1d)$$

$$\bar{x}_p = \frac{a_{xp} b_{xp}}{d_{xp}} \bar{x}_m, \quad (5.3.1e)$$

$$\bar{y}_p = \frac{a_{yp} b_{yp}}{d_{yp}(\bar{T})} \bar{y}_m, \quad (5.3.1f)$$

$$\bar{T} = \frac{p}{k_1 + k_2 \bar{x}_p}, \quad (5.3.1g)$$

The admissible steady states can be classified as,

- a hematopoietic steady state is defined when $\bar{y}_0 = \bar{y}_m = \bar{y}_p = 0$.
- a malignant steady state is defined when $\bar{x}_0 = \bar{x}_m = \bar{x}_p = 0$.
- a co-existing steady state is defined when $\bar{x}_0 > 0, \bar{y}_0 > 0, \bar{x}_m > 0, \bar{y}_m > 0, \bar{x}_p > 0, \bar{y}_p > 0$.

Proposition 5.3.1. A trivial steady state D_0 always exists,

$$D_0 = \left(0, 0, 0, 0, 0, 0, \frac{p}{k_1} \right) \quad (5.3.2)$$

Proof. Substituting $\bar{x}_0 = \bar{y}_0 = 0$ in Eqs. (5.3.1a-5.3.1g), $\bar{T} = \frac{p}{k_1}$ and the remaining variables at trivial steady state are zero. \square

Proposition 5.3.2. For $\bar{T}_H > \frac{d_{x0} + a_x}{r_x}$, a unique hematopoietic steady state D_H exists if and only if $\frac{a_x + d_{x0}}{r_x} < \frac{p}{k_1}$.

Proof. From Eq. 5.3.1,

$$\bar{x}_{0H} = \frac{1}{c_{xx}} \left(\frac{r_x \bar{T}_H}{d_{x0} + a_x} - 1 \right), \quad (5.3.3a)$$

$$\bar{x}_{mH} = \frac{a_x A_x(\bar{T}_H)}{b_{xp} + d_{xm}(\bar{T}_H)} \bar{x}_{0H}, \quad (5.3.3b)$$

$$\bar{x}_{pH} = \frac{a_{xp} b_{xp}}{d_{xp}} \bar{x}_{mH}, \quad (5.3.3c)$$

$$\bar{T}_H = \frac{p}{k_1 + k_2 \bar{x}_{pH}}. \quad (5.3.3d)$$

The admissibility of steady state necessitates the following inequality to be fulfilled,

$$\bar{T}_H > \frac{d_{x0} + a_x}{r_x}.$$

Substitute Eq. 5.3.3d in Eq. 5.3.3c, and use the resulting expression and Eq. 5.3.3a in Eq. 5.3.3b, we obtain a fourth order polynomial equation in \bar{x}_{mH} ,

$$\epsilon_{0H}\bar{x}_{mH}^4 + \epsilon_{1H}\bar{x}_{mH}^3 + \epsilon_{2H}\bar{x}_{mH}^2 + \epsilon_{3H}\bar{x}_{mH} + \epsilon_{4H} = 0 \quad (5.3.4)$$

where

$$\epsilon_{0H} = (k_2 a_{xp} b_{xp})^3 c_{xx} (a_x + d_{x0}) (\eta_{x1} + b_{xp}),$$

$$\epsilon_{1H} = b_{xp}^2 c_{xx} ((3k_1 + p(\eta_{x2} + \delta_{x2})) b_{xp} + \eta_{x1} (p\delta_{x2} + 3k_1)) (k_2 a_{xp})^2 (a_x + d_{x0}) d_{xp},$$

$$\epsilon_{2H} = c_{xx} ((3k_1^2 + 2p(\eta_{x2} + \delta_{x2})k_1 + p^2 \eta_{x2} \delta_{x2}) b_{xp} + (2(p\delta_{x2} + \frac{3}{2}k_1)) \eta_{x1} k_1) (a_x + d_{x0}) b_{xp} k_2 a_{xp} d_{xp}^2 + p\delta_{x1} a_x (b_{xp} k_2 a_{xp})^2 (a_x + d_{x0}) d_{xp},$$

$$\epsilon_{3H} = (\delta_{x2} p + k_1) c_{xx} ((\eta_{x2} p + k_1) b_{xp} + \eta_{x1} k_1) (a_x + d_{x0}) k_1 d_{xp}^3 + 2a_{xp} ((a_x + d_{x0}) k_1 + p\eta_{x2} r_x (\frac{a_x + d_{x0}}{r_x} - 1)) \delta_{x1} b_{xp} k_2 a_{xp} d_{xp}^2,$$

$$\epsilon_{4H} = -(-(a_x + d_{x0}) k_1 + p r_x) (\eta_{x2} p + k_1) a_{xp} p \delta_{x1} d_{xp}^3.$$

ϵ_{0H} , ϵ_{1H} and ϵ_{2H} are always positive whereas ϵ_{3H} and ϵ_{4H} can be positive or negative.

Using Descartes rule of sign, some of the cases are given in Table. 5.2.

Table 5.2 Descartes Rule of sign

Cases	ϵ_{0H}	ϵ_{1H}	ϵ_{2H}	ϵ_{3H}	ϵ_{4H}	Roots
1 st	+	+	+	+	-	1 pos real root
2 nd	+	+	+	-	-	1 pos real root
3 rd	+	+	+	+	+	No pos real root
4 th	+	+	+	-	+	0 or 2 pos real roots

Consider the 1st and 2nd cases where $\epsilon_{4H} < 0$ guarantees a unique positive real root.

$$\epsilon_{4H} < 0 \text{ implies } \frac{a_x + d_{x0}}{r_x} < \frac{p}{k_1}.$$

Consider 4th case where $\epsilon_{3H} < 0$ and $\epsilon_{4H} > 0$. $\epsilon_{3H} < 0$ if and only if $\frac{d_{x0} + a_x}{r_x} >$

$$\frac{a_x p^2 \delta_{x1} b_{xp} k_2 a_{xp}}{c_{xx} d_{xp} k_1^2 ((\eta_{x1} + b_{xp}) k_1 + p((\eta_{x2} + \delta_{x2}) b_{xp} + \eta_{x1} \delta_{x2})) + p b_{xp} (c_{xx} \delta_{x2} d_{xp} \eta_{x2} p + 2a_x a_{xp} \delta_{x1} k_2) k_1 + p^2 \eta_{x2} \delta_{x1} a_x k_2 a_{xp} b_{xp}}$$

and $\epsilon_{4H} > 0$ if and only if $\frac{a_x + d_{x0}}{r_x} > \frac{p}{k_1}$. It extends the possibility of two positive roots.

Hence, there exists a unique positive root of \bar{x}_{mH} if and only if $\frac{a_x + d_{x0}}{r_x} < \frac{p}{k_1}$. Given a unique positive \bar{x}_{mH} , we can obtain unique \bar{x}_{0H} , \bar{x}_{pH} and \bar{T}_H . \square

Proposition 5.3.3. For $\bar{T}_L > \frac{d_{y0} + a_y}{r_y}$, a unique malignant steady state exists if and only if $\frac{d_{y0} + a_y}{r_y} < \frac{p}{k_1}$.

Proof. From Eq. 5.3.1,

$$\bar{y}_{0L} = \frac{1}{c_{yy}} \left(\frac{r_y \bar{T}_L}{d_{y0} + a_y} - 1 \right), \quad (5.3.5a)$$

$$\bar{y}_{mL} = \frac{a_y A_y(\bar{T}_L)}{b_{yp} + d_{ym}} \bar{y}_{0L}, \quad (5.3.5b)$$

$$\bar{y}_{pL} = \frac{a_{yp} b_{yp}}{d_{yp}(\bar{T}_L)} \bar{y}_{mL}, \quad (5.3.5c)$$

$$\bar{T}_L = \frac{p}{k_1}. \quad (5.3.5d)$$

The admissibility of steady state necessitates,

$$\bar{T}_L > \frac{d_{y0} + a_y}{r_y}.$$

Substituting Eq. 5.3.5d into Eq. 5.3.5a we obtain,

$$\bar{y}_{0L} = \frac{1}{c_{yy}} \left(\frac{r_y \frac{p}{k_1}}{d_{y0} + a_y} - 1 \right). \quad (5.3.6)$$

Using the expression for \bar{y}_{0L} and value of \bar{T}_L in Eq. 5.3.5b and Eq. 5.3.5c, we obtain

$$\bar{y}_{mL} = \frac{p a_y \delta_{y1} \bar{y}_{0L}}{k_1 (b_{yp} + d_{ym}) (1 + \delta_{y2} \frac{p}{k_1})}, \quad (5.3.7)$$

and

$$\bar{y}_{pL} = \frac{a_{yp} b_{yp} \bar{y}_{mL}}{\frac{\eta_{y1}}{1 + \eta_{y2} \frac{p}{k_1}}} \quad (5.3.8)$$

Hence, a unique malignant state exists if and only if $\frac{d_{y0} + a_y}{r_y} < \frac{p}{k_1}$. □

A co-existing steady state follows from Eq. 5.3.1.

$$\bar{x}_{0C} + \frac{c_{xy}}{c_{xx}}\bar{y}_{0C} = \frac{1}{c_{xx}} \left(\frac{r_x \bar{T}_C}{d_{x0} + a_x} - 1 \right), \quad (5.3.9a)$$

$$\frac{c_{yx}}{c_{yy}}\bar{x}_{0C} + \bar{y}_{0C} = \frac{1}{c_{yy}} \left(\frac{r_y \bar{T}_C}{d_{y0} + a_y} - 1 \right) \quad (5.3.9b)$$

$$\bar{x}_{mC} = \frac{a_x A_x(\bar{T}_C)}{b_{xp} + d_{xm}(\bar{T}_C)} \bar{x}_{0C}, \quad (5.3.9c)$$

$$\bar{y}_{mC} = \frac{a_y A_y(\bar{T}_C)}{b_{yp} + d_{ym}} \bar{y}_{0C}, \quad (5.3.9d)$$

$$\bar{x}_{pC} = \frac{a_{xp} b_{xp}}{d_{xp}} \bar{x}_{mC}, \quad (5.3.9e)$$

$$\bar{y}_{pC} = \frac{a_{yp} b_{yp}}{d_{yp}(\bar{T}_C)} \bar{y}_{mC}, \quad (5.3.9f)$$

$$\bar{T}_C = \frac{p}{k_1 + k_2 \bar{x}_{pC}}, \quad (5.3.9g)$$

Solving Eq. 5.3.9a and Eq. 5.3.9b simultaneously we obtain,

$$\bar{x}_{0C} = \frac{1}{c_{xx}c_{yy} - c_{xy}c_{yx}} \left(c_{yy} \left(\frac{r_x \bar{T}_C}{d_{x0} + a_x} - 1 \right) - c_{xy} \left(\frac{r_y \bar{T}_C}{d_{y0} + a_y} - 1 \right) \right) \quad (5.3.10)$$

$$\bar{y}_{0C} = \frac{1}{c_{xx}c_{yy} - c_{xy}c_{yx}} \left(c_{xx} \left(\frac{r_y \bar{T}_C}{d_{y0} + a_y} - 1 \right) - c_{yx} \left(\frac{r_x \bar{T}_C}{d_{x0} + a_x} - 1 \right) \right) \quad (5.3.11)$$

where $c_{xx}c_{yy} \neq c_{xy}c_{yx}$.

Isolate x_{pC} from Eq. 5.3.9g and substitute into Eq. 5.3.9e,

$$\bar{x}_{mC} = \frac{d_{xp}}{k_2 a_{xp} b_{xp}} \left(\frac{p}{\bar{T}_C} - k_1 \right) \quad (5.3.12)$$

Using Eq. 5.3.10 and Eq. 5.3.12 in Eq. 5.3.9c,

$$\epsilon_{0C} \bar{T}_C^4 + \epsilon_{1C} \bar{T}_C^3 + \epsilon_{2C} \bar{T}_C^2 + \epsilon_{3C} \bar{T}_C + \epsilon_{4C} = 0, \quad (5.3.13)$$

where

$$\epsilon_{0C} = \delta_{x1} a_{xp} a_x k_2 \eta_{x2} (c_{xy} r_y (a_x + d_{x0}) - c_{yy} r_x (a_y + d_{y0})) b_{xp},$$

$$\epsilon_{1C} = -(\eta_{x2} \delta_{x2} k_1 (a_y + d_{y0}) (a_x + d_{x0}) (c_{xx} c_{yy} - c_{xy} c_{yx}) d_{xp} + \delta_{x1} a_{xp} a_x (((a_y \eta_{x2} + d_{y0} \eta_{x2} - r_y) c_{xy} - c_{yy} \eta_{x2} (a_y + d_{y0})) a_x + d_{x0} (a_y \eta_{x2} + d_{y0} \eta_{x2} - r_y) c_{xy} - c_{yy} (a_y + d_{y0}) (d_{x0} \eta_{x2} - r_x))) k_2) b_{xp},$$

$$\epsilon_{2C} = (a_y + d_{y0})(a_x + d_{x0})(c_{xx}c_{yy} - c_{xy}c_{yx})(((\eta_{x2}p - k_1)\delta_{x2} - \eta_{x2}k_1)b_{xp} - \eta_{x1}\delta_x k_1)d_{xp} - b_{xp}\delta_{x1}a_x k_2 a_{xp}(c_{xy} - c_{yy}),$$

$$\epsilon_{3C} = (a_y + d_{y0})(a_x + d_{x0})(c_{xx}c_{yy} - c_{xy}c_{yx})((\delta_{x2}p + \eta_{x2}p - k_1)b_{xp} + \eta_{x1}(\delta_{x2}p - k_1))d_{xp}$$

$$\epsilon_{4C} = d_{xp}p(a_y + d_{y0})(a_x + d_{x0})(c_{xx}c_{yy} - c_{xy}c_{yx})(\eta_{x1} + b_{xp}).$$

Identifying roots analytically is somehow cumbersome however, we may say that a positive root of \bar{T}_C leads to obtain the values of \bar{x}_{0C} , \bar{x}_{pC} , \bar{x}_{mC} , \bar{y}_{0C} , \bar{y}_{mC} and \bar{y}_{pC} . In addition, the necessary condition to obtain admissible D_C is that positive \bar{x}_{0C} and \bar{y}_{0C} exist.

5.3.2 Stability analysis

In this section, we examine the stability properties of the various steady states of ET. The Jacobian, J , of Eq. 5.2.1 is computed. Thus, for the steady states, the eigenvalues of the linearized system are obtained analytically and otherwise numerically. Avoid to introduce many mathematical notations, we use a_{ij} for all Jacobian matrices.

The Jacobian of system of Eq. 5.2.1 is

$$J = \begin{bmatrix} a_{11} & a_{12} & 0 & 0 & 0 & 0 & a_{17} \\ a_{21} & a_{22} & 0 & 0 & 0 & 0 & a_{27} \\ a_{31} & 0 & a_{33} & 0 & 0 & 0 & a_{37} \\ 0 & a_{42} & 0 & a_{44} & 0 & 0 & a_{47} \\ 0 & 0 & a_{53} & 0 & a_{55} & 0 & 0 \\ 0 & 0 & 0 & a_{64} & 0 & a_{66} & a_{67} \\ 0 & 0 & 0 & 0 & a_{75} & 0 & a_{77} \end{bmatrix} \quad (5.3.14)$$

where

$$a_{11} = \frac{r_x(1+c_{xy}\bar{y}_0)}{(1+c_{xx}\bar{x}_0+c_{xy}\bar{y}_0)^2}\bar{T} - a_x - d_{x0},$$

$$a_{12} = -\frac{r_x c_{xy}}{(1+c_{xx}\bar{x}_0+c_{xy}\bar{y}_0)^2}\bar{x}_0\bar{T},$$

$$a_{17} = \frac{r_x}{1+c_{xx}\bar{x}_0+c_{xy}\bar{y}_0}\bar{x}_0,$$

$$a_{21} = -\frac{r_y c_{yx}}{(1+c_{xx}\bar{x}_0+c_{xy}\bar{y}_0)^2}\bar{y}_0\bar{T},$$

$$a_{22} = \frac{r_y(1+c_{yx}\bar{x}_0)}{(1+c_{yx}\bar{x}_0+c_{yy}\bar{y}_0)^2}\bar{T} - a_y - d_{y0},$$

$$a_{27} = \frac{r_y}{1+c_{yx}\bar{x}_0+c_{yy}\bar{y}_0}\bar{y}_0,$$

$$a_{31} = \frac{a_x \delta_{x1}}{1+\delta_{x2}\bar{T}},$$

$$a_{33} = -b_{xp} - \frac{\eta_{x1}}{1+\eta_{x2}\bar{T}},$$

$$a_{37} = \frac{a_x \delta_{x1}}{(1+\delta_{x2}\bar{T})^2}\bar{x}_0 + \frac{\eta_{x1}\eta_{x2}}{(1+\eta_{x2}\bar{T})^2}\bar{x}_m,$$

$$a_{42} = \frac{a_y \delta_{y1}}{1+\delta_{y2}\bar{T}},$$

$$a_{44} = -b_{yp} - d_{ym},$$

$$a_{47} = \frac{a_y \delta_{y1}}{(1+\delta_{y2}\bar{T})^2}\bar{y}_0,$$

$$\begin{aligned}
a_{53} &= a_{xp}b_{xp}, \\
a_{55} &= -d_{xp}, \\
a_{64} &= a_{yp}b_{yp}, \\
a_{66} &= -\frac{\eta_{y1}}{1+\eta_{y2}\bar{T}}, \\
a_{67} &= \frac{\eta_{y1}\eta_{y2}}{(1+\eta_{y2}\bar{T})^2}\bar{y}_m, \\
a_{75} &= -k_2\bar{T}, \\
a_{77} &= -k_1 - k_2\bar{x}_p.
\end{aligned}$$

The Jacobian at D_0 is,

$$J_{D_0} = \begin{bmatrix} a_{11} & 0 & 0 & 0 & 0 & 0 & 0 \\ 0 & a_{22} & 0 & 0 & 0 & 0 & 0 \\ a_{31} & 0 & a_{33} & 0 & 0 & 0 & 0 \\ 0 & a_{42} & 0 & a_{44} & 0 & 0 & 0 \\ 0 & 0 & a_{53} & 0 & a_{55} & 0 & 0 \\ 0 & 0 & 0 & a_{64} & 0 & a_{66} & 0 \\ 0 & 0 & 0 & 0 & a_{75} & 0 & a_{77} \end{bmatrix} \quad (5.3.15)$$

where

$$\begin{aligned}
a_{11} &= \frac{p}{k_1}r_x - a_x - d_{x0}, \\
a_{22} &= \frac{p}{k_1}r_y - a_y - d_{y0}, \\
a_{31} &= \frac{p}{k_1} \left(\frac{a_x\delta_{x1}}{1+\delta_{x2}\frac{p}{k_1}} \right), \\
a_{33} &= -b_{xp} - \frac{\eta_{x1}}{1+\eta_{x2}\frac{p}{k_1}}, \\
a_{42} &= \frac{p}{k_1} \left(\frac{a_y\delta_{y1}}{1+\delta_{y2}\frac{p}{k_1}} \right), \\
a_{44} &= -b_{yp} - d_{ym}, \\
a_{53} &= a_{xp}b_{xp}, \\
a_{55} &= -d_{xp}, \\
a_{64} &= a_{yp}b_{yp}, \\
a_{66} &= -\frac{\eta_{y1}}{1+\eta_{y2}\frac{p}{k_1}}, \\
a_{75} &= -\frac{pk_2}{k_1}, \\
a_{77} &= -k_1.
\end{aligned}$$

Since J_{D_0} is a triangular matrix thus, eigenvalues are a_{11} , a_{22} , a_{33} , a_{44} , a_{55} , a_{66} and a_{77} . Five of the seven eigenvalues are negative but the remaining a_{11} and a_{22} may be positive negative or zero. Hence, D_0 is stable for $\frac{a_x+d_{x0}}{r_x} > \frac{p}{k_1}$ and $\frac{a_y+d_{y0}}{r_y} > \frac{p}{k_1}$.

The Jacobian at D_H is,

$$J_{D_H} = \begin{bmatrix} a_{11} & a_{12} & 0 & 0 & 0 & 0 & a_{17} \\ 0 & a_{22} & 0 & 0 & 0 & 0 & 0 \\ a_{31} & 0 & a_{33} & 0 & 0 & 0 & a_{37} \\ 0 & a_{42} & 0 & a_{44} & 0 & 0 & 0 \\ 0 & 0 & a_{53} & 0 & a_{55} & 0 & 0 \\ 0 & 0 & 0 & a_{64} & 0 & a_{66} & 0 \\ 0 & 0 & 0 & 0 & a_{75} & 0 & a_{77} \end{bmatrix} \quad (5.3.16)$$

$$a_{11} = \frac{r_x}{(1+c_{xx}\bar{x}_0)^2}\bar{T} - a_x - d_{x0},$$

$$a_{12} = -\frac{r_x c_{xy}}{(1+c_{xx}\bar{x}_0)^2}\bar{x}_0\bar{T},$$

$$a_{17} = \frac{r_x}{1+c_{xx}\bar{x}_0}\bar{x}_0,$$

$$a_{22} = \frac{r_y}{1+c_{yy}\bar{y}_0}\bar{T} - a_y - d_{y0},$$

$$a_{31} = \frac{a_x \delta_{x1}}{1+\delta_{x2}\bar{T}},$$

$$a_{33} = -b_{xp} - \frac{\eta_{x1}}{1+\eta_{x2}\bar{T}},$$

$$a_{37} = \frac{a_x \delta_{x1}}{(1+\delta_{x2}\bar{T})^2}\bar{x}_0 + \frac{\eta_{x1}\eta_{x2}}{(1+\eta_{x2}\bar{T})^2}\bar{x}_m,$$

$$a_{42} = \frac{a_y \delta_{y1}}{1+\delta_{y2}\bar{T}}\bar{T},$$

$$a_{44} = -b_{yp} - d_{ym},$$

$$a_{53} = a_{xp}b_{xp},$$

$$a_{55} = -d_{xp},$$

$$a_{64} = a_{yp}b_{yp},$$

$$a_{66} = -\frac{\eta_{y1}}{1+\eta_{y2}\bar{T}},$$

$$a_{75} = -k_2\bar{T},$$

$$a_{77} = -k_1 - k_2\bar{x}_p.$$

The Jacobian at D_L is,

$$J_{D_L} = \begin{bmatrix} a_{11} & 0 & 0 & 0 & 0 & 0 & 0 \\ a_{21} & a_{22} & 0 & 0 & 0 & 0 & a_{27} \\ a_{31} & 0 & a_{33} & 0 & 0 & 0 & 0 \\ 0 & a_{42} & 0 & a_{44} & 0 & 0 & a_{47} \\ 0 & 0 & a_{53} & 0 & a_{55} & 0 & 0 \\ 0 & 0 & 0 & a_{64} & 0 & a_{66} & a_{67} \\ 0 & 0 & 0 & 0 & a_{75} & 0 & a_{77} \end{bmatrix} \quad (5.3.17)$$

where

$$a_{11} = \frac{r_x}{1+c_{xy}\bar{y}_0}\bar{T} - a_x - d_{x0},$$

$$a_{21} = -\frac{r_y c_{yx}}{(1+c_{xy}\bar{y}_0)^2}\bar{y}_0\bar{T},$$

$$a_{22} = \frac{r_y}{(1+c_{yy}\bar{y}_0)^2}\bar{T} - a_y - d_{y0},$$

$$a_{27} = \frac{r_y}{1+c_{yy}\bar{y}_0}\bar{y}_0,$$

$$a_{31} = \frac{a_x \delta_{x1}}{1+\delta_{x2}\bar{T}},$$

$$\begin{aligned}
a_{33} &= -b_{xp} - \frac{\eta_{x1}}{1+\eta_{x2}\bar{T}}, \\
a_{42} &= \frac{a_y \delta_{y1}}{1+\delta_{y2}\bar{T}} \bar{T}, \\
a_{44} &= -b_{yp} - d_{ym}, \\
a_{47} &= \frac{a_y \delta_{y1}}{(1+\delta_{y2}\bar{T})^2} \bar{y}_0, \\
a_{53} &= a_{xp} b_{xp}, \\
a_{55} &= -d_{xp}, \\
a_{64} &= a_{yp} b_{yp}, \\
a_{66} &= -\frac{\eta_{y1}}{1+\eta_{y2}\bar{T}}, \\
a_{67} &= \frac{\eta_{y1} \eta_{y2}}{(1+\eta_{y2}\bar{T})^2} \bar{y}_m, \\
a_{75} &= -k_2 \bar{T}, \\
a_{77} &= -k_1 - k_2 \bar{x}_p.
\end{aligned}$$

The Jacobian at D_C is similar to J , except \bar{x}_0 and \bar{y}_0 are replaced by \bar{x}_{0C} and \bar{y}_{0C} respectively. Calculating eigenvalues analytically for the Jacobian J_{DH} , J_{DL} and J_{DC} is complicated. Therefore, we will find the stability of various steady state numerically.

We perform a lot of simulations through MATLAB for all parameters to observe the existing possible topologies. Fig. 5.3.1 illustrates the stability of steady states and shows that trajectories with different sets of initial conditions converge to the steady states. We vary the self-renewal rate of stem cells and the niche inhibiting factors. In each given case, a steady state is unique. The solution of the model is projected on (x_0, y_0) plane.

Fig. 5.3.1a illustrates that the trivial steady state is stable at $r_x = 10^{-7}$ and $r_y = 10^{-7}$ when there is no other steady state. At this point, we increase r_x resulting in the stable hematopoietic steady state at $r_x = 10^{-5}$ thus, the trivial steady state becomes unstable shown in Fig. 5.3.1b. This state corresponds to a healthy state. Instead of r_x , if we increase r_y , the stable malignant steady state appears at $r_y = 10^{-5}$ while the trivial steady state becomes unstable illustrated in Fig 5.3.1c. This state corresponds to a full blown malignant state. Hence, this investigation reveals that the self-renewal rates r_x and r_y may be crucial to obtain stable hematopoietic and malignant steady states.

For the default values of parameters where $r_x < r_y$, the malignant steady state is stable, whereas the trivial and hematopoietic steady states are unstable (See Fig 5.3.1d). Subsequently, increasing r_x and decreasing r_y , the hematopoietic steady state becomes stable and the malignant steady state becomes unstable at $r_x = 10^{-4}$ and $r_y = 10^{-5}$ (See Fig. 5.3.1e).

Consider the impact of inhibiting factors of stem cells when all parameters are at their default values. Increasing c_{yy} , a co-existing steady state appears at $c_{yy} = 10^{-4}$ and takes over the stability of malignant steady state (See Fig. 5.3.1f). Alternatively, decreasing c_{xx} , the special case of bistability is obtained at $c_{xx} = 3 \cdot 10^{-5}$ where both malignant and hematopoietic steady states are stable and the co-existing steady state is unstable (See Fig. 5.3.1g).

Hence, this investigation reveals the importance of stem cell parameters in order to obtain various steady states.

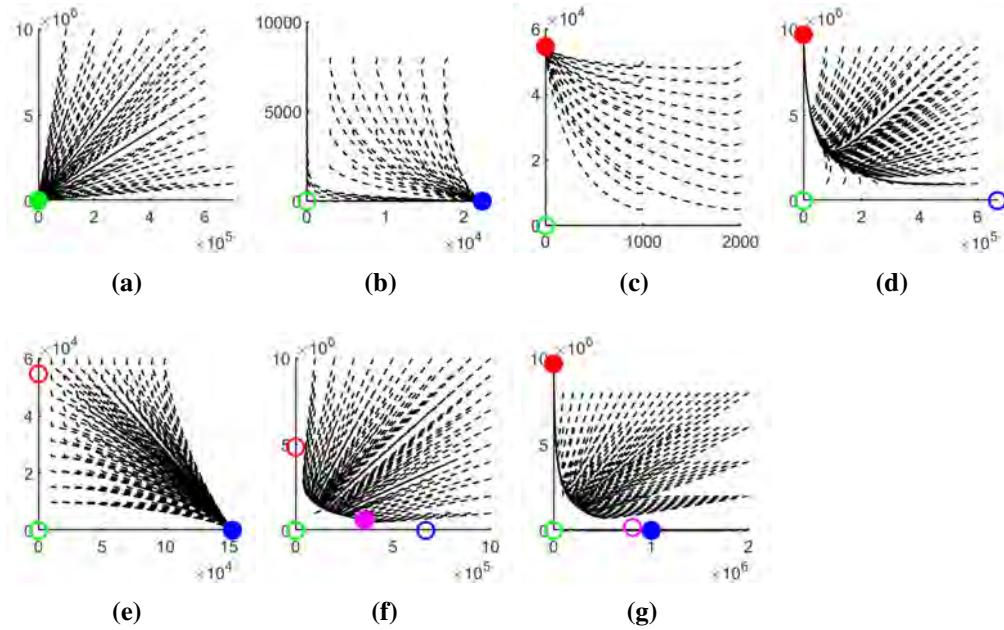


Fig. 5.3.1 The figure illustrates the trajectories for different initial conditions ultimately approach the stable steady states of the ET model. The solution of the model is projected on (x_0, y_0) plane. Full circles are stable steady states and open circles are unstable steady states. Green, blue, red and magenta correspond to trivial, hematopoietic, malignant and co-existing steady states respectively. x -axis denotes the number of hematopoietic stem cells whereas y -axis denotes the number of malignant stem cells. The trajectories are shown as black dotted lines. The panels are as follows, (a) $r_x = 10^{-7}$, $r_y = 10^{-7}$, (b) $r_x = 10^{-5}$, $r_y = 10^{-7}$, (c) $r_x = 10^{-7}$, $r_y = 10^{-5}$, (d) Default values, (e) $r_x = 1 \cdot 10^{-4}$, $r_y = 1 \cdot 10^{-5}$, (f) $c_{yy} = 10^{-4}$, (g) $c_{xx} = 3 \cdot 10^{-5}$. Note, in panel (g) the trajectories attract towards x_0 for very low values of y_0 .

5.3.3 Sensitivity Analysis

In this section, we perform a sensitivity analysis to explore the relationship between the input parameters and the outcome of the model. We take $c_{yy} = 10^{-4}$ while other parameters are fixed at their default values leading to a stable co-existing steady state. We choose a 10% variation in parameter values.

First, we focus on the parameters involved in stem cell dynamics. Fig. 5.3.2 shows that by decreasing (increasing), r_x , d_{y0} , c_{yy} and c_{yx} decreases (increases) the number of healthy cells (x_0 , x_m , x_p) while increases (decreases) the concentration of TPO and the number of malignant cells (y_0 , y_m , y_p). In contrast, decreasing (increasing) r_y , d_{x0} , c_{xx} and c_{xy} decreases (increases) the number of malignant, whereas the number of malignant cells and TPO concentration are increased (decreased).

Next, we observe the parameters involved in the TPO dynamics. Decreasing the TPO natural degradation rate k_1 increases the number of malignant cells (y_0 , y_m , y_p) and the concentration of TPO, whereas reducing platelet dependent TPO degradation

rate k_2 increases the number of healthy cells (x_0, x_m, x_p) , however it does not affect the TPO level. Finally, we observe that decreasing baseline production rate p decrease all types of cell count and the concentration of TPO or vice versa. It is mentioned that TPO parameters are less sensitive compared to stem cell parameters. In brief, this investigation shows that stem cell dynamics play a major role in the progression of ET.

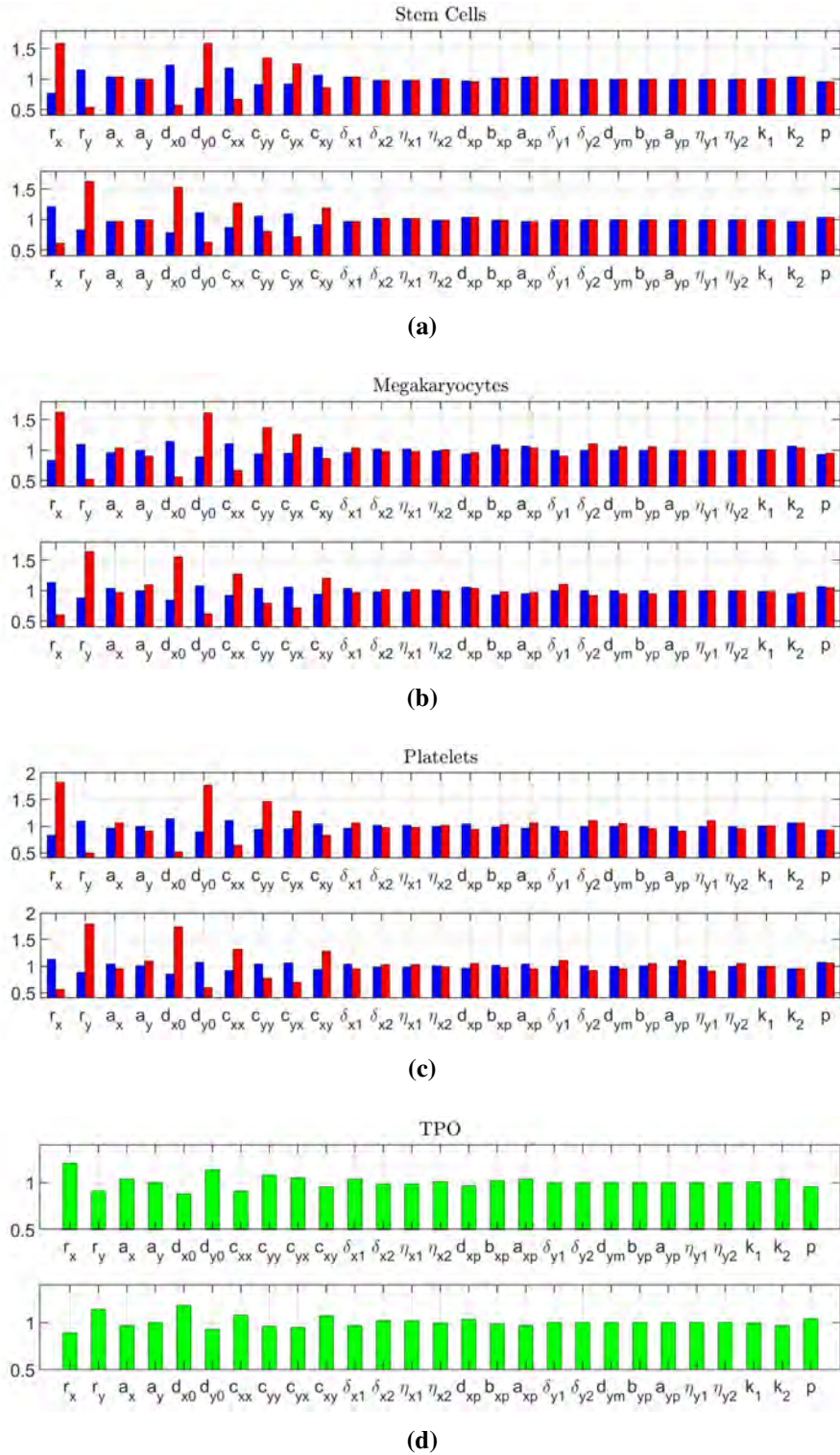


Fig. 5.3.2 Panels (a), (b), (c) and (d) show the change in HSC, MEG, PLT and TPO when parameters are decreased and increased by 10%. Blue, red and green denote healthy cell, malignant cells and TPO concentration respectively. The bars equal to 1 corresponds to the outcome for the default parameter values. Top panels correspond to decreasing a parameter by 10%, panel below corresponds to increasing a parameter by 10%.

In Table 5.3, we collect the most sensitive parameters (r_x , r_y , d_{x0} , d_{y0}) for a co-existing steady state values where $c_{yy} = 10^{-4}$. Table 5.3 summarizes the minimum and

maximum variation in the values of \bar{x}_{0C} , \bar{y}_{0C} , \bar{x}_{mC} , \bar{y}_{mC} , \bar{x}_{pC} , \bar{y}_{pC} and \bar{T}_C in percentage when parameters are perturbed by $\pm 10\%$. We have calculated numerical values by perturbing all parameters. However, we found that the self-renewal rates and death rates vary the steady state values most.

Table 5.3 The table shows the effect of the most sensitive parameters on co-existing steady state values. The first column shows the parameters varied by $\pm 10\%$ affecting the values given in the second row. The remaining percentages in the table show how much a corresponding value is varied.

	\bar{x}_{0C}	\bar{y}_{0C}	\bar{x}_{mC}	\bar{y}_{mC}	\bar{x}_{pC}	\bar{y}_{pC}	\bar{T}_C
	$3.55 \cdot 10^5$	$6.07 \cdot 10^5$	$1.01 \cdot 10^6$	$5.56 \cdot 10^7$	$2.01 \cdot 10^{11}$	$4.96 \cdot 10^{10}$	123.98
-10% r_x	-40%		-28%		-27%		+29%
-10% d_{x0}	+35%		+20%		+21%		-15%
-10% r_y		-35%		-36%		-40%	
-10% d_{y0}		+61%		+64%		+85%	
+10% r_x	+32%		+19%		+19%		-14%
+10% d_{x0}	-35%		-15%		-24%		+25%
+10% r_y		+53%		+55%		+73%	
+10% d_{y0}		-32%		-33%		-37%	

5.3.4 Numerical Analysis and Treatment Scenarios

This section discusses the treatment scenarios for different choices of parameters. For this purpose, we generate a variety of figures to characterize the steady states and their stability. In Fig. 5.3.3, we show the combination of parameters, which produces the interesting dynamics of the ET model. We explain the sub-figures of Fig. 5.3.3 subsequently.

- **Fig. 5.3.3a** illustrates the stability regions where the self-renewal rates of HSC r_x and MSC r_y are varied. In the right panel of Fig. 5.3.3a, denoted by D_T , the trivial steady state exists and is stable for small values of r_x and r_y . The left panel of Fig. 5.3.3a illustrates the stability regions when r_x and r_y are increased. Suppose a virtual subject is in the stability region $D_H^{T,L}$, where the hematopoietic steady state is stable and both trivial and malignant steady states are unstable. Increasing r_y changes a topology from a stable hematopoietic to a stable malignant steady state. A virtual subject approaches the stability region $D_L^{T,H}$, where the stable malignant and the unstable hematopoietic and trivial steady states exist. It suggests that the stem cell self-renewal rate is the important parameters for good prognosis.
- **Fig. 5.3.3b** illustrates the stability regions where a range of values of d_{x0} and d_{y0} is taken. Suppose a virtual subject is in the region $D_H^{T,L}$. At this point, increasing the death rate d_{x0} of HSC or decreasing the death rate d_{y0} of MSC moves a virtual subject in region $D_L^{H,T}$, corresponding to a worse situation. For larger values of d_{x0} , the hematopoietic steady state disappears whereas the malignant steady state is stable and the trivial steady state is unstable, D_L^T . However, D_H^T represents that

for larger values of d_{y0} , the malignant steady state vanishes and the hematopoietic steady state becomes stable, corresponding to a recovery of the disease. For large set of values for d_{x0} and d_{y0} , the trivial steady state exists and is stable, i.e., D_T .

- **Fig. 5.3.3c** illustrates the stability regions obtained by varying inhibiting factors c_{xx} and c_{yx} . The parameter c_{xx} denotes the inhibiting strength of x_0 for x_0 whereas c_{yx} denotes the inhibiting strength of x_0 for y_0 . For high values of c_{yx} and low values of c_{xx} , we observe the bi-stability region $D_{H,L}^{T,C}$ where both the hematopoietic and malignant steady states are stable and the co-existing and trivial steady states are unstable. However, an increase in c_{xx} makes the hematopoietic steady state unstable, whereas the co-existing steady state disappears $D_L^{T,H}$.
- Similarly, in **Fig. 5.3.3d**, for large values of c_{xy} , where the malignant steady state is stable, and the hematopoietic and trivial steady states are unstable, denoted by $D_L^{T,H}$. In region $D_C^{T,H,L}$, for large values of c_{yy} and a range of low values of c_{xy} , the co-existing steady state is stable and the remaining three steady states are unstable. Thus, the niche inhibiting factors may improve the diagnosis and reduce the disease load.

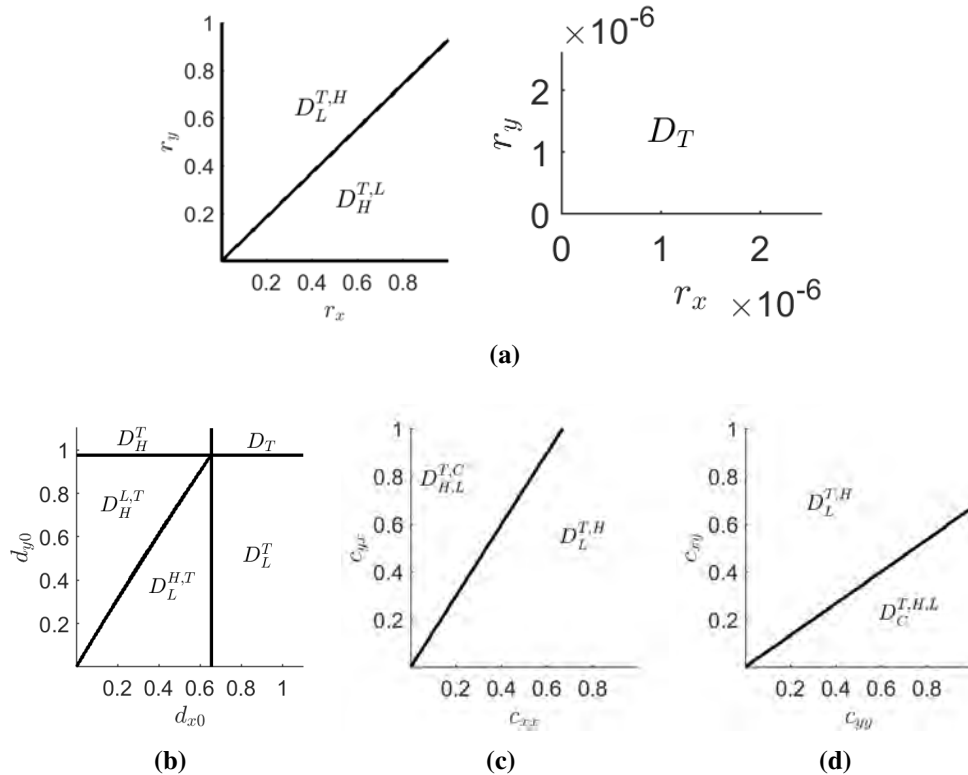


Fig. 5.3.3 The stability of the steady states, i.e. trivial, malignant, hematopoietic or coexistence, depending on the parameters involved in the stem cell dynamic. Panels (a), (b), (c) and (d) show a range of values for different pairs of parameters. The right panel (a) is zoomed in the left figure. The stable steady states are written as a subscript of D and unstable steady states are written as a superscript of D. All other parameter values are fixed at their default.

Data Fitting

A few data sets are available from a cohort of ET patients enrolled in the clinical trial “DALIAH”. Moreover, the data given in [79] represents an ET patient. The model trajectories compared to the available data of patients receiving interferon- α (IFN) are illustrated in Figure 5.3.4. In the model, we include the effect of IFN on stem cells. The simulation results compared to patient data validate our proposed model. We report deviated values from the default in tables 5.4 and 5.5.

In Fig. 5.3.4(a-c), we perturb the death rates of stem cells, d_{x0} and d_{y0} for data fitting. The values used for d_{x0} and d_{y0} correspond to region $D_H^{T,L}$ (Fig. 5.3.3b), where the hematopoietic steady state is stable and the malignant steady state is unstable. In addition, we identify a set of parameters given in Table. 5.4 for an ET patient that describes an excellent fitting of data before and after treatment (See Fig. 5.3.4d).

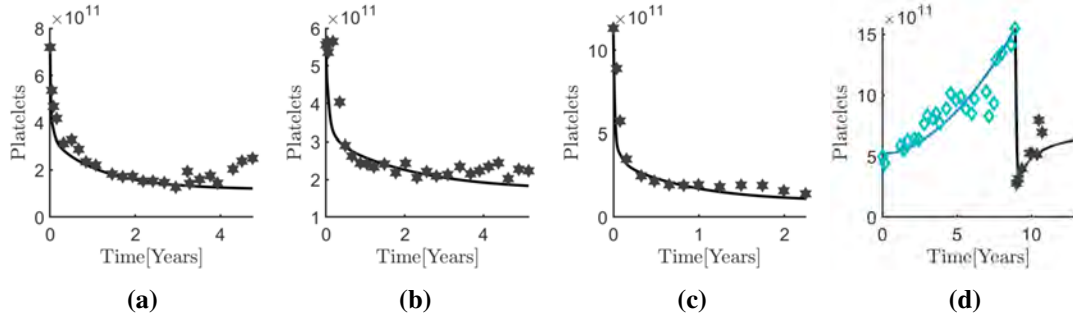


Fig. 5.3.4 The panels corresponding to ET patients treated with IFN are compared to the ET model. Data for the total platelet count ($x_p + y_p$) shown in green diamonds is before treatment whereas, data for platelet count are shown in dark grey stars curve during treatment. Model predictions are shown as full curves for platelet count (black treated and blue untreated). The data shown in panels (a), (b) and (c) are from the clinical trial “DALIAH”. The data shown in the panel (d) is extracted from [79].

Table 5.4 Parameter values for Figure 5.3.4d. The parameters in red are perturbed while fitting data during treatment.

Before treatment		After treatment	
Parameter	Value	Parameter	Value
r_x	$5 \cdot 10^{-4}$	r_x	$3 \cdot 10^{-2}$
r_y	$7.2 \cdot 10^{-4}$	r_y	$7.2 \cdot 10^{-4}$
a_y	$3.8 \cdot 10^{-4}$	a_y	$3.8 \cdot 10^{-4}$
d_{x0}	$2 \cdot 10^{-3}$	d_{x0}	$8 \cdot 10^{-4}$
d_{y0}	$2 \cdot 10^{-3}$	d_{y0}	$2 \cdot 10^{-1}$

Table 5.5 Parameter values for the Figure 5.3.4(a-c).

	Parameter	Value	Parameter	Value
Fi. 5.3.4a	d_{x0}	$2 \cdot 10^{-3}$	d_{y0}	$1 \cdot 10^{-2}$
Fi. 5.3.4b	d_{x0}	$3 \cdot 10^{-3}$	d_{y0}	$1 \cdot 10^{-2}$
Fi. 5.3.4c	d_{x0}	$1 \cdot 10^{-3}$	d_{y0}	$1 \cdot 10^{-2}$

In Silico Trials

The TPO receptor is usually used to increase the platelet count in immune thrombocytopenia. Importantly, TPO related *MPL* mutations are found in 1-3% ET cases [14; 89]. According to a few investigations, the feedback loop between TPO and megakaryocyte is affected, resulting in a subsequent increase of TPO serum levels in ET [51; 69; 98]. Also, thrombotic complications are often found in patients with ET. In order to prevent these complications, the typical drugs aim at reducing the platelet count. However, many novel mechanisms relating to high TPO levels and abnormal platelet production in ET are undiscovered in existing literature. Fig. 5.3.5 illustrates an in silico trial where TPO production is half of the default value. We observe that reducing TPO concentration reduces the total number of stem cells, megakaryocytes and platelets. These results offer to use TPO related drugs in ET patients for a short time preventing thrombotic complications. In contrast, the *JAK2V617F* allele burden is increased, which is critical for ET patients. However, we need clinical data to validate the results.

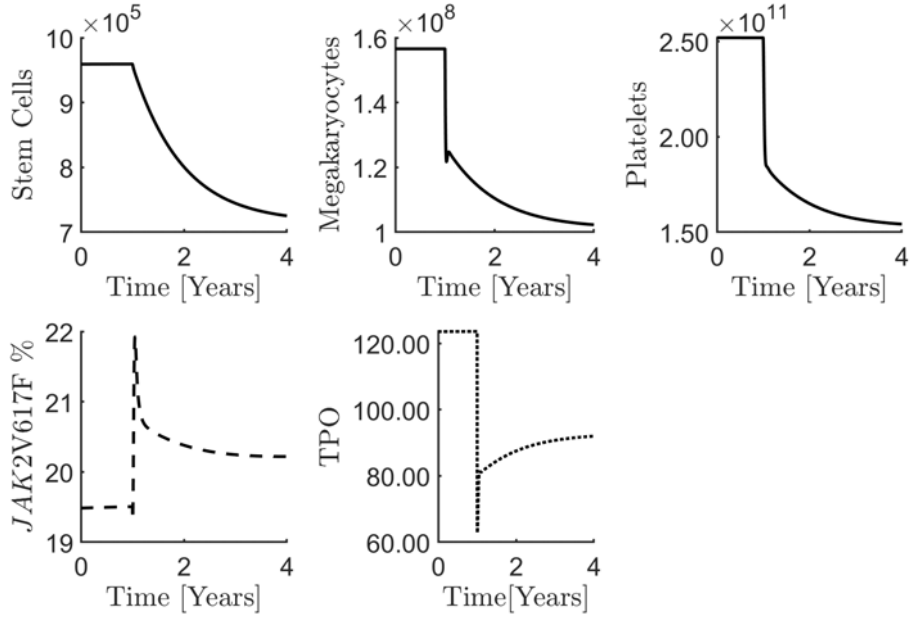


Fig. 5.3.5 An in silico TPO analysis. For a co-existing steady state, we set $c_{yy} = 10^{-3}$. After one year, set $p = 150$ (half of the default value) for treatment. The total cell count of stem cells, megakaryocytes and platelets is denoted by full black curve in the above panel, the $JAK2V617F$ is represented by dashed black curve and the concentration of TPO is represented in dotted black curve (below panel). The initial values are $(\bar{x}_{0C}, \bar{x}_{mC}, \bar{x}_{pC}, \bar{y}_{0C}, \bar{y}_{mC}, \bar{y}_{pC}, \bar{T}_C) = (3.56 \cdot 10^5, 1.01 \cdot 10^8, 2.02 \cdot 10^{11}, 6.02 \cdot 10^5, 5.52 \cdot 10^7, 4.91 \cdot 10^7, 123.57)$.

5.4 Conclusion

In this chapter, we propose a novel mathematical model describing the development of ET. The mechanism-based model incorporates both healthy and malignant cells with multiple feedback mediated by TPO. We have done an analytical investigation of the model wherever possible. The steady states and their stability are characterized using different stem cell parameters. Furthermore, a sensitivity analysis is performed to identify the sensitive parameters for the model's outcome. We have explored that the stem cell parameters are more sensitive to disease progression than the remaining parameters. Furthermore, we generate various bifurcation figures and found that set of stem cell parameters produce the most interesting dynamics of the model. Some of these figures are included in this chapter (See Fig. 5.3.3).

Several bio-medical literature theories have been proposed, associating blood cancer development with stem cell properties. ET is also thought to be a clonal disorder with origin in hematopoietic stem cells. In clinical practice, blood cancer therapy such as IFN reduces disease load by affecting the hematopoietic stem cells. The authors have reported that IFN increases the death rate of hematopoietic stem and progenitor cells [72]. IFN is also hypothesized to reduce the $JAK2V617F$ allele burden by targeting malignant stem cells [83]. Besides medical evidence, several authors have explored

the importance of stem cells for various hematological diseases through mathematical modelling [36; 66; 73; 95; 102; 103; 104; 110; 111]. Our results are in agreement with the perception that stem cell is a good candidate to prevent ET progression. Moreover, TPO therapy might be useful for reducing platelet count in the peripheral blood in order to avoid thrombotic complications. However, it can not switch from a malignant state to a healthy state.

CHAPTER 6

Mathematical modelling of erythropoiesis and thrombopoiesis with multiple EPO and TPO feedbacks

Mathematical modelling of erythropoiesis and thrombopoiesis with multiple EPO and TPO feedbacks

Zamra Sajid, Morten Andersen and Johnny T. Ottesen

Abstract

We propose a seven-dimensional mathematical model of erythropoiesis and thrombopoiesis. A key feature of the model is different cell populations incorporating several feedback loops that are mediated by erythropoietin (EPO) and thrombopoietin (TPO). The shared megakaryocyte-erythroid progenitor cell is an encouraging feature to investigate the coupled mechanism between erythroid and megakaryocyte lineage. The study contributes to understand the impact of various clinical investigations on these coupled dynamics. The subsystems of erythropoiesis and thrombopoiesis can be decoupled from the full model. These self-supporting subsystems are useful to investigate the independent mechanisms of erythrocytes and platelets. The model and its subsystems stipulate excellent results which adequately describe many critical situations such as recovery of the blood cells after phlebotomy, body's reaction to different administration regimens of EPO and TPO. We estimate the parameters from clinical data and identify the subset of parameters responsible for various clinical experiments. Furthermore, the subsystems are employed to evaluate parameters for the full model. In case where the coupling is required between erythropoiesis and thrombopoiesis, these subsystems cannot estimate the parameters and explain the full dynamics.

Keywords: mathematical modelling, EPO stimulating agents, TPO stimulants, megakaryocyte-erythroid progenitor, erythropoiesis, thrombopoiesis

1 Introduction

Hematopoietic stem cells (HSCs) are multipotent cells that produce blood cells required by the human body. Once an HSC differentiates, it undergoes a series of differentiation ultimately resulting in a large number of mature cells. This a process occurs in the bone marrow niche and is called hematopoiesis. In healthy individuals, approximately 10^{12} blood cells are produced every day to maintain

the steady state levels of the peripheral blood [1]. HSCs can regenerate themselves, often termed as self-renewal, meaning one HSC divide into two HSCs. In addition, one HSC may produce two daughters/progenitor cells, and it may differentiate into one HSC and one daughter cell. The hematopoietic stem cell niche is a particular environment where signals from the body carry out the differentiation of the required cell type. These differentiated cells are subdivided further into different categories of cells. For example, the myeloid cells include red blood cells (erythrocytes), white blood cells (leukocytes), and platelets (thrombocytes). Specific associated growth factors to distinct cell lineage are responsible for stimulating cell production and regeneration. Here, we focus on two cell types, red blood cells and megakaryocytes. Megakaryocytes (precursor of platelets) and erythrocytes differentiate from a shared precursor, the megakaryocyte-erythroid progenitor [16, 82], in response to glycoprotein hormones.

The erythropoietin (EPO) regulates the number of erythrocytes through a feedback loop. The kidneys secrete EPO in response to low oxygen levels in the blood. The EPO concentration increases the differentiation of late progenitor erythroid cells while it interrupts erythrocytes' apoptotic mechanism to balance their amount in the blood. Thus, the production and destruction of erythrocytes are maintained in healthy states by the level of EPO [2, 25, 33, 39, 71, 78, 83]. It means that the loss of function of the erythropoietin receptor may disrupt the production of erythrocytes. The erythrocyte life span is approximately 120 days in healthy individuals after macrophages envelop erythrocytes in the spleen [45, 66].

The principal hormone that regulates megakaryocyte and platelet development is thrombopoietin (TPO), produced by the liver. TPO stimulates the proliferation and differentiation of megakaryocyte precursors, promotes megakaryocyte maturation, decreases its apoptosis and stimulates the release of platelets via fragmentation of the mature megakaryocytes [17, 41]. TPO is presumed to be removed primarily from blood circulation by platelets. The half-life of TPO is estimated between 20 and 25 hours in [69] using data from [28]. However, in [40], the maximum half-life of TPO is given as 45 minutes. Furthermore, one mature megakaryocyte can give rise to between 1000 and 3000 platelets. The average platelet count for a normal human being is $290 \times 10^9/L$ of blood. Platelets have a life span of about 8 to 10 days.

The recent studies shed new light on alternative routes by which hematopoietic stem cells are differentiated into megakaryocytes. The studies suggest megakaryocyte-biased hematopoietic stem cells exist and can be triggered by extracellular signals such as TPO, which may differentiate directly into a megakaryocyte [57]. Also, TPO is thought to be responsible for the proliferation of megakaryocyte, and to some extent, erythroid cell lineage [68]. However, megakaryocyte lineage grew in the absence of EPO, which is consistent with the role of EPO in erythroid maturation. The TPO receptor gives a distinct separation as a marker between common myeloid and megakaryocyte/erythroid progenitors. In addition, it has also been shown that the TPO receptors increase the self-renewal of hematopoietic stem cells, especially under stress and inflammation [19].

1.1 Literature review of mathematical models

The blood and bone marrow sampling is easily accessible therefore, the hematopoietic system and its diseases have been studied extensively, and different mathematical models have been developed. Compartmental models are popular to describe the time evolution of the different hematopoietic cell types. In this type of model, each cell type is identified with one compartment, and its dynamics is described by one ordinary differential equation (ODE).

Several authors used compartmental models to investigate hematopoietic mechanisms such as phlebotomy or blood donation, erythropoiesis-stimulating agents (ESAs), etc., in healthy human beings. Some of the mathematical models described the regulation and formation of red blood cells and their supported mechanisms, such as EPO [10, 49, 77]. Among pioneers in mathematical modeling of hematopoiesis, an age-structured model for erythropoiesis following phlebotomy on normal human subjects is presented and experimental data on phlebotomized subjects are used to fit the parameters in the model [50]. In [23], the mathematical model consisted of different cell populations is presented to predict certain situations such as the recovery of the red blood cell mass after blood donation, the body's reaction to different ESAs, as EPO. The same group of authors presented the model which reflected hemoglobin dynamics in hemodialysis patients and predicted the hemoglobin response to ESAs therapy. In [77], a three-compartment model with a negative feedback mechanism for erythropoiesis was presented and physiological properties with the application of the RBC regeneration after a blood donation were captured. Afterward, the model was extended to identify optimal and individualized phlebotomy schedules in PV patients in [46].

A number of mathematical models are based on hematological diseases, [3, 7, 8, 15, 60]. In [48], a two-compartment model investigated quiescent and mitotic stem cells with constant delay in aplastic anemia and periodic hematopoiesis. The extended model has been used to investigate oscillation for parameter ranges observed in periodic chronic myeloid leukemia, cyclical neutropenia and thrombocytopenia [14, 48, 64]. In [42], a mathematical model of platelet, megakaryocyte, and TPO dynamics is presented. It contributes to the understanding of the origin of cyclic thrombocytopenia. In [69] an age-structured model with both normal and pathological platelet production is developed incorporating TPO. The authors numerically reproduce the human response to an injection of TPO. In [64], a mechanism based mathematical model of hematopoiesis is presented to investigate the platelet oscillations observed in cyclical thrombocytopenia. In [70], the authors presented a mathematical model describing the erythropoietic lineage under chemotherapy and EPO applications. Furthermore, compartment models have been used as a tool to study the dynamics of cancer cell populations [5, 6, 18, 22, 27, 59, 67, 76, 86].

1.2 Present study

Our attempt at modeling erythropoiesis and thrombopoiesis is not the first attempt. Many mathematical models exist in the literature, but none describes the

interacting mechanisms between erythrocytes and platelets with their corresponding growth factors EPO and TPO in healthy individuals. We aim to present a framework for developing a model regulating both erythrocyte and platelet production, which takes into account hematopoietic stem cells, megakaryocyte erythroid progenitor cell (MEP), erythrocytes (RBC), megakaryocytes (MEG) and platelets (PLT) with multi feedback from EPO and TPO on their dynamics. A non-linear ODE system captures the essential features via its compartment structure. We expect that such a mathematical model may be used in a clinical context to achieve personalized treatments. After formulating the important assumptions on the physiological process, we develop and analyze our novel mathematical model.

Assumptions on different mechanisms

1. **Niche feedback to HSCs:** HSCs self-renewal is inhibited by niche regulatory feedback [79] .
2. **TPO feedback to HSCs:** TPO stimulates HSCs by increasing the self-renewal [19] .
3. **TPO feedback to MEG:** TPO stimulates the production of MEG [26, 36, 38] while it inhibits the death rate of MEG [26, 51, 52, 85].
4. **TPO feedback to RBC:** The production of erythrocytes is stimulated by TPO [81].
5. **TPO removal mechanism:** The degradation of TPO occurs mainly by the platelet receptors. We further assume another clearance rate of TPO independent of platelet receptors [40, 43, 26].
6. **Production of RBC and PLT:** MEP differentiates into erythrocytes and megakaryocytes [16, 82]. The megakaryocyte is further fragmented into platelets. Generally, one megakaryocyte can produce between 1000 to 3000 platelets. It takes 5 to 7 days to mature megakaryocytes and shed platelets [17, 41].
7. **EPO feedback to MEG:** The production of MEG is inhibited by EPO [58].
8. **EPO feedback to RBC:** The production of erythrocytes is stimulated by EPO [2, 25, 33, 34, 39, 71] while the death rate is inhibited by EPO [25, 34, 71, 78, 83].

The proposed model captures the essential physiological processes for regulation of erythrocytes and platelets. We highlight the contemporary notion related to the effect of TPO on the self-renewal of HSC. The model's novel feature is the complex coupling of different mechanisms. In silico analysis provides insight into the link between erythropoiesis and thrombopoiesis by modulating EPO and TPO. The model will be shown to be in agreement with different categories of clinical data such as phlebotomy, ESAs, thrombopoietin stimulants, etc. Moreover,

subsystems of erythropoiesis and thrombopoiesis can be decoupled from the full system and may be compared to the experimental data. We observe a satisfied qualitative behavior of the model throughout the simulations. Based on estimates of parameters for a typical healthy individual, the presented model can be used to explore the changes in some of these parameters necessary to account for the dynamics of hematological diseases as done by several authors [14, 24, 42, 64]. The proposed model may also be extended from the healthy subjects to patients of MPNs by coupling the model to malignant cells using the similar approach by [5, 76]. It may help physicians to initiate therapy and observe patient's hematological parameters during treatment. However, a few particular challenges need to be addressed. For example, valid data of MPNs patients is required, including those who develop PV from ET over time. The underlying pathological dynamics have to be modeled, such as the feedback mechanisms of EPO and TPO in disease progression.

The presented paper is organized as; we derive the mathematical model in section 2. Next, in section 3, we present a brief mathematical analysis of the decoupled subsystems and the sensitivity analysis of the full model. In addition, we use data of healthy subjects from various clinical experiments as a benchmark for the model. Finally, the concluding remarks are given in section 4.

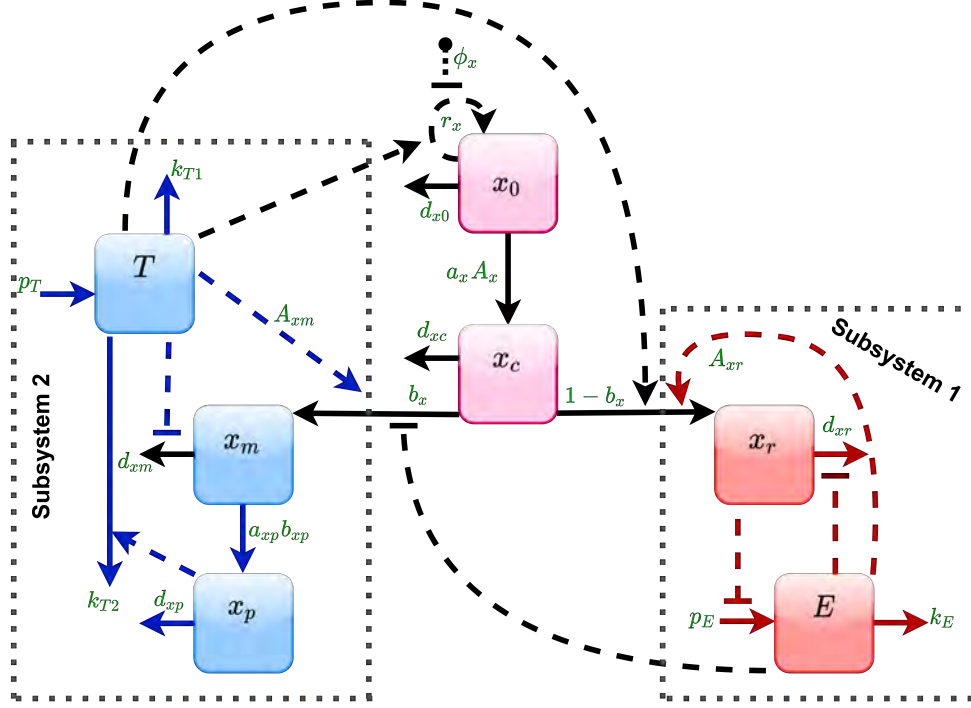


Figure 1: The boxes illustrate the variables of the conceptual model. Solid arrows represent the rates of the flows between and out of these compartments. Red and blue lines represent the mechanisms in subsystems 1 and 2 respectively. HSC (x_0) may self renew (r_x), die (d_{x0}) or differentiate (a_x). The stipulated line shows the inhibiting niche feedback ϕ_x on r_x . MEP (x_c) is produced with rate $a_x A_x$, may die (d_{xc}) or differentiate into MEG (x_m) and RBC (x_r) with fractions b_x and $1 - b_x$ respectively. The production (p_E) of EPO (E) is inhibited by RBC and EPO is degraded with rate k_E . EPO stimulates the proliferation (A_{xr}) and inhibits the death rate (d_{xr}) of RBC. MEG differentiates into platelets x_p with rate $a_{xp} b_{xp}$. MEG and PLT die with rates d_{xm} and d_{xp} respectively. TPO (T) stimulates the proliferation (A_{xm}) and inhibits the death rate (d_{xm}) of MEG while x_p stimulates the degradation of TPO k_{T2} . TPO is produced with baseline rate p_T and degradation rate k_{T1} . TPO stimulates the self-renewal of HSC and production of RBC whereas EPO inhibits the production of MEG. The two dotted boxes emphasize the two subsystems 1 and 2 describing the red blood cell - EPO subsystem and the platelet-megakaryocyte-TPO subsystem.

2 Mathematical model for erythropoiesis and thrombopoiesis

Based on the above assumptions, the model equations can be formulated. The resulting seven-dimensional compartment model consists of non-linear ordinary differential equations: the number of hematopoietic stem cells (x_0), the number of megakaryocyte-erythroid progenitors (x_c), the number of erythrocytes (x_r), the concentration of EPO (E), the number of megakaryocytes (x_m), the number of platelets (x_p) and the concentration of TPO (T). The conceptual model is

illustrated in Fig. 1. The resulting equations are,

$$\frac{dx_0}{dt} = (r_x T \phi_x(x_0) - d_{x0} - a_x)x_0, \quad (1a)$$

$$\frac{dx_c}{dt} = a_x A_x x_0 - b_x x_c - (1 - b_x)x_c - d_{xc}x_c, \quad (1b)$$

$$\frac{dx_m}{dt} = \frac{b_x}{1 + k_m E} A_{xm}(T)x_c - (b_{xp} + d_{xm}(T))x_m, \quad (1c)$$

$$\frac{dx_p}{dt} = a_{xp} b_{xp} x_m - d_{xp} x_p, \quad (1d)$$

$$\frac{dx_r}{dt} = (1 - b_x) A_{xr}(E) T x_c - d_{xr}(E) x_r, \quad (1e)$$

$$\frac{dE}{dt} = \frac{pE}{1 + k_0 x_r} - k_E E, \quad (1f)$$

$$\frac{dT}{dt} = p_T - (k_{T1} + k_{T2} x_p) T. \quad (1g)$$

r_x and d_{x0} represents self-renewal and death rates for HSC. Based on assumption 1, we take inhibiting niche feedback on self-renewal of HSC,

$$\phi_x = \frac{1}{1 + c_{xx} x_0}. \quad (2)$$

x_0 differentiates into x_c at the rate a_x . The progenitor cells between HSCs and MEP are implicitly considered by the multiplication factor A_x such that the resulting production rates of HSC become $a_x A_x$. Using assumption 6, the fraction of megakaryocytes and erythrocytes is denoted by b_x and $1 - b_x$. Moreover, d_{xc} represents the death rate of x_c .

Using assumption 7, k_m is the factor by which EPO inhibits the production of x_m whereas, by assumption 3, TPO stimulates the production of x_m and inhibiting the death rate of x_m given as,

$$A_{xm}(T) = \frac{\delta_{xm1}}{1 + \delta_{xm2} T} T, \quad (3)$$

$$d_{xm}(T) = \frac{\eta_{xm1}}{1 + \eta_{xm2} T}. \quad (4)$$

The fraction of x_m fragmented into x_p at the rate b_{xp} , a_{xp} is the number of fragmented platelets and d_{xp} denotes the death rate of x_p .

Considering assumption 8, EPO stimulates the production of erythrocytes while inhibiting their death rates as,

$$A_{xr}(E) = \frac{\delta_{xr1}}{1 + \delta_{xr2} E} E, \quad (5)$$

$$d_{xr}(E) = \frac{\eta_{xr1}}{1 + \eta_{xr2} E}. \quad (6)$$

The production of EPO, p_E is dependent on the number of erythrocytes x_r . Hence, a high number of x_r leads to a low level of EPO. EPO is degraded at the rate k_E . TPO is produced at the rate p_T and degraded at the rate k_{T1} and by platelets at $k_{T2}x_p$ (assumption 5). Finally, by assumptions 2 and 4, TPO stimulates HSC and RBC given in Eqs. 1a and 1e.

The default values of parameters and variables at steady state are given in Table 1.

Name	Value	Unit	Explanation	Reference
\bar{x}_0	$1.19 \cdot 10^4$	cells/kg	Normal HSC number	[48, 18, 27, 53]
\bar{x}_c	$1.34 \cdot 10^3$	cells/kg	Normal MEP number	-
\bar{x}_m	$1.89 \cdot 10^7$	cells/kg	Normal MEG number	-
\bar{x}_p	$1.99 \cdot 10^{11}$	cells/kg	Normal PLT number	[40]
\bar{x}_r	$5.21 \cdot 10^{12}$	cells/kg	Normal RBC number	[20, 66]
\bar{E}	6.87	U/L	EPO level	[49, 66]
\bar{T}	120.38	pg/ml	TPO level	[73]
Parameter	Value	Unit	Explanation	Reference
r_x	$5 \cdot 10^{-3}$	day ⁻¹	Self-renewal rate of HSC	[18]
a_x	$3.58 \cdot 10^{-5}$	day ⁻¹	Differentiation rate of HSC	-
d_{x0}	$2 \cdot 10^{-3}$	day ⁻¹	Death rate of HSC	[5, 59, 67]
c_{xx}	$2.48 \cdot 10^{-3}$	-	Inhibiting effect on HSC	-
A_x	$3.65 \cdot 10^3$	-	Multiplication factor for progenitor cells	-
d_{xc}	$1.7 \cdot 10^{-1}$	day ⁻¹	Death rate of MEP	-
b_x	$2.6 \cdot 10^{-1}$	day ⁻¹	Fraction of MEG	-
k_m	50	-	Factor affecting production of MEG	-
b_{xp}	$3.5 \cdot 10^{-1}$	-	Fraction MEG shedding PLT	-
a_{xp}	$3 \cdot 10^3$	-	MEG fragmented into PLT	[41, 17]
d_{xp}	$1 \cdot 10^{-1}$	day ⁻¹	Death rate of PLT	[66]
p_E	$1.56 \cdot 10^4$	day ⁻¹	Production rate of EPO	-
k_0	$5 \cdot 10^{-10}$	-	Factor affecting production of EPO	-
k_E	2.8	day ⁻¹	Degradation rate of EPO	[7, 10]
p_T	180	day ⁻¹	Production rate of TPO	-
k_{T1}	$5 \cdot 10^{-1}$	-	Random loss of TPO	-
k_{T2}	$5 \cdot 10^{-12}$	day ⁻¹	Degradation rate of TPO by PLT	-
δ_{xr1}	$3.06 \cdot 10^6$	-	Stimulation rate of RBC	-
δ_{xr2}	2.94	-	Factor affecting production of RBC	-
η_{xr1}	$1 \cdot 10^{-1}$	-	Factor affecting death rate of RBC	-
η_{xr2}	$5 \cdot 10^{-1}$	-	Factor affecting death rate of RBC	-
δ_{xm1}	$1 \cdot 10^6$	-	Factor stimulating production of MEG	-
δ_{xm2}	$1 \cdot 10^{-1}$	-	Factor affecting production of MEG	-
η_{xm1}	$3 \cdot 10^{-1}$	-	Factor affecting death rate of MEG	-
η_{xm2}	$9.4 \cdot 10^{-3}$	-	Factor affecting death rate of MEG	-
$A_{xr}(\bar{E})$	$3.25 \cdot 10^5$	-	Stimulation rate of RBC	-
$d_{xr}(\bar{E})$	$8.3 \cdot 10^{-3}$	day ⁻¹	Death rate of RBC	[10, 48]
$A_{xm}(\bar{T})$	$9.91 \cdot 10^5$	-	Stimulation rate of MEG	-
$d_{xm}(\bar{T})$	$1.46 \cdot 10^{-1}$	day ⁻¹	Death rate of MEG	[41, 17]

Table 1: List of the variables at steady state and parameters values

3 Results

This section provides various results related to subsystems of the model shown in Fig. 1, sensitivity analysis and the model calibration.

3.1 Analysis of Subsystems

Interestingly, erythropoiesis and thrombopoiesis subsystems can be independently analyzed from the full model. These subsystems are useful for estimating the important subsets of the full model parameters involved in the various clinical experiments. In addition, the subsystems are prioritized in clinical trials where the physicians are interested in observing hematological parameters specific to erythroid or megakaryocyte lineage. However, the drawback of the subsystems is that they are unable to represent the coupled mechanisms between erythropoiesis and thrombopoiesis.

Subsystems from the system of equations 1 can be decoupled and written in the form of two independent systems. As shown in Fig. 1, we introduce the subsystem 1,

$$\frac{dx_r}{dt} = A_{xr}(E) - d_{xr}(E)x_r, \quad (7a)$$

$$\frac{dE}{dt} = \frac{p_E}{1 + k_0 x_r} - k_E E, \quad (7b)$$

and the subsystem 2,

$$\frac{dx_m}{dt} = A_{xm}(T) - (b_{xp} + d_{xm}(T))x_m, \quad (8a)$$

$$\frac{dx_p}{dt} = a_{xp}b_{xp}x_m - d_{xp}x_p, \quad (8b)$$

$$\frac{dT}{dt} = p_T - (k_{T1} + k_{T2}x_p)T. \quad (8c)$$

We identify the subsystems' steady states and their stability.

- The unique steady state of the subsystem 1 is denoted by $S_1 = (\bar{x}_r, \bar{E}_r)$. Let, J_{S_1} be the Jacobian at S_1 . The determinant $\det(J_{S_1})$ is positive and trace $tr(J_{S_1})$ is negative, hence S_1 is always stable. The classification of the eigenvalues is given in Supplementary S1.

- The unique steady state of the subsystem 2 is denoted by $S_2 = (\bar{x}_m, \bar{x}_p, \bar{T}_p)$. The Jacobian J_{S_2} can be calculated at S_2 . By Routh Hurwitz criteria, S_2 is stable for $P_0P_1 > P_2$ and unstable for $P_0P_1 < P_2$ where,

$$P_0 = \frac{\eta_{xm1}}{1 + \eta_{xm2}\bar{T}_p} + b_{xp} + d_{xp} + k_{T2}\bar{x}_p + k_{T1},$$

$$P_1 = \left(\frac{\eta_{xm1}}{1 + \eta_{xm2}\bar{T}_p} + b_{xp} \right) (d_{xp} + k_{T2}\bar{x}_p + k_{T1}) + d_{xp}(k_{T2}\bar{x}_p + k_{T1}),$$

$$P_2 = d_{xp} \left(\frac{\eta_{xm1}}{1 + \eta_{xm2}\bar{T}_p} + b_{xp} \right) (k_{T2}\bar{x}_p + k_{T1}) + \dots$$

$$\left(\frac{\delta_{xm1}}{(1 + \delta_{xm2}\bar{T}_p)^2} + \frac{\eta_{xm1}\eta_{xm2}}{(1 + \eta_{xm2}\bar{T}_p)^2} \bar{x}_m \right) a_{xp}b_{xp}k_{T2}\bar{T}_p.$$

(See Supplementary S1 for details).

3.2 Sensitivity Analysis

After briefly describing the subsystems, we return to the full model. In clinical trials and practice, total cell counts are usually measured in blood samples. Therefore, we perform a sensitivity analysis to identify the sensitive parameters for the production of erythrocytes and platelets. We choose 10% variation in the default values given in Table 1 to observe the difference in the steady state values of RBC and PLT. (Detailed sensitivity analysis for all variables are given in Supplementary 3.2).

Fig. 2a shows that perturbing a_x , A_x and b_x change the number of platelets. However, the RBC count does not change more than the PLT count.

Fig. 2b illustrates the effect of parameters related to subsystem 1. By decreasing (increasing) δ_{xr1} and η_{xr2} , reduces (higher) the number of both erythrocytes and platelets, whereas decreasing (increasing) δ_{xr2} and η_{xr1} increases (decrease) the RBC and PLT count. This is interpreted as decreasing those parameters that reduce the number of erythrocytes resulted in high EPO levels. Hence, it reduces the production of megakaryocytes, followed by platelets (See Supplementary 3.2 for EPO levels). Furthermore, a high amount of RBC and a low number of PLT are obtained when variation in parameters increases the concentration of EPO (-10% in k_E , $+10\%$ in p_E and -10% in k_0) or vice versa. The parameters involved in the dynamics of EPO are more sensitive compared to others that appear in Fig 2b.

Fig 2c illustrates the effect of parameters included in subsystem 2. By decreasing δ_{xm1} , η_{xm2} , b_{xp} and a_{xp} decrease the average platelet count and increase the RBC count. In contrast, the average platelet count becomes high and the RBC count becomes low when δ_{xm2} , η_{xm1} and d_{xp} are decreased. Thus, these parameters impose an opposite effect on RBC and PLT count. In addition, the number of both erythrocytes and platelets is increased in response to high TPO levels, i.e. $+10\%$ in p_T , -10% in k_{T1} and k_{T2} . (See Supplementary 3.2 for TPO levels).

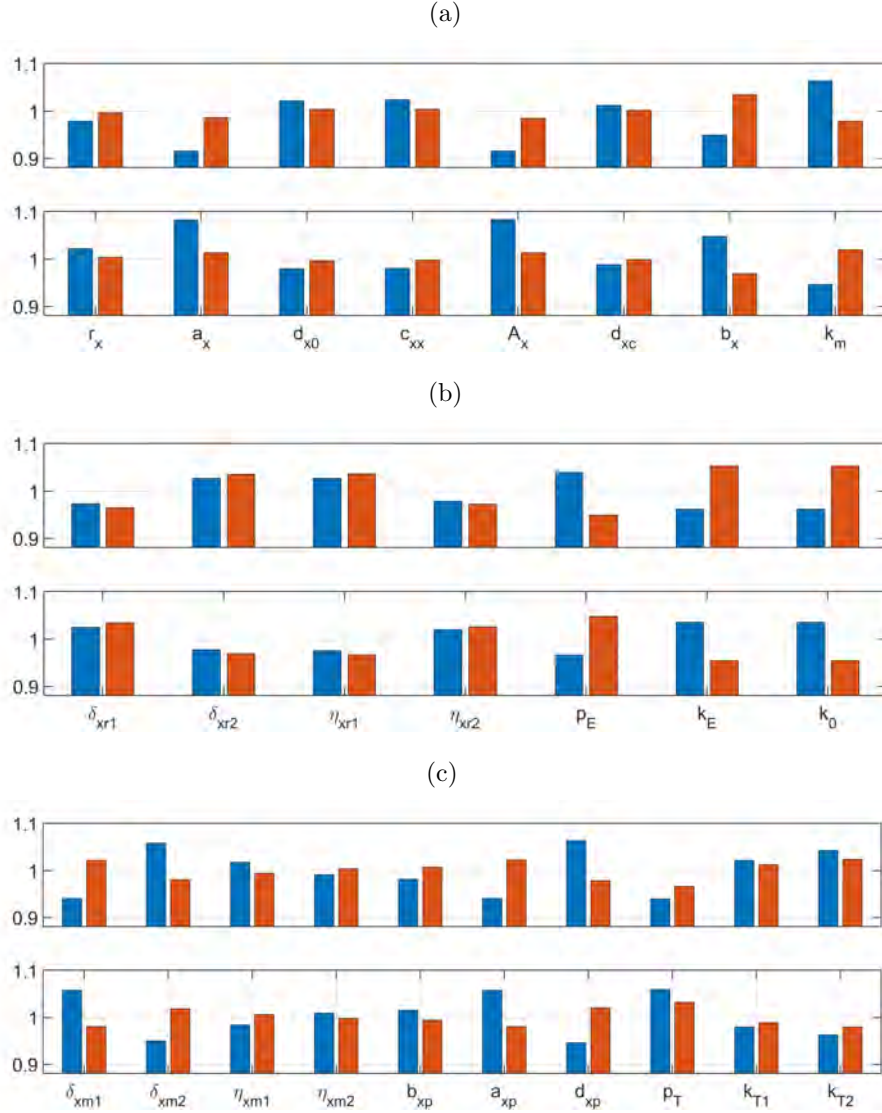


Figure 2: The top panels in (a), (b) and (c) show the relative effect in the number of RBC and PLT when parameters are decreased by 10%, whereas the bottom panels (a), (b) and (c) show the effect when parameters are increased by 10%. The values equal to 1 corresponds to the outcome for the default parameter values.

3.3 Calibration of the model

This section presents the calibration of the model using various data sets of healthy subjects. The hematological parameters can be easily measured in the clinic therefore, we focus on the erythrocyte and platelet count and concentration of EPO and TPO in the following simulations.

3.4 Phlebotomy

The process of drawing blood is known as phlebotomy. The reference range of total blood volume is 5 liters in a human where 450-550 ml is withdrawn when phlebotomy is performed. The clinical trial in [63] shows that the recovery of total hemoglobin in 29 healthy adults (male, 30 ± 10 years, 181 ± 7 cm, 76.6 ± 11.2 kg) takes at most two months. The erythrocytes are assumed to be at steady state when the procedure is performed. Data from [63] is shown in Fig. 3, where the hemoglobin is converted into the number of erythrocytes using mean MCV (mean corpuscular volume) value. (See Supplementary S3 for details). Fig. 3 shows simulations for a standard blood donation of 550 ml. The simulation starts in the steady state, and a half-liter of the blood (including erythrocytes and platelets) is removed due to blood donation at day seven. It shows that the erythrocytes count returns to the baseline within 60 days after blood donation. These results coincide with the findings given in [63].

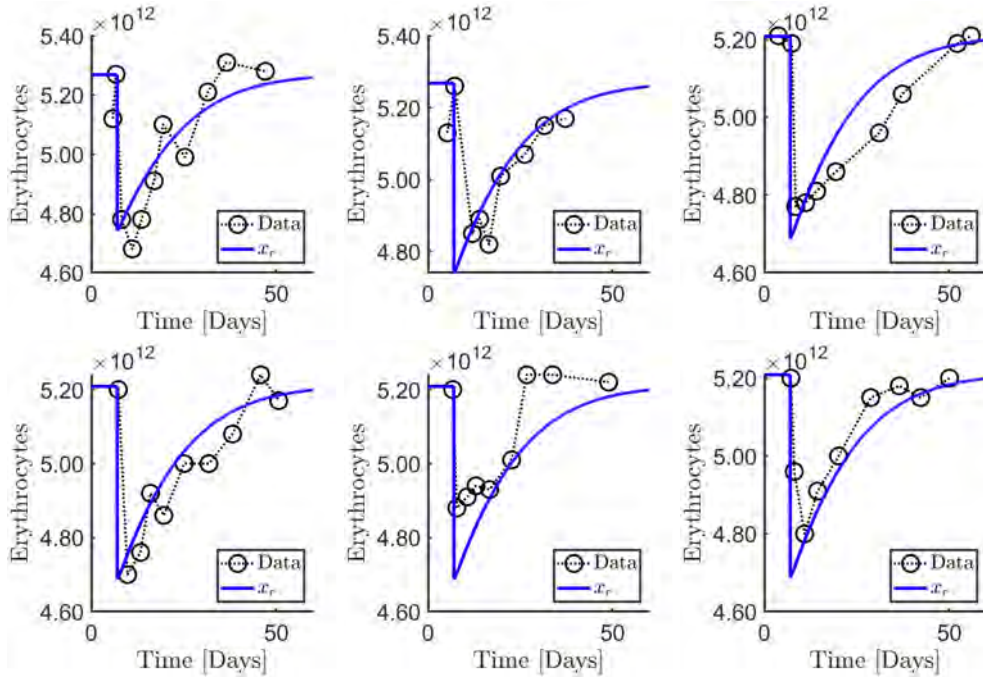


Figure 3: Data of erythrocytes (black circles) measurements over time for six subjects after phlebotomy at day seven [63]. The model curves are represented in blue. A half-liter of the total blood is drawn and erythrocytes reach their steady state level within 60 days after a few days. For the first panel we use, $\delta_{xr1} = 3.15 \cdot 10^6$. The middle and the bottom panels are obtained by the default values of the parameters.

Fig. 4 illustrates how the system responds to phlebotomy and drives back to the original state. We expect that erythrocytes and platelets are removed during phlebotomy. However, we can not find any evidence about EPO and TPO. Fig.

4 shows a minimal increase and decrease in the MEP and megakaryocyte count respectively. In addition, TPO and EPO concentrations are insignificant higher in response to the reduced erythrocyte and platelet count.

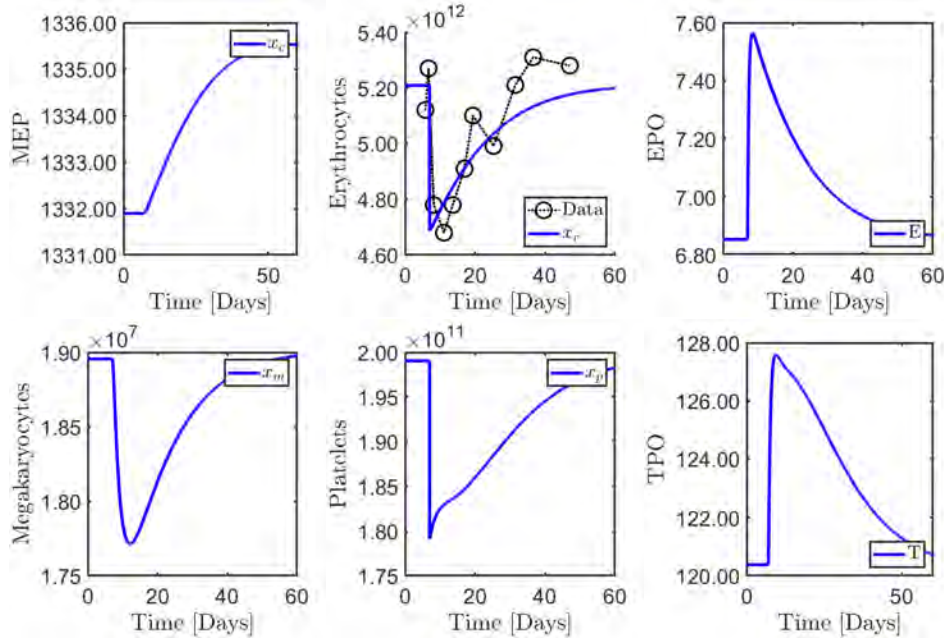


Figure 4: Model simulation during phlebotomy.

3.5 Erythropoiesis stimulating agents (ESAs).

In clinical trials, ESAs are adopted in stimulating the bone marrow to produce red blood cells. EPO is the famous erythropoiesis stimulating agents well known from doping. In healthy adults with normal hematocrit, injections of EPO around 60 IU kg^{-1} one to three times per week for 4–14 weeks increases the hematocrit [47]. Epoetin alpha is recombinant human erythropoietin (rHuEpo) and is nearly identical to EPO. In [13], changes in reticulocytes, hemoglobin and red blood cells are observed after subcutaneous dose (SC) of epoetin alpha.

Fig. 5 illustrates the administration of EPO dose and its effect on the erythrocyte dynamic. We compare the model output to the pharmacodynamics data of the study [75]. In this study SC dose of epoetin alpha is given three times weekly. However, the data for EPO is available only for the last 24 hours. The estimated parameters are taken from subsystem 1 (See Table S1 in Supplementary S1) except δ_{xr1} . We adjust δ_{xr1} to achieve steady state value for erythrocytes. The estimated δ_{xr1} for Fig. 5 is approximately equal to its default value. The estimated parameter values are given in Table 2. All other parameters are set at their default values.

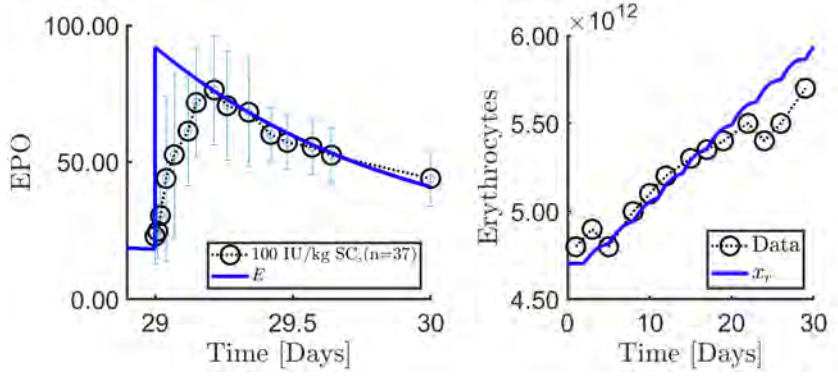


Figure 5: A data set generated from 37 patients is given in [75] after SC dose of epoetin alpha that is given 3 times weekly. The panel shows data (black circles) fitting for erythrocytes (geometric mean is given) and EPO (EPO data is available only for the last day of dose). The model simulations are illustrated in blue. The estimated parameter values are given in Table 2.

Parameter	Values	Parameters	Values	Parameters	Values
δ_{xr1}	$1.09 \cdot 10^6$	η_{xr1}	$2 \cdot 10^{-1}$	p_E	$5 \cdot 10^4$
k_E	1.1				

Table 2: Estimated parameter values for Fig.5

Fig. 6 illustrates data fitting for platelets and EPO where EPO is given intravenously (IV). The data points are taken from [30], and the platelet count rise is claimed after EPO dose. The measurement of platelet count is missing before EPO dose, and the last two data points show the increase in platelet count after 24 hours regardless of error bars. Thus, it is hard to say whether the number of platelets is increased or not after an IV dose of EPO. The authors observed an increase in TXB2 serum levels in response to EPO dose that may cause platelet activation. These markers may be useful for estimation of thromboembolic risk during EPO therapy. In Table. 3, we report deviated values from the default values.

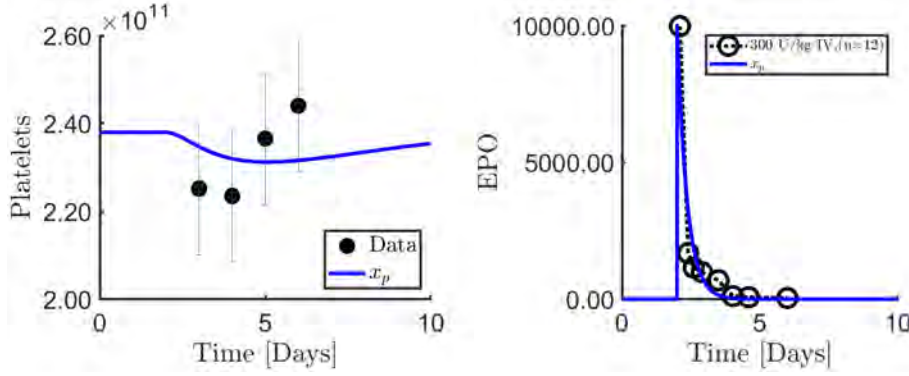


Figure 6: Data (black circles) of platelets and erythrocytes after IV dose of epoetin alpha [30], which enhances formation of red blood cells and also affects thrombopoiesis and platelet function. EPO is recorded before dose, however number of platelets are recorded after dose. The data for erythrocyte count is not available but rise in count is stated in [30]. The panels show data fitting for EPO and platelets. Black circles and blue curves denote data and model simulations respectively. The estimated parameter values are given in Table 3.

Parameter	Value	Parameter	Value	Parameter	Value
d_{x0}	$4.5 \cdot 10^{-2}$	a_x	$2.51 \cdot 10^{-5}$	c_{xx}	$1.49 \cdot 10^{-2}$
b_x	10^{-1}	a_{xp}	$1 \cdot 10^3$	d_{xp}	$2.5 \cdot 10^{-1}$
k_{T2}	$8 \cdot 10^{-12}$	δ_{xm1}	$1.1 \cdot 10^7$	δ_{xm2}	1
δ_{xr1}	$2.7 \cdot 10^{11}$	η_{xr1}	$2.2 \cdot 10^{-3}$		

Table 3: Estimated parameter values for Fig.6

Despite its use in healthy individuals, EPO therapy is used in many diseases such as anemia. EPO injections are used in anemia when a patient suffers from very low red blood cell counts.

3.6 Thrombopoietin stimulants

TPO is the primary physiological hormone that regulates megakaryocyte and platelet development. Another fact is that TPO enables HSC maintenance as well. The thrombopoietin receptor TPO-RAs is the platelet growth factor commonly used to increase the platelet count in immune thrombocytopenia [4, 84]. In [32], the recombinant human thrombopoietin (rhTPO) is experimented to regulate megakaryopoiesis and erythropoiesis in severe aplastic anemia patients hence, the need for blood transfusion is reduced.

In [28], one week after SC injection of thrombopoietic recombinant ($1 \mu\text{g kg}^{-1}$), megakaryopoiesis becomes double, leading to doubling of platelets on day

12. All values return to baseline after four weeks. Fig. 7 illustrates the data fitting for platelet count and TPO levels taken from [28]. The platelet count is increased for a few days and then returned to the initial value within 30 days while TPO level reaches its steady state within 5 days.

Another novel thrombopoietin receptor ligand AMG 531, is investigated through a single IV or SC injection in healthy subjects [80]. AMG 531 is a thrombopoiesis-stimulating protein. Since it is known to stimulate production of megakaryocytes in the same way as TPO, we suppose that the same TPO dose is induced as in [28] and observe the effect on platelet count in Fig. 8. The estimated parameters are taken from subsystem 2 (Table S1). All other parameters are set at their default values except $\eta_{xr1} = 2.2 \cdot 10^{-2}$.

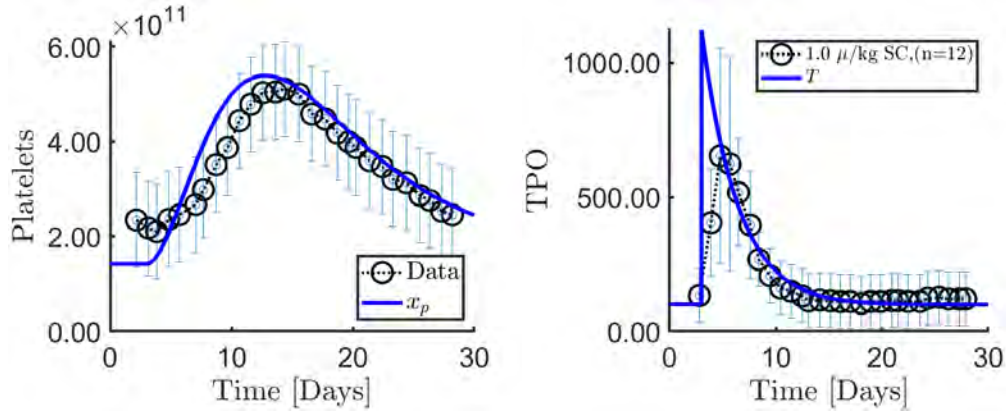


Figure 7: In silico analysis of subcutaneous injection of TPO or PEG-rHuMGDF ($3\mu g/kg$). Data (black circles) of platelets and TPO is given [28]. The model simulations are denoted by blue versus time. The panel shows data fitting for platelets and TPO. The estimated values are given in Table S1.

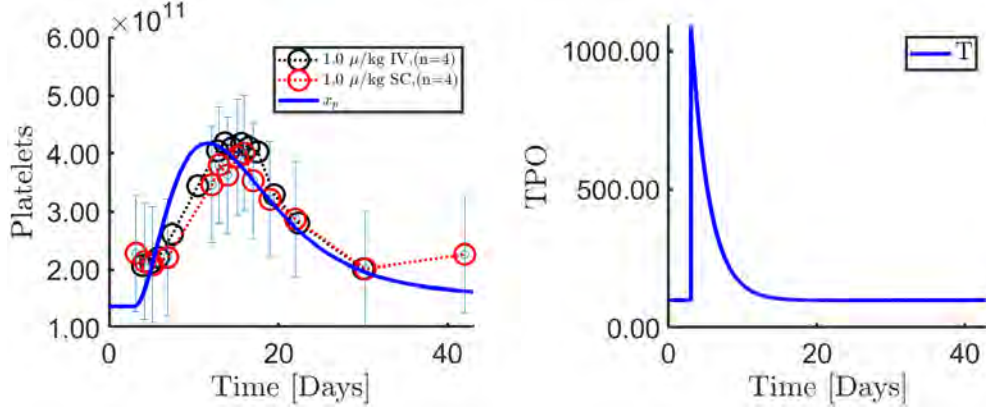


Figure 8: Data of platelet count is given after IV and SC injection of AMG 531 [80]. The black circles represent intravenous dose whereas red circles show subcutaneous dose of TPO receptor AMG 531.

4 Discussion and Conclusions

In this article, a mathematical model incorporating erythrocytes and platelets with multiple EPO and TPO feedbacks is proposed. Moreover, the interacting mechanisms of erythropoiesis and thrombopoiesis are considered. All the biological mechanisms can not be taken into account for our model, however, the essential physiological properties have been captured. The model consists of three ODEs (HSC, MEP and MEG) describing the bone marrow dynamics, and four ODEs of RBC, PLT, EPO and TPO for blood dynamics. Interestingly, the subsystems of erythropoiesis and thrombopoiesis can be decoupled from the full model. The simplified structures of subsystems allow us to perform mathematical investigations and find their steady states. Each of these subsystems has a unique positive steady state and stability conditions of these steady states are covered in supplementary S1.

Sensitivity analysis identifies the sensitive and insensitive parameters for the model variables. Fig. 2 given in section 3.2 describes the effect of 10% variation of parameters on the number of erythrocytes and platelets, and Fig. S6 given in supplementary S2 illustrates the effect of 10% variation of parameters on the full system. Now we summarize the results from sensitivity analysis shown in Fig. 2. The influence of varying the parameters involved in HSC and MEP (a_x , A_x and b_x) is less on the RBC count than on the PLT count. Considering the effect of the parameters included in subsystem 1 (erythropoiesis) on the full model, we can observe that the parameters involved in EPO dynamics are more sensitive as compared to other parameters of subsystem 1. Increasing EPO concentration (-10% k_E , +10% p_E and -10% k_0) increases the RBC count and decreases the PLT count or vice versa. Considering the effect of parameters contained in subsystem 2 (thrombopoiesis) on the full model, the number of both RBC and PLT count is increased in response to high TPO levels by perturbing +10% p_T , -10% k_{T1} and

-10% k_{T2} . However, the remaining parameters (δ_{xm1} , δ_{xm2} , η_{xm1} , η_{xm2} , a_{xp} , b_{xp} and d_{xp}) impose opposite effects on the RBC and PLT count, i.e., if RBC count is decreased, the PLT count is increased or vice versa.

Furthermore, we calibrate the model by fitting to various experimental data sets. The appropriate fitting of data is an appealing feature of the model. Fig. 3 illustrates that for the default values of parameters, we are able to fit phlebotomy data for four subjects. In contrast, a little change is required in δ_{xr1} for adjusting the initial values for two data sets. Furthermore, the subsystems are in excellent agreement with the data. These subsystems help us in estimating parameters of the full model in many situations where the coupling between the two subsystems is of no interest. For instance, Fig. S3 illustrates the effect of EPO therapy on erythrocytes in subsystem 1. The estimated values of η_{xr1} , p_E and k_E are used for data fitting in the full model (See Fig. 5). Similarly, Fig. S4 and Fig. S5 illustrate the data fitting in subsystem 2 where TPO dose stimulates the platelet count. We use these estimated parameter values for data fitting in the full model (See Fig. 7 and Fig. 8). However, a drawback of these nested models is their inability to capture the coupled mechanisms of full model. For example, in [30], the authors were interested in investigating PLT count when EPO injection is given (See Fig. 6). In such situations, our full model is useful to interpret the outcomes of clinical trials.

Besides data fitting, we conduct several other *in silico* experiments for a virtual subject (See supplementary section S4). For example, Fig. S7 and Fig. S8 show the transfusion of red blood cells and platelets. These procedures are primarily preferred for hematological diseases because such *in vivo* experiments are critical for healthy individuals. Fig. S7 illustrates that red blood cell transfusion stimulates the megakaryocytes and platelets and, ultimately, increase in platelet count increases the TPO degradation rate. Furthermore, Fig. S8 represents that transfusing platelets increase TPO degradation, resulting in the reduced MEP, MEG and RBC count, however, the EPO concentration is increased due to low number of erythrocytes. Similarly, plateletpheresis imposes the opposite effects on the dynamics of model (See Fig. S9). Note, our model indicates that HSC remains unaffected with these procedures. The mechanism affecting HSC during blood transfusion and apheresis are not yet well understood. Therefore, we might not interpret this effect accurately in a physiological sense. The academic community has extensively explored the independent reactions of EPO and TPO dose. However, little research [61, 62] has been carried out to investigate the synergy between EPO and TPO. We simulate this combined effect of EPO and TPO dose in Fig. S10. The analysis shows that HSC, MEP and RBC count are increased, whereas, the MEG and PLT count is first decreased, and then after a few days, the number of MEG and PLT is increased. However, when the TPO dose is given alone, we have not seen this sudden drop in MEG and PLT count. According to our perception, this sudden drop can be eliminated by decreasing k_m that reduces the inhibiting strength of EPO to MEG.

In summary, the presented model has the novel feature of simulating and replicating the coupled dynamics of erythropoiesis and thrombopoiesis. The adaptations necessary to combine them are discussed in detail. We demonstrate

how the proposed model and its subsystems can develop clinically meaningful predictions regarding EPO and TPO applications. The overall analysis strengthens the argument that our model is a valid candidate in clinical settings for various experiments. As a future perspective, the model can be extended for multiple hematological diseases where we may include the different pathological aspects for the novel intervention strategies.

Supplementary Materials

S1 Analysis of subsystems

S1.1 Erythropoiesis subsystem: Subsystem 1

The subsystem 1 reads,

$$\frac{dx_r}{dt} = A_{xr}(E) - d_{xr}(E)x_r, \quad (\text{S1a})$$

$$\frac{dE}{dt} = \frac{p_E}{1 + k_0 x_r} - k_E E, \quad (\text{S1b})$$

Steady states

Consider the system of Eqs (S1). Expressions for steady state solutions are,

$$\bar{x}_r = \frac{\delta_{xr1} \bar{E}_r (1 + \eta_{xr2} \bar{E}_r)}{\eta_{xr1} (1 + \delta_{xr2} \bar{E}_r)}, \quad (\text{S2})$$

$$\bar{E}_r = \frac{p_E}{k_E (1 + k_0 \bar{x}_r)}. \quad (\text{S3})$$

Substituting expression for \bar{E}_r in Eq. S2,

$$k_0 k_E \delta_{xr1} \eta_{xr2} E^3 + k_E (k_0 \delta_{xr1} + \delta_{xr2} \eta_{xr1}) E^2 + \eta_{xr1} (-p_E \delta_{xr2} + k_E) E - p_E \eta_{xr1} = 0, \quad (\text{S4})$$

Since the coefficients in the first two terms i.e. $k_0 k_E \delta_{xr1} \eta_{xr2}$ and $k_E (k_0 \delta_{xr1} + \delta_{xr2} \eta_{xr1})$ are positive whereas the last term $-p_E \eta_{xr1}$ is negative. Thus, by using Descartes' rule of sign, there exists exactly one positive root of Eq. S4, such that $E_{r+} = E_r$. Using Eq. S3, we get

$$\bar{x}_r = \frac{1}{k_0} \left(\frac{p_E}{k_E \bar{E}_r} - 1 \right). \quad (\text{S5})$$

Hence, a unique steady state is denoted by $S_1 = (\bar{x}_r, \bar{E}_r)$.

Stability

The stability of the steady states of subsystem 1 is easily characterized. The Jacobian matrix of the subsystem 1 at S_1 is,

$$J_{S_1} = \begin{bmatrix} -\frac{\eta_{xr1}}{1 + \eta_{xr2} \bar{E}_r} & \frac{\delta_{xr1}}{(1 + \delta_{xr2} \bar{E}_r)^2} + \frac{\eta_{xr1} \eta_{xr2}}{(1 + \eta_{xr2} \bar{E}_r)^2} \bar{x}_r \\ -\frac{p_E k_0}{(k_0 \bar{x}_r + 1)^2} & -k_E \end{bmatrix} \quad (\text{S6a})$$

The determinant of the Jacobian at (\bar{x}_r, \bar{E}_r) is,
 $\det(J_{S_1}) = \frac{k_E \eta_{xr1}}{1 + \eta_{xr2} \bar{E}_r} \frac{\delta_{xr1}}{(1 + \delta_{xr2} \bar{E}_r)^2} + \frac{\eta_{xr1} \eta_{xr2}}{(1 + \eta_{xr2} \bar{E}_r)^2} \frac{p_E k_0}{(k_0 \bar{x}_r + 1)^2} \bar{x}_r$ is always positive.

The trace of the Jacobian,

$$tr(J_{S_1}) = -k_E - \frac{\eta_{xr1}}{1 + \eta_{xr2}\bar{E}_r}$$

is always negative. Therefore, no further condition is necessary to guarantee stability of the steady state.

We further find the eigenvalues of the system

$$\lambda_{1,2} = -\frac{tr(J) \pm \sqrt{tr^2 - 4det}}{2}$$

For $tr^2 < 4det$, the obtained eigenvalues are pair of complex conjugates, whereas $tr^2 > 4det$ gives negative real eigenvalues. Fig. S1 is an example showing the trajectories attract towards a stable steady state.

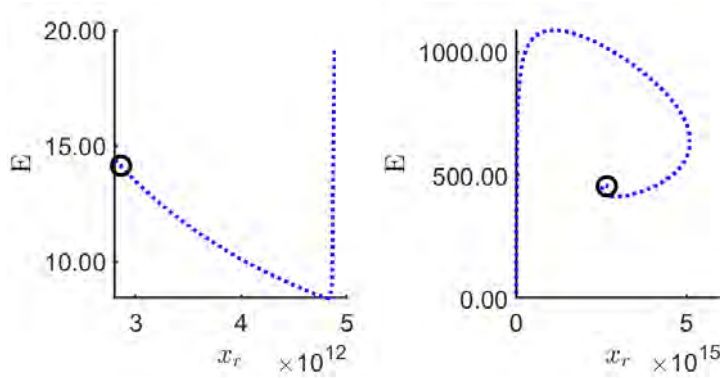


Figure S1: In the left panel, $k_E = 3$ gives two negative real eigenvalues. Decreasing k_E up to $k_E = 10^{-4}$ transforms the real eigenvalues into complex eigenvalues with negative real parts. The resulting trajectories are shown in the right panel.

S1.2 Thrombopoiesis subsystem: Subsystem 2

The subsystem 2 reads,

$$\frac{dx_m}{dt} = A_{xm}(T) - (b_{xp} + d_{xm}(T))x_m, \quad (S7a)$$

$$\frac{dx_p}{dt} = a_{xp}b_{xp}x_m - d_{xp}x_p, \quad (S7b)$$

$$\frac{dT}{dt} = p_T - (k_{T1} + k_{T2}x_p)T. \quad (S7c)$$

Steady states

Consider the system of Eqs (S7). Expressions for steady state solutions are,

$$\bar{x}_m = \frac{\frac{\delta_{xm1}\bar{T}_p}{1 + \delta_{xm2}\bar{T}_p}}{b_{xp} + \frac{\eta_{xm1}}{1 + \eta_{xm2}\bar{T}_p}}, \quad (S8)$$

$$\bar{x}_p = \frac{a_{xp}b_{xp}}{d_{xp}}\bar{x}_m, \quad (\text{S9})$$

$$\bar{T}_p = \frac{p_T}{(k_{T1} + k_{T2}\bar{x}_p)}. \quad (\text{S10})$$

Substitute expression for \bar{x}_p and \bar{T}_p in Eq. S8,

$$\epsilon_3 x_m^3 + \epsilon_2 x_m^2 + \epsilon_1 x_m + \epsilon_0 = 0 \quad (\text{S11})$$

where,

$$\epsilon_3 = b_{xp}^2 (b_{xp} + \eta_{xm1}) a_{xp}^2 k_{T2}^2,$$

$$\epsilon_2 = a_{xp} k_{T2} ((\delta_{xm2} + \eta_{xm2}) p_T + 2k_{T1}) b_{xp} + \eta_{xm1} (p_T \delta_{xm2} + 2k_{T1}) b_{xp} d_{xp},$$

$$\epsilon_1 = ((\eta_{xm2} p_T + k_{T1}) b_{xp} (p_T \delta_{xm2} + k_{T1}) + k_{T1} \eta_{xm1} (p_T \delta_{xm2} + k_{T1})) d_{xp}^2 \dots$$

$$- a_{xp} k_{T2} \delta_{xm1} p_T b_{xp} d_{xp},$$

$$\epsilon_0 = -\delta_{xm1} p_T (\eta_{xm2} p_T + k_{T1}) d_{xp}^2.$$

Since ϵ_3 and ϵ_2 are positive, whereas ϵ_0 is negative. Thus, by using Descartes' rule of sign there exists exactly one positive root of Eq. S11 such that, $\bar{x}_{m+} = \bar{x}_m$. Using \bar{x}_m , we get \bar{x}_p and \bar{T}_p .

Hence, a unique steady state is denoted by $S_2 = (\bar{x}_m, \bar{x}_p, \bar{T}_p)$.

Stability

The Jacobian matrix of the subsystem 2 at S_2 is,

$$J_{S_2} = \begin{bmatrix} -\frac{\eta_{xm1}}{1+\eta_{xm2}\bar{T}_p} - b_{xp} & 0 & \frac{\delta_{xm1}}{(1+\delta_{xm2}\bar{T}_p)^2} + \frac{\eta_{xm1}\eta_{xm2}}{(1+\eta_{xm2}\bar{T}_p)^2} \bar{x}_m \\ a_{xp}b_{xp} & -d_{xp} & 0 \\ 0 & -k_{T2}\bar{T}_p & -k_{T2}\bar{x}_p - k_{T1} \end{bmatrix} \quad (\text{S12a})$$

The characteristic polynomial equation is

$$\lambda^3 + P_0\lambda^2 + P_1\lambda + P_2 = 0$$

where,

$$P_0 = \frac{\eta_{xm1}}{1+\eta_{xm2}\bar{T}_p} + b_{xp} + d_{xp} + k_{T2}\bar{x}_p + k_{T1},$$

$$P_1 = \left(\frac{\eta_{xm1}}{1+\eta_{xm2}\bar{T}_p} + b_{xp} \right) (d_{xp} + k_{T2}\bar{x}_p + k_{T1}) + d_{xp} (k_{T2}\bar{x}_p + k_{T1}) \text{ and}$$

$$P_2 = d_{xp} \left(\frac{\eta_{xm1}}{1+\eta_{xm2}\bar{T}_p} + b_{xp} \right) (k_{T2}\bar{x}_p + k_{T1}) + \left(\frac{\delta_{xm1}}{(1+\delta_{xm2}\bar{T}_p)^2} + \frac{\eta_{xm1}\eta_{xm2}}{(1+\eta_{xm2}\bar{T}_p)^2} \bar{x}_m \right) a_{xp} b_{xp} k_{T2} \bar{T}_p$$

By Routh Hurwitz criteria, all roots lie in the left half plane for $P_0 > 0$, $P_2 > 0$ and $P_0 P_1 > P_2$. P_0 and P_2 are always positive for positive values of parameters. However, a steady state may be unstable when $P_0 P_1$ is less than P_2 . Following are a few examples where the trajectories attract towards a stable steady state. We perform a series of simulations with physiologically acceptable parameter values, but none of the results provide us an unstable steady state.

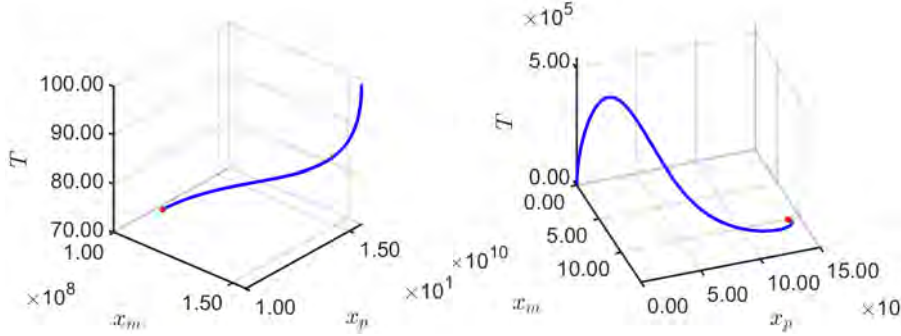


Figure S2: In the left panel, $p_T = 30$ gives three negative real eigenvalues. Increasing p_T provides a negative real and a pair of complex eigenvalues with negative real parts. In the right panel $p_T = 4 \cdot 10^5$.

Numerical Results for Subsystems

In this section, we estimate the model parameters of the subsystems for the experimental data extracted from [75] and [28].

In [75], epoetin alpha is given subcutaneously three times weekly for four weeks to 37 healthy males. The geometric mean of RBC is shown over time however, the data for EPO is available only for the last day (See Fig.S3). In [28], the subcutaneous dose of PEG-rHuMGDF is given to 12 healthy volunteers, and a rise in platelet count and megakaryocyte mass is observed. PEG-rHuMGDF and rHuTPO are two thrombopoietic growth factors and are thought to increase platelets' concentrations equivalently [56]. Due to lack of data, we use PEG-rHuMGDF data for TPO in our simulations (See Fig.S4). The estimated parameter values are given in Table. S1. Fig. S5 shows the effect of AMG 531 (SC and IV) dose on the platelet and megakaryocyte count. AMG 531 is a TPO receptor ligand and has the equivalent ability, like TPO, to bind to Mpl and activate the JAK-STAT pathway.

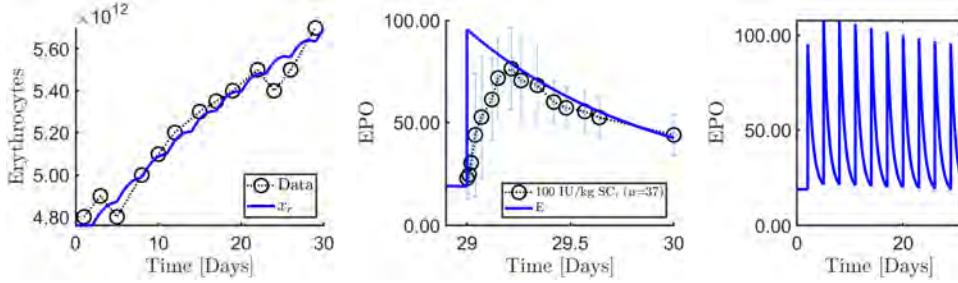


Figure S3: A data set generated from 37 patients is given in [75]. Subcutaneous dose of epoetin alpha is given 3 times weekly. The left figure shows data fitting for erythrocytes (geometric mean is given), the middle figure shows data fitting for EPO (EPO data is available only for the last day of dose) and the right figure shows EPO curves for 30 days.

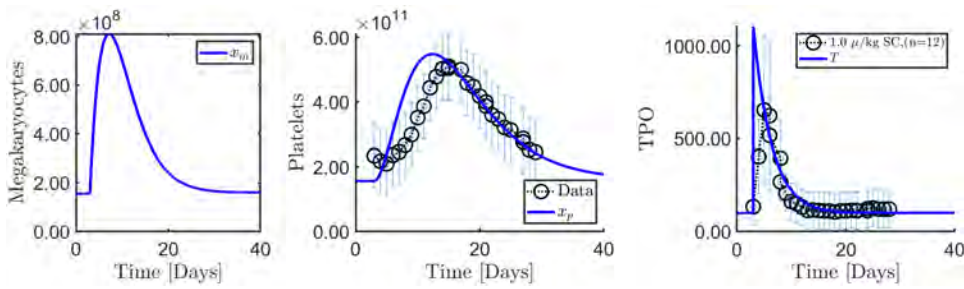


Figure S4: In silico analysis of subcutaneous injection of TPO or PEG-rHuMGDF ($3\mu g/kg$). Data points are taken from [28]. The panels show TPO effect on megakaryocytes, platelets and TPO.

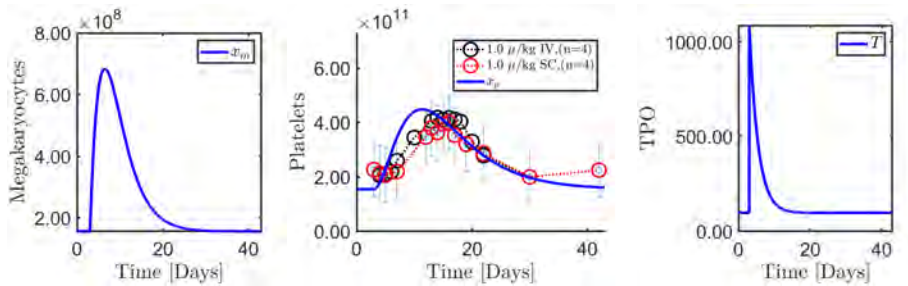


Figure S5: Data points are taken from [80]. The panel shows data fitting for platelets when TPO is induced. The black circles represent intravenous dose whereas red circles show subcutaneous dose of TPO receptor AMG 531. All parameter values are similar to Fig. S4 except k_{T1} .

	Parameter	Value	Parameter	Value
Subsystem 1	δ_{xr1}	$2.7 \cdot 10^{11}$	δ_{xr2}	2.94
	η_{xr1}	$2 \cdot 10^{-1}$	η_{xr2}	$5 \cdot 10^{-1}$
	p_E	$5 \cdot 10^4$	k_0	$5 \cdot 10^{-10}$
	k_E	1.1		
Subsystem 2	b_{xp}	$1.5 \cdot 10^{-1}$	a_{xp}	$1 \cdot 10^3$
	d_{xp}	$1.5 \cdot 10^{-1}$	p_T	30
	k_{T1}	$2.9 \cdot 10^{-1}$	k_{T2}	$3 \cdot 10^{-14}$
	Fig. S4	δ_{xm1}	$4 \cdot 10^5$	δ_{xm2}
Fig. S5	η_{xm1}	$2 \cdot 10^{-1}$	η_{xm2}	$9.4 \cdot 10^{-3}$
	k_{T1}	$4 \cdot 10^{-1}$		

Table S1: Estimated parameter values for Figs. S3, S4, S5

S2 Sensitivity Analysis

We perform a sensitivity analysis to identify the sensitive parameters for the variables involved in the model (See Fig. S6). We choose a 10% variation in the default values given in Table 1 to observe the difference in the cell count and concentration of EPO and TPO.

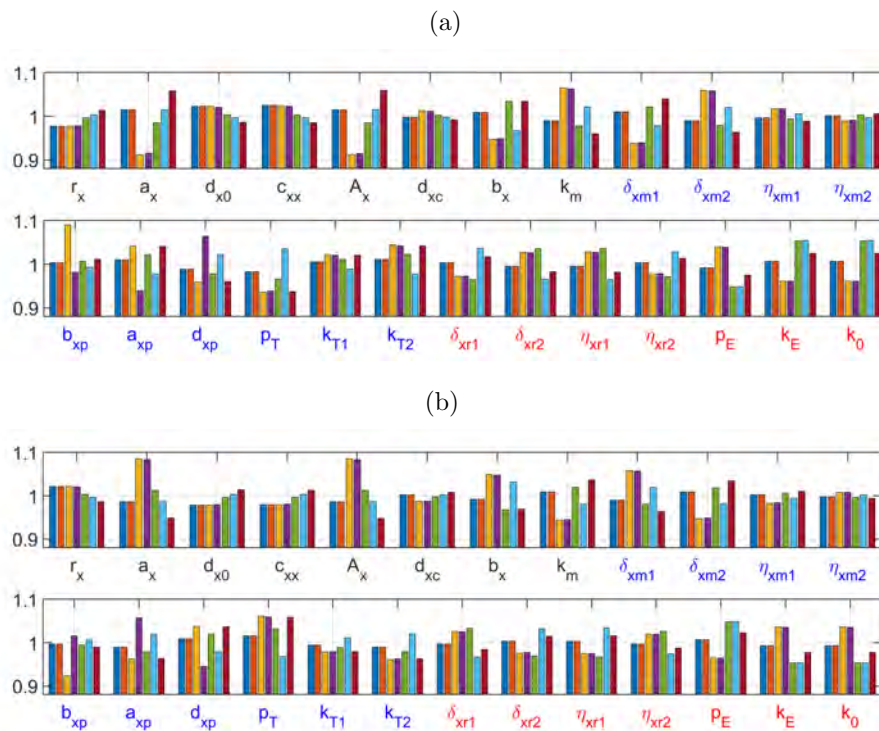


Figure S6: Panels (a) and (b) show the effect when parameters are decreased and increased by 10% respectively. For each parameters, seven columns are shown; blue, red, mustard, purple, green, light blue and maroon correspond to the average of x_0 , x_c , x_m , x_p , x_r , E and T . Parameters in red represent the subsystem 1 and parameters in blue represent the subsystem 2.

S3 Hematological parameters:

The average blood volume in an adult is 4 to 6 liters: women have 4 to 5 liters, and men 5 to 6 liters. This blood volume represents about 8% of total body weight. Blood has a pH between 7.35 and 7.45, and it is composed of 55% plasma (the fluid portion) and 45% formed elements or cells. Of the 45% cellular components, approximately 44% of the cells are red blood cells, whereas only 1% are white blood cells and platelets. Plasma is composed of about 91.5% water and 8.5% solutes (kind of proteins). The proportion of blood occupied by red blood cells measured using hematocrit is called erythrocytes volume percentage (EVP). It is usually expressed as a percentage of the total blood volume. The reference range of hematological parameters for healthy individuals is given in table S2.

Hemoglobin (Hb) consists of a heme group (iron-containing oxygen-transport metalloprotein in the red blood cells). Additionally, a pair of globin chains carry oxygen to the rest of the body. In humans, hemoglobin

is typically used to evaluate red blood cell mass. Hematocrit (Ht) is defined as the volume percentage of red blood cells, and measurements depend upon the red blood cells' size. There are other Ht names, such as packed cell volume (PCV) or erythrocyte volume fraction (EVF).

Since red blood cells are approximately 33% hemoglobin, the Hb concentration of whole blood is typically about one-third of the Ht. In vitro hemolysis, a Ht can be estimated from Hb measurement such as

$$Ht = \frac{Hg}{3} \quad (S13)$$

Mean corpuscular volume (MCV), mean corpuscular haemoglobin (MCH) and mean corpuscular haemoglobin concentration (MCHC) is termed as red blood cell indices. MCV is the size of red blood cells and expressed as femtoliters (10^{15} fl). The average values for MCV are 87 ± 7 fl. MCH quantifies the amount of hemoglobin per red blood cell. The normal values for MCH are 29 ± 2 picograms (pg) per cell. MCHC correlates the hemoglobin with the volume of a cell. It is expressed as g/dl of red blood cells or as a percentage value. The normal values for MCHC are 34 ± 2 g/dl. In [63], a minimal difference is observed in MCH measurements for all subjects. In addition, MCV is measured before, and after phlebotomy in [35], the standard deviation from the mean is 88.4 ± 0.8 fl. Hence, it is concluded that the arithmetic mean of MCH and MCV values can be used in the following formulas.

$$Number\ of\ Erythrocytes = \frac{Ht}{MCV} \times 10^{12} \quad (S14a)$$

$$Number\ of\ Erythrocytes = \frac{Hg}{MCH} \times 10^{12} \quad (S14b)$$

Category	Reference range
Red blood cells (RBCs)	4.2 to 5.4×10^{12} /L (females), 4.7 to 6.1×10^{12} / L (males)
Hematocrit (Hct)	37% to 47% (females), 42% to 52% (males)
White blood cells (WBCs)	4.8 to 10.8×10^9 /L
Platelets (PLTs)	150 to 400×10^9 /L
EPO	6-16 IU/L
Tpo	81.25-237.7 pg/ml

Table S2: Reference range for hematological parameters

S4 Simulations

We use default parameter values for all the simulations below.

S4.1 Transfusion of red blood cells

The transfusion of red blood cells is performed in order to achieve a rapid increase in the supply of oxygen to the tissues when the concentration of hemoglobin (Hb) is low and the oxygen carrying capacity is reduced. The critical patients suffering from an iron deficiency or anemia are also advised for red blood cell transfusion. The procedure is also associated with the increased risk of thrombotic events but the underlying mechanisms are poorly understood. Some of the research shed light on the platelet activation and aggregation after red blood cell transfusion in healthy and ill individuals [72]. However, its effect on the megakaryopoiesis and hematopoietic stem cells are yet to be revealed.

Fig. S7 illustrates the outcome of the model when 10% erythrocytes are induced at a steady state. The concentration of EPO and TPO is decreased. Due to a decrease in TPO levels, megakaryocytes and platelets count are increased but still in the reference range. However, the red blood cell transfusion shows no effect on HSC count therefore, we do not include the figure for HSC.

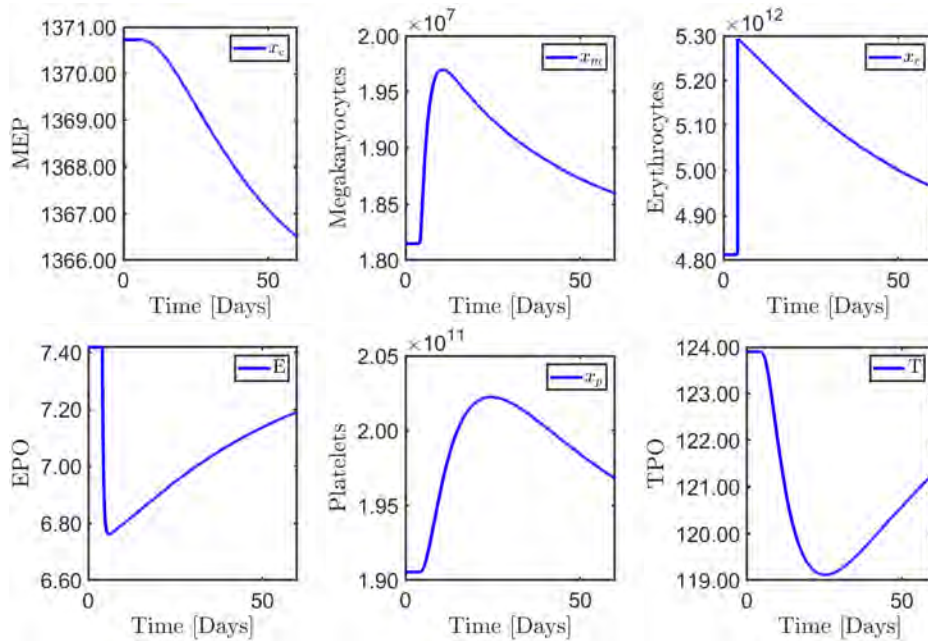


Figure S7: In silico analysis of 1 unit (9%-10%) of RBC transfusion.

S4.2 Platelet transfusion and Plateletpheresis

Platelet transfusion is the process of transfusing platelets to persons having platelet levels less than $10 \times 10^9/L$. Such therapy is mainly applied to patients with thrombocytopenia. It is also hypothesized that transfusing platelets

decreases TPO concentration, which eventually supports the evidence of TPO clearance through platelets [55, 21]. In [21], it is investigated that platelet count and TPO concentration are inversely correlated. After the transfusion, the number of platelets is increased immediately and then started to decrease. Conversely, TPO levels are reduced significantly but then returned to steady state level in almost three days.

In Figure S8, we show *in silico* analysis of platelet transfusion. We notice that platelet transfusion results in decreasing the concentration of TPO. In addition, we can observe the dynamics of erythropoiesis. The number of erythrocytes is reduced, and as a result, the concentration of EPO is increased while MEP count decreases slightly. We exclude a figure illustrating HSC count since HSC count is almost constant.

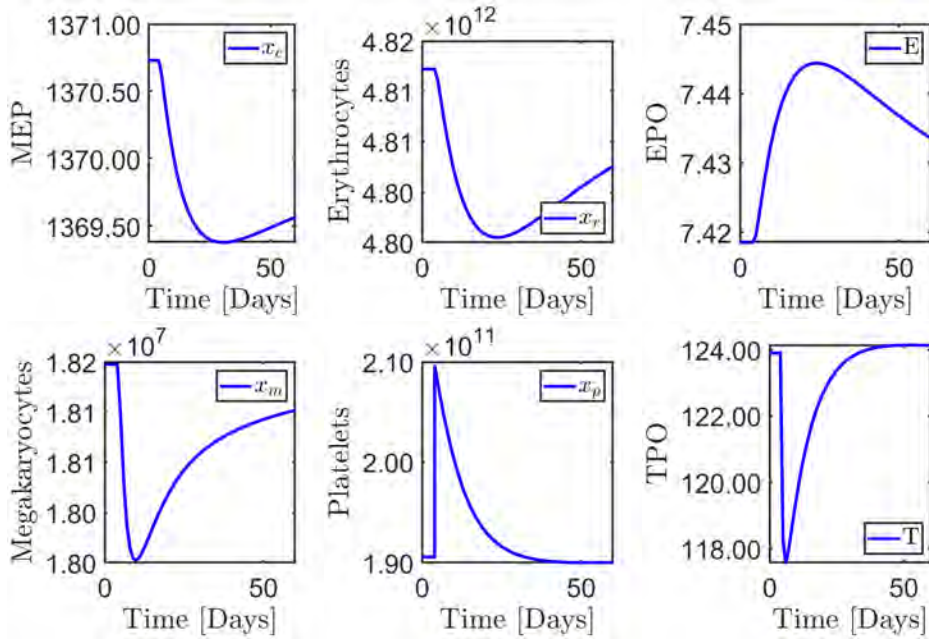


Figure S8: *In silico* analysis of platelet transfusion. 10% platelets are transfused.

Plateletpheresis is the process used in blood donation separating the platelets and returning the rest of the blood to the donor. It may also be used to treat patients with thrombocytosis. Plateletpheresis is performed in four MPN patients with extreme thrombocytosis and platelet counts are decreased within 1 to 3 sessions without any adverse effects [11]. Fig. S9 illustrates that removing platelets increases the number of erythrocytes. It is associated to the risk of thrombosis if the elevation is too high.

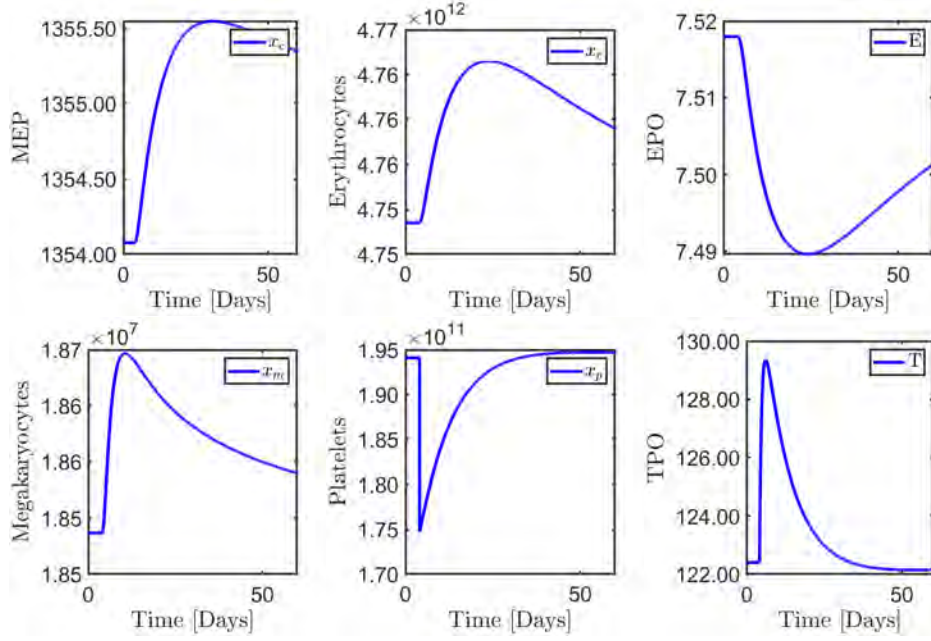


Figure S9: In silico analysis of plateletpheresis. 10% platelets are removed.

S4.3 Combination of EPO and TPO dose

Several clinical experiments are held to investigate the effects of EPO and TPO alone or in combination with each other on the stimulation of erythroid-megakaryocyte progenitors and HSC [37, 54, 61, 62, 74]. We are able to perform such experiments in our model. In Fig. S10, we inject EPO and TPO at the same time. We suppose EPO (100 U/l) and TPO (1000 pg/ml) dose equivalent to clinical trials performed in [75] and [28]. Fig. S10 illustrates that the combination of EPO and TPO dose stimulates HSC and MEP, resulting in erythrocyte production. In contrast, megakaryocyte and platelet count first decrease, and within 5 to 10 days, they become higher than the previous level.

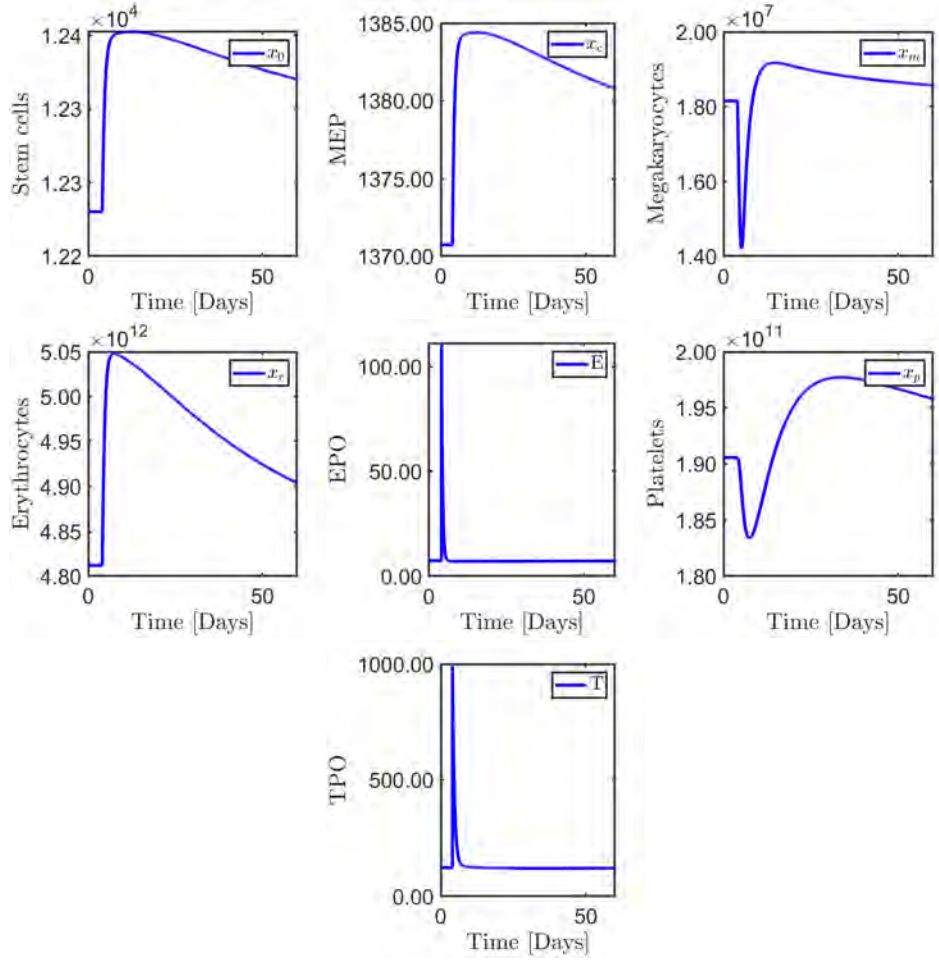


Figure S10: Combination of EPO and TPO dose.

References

- [1] Abkowitz JL, Catlin SN, Mc Callie MT and Gutter P Evidence that the number of hematopoietic stem cells per animal is conserved in mammals. *Blood*, 03-0822.
- [2] Adamson J. 1974 The relationship of erythropoietin and iron metabolism to red blood cell production in humans. *Semin. Oncol*, 21, 9-15.
- [3] Adimy M, Crauste F and Ruan S. 2006. Modelling hematopoiesis mediated by growth factors with applications to periodic haematological diseases. *Bull Math Biol*, 68:2321–2351.
- [4] Al-Samkari H and Kuter DJ. 2019. Optimal use of thrombopoietin receptor agonists in immune thrombocytopenia. *Therapeutic Advances in Hematology*.
- [5] Andersen M, Sajid Z, Pedersen RK, Gudmand-Hoeyer J, Ellervik C, Skov V, Kjær L, Pallisgaard N, Kruse TA, Thomassen M, Troelsen J, Hasselbalch HC and Ottesen JT. 2017. Mathematical modelling as a proof of concept for MPNs as a human inflammation model for cancer development. *Plos One*.
- [6] Andersen M, Hasselbalch H, Kjaer L, Skov V and Ottesen JT. 2020. Global dynamics of healthy and cancer cells competing in the hematopoietic system. *Mathematical Biosciences* 626, 1-15.
- [7] Angulo O, Crauste F and López-Marcos JC. 2018. Numerical integration of an erythropoiesis model with explicit growth factor dynamics. *Journal of Computational and Applied Mathematics*, 330: 770-782.
- [8] Banks HT, Bliss KM and Tran H. 2012. Modelling Red Blood Cell and Iron Dynamics in Patients with Chronic Kidney Disease. *North Carolina State University. Center for Research in Scientific Computation*.
- [9] Beer PA, Campbell PJ and Scott LM. 2008. MPL mutations in myeloproliferative disorders: analysis of the PT-1 cohort. *Blood*, 112:141-9.
- [10] Belair J, Mackey MC and Mahaffy JM. 1995. Age-structured and two delay models for erythropoiesis. *Math. Biosci.* 128, 317-346.
- [11] Boddu P, Falchi L, Hosing C, Newberry K, Bose P and Verstovsek S. 2017. The role of thrombocytapheresis in the contemporary management of hyperthrombocytosis in Myeloproliferative Neoplasms: A case based study review. *Leuk Res*, 58: 14–22.

- [12] Campbell PJ and Green AR. 2006. The myeloproliferative disorders. *N. Engl. J. Med.*, 355: 2452–2466.
- [13] Cheung W, Minton N and Gunawardena K. 2001. Pharmacokinetics and pharmacodynamics of epoetin alpha once weekly and three times weekly. *European Journal Pharmacol*, 57: 411-418.
- [14] Colijn C and Mackey MC. 2005. A mathematical model of hematopoiesis: II. Cyclical neutropenia. *Journal of Theoretical Biology*, 237 133–146.
- [15] Crauste F, Pujo-Menjouet L, Genieys S, Molina C and Gandrillon O. 2008. Adding self-renewal in committed erythroid progenitors improves the biological relevance of a mathematical model of erythropoiesis. *Journal of Theoretical Biology*, 250:322–338.
- [16] Debili N, Coulombel L, Croisille L, Katz A, Guichard J, Breton-Gorius. 1996. J, et al. Characterization of a bipotent erythro-megakaryocytic progenitor in human bone marrow. *Blood*, 88:1284–1296.
- [17] Deutsch VR and Tomer A. 2006. Megakaryocyte development and platelet production. *British Journal of Haematology*, 134, 453–466.
- [18] Dingli D and Michor F. 2006. Successful Therapy Must Eradicate Cancer. *Stem Cells*, 24(12): 2603.
- [19] Edvardsson L, Dykes J and Olofsson T. 2006. Isolation and characterization of human myeloid progenitor populations–TpoR as discriminator between common myeloid and megakaryocyte/erythroid progenitors. *Exp Hematol*, 34(5): 599-609.
- [20] Erslev AJ. 1990. Production of erythrocytes. *Haematology*, pages 389–397.
- [21] Folman CC, de Jong SM, de Haas M and von dem Borne AE. 2001. Analysis of the kinetics of TPO uptake during platelet transfusion. *Transfusion*, 41:517-521.
- [22] Foo J, Drummond MW, Clarkson B, Holyoake T and Michor F. 2009. Eradication of Chronic Myeloid Leukemia Stem Cells: A Novel Mathematical Model predicts no therapeutic benefit of adding G-CSF to Imatinib. *PLoS Comput Biol* 5(9).
- [23] Fuertinger DH, Kappel F, Thijssen S, Levin N and Kotanko P. 2013. A model of erythropoiesis in adults with sufficient iron availability. *J. Math. Biol.*, 66: 1209–1240.

- [24] Fuertinger DH, Kappel F, Zhang H, Thijssen S and Kotanko P. 2017. Prediction of hemoglobin levels in individual hemodialysis patients by means of a mathematical model of erythropoiesis. *Plos One*.
- [25] Granziero L, Ghia P, Circosta P, Gottardi D, Strola G, Geuna M, Montagna L, Piccoli P, Chilosi M and Caligaris-Cappio F. 2001. Survivin is expressed on CD40 stimulation and interfaces proliferation and apoptosis in B-cell chronic lymphocytic leukemia. *Blood*, 97, 9: 2777-2783.
- [26] Guttia U, Pasupuletib SR, Sahub I, Kotipallib A, Undib RB, Kandib R, Saladia RGV and Guttib RK. 2016. Erythropoietin and thrombopoietin mimetics: Natural alternatives to erythrocyte and platelet disorders. *Critical Reviews in Oncology/Hematology*, vol:108, 175–186.
- [27] Haeno H, Levine RL, Gilliland DG and Michor F. 2009. A progenitor cell origin of myeloid malignancies. *Proceedings of the National Academy of Sciences of the United States of America*, 106(39):16616-16621.
- [28] Harker LA, Roskos LK, Marzec UM, Carter RA, Cherry JK, Sundell B, Cheung EN, Terry D and Sheridan W. 2000. Effects of megakaryocyte growth and development factor on platelet production, platelet life span, and platelet function in healthy human volunteers. *Blood*, vol 95, 8.
- [29] Hasselbalch HC. 2013. Chronic inflammation as a promotor of mutagenesis in essential thrombocythemia, polycythemia vera and myelofibrosis. A human inflammation model for cancer development? *Leukemia Research*, 37: 214–220.
- [30] Heinisch BB, Vcelar B, Kapiotis S, Blann A, Wolzt M, Sillermatula JM and Jilma B. 2012. The effect of erythropoietin on platelet and endothelial activation markers: A prospective trial in healthy volunteers. *Platelets*, 23(5): 352–358.
- [31] Horikawa Y, Matsumura I, Hashimoto K, Shiraga M, Kosugi S, Tadokoro S, Kato T, Miyazaki H, Tomiyama Y, Kurata Y, Matsuzawa Y and Kanakura Y . 1997. Markedly reduced expression of platelet c-mpl receptor in essential thrombocythemia. *Blood*, 90: 4031–4038.
- [32] Huang J and Tefferi A. 2009. Erythropoiesis stimulating agents have limited therapeutic activity in transfusion-dependent patients with primary myelofibrosis regardless of serum erythropoietin level. *Eur J Haematol*, 83 (2): 154-5.
- [33] Iiyama M, Kakihana K, Kurosu T and Miura O. 2006. Reactive oxygen species generated by hematopoietic cytokines play roles in activation of receptor- mediated signaling and in cell cycle progression. *Cellular Signalling* 18, 2: 174-182.

- [34] Jelkmann W. 2013. Physiology and pharmacology of erythropoietin. *Transfus Med Hemother*, 40:302–309.
- [35] Johansson P and Andreasson B. 2006. Hydroxyurea therapy increases plasma erythropoietin in patients with essential thrombocythaemia or polycythaemia vera. *Clin. Lab. Haem.* 28: 233-236.
- [36] Kaushansky K. 1995. Thrombopoietin: the primary regulator of platelet production. *Blood*, 86 : 419–431.
- [37] Kaushansky K, Broudy VC, Grossmann A, Humes J, Lin N, Ren HP, Bailey MC, Papayannopoulou T, Forstrom JW and Sprugel KH. 1995. Thrombopoietin expands erythroid progenitors, increases red cell production, and enhances erythroid recovery after myelosuppressive therapy. *J Clin Invest*, 96(3):1683-7.
- [38] Kaushansky K. 1998. Drug Therapy. *The New England Journal of Medicine*.
- [39] Krantz SB. 1991. Erythropoietin. *Blood*, 77(3): 419–434.
- [40] Kuter DJ. 1996. The physiology of platelet production. *Stem Cells*, 14, 88-101.
- [41] Kuter DJ and Gernsheimer TB. 2009. Thrombopoietin and Platelet Production in Chronic Immune Thrombocytopenia. *Hematol Oncol Clin North Am*, 23(6): 1193–1211.
- [42] Langlois GP, Morgan Craig, Antony R. Humphries, Michael C. Mackey, Joseph M. Mahaffy, Jacques Bélair, Thibault Moulin, Sean R. Sinclair and Liangliang Wang. 2017. Normal and pathological dynamics of platelets in humans. *Journal of Mathematical Biology*, 75 (6-7): 1411-1462.
- [43] Li J, Xia Y and Kuter DJ. 1999. Interaction of thrombopoietin with the platelet c-mpl receptor in plasma: binding, internalization, stability and pharmacokinetics. *British Journal of Haematology*, 106, 345-356.
- [44] Li N, Yao QM and Gale RP. 2015. Frequency and allele burden of CALR mutations in Chinese with essential thrombocythemia and primary myelofibrosis without JAK2(V617F) or MPL mutations. *Leuk Res*, 39:510-4.
- [45] Lichtman MA, Beutler E, Kipps TJ, Seligsohn U, Kaushansky K and Prchal JT. 2006. Williams Hematology. McGraw-Hill: New York, NY, USA.

- [46] Lilienthal P, Tetschke M, Schalk E, Fischer T and Sager S. 2020. Optimized and Personalized Phlebotomy Schedules for Patients Suffering From Polycythemia Vera. *Frontiers in physiology*.
- [47] Lundby C and Olsen NV. 2011. Effects of recombinant human erythropoietin in normal humans. *J Physiol* 589.6 pp 1265–1271.
- [48] Mackey M. 1978. Unified hypothesis of the origin of aplastic anaemia and periodic hematopoiesis. *Blood*, 51, 941–956.
- [49] Mahaffy JM. 1999. Age-structured modelling of haematopoiesis. *San Diego State University*.
- [50] Mahaffy JM, Polk SW and Roeder RK. 1999. An age-structured model for erythropoiesis following a phlebotomy. *Tech. Rep. CRM-2598, Department of Mathematical Sciences, San Diego State University, San Diego, CA 92182-0314*.
- [51] Majka M, Ratajczak J, Gewirtz AM, Ratajczak MZ. 2000. PI-3K-AKT axis inhibits apoptosis in normal human megakaryoblasts and is efficiently activated by thrombopoietin. *Experimental Hematology*, Vol.28(12), pp.1492-1492.
- [52] Majka M, Janowska-Wieczorek A, Ratajczak J, Kowalska MA, Vilaire G, Pan ZK, Honczarenko M, Marquez LA, Poncz M and Ratajczak MZ. 2000. Stromal-derived factor 1 and thrombopoietin regulate distinct aspects of human megakaryopoiesis. *Blood*, Vol.86(13).
- [53] Marciniak-Czochra A, Stiehl T, Ho AD, Jäger W and Wagner W. 2009. Modelling of asymmetric cell division in hematopoietic stem cells—regulation of self-renewal is essential for efficient repopulation. *Stem Cells Dev*, 18 (3), 377-85.
- [54] McDonald TP, Cottrell MB, Clift RE, Cullen WC and Lin FK. 1987. High doses of recombinant erythropoietin stimulate platelet production in mice. *Exp Hematol*, 15(6):719-21.
- [55] Moller P, Andersson PO, Andersson AC and Wadenvik H. 2000. Plasma thrombopoietin concentrations in response to platelet transfusion therapy. *Acta Haematol*, 102(3):131-4.
- [56] Murphy MJ Jr, Kuter DJ. 1998. Thrombopoietin: from molecule to medicine. *Stem Cells*, 16: 1-257.
- [57] Noetzli LJ, French SL and Machlus KR. 2019. New insights into the differentiation of megakaryocytes from hematopoietic progenitors. *Arterioscler Thromb Vasc Biol*, 39: 1288- 1300.

- [58] Obama K, Maruyama Y, Osame M. 1999. The correlation between erythropoiesis and thrombopoiesis as an index for pre-operative autologous blood donation. *Transfusion science* 21, 207-210.
- [59] Ottesen JT, Sajid Z, Pedersen RK, Gudmand-Hoeyer J, Bangsgaard KO, Skov V, Kjær L, Knudsen TA, Pallisgaard N, Kruse TA, Thomassen M, Troelsen J, Hasselbalch HC and Andersen M. 2019. Bridging blood cancers and inflammation: The reduced Cancitis model. *Journal of Theoretical Biology*, 465: 90-108.
- [60] Pantel, K, Loeffler M, Bungart B and Wichmann HE. 1990. A mathematical model of erythropoiesis in mice and rats. Part 4: Differences between bone marrow and spleen. *Cell Proliferation*, 23 (4):283-297.
- [61] Papayannopoulou T, Brice M, Farrer D and Kaushansky K. 1996. Insights into the cellular mechanisms of erythropoietin-thrombopoietin synergy. *Exp Hematol*, 24(5):660-9.
- [62] Papayannopoulou T and Kaushansky K. 2016. Evolving insights into the synergy between erythropoietin and thrombopoietin and the bipotent Erythroid/Megakaryocytic progenitor cell. *Exp Hematol*, 44(8): 664–668.
- [63] Pottgiesser T, Specker W, Umhau M, Dickhuth HH, Roecker K and Schumacher YO. 2008. Recovery of hemoglobin mass after blood donation. *Transfusion*, vol:48.
- [64] Raluca Apostu and Michael C. Mackey. 2008. Understanding cyclical thrombocytopenia: A mathematical modeling approach. *Journal of Theoretical Biology*, 251, 297–316.
- [65] Emmons RVB, Reid DM, Cohen RL, Meng G, Young NS, Dunbar CE and Shulman NR. 1996. Human thrombopoietin levels are high when thrombocytopenia is due to megakaryocyte deficiency and low when due to increased platelet destruction. *Blood*, Vol 87, No 10, pp 4068-4071.
- [66] Rodak BF, Fritsma GA and Doig K. 2008. Hematology: Clinical principles and applications.
- [67] Sajid Z, Andersen M and Ottesen JT. 2019. Mathematical analysis of the Cancitis model and the role of inflammation in blood cancer progression. *Mathematical Biosciences and Engineering*, 16 (6): 8268–8289.
- [68] Sanada C, Xavier-Ferrucio J, Lu YC, Min E, Zhang P, Zou S, Kang E, Zhang M, Zerfati G, Gallagher PG and Krause DS. 2016. Adult human megakaryocyte-erythroid progenitors are in the CD34+1CD38mid fraction. *Blood*, 128(7): 923-933.

- [69] Santilladns M, Mahaffay JM, Belair J and Mackey MC. 2000. Regulation of Platelet Production: The Normal Response to Perturbation and Cyclical Platelet Disease. *Journal of Theoretical Biology*, 206, 585-603.
- [70] Schirm S, Engel C, Loeffler M, Scholz M. 2013. A Biomathematical Model of Human Erythropoiesis under Erythropoietin and Chemotherapy Administration. *PloS One*.
- [71] Silva M, Grillot D, Benito, Richard C, Nunez G and Fernandez- Luna J. 1996. Erythropoietin can promote erythroid progenitor survival by repressing apoptosis through bcl-1 and bcl-2. *Blood*, 88, 1576-1582.
- [72] Silvain J, Pena A, Cayla G, Brieger D, Bellemain-Appaix A, Chastre T, Vignalou JP, Beygui F, Barthelemy O, Collet JP, Montalescot G. 2010. Impact of red blood cell transfusion on platelet activation and aggregation in healthy volunteers: results of the TRANSFUSION study. *European Heart Journal* , 31, 2816–2821.
- [73] Singh A, Verma A, Nityanand S, Chaudhary R and Elhence P. 2015. Circulating thrombopoietin levels in normal healthy blood donors and in aplastic anemia patients in relation to disease severity *Asian J Transfus Sci*, 9(1): 70–73.
- [74] Sitnicka E, Lin N, Priestley GV, Fox N, Broudy VC, Wolf NS, Kaushansky K The effect of thrombopoietin on the proliferation and differentiation of murine hematopoietic stem cells. 1996. *Blood*, 87(12):4998-5005.
- [75] Sorgel F, Thyroff-Friesinger U, Vetter A, Vens- Cappell B and Kinzig M. 2009. Bioequivalence of HX575 (Recombinant Human Epoetin Alfa) and a Comparator Epoetin Alfa after Multiple subcutaneous administrations. *Pharmacology*, 83:122–130.
- [76] Stiehl T and Marciniak-Czochra A. 2012 Mathematical modelling of leukemogenesis and cancer stem cell dynamics. *Math. Model. Nat. Phenom*, 7, 166–202.
- [77] Tetschke M, Lilienthal P, Pottgiesser T, Fischer T, Schalk E and Sager S. 2018. Mathematical Modeling of RBC Count Dynamics after Blood Loss. *Processes*, 6, 157.
- [78] Testa U. 2004. Apoptotic mechanism in the control of erythropoiesis. *Leukemia* 18, 7: 1176-1199.
- [79] Walkley C, Shea J, Sims N, Purton L and Orkin S. 2007. Rb regulates interactions between hematopoietic stem cells and their bone marrow micro-environment, *Cell*, 129: 1081-95.

- [80] Wang B, Nichol JL and Sullivan JT. 2004. Pharmacodynamics and pharmacokinetics of AMG 531, a novel thrombopoietin receptor ligand. *Clinical pharmacology and therapeutics*.
- [81] Wang H, Dong Q, Fu R, Qu W, Ruan E, Wang G, Liu H, Wu Y, Song J, Xing L, Guan J, Li L and Shao Z. 2015. Recombinant human thrombopoietin treatment promotes hematopoiesis recovery in patients with severe aplastic anemia receiving immunosuppressive therapy. *Hindawi Publishing Corporation BioMed Research International*, Article ID 597293, 6 pages.
- [82] Weissman IL, Anderson DJ and Gage F. 2001. Stem and progenitor cells: origins, phenotypes, lineage commitments, and transdifferentiations. *Cell Dev Biol*, 17:387–403.
- [83] Weitzman JB, Fiette L, Matsuo K and Yaniv M. 2000. JunD protects cells from p53- dependent senescence and apoptosis. *Mol Cell*, 6, 5: 1109-1119.
- [84] Wormanna B. 2013. Clinical Indications for Thrombopoietin and Thrombopoietin-Receptor Agonists. *Transfus Med Hemothe*, 40:319–325.
- [85] Zauli G, Vitale M, Falcieri E, Gibellini D, Bassini A, Celeghini C, Columbaro M and Capitani S. 1997. In vitro senescence and apoptotic cell death of human megakaryocytes. *Blood*, 90, 2234-2243.
- [86] Zhang J, Fleischman AG and Wodarz D. 2017. Determining the role of inflammation in the selection of *JAK2* mutant cells in myeloproliferative neoplasms. *J. Theor. Biol*, 425: 43–52.

Bibliography

- [1] Abkowitz JL, Catlin SN, Mc Callie MT and Gutterop P Evidence that the number of hematopoietic stem cells per animal is conserved in mammals. *Blood*, 03-0822.
- [2] Adamson J. 1968. The Erythropoietin/Haematocrit relationship in normal and polycythemia man: Implications of marrow regulation. *Blood*, Vol 32 No. 4.
- [3] Adamson J. 1974. The relationship of erythropoietin and iron metabolism to red blood cell production in humans. *Semin. Oncol*, 21, 9-15.
- [4] Adimy M, Crauste F and Ruan S. 2006. Modelling hematopoiesis mediated by growth factors with applications to periodic haematological diseases. *Bull Math Biol*, 68:2321–2351.
- [5] Adimy M and Crauste F. 2007. Modelling and asymptotic stability of a growth factor-dependent stem cells dynamics model with distributed delay. *Discrete and Continuous Dynamical Systems*, 1(1).
- [6] Arachchillage DR and Laffan M. 2019. Pathogenesis and management of thrombotic disease in Myeloproliferative Neoplasms. *Semin Thromb Hemost*, 45(06): 604-611
- [7] Andersen M, Sajid Z, Pedersen RK, Gudmand-Hoeyer J, Ellervik C, Skov V, Kjær L, Pallisgaard N, Kruse TA, Thomassen M, Troelsen J, Hasselbalch HC and Ottesen JT. 2017. Mathematical modelling as a proof of concept for MPNs as a human inflammation model for cancer development. *Plos One*.
- [8] Andersen M, Hasselbalch H, Kjaer L, Skov V and Ottesen JT. 2020. Global dynamics of healthy and cancer cells competing in the hematopoietic system. *Mathematical Biosciences* 626, 1-15.
- [9] Angulo O, Crauste F and López-Marcos JC. 2018. Numerical integration of an erythropoiesis model with explicit growth factor dynamics. *Journal of Computational and Applied Mathematics*, 330: 770-782.
- [10] Arber DA, Orazi A, Hasserjian R, Thiele J, Borowitz MJ, Le Beau MM, Bloomfield CD, Cazzola M and Vardiman JW. 2016. The 2016 revision to the World Health Organization classification of myeloid neoplasms and acute leukemia. *Blood*, 127 (20): 2391–2405.
- [11] Banks HT, Bliss KM and Tran H. 2012. Modelling red blood cell and iron dynamics in patients with chronic kidney disease. *North Carolina State University. Center*

for Research in Scientific Computation.

- [12] Barbui T, Barosi G and Birgegard G. 2011. Philadelphia-negative classical myeloproliferative neoplasms: critical concepts and management recommendations from European Leukemia Net. *J Clin Oncol*, 29:761-70.
- [13] Barbui T, Finazzi G and Falanga A. 2013. Myeloproliferative neoplasms and thrombosis. *Blood*, vol. 122, no. 13, pp. 2176–2184.
- [14] Beer PA, Campbell PJ and Scott LM. 2008. MPL mutations in myeloproliferative disorders: analysis of the PT-1 cohort. *Blood*, 112:141-9.
- [15] Belair J, Mackey MC and Mahaffy JM. 1995. Age- structured and two delay models for erythropoiesis. *Math. Biosci.* 128, 317-346.
- [16] Bjørn ME, Stricker K, Kjær L, Ellemann K, and Hasselbalch HC. 2014. Combination therapy with interferon and JAK1- 2 inhibitor is feasible: proof of concept with rapid reduction in JAK2V617F-allele burden in polycythemia vera, *Leukemia Research Reports*, vol. 3, no. 2, pp. 73–75.
- [17] Boddu P, Falchi L, Hosing C, Newberry K, Bose P and Verstovsek S. 2017. The role of thrombocytapheresis in the contemporary management of hyperthrombocytosis in Myeloproliferative Neoplasms: A case based study review. *Leuk Res*, 58: 14–22.
- [18] Bohlius J, Tonia T and Schwarzer G. 2010. Twist and shout: one decade of meta-analyses of erythropoiesis-stimulating agents in cancer patients. *Acta Haematol*, 125(1–2): 55–67.
- [19] Borge OJ, Ramsfjell V, Veiby OP, Murphy MJ, Lok S and Jacobsen SE. 1996. Thrombopoietin, but not erythropoietin promotes viability and inhibits apoptosis of multipotent murine hematopoietic progenitor cells in vitro. *Blood*, 88: 2859-2870.
- [20] Bradford G, Williams B, Rossi R and Bertoncello I. 1997. Quiescence, cycling and turnover in the primitive haematopoietic stem cell compartment. *Exper. Hematol*, 25. 445-453.
- [21] Branchog I, Kutti J, Ridell B, Swolin B and Weinfeld A. 1975. The relation of thrombokinetics to bone marrow megakaryocytes in idiopathic thrombocytopenic purpura (ITP). *Blood*, 45: 552-562.
- [22] Campbell PJ and Green AR. 2006. The myeloproliferative disorders. *N. Engl. J. Med*, 355: 2452–2466.
- [23] Carneskog J, Kutti J, Wadenvik H, Lundberg PA and Lindstedt G. 1998. Plasma erythropoietin by high-detectability immune-radiometric assay in untreated and treated patients with Polycythemia vera and essential thrombocythemia. *Eur J. Haematol*, 60:278-82.
- [24] Clapp G, Lepoutre T and El Cheikh R. 2015. Implication of autologous immune system in bcr-abl transcript variations in chronic myelogenous leukemia patients treated with imatinib, *Cancer Res*, 75, 4053–4062.

- [25] Colijn C and Mackey MC. 2005. A mathematical model of hematopoiesis—I. Periodic chronic myelogenous leukemia. *Journal of Theoretical Biology*, 237: 117-132.
- [26] Colijn C and Mackey MC. 2005. A mathematical model of hematopoiesis: II. Cyclical neutropenia. *Journal of Theoretical Biology*, 237 133–146.
- [27] Crauste F, Pujo-Menjouet L, Genieys S, Molina C and Gandrillon O. 2008. Adding self-renewal in committed erythroid progenitors improves the biological relevance of a mathematical model of erythropoiesis. *Journal of Theoretical Biology*, 250:322–338.
- [28] Debeljak N, Solar P and Sytkowski AJ. 2014 Erythropoietin and cancer: the unintended consequences of anemia correction. *Front Immunol*, 5:563.
- [29] Demin I, Crauste F, Gandrillon O and Volpert V. 2010. A multi-scale model of erythropoiesis. *Journal of Biological Dynamics*, 4:1, 59-70.
- [30] Dingli D and Michor F. 2006. Successful therapy must eradicate cancer. *Stem Cells*, 24(12): 2603.
- [31] Eaton DL and De Sauvage FJ. 1997. Thrombopoietin: the primary regulator of megakaryocytopoiesis and thrombopoiesis. *Exp. Hematol*, 25, 1-7.
- [32] Edvardsson L, Dykes J and Olofsson T. 2006. Isolation and characterization of human myeloid progenitor populations—TpoR as discriminator between common myeloid and megakaryocyte/erythroid progenitors. *Exp Hematol*, 34(5):599-609.
- [33] Erslev AJ. 1990. Production of erythrocytes. *Haematology*, pages 389–397.
- [34] Farrell F and Lee A. 2004. The erythropoietin receptor and its expression in tumour cells and other tissues. *The Oncologist*, 9: 18-30.
- [35] Finazzi G and Barbui T. 2007. How I treat patients with polycythemia vera. *Blood*, 109 (12): 5104-11.
- [36] Foo J, Drummond MW, Clarkson B, Holyoake T and Michor F. 2009. Eradication of chronic myeloid leukemia stem cells: A novel mathematical model predicts no therapeutic benefit of adding G-CSF to imatinib. *PLoS Comput Biol* 5(9).
- [37] Erickson-Miller CL, Chadderton A, Gibbard A, Kirchner J, Pillarisetti K, Baker K, Pandite L, El-Hariry I, Kamel YM, Liu Y, Martin A and Messam C. 2010. Thrombopoietin receptor levels in tumor cell lines and primary tumors. *Journal of Oncology*.
- [38] Fuertinger DH, Kappel F, Thijssen S, Levin N and Kotanko P. 2013. A model of erythropoiesis in adults with sufficient iron availability. *J. Math. Biol*, 66: 1209–1240.
- [39] Fuertinger DH, Kappel F, Zhang H, Thijssen S and Kotanko P. 2017. Prediction of hemoglobin levels in individual hemodialysis patients by means of a mathematical model of erythropoiesis. *Plos One*.
- [40] Granziero L, Ghia P, Circosta P, Gottardi D, Strola G, Geuna M, Montagna L,

- Piccoli P, Chilosi M and Caligaris-Cappio F. 2001. Survivin is expressed on CD40 stimulation and interfaces proliferation and apoptosis in B-cell chronic lymphocytic leukemia. *Blood*, 97, 9: 2777-2783.
- [41] Griesshammer M, Hornkohl A, Nichol JL, Hecht T, Raghavachar A, Heimpel H and Schrezenmeier H. 1998. High levels of thrombopoietin in sera of patients with essential thrombocythemia: Cause or consequence of abnormal platelet production? *Ann Hematol* 77:211-215
- [42] Gentry SN and Jackson TL. 2013. A mathematical model of cancer stem cell driven tumor initiation: implications of niche size and loss of homeostatic regulatory mechanisms. *PloS One*, 8(8): 71128.
- [43] Haeno H, Levine RL, Gilliland DG and Michor F. 2009. A progenitor cell origin of myeloid malignancies. *Proceedings of the National Academy of Sciences of the United States of America*, 106(39):16616-16621.
- [44] Hasselbalch HC. 2012. Perspectives on chronic inflammation in essential thrombocythemia , polycythemia vera , and myelofibrosis: is chronic inflammation a trigger and driver of clonal evolution and development of accelerated atherosclerosis and second cancer? *Blood*, 119: 3219–3226.
- [45] Hasselbalch HC. 2013. Chronic inflammation as a promotor of mutagenesis in essential thrombocythemia, polycythemia vera and myelofibrosis. A human inflammation model for cancer development? *Leukemia Research*, 37: 214–220.
- [46] Hasselbalch HC. 2013. The role of cytokines in the initiation and progression of myelofibrosis. *Cytokine and Growth Factor Reviews*, vol. 24, no. 2, pp. 133–145.
- [47] Hasselbalch HC. 2014. Perspectives on the impact of JAK-inhibitor therapy upon inflammation-mediated comorbidities in myelofibrosis and related neoplasm. *Expert Review of Hematology*, vol. 7, no. 2, pp. 203–216.
- [48] Hasselbalch HC and Bjørn ME. 2015. MPNs as inflammatory diseases: The evidence, consequences, and perspectives. *Hindawi Publishing Corporation Mediators of Inflammation*, Article ID 102476, 16 pages.
- [49] Hattangadi SM, Wong P, Zhang L, Flygare J and Lodish HF. 2011. From stem cell to red cell: regulation of erythropoiesis at multiple levels by multiple proteins, RNAs, and chromatin modifications. *Blood*, 118(24):6258-68.
- [50] Heinisch BB, Vcelar B, Kapiotis S, Blann A, Wolzt M, Sillermatula JM and Jilma B. 2012. The effect of erythropoietin on platelet and endothelial activation markers: A prospective trial in healthy volunteers. *Platelets*, 23(5): 352–358.
- [51] Horikawa Y, Matsumura I, Hashimoto K, Shiraga M, Kosugi S, Tadokoro S, Kato T, Miyazaki H, Tomiyama Y, Kurata Y, Matsuzawa Y and Kanakura Y . 1997. Markedly reduced expression of platelet c-mpl receptor in essential thrombocythemia. *Blood*, 90: 4031–4038.
- [52] Huang J and Tefferi A. 2009. Erythropoiesis stimulating agents have limited ther-

- apeutic activity in transfusion-dependent patients with primary myelofibrosis regardless of serum erythropoietin level. *Eur J Haematol*, 83 (2): 154-5.
- [53] Hurtado-Nedelec M. 2013. Increased reactive oxygen species production and p47phox phosphorylation in neutrophils from myeloproliferative disorders patients with JAK2 (V617F) mutation. *Haematologica*, 98, 1517– 1524.
- [54] Iiyama M, Kakihana K, Kurosu T and Miura O. 2006. Reactive oxygen species generated by hematopoietic cytokines play roles in activation of receptor-mediated signaling and in cell cycle progression. *Cellular Signalling* 18, 2: 174-182.
- [55] Jelkmann W. 2013. Physiology and pharmacology of erythropoietin. *Transfus Med Hemother*, 40:302–309.
- [56] Johansson P and Andreasson B. 2006. Hydroxyurea therapy increases plasma erythropoietin in patients with essential thrombocythaemia or polycythaemia vera. *Clin. Lab. Haem.* 28: 233-236.
- [57] King KY, Matatall KA, Shen CC, Goodell MA, Swierczek SI, Prchal JT. 2015. Comparative long-term effects of interferon α and hydroxyurea on human hematopoietic progenitor cells, *International Society for Experimental Hematology*, 43: 912–918.
- [58] Komarova NL. 2013. Principles of regulation of self-renewing cell lineages, *Plos One*, 8.
- [59] Komarova NL and van den Driessche P. 2015. Stability of control networks in autonomous homeostatic regulation of stem cell lineages, *Math. Oncol*, 80, 1345–1365.
- [60] Kaushansky K. 1995. Thrombopoietin: the primary regulator of platelet production. *Blood*, 86 : 419–431.
- [61] Kim YM, Koo BK, Jeong HW, Yoon MJ, Song R, Shin J, Jeong DC, Kim SH and Kong YY. 2008. Defective Notch activation in micro-environment leads to myeloproliferative disease, *Blood*, 112 (12): 4628-38 .
- [62] Kim P, Lee P, and Levy D. 2008. Dynamics and potential impact of the immune response to chronic myelogenous leukemia. *PLoS Comput Biol*, 4.
- [63] Krantz SB. 1991. Erythropoietin. *Blood*, 77(3): 419–434.
- [64] Kristinsson SY, Landgren O and Samuelsson J. 2010. Autoimmunity and the risk of myeloproliferative neoplasms. *Haematologica* 95: 1216–1220.
- [65] Kuter DJ. 1996. The physiology of platelet production. *Stem Cells*, 14, 88-101.
- [66] Kuter DJ and Gernsheimer TB. 2009. Thrombopoietin and platelet production in chronic immune thrombocytopenia. *Hematol Oncol Clin North Am*, 23(6): 1193–1211. doi:10.1016/j.hoc.2009.09.001.
- [67] Langlois GP, Morgan Craig, Antony R. Humphries, Michael C. Mackey, Joseph M. Mahaffy, Jacques Bélair, Thibault Moulin, Sean R. Sinclair and Liangliang Wang. 2017. Normal and pathological dynamics of platelets in humans. *Journal*

- of Mathematical Biology*, 75 (6-7): 1411-1462.
- [68] Leder K, Holland E and Michor F. 2010 The therapeutic implications of plasticity of the cancer stem cell phenotype. *PLoS One*, 5, e14366.
- [69] Li N, Yao QM and Gale RP. 2015. Frequency and allele burden of CALR mutations in Chinese with essential thrombocythemia and primary myelofibrosis without JAK2(V617F) or MPL mutations. *Leuk Res*, 39:510-4.
- [70] Lichtman MA, Beutler E, Kipps TJ, Seligsohn U, Kaushansky K and Prchal JT. 2006. *Williams Hematology*. McGraw-Hill: New York, NY, USA.
- [71] Loeffler M, Pantel K, Wulff H and Wichmann HE. 1989. A mathematical model of erythropoiesis in mice and rats. Part 1. Structure of the model. *Cell Tissue Kinetics*, 22:13–30
- [72] Lu M, Zhang W, Li Y. 2010. Interferon-alpha targets JAK2V617F positive hematopoietic progenitor cells and acts through the p38 MAPK pathway. *Exp Hematol*, 38:472–480.
- [73] Mackey M. 1978. Unified hypothesis of the origin of aplastic anaemia and periodic hematopoiesis. *Blood*, 51, 941–956.
- [74] Mahaffy JM, Belair J and Mackey MC. 1998. Hematopoietic model with moving boundary condition and state dependent delay: Applications in Erythropoiesis. *J. theor. Biol*, 190: 135-146.
- [75] Mahaffy JM. 1999. Age-structured modelling of haematopoiesis. *San Diego State University*.
- [76] Mahaffy JM, Polk SW and Roeder RK. 1999. An age-structured model for erythropoiesis following a phlebotomy. *Tech. Rep. CRM-2598, Department of Mathematical Sciences, San Diego State University, San Diego, CA 92182-0314*.
- [77] Marciniak-Czochra A, Stiehl T, Ho AD, Jäger W and Wagner W. 2009. Modelling of asymmetric cell division in hematopoietic stem cells—regulation of self-renewal is essential for efficient repopulation. *Stem Cells Dev*, 18 (3), 377-85.
- [78] Meiss JD. 2007. *Differential Dynamical Systems*.
- [79] Michiels JJ, Schroyens W, Lindemans J, Kate FWJT, Lam KH and De Raeve H. 2014. The Erythrocyte count on top of bone marrow histology discriminates Essential Thrombocythemia and Polycythemia Vera in JAK2V617F mutated prefibrotic Myeloproliferative Neoplasm with no or minor splenomegaly. *Journal of Haematology and Thromboembolic Diseases*, 2:4.
- [80] Michor F, Iwasa Y and Nowak MA. 2004. Dynamics of cancer progression. *Nature Rev. Cancer*, 4, 197–205.
- [81] Michor F, Hughes T, Iwasa Y, Branford S, Shah N, Sawyers C and Novak M. 2015. *Dynamics of chronic myeloid leukaemia*. *Nature* 435, 1267–1270.
- [82] Motoji T, Takanashi M and Motomura S. 1996. Growth stimulatory effect of thrombopoietin on the blast cells of acute myelogenous leukaemia. *British Jour-*

- nal of Haematology*, vol. 94, no. 3, pp. 513–516.
- [83] Mullally A, Bruedigam C, Poveromo L, Heidel FH, Purdon A, Vu T, Austin R, Heckl D, Breyfogle LJ, Kuhn CP, Kalaitzidis D, Armstrong SA, Williams DA, Hill GR, Ebert BL, Lane SW. 2013. Depletion of Jak2V617F myeloproliferative neoplasm-propagating stem cells by interferon- α in a murine model of polycythemia vera. *Blood*, 121 (18): 3692–3702.
- [84] Murayama T, Imoto S, Natazuka T, Chihara K, Matsui T. 1998. Proliferative reaction of myelogenous leukemia cells with cytokines G-CSF, GM-CSF, M-CSF, SCF and TPO. *Leukemia Research* 22, 557–560.
- [85] Osterborg A, Aapro M, Cornes P, Haselbeck A, Hayward CR and Jelkmann W. 2007. Preclinical studies of erythropoietin receptor expression in tumour cells: impact on clinical use of erythropoietic proteins to correct cancer-related anaemia. *Eur J Cancer*, 43 (3): 510–519.
- [86] Ottesen JT, Sajid Z, Pedersen RK, Gudmand-Hoeyer J, Bangsgaard KO, Skov V, Kjær L, Knudsen TA, Pallisgaard N, Kruse TA, Thomassen M, Troelsen J, Hasselbalch HC and Andersen M. 2019. Bridging blood cancers and inflammation: The reduced Cancitis model. *Journal of Theoretical Biology*, 465: 90-108.
- [87] Pantel, K, Loeffler M, Bungart B and Wichmann HE. 1990. A mathematical model of erythropoiesis in mice and rats. Part 4: Differences between bone marrow and spleen. *Cell Proliferation*, 23 (4): 283-297.
- [88] Passamonti F, Griesshammer M and Palandri F. 2017. Ruxolitinib for the treatment of inadequately controlled polycythaemia vera without splenomegaly (RESPONSE-2): a randomised, open-label, phase 3b study. *Lancet Oncol*, 18 (1): 88-99.
- [89] Pardanani AD, Levine RL and Lasho T. 2006. MPL515 mutations in myeloproliferative and other myeloid disorders: a study of 1182 patients. *Blood*, 108:3472-6.
- [90] Pedersen RK, Andersen M, Knudsen TA, Sajid Z, Gudmand-Hoeyer J, Dam MJB, Skov V, Kjær L, Ellervik C, Larsen TS, Hansen D, Pallisgaard N, Hasselbalch HC and Ottesen JT. 2020. Data-driven analysis of JAK2V617F kinetics during interferon α 2 treatment of patients with polycythemia vera and related neoplasms. *Cancer Medicine*, 00:1–13.
- [91] Pinho S, Frenette PS. 2019 Haematopoietic stem cell activity and interactions with the niche. *Molecular Cell Biology*, Volume 20.
- [92] Pourcelot E. 2015. Cytokine profiles in polycythemia vera and essential thrombocythemia patients: Clinical implications. *Exp. Hematol*, 42, 360–368.
- [93] Pradhan A, Lambert QT, Griner LN and Reuther GW. 2010. Activation of JAK2-V617F by components of heterodimeric cytokine Receptors. *J. Biol. Chem*, 285, 16651–16663.
- [94] Pujo-Menjouet L, Bernard S and Mackey M. 2005. Long period oscillations in a

- G0 model of hematopoietic stem cells. *SIAM J Appl Dyn Syst* 4, 312–332.
- [95] Raluca Apostu and Michael C. Mackey. 2008. Understanding cyclical thrombocytopenia: A mathematical modeling approach. *Journal of Theoretical Biology*, 251, 297–316.
- [96] Ratajczak MZ, Ratajczak J, Marlicz W, Pletcher CH Jr, Machalinski B, Moore J, Hung H and Gewirtz AM. 1997. Recombinant human thrombopoietin (TPO) stimulates erythropoiesis by inhibiting erythroid progenitor cell apoptosis. *Br. J. Haematol*, 98, 8-17.
- [97] Ritchie A, Vadhan-Raj S and Broxmeyer HE. 1996. Thrombopoietin suppresses apoptosis and behaves as a survival factor for the human growth factor-dependent cell line, M07e. *Stem Cells*, 14, 330-336.
- [98] Emmons RVB, Reid DM, Cohen RL, Meng G, Young NS, Dunbar CE and Shulman NR. 1996. Human thrombopoietin levels are high when thrombocytopenia is due to megakaryocyte deficiency and low when due to increased platelet destruction. *Blood*, Vol 87, No 10, pp 4068-4071.
- [99] Rodak BF, Fritsma GA and Doig K. 2008. Hematology: Clinical principles and applications.
- [100] Rovida E, Marzi I, Cipolleschi MG and Sbarba PD. 2014. One more stem cell niche: how the sensitivity of chronic myeloid leukemia cells to imatinib mesylate is modulated within a “hypoxic” environment. *Hypoxia*, 1-10.
- [101] Rumi E, Pietra D and Ferretti V. 2014. JAK2 or CALR mutation status defines subtypes of essential thrombocythemia with substantially different clinical course and outcomes. *Blood*, 123:1544-51.
- [102] Sajid Z, Andersen M and Ottesen JT. 2019. Mathematical analysis of the Cancitis model and the role of inflammation in blood cancer progression. *Mathematical Biosciences and Engineering*, 16 (6): 8268–8289.
- [103] Sajid Z, Andersen M and Ottesen JT. 2020. System dynamics of cancer in erythropoiesis with multiple Epo feedbacks. *System Dynamics Review*, published.
- [104] Sajid Z, Andersen M and Ottesen JT. 2020. Dynamics of erythropoiesis with multiple Epo feedbacks in blood cancer with stem cell competition. *Journal of Theoretical Biology*, Submitted
- [105] Sajid Z, Andersen M and Ottesen JT. 2020. Mathematical modelling of erythropoiesis and thrombopoiesis with multiple EPO and TPO feedbacks. *Submitted*
- [106] Santar CG, Desmond R, Feng X, Bat T, Chen J, Heuston E, Mizukawa B, Mulloy JC, Bodine DM, Laroche A, Dunbar CE. 2015. Functional niche competition between normal hematopoietic stem and progenitor cells and myeloid Leukemia Cells. *Stem Cells*, 33(12): 3635-42.
- [107] Santilladns M, Mahaffay JM, Belair J and Mackey MC. 2000. Regulation of platelet production: The normal response to perturbation and cyclical platelet dis-

- ease. *Journal of Theoretical Biology*, 206, 585-603.
- [108] Silva M, Grillot D, Benito, Richard C, Nunez G and Fernandez- Luna J. 1996. Erythropoietin can promote erythroid progenitor survival by repressing apoptosis through bcl-1 and bcl-2. *Blood*, 88, 1576-1582.
- [109] Squizzato A, Romualdi E and Passamonti F. 2013 Antiplatelet drugs for polycythaemia vera and essential thrombocythaemia. *Cochrane Database Syst Rev* 4: CD006503.
- [110] Stiehl T and Marciniak-Czochra A. 2012 Mathematical modelling of leukemogenesis and cancer stem cell dynamics. *Math. Model. Nat. Phenom*, 7, 166–202.
- [111] Stiehl T, Baran N, Ho AD, Marciniak-Czochra A. 2015. Cell division patterns in acute myeloid leukemia stem-like cells determine clinical course: A model to predict patient survival. *Cancer Research*, 75 (6): 940-949.
- [112] Stiehl T, Ho AD and Marciniak-Czochra A. 2018. Mathematical modelling of the impact of cytokine response of acute myeloid leukemia cells on patient prognosis. *Sci. Rep.*, 2809.
- [113] Stoffel R, Wiestner A and Skoda RC. 1996. Thrombopoietin in Thrombocytopenic Mice: Evidence Against Regulation at the mRNA Level and for a Direct Regulatory Role of Platelets. *Blood*, Vol 87, No 2: pp 567-573.
- [114] Tafuri A, Lemoli RM, Petrucci MT, Ricciardi MR, Fogli M, Bonsi L, Ariola C, Strippoli P, Gregorj C, Petti MC, Tura S, Mandelli F and Bagnara GP. 1999. Thrombopoietin and interleukin 11 have different modulatory effects on cell cycle and programmed cell death in primary acute myeloid leukemia cells. *Experimental Hematology* 27, 1255–1263.
- [115] Tanimukai S, Kimura T, Sakabe H, Ohmizono Y, Kato T, Miyazaki H, Yamagishi H and Sonoda Y. 1997. Recombinant human c-Mpl ligand (Thrombopoietin) not only acts on megakaryocyte progenitors, but also on erythroid and multi potential progenitors in vitro. *Exp. Hematol.*, 25, 1025-1033.
- [116] Tefferi A, Rumi E, Finazzi G, Gisslinger H, Vannucchi AM, Rodeghiero F. 2013. Survival and prognosis among 1545 patients with contemporary polycythemia vera: an international study. *Leukemia*, 27(9):1874–81.
- [117] Tefferi A, Lasho TL and Finke CM. 2014. CALR vs JAK2 vs MPL-mutated or triple-negative myelofibrosis: clinical, cytogenetic and molecular comparisons. *Leukemia*, 28:1472-7.
- [118] Tetschke M, Lilienthal P, Pottgiesser T, Fischer T, Schalk E and Sager S. 2018. Mathematical modeling of RBC count dynamics after blood loss. *Processes*, 6, 157.
- [119] Testa U. 2004. Apoptotic mechanism in the control of erythropoiesis. *Leukemia* 18, 7: 1176-1199.
- [120] van Genderen PJJ and Michiels JJ. 1993. Primary thrombocythemia: diagnosis, clinical manifestations and management. *Ann Hematol*, 67:57–62.

- [121] Walenda T, Stiehl T, Braun H, Frobel J, Ho AH, Schroeder T, Goecke TW, Rath B, Germing U, Marciniak-Czochra A and Wagner W. 2014. Feedback signals in Myelodysplastic Syndromes: Increased self-renewal of the malignant clone suppresses normal hematopoiesis. *PLoS Computational Biology*, 10 (4).
- [122] Walkley C, Shea J, Sims N, Purton L and Orkin S. 2007. Rb regulates interactions between hematopoietic stem cells and their bone marrow micro-environment, *Cell*, 129: 1081-95.
- [123] Wan PX, Wang BW, Wang ZC. 2015 Importance of the stem cell microenvironment for ophthalmological cell-based therapy. *World J Stem Cells*, 7(2): 448-460.
- [124] Weitzman JB, Fiette L, Matsuo K and Yaniv M. 2000. JunD protects cells from p53- dependent senescence and apoptosis. *Mol Cell*, 6, 5: 1109-1119.
- [125] Wichmann HE, Loeffler M, Pantel K and Wulff HH. 1989. A mathematical model of erythropoiesis in mice and rats. Part 2. Stimulated erythropoiesis. *Cell Tissue Kinetics*, 22:31–49.
- [126] Wulff H, Wichmann HE, Pantel K and Loeffler M. 1989. A mathematical model of erythropoiesis in mice and rats. Part 3: suppressed erythropoiesis. *Cell Tissue Kinetics*, 22:51–61.
- [127] Yang J, Axelrod DE and Komarova NL. 2017. Determining the control networks regulating stem cell lineages in colonic crypts, *J. Theor. Biol.*, 429, 190–203.
- [128] Zauli G, Vitale M, Falcieri E, Gibellini D, Bassini A, Celeghini C, Columbaro M and Capitani S. 1997. In vitro senescence and apoptotic cell death of human megakaryocytes. *Blood*, 90, 2234-2243.
- [129] Zhang J, Fleischman AG and Wodarz D. 2017. Determining the role of inflammation in the selection of *JAK2* mutant cells in myeloproliferative neoplasms. *J. Theor. Biol*, 425: 43–52.
- [130] Ziegler AK, Grand J, Stangerup I, Nielsen HJ, Dela F, Magnussen K and Helge JW. 2014. Time course for the recovery of physical performance, blood hemoglobin, and ferritin content after blood donation. *Transfusion* vol 55.

Appendix A

Mathematical modelling as a proof of concept for MPNs as a human inflammation model for cancer development

RESEARCH ARTICLE

Mathematical modelling as a proof of concept for MPNs as a human inflammation model for cancer development

Morten Andersen¹, Zamra Sajid¹, Rasmus K. Pedersen¹, Johanne Gudmand-Hoeyer¹, Christina Ellervik², Vibe Skov³, Lasse Kjær³, Niels Pallisgaard⁴, Torben A. Kruse⁵, Mads Thomassen⁵, Jesper Troelsen¹, Hans Carl Hasselbalch^{3*}, Johnny T. Ottesen¹

1 Department of Science and Environment, Roskilde University, Roskilde, Denmark, **2** Department of Laboratory Medicine at Boston Children's Hospital, Boston, Massachusetts, United States of America, **3** Department of Hematology, Zealand University Hospital, University of Copenhagen, Roskilde, Denmark, **4** Department of Pathology, Zealand University Hospital, University of Copenhagen, Roskilde, Denmark, **5** Department of Clinical Genetics, Odense University Hospital, Odense, Denmark

* hans.hasselbalch@gmail.com



OPEN ACCESS

Citation: Andersen M, Sajid Z, Pedersen RK, Gudmand-Hoeyer J, Ellervik C, Skov V, et al. (2017) Mathematical modelling as a proof of concept for MPNs as a human inflammation model for cancer development. PLoS ONE 12(8): e0183620. <https://doi.org/10.1371/journal.pone.0183620>

Editor: Pal Bela Szecsi, Holbæk Hospital, DENMARK

Received: March 16, 2017

Accepted: August 8, 2017

Published: August 31, 2017

Copyright: © 2017 Andersen et al. This is an open access article distributed under the terms of the [Creative Commons Attribution License](https://creativecommons.org/licenses/by/4.0/), which permits unrestricted use, distribution, and reproduction in any medium, provided the original author and source are credited.

Data Availability Statement: All relevant data are within the paper and its Supporting Information files.

Funding: The authors received no specific funding for this work.

Competing interests: C. Ellervik, V. Skov, L. Kjær, T.A. Kruse, M. Thomassen, M. Andersen, J.T. Ottesen, J. Troelsen, Z. Sajid, R.K. Pedersen and J. Gudmand-Hoeyer have no conflicts of interest to disclose. N. Pallisgaard has the following to

Abstract

The chronic Philadelphia-negative myeloproliferative neoplasms (MPNs) are acquired stem cell neoplasms which ultimately may transform to acute myelogenous leukemia. Most recently, chronic inflammation has been described as an important factor for the development and progression of MPNs in the biological continuum from early cancer stage to the advanced myelofibrosis stage, the MPNs being described as ^aA Human Inflammation Model for Cancer Development^a. This novel concept has been built upon clinical, experimental, genomic, immunological and not least epidemiological studies. Only a few studies have described the development of MPNs by mathematical models, and none have addressed the role of inflammation for clonal evolution and disease progression. Herein, we aim at using mathematical modelling to substantiate the concept of chronic inflammation as an important trigger and driver of MPNs. The basics of the model describe the proliferation from stem cells to mature cells including mutations of healthy stem cells to become malignant stem cells. We include a simple inflammatory coupling coping with cell death and affecting the basic model beneath. First, we describe the system without feedbacks or regulatory interactions. Next, we introduce inflammatory feedback into the system. Finally, we include other feedbacks and regulatory interactions forming the inflammatory-MPN model.

Using mathematical modeling, we add further proof to the concept that chronic inflammation may be both a trigger of clonal evolution and an important driving force for MPN disease progression. Our findings support intervention at the earliest stage of cancer development to target the malignant clone and dampen concomitant inflammation.

disclose: consulting or advisory role for Qiagen and Novartis, participated in speakers bureau (Novartis and Roche), research funding (Incyte and Novartis), holds a patent (patent pending on contamination control of lymphocyte DNA when measuring cell free DNA in liquid biopsies), travel and accommodation (Novartis). H.C. Hasselbalch has the following to disclose: invited speaker and advisory role (Gilead), research funding (Novartis), travel and accommodation (Gilead, PharmaEssentia, Novartis). This does not alter our adherence to PLOS ONE policies on sharing data and materials.

Introduction

The classic chronic Philadelphia-negative myeloproliferative neoplasms (MPNs) include essential thrombocythemia (ET), polycythemia vera (PV) and primary myelofibrosis (PMF), which are acquired stem cell neoplasms [1]. Most patients live with their MPNs for decades although with a huge morbidity burden due to a high risk of thrombosis with cardiovascular complications and a massive comorbidity burden as well due to an increased propensity to develop autoimmune and chronic inflammatory diseases [2±4], including a 40% increased risk of second cancers [5,6]±not only after the MPN-diagnosis but also prior to the MPN-diagnosis [7]. Several years prior to the MPN-diagnosis these patients also have an increased risk of cardiovascular, autoimmune and inflammatory diseases [8,9]. Furthermore, the MPNs have an inherent risk of transformation to acute myelogenous leukemia (AML) and myelodysplastic syndrome (MDS) [10].

During the last decade major breakthroughs have occurred in the understanding of the pathogenesis of the MPNs, the most important being the identification of the somatic clonal markers±JAK2, MPL and CALR [11±18]. The findings of several other mutations already at the time of MPN-diagnosis, with the emergence of additional mutations in the advanced transforming stages of MPNs [17,18], all support the concept of a biological continuum from the early cancer stages (ET/PV) to the advanced cancer stages (myelofibrosis or AML) [1,19,20]. Chronic inflammation is the common link between common diseases such as atherosclerosis, the metabolic syndrome, type II diabetes mellitus and cancer, in which the JAK-STAT- signalling and the NF-κB pathways are activated and have major roles in disease progression [21±28]. These pathways are activated in MPNs as well. Most recently, the MPNs have been described as “Inflammatory Diseases” [4] and “A Human Inflammation Model For Cancer Development” [29] reflecting chronic inflammation to be a major driving force for clonal evolution and disease progression in MPNs [30±39]. This novel concept is built upon a platform, which has combined data from studies in several research fields and disciplines within MPNs—clinical [3±9,29±53], experimental [54±63], genomic [64±70], immunological [71±74] and not least epidemiological studies [3,5±7,75±77].

Another research field—mathematical modelling of cancer development—has not been applied to a similar extent within MPNs until very recently [78,79] and not in the context of investigating the concept of MPNs as “A Human Inflammation Model for Cancer Development”. Mathematical modelling of cancer development has provided new insights regarding cancer initiation and progression [80±89]. In this context, mathematical modelling has a huge potential to support or disprove understanding of research data on pathogenetic factors of significance for cancer development but also in regard to providing supportive evidence for a drug to be used in cancer therapy and accordingly a novel tool in evidence-based medicine [90±92]. Mathematical modelling of chronic inflammation as the trigger and driver of MPNs has never been investigated. Although the concept of MPNs as “inflammatory diseases” is being increasingly recognized, additional proof of this novel concept by mathematical modelling might be of utmost importance not only for our understanding of the pathogenesis of these neoplasms, but also in regard to diagnosis and treatment. Herein, we for the first time by mathematical modelling add further proof of the concept that MPNs may be both triggered and driven by chronic inflammation. We discuss the perspectives of our findings, which might implicate intervention at the earliest stage of cancer development (ET, PV) to target the malignant clone and dampen concomitant inflammation when the tumor burden is minimal, and accordingly, the outcome of treatment is logically most favorable.

Methods

The system describes the proliferation from stem cells to mature cells including mutations of healthy stem cells to become malignant stem cells. We include regulatory interactions (e.g. niche growth effects) and inflammation coping with cell death, inflammatory cytokines, and neutrophils. In order to design an inflammatory MPN model, we build on the coupled dynamics of inflammation and cancer progression as depicted in Fig 1.

The model

Most previous studies attempting to model the role of inflammation and immune deregulation in cancer progression consider solid tumors and couple the T-cell and natural killer (NK) cell dynamics to a logistic growth of a tumor. They mainly describe quite simplified versions of the adaptive immune response without explicitly considering the underlying cancer growth dynamics [93+98]. In contrast to all these models, our model is the first which couples the principles underlying actual cell dynamics to a basal inflammatory response. This response is seen for a normal infection, where the amount of dead cells provokes the immune response and stimulates the renewal of stem cells. Despite this complex coupling, the model is kept as simple as possible still allowing the relevant quantities to be described. Thus, the goal is to describe an important coupling between MPN development and the inflammatory response at

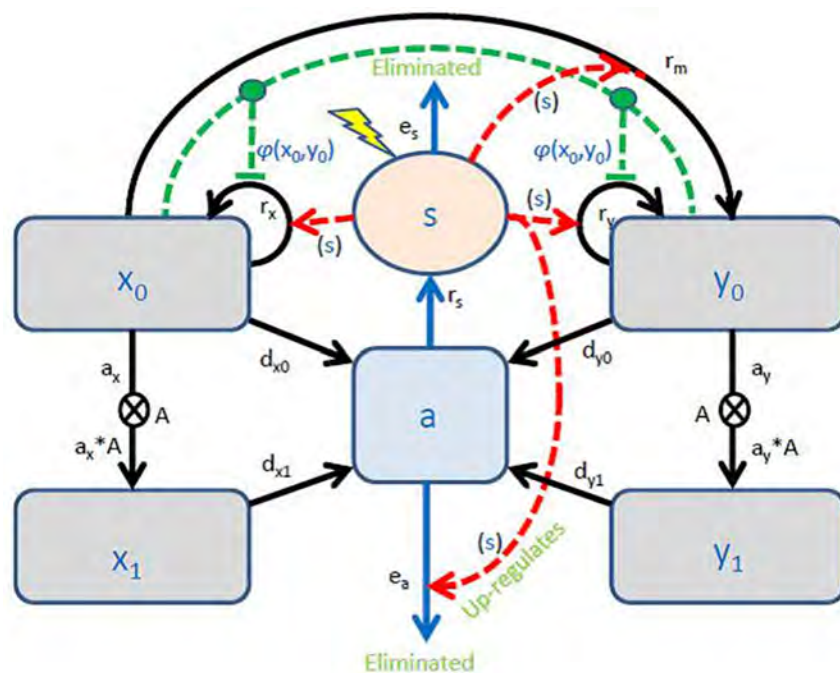


Fig 1. The conceptual model. Light gray boxes (symbolized x_0 , x_1 , y_0 , and y_1) illustrate the compartments of the basic model, and the black arrows the rates of the flows between these compartments. Here x_0 denotes the number of HSC, x_1 that of HMS, y_0 that of MPN SC, and y_1 the number of MPN MC. The light blue compartment (symbolized a) contains all dead cells and the light orange compartment (symbolized s) the inflammatory level, i.e. the immune response. Blue arrows from these represent related rates of flows. Red stipulated arrows going from the inflammatory compartment represent effects of the cytokines (or neutrophils when eliminating dead cells) modulating rates of the basic model. Two additional rates (depending on x_0 and y_0) appearing as red stipulated arrows represent the bone marrow niches symbiosis with the stem cells modulating the self-renewal rates. Note, stem cells leaving their respective compartments enter the corresponding mature cell-pools as multiplied by the progenitor amplification factor (A).

<https://doi.org/10.1371/journal.pone.0183620.g001>

a quantitatively conceptual level. Hence, the complicated mathematical question of model identifiability and accurate parameter estimation will be addressed elsewhere. Nevertheless, we include some model calibration and validation after presenting the model to justify and demonstrate the strength of the model.

Basically, our model consists of four pools of cells; the hematopoietic stem cells (HSC), the hematopoietic mature cells (HMC), the MPN-mutated stem cells (MPN SC) and the MPN mature cells (MPN MC). The number of these cells are denoted $x_0, x_1, y_0,$ and y_1 respectively, where x refers to normal hematopoietic cells and y to MPN hematopoietic cells, while index 0 refers to stem cells and index 1 to mature cells. A single stem cell (SC) may proliferate in three ways; symmetric self-renewal (having two stem cells as offspring), asymmetric self-renewal (turning into one stem cell and one progenitor cell), and symmetric differentiation (giving rise to two progenitor cells). The progenitor cells cannot be ignored, however, we consider the progenitor cells simply as intermedia multiplication steps describing the way stem cells generate mature cells. In the model, the generations or continuum of progenitor cells will be implicitly accounted for as each stem cell will generate a number of mature cells by an amplification factor, $A (= 2^k$ if there are k generations of progenitor cells). Feedbacks from or to progenitor cells are ignored or integrated into the other included feedbacks.

The present focus is on the ensemble of each cell type and not the individual cells; thus the governing laws will be for the pools of cells, in science denoted compartments [99]. Mathematically, the dynamics will be described by non-linear ordinary differential equations respecting conservation laws. The HSC self-renews with rate r_x and the malignant MPN SC self-renews with rate r_y . Furthermore, HSC may be transformed by cell division by a rate a_x whereas the MPN SC does so with a rate a_y . The mature cells are multiply generated, i.e. the HMC are generated with a rate $a_x \cdot A_x$ and the MPN MC with a rate $a_y \cdot A_y$. Finally, all cell types may die; stem cells with a lower rate and mature cells with a higher rate. The turnover (or mortality) rates are $d_{x0}, d_{x1}, d_{y0},$ and d_{y1} for the HSC, HMC, MPN SC, and MPN MC, respectively. Except for the mutation part and the multiplication factor, this duplicates the structure of the model proposed by Dingli and Michor (they silently used $A = 1$) [92].

A small probability r_m describes the mutation of HSC into MPN SC. In that case, r_m is not the probability of a single mutation but possibly a serial sequence of mutations turning the HSC into a cancer cell capable of self-renewal, by definition an MPN SC, where a mutation is expected to be described by a Poisson process [100]. The probability for one mutation is about 10^{-7} per year per cell [101]. However, not all mutations are malignant; only mutations which happen on particular locations (i.e. at specific nucleic acids) of the DNA cause MPN relevant mutations. Inflammation increases the risk of mutations, including smoking, exposure to ultraviolet light or certain chemicals [49,50,101±104]. It is this small probability which violates a possible deterministic description with a simple mutation rate. Except for the mutation part, the model will be deterministic and continuous. In most of our work, we studied the development right after the first malignant mutation has occurred (denoted the first insult). In these cases, the simulations start with one malignant stem cell. Meanwhile, the number of all other cells are in a healthy steady state with the mutation rate put to zero. The approach is justified by the fact that including a non-zero mutation rate did not affect the outcome of the model.

The equations are all of the general form,

$$\left\{ \begin{array}{l} \text{Change in amount of a} \\ \text{compartment per time} \end{array} \right\} = \left\{ \begin{array}{l} \text{rate of generation times} \\ \text{the generating source} \end{array} \right\} - \left\{ \begin{array}{l} \text{rate of elimination times the amount} \\ \text{in the compartment considered} \end{array} \right\}$$

resulting in specific systems of ordinary differential equations as given in [S1 Appendix](#).

Whenever cells die the debris have to be engulfed by phagocytic cells, e.g. neutrophils and macrophages while a hierarchic cascade of pro- and anti-inflammatory cytokines are released [96±98,110]. Following the parsimonious principle, we let the dead cells (a) up-regulate the amount of phagocytic cells (s) with rate constant r_s per dead cell while they are eliminated with a rate e_s . In addition, endotoxins, smoking and other environmental factors may add to the inflammatory response; thus we add such a term (characterized by the lightning symbol in Fig 1). Since MPNs develop on time-scale years and inflammatory immune processes are fast (on time-scale hours-days), we assume that the amount of phagocytic cells is balanced by the cytokines levels in a fixed ratio. Thus, the cytokine level is proportional to the phagocytic level why the inflammatory compartment (s) represents both (up to a possible proportionality constant which may be incorporated into the rate constants). Meanwhile, the amount of dead cells is down-regulated as a second order elimination process, $-e_a \cdot a \cdot s$, with rate constant e_a . Dead cells are produced by $d_0 \cdot x_0 + d_{y_0} \cdot y_0 + d_{x_1} \cdot x_1 + d_{y_1} \cdot y_1$ per time denoted the turnover, which is assessed by the plasma concentration of lactic dehydrogenase (LDH). It is well-known that the inflammatory level affects the mutation rate [104] and the self-renewal rates [105]. For simplicity, we take these to be proportional with the inflammatory level (of course saturation may occur) but since the level (a) settles at constant levels so does the inflammatory level (s), which may be thought of as the amount of inflammatory cytokines which have been shown to be increased in patients with MPNs and several in a step-wise manner from controls over the early cancer stages (ET, PV) to the advanced cancer stage±myelofibrosis (PMF) (S1 Appendix) [40±46]. Thus, it turns out that various specific cytokines (IL-1β, IL-1RA, IL-2R, IL-6, IL-8, IL-10, IL-12) and C-reactive protein (CRP)±a conventional biomarker of inflammation±are linearly correlated with the inflammatory level (s). These cytokines have been chosen for validation of our model since elevated levels of several of these cytokines have been associated with an inferior survival [44]. Likewise, elevated levels of CRP have been shown to be associated with shortened leukemia-free survival in patients with myelofibrosis [42]. Of note, the inflammatory cytokine IL-8 have been reported to be of particular interest in the context of MPN pathogenesis [57±60]. These extra pools of cells are depicted in Fig 1 along with the rates governing the dynamics. This establishes the coupled inflammatory-MPN model. The full system of mathematical equations, representing the model is described in Table B in S1 Appendix including default parameter values.

Model calibration, validation, and results

The model is inspired by Dingli and Michor, and therefore the parameter values are based upon their values [92]. However, we have adjusted them to obtain more appropriate saturation levels in agreement with data (see Fig 2 and the reported values in Table C in S1 Appendix). First, the model is calibrated to the situation of no MPN cancer cells ($y_{0i} = 0$ and $y_{1i} = 0$). In this situation, we expect a stable steady state such that the number of HSC is approximately 10^4 and that of HMC is approximately 10^{10} . These choices are compromises between reported values for the number of HSC [78, 86, 88, 89, 92].

From the steady state condition we have the number of dead cells to be $a_x = \frac{d_{x_0} x_0 + d_{x_1} x_1}{e_a s} \approx 10^3$. We further expect $r_x > d_{x_0} + a_x$ and $d_{x_0} \ll d_{x_1}$. When allowing for MPN development the healthy state becomes unstable when perturbed by the malignant stem cells. Thus, we expect $r_y > r_x$.

In the final stage the in silico patient will have vanishing hematopoietic cells and the MPN cells will approach a stable steady state with a higher amount of MPN cells than normal hematopoietic cells in the healthy steady state. This is accomplished by choosing all the c-

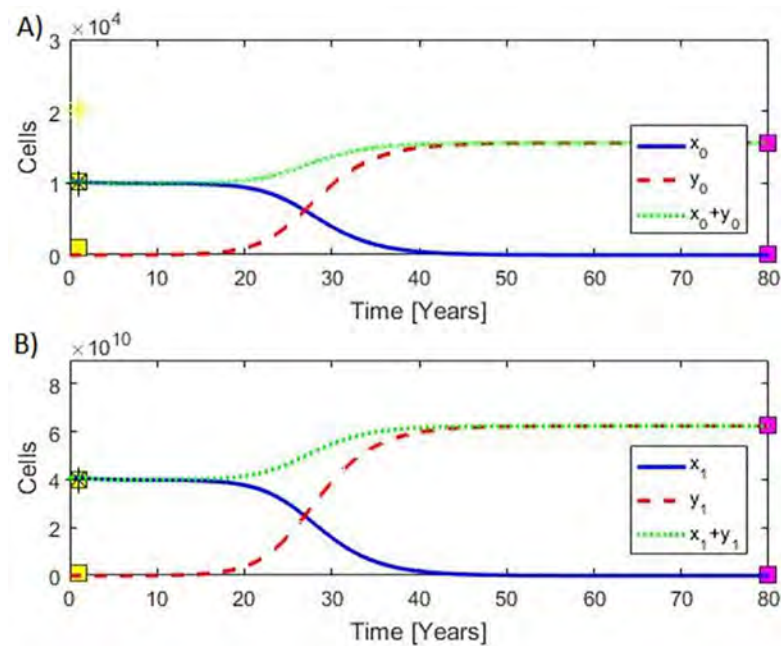


Fig 2. Model calibration. A) Plateaus to the left show the amount of hematopoietic stem cells x_0 (upper plateau) and that for MPN stem cells y_0 (lower plateau) whereas the plateaus to the right show the amount of hematopoietic stem cells x_0 (lower plateau) and MPN stem cells y_0 (upper plateau). B) Plateaus to the left show the amount of hematopoietic mature cells x_1 (upper plateau) and that for MPN mature cells y_1 (lower plateau) whereas the plateaus to the right show the amount of hematopoietic mature cells x_1 (lower plateau) and MPN mature cells y_1 (upper plateau). The yellow and purple boxes show our data used for calibrating (and validating) the model with further details in [S1 Appendix](#). Yellow boxes show our ‘no MPN cancer values’, and purple boxes show our ‘full blown’ MPN values in the advanced myelofibrosis stage. Yellow position marker shows the number of hematopoietic stem cells as used by Dingli & Michor [92], and black position markers show the number of cells as used by Gentry et al. [86].

<https://doi.org/10.1371/journal.pone.0183620.g002>

values equal in order to keep the model as simple as possible and the number of parameters as few as possible. Likewise, the parsimonious principle suggests $d_{y0} = d_{x0}$, $a_y = a_x$ and $A_y = A_x$.

The JAK2V617F allele burden has been reported to have median values of 7% (95% CL $2 \pm 15\%$; range $1 \pm 39\%$), 33% (95% CL $20 \pm 40\%$; range $1 \pm 92\%$) and 67% (95% CL $52 \pm 95\%$; range $37 \pm 99\%$) in ET, PV and PMF patients, respectively [19]. It follows that the model output perfectly resamples these dynamic changes in the JAK2V617F mutational load (Fig 3). Additional details are given in the [S1 Appendix](#) section.

All these attempts in calibrating the model may simultaneously be considered as validation since they performed successfully. However, the model may be validated further by predicting affected cytokine levels from the inflammatory level. As indicators of the inflammatory level, we refer to those cytokines, which are considered most important in the context of MPNs: IL-1 β , IL-1RA, IL-2R, IL-6, IL-8, IL-10, IL-12 and the inflammation biomarker CRP which all turned out to be linearly correlated with the inflammatory level (s).

For the specific cytokines (C_i) tabulated in the [S1 Appendix](#), we have ‘Normal’, ‘PV’, and ‘PMF’ median values (m_{ij} , where index i specifies the cytokine and index j refers to ‘Normal’, ‘PV’ and ‘PMF’ states) for each. Then we find k_{i1} and k_{i2} such that $m_{ij} = k_{i1} s_j + k_{i2}$ where s_j is the value of s at year t_j . Similarly, LDH values were demonstrated to be correlated and compared to the total rate of dying cells $DI = dx_0x_0 + dx_1x_1 + dy_0y_0 + dy_1y_1$. The results are summarized

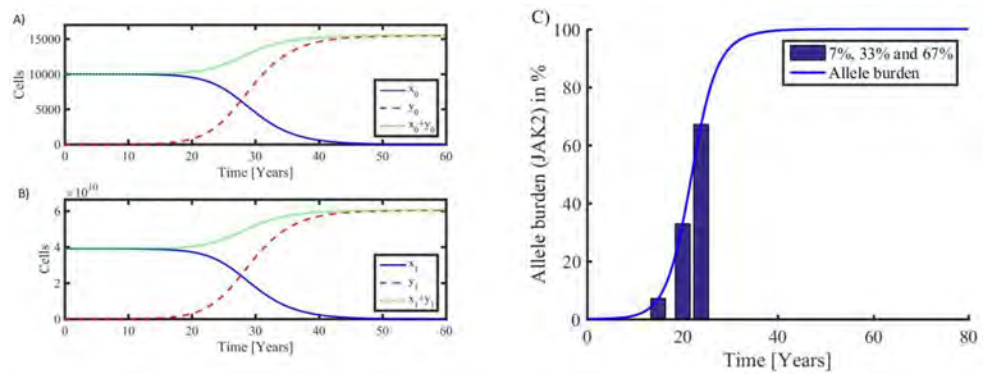


Fig 3. Left: Typical development in stem cells (top panel A) and mature cells (bottom panel B). Healthy hematopoietic cells (full blue curves) dominate in the early phase where the number of malignant cells (stipulated red curves) are few. The total number of cells is also shown (dotted green curves). When a stem cell mutates without repairing mechanisms, a slowly increasing exponential growth starts. At a certain stage, the malignant cells become dominant, and the healthy hematopoietic cells begin to show a visible decline. Finally, the composition between the cell types results in a takeover by the malignant cells, leading to an exponential decline in hematopoietic cells and ultimately their extinction. The development is driven by an approximately exponential increase in the MPN stem cells, and the development is closely followed by the mature MPN cells. **Right:** The corresponding allele burden (7%, 33% and 67% corresponding to ET, PV, and PMF, respectively) defined as the ratio of MPN mature cells to the total number of mature cells.

<https://doi.org/10.1371/journal.pone.0183620.g003>

in Fig 4 which shows that the model predicts data very well. Only IL-6 seems to be less well predicted.

Disallowing potential mutations and having no MPN-stem cells initially forces the model system into a steady state where solutions are all constant after a possible initial transient event. Introducing a mutation probability introduces a fatal malignant state; the higher the mutation probability is the faster the malignant state develops. A typical scenario is shown in Fig 3A along with a curve of the allele burden development (Fig 3B). The Figure depicts both

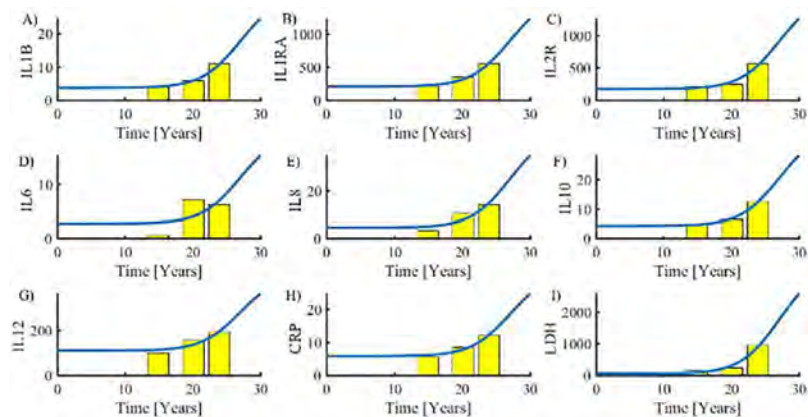


Fig 4. Model validation. Cytokines A) IL-1 β , B) IL-1RA, C) IL-2R, D) IL-6, E) IL-8, F) IL-10, G) IL-12 and H) C-reactive proteins (CRP) are approximately linearly correlated with the inflammatory level s . For the specific cytokines, we have from left to right 'Normal', 'PV', and 'PMF' median values (yellow columns) for comparison based on the predicted inflammatory level s (full blue curve) as a function of time after the first insult. I) Similarly, LDH is correlated with and compared to the total rate of dying cells $DI = dx_0x_0 + dx_1x_1 + dy_0y_0 + dy_1y_1$.

<https://doi.org/10.1371/journal.pone.0183620.g004>

modeling of the development of MPN from normal HSC and the early MPN diseases stages (ET/PV) to the advanced myelofibrosis stage.

Having a continuous mutation rate, it will take 24 years for the disease to develop to an allele burden of 7% (e.g. ET) and after additional four years the allele burden reaches 33% (e.g. transformation of ET to PV) to become 67% (e.g. transformation of PV to post-PV myelofibrosis) at year 36 after the first stem cell mutation. Disallowing mutations in the model and initially including a single malignant stem cell and no malignant mature cells shifts the allele burden curve by one year to the left on the time axis.

Thus, the mutation of an HSC to MPN SC triggers the disease. Once an MPN stem cell is established the disease can progress without further mutations.

The baseline inflammatory load (stimulus) is arbitrarily set to 7 pg/ml per day during normal circumstances. It is an exogenous stimulation of the immune system, which leads to an inflammatory level of 3.61 pg/ml, increasing to 3.66 pg/ml in MPNs. This corresponds to a baseline of 700 dead cells (in the hematopoietic steady state) before MPN develops remarkably. A doubling of the baseline inflammatory level is directly affecting the inflammation load (cytokine level) and thereby affecting the rest of the system as dictated by the model equations. In Fig 5 is depicted that shortening the exposure time of inflammation load is associated with deceleration of disease progression.

Discussion

Chronic inflammation is characterized by persistently activated immune cells, DNA damage, tissue destruction, remodeling and fibrosis [106]. In patients with MPNs, these processes are exemplified by the advanced myelofibrosis stage [4, 29], which accordingly might be considered to develop as the consequence of chronic inflammation in the bone marrow—the inflamed bone marrow and “the wound that won’t heal” [4, 29, 107, 108]. Herein, we for the first time use mathematical modelling to substantiate the concept that MPN progression is facilitated by chronic inflammation and that ET and PV are linked through increasing JAK2V617F allele burden [19] which is destined to happen as time increases without interference. Importantly, we were able to create the inflammation-MPN model based upon current knowledge on the interactions between inflammatory cytokines, hematopoietic stem cells and progenitors, and the bone marrow microenvironment [31±33, 35±37, 105]. By mathematical modelling of all these interactions, our integrated inflammation-MPN model was created. The model was validated from current data on circulating inflammatory cytokines in MPNs [40, 44±46], thereby substantiating inflammation to be a highly potent stimulus for clonal evolution and cancer progression in MPNs. In the context that elevated CRP levels have been shown to be associated with shortened leukemia-free survival in myelofibrosis [42], it is of interest that our model was excellently validated by data on CRP levels in the different MPN disease stages as well.

Mathematical modelling has been used to describe the impact of chronic inflammation and immune deregulation in aging [109] and several diseases, including type 1 diabetes mellitus [110], rheumatoid arthritis [96] and colitis-associated colon cancer [111]. Based upon the known association between respiratory infections and chronic inflammation, Herald described a general model of inflammation [97]. In this model, a system of nonlinear ordinary differential equations was used to describe interactions between macrophages, inflammatory and anti-inflammatory cytokines and bacteria. Though initiated by bacteria as the stimulus to trigger chronic inflammation, their study focused on chronic inflammation in the absence of pathogens as well [97]. Of note, even small changes in parameters of importance for inflammatory cytokine production and macrophage sensitivity to cytokines resulted in dramatically different

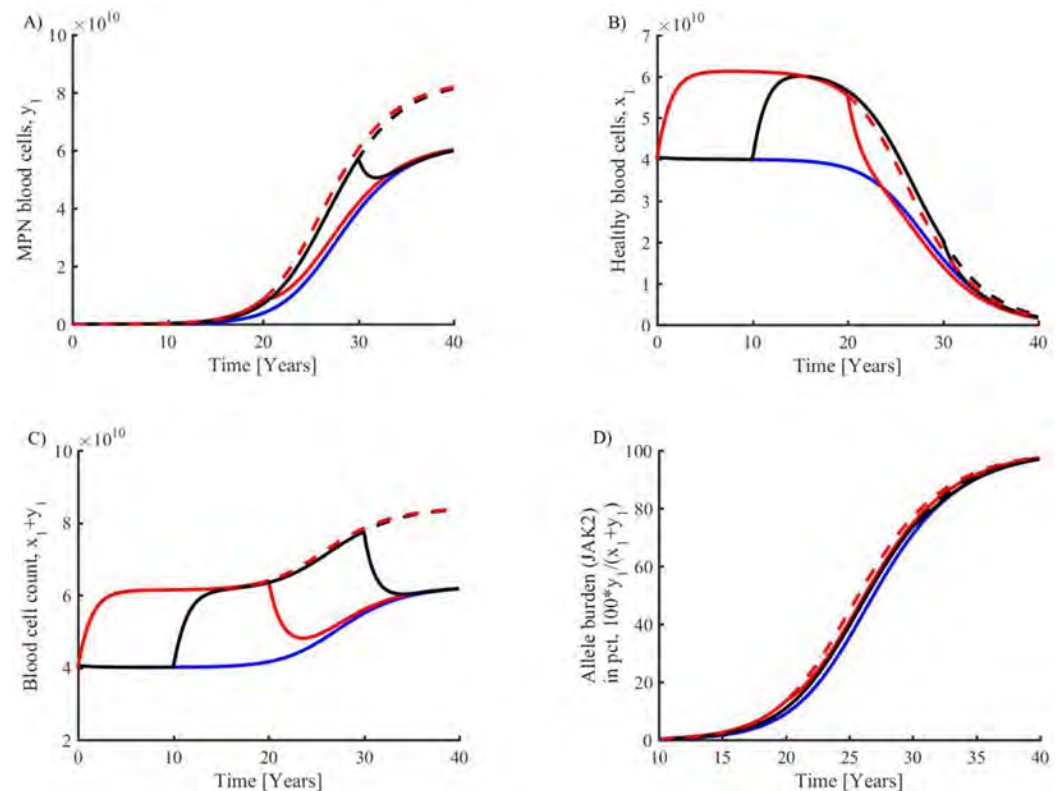


Fig 5. Investigation of increased inflammatory load at various onsets and durations. Blue curve is default parameters corresponding to Fig 3, red dotted is a doubling of inflammatory load, full red curve is a doubling of inflammatory load in year 0 ± 20 , then back to default level, black dotted curve is inflammatory doubling from year 10, the full black is inflammatory doubling year 10 ± 30 . **Upper:** Increasing inflammatory load has a boosting effect on MPN MC (A) as well as on HMC (B). **Lower:** Displaying the results in terms of the clinically available quantity, total blood cell count, also shows a boosted effect with increasing inflammatory load (C). The allele burden of JAK2 mutated blood cells similarly shows that increased inflammation increases disease development (D). There is a clear effect of MPN promotion with increasing inflammatory load, earlier onset, and exposure time. Lowering inflammatory load makes disease progression less rapid. Maintaining a doubling (red dotted curve) shifts the allele burden curve to the left by two years. Shortening the exposure time of inflammatory load weakens the disease progression. The inflammation has a fast impact on the total number of blood cells, which typically changes by 25% within the first year after doubling or reducing the inflammatory load by 50%.

<https://doi.org/10.1371/journal.pone.0183620.g005>

model behaviors [97]. According to this model chronic inflammation is not triggered when the immune system is functioning properly. However, in patients with a dysfunction of the immune system positive feedback of the inflammatory cytokine network is prone to induce chronic inflammation. Furthermore, if the macrophage population is more sensitive to inflammatory cytokines small perturbations initiated by the inflammation stimulus will also lead to chronic inflammation [97]. In this context, it is intriguing to consider if the inherited genetic predisposition to acquire the JAK2V617F-mutation due to the haplotype 46/1 [112±117], which also confers an increased risk of (other) inflammatory diseases (e.g. Crohns' disease) [118,119] and /or acquired genetic instability due to sustained chronic inflammation (chronic inflammatory diseases or toxin exposure (e.g. smoking) might further increase the risk of developing MPN—a hypothesis originally proposed by Hermouet et al [33,35]. Importantly, the hypersensitivity of clonal MPN-cells to exogenous and endogenous growth factors and inflammatory cytokines might also more easily lead to a chronic inflammatory state—similar to the increased sensitivity of the macrophage population leading to chronic inflammation in the

Herald model and also implemented in the Hermouet model, implying an enhanced myelomonocytic response to cytokine stimulation [33,35].

In the Herald model and the model described by Nielsen et al in regard to type 1 diabetes mellitus, the macrophages constituted an important compartment [97,110]. The monocyte-macrophage cell lineage is of major importance in the context of inflammation and cancer development. In our MPN-inflammation model bone marrow macrophages are also of utmost importance—both in regard to release of inflammatory cytokines, but also in regard to the development of myelofibrosis. Thus, in MPNs the monocyte-macrophage cell— together with the megakaryocyte (MK) cell lineage—are considered to be responsible for the development of myelofibrosis by the release of a number of growth factors and inflammatory cytokines that stimulate fibroblast proliferation [36,120,121]. The “Herald Model” is in several aspects equivalent to our model when considering substituting “bacteria” in the “Herald Model” by any noxious inflammatory stimulus. In fact, we implement yet another cell lineage—the MKs—as the source of a continuous release of products that stimulate the vicious inflammation circle, implying ultimately the development of cancer—the MPNs. As previously outlined, our mathematical modelling of the concept of chronic inflammation in MPNs is also supported by the elegant model described by Hermouet and co-workers [33,35], in which the *JAK2 46/1* haplotype was proposed as a marker of inappropriate myelomonocytic response to cytokine stimulation, leading to increased risk of inflammation, myeloid neoplasms, and impaired defense against infection [33]. Indeed, the Hermouet model for chronic inflammation [33,35] fits exceedingly well with the Herald model of general inflammation [97] and our mathematical modelling of MPNs as “A Human Inflammation Mode for Cancer Development [29±32]. In this regard, chronic inflammation and immune deregulation in MPNs might act as a trigger for later development of AML and MDS in line with the known association of inflammatory signaling and cancer [24±27]. The above models are additionally supported by the hypothetical model by Takizawa et al. (2010) [122], describing how chronic inflammatory processes might impinge on hematopoiesis, potentially fostering hematopoietic stem cell diseases, including MPNs. By inducing high proliferation of most HSCs, chronic inflammation might give rise to both exhaustion of the HSC pool and an even greater risk to accumulate genetic alterations in HSCs. Furthermore, by inflammatory stimuli from the bone marrow microenvironment these genetically altered HSCs might be rescued or “cancer cell niche” for later development of a hematological cancer [122].

The perspectives of our study are several. In the context that myelomonocytic cells (granulocytes, macrophages, monocytes) and MKs are all deeply involved in cancer development and progression [123,124], chronic inflammation is associated with premature atherosclerosis (atherothrombosis) [21±23, 29,30], in which both platelets and monocytes are highly important (monocytes a link between atherosclerosis and cancer [28]) and platelets are intimately involved in the metastatic process in cancer [124]—and likely in MPNs as well [125]—the avenue is opened for studying all these aspects by using mathematical modelling of current knowledge of the impact of chronic inflammation and immune deregulation in patients with MPNs. Ultimately, mathematical modelling may also be able to substantiate which agents to be used in MPNs in order to induce “minimal residual disease” [125±129] and the importance of early intervention with agents that directly target both the malignant clone (interferon-alpha2) [126±129] and the inflammatory process (JAK1-2 inhibition with e.g. ruxolitinib) [130].

In conclusion, we have for the first time applied mathematical modelling as a tool to deliver the proof of concept that chronic inflammation is closely linked to the development of the MPNs—myeloproliferative cancers which today are considered to be “chronic inflammatory diseases”, in which chronic inflammation may be a driving force for clonal expansion and

ultimately the development of AML [4, 29±32,39]. Studies are ongoing to elucidate the above perspectives by mathematical modelling. In this regard, mathematical modelling of resolution of inflammation may be highly important [98] and useful to support the decision-making which agents to use in the future for patients with MPNs in order to induce minimal residual disease and hopefully cure.

Supporting information

S1 Appendix.
(DOCX)

Author Contributions

Conceptualization: Morten Andersen, Christina Ellervik, Vibe Skov, Lasse Kjñr, Niels Pallisgaard, Torben A. Kruse, Mads Thomassen, Jesper Troelsen, Hans Carl Hasselbalch, Johnny T. Ottesen.

Data curation: Morten Andersen, Johnny T. Ottesen.

Formal analysis: Morten Andersen, Zamra Sajid, Rasmus K. Pedersen, Johanne Gudmand-Hoeyer, Johnny T. Ottesen.

Investigation: Morten Andersen, Hans Carl Hasselbalch, Johnny T. Ottesen.

Methodology: Morten Andersen, Christina Ellervik, Vibe Skov, Lasse Kjñr, Niels Pallisgaard, Torben A. Kruse, Mads Thomassen, Jesper Troelsen, Hans Carl Hasselbalch, Johnny T. Ottesen.

Resources: Morten Andersen, Johnny T. Ottesen.

Software: Morten Andersen, Zamra Sajid, Rasmus K. Pedersen, Johanne Gudmand-Hoeyer, Johnny T. Ottesen.

Supervision: Hans Carl Hasselbalch, Johnny T. Ottesen.

Validation: Morten Andersen, Vibe Skov, Lasse Kjñr, Hans Carl Hasselbalch, Johnny T. Ottesen.

Visualization: Morten Andersen, Hans Carl Hasselbalch, Johnny T. Ottesen.

Writing ± original draft: Morten Andersen, Hans Carl Hasselbalch, Johnny T. Ottesen.

Writing ± review & editing: Morten Andersen, Zamra Sajid, Rasmus K. Pedersen, Johanne Gudmand-Hoeyer, Christina Ellervik, Vibe Skov, Lasse Kjñr, Niels Pallisgaard, Torben A. Kruse, Mads Thomassen, Jesper Troelsen, Hans Carl Hasselbalch, Johnny T. Ottesen.

References

1. Campbell PJ, Green AR. The myeloproliferative disorders. *N Engl J Med.* 2006; 355 (23): 2452±2466. <https://doi.org/10.1056/NEJMra063728> PMID: 17151367
2. Marchioli R, Finazzi G, Landolfi R, Kutti J, Gisslinger H, Patrono C, et al. Vascular and neoplastic risk in a large cohort of patients with polycythemia vera. *J Clin Oncol.* 2005; 23: 2224±2232. <https://doi.org/10.1200/JCO.2005.07.062> PMID: 15710945
3. Kristinsson SY, Landgren O, Samuelsson J Björkholm M, Goldin LR. Autoimmunity and the risk of myeloproliferative neoplasms. *Haematologica.* 2010; 95(7): 1216±1220. <https://doi.org/10.3324/haematol.2009.020412> PMID: 20053870
4. Hasselbalch HC, Bjørn ME. MPNs as Inflammatory Diseases: The Evidence, Consequences, and Perspectives. *Mediators Inflamm.* 2015: 102476. <https://doi.org/10.1155/2015/102476> PMID: 26604428

5. Frederiksen H, Farkas DK, Christiansen CF, Hasselbalch HC, Sørensen HT. Chronic myeloproliferative neoplasms and subsequent cancer risk: a Danish population-based cohort study. *Blood*. 2011; 118(25): 6515±6520. <https://doi.org/10.1182/blood-2011-04-348755> PMID: 22039256
6. Frederiksen H, Farkas DK, Christiansen CF, Larsen TS, Hasselbalch HC, Stentoft J, et al. Survival of patients with chronic myeloproliferative neoplasms and new primary cancers: a population-based cohort study. *Lancet Haematol*. 2015; 2(7): e289±296. [https://doi.org/10.1016/S2352-3026\(15\)00092-7](https://doi.org/10.1016/S2352-3026(15)00092-7) PMID: 26688384
7. Pettersson H, Knutsen H, Holmberg E, Andreasson B. Increased incidence of another cancer in myeloproliferative neoplasms patients at the time of diagnosis. *Eur J Haematol*. 2015; 94(2): 152±156. <https://doi.org/10.1111/ejh.12410> PMID: 25039361
8. Enblom A, Lindskog E, Hasselbalch HC, Hersby D, Bak M, Tetu J, et al. High rate of abnormal blood values and vascular complications before diagnosis of myeloproliferative neoplasms. *Eur J Intern Med*. 2015; 26(5): 344±347. <https://doi.org/10.1016/j.ejim.2015.03.009> PMID: 25863408
9. Sørensen AL, Hasselbalch HC. Antecedent cardiovascular disease and autoimmunity in Philadelphia-negative chronic myeloproliferative neoplasms. *Leuk Res*. 2016; 41: 27±35. <https://doi.org/10.1016/j.leukres.2015.11.017> PMID: 26718091
10. Bjorkholm M, Derolf AR, Hultcrantz M, Kristinsson SY, Ekstrand C, Goldin LR. Treatment-related risk factors for transformation to acute myeloid leukemia and myelodysplastic syndromes in myeloproliferative neoplasms. *J Clin Oncol*. 2011; 29(17): 2410±2415. <https://doi.org/10.1200/JCO.2011.34.7542> PMID: 21537037
11. James C, Ugo V, Le Couédic J-P, Staerk J, Delhommeau F, Lacout C, et al. A unique clonal JAK2 mutation leading to constitutive signalling causes polycythaemia vera. *Nature*. 2005; 434: 1144±1148. <https://doi.org/10.1038/nature03546> PMID: 15793561
12. Kralovics R, Passamonti F, Buser AS, Teo SS, Tiedt R, Passweg JR, et al. A gain-of-function mutation of JAK2 in myeloproliferative disorders. *N Engl J Med*. 2005; 352(17): 1779±1790. <https://doi.org/10.1056/NEJMoa051113> PMID: 15858187
13. Baxter EJ, Scott LM, Campbell PJ, East C, Fourouclas N, Swanton S, et al. Acquired mutation of the tyrosine kinase JAK2 in human myeloproliferative disorders. *Lancet*. 2005; 365(9464): 1054±1061.
14. Levine RL, Wadleigh M, Cools J, Ebert BL, Wernig G, Huntly BJ, et al. Activating mutation in the tyrosine kinase JAK2 in polycythemia vera, essential thrombocythemia, and myeloid metaplasia with myelofibrosis. *Cancer Cell*. 2005; 7(4): 387±397. <https://doi.org/10.1016/j.ccr.2005.03.023> PMID: 15837627
15. Klampfl T, Gisslinger H, Harutyunyan AS, et al. Somatic mutations of calreticulin in myeloproliferative neoplasms. *N Engl J Med*. 2013; 369(25): 2379±2390. <https://doi.org/10.1056/NEJMoa1311347> PMID: 24325356
16. Nangalia J, Massie CE, Baxter EJ, Nivarthi H, Rumi E, Milosevic JD, et al. Somatic CALR mutations in myeloproliferative neoplasms with nonmutated JAK2. *N Engl J Med*. 2013; 369(25): 2391±2405. <https://doi.org/10.1056/NEJMoa1312542> PMID: 24325359
17. Cazzola M, Kralovics R. From Janus kinase 2 to calreticulin: The clinically relevant genomic landscape of myeloproliferative neoplasms. *Blood*. 2014; 123(24): 3714±3719. <https://doi.org/10.1182/blood-2014-03-530865> PMID: 24786775
18. Lundberg P, Karow A, Nienhold R, Looser R, Hao-Shen H, Nissen I, et al. Clonal evolution and clinical correlates of somatic mutations in myeloproliferative neoplasms. *Blood*. 2014; 123(14): 2220±2228. <https://doi.org/10.1182/blood-2013-11-537167> PMID: 24478400
19. Larsen TS, Pallisgaard N, Møller MB, Hasselbalch HC. The JAK2 V617F allele burden in essential thrombocythemia, polycythemia vera and primary myelofibrosis: Impact on disease phenotype. *Eur J Haematol*. 2007; 79(6): 508±515. <https://doi.org/10.1111/j.1600-0609.2007.00960.x> PMID: 17961178
20. Barosi G, Rosti V, Bonetti E, Campanelli R, Carolei A, Catarsi P, et al. Evidence that Prefibrotic Myelofibrosis Is Aligned along a Clinical and Biological Continuum Featuring Primary Myelofibrosis. *PLoS One*. 2012; 7(4): e35631. <https://doi.org/10.1371/journal.pone.0035631> PMID: 22536419
21. Danesh J, Whincup P, Walker M, Lennon L, Thomson A, Appleby P, et al. Low grade inflammation and coronary heart disease: prospective study and updated meta-analyses. *BMJ*. 2000; 321: 199±204. PMID: 10903648
22. Ridker PM, Cushman M, Stampfer MJ, Tracy RP, Hennekens CH. Plasma concentration of C-reactive protein and risk of developing peripheral vascular disease. *Circulation*. 1998; 97(5): 425±428. PMID: 9490235
23. Brevetti G, Giugliano G, Brevetti L, Hiatt WR. Inflammation in peripheral arterial disease. *Circulation*. 2010; 122: 1862±1875. <https://doi.org/10.1161/CIRCULATIONAHA.109.918417> PMID: 21041698
24. Hanahan D, Weinberg RA. The hallmarks of cancer. *Cell*. 2000; 100(1): 57±70. PMID: 10647931

25. Pikarsky E, Porat RM, Stein I, Abramovitch R, Amit S, Kasem S, et al. NF-kappaB functions as a tumour promoter in inflammation associated cancer. *Nature*. 2004; 431(7007): 461±466. <https://doi.org/10.1038/nature02924> PMID: 15329734
26. Karin M, Greten FR. NF-kappaB: linking inflammation and immunity to cancer development and progression. *Nat Rev Immunol*. 2005; 5(10): 749±759. <https://doi.org/10.1038/nri1703> PMID: 16175180
27. Mantovani A, Garlanda C, Allavena P. Molecular pathways and targets in cancer-related inflammation. *Ann Med*. 2010; 42(3): 161±170. <https://doi.org/10.3109/07853890903405753> PMID: 20384432
28. Pittet MJ, Swirski FK. Monocytes link atherosclerosis and cancer. *Eur J Immunol*. 2011; 41(9): 2519±2522. <https://doi.org/10.1002/eji.201141727> PMID: 21952809
29. Hasselbalch HC. Chronic inflammation as a promotor of mutagenesis in essential thrombocythemia, polycythemia vera and myelofibrosis. A human inflammation model for cancer development? *Leuk Res*. 2013; 37(2): 214±220. <https://doi.org/10.1016/j.leukres.2012.10.020> PMID: 23174192
30. Hasselbalch HC. Perspectives on chronic inflammation in essential thrombocythemia, polycythemia vera, and myelofibrosis: is chronic inflammation a trigger and driver of clonal evolution and development of accelerated atherosclerosis and second cancer? *Blood*. 2012; 119: 3219±3225. <https://doi.org/10.1182/blood-2011-11-394775> PMID: 22318201
31. Hasselbalch HC. The role of cytokines in the initiation and progression of myelofibrosis. *Cytokine Growth Factor Rev*. 2013; 24(2): 133±145. <https://doi.org/10.1016/j.cytogfr.2013.01.004> PMID: 23415024
32. Hasselbalch HC. A role of NF-E2 in chronic inflammation and clonal evolution in essential thrombocythemia, polycythemia vera and myelofibrosis? *Leuk Res*. 2014; 38(2): 263±266. <https://doi.org/10.1016/j.leukres.2013.07.002> PMID: 23932394
33. Hermouet S, Vilaine M. The JAK2 46/1 haplotype: a marker of inappropriate myelomonocytic response to cytokine stimulation, leading to increased risk of inflammation, myeloid neoplasm, and impaired defense against infection? *Haematologica*. 2011; 96(11): 1575±1579. <https://doi.org/10.3324/haematol.2011.055392> PMID: 22058280
34. Hermouet S, Hasselbalch HC, Čokić V. Mediators of Inflammation in Myeloproliferative Neoplasms: State of the Art. *Mediators Inflamm*. 2015; 964613. <https://doi.org/10.1155/2015/964613> PMID: 26681841
35. Hermouet S, Bigot-Corbel E, Gardie B. Pathogenesis of Myeloproliferative Neoplasms: Role and Mechanisms of Chronic Inflammation. *Mediators Inflamm*. 2015; 145293. <https://doi.org/10.1155/2015/145293> PMID: 26538820
36. Desterke C, Martinaud C, Ruzehaji N, Le Bousse-Kerdilès MC. Inflammation as a Keystone of Bone Marrow Stroma Alterations in Primary Myelofibrosis. *Mediators Inflamm*. 2015; 415024. <https://doi.org/10.1155/2015/415024> PMID: 26640324
37. Čokić VP, Mitrović-Ajtić O, Beleslin-Čokić BB, Marković D, Buač M, Diklić M, et al. Proinflammatory Cytokine IL-6 and JAK-STAT Signaling Pathway in Myeloproliferative Neoplasms. *Mediators Inflamm*. 2015; 453020. <https://doi.org/10.1155/2015/453020> PMID: 26491227
38. Geyer HL, Dueck AC, Scherber RM, Mesa R. Impact of Inflammation on Myeloproliferative Neoplasm Symptom Development. *Mediators Inflamm*. 2015; 284706. <https://doi.org/10.1155/2015/284706> PMID: 26538823
39. Koschmieder S, Mughal TI, Hasselbalch HC, Barosi G, Valent P, Kiladjian JJ, et al. Myeloproliferative neoplasms and inflammation: whether to target the malignant clone or the inflammatory process or both. *Leukemia*. 2016; 30(5): 1018±1024. <https://doi.org/10.1038/leu.2016.12> PMID: 26854026
40. Panteli KE, Hatzimichael EC, Bouranta PK, Katsaraki A, Seferiadis K, Stebbing, et al. Serum interleukin (IL)-1, IL-2, sIL-2Ra, IL-6 and thrombopoietin levels in patients with chronic myeloproliferative diseases. *Br J Haematol*. 2005; 130: 709±715. <https://doi.org/10.1111/j.1365-2141.2005.05674.x> PMID: 16115126
41. Barbui T, Carobbio A, Finazzi G, Vannucchi AM, Barosi G, Antonioli E et al. Inflammation and thrombosis in essential thrombocythemia and polycythemia vera: different role of C-reactive protein and pentraxin 3. *Haematologica*. 2011; 96: 315±318. <https://doi.org/10.3324/haematol.2010.031070> PMID: 21173097
42. Barbui T, Carobbio A, Finazzi G, Guglielmelli P, Salmoiraghi S, Rosti V et al., Elevated C-reactive protein is associated with shortened leukemia-free survival in patients with myelofibrosis. *Leukemia*. 2013; 27(10): 2084±6. <https://doi.org/10.1038/leu.2013.207> PMID: 23828261
43. Verstovsek S, Kantarjian H, Mesa RA, Pardanani AD, Cortes-Franco J, Thomas DA, et al. Safety and efficacy of INCB018424, a JAK1 and JAK2 inhibitor, in myelofibrosis. *N Engl J Med*. 2010; 363: 1117±1127. <https://doi.org/10.1056/NEJMoa1002028> PMID: 20843246

44. Tefferi A, Vaidya R, Caramazza D, Finke C, Lasho T, Pardanani A. Circulating interleukin (IL)-8, IL-2R, IL-12, and IL-15 levels are independently prognostic in primary myelofibrosis: a comprehensive cytokine profiling study. *J Clin Oncol*. 2011; 1356±1363. <https://doi.org/10.1200/JCO.2010.32.9490> PMID: 21300928
45. Vaidya R, Gangat N, Jimma T, Finke CM, Lasho TL, Pardanani A, et al. Plasma cytokines in polycythemia vera: phenotypic correlates, prognostic relevance, and comparison with myelofibrosis. *Am J Hematol*. 2012; 87(11): 1003±5. <https://doi.org/10.1002/ajh.23295> PMID: 22965887
46. Pourcelot E, Trocme C, Mondet J, Bailly S, Toussaint B, Mossuz P. Cytokine profiles in polycythemia vera and essential thrombocythemia patients: Clinical implications. *Experimental Hematol*. 2014; 42: 360±368.
47. Christensen AS, Møller JB, Hasselbalch HC. Chronic kidney disease in patients with the Philadelphia-negative chronic myeloproliferative neoplasms. *Leuk Res*. 2014; 38(4): 490±495. <https://doi.org/10.1016/j.leukres.2014.01.014> PMID: 24630365
48. Bak M, Sørensen TL, Meulengracht Flachs E, Zwisler AD, Juel K, Frederiksen H, et al: Age-Related Macular Degeneration in Patients with Chronic Myeloproliferative Neoplasms: A Nationwide Population-Based Cohort Study. *JAMA Ophthalmol*. 2017; 135(8):835±843. <https://doi.org/10.1001/jamaophthalmol.2017.2011> PMID: 28655032
49. Hasselbalch HC. Smoking as a contributing factor for development of polycythemia vera and related neoplasms. *Leuk Res*. 2015; 015 Sep 9.
50. Lindholm Sørensen A, Hasselbalch HC. Smoking and Philadelphia-negative chronic myeloproliferative neoplasms. *Eur J Haematol*. 2016; 97(1): 63±69. <https://doi.org/10.1111/ejh.12684> PMID: 26384085
51. Andersen CL, Bjørn ME, McMullin MF, Harrison C, Samuelsson J, Ejerblad E et al. Circulating YKL-40 in patients with essential thrombocythemia and polycythemia vera treated with the novel histone deacetylase inhibitor vorinostat. *Leuk Res*. 2014; 38(7): 816±821. <https://doi.org/10.1016/j.leukres.2014.04.002> PMID: 24836761
52. Bjørn ME, Andersen CL, Jensen MK, Hasselbalch HC. Circulating YKL-40 in myelofibrosis a potential novel biomarker of disease activity and the inflammatory state. *Eur J Haematol*. 2014; 93(3): 224±228. <https://doi.org/10.1111/ejh.12332> PMID: 24689875
53. Bjørn ME, Hasselbalch HC. The Role of Reactive Oxygen Species in Myelofibrosis and Related Neoplasms. *Mediators Inflamm*. 2015; 648090. <https://doi.org/10.1155/2015/648090> PMID: 26538833
54. Fleischman AG, Aichberger KJ, Luty SB, Bumm TG, Petersen CL, Doratotaj S, et al: TNF α facilitates clonal expansion of JAK2V617F positive cells in myeloproliferative neoplasms. *Blood*. 2011; 118: 6392±6398. <https://doi.org/10.1182/blood-2011-04-348144> PMID: 21860020
55. Lu M, Xia L, Liu YC, Hochman T et al: Lipocalin produced by myelofibrosis cells affects the fate of both hematopoietic and marrow microenvironmental cells. *Blood*. 2015; 126: 972±982. <https://doi.org/10.1182/blood-2014-12-618595> PMID: 26022238
56. Kleppe M, Kwak M, Koppikar P, Riestler M, Keller M, Bastian L et al. JAK-STAT pathway activation in malignant and nonmalignant cells contributes to MPN pathogenesis and therapeutic response. *Cancer Discov*. 2015; 5: 316±331. <https://doi.org/10.1158/2159-8290.CD-14-0736> PMID: 25572172
57. Kaufmann KB, Grunder A, Hadlich T, Wehrle J, Gothwal M, Bogeska R, et al: A novel murine model of myeloproliferative disorders generated by overexpression of the transcription factor NF-E2. *J Exp Med*. 2012; 209: 35±50. <https://doi.org/10.1084/jem.20110540> PMID: 22231305
58. Jutzi JS, Bogeska R, Nikoloski G, Schmid CA, Seeger TS, Stegelmann F et al: MPN patients harbor recurrent truncating mutations in transcription factor NF-E2. *J Exp Med*. 2013; 210: 1003±1019. <https://doi.org/10.1084/jem.20120521> PMID: 23589569
59. Jutzi JS, Pahl HL. The hen or the egg: inflammatory aspects of murine MPN models. *Mediators Inflamm*. 2015; 2015:101987. <https://doi.org/10.1155/2015/101987> PMID: 26543325
60. Wehrle J, Seeger TS, Schwemmers S, Pfeifer D, Bulashevskaya A, Pahl HL. Transcription factor nuclear factor erythroid-2 mediates expression of the cytokine interleukin 8, a known predictor of inferior outcome in patients with myeloproliferative neoplasms. *Haematologica*. 2013; 98: 1073±1080. <https://doi.org/10.3324/haematol.2012.071183> PMID: 23445878
61. Roelz R, Pilz IH, Mutschler M, Pahl HL. Of mice and men: human RNA polymerase III promoter U6 is more efficient than its murine homologue for shRNA expression from a lentiviral vector in both human and murine progenitor cells. *Exp Hematol*. 2010; 38: 792±797. <https://doi.org/10.1016/j.exphem.2010.05.005> PMID: 20685233
62. Zhang Y, Liu X, McHale C, Li R, Zhang L, Wu Y et al. Bone marrow injury induced via oxidative stress in mice by inhalation exposure to formaldehyde. *PLoS One*. 2013; 8: e74974. <https://doi.org/10.1371/journal.pone.0074974> PMID: 24040369

63. Zhang Q, Zhao K, Shen Q, Han Y, Gu Y, Li X, et al: Tet2 is required to resolve inflammation by recruiting Hdac2 to specifically repress IL-6. *Nature*. 2015; 525: 389±393. <https://doi.org/10.1038/nature15252> PMID: 26287468
64. Skov V, Larsen TS, Thomassen M, Riley CH, Jensen MK, Bjerrum OW, et al: Whole-blood transcriptional profiling of interferon-inducible genes identifies highly upregulated IFI27 in primary myelofibrosis. *Eur J Haematol*. 2011; 87(1): 54±60. <https://doi.org/10.1111/j.1600-0609.2011.01618.x> PMID: 21447007
65. Skov V, Riley CH, Thomassen M, Larsen TS, Jensen MK, Bjerrum OW, et al: Whole blood transcriptional profiling reveals significant down-regulation of human leukocyte antigen class I and II genes in essential thrombocythemia, polycythemia vera and myelofibrosis. *Leuk Lymphoma*. 2013; 54(10): 2269±2273. <https://doi.org/10.3109/10428194.2013.764417> PMID: 23302045
66. Skov V, Thomassen M, Riley CH, Jensen MK, Bjerrum OW, Kruse TA, et al: Gene expression profiling with principal component analysis depicts the biological continuum from essential thrombocythemia over polycythemia vera to myelofibrosis. *Exp. Hematol*. 2012; 40(9): 771±780. <https://doi.org/10.1016/j.exphem.2012.05.011> PMID: 22659388
67. Skov V, Larsen TS, Thomassen M, Riley CH, Jensen MK, Bjerrum OW, et al: Molecular profiling of peripheral blood cells from patients with polycythemia vera and related neoplasms: identification of deregulated genes of significance for inflammation and immune surveillance. *Leuk Res*. 2012; 36(11): 1387±1392. <https://doi.org/10.1016/j.leukres.2012.07.009> PMID: 22877729
68. Hasselbalch HC, Thomassen M, Riley CH, Kjær L, Larsen TS, Jensen MK, et al: Whole blood transcriptional profiling reveals deregulation of oxidative and antioxidative defence genes in myelofibrosis and related neoplasms. Potential implications of downregulation of Nrf2 for genomic instability and disease progression. *PLoS One*. 2014; 14; 9(11):e112786. <https://doi.org/10.1371/journal.pone.0112786> PMID: 25397683
69. Skov V, Burton M, Thomassen M, Larsen TS, Riley CH, Madelung AB et al. A 7-Gene Signature Depicts The Biochemical Profile of Early Prefibrotic Myelofibrosis. *Plos One*. 2016; 11(8): e0161570. <https://doi.org/10.1371/journal.pone.0161570> PMID: 27579896
70. Ciaffoni F, Cassella E, Varricchio L, Massa M, Barosi G, Migliaccio AR. Activation of non-canonical TGF-β1 signaling indicates an autoimmune mechanism for bone marrow fibrosis in primary myelofibrosis. *Blood Cells Mol Dis*. 2015; 54(3): 234±41 <https://doi.org/10.1016/j.bcmd.2014.12.005> PMID: 25703685
71. Riley CH, Jensen MK, Brimnes MK, Hasselbalch HC, Bjerrum OW, Straten PT, et al. Increase in circulating CD4(+) CD25(+) Foxp3(+) T cells in patients with Philadelphia-negative chronic myeloproliferative neoplasms during treatment with IFN-alpha. *Blood*. 2011; 118(8): 2170±2173. <https://doi.org/10.1182/blood-2011-03-340992> PMID: 21708889
72. Riley CH, Hansen M, Brimnes MK, Hasselbalch HC, Bjerrum OW, Svane IM, et al. Expansion of circulating CD56bright natural killer cells in patients with JAK2-positive chronic myeloproliferative neoplasms during treatment with interferon-α. *Eur J Haematol*. 2015; 94(3): 227±234. <https://doi.org/10.1111/ejh.12420> PMID: 25082025
73. Riley CH, Brimnes MK, Hansen M, Jensen MK, Hasselbalch HC, Kjaer L, et al: Interferon-alpha induces marked alterations in circulating regulatory T cells, NK cell subsets and dendritic cells in patients with JAK2-positive essential thrombocythemia and polycythemia vera. *Eur J Haematol*. 2016; 97(1): 83±92. <https://doi.org/10.1111/ejh.12687> PMID: 26385526
74. Barosi G. An immune dysregulation in MPN. *Curr Hematol Malig Rep*. 2014; 9(4): 331±339. <https://doi.org/10.1007/s11899-014-0227-0> PMID: 25139710
75. Titmarsh GJ, McMullin MF, McShane CM, Clarke M, Engels EA, Anderson LA, et al: Community-acquired infections and their association with myeloid malignancies. *Cancer Epidemiol*. 2014; 38(1): 56±61. <https://doi.org/10.1016/j.canep.2013.10.009> PMID: 24275260
76. Nielsen C, Birgens HS, Nordestgaard BG, Kjaer L, Bojesen SE. The JAK2 V617F somatic mutation, mortality and cancer risk in the general population. *Haematologica*. 2011; 96(3): 450±453. <https://doi.org/10.3324/haematol.2010.033191> PMID: 21160067
77. Nielsen C, Bojesen SE, Nordestgaard BG, Kofoed KF, Birgens HS. JAK2V617F somatic mutation in the general population: myeloproliferative neoplasm development and progression rate. *Haematologica*. 2014; 99(9): 1448±1455. <https://doi.org/10.3324/haematol.2014.107631> PMID: 24907356
78. Haeno H, Levine RL, Gilliland DG, Michor F. A progenitor cell origin of myeloid malignancies. *Proc Natl Acad Sci U S A*. 2009; 106(39): 16616±16621. <https://doi.org/10.1073/pnas.0908107106> PMID: 19805346
79. Attolini CS, Cheng YK, Beroukhim R, Getz G, Abdel-Wahab O, Levine RL, et al. A mathematical framework to determine the temporal sequence of somatic genetic events in cancer. *Proc Natl Acad Sci U S A*. 2010; 107(41): 17604±17609. <https://doi.org/10.1073/pnas.1009117107> PMID: 20864632

80. Michor F, Iwasa Y, Nowak MA. Dynamics of cancer progression. *Nature Reviews Cancer*. 2004; 4: 197±205. <https://doi.org/10.1038/nrc1295> PMID: 14993901
81. Michor F, Hughes TP, Iwasa Y, Branford S, Shah NP, Sawyers CL. Dynamics of chronic myeloid leukaemia. *Nature*. 2005; 435: 1267±1270. <https://doi.org/10.1038/nature03669> PMID: 15988530
82. De Pillis LG, Radunskaya AE, Wiseman CL. A validated mathematical model of cell-mediated immune response to tumor growth. *Cancer Research*. 2005; 65(17): 7950±7958. <https://doi.org/10.1158/0008-5472.CAN-05-0564> PMID: 16140967
83. Michor F. Mathematical models of cancer stem cells. *J Clin Oncol*. 2008; 26(17): 2854±2861. <https://doi.org/10.1200/JCO.2007.15.2421> PMID: 18539964
84. Stiehl T, Marciniak-Czochra A. Characterization of stem cells using mathematical models of multistage cell lineages. *Mathematical and Computer Modelling*. 2011; 53(7±8): 1505±1517.
85. Stiehl T, Marciniak-Czochra A. Mathematical Modeling of Leukemogenesis and Cancer Stem Cell Dynamics. *Math Model Nat Phenom*. 2012; 7(1): 166±202.
86. Gentry SN, Jackson TL. A mathematical model of cancer stem cell driven tumor initiation: implications of niche size and loss of homeostatic regulatory mechanisms. *Plos One*. 2013; 8(8): e71128. <https://doi.org/10.1371/journal.pone.0071128> PMID: 23990931
87. Walenda T, Stiehl T, Braun H, Fröbel J, Ho AD, Schroeder T, et al: Feedback Signals in Myelodysplastic Syndromes: Increased Self-Renewal of the Malignant Clone Suppresses Normal Hematopoiesis. *PLoS Comput Biol*. 2014; 10(4): e1003599. <https://doi.org/10.1371/journal.pcbi.1003599> PMID: 24763223
88. Stiehl T, Baran N, Ho AD, Marciniak-Czochra A. Cell Division Patterns in Acute Myeloid Leukemia Stem-like Cells Determine Clinical Course: A Model to Predict Patient Survival. *Cancer Research*. 2015; 75(6): 940±994. <https://doi.org/10.1158/0008-5472.CAN-14-2508> PMID: 25614516
89. Stiehl T, Lutz C, Marciniak-Czochra A. Emergence of heterogeneity in acute leukemias. *Biology Direct*. 2016; 11: 51. <https://doi.org/10.1186/s13062-016-0154-1> PMID: 27733173
90. Goldie JH, Coldman AJ. A mathematic model for relating the drug sensitivity of tumors to their spontaneous mutation rate. *Cancer Treatment Reports*. 1979; 63: 1727±1733. PMID: 526911
91. Goldie JH, Coldman AJ. Quantitative model for multiple levels of drug resistance in clinical tumors. *Cancer Treatment Reports*. 1983; 67: 923±931. PMID: 6627236
92. Dingli D, Michor F. Successful therapy must eradicate cancer stem cells. *Stem Cells*. 2006; 24(12): 2603±2610. <https://doi.org/10.1634/stemcells.2006-0136> PMID: 16931775
93. De Pillis LG and Radunskaya A: The dynamics of an optimal controlled tumor model: a case study. *Mathematical and computer modelling*. 2003; 37: 1221±1244.
94. Saleem M, Agrawal T: Complex dynamics in a mathematical model of tumor growth with time delays in cell proliferation. *International Journal of Scientific and Research Publications*. 2012; 2(6): 1±7.
95. Nielsen KH, Pociot FM, Ottesen JT. Bifurcation Analysis of an Existing Mathematical Model Reveals Novel Treatment Strategies and Suggests Potential Cure for Type 1 Diabetes. *Mathematical Medicine and Biology*. 2014; 31(3): 205±225. <https://doi.org/10.1093/imammb/dqt006> PMID: 23620354
96. Baker M, Denman-Johnson S, Brook BS, Gaywood I, Owen MR. Mathematical modelling of cytokine-mediated inflammation in rheumatoid arthritis. *Mathematical Medicine and Biology*. 2013. 30: 311±337. <https://doi.org/10.1093/imammb/dqs026> PMID: 23002057
97. Herald MC. General Model of Inflammation. *Bulletin of Mathematical Biology*. 2010; 72: 765±779. <https://doi.org/10.1007/s11538-009-9468-9> PMID: 19851812
98. Dunster JL, Byrne HM, King JR. The Resolution of Inflammation: A Mathematical Model of Neutrophil and Macrophage Interactions. *Bull Math Biol*. 2014; 76: 1953±1980. <https://doi.org/10.1007/s11538-014-9987-x> PMID: 25053556
99. Jacquez JA, Simon CP. Qualitative Theory of Compartmental Systems. *SIAM Review*. 1993; 35(1): 43±79.
100. Michor F, Iwasa Y, Nowak MA. The age incidence of chronic myeloid leukemia can be explained by a one-mutation model. *Proc Natl Acad Sci USA*. 2006; 103: 14931±14934. <https://doi.org/10.1073/pnas.0607006103> PMID: 17001000
101. Jackson AL, Loeb LA. The mutation rate and cancer. *Genetics*. 1998; 148: 1483±1490. PMID: 9560368
102. Cooke MS, Evans MD, Dizdaroglu M, Lunec J. Oxidative DNA damage: mechanisms, mutation, and disease. *FASEB J*. 2003; 17: 1195±1214. <https://doi.org/10.1096/fj.02-0752rev> PMID: 12832285
103. Ferguson LR. Chronic inflammation and mutagenesis. *Mutat Res*. 2010; 690: 3±11. <https://doi.org/10.1016/j.mrfmmm.2010.03.007> PMID: 20223251

104. Kiraly O, Gong G, Olipitz W, Muthupalani S, Engelward BP. Inflammation-Induced Cell Proliferation Potentiates DNA Damage-Induced Mutations in Vivo. *Plos Genet.* 2015; 11(2):e100490.
105. King KY, Goodell MA. Inflammatory modulation of hematopoietic stem cells: viewing the hematopoietic stem cell as a foundation for the immune response. *Nat Rev Immunol.* 2014; 11(10): 685±692.
106. Rockey DC, Bell PD, Hill JA. Fibrosis: A Common Pathway to Organ Injury and Fibrosis. *N Engl J Med.* 2015; 372: 1138±1149. <https://doi.org/10.1056/NEJMra1300575> PMID: 25785971
107. Dvorak HF. Tumors: wounds that do not heal, Similarities between tumor stroma generation and wound healing. *N Engl J Med.* 1986; 315(26): 1650±1659. <https://doi.org/10.1056/NEJM198612253152606> PMID: 3537791
108. Dvorak HF. Tumors: wounds that do not heal-redux. *Cancer Immunology Research.* 2015; 3(1): 1±11. <https://doi.org/10.1158/2326-6066.CIR-14-0209> PMID: 25568067
109. Nikas JB. Inflammation and Immune System Activation in Aging: A Mathematical Approach. *Scientific Reports.* 2013; 3: 3254: 1±7. <https://doi.org/10.1038/srep03254> PMID: 24247109
110. Nielsen KH, Pociot FM, Ottesen JT. Bifurcation analysis of an existing mathematical model reveals novel treatment strategies and suggests potential cure for type 1 diabetes. *Math Med Biol.* 2014; 31(3): 205±225. <https://doi.org/10.1093/imammb/dqt006> PMID: 23620354
111. Lo WC, Martin EW Jr, Hitchcock CL, Friedman A. Mathematical model of colitis-associated colon cancer. *J Theor Biol.* 2013; 317: 20±29. <https://doi.org/10.1016/j.jtbi.2012.09.025> PMID: 23026764
112. Pardanani A, Fridley BL, Lasho TL, Gilliland DG, Tefferi A. Host genetic variation contributes to phenotypic diversity in myeloproliferative disorders. *Blood.* 2008; 111(5): 2785±2789. <https://doi.org/10.1182/blood-2007-06-095703> PMID: 18006699
113. Kilpivaara O, Mukherjee S, Schram AM, Wadleigh M, Mullally A, Ebert BL, et al. A germline JAK2 SNP is associated with predisposition to the development of JAK2(V617F)-positive myeloproliferative neoplasms. *Nat Genet.* 2009; 41(4): 455±459. <https://doi.org/10.1038/ng.342> PMID: 19287384
114. Jones AV, Chase A, Silver RT, Oscier D, Zoi K, Wang YL, et al: JAK2 haplotype is a major risk factor for the development of myeloproliferative neoplasms. *Nat Genet.* 2009; 41(4): 446±449. <https://doi.org/10.1038/ng.334> PMID: 19287382
115. Olcaydu D, Harutyunyan A, Jäger R, Berg T, Gisslinger B, Pabinger I, et al: A common JAK2 haplotype confers susceptibility to myeloproliferative neoplasms. *Nat Genet.* 2009; 41(4): 450±454. <https://doi.org/10.1038/ng.341> PMID: 19287385
116. Cross NC. Genetic and epigenetic complexity in myeloproliferative neoplasms. *Hematology Am Soc Hematol Educ Program.* 2011; 208±214. <https://doi.org/10.1182/asheducation-2011.1.208> PMID: 22160036
117. Tapper W, Jones AV, Kralovics R, Harutyunyan AS, Zoi K, Leung W, et al: Genetic variation at MECOM, TERT, JAK2 and HBS1L-MYB predisposes to myeloproliferative neoplasms. *Nat Commun.* 2015; 6: 6691. <https://doi.org/10.1038/ncomms7691> PMID: 25849990
118. Barrett JC, Hansoul S, Nicolae DL, Cho JH, Duerr RH, Rioux JD, et al: Genome-wide association defines more than 30 distinct susceptibility loci for Crohn's disease. *Nat Genet.* 2008; 40(8): 955±962. <https://doi.org/10.1038/ng.175> PMID: 18587394
119. Ferguson LR, Han DY, Fraser AG, Huebner C, Lam WJ, Morgan AR, et al: Genetic factors in chronic inflammation: single nucleotide polymorphisms in the STAT-JAK pathway, susceptibility to DNA damage and Crohn's disease in a New Zealand population. *Mutat Res.* 2010; 690(1±2): 108±115. <https://doi.org/10.1016/j.mrfmmm.2010.01.017> PMID: 20109474
120. Martyre MC, Romquin N, Le Bousse-Kerdiles MC, Chevillard S, Benyahia B, Dupriez B, et al. Transforming growth factor-beta and megakaryocytes in the pathogenesis of idiopathic myelofibrosis. *Br J Haematol.* 1994; 88(1): 9±16. PMID: 7803262
121. Tefferi A. Myelofibrosis with myeloid metaplasia. *N Engl J Med.* 2000; 27; 342(17): 1255±1265. <https://doi.org/10.1056/NEJM200004273421706> PMID: 10781623
122. Takizawa H, Boettcher S, Manz MG. Demand-adapted regulation of early hematopoiesis in infection and inflammation. *Blood.* 2012; 119(13): 2991±3002. <https://doi.org/10.1182/blood-2011-12-380113> PMID: 22246037
123. Parihar A, Eubank TD, Doseff AI. Monocytes and macrophages regulate immunity through dynamic networks of survival and cell death. *J Innate Immun.* 2010; 2: 204±215. <https://doi.org/10.1159/000296507> PMID: 20375558
124. Leblanc R, Peyruchaud O. Metastasis: new functional implications of platelets and megakaryocytes. *Blood.* 2016; 128(1): 24±31. <https://doi.org/10.1182/blood-2016-01-636399> PMID: 27154188
125. Hasselbalch HC. The platelet-cancer loop in myeloproliferative cancer. Is thrombocytopenia an enhancer of cancer invasiveness and metastasis in essential thrombocythemia, polycythemia vera

- and myelofibrosis? *Leuk Res.* 2014; 38(10): 1230±1236. <https://doi.org/10.1016/j.leukres.2014.07.006> PMID: 25149709
126. Hasselbalch HC. A new era for IFN- α in the treatment of Philadelphia-negative chronic myeloproliferative neoplasms. *Expert Rev Hematol.* 2011; 4(6): 637±655. <https://doi.org/10.1586/EHM.11.63> PMID: 22077528
 127. Silver RT, Kiladjian J-J, Hasselbalch HC. Interferon and the treatment of polycythemia vera, essential thrombocythemia and myelofibrosis. *Expert Rev Hematol.* 2013; 6(1): 49±58. <https://doi.org/10.1586/ehm.12.69> PMID: 23373780
 128. Rank C, Bjerrum O, Larsen T, Kjær L, de Stricker K, Riley CH, et al: Minimal residual disease after long-term interferon-alpha2 treatment: a report on hematological, molecular and histomorphological response patterns in 10 patients with essential thrombocythemia and polycythemia vera. *Leuk Lymphoma.* 2015; 1±7.
 129. Kiladjian JJ, Giraudier S, Cassinat B. Interferon-alpha for the therapy of myeloproliferative neoplasms: targeting the malignant clone. *Leukemia.* 2016; 30(4): 776±781. <https://doi.org/10.1038/leu.2015.326> PMID: 26601783
 130. Hasselbalch HC. Perspectives on the impact of JAK-inhibitor therapy upon inflammation-mediated comorbidities in myelofibrosis and related neoplasms. *Expert Rev Hematol.* 2014; 7(2): 203±216. <https://doi.org/10.1586/17474086.2013.876356> PMID: 24524202

Appendix B

Bridging blood cancers and inflammation: The reduced Cancitis model



Bridging blood cancers and inflammation: The reduced Cancitis model

Johnny T. Ottesen^{a,*}, Rasmus K. Pedersen^a, Zamra Sajid^a, Johanne Gudmand-Hoyer^a,
 Katrine O. Bangsgaard^a, Vibe Skov^b, Lasse Kjær^b, Trine A. Knudsen^b, Niels Pallisgaard^b,
 Hans C. Hasselbalch^b, Morten Andersen^a

^a Department of Science and Environment, Roskilde University, Denmark

^b Department of Hematology, Zealand University Hospital, University of Copenhagen, Denmark



ARTICLE INFO

Article history:

Received 5 April 2018

Revised 11 December 2018

Accepted 2 January 2019

Available online 4 January 2019

ABSTRACT

A novel mechanism-based model - the Cancitis model - describing the interaction of blood cancer and the inflammatory system is proposed, analyzed and validated. The immune response is divided into two components, one where the elimination rate of malignant stem cells is independent of the level of the blood cancer and one where the elimination rate depends on the level of the blood cancer. A dimensional analysis shows that the full 6-dimensional system of nonlinear ordinary differential equations may be reduced to a 2-dimensional system - the reduced Cancitis model - using Fenichel theory. The original 18 parameters appear in the reduced model in 8 groups of parameters. The reduced model is analyzed. Especially the steady states and their dependence on the exogenous inflammatory stimuli are analyzed. A semi-analytic investigation reveals the stability properties of the steady states. Finally, positivity of the system and the existence of an attracting trapping region in the positive octahedron guaranteeing global existence and uniqueness of solutions are proved. The possible topologies of the dynamical system are completely determined as having a Janus structure, where two qualitatively different topologies appear for different sets of parameters. To classify this Janus structure we propose a novel concept in blood cancer - a reproduction ratio \mathcal{R} . It determines the topological structure depending on whether it is larger or smaller than a threshold value. Furthermore, it follows that inflammation, affected by the exogenous inflammatory stimulation, may determine the onset and development of blood cancers. The body may manage initial blood cancer as long as the self-renewal rate is not too high, but fails to manage it if an inflammation appears. Thus, inflammation may trigger and drive blood cancers. Finally, the mathematical analysis suggests novel treatment strategies and it is used to discuss the *in silico* effect of existing treatment, e.g. interferon- α or T-cell therapy, and the impact of malignant cells becoming resistant.

© 2019 Elsevier Ltd. All rights reserved.

1. Introduction

Formation of blood cells, hematopoiesis, takes place in the bone marrow by cell division of hematopoietic stem cells (HSCs). Mutations of HSCs may lead to cancerous stem cells causing blood cancers, which ultimately suppress production of healthy blood cells (Chen et al., 2011; Dingli et al., 2007). The myeloproliferative neoplasms (MPNs) are disorders emanating from the bone marrow and predominantly consist of chronic myelogenous leukemia (CML), essential thrombocythemia (ET), polycythemia vera (PV), and primary myelofibrosis (PMF) (Campbell and Green, 2006). Despite similarities, common theoretical considerations can be applied, since the diseases share clonal hematopoiesis as a hallmark

and are strongly influenced by - and coupled with - the inflammatory response of the immune system (Desterke et al., 2015).

In this article we develop a model of the system underlying the blood cancer diseases coupled to the inflammatory response system. The model presented in Andersen et al. (2017) is used as a starting point and only what is truly important for the purpose of the model is included.

Most cancers are developed somewhat similarly in the early avascular phase before tumor size plays a role (Wilkie, 2013; Wodarz and Komarova, 2014). Thus, the present model may be adapted for early cancer more generally despite it being developed specifically for blood cancers. Some blood cancers are curable, while others, such as MPNs, are more challenging (Abdel-Wahab et al., 2010; Spivak, 2017). Thus, special attention will be on MPNs although the risk of getting MPNs is relatively low.

In Andersen et al. (2017), a novel and mechanism-based model of blood cancers coupled to the inflammatory response of the

* Corresponding author.

E-mail address: Johnny@ruc.dk (J.T. Ottesen).

immune system was proposed. The model is to our knowledge the first of its kind and furthermore generic in the sense that it describes blood cancer in general. Shortly after, Komarova et al. published a simplified approach to discuss the role of inflammation in MPNs (Zhang et al., 2017). They included stem cell dynamics and bone marrow niche feedback, but describe the inflammation as a fixed parameter independent of the actual cancer development, i.e. independent of the immune response to the cancer cells. This approach is somewhat similar to the 2-dimensional approach taken in Flå et al. (2015), where a simple model of stem cell dynamics including bone marrow niche feedback, but without including inflammation, was investigated.

In Andersen et al. (2017), T-cells were not explicitly considered, but in the present study we include the effect of these cells. Accumulated evidence has indicated that the immune system may recognize and eliminate malignant cells (Parish, 2003; Smyth et al., 2001) acting as a control mechanism for maintaining homeostasis. This effect is called immune surveillance, a concept attributed to Thomas and MacFarlane in the late 1950s although a similar idea was promoted by Ehrlich already in 1909. Today it is refined into the concept of immunoediting (Ribatti, 2017).

An early mathematical model describing interaction of tumor cells and effector cells (killer cells) for BCL1 lymphoma was presented by Kuznetsov and Knott (2001) continuing the work from Kuznetsov and Makalin (1994) and was based on a logistic growth equation to describe the intrinsic dynamics.

Several models of the role of inflammation in general cancer progression have since been studied. Most of these modeling attempts consider solid tumors and couples the T-cell and natural killer (NK) cell dynamics to a logistic growth description of tumors. The models in (Arciero et al., 2004; Baker et al., 2013; Bangsgaard et al., 2017; Bangsgaard and Ottesen, 2017; Borges et al., 2014; Cosentino and Bates, 2012; De Pillis et al., 2005; Dunster et al., 2014; Hanson et al., 0000; Herald, 2010; Katak, 2014; Kirschner and Panette, 1998; Moore and Li, 2004; Nanda et al., 2007; Nielsen, 0000; Nielsen et al., 2013; Pillis et al., 2006; Pillis and Radunskaya, 2003; Saleem and Agrawal, 2012; Sarkar and Banerjee, 2005) are simplified models describing how solid cancers may stimulate the T-cell dynamics, while the cancer dynamics are decoupled from the rest of the system, simply described as logistic growth or similar. The works by Kuznetsov and Knott (2001), Zhang et al. (2017), Moore and Li (2004) and Nanda et al. (2007) and the excellent books by Wodarz and Komarova (2014) and Komarova and Wodarz (2014) point toward the direction taken in the present paper.

Clapp et al. (2015) consider a 5D model including active and quiescent stem cells, progenitor cells, mature cells and one immune compartment to describe chronic myelogenous leukemia. The active stem cell pool is based on the logistic growth equation omitting interactions with the normal hematopoietic cells. Recently Besse et al. (2018) investigate a simplified version of this model. Simultaneously Talkington A and Durrett (2018) compared four models of acute lymphocytic leukemia, namely those by Kuznetsov and Makalin (1994), Kirschner and Panette (1998), Dong et al. (2014), and Moore and Li (2004). The purpose was to study modified T-cells engineered to recognize CD19 surface marker clinically, resulting in partial success in virtual treatment of the disease. All four models predict a positive effect of the treatment. Historically, a few important models addressing tyrosine kinase inhibitors (TKI), e.g. imatinib, in treating chronic myelogenous leukemia have appeared. Michor et al. (2005) explained incomplete eradication of CML under TKI treatment by resistance. Komarova and Wodarz (2007) incorporated quiescent stem cells and the development of resistance to treatment. Using an agent-based model, Roeder et al. (2006) describe competition between leukemic stem cells and normal hematopoi-

etic stem cells and included the effect of TKIs on the competition. Long-term effect of the immune response was modeled by Kim et al. (2008) by adding an unspecific immune component to the model by Michor et al. (2005).

Recently, Brady et al. suggested an inflammatory model coupled to the autonomic regulation of the cardiovascular system for healthy subjects exposed to intravenous injection of lipopolysaccharide (LPS) to stimulate an inflammatory response. Simultaneously, Bangsgaard and Ottesen (2017) suggested a detailed inflammatory response model coupled to the Hypothalamic–Pituitary–Adrenal axis allowing an exogenous stimuli. This so-called ITIS model contains eight time-dependent variables: Endotoxin, phagocytic cells, pro- and anti-inflammatory cytokines (a broad category of signaling molecules consisting of small proteins): TNF- α , IL-10, TGF- β , CRH, ACTH and cortisol. The ITIS model is capable of reproducing available data and has served as an inspiration in the present work, but in a suitable simplified form.

The outline of the paper is as follows. In Section 2 the model is presented and in Section 2.1 it is expanded by explicitly including a description of the interaction with immune response effector cells such as T-cells. The model is put on a dimensionless form and based on a separation of time scales, a two-dimensional model - the reduced Cancitis model - is suggested in Section 3. The reduced Cancitis model is analyzed in Section 4. Admissible steady states are derived and in Section 4.1 their stability properties are examined depending on the external inflammatory stimuli. A complete analysis of the topology of the dynamical system is presented, showing a Janus topology¹ An attracting trapping region is constructed in Section 4.2 establishing global existence and uniqueness of solutions. A treatment plan by T-cell gene therapy appear in Section 4.3 along with a description of how the phase plane varies with increasing external inflammatory stimuli. Special focus is on the role of the level of external inflammatory stimuli and its effect on existence and stability of healthy and unhealthy steady states of the model. The various findings are discussed and conclusions made in Section 5. Finally, some cumbersome derivations related to the steady states are presented in Appendix A and Appendix B.

2. The model

As in the previous model presented in Andersen et al. (2017), focus will be on ensembles of each cell type and not the individual cells. Hence, the governing laws will be for the pools of cells, commonly denoted compartments. The compartments encompass the healthy hematopoietic stem cells in the bone marrow, the healthy hematopoietic mature cells in the blood, the malignant stem cells in the bone marrow, the malignant mature cells in blood, the pool of dead cells and the resulting debris not yet cleared, and a variable describing the immune system activity level, which correlates with the associated cytokines related to the disease. In what follows we will denote healthy hematopoietic cells shortly as hematopoietic cells in contrast to e.g. malignant cells. As we are aiming for an integrated mechanism-based model for blood cancers, competition between cell types is crucial. The function of the immune system to handle dead cells constitutes an effective feedback mechanism regulating the stem cell reproduction whereas the specific T-cell response fights the cancer cells. The aggregated immune response is known to correlate with the disease state of the blood cancer. Mathematically the dynamics is described by nonlinear ordinary differential equations respecting conservation laws as illustrated in Fig. 1.

¹ Named after the ancient Greek God Janus having two faces meaning that two different topologies exists.

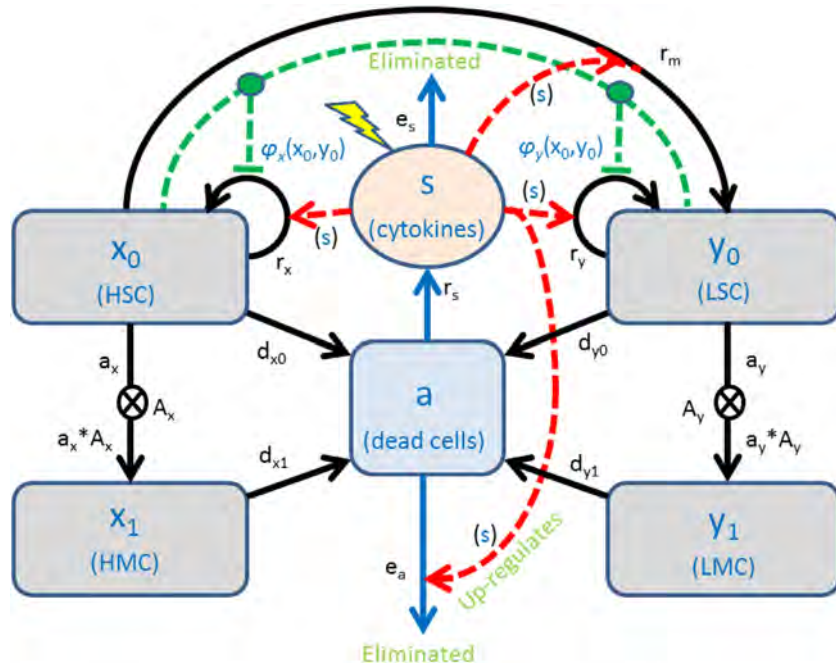


Fig. 1. The conceptual model corresponding to Eq. (1). Light gray boxes (symbolized x_0 , x_1 , y_0 , and y_1 for the hematopoietic stem cells (HSC), the hematopoietic mature cells (HMC), the leukemic stem cells (LSC), and the leukemic mature cells (LMC), respectively) illustrate the compartments of the basic model and the black arrows the rates of the flows between these compartments. Stem cells differentiating into progenitor cells reduce the amount of these with rates a_x and a_y and enter the corresponding mature cell-pools as these rates are multiplied by progenitor application factors (A_x and A_y , respectively, and symbolized by \otimes -symbols). All cells may undergo apoptosis and their death rates are indicated by black arrows labeled with a d index and the corresponding variable. A normal hematopoietic stem cell may mutate into a malignant stem cell with an effective probability r_m indicated by a black arrow. The light blue compartment (symbolized a) contains all dead cells and the light orange compartment (symbolized s) the inflammatory level, i.e. the immune response. Blue arrows from these represent related rates of flow: e_a is the second order elimination rate of debris, e_s is the elimination rate of the inflammatory activity, and r_s is the rate by which dead cells stimulate the inflammatory response. Red stipulated arrows (marked by (s)) going from the inflammatory compartment represent effects of the cytokines (or neutrophils when eliminating dead cells) modulating the rates of the basic model. The green stipulated lines represent the bone marrow niche inhibition (depending on x_0 and y_0 , see text) modulating the self-renewal rates, r_x and r_y . (For interpretation of the references to colour in this figure legend, the reader is referred to the web version of this article.)

Using symbols as in Fig. 1 and letting dot denote the time derivative, the mathematical equations are,

$$\dot{x}_0 = (r_x \phi_x(x_0, y_0) s - d_{x_0} - a_x) x_0 - r_m s x_0 \quad (1a)$$

$$\dot{x}_1 = a_x A_x x_0 - d_{x_1} x_1 \quad (1b)$$

$$\dot{y}_0 = (r_y \phi_y(x_0, y_0) s - d_{y_0} - a_y) y_0 + r_m s x_0 \quad (1c)$$

$$\dot{y}_1 = a_y A_y y_0 - d_{y_1} y_1 \quad (1d)$$

$$\dot{a} = d_{x_0} x_0 + d_{y_0} y_0 + d_{x_1} x_1 + d_{y_1} y_1 - e_a a s \quad (1e)$$

$$\dot{s} = r_s a - e_s s + I \quad (1f)$$

The time dependent variables x_0 , x_1 , y_0 , y_1 , a , and s denote the amount of (healthy) hematopoietic stem cells (HSC), (healthy) hematopoietic mature cells (HMC), malignant stem cells (LSC), malignant mature cells (LMC), dead cells, and the cytokine level, an abstract quantity describing the activity level of the immune system, respectively. Whenever cells undergo apoptosis, the debris has to be engulfed by phagocytic cells, e.g. neutrophils and macrophages, which are regulated by the release of a hierarchic cascade of pro- and anti-inflammatory cytokines (Dunster et al., 2014; Herald, 2010; Kirschner and Panette, 1998). Following the parsimonious principle, we let the dead cells (a) up-regulate the amount of phagocytic cells (s) with rate constant r_s , while they are eliminated with a rate e_s . In addition, endotoxins, smoking and other environmental factors may add to the inflammatory response; thus we add a term (characterized by the lightning symbol in Fig. 1). Since MPNs develop on a time-scale of years and

inflammatory immune processes are on a time-scale of hours-days (Bangsgaard et al., 2017; Cavaillon, 1994; Chow et al., 2005; Clodi et al., 2008), we may assume a QSSA, implying that the ratio of the amount of phagocytic cells and the cytokines are fixed. Thus, the cytokine level is proportional to the phagocytic level and the inflammatory compartment (s) represents both.

The dynamics of the hematopoietic stem cells (x_0) are governed by the self-renewal rate r_x , the death rate d_{x_0} , and the division into progenitor cells with rate a_x . The inhibiting niche feedback in the bone marrow, represented by the function ϕ_x , controls cell division in a healthy individual and allows for competition between healthy and cancerous stem cells when both are present (see below). Furthermore, inflammation stimulates self-renewal and is assumed to be proportional with the cytokine level. This reflects the fact that an increase in hematopoietic cell death instigates the birth of extra cells. Finally, the stem cells may mutate with a mutation rate r_m , which is believed to increase with inflammation (Andersen et al., 2017; Brianna M. Craver et al., 2018; Desterke et al., 2015; Hasselbalch, 2012; 2014; Hasselbalch and Bjoern, 2015; Hermouet et al., 2015; Koschmieder et al., 2016; Voit, 2013; Wilkie, 2013; Wodarz and Komarova, 2014; Zhang et al., 2017).

The dynamics of the malignant stem cells (y_0) are governed similarly and we use the same symbols with a y -index instead of an x -index to denote the corresponding rates. The only difference is that mutation of hematopoietic stem cells add to the number of malignant cells and is proportional to the number of hematopoietic stem cells. In addition, we will later allow the death rate d_{y_0} to be y_0 -dependent.

If no mutations occur, stem cells divide either into two stem cells of the same type as the mother cell, into two progenitor cells, or divide into one of each. Progenitor cells differentiate further into

new and gradually more and more mature progenitor cells in a number of generations (k) to ultimately divide into fully matured cells (i.e. cells which do not divide further). The progenitor cells are not explicitly considered in the model. However, a stem cell dividing into two progenitor cells, so-called symmetric division, will at the end give rise to $A = 2^k$ mature cells, which we denote as the multiplication factor. Hence, the change in hematopoietic mature cells per time becomes $a_x A_x$ times the amount of hematopoietic stem cells, where we denote A_x the multiplication factor for the hematopoietic cells, which in general is larger than 2^k . Simultaneously, hematopoietic mature cells undergo apoptosis with a constant rate d_{x_1} .

Again, the change in malignant mature cells per time is similar to that of the hematopoietic mature cells, but with index y instead of x .

The change in the amount of dead cells per time is given by the death rates times the number of cells in the aforementioned compartments minus the clearing by the immune system. This clearing is taken to be a second order equation in the number of dead cells and the amount of cytokines, representing the activity of the immune system, eliminating the dead cells with an elimination rate e_a .

The stimulation of the immune system is proportional to the amount of dead cells with rate r_s whereas the elimination is taken to be proportional to the amount of cytokines with rate e_s . We emphasize that the immune system is stimulated by an increased number of cancer cells by this feedback mechanism. In addition we include the possibility of an exogene stimulation of the immune system $I(t)$, where we indicate that this stimulation may change over time t . This exogene stimulation may be taken as anything provoking the immune system, e.g. infections, smoking or pollution. In many mathematical considerations, we will take the inflammatory load I to be piecewise constant to allow for analytical results.

Finally, the bone marrow niche feedback functions are in general decreasing functions of the individual stem cell types. We choose

$$\phi_x = \phi_x(x_0, y_0) = \frac{1}{1 + c_{xx}x_0 + c_{xy}y_0} \tag{2a}$$

$$\phi_y = \phi_y(x_0, y_0) = \frac{1}{1 + c_{yx}x_0 + c_{yy}y_0}, \tag{2b}$$

where c_{ij} describes the inhibitory strength of the signaling bone marrow niche feedback from cell type j onto cell type i . It is generally assumed that $c_{yy} \leq c_{yx} < c_{xy} \leq c_{xx}$, since leukemic cells are less sensitive to inhibitive niche feedback than healthy hematopoietic cells. Similar to Flå et al. (2015), our investigations show no qualitative difference in observed model output when using various functional forms of the negative feedback.

Motivated by the biology where numbers of cells and concentrations are required to be non-negative numbers, we will use the terminology that a steady state is **admissible** if and only if all components are non-negative i.e. if and only if the steady state is in the non-negative octahedron. We denote a steady state as **appropriate** if and only if it does not require a degenerated set of parameters, i.e. a set of parameters where an equality constraint is imposed on the parameters whereas inequalities constrains are allowed. The reason is that such a set of parameters are not robust to perturbations and thus biologically unlikely to exist. However, non-appropriate steady states may still be of interest since they divide possible situations of interest like e.g. bifurcation points do.

In most considerations, we take the mutation rate to be zero to ease the analytical analysis. Hence, we start our system in a steady state related to none malignant cells and introduce a single malignant stem cell initially. Thus the initial condition will be that of

a (healthy) hematopoietic steady state except one malignant stem cell is added to that state.

The model stated in Eqs. (1) and (2) is presented in (Andersen et al., 2017) and will be analyzed in detail elsewhere. For later use it is sufficient to know that two admissible hematopoietic steady states (defined as one having $y_0 = 0$, but $x_0 \neq 0$) may exist depending on the level of exogenous inflammatory stimuli I ,

$$E_{H\pm} = (x_{0H\pm}, x_{1H\pm}, y_{0H\pm}, y_{1H\pm}, a_{H\pm}, s_{H\pm}), \tag{3}$$

where $x_{0H\pm} = \frac{s_{H\pm} - \alpha_x}{\alpha_x c_{xx}}$, $x_{1H\pm} = \frac{a_x A_x}{d_{x_1}} x_{0H\pm}$, $y_{0H\pm} = 0$, $y_{1H\pm} = 0$, $a_{H\pm} = \frac{e_s s_{H\pm} - I}{r_s}$, and $s_{H\pm} = \frac{1}{2} \left(\zeta_{H_1} \pm \sqrt{\zeta_{H_1}^2 - 4\zeta_{H_2}} \right)$, with $\zeta_{H_1} = \frac{I}{e_s} + \frac{\zeta_{H_2}}{\alpha_x}$, $\zeta_{H_2} = \frac{\beta_x r_s}{e_a e_s c_{xx}}$, $\alpha_x = \frac{a_x + d_{x_0}}{r_x}$, and $\beta_x = a_x A_x + d_{x_0}$. These steady state coordinates will be used for turning the model into proper dimensionless form.

2.1. Model extension: Including the T-cell response

Whenever cells die, the debris have to be engulfed by phagocytic cells, e.g. neutrophils and macrophages and a hierarchic cascade of pro- and anti-inflammatory cytokines are released. Apoptosis is mediated by the immune system and is included in the Cancitis model. The immune response may be split into two parts namely the innate immune response and the adaptive immune response (McComb et al., 2013). The innate immune response provides an immediately but non-specific response. The innate response consists of granulocytes, dendrites, macrophages and natural killer cells.

The adaptive immune response is activated by the innate immune response. Thus a delay is introduced from exposure to maximal response and this delay may be up to 7 days (McComb et al., 2013). The adaptive immune response includes B-cells and T-cells also denoted lymphocytes. We include naive T-cells and effector T-cells, since these have an important role in inhibiting the development of cancer (Murphy and Travers, 2012). Effector T-cells are responsible for a direct defense, where they induce death to the malignant cells. Naive T-cells are activated by antigen presenting cells (APC). A QSSA suggests itself, since we are interested in the time-scale of years and the time-scale of the adaptive immune response is of order of days.

The presence of foreign antigens in the body may be sensed by the naive T-cells (T_n). This will start a cascade of up-regulating cells and molecules in the immune system, among these effector T-cells (T_e), e.g. CD8⁺ T-cells, and NK-cells. These specifically attack and destroy the identified foreign cells (necrosis). The process from identification to attack happens on a time-scale of a week, however, the effector cells have memories to recognize the identified cells afterwards. This process is known as immune surveillance.

Inspired by Moore and Li (2004) and Nanda et al. (2007), we let the naive T-cells identify the cancer cells (we let temporarily y denote the number of such, which in our case will be y_0 or y_1). These T-cells are transformed into effector cells proportional to the product of the number of naive T-cells and cancer cells with rate, k_n . Naive T-cells may produce α_n effector cells per transforming naive T-cell. A linear elimination of naive T-cells appear simultaneously with rate ηk_n . The naive T-cells are produced at a constant rate p_n , whereas effector cells are eliminated proportional to T_e with rate γ_e . Thus,

$$\dot{T}_n = p_n - k_n T_n (y + \eta) \tag{4}$$

and

$$\dot{T}_e = \alpha_n k_n T_n y - \gamma_e T_e. \tag{5}$$

The pool of effector cells (T_e) eliminate the cancer cells as a second order reaction with rate γ_y . Letting 'growth' denote the aforementioned dynamics of cancer cells without explicitly including the

T-cells, i.e. the right hand side of Eq. (1c) or (1d), the governing equation of malignant cells become

$$\dot{y} = \text{growth} - \gamma_y T_e y. \tag{6}$$

The fast T-cell response compared to the slow timescale of MPNs development justify a QSSA, thus

$$T_e \approx \frac{\alpha_n p_n}{\gamma_e} \frac{y}{y + \eta} \tag{7}$$

and

$$\dot{y} = \text{growth} - \frac{\gamma_y \alpha_n p_n}{\gamma_e} \frac{y^2}{\eta + y} \approx \text{growth} - \tilde{d}_y y^2, \tag{8}$$

with $\tilde{d}_y = \frac{\gamma_y \alpha_n p_n}{\gamma_e \eta}$ and where the approximation holds if $y \ll \eta$. Hence, using the approximation in Eq. (8) the death rate d_y in the 'growth' part may be substituted by

$$d_y \rightarrow \hat{d}_y + \tilde{d}_y \frac{\eta y}{\eta + y} \approx \hat{d}_y + \tilde{d}_y \cdot y \tag{9}$$

for $y \ll \eta$ where $\hat{d}_y = d_y$. Thus, the constant mortality rate is changed by adding a death rate which is linear in y . In fact, this may be considered as a general approximation of a possible y -dependent death rate by its first order Taylor expansion. We emphasize that this expression is desirable, since it is still simple, but includes an important effect for non-vanishing values of y . A reasonable choice is to take $\hat{d}_y = d_{y_0}$ and $\tilde{d}_y \sim 10^{-6} \text{ day}^{-1}$ as default values. These estimates are based on requiring the two elimination terms to be of the same order and equal to that for normal hematopoietic stem cells, which is approximately 0.002 cell per day (Andersen et al., 2017; Dingli and Michor, 2006).

Hence, the leukemic model in Eq. (1) still holds with d_{y_0} substituted by $\hat{d}_{y_0} + \tilde{d}_{y_0} \cdot y_0$ where we assume that the most impor-

tant effect is on the stem cell compartment, which drives the cancer development. The previous analytical results obtained are corrupted by the extension allowing the death rate to be y_0 dependent. We therefore seek a suitable model reduction (obtained in Eq. (10)) allowing a more thorough analysis.

2.2. Model validation

In the stable hematopoietic steady state, the numbers of stem cells and mature cells are taken to be approximately 10^4 and $4 \cdot 10^{10}$, respectively, which are compromises between reported values (Dingli and Michor, 2006; Gentry and Jackson, 2013; Haeno et al., 2009a; 2009b; Stiehl et al., 2015; 2016). In the final stage of full blown cancer, the number of hematopoietic cells is vanishing and the cancer cells will approach a stable steady state with a higher amount of cells than in the healthy steady state. The absolute values are more uncertain but we have aimed for 10^5 cancer stem cells and 10^{13} mature cancer cells as reported in Dingli and Michor (2006). In clinical practice JAK2V617 allele burden and the total cell count in the blood are usually measured. Whereas the total cell count is $x_1 + y_1$, the JAK2V617 allele burden is taken as $\frac{y_1}{x_1 + y_1}$.

The JAK2V617 allele burden has been reported to have median values of 7% (95% CI 2–15% and range 1–39%), 33% (95% CI 20–40% and range 1–92%), and 67% (95% CI 52–95% and range 37–99%) in ET, PV and PMF patients, respectively (Larsen et al., 2007).

The model is calibrated to resample this dynamic in the JAK2V617F allele burden, which gives predictions, t_{ET} , t_{PV} , and t_{PMF} for when ET, PV and PMF appear, respectively. For illustrations of cell counts and allele burden see Fig. 2 Cytokines as IL-1 β , IL-1RA, IL-2R, IL-6, IL-8, IL-10, and IL-12 are considered to be specific indicators of the inflammatory level during MPN, whereas C-reactive

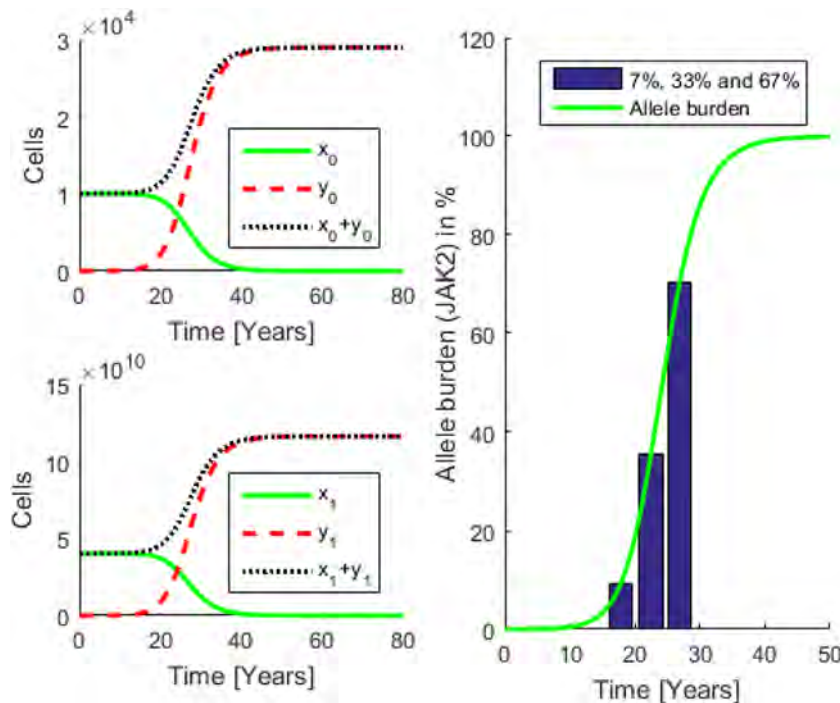


Fig. 2. Left: Typical development in stem cells (top left) and mature cells (bottom left). Healthy hematopoietic cells (full green curves) dominate in the early phase where the malignant cells (stipulated red curves) are few in number. The total number of cells is also shown (dotted black curves). When a stem cell mutates and escapes repairing mechanisms, it approximately starts a slowly increasing exponential growth (at $t = 0$). At a certain stage, the malignant cells become dominant and the healthy hematopoietic cells begin to show a visible decline. Finally, the competition between the cell types results in a takeover by the malignant cells, leading to an approximately exponential decline in the amount of normal hematopoietic cells and ultimately their extinction. The development is closely followed by the mature cells. Right: The corresponding allele burden (7%, 33% and 67% corresponding to ET, PV and PMF, respectively, shown as blue columns) defined as the ratio of MPN mature cells to the total number of mature cells. The full green curve illustrates the continuous model prediction. Default parameter values from Tables 1 and 2 have been used. (For interpretation of the references to colour in this figure legend, the reader is referred to the web version of this article.)

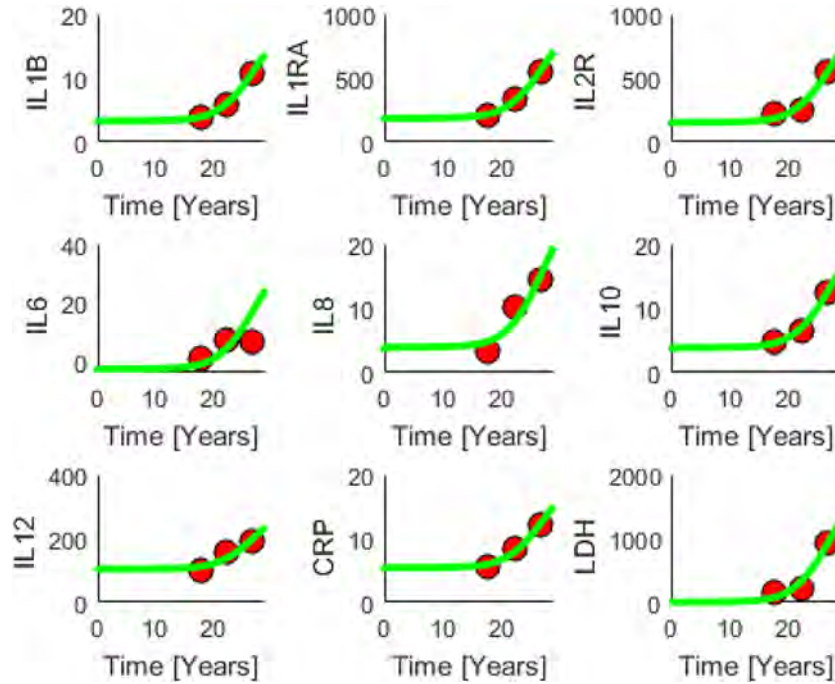


Fig. 3. Model validation. Cytokines from upper left to lower right; IL-1 β , IL-1RA, IL-2R, IL-6, IL-8, IL-10, IL-12 as well as the plasma concentration of C-reactive protein (CRP) are approximately linearly correlated with the inflammatory level s , whereas lactic dehydrogenase (LDH) is linearly correlated with and compared to the total amount of dying cells per time $D = d_{x_0}x_0 + d_{x_1}x_1 + d_{y_0}y_0 + d_{y_1}y_1$. On each subplot data are shown (red dots encircled by black) at predicted times for ET, PV and PMF (left to right), estimated from the allele burden in Fig. 2. On each subplot, model predictions are shown (full green curve). Default parameter values from Tables 1 and 2 have been used. (For interpretation of the references to colour in this figure legend, the reader is referred to the web version of this article.)

Table 1
Default parameter values ($r_m = 0$) from Andersen et al. (2017).

Parameter	Value	Unit	Parameter	Value	Unit
r_x	$8.7 \cdot 10^{-4}$	day $^{-1}$	r_y	$1.3 \cdot 10^{-3}$	day $^{-1}$
a_x	$1.1 \cdot 10^{-5}$	day $^{-1}$	a_y	$1.1 \cdot 10^{-5}$	day $^{-1}$
A_x	$4.7 \cdot 10^{13}$	-	A_y	$4.7 \cdot 10^{13}$	-
d_{x_0}	$2 \cdot 10^{-3}$	day $^{-1}$	d_{y_0}	$2 \cdot 10^{-3}$	day $^{-1}$
d_{x_1}	129	day $^{-1}$	d_{y_1}	129	day $^{-1}$
c_{xx}	$5.6 \cdot 10^{-5}$	-	c_{yx}	$5.2 \cdot 10^{-5}$	-
c_{xy}	$5.4 \cdot 10^{-5}$	-	c_{yy}	$5.0 \cdot 10^{-5}$	-
e_s	2	day $^{-1}$	r_s	$3 \cdot 10^{-4}$	day $^{-1}$
e_a	$2 \cdot 10^9$	day $^{-1}$	I	7	day $^{-1}$

Table 2
Default dimensionless parameter values ($r_m = 0$).

Parameter	Value	Parameter	Value
R	1.49	J (baseline)	0.76
D_0	1.00	D_1	0.10
C_x	0.93	C_y	1.08
B_x	0.06	B_y	0.07

protein (CRP) is a general inflammation biomarker. All these have been shown to correlate with MPN states ET, PV and PMF. (Tefferi et al., 2011; Vaidya et al., 2012) Thus we assume linear correlations between each of these and the inflammatory level s . In addition, LDH values, which express the total rate of dying cells per time ($D = d_{x_0}x_0 + d_{x_1}x_1 + d_{y_0}y_0 + d_{y_1}y_1$) were demonstrated to be correlated to the MPN states ET, PV and PMF (Larsen et al., 2007).

The model outputs are compared to the data in Fig. 3. using the estimated instances t_{ET} , t_{PV} , and t_{PMF} for ET, PV and PMF, respectively. The model predictions are in a remarkable accordance with the data.

3. The reduced Cancitis model

The extended model is brought into dimensionless form by scaling the variables of the model. A time scale separation argument is used to obtain a reduced model, corresponding to setting the time derivative of x_1 , y_1 , a , and s to zero. The four dependent variables may then be solved in terms of x_0 and y_0 . As this approach is well known and straightforward, the derivation is shown in Appendix A. Analyzing the resulting Eqs. (10) in terms of the scaled hematopoietic stem cells, X_0 , and the scaled cancerous stem cells, Y_0 , is the focus of the rest of the paper.

$$X_0' = \left(\frac{J + \sqrt{J^2 + 2B_x X_0 + 2B_y Y_0}}{1 + X_0 + C_y Y_0} - 1 \right) X_0 \quad (10a)$$

$$Y_0' = \left(R \frac{J + \sqrt{J^2 + 2B_x X_0 + 2B_y Y_0}}{1 + C_x X_0 + Y_0} - D_0 - D_1 Y_0 \right) Y_0 \quad (10b)$$

where $J = \frac{I}{2e_s} \frac{r_x}{d_{x_0} + a_x}$, $R = \frac{r_y}{r_x}$, $D_0 = \frac{\hat{d}_{y_0} + a_y}{d_{x_0} + a_x}$, $D_1 = \frac{\hat{d}_{y_0}}{c_{yy}} \frac{1}{d_{x_0} + a_x}$, $C_x = \frac{c_{yx}}{c_{xx}}$, $C_y = \frac{c_{xy}}{c_{yy}}$, $2B_x = b_{x_0} + b_{x_1} \approx b_{x_1} = \frac{a_x A_x}{c_{xx}} \frac{r_s}{e_s e_a} \frac{r_x}{d_{x_0} + a_x} \sim 10^{-1}$, and $2B_y = b_{y_0} + b_{y_1} \approx b_{y_1} = \frac{a_y A_y}{c_{yy}} \frac{r_s}{e_s e_a} \frac{r_x}{d_{x_0} + a_x} \sim 10^{-1}$. Notice, the ratio between B_x and B_y is the ratio between the rate by which the corresponding mature cells are produced normalized by their self-inhibitory factor (carrying capacity). The default dimensionless parameter values are listed in Table 2. Note, the reduced model involves 8 parameters where D_1 describe the strength of the Y_0 dependent elimination term in dimensionless form. The numerator in Eq. (10) corresponds to the scaled cytokine level and the denominators express the stem cell niche interactions allowing for different competitive advantages of hematopoietic and cancerous cells. The death rate of hematopoietic stem cells has been normalized to 1, whereas a different rate is allowed for cancer stem cells (D_0) as well as an extra

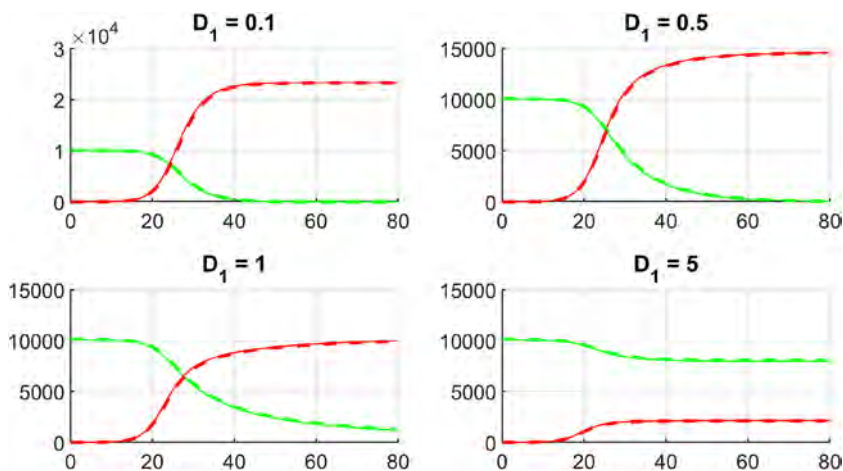


Fig. 4. Comparison of the reduced model (stipulated curves) and the full model (full curves) for dimensionless values $D_1 = 0.1, 0.5, 1, 5$. Green curves show hematopoietic stem cell counts and red curves show malignant stem cell counts versus time in years. All quantities are in dimensional variables. (For interpretation of the references to colour in this figure legend, the reader is referred to the web version of this article.)

degradation term ($D_1 Y_0$) corresponding to the T-cell response. We emphasize the local existence and uniqueness of solutions in the non-negative octahedron. Subsequently, we will focus on the impact of the dimensionless inflammatory stimuli J .

Fig. 4 illustrates that the reduced Cancitis model agrees excellently with the full model for various values of D_1 . As seen, an increase in the Y_0 -dependent death rate, corresponding to how aggressively the effector cells eliminate the malignant stem cells, conjures a bearable co-existing state. Higher values of D_1 yields a lower burden of malignant cells. This is in accordance with the concept of immune surveillance (as illustrated in Fig. 4 for $D_1 = 5$), (Ribatti, 2017). If resistance appears, i.e. the malignant cells become immune to the effector cells, it agrees with the concept of immunoediting (Ribatti, 2017); In the first phase, malignant cells are killed (not pictured in Fig. 4), in the second phase, a pseudo-equilibrium between immune and malignant cells appears (as for $D_1 = 5$ in Fig. 4), and finally the third phase - the escape phase - develops, where the co-existing pseudo-steady state disappears due to an absence of a sufficient immune response. In the escape phase, the disease ultimately gives symptoms and it may become clinically detected (as for $D_1 = 0.1$ in Fig. 4). The absence of a sufficient immune response is believed to be caused by a down-regulation or loss of an expression of malignant antigens, an up-regulated resistance of malignant cells, an increased expression of pro-survival genes, or the development of an immunosuppressive malignant cell microenvironment. (Ribatti, 2017).

4. Analysis and results

We study the effect of the dimensionless inflammatory load J on the possible steady states and their stability for the reduced Cancitis model in Eq. (10). Thus, we start by investigating the existence of steady states. By definition

- A trivial steady state is defined as having $X_0 = Y_0 = 0$.
- A (purely) hematopoietic steady state is defined as having $Y_0 = 0$, but $X_0 > 0$.
- A (purely) leukemic steady state is defined as having $X_0 = 0$, but $Y_0 > 0$.
- A co-existing steady state is defined as having $X_0 > 0$ and $Y_0 > 0$.

Note, non-negativity of X_0 and Y_0 implies non-negativity of the derived variables X_1, Y_1, A , and S_+ given by Eq. (A.9). Straight forward, but tedious computations (see Appendix B) give analytical results for the steady states, which are summarized as,

- An admissible **trivial steady state** always exists,

$$F_0 = (0, 0). \tag{11}$$

- Admissible **hematopoietic steady states**, $F_H = (X_{0H}, 0)$ are solutions to

$$\frac{J + \sqrt{J^2 + 2B_x X_{0H}}}{1 + X_{0H}} - 1 = 0, \tag{12}$$

with $X_{0H} > 0$. For certain combinations of parameter values two solutions may exist,

$$X_{0H\pm} = J + B_x - 1 \pm \sqrt{(J + B_x - 1)^2 + 2J - 1}. \tag{13}$$

For $F_{H\pm}$ to be admissible all components have to be real and non-negative and X_0 have to be positive. This gives rise to some restrictions given as inequalities in the level of exogenous inflammatory stimuli.

- For $B_x < \frac{1}{2}$ no admissible hematopoietic steady state exists for $J \leq \frac{1}{2}$. A bifurcation happens at $J = \frac{1}{2}$ such that for $J > \frac{1}{2}$ a unique, admissible hematopoietic steady state, X_{0H+} , exists with $X_{0H+}(J) \rightarrow 0$ for $J \rightarrow \frac{1}{2}$ and $X_{0H+}(J)$ being an increasing function.

Note, both the existence and the value of X_{0H+} only depends on the two parameters J and B_x . Remarkably, increasing the dimensionless rate $B_x \approx \frac{r_s}{c_{xx} e_3 e_a}$, by which the normal cells stimulate the dead cell pool, leads to an increase in the amount of normal cells X_{0H+} at the hematopoietic steady state value.

- Admissible **purely leukemic steady states**, $F_L = (0, Y_{0L})$, are the solutions of

$$R \frac{J + \sqrt{J^2 + 2B_y Y_{0L}}}{1 + Y_{0L}} - D_0 - D_1 Y_0 = 0, \tag{14}$$

with $Y_{0L} > 0$.

- For $J > \frac{1}{2} \frac{D_0}{R}$ a unique, admissible leukemic steady state exists. Then $Y_{0L}(J)$ is increasing in J .
- For $B_y < \frac{1}{2} \frac{D_0}{R} \left(\frac{D_0}{R} + \frac{D_1}{R} \right)$, and $J < \frac{1}{2} \frac{D_0}{R}$ no leukemic steady states exist.
- For default parameter values, $B_y < \frac{1}{2} \frac{D_0}{R} \left(\frac{D_0}{R} + \frac{D_1}{R} \right)$ and increasing inflammatory stimuli passing the critical value $J_{crit} = \frac{1}{2} \frac{D_0}{R}$, a leukemic steady state is created. This happens as $Y_0(J)$ increases from 0 with increasing J .

Note, both the existence and the value of a leukemic steady state only depends on the four parameters $J, \frac{D_0}{R}, \frac{D_1}{R}$, and B_y .

• **Co-existing steady states**, $F_C = (X_{0C}, Y_{0C})$, may exist, being the solutions of

$$J + \sqrt{J^2 + 2B_x X_{0C} + 2B_y Y_{0C}} = 1 + X_{0C} + C_y Y_{0C} \tag{15}$$

and

$$J + \sqrt{J^2 + 2B_x X_{0C} + 2B_y Y_{0C}} = (1 + C_x X_{0C} + Y_{0C}) \left(\frac{D_0}{R} + \frac{D_1}{R} Y_{0C} \right), \tag{16}$$

where $X_{0C} > 0$ and $Y_{0C} > 0$. X_{0C} can be computed directly, if Y_{0C} is known,

$$X_{0C} = \frac{(1 + Y_{0C}) \left(\frac{D_0}{R} + \frac{D_1}{R} Y_{0C} \right) - C_y Y_{0C}}{1 - C_x \left(\frac{D_0}{R} + \frac{D_1}{R} Y_{0C} \right)}. \tag{17}$$

Candidates for Y_{0C} are solutions to a fourth order polynomial with intricate expressions for the coefficients not easily investigated analytically. The co-existing steady state is not created by a bifurcation through (0,0) as no solution to (15) and (16) exists for (X_{0C}, Y_{0C}) approaching this point. Instead the co-existing steady state bifurcates from either the hematopoietic or the leukemic steady state, depending on the stability properties of these.

4.1. Stability considerations

In this section, we examine the stability properties of the various admissible steady states of the reduced model. The stability of the steady states are equivalent to the stability of the linearized equations near the steady state, if the steady state is hyperbolic, i.e. if no eigenvalue of the matrix of the linearized system has real part equal to zero. The Jacobian, \mathcal{J} , of Eq. (10) is computed analytically at most of the steady states, see below. Thus, for these steady states, the eigenvalues of the linearized system are easily obtained analytically and otherwise numerically. If all eigenvalues have negative real part, the steady state is stable and attracts neighbouring solutions, while if at least one eigenvalue has positive real part, the steady state is unstable. For the trivial steady state, the leukemic steady state and the hematopoietic steady state, \mathcal{J} is calculated analytically and becomes triangular, thus the eigenvalues can be directly read off from the diagonal.

In this section, we focus on cases that may be investigated analytically and in accordance with the default parameters we therefore assume,

$$B_x < \frac{1}{2}, \quad \text{and} \quad B_y < \frac{1}{2} \frac{D_0}{R} \left(\frac{D_0}{R} + \frac{D_1}{R} \right), \tag{18}$$

which were also used in the previous section for clear statements on existence of a hematopoietic and a leukemic steady state, respectively. In the following, we investigate the stability of the steady states.

First, consider the **trivial steady state**. At F_0 the Jacobian for the trivial steady states becomes,

$$\mathcal{J}_0 = 2 \begin{bmatrix} J - \frac{1}{2} & 0 \\ 0 & R \left(J - \frac{D_0}{2R} \right) \end{bmatrix}. \tag{19a}$$

with eigenvalues $\lambda_1 = J - \frac{1}{2}$ and $\lambda_2 = J - \frac{D_0}{2R}$. Evidently, the two eigenvalues are negative if and only if $J < \min\{\frac{1}{2}, \frac{D_0}{2R}\}$. Compared to the previous section this implies that the trivial steady state is stable only if there are no leukemic or hematopoietic steady states.

Secondly, consider the **hematopoietic steady state** and the corresponding Jacobian, \mathcal{J}_H , with the form

$$\mathcal{J}_H = \begin{bmatrix} \lambda_{H1} & \mathcal{J}_H(1, 2) \\ 0 & \lambda_{H2} \end{bmatrix}, \tag{20a}$$

where

$$\mathcal{J}_H(1, 2) = X_{0H+} \frac{B_y(1 + X_{0H+}) - C_y \sqrt{J^2 + 2B_x X_{0H+}} \left(J + \sqrt{J^2 + 2B_x X_{0H+}} \right)}{\sqrt{J^2 + 2B_x X_{0H+}} (1 + X_{0H+})^2}. \tag{21}$$

The Jacobian is an upper triangular matrix with vanishing entry (2,1), i.e. $\mathcal{J}_H(2, 1) = 0$, and the eigenvalues are given by the diagonal entries. The first eigenvalue $\lambda_{H1} = \mathcal{J}_H(1, 1)$ has corresponding eigenvector pointing along the X_0 - axis. The expression of λ_{H1} can be formulated

$$\lambda_{H1} = \frac{X_{0H+}}{(1 + X_{0H+}) \sqrt{J^2 + 2B_x X_{0H+}}} \left(-\sqrt{(J + B_x - 1)^2 + 2J - 1} \right). \tag{22}$$

Whenever the hematopoietic steady state is admissible, $X_{0H+} > 0$ corresponding to $J > \frac{1}{2}$, the eigenvalue is negative, $\lambda_{H1} < 0$. Thus, if the dynamics is restricted to the X_0 -axis then X_{0H+} is stable. This is a desirable property of the model as it illustrates that homeostasis is maintained prior to a mutation providing a malignant stem cell.

The other eigenvalue is

$$\lambda_{H2} = R \left(\frac{1 + X_{0H+}}{1 + C_x X_{0H+}} - \frac{D_0}{R} \right). \tag{23}$$

As X_{0H+} does neither depend on C_x nor $\frac{D_0}{R}$ a direct inspection of Eq. (23) yields that increasing C_x or $\frac{D_0}{R}$ has a stabilizing effect.

Since X_{0H+} increases from 0, as J increases from $\frac{1}{2}$, the hematopoietic steady state bifurcating from the trivial steady state is stable if $\frac{D_0}{R} > 1$ and unstable if $\frac{D_0}{R} < 1$ for J in a neighborhood of and larger than $\frac{1}{2}$. Note, if $C_x \geq 1$ then $\frac{1 + X_{0H+}}{1 + C_x X_{0H+}} \leq 1$. Hence, if $\frac{D_0}{R} > 1$ and $C_x \geq 1$, which corresponds to the malignant cells are inhibited more than the hematopoietic cells by the niche feedback, then the hematopoietic steady state is stable for arbitrarily large X_{0H+} . For $C_x < \frac{R}{D_0} < 1$, the stable hematopoietic steady state will turn unstable for sufficiently large J , since λ_{H2} approaches $C_x^{-1} - \frac{D_0}{R} > 0$ as X_{0H+} increases unboundedly with J . Rewriting $\lambda_{H2} = 0$ by use of Eq. (12) one arrives at the criterion

$$R \frac{J + \sqrt{J^2 + 2B_x X_0 + 2B_y Y_0}}{1 + C_x X_0 + Y_0} - D_0 - D_1 Y_0 = 0 \tag{24}$$

at $Y_0 = 0$ corresponding to the coexisting steady state being extended to the Y_0 axis (see expression (16)). This means that the hematopoietic steady state changes stability when it crosses a branch of the co-existing steady state on the X_0 -axis and is unstable for large values of X_{0H+} corresponding to large values of J . The criterion $\lambda_{H2} = 0$ is easily solved for a critical X_{0H+} -value, X_c ,

$$X_c = \frac{\frac{D_0}{R} - 1}{1 - \frac{D_0}{R} C_x}. \tag{25}$$

As X_{0H+} is an invertible function of J , Eq. (25) may be expressed as a threshold value of J ,

$$J_c = \frac{X_c^2 + 2(1 - B_x)X_c + 1}{2(1 + X_c)}. \tag{26}$$

Thirdly, consider the **purely leukemic steady state**, and the corresponding Jacobian, \mathcal{J}_L ,

$$\mathcal{J}_L = \begin{bmatrix} \lambda_{L1} & 0 \\ \mathcal{J}_L(2, 1) & \lambda_{L2} \end{bmatrix}, \tag{27a}$$

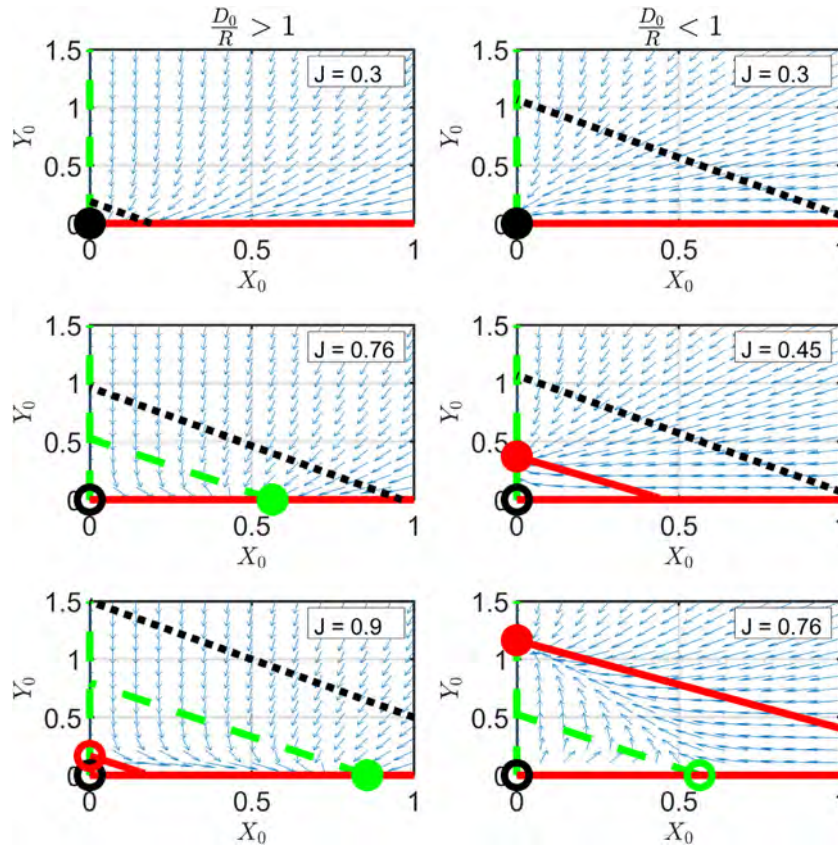


Fig. 5. Phase plane diagram for the hematopoietic cells (X_0) and the leukemic cells (Y_0). The cases corresponding to analytical results of the trivial, hematopoietic and leukemic steady states and their stability are shown. J increases from top row to bottom row illustrating the sequence of bifurcations for increasing J in the two cases $\frac{D_0}{R} > 1$ and $\frac{D_0}{R} < 1$. Full circles are stable steady states, open circles are unstable steady states. The black dotted line is the boundary of the analytical trapping region, the red curve is nullcline of \dot{Y}_0 , and the green stipulated curve is the nullcline of \dot{X}_0 . In the left column the hematopoietic steady state is stable independently of the presence of a leukemic steady state whereas in the right column, the leukemic steady state is stable. We emphasize that the trapping region generally depends on D_0 and J as well as $R, B_x, B_y, C_x,$ and C_y . On some subplots the dotted black line lies outside the visible range. (For interpretation of the references to colour in this figure legend, the reader is referred to the web version of this article.)

with

$$\mathcal{J}_L(2, 1) = RY_{OL} \frac{B_x(1 + Y_{OL}) - C_x\sqrt{J^2 + 2B_yY_{OL}}(J + \sqrt{J^2 + 2B_yY_{OL}})}{\sqrt{J^2 + 2B_yY_{OL}}(1 + Y_{OL})^2} \quad (28)$$

The Jacobian is a lower triangular matrix. Since entry (1,2) vanish, $\mathcal{J}_L(1, 2) = 0$, the Y_0 -axis is the eigenvector direction for the eigenvalue $\lambda_2 = \mathcal{J}_L(2, 2)$ evaluated at the leukemic steady state. Using the restrictions on B_y from inequality (18) we get

$$\lambda_{L2} = Y_{OL} \left(\frac{RB_y}{\sqrt{J^2 + 2B_yY_{OL}}(1 + Y_{OL})} - R \frac{J + \sqrt{J^2 + 2B_yY_{OL}}}{(1 + Y_{OL})^2} - D_1 \right) \leq -D_1Y_{OL}^2, \quad (29)$$

so the leukemic steady state is stable along the direction of the Y_0 -axis. The other eigenvalue is

$$\lambda_{L1} = \left(\frac{D_0}{R} + \frac{D_1}{R}Y_{OL} \right) \frac{1 + Y_{OL}}{1 + C_yY_{OL}} - 1. \quad (30)$$

As Y_{OL} increases from 0 as J increases from $\frac{1}{2} \frac{D_0}{R}$, then $\lambda_{L1} < 0$ if $\frac{D_0}{R} < 1$ and $\lambda_{L1} > 0$ if $\frac{D_0}{R} > 1$, for J values near $\frac{1}{2} \frac{D_0}{R}$. Increasing C_y has a stabilizing effect by decreasing λ_{L1} . Contrary to the hematopoietic case, an initial negative λ_{L1} will inevitably become positive for increasing J , after which Y_{OL} increases unboundedly causing the first term in Eq. (30) to become larger than one.

The analytical results for existence and stability of the trivial, hematopoietic and leukemic steady states are summarised in Fig. 5.

Lastly, consider the **co-existing steady state**. The admissible co-existing steady states are calculated numerically as a function of J and so is the Jacobian and its eigenvalues using the parameter values in Table 2 for the remaining parameters when nothing else is specified. The results are summarized in Fig. 8 and admissible co-existing steady states are stable for $J > 3.636$ approximately. The model implies that the ratio between R and the cell death rate D_0 is important. If the ratio between D_0 and R is less than one, the leukemic steady state is stable when created and occurs before the unstable hematopoietic steady state for J increasing until the co-existing steady state may take over the stability and bifurcate from the leukemic steady state. This is not to say that an increase in the inflammatory load cures the *in silico* patient or that it reduces the impact of the disease. Instead the co-existing steady state level of the malignant cells saturates approximately at the level as the level of malignant cells at the full leukemic steady state at the bifurcation point. Thus the tumor burden is not decreased, but is only prevented from increasing significantly. See Figs. 6 and 8. This model based hypothesis may seem a little counter-intuitive and deserves clinical testing. Conversely, if the ratio between D_0 and R is larger than one, the hematopoietic steady state is born stable and occurs before the unstable leukemic steady state occurs for J increasing until the co-existing steady state may take over the stability of - and bifurcate from - the hematopoietic steady state, see Fig. 7. Hence we emphasize that the dynam-

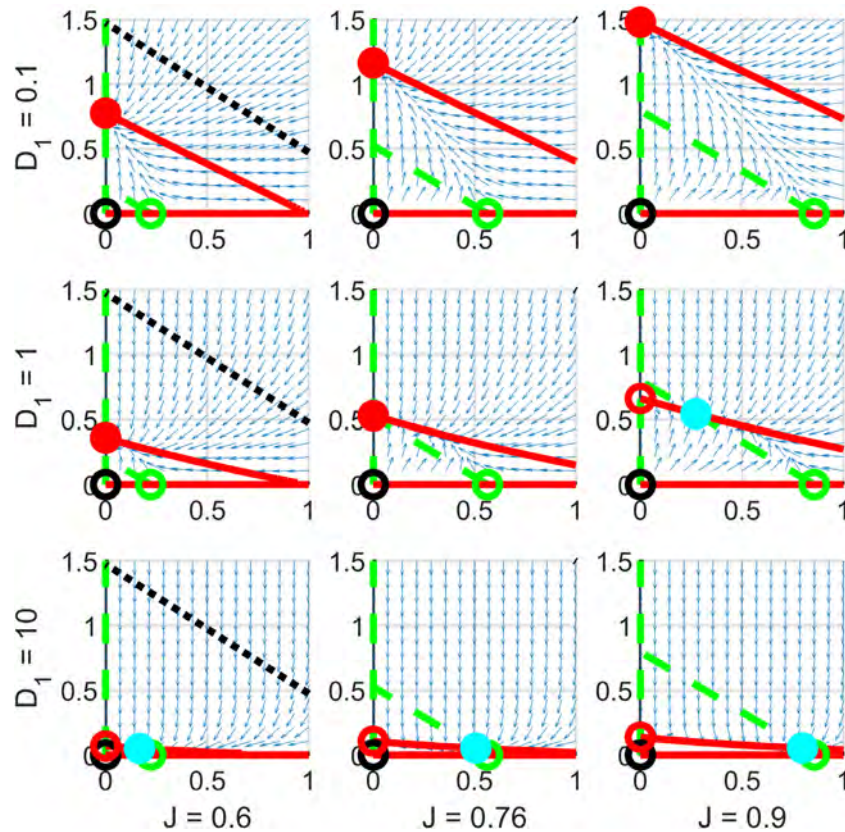


Fig. 6. Illustration of the dynamics in a (X_0, Y_0) -phase plane. Each row corresponds to $D_1 = 0.1, 1, 10$, respectively, whereas each column corresponds to $J = 0.60, 0.76, 0.90$, respectively. Red curves are Y_0 nullclines (includes the X_0 -axis) and blue stipulated curves are X_0 nullclines (includes the Y_0 -axis). Open circles represent unstable steady states whereas full circles represent stable steady states. The black circle is the trivial steady state, the green circle the hematopoietic steady state, the red the purely leukemic steady state, and cyan the co-existing steady state. The attracting trapping region is indicated on each palette by the coordinate axis and a black dotted line, which increases with J but has slope -1 (the black dotted line may fall outside the visible range on some subplots). The flows are indicated by the normalized slope field with arrows. (For interpretation of the references to colour in this figure legend, the reader is referred to the web version of this article.)

ics of the system is rather different depending on whether the ratio between D_0 and R is less than or greater than one. Thus increasing the ratio D_0 to R or increasing the ratio of D_1 to R , as illustrated in Fig. 7, represent very appealing candidates for treatment. Eq. (B.11) is equivalent to Eq. (B.18) with $X_0 = 0$, thus the leukemic steady state and the co-existing steady state equals for $X_0 = 0$. By the implicit function theorem it follows that for $Y_0 \geq Y_{0L}$ the derivative of $X_0 = X_0(Y_0)$ with respect to Y_0 is positive corresponding to an increasing steady state trajectory in J .

The possible topologies are summarized in Figs. 6 and 7. The corresponding bifurcation diagram are depicted in Fig. 8. Continuous animations for varying J for different fixed values of D_0 and D_1 may be found at <http://dirac.ruc.dk/cancitis/> together with an animated bifurcation diagram (see Section 4.3 for further discussions). We refer to the topology of the dynamical system as Janus topology, since it has two faces, i.e. two different topologies for different set of parameters.

4.2. Existence of an attracting trapping region for the reduced Cancitis model

A trapping region is a compact set with the property that orbits starting in the trapping region cannot escape the region. An attracting trapping region is a trapping region which is attracting, i.e. orbits starting outside the trapping region will enter the trapping region (in finite time). An attracting trapping region is a suitable feature for a biological system, since it guaranties some basic

well-behavior of the system such as boundedness of solutions and global existence in time (Robinson, 1999).

An attracting trapping region exists in the non-negative octahedron for the reduced Cancitis model in Eq. (10) (will be shown below). As a consequence the steady states lies in this trapping region.

For some parameter values, $X'_0 < 0$ and $Y'_0 < 0$ for any X_0 and Y_0 . The idea is to show that $X'_0 < 0$ and $Y'_0 < 0$, for large $X_0 + Y_0$ for all parameter values.

Let

$$K = \max\{J, \sqrt{2B_x}, \sqrt{2B_y}\} \quad \text{and} \quad L = \min\{1, C_x, C_y\}. \quad (31)$$

Thus, $J^2, 2B_x, 2B_y < K^2$ and $1, C_x, C_y > L$, which implies

$$\frac{J + \sqrt{J^2 + 2B_x X_0 + 2B_y Y_0}}{1 + X_0 + C_y Y_0} - 1 < \frac{K}{L} \frac{1 + \sqrt{1 + X_0 + Y_0}}{1 + X_0 + Y_0} - 1, \quad (32)$$

and

$$\begin{aligned} R \frac{J + \sqrt{J^2 + 2B_x X_0 + 2B_y Y_0}}{1 + C_x X_0 + Y_0} - D_0 - D_1 Y_0 \\ < R \frac{K}{L} \frac{1 + \sqrt{1 + X_0 + Y_0}}{1 + X_0 + Y_0} - D_0 \end{aligned} \quad (33)$$

Consider therefore (for $\alpha > 0$)

$$\alpha \frac{1 + \sqrt{1 + X_0 + Y_0}}{1 + X_0 + Y_0} - 1, \quad (34)$$

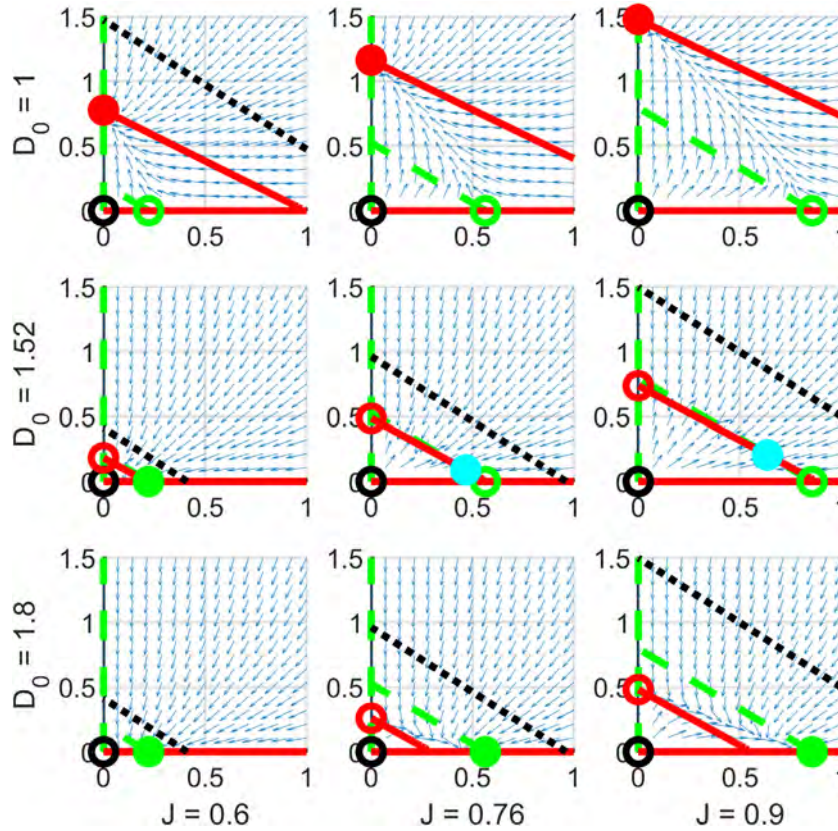


Fig. 7. Illustration of the dynamics in the (X_0, Y_0) phase plane. Each row corresponds to $D_0 = 1, 1.52, 1.8$, respectively, whereas each column corresponds to $J = 0.60, 0.76, 0.90$, respectively. R is set to its default value 1.49. Red curves are Y_0 nullclines (and include the X_0 -axis) and green stipulated curves are X_0 nullclines (and include the Y_0 -axis). Open circles represent unstable steady states whereas full circles represent stable steady states. The black circle is the trivial steady state, the green circle the hematopoietic steady state, the red circle the purely leukemic steady state, and the cyan circle the co-existing steady state. The attracting trapping region is indicated on each palette (surrounded by the coordinate axis and a black dotted line, which may fall outside the visible range). The trapping region decreases with D_0 and increases with J , but has slope -1 . The flows are indicated by the normalized slope field with arrows. (For interpretation of the references to colour in this figure legend, the reader is referred to the web version of this article.)

and introduce

$$z = \sqrt{1 + X_0 + Y_0}. \tag{35}$$

As X_0 and Y_0 are non negative, the minimal, allowed value of z is 1. Expression (34) is negative if and only if

$$z^2 - \alpha z - \alpha > 0. \tag{36}$$

For any $\alpha > 0$ there is exactly one positive solution to $z^2 - \alpha z - \alpha = 0$, being $\frac{1}{2}(\alpha + \sqrt{\alpha^2 + 4\alpha})$. Any larger z value fulfills (36) and since $z \geq 1$ is required we get

$$z_{crit} = \max \left\{ \frac{1}{2}(\alpha + \sqrt{\alpha^2 + 4\alpha}), 1 \right\}. \tag{37}$$

Solving for $X_0 + Y_0$ this implies that the bound M is

$$M = z_{crit}^2 - 1, \tag{38}$$

i.e. for $X_0 + Y_0 > M$ are $X'_0 < 0$ and $Y'_0 < 0$. Note that we may chose

$$\alpha = \frac{\max\{1, \frac{R}{D_0}\} \cdot \max\{J, \sqrt{2B_x}, \sqrt{2B_y}\}}{\min\{1, C_x, C_y\}}. \tag{39}$$

Thus, $M \geq 0$ and the triangle defined by the X_0 -axis, the Y_0 -axis and the line $X_0 + Y_0 = M$ thus define an attractive trapping region for Eq. (10). We emphasize that M generally depends on D_0 and J as well as $R, B_x, B_y, C_x,$ and C_y .

4.3. Phase plane analysis and treatments

In the present work, we mainly focus on analyzing the impact of the inflammatory stimuli J , modifying the T-cell independent death rate D_0 , and modifying the T-cell response represented by D_1 rather than a complete analysis of real treatments. However, several treatment scenarios are possible, e.g. T-cell therapy. Interferon- α treatment among other things stimulates the immune system, whereby the effect of the effector T-cells become strengthened.

The reduced model has been investigated numerically for various choices of parameters. The default parameters, as given in Table 2, have been used when nothing else is stated.

First consider the default case $\frac{D_0}{R} < 1$ as illustrated in Fig. 6 showing the phase plane for various J and D_1 . A trivial steady state F_0 is found to always exist, and, for sufficiently low inflammatory stimuli J , it is stable. For J greater than $\frac{D_0}{2R}$, a purely leukemic steady state F_L becomes admissible and the leukemic cells increase in numbers with increasing J . For choices of J where only F_L and F_0 are admissible, the leukemic steady state is found to be stable, whereas the trivial state is unstable. It is worth emphasizing that the purely leukemic steady states in general only depend on the four clusters of parameters $\frac{D_0}{R}, \frac{D_1}{R}, \frac{J}{D_1}, B_y,$ and J .

For J greater than $\frac{1}{2}$, an unstable hematopoietic steady state, F_{H+} , becomes admissible. In absence of mutations, i.e. no malignant cells present, the hematopoietic steady state appears stable. Being a saddle point with stable manifold along the X_0 -axis and the unstable manifold having a nonvanishing Y_0 -component, a per-

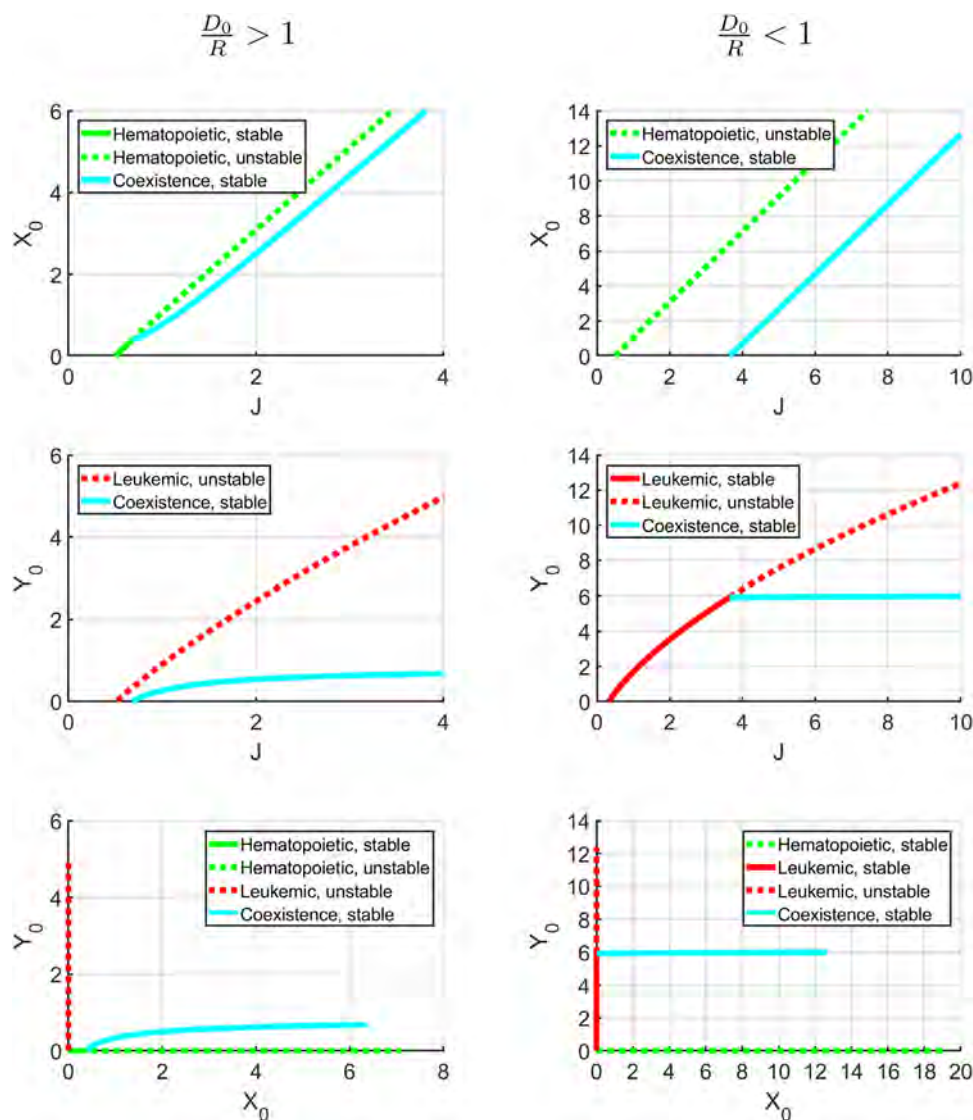


Fig. 8. Left column shows the bifurcation diagrams for the case $\frac{D_0}{R} > 1$ and the right column shows the corresponding for $\frac{D_0}{R} < 1$ (the default case). The bifurcation diagrams showing the appearance and stability of the admissible steady states depending on the bifurcation parameter J . The top panel shows X_0 , the middle panel shows Y_0 , and the lower panel shows the J -trajectory of the admissible steady states in a (X_0, Y_0) phase plane having the range on the axis as in the other figures above. Green curves are the hematopoietic steady states, red curves are the purely leukemic steady states, and cyan curves are the co-existing steady states. At the origin a trivial steady state always exists. It is stable for some values of J and unstable for others thus it is not shown on the figure. Dotted curves mean that the corresponding steady state is unstable, while full curves indicate that the corresponding steady state is stable. For the left column $J \in [0; 4]$, while for the right column $J \in [0; 10]$. (For interpretation of the references to colour in this figure legend, the reader is referred to the web version of this article.)

turbation with malignant cells may cause the state to be repelling away from the hematopoietic steady state. As was shown analytically, F_{H+} only depends on the two parameters J and B_x and for fixed B_x , X_{0H+} increases with J .

As shown in Fig. 6, an admissible co-existence steady state, F_C may exist, which is dependent on both J and D_1 . While it has been found to exist for sufficiently high J , regardless of realistic values of D_1 , the existence of F_C does require very large values of J for $D_1 \leq 0.1$. For default parameter values (e.g. $D_1 = 0.1$), the co-existing steady state occurs for J larger than J_C given by Eq. (26). The co-existing steady state is stable and bifurcates from the leukemic steady state which loses its stability and becomes unstable. For increasing J , F_C moves away from F_L with increasing X_0 . For D_1 around 1 or greater, the co-existence steady state might represent a possible preferable situation to the full-blown leukemic state F_L . For large choices of D_1 , such as $D_1 = 10$ shown in Fig. 6, F_C is in close proximity of F_{H+} for most realistic choices of J , leading to a co-existence steady state, which can be interpreted

as having a small number of leukemic cells, which are held back from increasing due to a strong T-cell response. In the case where the co-existence steady state exists, it is found numerically to be stable, while the leukemic steady state F_L becomes unstable whenever the co-existing steady state becomes admissible. Thus, for any situation where a co-existence steady state is admissible, the system will move towards this state.

Increasing B_y , D_0 or D_1 and decreasing R cause the leukemic steady state to appear at higher values of J while increasing B_x causes the hematopoietic steady state to occur for lower values of J . Thus, the model identifies important parameters for potential protection to prevent a leukemic outbreak.

Next, consider the case $\frac{D_0}{R} > 1$ in contrast to the default case. Phase plane portraits are shown in Fig. 7 for various J and D_0 . The situation is analogous to the default case except the order in which the hematopoietic steady state and the leukemic steady state occur are interchanged along with their stability properties. Thus the hematopoietic steady state bifurcates from the trivial steady state

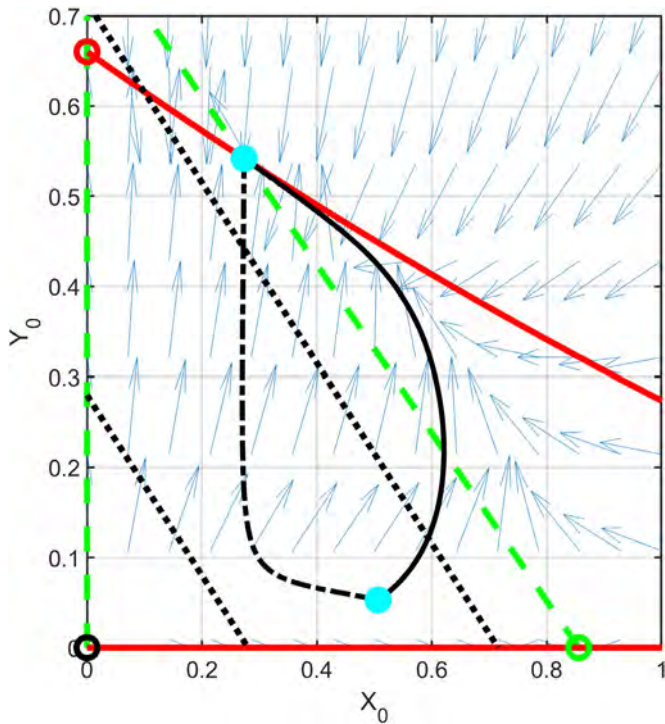


Fig. 9. An *in silico* treatment of a virtual patient having $(D_1, J) = (1, 0.9)$. The treatment combines gene therapy, by increasing D_1 to 10, and an anti-inflammatory treatment, by lowering J from 0.9 to 0.76. Hereby the virtual patient is moved from a co-existing steady state (upper cyan dot) with high malignant cell counts, $(X_0, Y_0) = (0.27, 0.55)$ corresponding to $(D_1, J) = (1, 0.9)$, toward a co-existing steady state (lower cyan dot) with low malignant cell count and normalized hematopoietic cell count, $(X_0, Y_0) = (0.51, 0.05)$ corresponding to $(D_1, J) = (10, 0.76)$. This treatment path (stipulated black curve) do not follow the displayed slope field. Thereafter treatment is put on pause and the virtual patient follows the flow back toward the original co-existing steady state (full black curve), $(X_0, Y_0) = (0.27, 0.55)$. Full red lines show the Y_0 nullcline and the stipulated green lines show the X_0 nullcline. The open circles illustrate the unstable steady states (black for the trivial, red for the leukemic, and green for the normal hematopoietic steady state). The black dotted lines bound the region, which represents the total leukocyte count considered to be normal. Above the upper boundary the risk of thrombosis is considered high and below the lower boundary the immune system is considered to be dysfunctional. (For interpretation of the references to colour in this figure legend, the reader is referred to the web version of this article.)

and takes over the stability for increasing J shown in the second and third row of Fig. 7. For larger J -values, the leukemic steady state bifurcates from the trivial one as an unstable steady state and it remains unstable for larger J . For even larger values of J , the co-existing steady state bifurcates from the hematopoietic steady state and it takes over the stability leaving the hematopoietic steady state unstable. For increasing J , it slowly moves away from the hematopoietic steady state. Compared to the default case, $\frac{D_0}{R} < 1$, this is not necessarily lethal, since X_{0C} stays relatively close to X_{0H} and $Y_{0C} \ll Y_{0L}$.

Returning to the case $\frac{D_0}{R} < 1$, a scenario of an *in silico* treatment of a virtual patient having $(D_1, J) = (1, 0.9)$ is illustrated in Fig. 9. The treatment combines a strengthened T-cell effect (interferon or T-cell therapy) by increasing D_1 to 10 and an anti-inflammatory treatment, which lowers J from 0.9 to 0.76. Thus, the virtual patient is moved from a co-existing steady state with high malignant cell counts, $(X_0, Y_0) = (0.27, 0.55)$ towards a co-existing steady state with low malignant cell counts and normalized hematopoietic cell counts, $(X_0, Y_0) = (0.51, 0.05)$. This treatment path (stipulated curve) does not follow the displayed slope field shown, corresponding to $(D_1, J) = (1, 0.9)$. It takes approximately 5 years for the treatment to lower Y_0 to 15%, but almost 20 years to increase X_0 to near normal amount. The total cell

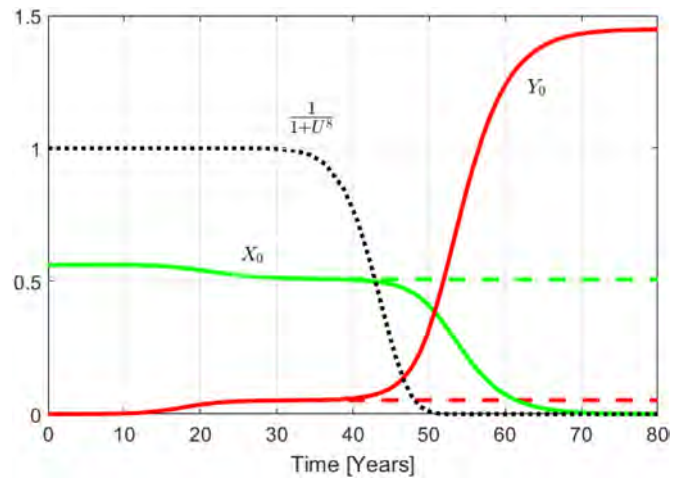


Fig. 10. Effects of resistance of malignant stem cells to T-cell elimination. The dotted lines show the cancer development toward the co-existing steady state in absence of resistance whereas the full lines show the development when resistance develops. Green curves represent the hematopoietic stem cell counts (X_0) and the red curves represent the malignant stem cell counts (Y_0). Parameters are as for Fig. 4 but with $D_1 = 10$. Black dotted line shows the inhibiting factor $\frac{1}{1+U^8}$ over time, reducing the population death due to resistance. All quantities are shown in dimensionless units except time which is in years. See Section 5 for further discussion. (For interpretation of the references to colour in this figure legend, the reader is referred to the web version of this article.)

count ($X_0 + Y_0$) is fairly well controlled during this treatment process, which is essential to prevent high risk of thrombosis. Thereafter treatment is put on pause and the virtual patient follows the flow back toward the original co-existing steady state, $(X_0, Y_0) = (0.27, 0.55)$. It takes about 20 years for Y_0 to pass 0.5 corresponding to 10% below the original amount. The time interval of treatment and relapse are both quite large and it is likely that the malignant cells develop resistance during such time span. On the other hand, these time scales are comparable to clinical experiences.

To explicitly include resistance in the model, we assume that the exposure,

$$U = \int_0^t Y_0(t) dt, \tag{40}$$

of malignant stem cells drives the development of resistance. Furthermore, we assume that resistance inhibits the Y_0 -dependent death rate D_1 by a decreasing Hill-function in the exposure, as it is associated with a reduced T-cell elimination of the malignant cells. Thus, the death rate, D_1 , in Eq. (10b) is substituted by,

$$\frac{D_1}{1 + U^8}. \tag{41}$$

We note that, as exposure increases, the effective death rate in Eq. (41) decreases, leading to an increase in Y_0 , which further increases exposure and so on. Initially, the development will be like that seen for the co-existing steady state (as shown in Fig. 4 for $D_1 = 5$), but as the exposure increases, resistance develops and the dynamic starts to deviate from that without resistance. Thus, after approaching the co-existing steady state for a while the cancer development begins to increase approximately as an exponential-function (for the second time) before finally reaching the saturation level, corresponding to full blown cancer, as seen in Fig. 10. Meanwhile, the hematopoietic cells show a reciprocal development. Overall, the co-existing stable steady state is approached in the first phase of the development, while resistance develops. When resistance becomes influential, around year 30, the co-existing steady state disappears and in the next phase the full blown cancer develops. Thus, the developed resistance destroys the

effect of the therapy over time. We have chosen the Hill power to be 8 in Eq. (41). Choosing it larger does not change the numerical output significantly and choosing it smaller makes the dormancy state, i.e. the temporary plateau between year 25 and 40 in Fig. 10, shorter and resistance will start a bit earlier. For $U = 1$, expression (41) takes the saturation value $\frac{1}{2}D_1$. This half saturation value corresponds approximately to year 42 at Fig. 10.

A specific finding deserves to be emphasized: A dimensionless stem cell reproduction ratio \mathcal{R} exists, which determines how robust the hematopoietic condition may be and how disastrously a potential blood cancer disease will develop. This is similar to the concept of a reproduction number in epidemiology describing whenever an epidemic outbreak may occur. In our case, the reproduction ratio consists of a combination of six physiological parameters from the dimensional form of the full model. Inspired by the different topologies discussed above, we define the reproduction ratio as the inverse of $\frac{D_0}{R}$,

$$\mathcal{R} = \left(\frac{D_0}{R}\right)^{-1} = \frac{\left(\frac{r_y}{\hat{d}_{y0} + a_y}\right)}{\left(\frac{r_x}{d_{x0} + a_x}\right)} \quad (42)$$

Thus for, $\mathcal{R} > 1$ we have a more serious situation than for $\mathcal{R} < 1$, showing that if the reproduction ratio exceeds the threshold, $\mathcal{R}_0 = 1$ it is more disastrous than if it is below \mathcal{R}_0 . Physiologically, the reproduction ratio \mathcal{R} tells us that the situation is worse if malignant stem cells have a better fitness than the hematopoietic stem cells. The intuitive interpretation in most bio-medical literature attributes the main cause for cancer development to the frequency of stem cell division. Our fitness concept, the ratio between the self-renewal rate and the sum of the death rate and the proliferation rate, is far more nuanced, but is in agreement with the literature and thus confirming our results. To force the model from a regime of highly disastrously development into a regime of less disastrously development we may simply focus on how to manipulate the reproduction ratio, \mathcal{R} , for the specific system under consideration to become less than the threshold value of \mathcal{R} . The threshold concept depends on six parameters, which offer independent manipulation possibilities. Alternatively, one may consider the fitness of hematopoietic cells as a given fitness threshold value for a specific system. Thus the development of a given mutation is determined by the fitness value of that mutation compared to that of the hematopoietic cells.

In addition to the primary reproduction ratio \mathcal{R} , a secondary reproduction number, \mathcal{S} , important for the dynamics of the system as it appears in most analytical expressions (see Appendix B), is,

$$\mathcal{S} = \left(\frac{D_1}{R}\right)^{-1} = \frac{\left(\frac{r_y C_{yy}}{\bar{y}_0}\right)}{\left(\frac{r_x}{d_{x0} + a_x}\right)}. \quad (43)$$

This secondary reproduction number, \mathcal{S} , describes the T-cell dependent fitness of the malignant stem cells relative to the afore defined fitness of the hematopoietic stem cells, whereas the primary reproduction ratio, \mathcal{R} , compares the T-cell independent fitness of malignant stem cells to that of hematopoietic stem cells.

Increasing the inflammatory stimuli J accelerates and drives the blood cancer in general. Vice versa, the blood cancer itself induces an inflammatory response, and thus the coupled system introduces a negative spiral with respect to the disease development. For further details on this see (Andersen et al., 2017).

5. Discussion and conclusion

A novel mechanism-based model - the Cancitis model - describing the interaction of blood cancer and the inflammatory system is proposed. The immune response is divided into two components, one where the elimination rate of malignant stem cells is independent of the size of the cancer (Y_0 -independent death rate) and one where the elimination rate depends on the size of the cancer (Y_0 -dependent death rate). The model confirms that inflammation may accelerate and drive a cancer beyond the fact that the presence of a cancer induces an inflammatory response. A dimensional analysis shows that the full 6-dimensional system of nonlinear ordinary differential equation may be reduced to a 2-dimensional system - the reduced Cancitis model. In terms of Fenichel theory this is known as the reduced model or the slow manifold approximation. This is a very good approximation and is appropriate for MPNs in particular, since these diseases develop slowly. The original parameters appear in the reduced model in clusters, showing the important grouping of parameters. The reduced model allows for a highly analytical investigation of steady states and their dependence especially on the inflammatory stimuli J , the Y_0 -independent death rate (D_0) and the Y_0 -dependent death rate (D_1). A semi-analytic investigation reveals the stability properties of the steady states. Finally, we prove positivity of the system and the existence of an attracting trapping region in the positive octahedron guaranteeing global existence and uniqueness of solutions. For the reduced Cancitis model, the possible topologies are completely described as having a Janus structure, where two qualitatively different topologies appear for different sets of parameters given by \mathcal{R} . In the important work by Stiehl and Marciniak-Czochra (2012), a model without immune interaction is presented. The authors discuss a fraction similar to \mathcal{R} given in Eq. (42) and shows that it is important for the dynamics of the system. However, this model involved explicitly the hierarchy of progenitor cells, whereby a lot of unknown parameters are introduced, thus their results appear as a more qualitative analysis involving all these parameters. The relative simplicity of our model, due to the parsimonious principle and the model reduction, make it possible to state sharp criteria involving \mathcal{R} , which along with another threshold \mathcal{S} given in Eq. (43) deliver a complete topological analysis of the possible dynamics.

For the default parameters, a trivial steady state F_0 always exist. Starting by no stimulation J of the inflammatory system, only the trivial steady state is stable. Increasing J will turn this trivial steady state into an unstable steady state while a leukemic steady state appears. If J is increased further, an unstable hematopoietic steady state occurs. In absence of mutations, i.e. no malignant cells, the hematopoietic steady state is stable. Being a saddle point, a perturbation of the hematopoietic steady state with malignant cells may cause the state to be repelling away from the hematopoietic steady state. At the bifurcation, the purely leukemic steady state takes over the stability turning the trivial steady state into an unstable state. Both the hematopoietic steady state and the leukemic steady state start at the trivial steady state and move away from it with increasing values of J . A co-existing steady state bifurcates from the leukemic one for even higher values of J and simultaneously the leukemic steady state loses its stability. For increasing values of J , the co-existing steady state moves towards higher X_0 -values and with only a minor increase in Y_0 . Increasing D_1 also decreases Y_0 , thus representing an attractive disease condition compared to full blown blood cancer.

We emphasize that the choice of default parameter values for C_x and C_y make the highest order coefficient in Eq. (B.23), given in expression (B.24), relatively small, since $C_x C_y \approx 1$. As a consequence, not only the roots of Eq. (B.23), but also the number of real roots become sensitive to these parameter values. Thus some caution is needed; A considerable change in parameters may not only change

the stability properties, but also the number of possible co-existing steady states. The outbreak of blood cancer in general is commonly considered to occur when the ratio of the self-renewal rates, R , exceeds a threshold value, frequently taken to be one. However, the model implies that the ratio between R and the cell death rates D_0 and D_1 should rather be considered. In fact, the analysis motivates the definition of a primary and a secondary reproduction ratio, \mathcal{R} and \mathcal{S} , respectively, crucially for topology of the dynamics of the system. If \mathcal{R} is larger than one, the leukemic steady state appears first and the hematopoietic steady state later for increasing J . The leukemic steady state is stable until the co-existing steady state may take over. If instead, \mathcal{R} is less than one, the hematopoietic steady state appears first and the leukemic steady state later with respect to increasing J . Thus the hematopoietic steady state is stable until the co-existing steady state takes over while the leukemic steady state remains unstable. Inflammation is presumably another important quantity for the onset and development of blood cancer, greatly influenced by the inflammatory stimulation J (Andersen et al., 2017; Brianna M. Craver et al., 2018; Desterke et al., 2015; Hasselbalch, 2012; 2014; Hasselbalch and Bjoern, 2015; Hermouet et al., 2015; Koschmieder et al., 2016; Wodarz and Komarova, 2014; Zhang et al., 2017). This suggests that the body may manage initial leukemia as long as the self-renewal rate is not too high, but fails to manage it if an inflammation appears. These findings suggest combining treatment with anti-inflammatory treatment. Thus inflammation may trigger and drive blood cancers including MPNs.

It is interesting that decreasing the inflammatory stimuli for $\mathcal{R} > 1$ may not be a good first step in treatment of such patients. Instead D_1 should be increased first and subsequently the inflammatory stimuli may be reduced. However, for $\mathcal{R} < 1$ the inflammatory stimuli may be reduced simultaneously with increasing D_0 .

We note that, increasing the inflammatory stimuli (J) increases $J = \frac{I}{2e_s \bar{s}} = I \frac{(r_x/e_s)}{d_{x0} + a_x} = \frac{I}{e_s} \frac{r_x}{d_{x0} + a_x}$. An increase in the rate r_x increases the amount of hematopoietic stem cells, which quickly increases the amount of mature hematopoietic cells, thus leading to an indirect increase in the amount of dead cells (for unchanged values of d_{x0} and a_x). An increase in the amount of dead cells stimulates the inflammation, whereas e_s eliminates the debris of the dead cells. Thus increasing the fraction r_x/e_s eventually increases the inflammation. This may suggest that drugs helping the inflammatory response in eliminating the debris more effectively may decrease J . However, the denominator $d_{x0} + a_x$ denotes the rate at which hematopoietic stem cells are reduced, due to apoptosis and proliferation into progenitor cells. Hence, an increase in either d_{x0} or a_x will decrease J . The reason why is that a decrease in x_0 in the long term leads to a decrease in x_1 and thus a decrease in the amount of dead cells, a , whereby the inflammatory response become less stimulated. Hence, treatment affecting the stem cells by increasing the natural death rate d_{x0} may decrease the inflammatory response and thereby help reduce the cancer. In combination, the competition between self-renewal rate r_x and the elimination of hematopoietic stem cells $d_{x0} + a_x$ is reflected in the ratio $\frac{r_x}{d_{x0} + a_x}$. Likewise, the competition between the inflammatory load I and the elimination rate of debris by the immune response e_s is reflected in the ratio $\frac{I}{e_s}$. Thus increasing these ratios increase J . This is surprising, since intuitively one would guess that treatment should primarily affect the malignant stem cells and leave the normal hematopoietic stem cell as unaffected as possible. Of course, affecting the amount of normal hematopoietic stem cells has other impacts apart from just affecting J , due to the direct competition between the cell types. Increased J also affect the self-renewal rate for the malignant stem cells. Since the stem cell self-renewal is proportional to J in both cases, the malignant cells benefit most, due to an expected higher baseline self-renewal rate of the ma-

lignant stem cells r_y than for the normal hematopoietic stem cells r_x .

The specific inclusion of the T-cells in the immune response has its roots in gene therapy and interferon- α treatment. In gene therapy a patients own T-cells are modified outside the body and re-injected to fight the cancer. As shown, it is in principle a very effective instrument, but in practice it has limited function, since cancer cells almost always develop resistance, by modifying the recognizable surface receptors used by the naive T-cells to identify the cancer cells. Without being recognized by naive T-cells, the effector cells will not attack the cancer cells making this defence weak. Interestingly, even if resistance did not occur, the model predicts that T-cell therapy does not cure the patient, but only keeps the cancer in an iron grip at the co-existing steady state securing limited growth of cancer for a while. When resistance occurs the grip loosens and a fatal growth begins despite continued T-cell therapy as illustrated on Fig. 10. The fact is that increasing D_1 by a T-cell therapy may turn a full blown leukemic (stable) steady state into a co-existing (stable) steady state or even for high dose therapy into a healthy (stable) hematopoietic steady state temporarily as illustrated in Fig. 7. It takes some years (e.g. 5 years) as illustrated in Fig. 9. However, without changing the parameters permanently (e.g. D_1) the cancer recurs either because the cancerous stem cells are not completely eradicated or as soon as a new mutation (surviving repair mechanisms) appears. For a supplementary discussion reaching the same conclusion see (Michor et al., 2006). However, for the case of all cancerous stem cells to be completely eliminated 20 years of treatment may be needed. In fact, due to the detection limit, one can never be sure that the cancer is completely eradicated. A detection limit of 1% of 10^{10} mature cells (or 10^4 stem cells) corresponds to 10^8 mature cells (or 100 stem cells). Thus, to guarantee an eradication of the malignant stem cells requires a detection limit lower than 0.01%. However, T-cell therapy may be suitable in combination with other treatment.

In the groundbreaking work by Kuznetsov and Knott (2001) and Kuznetsov and Makalin (1994), the intrinsic dynamics of the cells themselves was not considered, but was simply taken as logistic growths independent of the other cell types. In contrast to this, we describe the common dynamics of all cell types based on the underlying biological mechanisms. We include the effect of cancerous cells on normal cells and vice versa, their interaction with the dead cells, the dead cells interaction with the immune system, the interaction of the immune system with the replication of (living) cells, and specifically the interaction between cancerous cells and the adaptive immune system, mediated by T-cells and other killer cells. In this way the presented model deviates from the general models in (Arciero et al., 2004; Baker et al., 2013; Borges et al., 2014; Cosentino and Bates, 2012; De Pillis et al., 2005; Dunster et al., 2014; Hanson et al., 0000; Herald, 2010; Katak, 2014; Kirschner and Panette, 1998; Moore and Li, 2004; Nanda et al., 2007; Nielsen, 0000; Nielsen et al., 2013; Pillis et al., 2006; Pillis and Radunskaya, 2003; Saleem and Agrawal, 2012; Sarkar and Banerjee, 2005). Thus co-existing states are explicitly shown to be possible as it is shown how such states depends on the important parameters, i.e. inflammatory load and the two relevant death rates. It is shown that in case resistance is considered, this co-existing state is merely a dormancy state and ultimately develops into the full blown cancer state. It is interesting that our mechanism-based multi-cell model confirms previous conclusion that immunotherapy does not completely eradicate malignant cells predicted by Kuznetsov and Knott (2001). This is an important subject as pointed out by Dingli and Michor (2006).

Besides having a strengthening effect on the effector cells, interferon- α also affects other parts of the cancer-immune system in a constructive synergistic way, which may make the treatment even more effective. A full discussion of how various treatments

affect blood cancer and treatment optimization will be addressed in subsequent papers.

Appendix A. Dimensionless form of six dimensional model

Formulating equations on dimensionless form may reduce the number of free parameters by grouping the original parameters into clusters of parameters, the dimensionless parameters. Simultaneously the dimensionless form may suggest a model reduction using Fenichel theory from geometric singular perturbation theory (Kuehn, 2015).

All variables in Eqs. (1) and (2) are scaled by a constant having the unit of the variable, if any, and it is denoted with same symbol as the variable, but with a bar above. Likewise, the corresponding dimensionless variable is denoted with the corresponding capital letter and with index as the original symbol. Thus we put $x_0 = \bar{x}_0 X_0$, $x_1 = \bar{x}_1 X_1$, $y_0 = \bar{y}_0 Y_0$, $y_1 = \bar{y}_1 Y_1$, $a = \bar{a}A$, $s = \bar{s}S$, and $t = \bar{t}T$, with X_0, X_1, Y_0, Y_1, A, S , and T , the dimensionless variables and $\bar{x}_0, \bar{x}_1, \bar{y}_0, \bar{y}_1, \bar{a}, \bar{s}$, and \bar{t} the scaling constants carrying the dimensions. Hence the extended model of the differential system in (1) and (2) in the new dimensionless variables reads,

$$X_0' = \bar{t} \left(\frac{\bar{s}r_x}{1 + (c_{xx}\bar{x}_0 X_0 + c_{xy}\bar{y}_0 Y_0)} - d_{x_0} - a_x \right) X_0 \quad (A.1a)$$

$$X_1' = \bar{t} \left(\frac{\bar{x}_0}{\bar{x}_1} a_x A_x X_0 - d_{x_1} X_1 \right) \quad (A.1b)$$

$$Y_0' = \bar{t} \left(\frac{\bar{s}r_y}{1 + (c_{yx}\bar{x}_0 X_0 + c_{yy}\bar{y}_0 Y_0)} - d_{y_0}(Y_0) - a_y \right) Y_0 \quad (A.1c)$$

$$Y_1' = \bar{t} \left(\frac{\bar{y}_0}{\bar{y}_1} a_y A_y Y_0 - d_{y_1} Y_1 \right) \quad (A.1d)$$

$$A' = \bar{t} \left(d_{x_0} \frac{\bar{x}_0}{\bar{a}} X_0 + d_{y_0}(Y_0) \frac{\bar{y}_0}{\bar{a}} Y_0 + d_{x_1} \frac{\bar{x}_1}{\bar{a}} X_1 + d_{y_1} \frac{\bar{y}_1}{\bar{a}} Y_1 - e_a \bar{s} A S \right) \quad (A.1e)$$

$$S' = \bar{t} \left(r_s \frac{\bar{a}}{\bar{s}} A - e_s S + \frac{I}{\bar{s}} \right) \quad (A.1f)$$

putting the mutation rate r_m to zero and where $d_{y_0}(Y_0) = \hat{d}_{y_0} + \hat{d}_{y_0} \bar{y}_0 \cdot Y_0$. Here prime denote the derivative with respect to the dimensionless time variable T . To simplify the hematopoietic steady state E_{H+} in Eq. (3), as much as we can, we choose

$$\bar{s} = \frac{d_{x_0} + a_x}{r_x} \sim 1 \quad (A.2a)$$

$$\bar{a} = \frac{e_s \bar{s}}{r_s} \sim 10^4 \quad (A.2b)$$

$$\bar{x}_0 = \frac{1}{c_{xx}} \sim 10^4 \quad (A.2c)$$

$$\bar{x}_1 = \frac{a_x A_x}{c_{xx} d_{x_1}} \sim 10^{11} \quad (A.2d)$$

$$\bar{y}_0 = \frac{1}{c_{yy}} \sim 10^4 \quad (A.2e)$$

$$\bar{y}_1 = \frac{a_y A_y}{c_{yy} d_{y_1}} \sim 10^{11} \quad (A.2f)$$

$$\bar{t} = \frac{1}{d_{x_0} + a_x} \sim 10^3 \text{ day} \quad (A.2g)$$

where the order is stated after the \sim symbol based on the default parameter values in Table 1. These values are in accordance with those reported in the literature where they are estimated to obtain observed cell counts, see (Gentry and Jackson, 2013; Haeno et al., 2009a; Stiehl et al., 2015). In addition, we have used 700 as a normal number of dead cells. For further details see (Andersen et al., 2017). Hence, system (A.1) becomes

$$X_0' = \left(\frac{S}{1 + (X_0 + \frac{c_{xy}}{c_{yy}} Y_0)} - 1 \right) X_0 \quad (A.3)$$

$$Y_0' = \left(\frac{r_y}{r_x} \frac{S}{1 + (\frac{c_{yx}}{c_{xx}} X_0 + Y_0)} - \frac{d_{y_0}(Y_0) + a_y}{d_{x_0} + a_x} \right) Y_0 \quad (A.4)$$

$$\epsilon_1 X_1' = (X_0 - X_1) \quad (A.5)$$

$$\epsilon_1 Y_1' = \frac{d_{y_1}}{d_{x_1}} (Y_0 - Y_1) \quad (A.6)$$

$$\epsilon_2 S' = \left(A - S + \frac{I}{e_s \bar{s}} \right) \quad (A.7)$$

$$\epsilon_2 \epsilon_3 A' = (b_{x_0} X_0 + b_{y_0}(Y_0) Y_0 + b_{x_1} X_1 + b_{y_1} Y_1 - AS) \quad (A.8)$$

where $\epsilon_1 = \frac{r_x}{d_{x_1}} \bar{s} \sim 10^{-5}$, $\epsilon_2 = \frac{r_x}{e_s} \bar{s} \sim 10^{-3}$, $\epsilon_3 = \frac{e_s}{e_a \bar{s}} \sim 10^{-10}$, $b_{x_0} = d_{x_0} \frac{\bar{x}_0 \bar{t}}{\bar{s} \bar{a}} \frac{d_{x_0} + a_x}{e_a} \sim 10^{-13}$, $b_{x_1} = d_{x_1} \frac{\bar{x}_1 \bar{t}}{\bar{s} \bar{a}} \frac{d_{x_0} + a_x}{e_a} \sim 10^{-1}$, $b_{y_0} = (\hat{d}_{y_0} + \hat{d}_{y_0} \bar{y}_0) \frac{\bar{y}_0 \bar{t}}{\bar{s} \bar{a}} \frac{d_{x_0} + a_x}{e_a} \sim 10^{-13}$, and $b_{y_1} = d_{y_1} \frac{\bar{y}_1 \bar{t}}{\bar{s} \bar{a}} \frac{d_{x_0} + a_x}{e_a} \sim 10^{-1}$. In addition $\frac{d_{y_1}}{d_{x_1}} \sim 1$, $\frac{c_{xy}}{c_{yy}} \sim 1$, $\frac{r_y}{r_x} \sim 1$, $\frac{d_{y_0} + a_y}{d_{x_0} + a_x} \sim 1$, and $\frac{1}{e_s \bar{s}} \sim 1^{-1}$.

We emphasize that the dimensionless variable X_0, X_1, Y_0, Y_1, S and A are all of the same order, since each are normalized by their 'maximal carrying capacity'.

A1. The reduced extended model - the reduced Cancitis model

The system is initially close to the unstable hematopoietic steady state and the development of MPNs is slow, thus we are interested in the reduced system. A naive QSSA may be performed but since several time scales are involved one should be careful. By Fenichel theory the Eqs. (A.3–A.8) involving small epsilon terms may be studied in the limit of vanishing left hand sides, whereby we obtain the reduced Cancitis model, i.e. the slow manifold approximation. Thus from Eq. (A.5–A.6) we obtain the algebraic relations,

$$X_1 = X_0. \quad (A.9a)$$

$$Y_1 = Y_0. \quad (A.9b)$$

Using this in Eq. (A.8) gives

$$\epsilon_4 A' = (2B_x X_0 + 2B_y Y_0 - AS) \quad (A.10a)$$

with $\epsilon_4 = \epsilon_2 \epsilon_3 \sim 10^{-13}$, $2B_x = b_{x_0} + b_{x_1} \approx b_{x_1} \sim 10^{-1}$, and $2B_y = b_{y_0} + b_{y_1} \approx b_{y_1} \sim 10^{-1}$. Thus we will consider B_y to be independent of Y_0 in what follows.

Thus, from Eq. (A.7) and (A.10a),

$$S = J \pm \sqrt{J^2 + 2B_x X_0 + 2B_y Y_0} \equiv S_{\pm} \quad (A.11)$$

where only S_+ is non-negative allowing us to disregard the possibility of $S = S_-$ in what follows and thus by substituting S_+ from Eq. (A.11) into the right hand side of Eq. (A.7) and putting this equal to zero we get,

$$A = \sqrt{J^2 + 2B_x X_0 + 2B_y Y_0} \quad (A.12)$$

which is always non-negative and where $J = \frac{I}{2e_s \bar{s}}$.

Hence, the reduced Cancitis model becomes a closed system in X_0 and Y_0 ,

$$X_0' = \left(\frac{J + \sqrt{J^2 + 2B_x X_0 + 2B_y Y_0}}{1 + X_0 + C_y Y_0} - 1 \right) X_0 \tag{A.13a}$$

$$Y_0' = \left(R \frac{J + \sqrt{J^2 + 2B_x X_0 + 2B_y Y_0}}{1 + C_x X_0 + Y_0} - D_0 - D_1 Y_0 \right) Y_0 \tag{A.13b}$$

where $R = \frac{r_y}{r_x}$, $D_0 = \frac{d_{y_0+a_y}}{d_{x_0+a_x}}$, $D_1 = \frac{d_{y_0} \bar{y}_0}{d_{x_0+a_x}}$, $C_x = \frac{c_{yx}}{c_{xx}}$, and $C_y = \frac{c_{xy}}{c_{yy}}$. The default dimensionless parameter values are listed in Table 2 and we note that all values are of order one. Note, the reduced model involves 8 parameters (including J) where D_1 describe the strength of the Y_0 dependent elimination term in dimensionless form. We emphasize the local existence and uniqueness of solution in the non-negative octahedron. Subsequently we will focus on the impact of the dimensionless inflammatory stimuli J .

Appendix B. Derivations of admissible Steady states

From Eq. (10a) the **hematopoietic steady state** $F_H = (X_0, 0)$ exist if and only if

$$J + \sqrt{J^2 + 2B_x X_0} = 1 + X_0, \tag{B.1}$$

i.e. if and only if

$$\sqrt{J^2 + 2B_x X_0} = X_0 + 1 - J. \tag{B.2}$$

Disregarding the possibility of double roots a solution exist if and only if $J < X_0 + 1$ (which have to be checked subsequently) given by,

$$X_0^2 - 2(J + B_x - 1)X_0 - (2J - 1) = 0, \tag{B.3}$$

i.e.

$$X_0 = (J + B_x - 1) \pm \sqrt{(J + B_x - 1)^2 + (2J - 1)} \tag{B.4a}$$

$$= (J + B_x - 1) \pm \sqrt{(J + B_x)^2 - 2B_x}. \tag{B.4b}$$

These roots are real if and only if $J \geq -B_x + \sqrt{2B_x}$, a trivial statement for $B_x > 2$ or $J > \frac{1}{2}$, which is not the case for the default parameters.

Putting $J_{H,1} = \frac{1}{2}$ and $J_{H,2} = 1 - B_x$ we may rewrite Eq. (B.3) as,

$$X_0^2 - 2(J - J_2)X_0 - 2(J - J_1) = 0, \tag{B.5a}$$

Applying Descartes' rule of signs gives that $X_{0+} > 0$ if and only if $J > \min\{J_1, J_2\}$ ($= \frac{1}{2}$ for default parameter values) and $X_{0-} > 0$ if and only if $J_2 < J < J_1$, requiring $B_x > \frac{1}{2}$ (which is not the default case).

The earlier condition $J < X_0 + 1$ may be examined and is equivalent to requiring,

$$\mp \sqrt{(J + B_x)^2 - 2B_x} < B_x, \tag{B.6a}$$

which is trivially fulfilled for X_{0+} . For X_{0-} , this gives

$$J < J_0 \equiv -B_x + \sqrt{B_x^2 + 2B_x}, \tag{B.7}$$

since J is restricted to be positive for physiological reasons.

Hence, F_{H+} is admissible if and only if $J > \min\{J_1, J_2\}$ ($= \frac{1}{2}$ for default parameter values) while F_{H-} is admissible if and only if

$$-B_x + \sqrt{2B_x} < J < -B_x + \sqrt{B_x^2 + 2B_x} \tag{B.8a}$$

and

$$1 - B_x < J < \frac{1}{2} \tag{B.9a}$$

i.e. if and only if

$$-B_x + \sqrt{2B_x} < J < \frac{1}{2} \text{ and } B_x > \frac{1}{2}, \tag{B.10a}$$

which is not in accordance with the default parameter values, meaning that in realistic cases only F_{H+} may be admissible.

The **Purely leukemic steady states** are the solutions of $g(Y_0, J) = 0$ with

$$g(Y_0, J) = R \frac{J + \sqrt{J^2 + 2B_y Y_0}}{1 + Y_0} - D_0 - D_1 Y_0, \tag{B.11}$$

where g is increasing with J . Inserting $Y_0 = 0$ give

$$J_{crit} = \frac{1}{2} \frac{D_0}{R}. \tag{B.12}$$

As $g(y, J)$ is increasing in J , $g(0, J) > 0$ for $J > J_{crit}$. For any fixed J , $g(y, J) < 0$ for y sufficiently large. Since g is continuous, the intermediate value theorem ensures that for any fixed $J > J_{crit}$ there exists a y satisfying $g(y, J) = 0$ i.e. a solution exists to (B.11).

Solutions of (B.11) are roots in the fourth order polynomial

$$\alpha_1 Y_0^4 + \alpha_2 Y_0^3 + \alpha_3 Y_0^2 + \alpha_4 Y_0 + \alpha_5 = 0, \tag{B.13}$$

with the constraint

$$\left(\frac{D_0}{R} + \frac{D_1}{R} Y_0 \right) (Y_0 + 1) > J. \tag{B.14}$$

where

$$\alpha_1 = \left(\frac{D_1}{R} \right)^2 \tag{B.15a}$$

$$\alpha_2 = 2 \frac{D_1}{R} \left(\frac{D_1}{R} + \frac{D_0}{R} \right) \tag{B.15b}$$

$$\alpha_3 = \left(\frac{D_0}{R} \right)^2 + \left(\frac{D_1}{R} \right)^2 + 2 \frac{D_1}{R} \left(2 \frac{D_0}{R} - J \right) \tag{B.15c}$$

$$\alpha_4 = 2 \left(\left(\frac{D_0}{R} - J \right) \left(\frac{D_0}{R} + \frac{D_1}{R} \right) - B_y \right) \tag{B.15d}$$

$$\alpha_5 = \frac{D_0}{R} \left(\frac{D_0}{R} - 2J \right). \tag{B.15e}$$

Note that $\alpha_1 > 0$, $\alpha_2 > 0$. For large J , α_3 , α_4 , α_5 are all negative so by Descartes' rule of sign there is exactly one positive root to the polynomial in this case showing that a leukemic steady state is inevitable for large inflammatory stimuli J .

Consider now $B_y < \frac{1}{2} \frac{D_0}{R} \left(\frac{D_0}{R} + \frac{D_1}{R} \right)$. The coefficients α_3 , α_4 , α_5 change sign once with increasing J . The root $J_{L,5}$ of $\alpha_5(J)$ being $\frac{1}{2} \frac{D_0}{R}$, is smaller than the root $J_{L,4}$ of $\alpha_4(J)$, which again is smaller than the root $J_{L,3}$ of $\alpha_3(J)$. This implies that as α_5 crosses zero a unique leukemic steady state is generated and it persists for any larger J values as there is exactly one sign change in the coefficients of the polynomial for any $J > \frac{1}{2} \frac{D_0}{R}$. Solving $\alpha_5 = 0$ gives (B.12). Thus the leukemic steady state emerges at $Y_0 = 0$ for $J = J_{crit}$.

For $B_y > \frac{1}{2} \frac{D_0}{R} \left(\frac{D_0}{R} + \frac{D_1}{R} \right)$, then α_3 remains positive for $J > J_{L,4}$ while α_4 and α_5 behave like in the previous case. Contrary to the previous case there exists a J between $J_{L,4}$ and $J_{L,5}$ such that $\alpha_4 < 0$ and $\alpha_5 > 0$. Hence, there are two sign changes in the coefficients of the polynomial, which indicate 0 or 2 roots. As J is increased such that $\alpha_5 < 0$ there is one sign change in the coefficients for all larger values of J .

The criterion $\alpha_5 > 0$ thus guarantees a unique, positive root to (B.13). Since at least one solution to (B.11) exists in this case, the root of the polynomial must satisfy (B.11).

As the polynomial on the left hand side of (B.13) is decreasing in J and the unique root for $J > \frac{1}{2} \frac{D_0}{R}$ occurs with a positive slope,

an increase in J must increase the value of the root i.e. $Y_{0L}(J)$ is increasing for any $J > \frac{1}{2} \frac{D_0}{R}$.

Notice, putting $g = 0$ in Eq. (B.11) is equivalent to Eq. (B.18) with $X_0 = 0$. Thus the leukemic steady state and the co-existing steady state are equal for $X_0 = 0$. By implicit function theorem it follows that for $Y_0 \geq Y_{0L}$ the derivative of $X_0 = X_0(Y_0)$ with respect to Y_0 is positive corresponding to an increasing steady state trajectory in J .

From Eq. (10) **co-existing steady states** $F_C = (X_0, Y_0)$ having positive components exist if and only if

$$J + \sqrt{J^2 + 2B_x X_0 + 2B_y Y_0} = 1 + X_0 + C_y Y_0 \tag{B.16}$$

and

$$J + \sqrt{J^2 + 2B_x X_0 + 2B_y Y_0} = (1 + C_x X_0 + Y_0) \left(\frac{D_0}{R} + \frac{D_1}{R} Y_0 \right). \tag{B.17}$$

Assuming solutions exist the equations are equivalent to,

$$1 + X_0 + C_y Y_0 = \left(\frac{D_0}{R} + \frac{D_1}{R} Y_0 \right) (1 + C_x X_0 + Y_0) \tag{B.18}$$

and

$$\sqrt{J^2 + 2B_x X_0 + 2B_y Y_0} = 1 + X_0 + C_y Y_0 - J. \tag{B.19}$$

Disregarding the possibility of double roots a solution exist if and only if

$$1 + X_0 + C_y Y_0 > J, \tag{B.20}$$

and

$$(1 + C_x X_0 + Y_0) \left(\frac{D_0}{R} + \frac{D_1}{R} Y_0 \right) > J, \tag{B.21}$$

which have to be checked subsequently.

Isolating X_0 in (B.18)

$$X_0 = \frac{(1 + Y_0) \left(\frac{D_0}{R} + \frac{D_1}{R} Y_0 \right) - C_y Y_0 - 1}{1 - C_x \left(\frac{D_0}{R} + \frac{D_1}{R} Y_0 \right)} \tag{B.22}$$

for non-vanishing denominator and substituting it into (B.19) gives the fourth order polynomial in Y_0 ,

$$\eta_0 Y_0^4 + \eta_1 (J - J_{C,1}) Y_0^3 + \eta_2 (J - J_{C,2}) Y_0^2 + \eta_3 (J - J_{C,3}) Y_0 + \eta_4 (J - J_{C,4}) = 0. \tag{B.23}$$

where

$$\eta_0 = - \left(\frac{D_1}{R} \right)^2 (C_x C_y - 1)^2 \tag{B.24}$$

$$\eta_1 = -2 \frac{D_1}{R} \left(C_x \frac{D_1}{R} - C_x^2 C_y \frac{D_1}{R} \right) \tag{B.25}$$

$$\eta_2 = \left(\left(4 \frac{D_0 D_1}{R^2} C_y + 2 \frac{D_1^2}{R^2} \right) C_x^2 + (-2 \frac{D_1^2}{R^2} - 2 \frac{D_1}{R} C_y - 4 \frac{D_0 D_1}{R^2}) C_x + 2 \frac{D_1}{R} \right) \tag{B.26}$$

$$\eta_3 = \left((2 C_y \frac{D_0^2}{R^2} + 4 \frac{D_0 D_1}{R^2}) C_x^2 + (-2 C_y \frac{D_0}{R} - 2 \frac{D_0^2}{R^2} - 4 \frac{D_0 D_1}{R^2}) C_x + (-2 \frac{D_1}{R}) C_x + 2 \left(\frac{D_0}{R} + \frac{D_1}{R} \right) \right) \tag{B.27}$$

$$\eta_4 = \left((2 \frac{D_0^2}{R^2}) C_x^2 + (-2 \frac{D_0^2}{R^2} - 2 \frac{D_0}{R}) C_x + 2 \frac{D_0}{R} \right) \tag{B.28}$$

and

$$J_{C,1} = \frac{1}{\eta_1} \left((-2 C_y^2 \left(\frac{D_0}{R} \right) + B_y \left(\frac{D_1}{R} \right) - 2 C_y \left(\frac{D_1}{R} \right)) C_x^2 + \left(2 \left(\frac{D_1}{R} \right) + 2(2 D_0 + D_1) \frac{C_y}{R} - B_x \frac{D_1}{R} \right) C_x + \frac{2}{R} (D_0 + D_1) \right) \tag{B.29}$$

$$J_{C,2} = \frac{1}{\eta_2} \left((C_y^2 \left(\frac{D_0}{R} \right)^2 + 2 \frac{D_0 D_1}{R^2} (2 C_y - B_y) + \frac{D_1^2}{R^2}) C_x^2 + \left(\frac{D_1^2}{R^2} (B_x - 2) - 2 C_y \frac{D_0^2}{R^2} - \frac{D_1}{R} (C_y B_x - 2 B_y) \right) C_x \right) + \frac{1}{\eta_2} \left(\frac{D_0 D_1}{R^2} (2 B_x - 4 C_y - 4) C_x - \frac{D_1}{R} B_x + 4 \frac{D_0 D_1}{R^2} + \frac{1}{R^2} (D_0^2 + D_1^2) \right) \tag{B.30}$$

$$J_{C,3} = \frac{1}{\eta_3} \left(\frac{D_0^2}{R^2} (2 C_y - B_y) + 2 \frac{D_0 D_1}{R^2} \right) C_x^2 + \left(\frac{D_0}{R} (-B_x C_y + 2 B_y) - \frac{D_0^2}{R^2} (-B_x + 2 C_y + 2) - \frac{D_0 D_1}{R^2} (-2 B_x + 4) \right) C_x - \frac{1}{\eta_3} \left(\left(\frac{D_1}{R} B_x \right) C_x - \left(\frac{D_0}{R} + \frac{D_1}{R} \right) B_x + B_x C_y - B_y + 2 \frac{D_0}{R^2} (D_0 + D_1) \right), \tag{B.31}$$

$$J_{C,4} = \frac{1}{\eta_4} \left(\frac{D_0^2}{R^2} C_x^2 - \left(2 \frac{D_0^2}{R^2} + \frac{D_0}{R} B_x - B_x \frac{D_0^2}{R^2} \right) C_x - \frac{D_0}{R} B_x + B_x + \frac{D_0^2}{R^2} \right). \tag{B.32}$$

For default values of parameters, Eq. (B.23) becomes

$$8.72 \cdot 10^{-6} Y_0^4 - 3.68 \cdot 10^{-3} (J + 0.61) Y_0^3 + 4.39 \cdot 10^{-2} (J + 1.06) Y_0^2 + (J - 0.71) Y_0 - 4(J - 0.27) = 0. \tag{B.33}$$

From the default parameters it follows that $J_{C,2} < J_{C,1} < 0 < J_{C,4} < J_{C,3} < J$ and by Descartes' rule of sign there exists one or three positive and real root if and only if $J > J_{C,4}$. From numeric considerations it follows that the number of positive Y_0 -roots are three. However, two of these cause X_0 to be negative in accordance with Eq. (B.20–B.21). Thus exactly one co-existing steady state exist.

References

Abdel-Wahab, O., Manshour, T., Patel, J., Harris, K., Yao, J., Hedvat, C., Heguy, A., Bueso-Ramos, C., Kantarjian, H., Levine, R.L., Verstovsek, S., 2010. Genetic analysis of transforming events that convert chronic myeloproliferative neoplasms to leukemias. *Cancer Res.* 70 (2), 447–452. doi:10.1158/0008-5472.CAN-09-3783.

Andersen, M., Sajid, Z., Pedersen, R., Gudmand-Hoeyerj Ellervik, C., Skov, V., Kjær, L., Pallisgaard, N., Kruse, T., Thomassen, M., Troelsen, J., Hasselbalch, H., Ottesen, J., 2017. Mathematical modelling as a proof of concept for MPNs as a human inflammation model for cancer development. *PLoS ONE* 12 (8), 1–18. doi:10.1371/journal.pone.0183620.

Arciero, J., Jackson, T., Kirschner, D., 2004. A mathematical model of tumor-immune evasion and siRNA treatment. *Discrete Continuous Dyn. Syst.-Series B* 4 (1), 39–58.

Baker, M., Denman-Johnson, B.B., Owen, M., 2013. Mathematical modelling of cytokine-mediated inflammation in rheumatoid arthritis. *Math. Med. Biol.* 30, 311–337.

Bangsgaard, E., Hjorth, P., Olufsen, M., Mehlsen, J., Ottesen, J., 2017. Integrated inflammatory stress (ITIS) model. *Bull. Math. Biol.* 79 (7), 1487–1509. doi:10.1007/s11538-017-0293-2.

Bangsgaard, E., Ottesen, J., 2017. Patient specific modeling of the HPA axis related to clinical diagnosis of depression. *Math. Biosci.* 287, 24–35. 10.1016/j.mbs.2016.10.007.

Besse, A., GD, C., Bernard, S., Nicolini, F., Levy, D., Lepoutre, T., 2018. Stability analysis of a model of interaction between the immune system and cancer cells in chronic myelogenous leukemia. *Bull. Math. Biol.* 80, 1084–1110.

- Borges, F., Iarosz, K., Ren, H., Batista, A., Baptista, M., Vianna, R., Lopes, S., Grebogi, C., 2014. Model for tumor growth with treatment by continuous pulsed chemotherapy. *Biosystems* 116, 43–48.
- Brady, R., Frank-Ito, D., Tran, H., Janum, S., Møller, K., Brix, S., Ottesen, J., Mehlsen, J., Olufsen, M., Math. Modell. Natural Phenom. (In process).
- Brianna M. Craver, B., Alaoui, K., Scherber, R., Fleischman, A., 2018. The critical role of inflammation in the pathogenesis and progression of myeloid malignancies. *Cancers* 10(4), 1–18.
- Campbell, P., Green, A., 2006. The myeloproliferative disorders. *N. Engl. J. Med.* 355, 2452–2466.
- Cavaillon, J.M., 1994. Cytokines and macrophages. *Biomed. Pharmacother.* 48, 445–453.
- Chen, S.-Y., Huang, Y.-C., Liu, S.-P., Tsai, F.-J., Shyu, W.-C., Lin, S.-Z., 2011. An overview of concepts for cancer stem cells. *Cell Transplant.* 20 (1), 113–120.
- Chow, C.C., Clermont, G., Kumar, R., Lagoa, C., Tawadrous, Z., Gallo, D., Betten, B., Bartels, J., Constantine, G., Fink, M.P., Billiar, T.R., Vodovotz, Y., 2005. The acute inflammatory response in diverse shock states. *Shock* 24 (1), 74–84. doi:10.1097/01.shk.0000168526.97716.f3.
- Clapp, G., Lepoutre, T., El Cheikh, R., Bernard, S., Ruby, J., Labussiere-Wallet, H., Nicolini, F., Levy, D., 2015. Implication of autologous immune system in bcr-abl transcript variations in chronic myelogenous leukemia patients treated with imatinib. *Cancer Res.* 75 (19), 4053–4062.
- Clodi, M., Vila, G., Geyeregger, R., Riedl, M., Stulnig, T.M., Struck, J., Luger, T.A., Luger, A., 2008. Oxytocin alleviates the neuroendocrine and cytokine response to bacterial endotoxin in healthy men. *Am. J. Physiol. Endocrinol. Metab.* 295, 686–691.
- Cosentino, Bates, 2012. *Feedback Control in System Biology*. CRC press.
- De Pillis, L.G., Radunskaya, A.E., Wiseman, C.L., 2005. A validated mathematical model of cell-mediated immune response to tumor growth. *Cancer Res.* 65 (17), 7950–7958. doi:10.1158/0008-5472.CAN-05-0564.
- Desterke, C., Martinaud, C., Ruzehaji, N., Le Bousse-Kerdilès, M.C., 2015. Inflammation as a keystone of bone marrow stroma alterations in primary myelofibrosis. *Mediators Inflamm.* 2015, pp.16. doi:10.1155/2015/415024.
- Dingli, D., Michor, F., 2006. Successful therapy must eradicate cancer stem cells. *Stem Cells* 24 (12), 2603–2610. doi:10.1634/stemcells.2006-0136.
- Dingli, D., Traulsen, A., Michor, F.L., 2007. (A)symmetric stem cell replication and cancer. *PLoS Comput. Biol.*
- Dong, Y., Miyazaki, R., Takeuchi, Y., 2014. Mathematical modeling on helper t cells in a tumor immune system. *Discrete Continuous Dyn. Syst. Series B* 19, 55–71.
- Dunster, J., HM, B., King, J., 2014. The resolution of inflammation: a mathematical model of neutrophil and macrophage interactions. *Bull. Math. Biol.* 76, 1953–1980.
- Flå, T., Rupp, F., Woywod, C., 2015. Bifurcation patterns in generalized models for the dynamics of normal and leukemic stem cells with signaling. *Math. Methods Appl. Sci.* 38 (16), 3392–3407. doi:10.1002/mma.3345.
- Gentry, S.N., Jackson, T.L., 2013. A mathematical model of cancer stem cell driven tumor initiation: implications of niche size and loss of homeostatic regulatory mechanisms. *PLoS one* 8 (8), e71128. doi:10.1371/journal.pone.0071128.
- Haeno, H., Levine, R.L., Gilliland, D.G., Michor, F., 2009. A progenitor cell origin of myeloid malignancies. *Proc. Natl. Acad. Sci. U.S.A.* 106, 16616–16621. doi:10.1073/pnas.0908107106.
- Haeno, H., Levine, R.L., Gilliland, D.G., Michor, F., 2009. A progenitor cell origin of myeloid malignancies - SUPPORTING INFO. *PNAS* (i).
- Hanson, S., Grimes, D., Taylor-King, J., Bauer, B., Warman, P., Frankenstein, Z., Kaznatcheev, A., Bonassar, M., Cannataro, V., Motawe, Z., Lima, E., Kim, S., Davila, M., Araujo, A., Toxicity Management in CAR T cell therapy for B-ALL: Mathematical modelling as a new avenue for improvement. doi:10.1101/049908.
- Hasselbalch, H., 2012. Perspectives on chronic inflammation in essential thrombocythemia, polycythemia vera, and myelofibrosis: is chronic inflammation a trigger and driver of clonal evolution and development of accelerated atherosclerosis and second cancer? *Blood* 119, 3219–3225.
- Hasselbalch, H., 2014. A role of nf- κ B in chronic inflammation and clonal evolution in essential thrombocythemia, polycythemia vera and myelofibrosis? *Leuk. Res.* 38 (2), 263–266. doi:10.1016/j.leukres.2013.07.002.
- Hasselbalch, H., Bjoern, M., 2015. Mps as inflammatory diseases: the evidence, consequences, and perspectives. *Mediators Inflamm.* 1–16. doi:10.1155/2015/102476.
- Herald, M., 2010. General model of inflammation. *Bull. Math. Biol.* 72, 765–779.
- Hermouet, S., Bigot-Corbel, E., Gardie, B., 2015. Pathogenesis of myeloproliferative neoplasms: role and mechanisms of chronic inflammation. *Mediators Inflamm.* 1–16. doi:10.1155/2015/145293.
- Katak, S., 2014. Mathematical modeling and analysis of tumor-immune system interaction by using lokta-Volterra predator-prey like model with piecewise constant arguments. *Period. Eng. Natural Sci.* 2 (1), 7–12.
- Kim, P., Lee, P., Levy, D., 2008. Dynamics and potential impact of the immune response to chronic myelogenous leukemia. *PLoS Comput. Biol.* 4 (6), e1000095.
- Kirschner, D., Panette, J., 1998. Modeling immunotherapy of tumor-immune interaction. *J. Math. Biol.* 37, 235–252.
- Komarova, N., Wodarz, D., 2007. Effect of cellular quiescence on the success of targeted cml therapy. *PLoS one* 48, e990.
- Komarova, N., Wodarz, D., 2014. *Birkhuser Basel, Springer Science+Business Media New York* doi:10.1007/978-1-4614-8301-4.
- Koschmieder, S., Mughal, T., Hasselbalch, H., Barosi, G., Valent, P., Kiladjian, J.-J., Jerczynski, G., Gisslinger, H., Jutzi, J., Pahl, J., Hehlmann, R., Vannucchi, A., Cervantes, F., Silver, R., Barbui, T., 2016. Myeloproliferative neoplasms and inflammation: whether to target the malignant clone or the inflammatory process or both. *Leukemia* 30 (5). doi:10.1038/leu.2016.12. 1018–24
- Kuehn, C., 2015. *General Fenichel Theory*, 191.
- Kuznetsov, V., Knott, C., 2001. Modeling tumor regrowth and immunotherapy. *Math. Comput. Model.* 33, 1275–1297.
- Kuznetsov, V., Makalin, I., 1994. Nonlinear dynamics of immunogenic tumors: parameter estimation and global bifurcation analysis. *Bull. Math. Biol.* 56 (2), 295–321.
- Larsen, T., Pallisgaard, N., Moeller, M., Hasselbalch, H., 2007. The JAK2V617F allele burden in essential thrombocythemia, polycythemia vera and primary myelofibrosis-impact on disease phenotype. *Eur. J. Haematol.* 79 (6), 508–515.
- McComb, S., Thiriot, A., Krishnan, L., Stark, F., 2013. Introduction to the Immune System, 1061. Humana Press, Totowa, NJ doi:10.1007/978-1-62703-589-7_1.
- Michor, F., Hughes, P. T., Iwasa, Y., Branford, S., Shah, N.P., Sawyers, C.L., Nowak, M.A., 2005. Dynamics of chronic myeloid leukaemia. *Nature* 435 (7046), 1267–1270. doi:10.1038/nature03669.
- Michor, F., Iwasa, Y., MA., N., 2006. The age incidence of chronic myeloid leukemia can be explained by a one-mutation model. *Proc. Natl. Acad. Sci. USA* 103, 14931–14934.
- Moore, H., Li, N., 2004. A mathematical model for chronic myelogenous leukemia (CML) and T cell interaction. *J. Theo. Biol.* 227, 513–523.
- Murphy, K., Travers, P., 2012. *Janeway's immunobiology*, 8th ed. Garland Science, New York.
- Nanda, S., Moore, H., Lenhart, S., 2007. Optimal control of treatment in a mathematical model of chronic myelogenous leukemia. *Math. Biosci.* 210, 143–156.
- Nielsen, K. H., Using Mathematical Modeling to Explore Glucotoxicity as a Precipitating Factor in Type 1 Diabetes as well as a Cause of Low-Grade Autoinflammation in Type 2 Diabetes Hyperglycemia as a Trigger for Autoimmune Diabetes. Ph.D. thesis.
- Nielsen, K.H., Ottesen, J.T., Pociot, F., 2013. Using Mathematical Modeling to Explore Glucotoxicity as a Precipitating Factor in Type 1 Diabetes as well as a Cause of Low-Grade Autoinflammation in Type 2 Diabetes Hyperglycemia as a Trigger for Autoimmune Diabetes.
- Parish, C., 2003. Cancer immunotherapy: the past, the present and the future. *Immunol. Cell Biol.* 81, 106–113.
- Pillis, L., Gu, W., Radunskaya, 2006. Mixed immunotherapy and chemotherapy of tumors: modeling applications and biological interpretations. *J. Theor. Biol.* 238, 841–862.
- Pillis, L., Radunskaya, A., 2003. The dynamics of an optimal controlled tumor model: a case study. *Math. Comput. Model.* 37, 1221–1244.
- Ribatti, D., 2017. The concept of immune surveillance against tumors: the first theories. *Oncotarget* 8 (4), 7175–7180.
- Robinson, C., 1999. *Dynamical Systems, Stability, Symbolic Dynamics, and Chaos*, Second CRC Press, Boca Raton, Fla.
- Roeder, I., Horn, M., Glauche, Hochhaus, A., Mueller, M., Loeffler, M., 2006. Dynamic modeling of imatinib treated chronic myeloid leukemia: functional insights and clinical implications. *Nat. Med.* 12 (10), 1181–1184.
- Saleem, M., Agrawal, 2012. Complex dynamics in a mathematical model of tumor growth with time delays in cell proliferation. *Int. J. Sci. Res. Publ.* 2 (6), 1–7.
- Sarkar, R., Banerjee, 2005. Cancer self remission and tumor stability – a stochastic approach. *Math. Biosci.* 196, 65–81.
- Smyth, M., Godfrey, D., Trapani, J., 2001. A fresh look at tumor immunosurveillance and immunotherapy. *Nat. Immunol.* 2, 293–299.
- Spivak, J., 2017. Myeloproliferative neoplasms. *N. Engl. J. Med.* 376 (22), 2168–2181. doi:10.1056/NEJMra1406186.
- Stiehl, T., Baran, N., Ho, A.D., Marciniak-Czochra, A., 2015. Cell division patterns in acute myeloid leukemia stem-like cells determine clinical course: A Model to predict patient survival. *Cancer Res.* 75 (6), 940–949. doi:10.1158/0008-5472.CAN-14-2508.
- Stiehl, T., Lutz, C., Marciniak-Czochra, A., 2016. Emergence of heterogeneity in acute leukemias. *Biol. Direct* 11 (51), 1–19. doi:10.1186/s13062-016-0154-1.
- Stiehl, T., Marciniak-Czochra, A., 2012. Mathematical modeling of leukemogenesis and cancer stem cell dynamics. *Math. Model. Nat. Phenom.* 7 (1), 166–202.
- Talkington, A., Dantoin, C., Durrett, R., 2018. Ordinary differential equation models for adaptive immunotherapy. *Bull. Math. Biol.* 80, 1059–1083.
- Tefferi, A., Vaidya, R., Caramazza, D., Finke, C., Lasho, T., Pardanani, A., 2011. Circulating interleukin (il)-8, il-2r, il-12, and il-15 levels are independently prognostic in primary myelofibrosis: a comprehensive cytokine profiling study. *J. Clin. Oncol.* 29, 1356–1363.
- Vaidya, R., Gangat, N., Jimma, T., Finke, C.M., Lasho, T.L., Pardanani, A., Tefferi, A., 2012. Plasma cytokines in polycythemia vera: phenotypic correlates, prognostic relevance, and comparison with myelofibrosis. *Am. J. Hematol.* 87 (11), 1003–1005. doi:10.1002/ajh.23295.
- Voit, E., 2013. *A First Course in System Biology*. Garland Science, Taylor & Francis Group, New York and London.
- Wilkie, K., 2013. *Systems Biology of Tumor Dormancy*. Chapter 10. A Review of Mathematical Models of Cancer-immune Interactions in the Context of Tumor Dormancy, 734. Springer-Verlag, New York doi:10.1007/978-1-4614-1445-2.
- Wodarz, D., Komarova, N., 2014. *World Scientific Publishing*.
- Zhang, J., Fleischman, A.G., Wodarz, D., Komarova, N.L., 2017. Determining the role of inflammation in the selection of JAK2 mutant cells in myeloproliferative neoplasms. *J. Theor. Biol.* doi:10.1016/j.jtbi.2017.05.012.

Appendix C

Data-driven analysis of *JAK2V617F* kinetics during interferonalpha2 treatment of patients with polycythemia vera and related neoplasms

Data-driven analysis of *JAK2V617F* kinetics during interferon-alpha2 treatment of patients with polycythemia vera and related neoplasms

Rasmus K. Pedersen¹  | Morten Andersen¹  | Trine A. Knudsen²  | Zamra Sajid¹  |
 Johanne Gudmand-Hoeyer¹  | Marc J. B. Dam¹  | Vibe Skov²  | Lasse Kjær²  |
 Christina Ellervik^{3,4,5,6}  | Thomas S. Larsen⁷  | Dennis Hansen⁷  | Niels Pallisgaard⁸ |
 Hans C. Hasselbalch²  | Johnny T. Ottesen¹ 

¹Department of Science and Environment, Roskilde University, Roskilde, Denmark

²Department of Haematology, Zealand University Hospital, Roskilde, Denmark

³Department of Production, Research, and Innovation, Region Zealand, Sorø, Denmark

⁴Faculty of Health and Medical Sciences, University of Copenhagen, Copenhagen, Denmark

⁵Department of Pathology, Harvard Medical School, Boston, FL, USA

⁶Department of Laboratory Medicine, Boston Children's Hospital, Boston, FL, USA

⁷Department of Hematology, Odense University Hospital, Odense, Denmark

⁸Department of Surgical Pathology, Zealand University Hospital, Roskilde, Denmark

Correspondence

Johnny T. Ottesen, Department of Science and Environment, Roskilde University, Universitetsvej 1, 4000 Roskilde, Denmark. Email: johnny@ruc.dk

Funding information

OEUH Frie Forskningsmidler. OEUH-Region Sjælland Fælles Forskningspulje. Fonden til Lægevidenskabens Fremme. Ellen og Aage Fausbølls Helsefond af 1975. Swedish Orphan. Den Forskningsfremmende Pulje for Kliniske Professorer ansat i Region Sjælland og ved Institut for Klinisk Medicin, Københavns Universitet. Regions Sjællands Sundhedsvidenskabelige Forskningsfond.

Abstract

Treatment with PEGylated interferon-alpha2 (IFN) of patients with essential thrombocythemia and polycythemia vera induces major molecular remissions with a reduction in the *JAK2V617F* allele burden to undetectable levels in a subset of patients. A favorable response to IFN has been argued to depend upon the tumor burden, implying that institution of treatment with IFN should be as early as possible after the diagnosis. However, evidence for this statement is not available. We present a thorough analysis of unique serial *JAK2V617F* measurements in 66 IFN-treated patients and in 6 untreated patients. Without IFN treatment, the *JAK2V617F* allele burden increased exponentially with a period of doubling of 1.4 year. During monotherapy with IFN, the *JAK2V617F* allele burden decreased mono- or bi-exponentially for 33 responders of which 28 patients satisfied both descriptions. Bi-exponential description improved the fits in 19 cases being associated with late *JAK2V617F* responses. The decay of the *JAK2V617F* allele burden during IFN treatment was estimated to have half-lives of 1.6 year for the monoexponential response and 1.0 year in the long term for the bi-exponential response. In conclusion, through data-driven analysis of the *JAK2V617F* allele burden, we provide novel information regarding the *JAK2V617F* kinetics during IFN-treatment, arguing for early intervention.

This is an open access article under the terms of the Creative Commons Attribution License, which permits use, distribution and reproduction in any medium, provided the original work is properly cited.

© 2020 The Authors. *Cancer Medicine* published by John Wiley & Sons Ltd.

KEYWORDS

early treatment, essential thrombocythemia, interferon-alpha2, *JAK2V617F* kinetics, myeloproliferative neoplasms, polycythemia vera, primary myelofibrosis

1 | INTRODUCTION

The classic Philadelphia chromosome-negative chronic myeloproliferative neoplasms (MPNs) encompass essential thrombocythemia (ET), polycythemia vera (PV), and primary myelofibrosis (PMF), including early prefibrotic myelofibrosis. These neoplasms arise due to an acquired stem cell insult with ensuing clonal myeloproliferation in the biological continuum from the early cancer stages (ET and PV) to the advanced myelofibrosis stage¹ and ultimately leukemic transformation.^{2,3}

Molecular markers for MPNs include *JAK2V617F*, *CALR* -and *MPL*-mutations. These mutations are the so-called driver mutations whereas additional mutations (e.g., *ASXL1*, *TET2*) are frequently recorded in the more advanced disease stages with severe myelofibrosis.⁴⁻¹² The *JAK2V617F* mutation associates with laboratory (hemoglobin level, leukocyte count, platelet count, CD34+ count, serum lactic dehydrogenase, and in vivo granulocyte and platelet activation) and clinical (pruritus, thrombosis, spleen size) outcomes^{8,13-25} and prognosis.^{13,17} Accordingly, a new concept of these diseases as a biological continuum from ET over PV to PMF has emerged, implying the *JAK2V617F* mutational load to reflect the tumor burden as assessed by a rising leukocyte count and increasing splenomegaly during disease progression toward myelofibrotic and leukemic transformation.²⁶ However, this hypothesis on the biological continuum is still being debated.

Interferon-alpha2 (IFN) has been used in the treatment of MPNs for about 30 years and several studies have convincingly demonstrated that this agent is safe and highly efficacious in normalizing elevated cell counts.²⁷⁻⁵² Indeed, prolonged treatment (about 5 years) may be followed by polyclonal hematopoiesis, normalization of the bone marrow and low-burden *JAK2V617F* in a subset of patients, even being sustained for 2-3 years after discontinuation of IFN.^{36,48}

These highly encouraging results have been the focus of increasing interest, since we may enter a new era with “Minimal Residual Disease” (MRD) as a novel treatment goal.^{36,44,48}

Early treatment to reduce or eradicate the malignant clone is of paramount importance for achievement of MRD or cure in all cancers. However, in MPNs a “watch and

wait” strategy is used in “low-risk” patients allowing the malignant clone to expand with the inherent risk of increasing genomic instability, sub-clone formation, resistance to treatment and disease progression from the early cancer stages (ET and PV) to the advanced metastatic cancer stage—myelofibrosis with bone marrow failure and ultimately leukemic transformation.

In recent years, the “watch and wait” strategy has been challenged by reports demonstrating the potential of IFN to induce MRD in an increasing number of patients.^{36,44,48} Furthermore, these studies also indicate that early treatment with IFN increases the chance of sustained hematological and molecular remissions. However, evidence for this statement is lacking.

As noted above, changes in the *JAK2V617F* allele burden before and during IFN-treatment have been studied extensively, whereas the time-scale kinetics of these changes still remain to be identified and described in detail.

In this study, we predict the *JAK2V617F* kinetics during IFN-treatment through data-driven analysis of serial *JAK2V617F* measurements in MPN patients receiving cytoreductive treatment with IFN only and patients being observed without cytoreduction. Evidence for tumor burden reduction through early intervention with IFN is provided, thereby challenging the “watch and wait” strategy commonly applied to low-risk MPN patients.

2 | METHODS

2.1 | Study design

2.1.1 | Prospective study

Data were obtained from two different study populations. *JAK2V617F* observations during PEGylated r-IFN α (IFN) monotherapy were obtained from 120 patients enrolled in the DALIAH trial (#EudraCT 2011-001919-31), which is an ongoing Danish multicenter prospective randomized open-label phase III clinical trial comparing IFN with hydroxyurea in MPN patients. Enrollment began in February 2012 and was completed in July 2015. Patients are followed for five years. The DALIAH trial was approved by the Danish Regional Science Ethics Committee and by the Danish Medicines Agency.

The clinical characteristics of the patients used in later analysis is shown in Table 1.

TABLE 1 Prospective study. Baseline demographics and clinical characteristics of *JAK2V617F* positive patients from the DALIAH trial randomized to IFN. Only patients with four or more measurements of the *JAK2V617F* allele burden are included

Characteristics	ET (n = 15)	PV (n = 39)	Pre-MF (n = 5)	PMF (n = 7)	Total (n = 66)
IFN type (IFN α -2a/ IFN α -2b)	10/5	21/18	3/2	2/5	36/30
Age (y)	53 (43-64)	64 (52-69)	62 (59-65)	64 (51-65)	62 (51-67)
Gender, male	6 (40)	20 (51)	3 (60)	6 (86)	35 (53)
History of major thrombotic event	0 (0)	12 (31)	1 (20)	2 (29)	15 (23)
<i>JAK2V617F</i> allele burden (%)	15 (10-21)	44 (22-62)	35 (19-40)	51 (50-88)	37 (19-51)
Haematocrit (vol%)	44 (39-47)	55 (48-59)	45 (41-45)	49 (37-51)	49 (45-55)
Haemoglobin (mmol/L)	9.0 (8.3-9.7)	11.4 (10.0- 12.3)	9.2 (8.6-9.5)	9.6 (7.2-10.2)	9.9 (9.1-11.8)
Platelets ($\times 10^9/L$)	730 (626-887)	538 (343-670)	681 (667-776)	460 (351-611)	611 (413-739)
White blood cells ($\times 10^9/L$)	8.9 (7.6-11.9)	9.9 (8.4-13.2)	9.2 (8.6-9.5)	10.8 (5.5-17.4)	9.7 (8.2-12.9)
Plasma lactate dehydrogenase (U/L)	193 (164-210)	229 (199-304)	281 (181-342)	367 (284-643)	222 (189-308)
Splenomegaly (≥ 13 cm by US)	2/9 (22)	11/26 (42)	1/4 (25)	7/7 (100)	21/46 (46)
Disease-related symptoms ^a	8 (53)	24 (62)	1 (20)	3 (43)	36 (55)
Phlebotomy before enrolment	2 (13)	35 (90)	1 (20)	4 (57)	42 (64)
Low-risk disease ^b	10 (67)	13 (33)	1 (20)	3 (43)	27 (41)

Note: Data are median (IQR) and n (%)

^aConstitutional symptoms, microvascular disturbances and pruritus

^bAge ≤ 60 y of age, platelets ≤ 1500 ($\times 10^9/L$) and no prior major thrombosis

2.1.2 | Retrospective study

We retrospectively obtained information on *JAK2V617F* kinetics in six untreated (i.e., no cytoreductive therapy) MPN patients followed at the outpatient clinic at the Department of Haematology, Zealand University Hospital, Denmark. Four patients had previously received cytoreductive therapy with either r-IFN α -2a (Pegasys[®]) or r-IFN α -2b (PegIntron[®]) (n = 2) or monotherapy with both HU and r-IFN α -2a (n = 2) according to standard care, but had discontinued therapy due to intolerability (r-IFN α -2a: n = 2, HU: n = 2) and/or hematologic response in concert with a low *JAK2V617F* allele burden (r-IFN α -2a: n = 1, r-IFN α -2b: n = 1). Patient (A) discontinued treatment due to *JAK2V617F* $< 1\%$ for more than 1 year after r-IFN α -2b exposure and patient C discontinued r-IFN α -2a due to complete hematologic response in concert with a low *JAK2V617F* allele burden (6%). Two patients had not received any prior cytoreductive treatment. At the time of inclusion in the study all untreated patients had been off

cytoreductive treatment for at least 0.5 months (median: 1.2 month; range 0.5-5.3 months).

Patients were evaluated for enrollment when attending regular appointments between 1st of May 2018 and 15th of December 2018.

Written informed consent was provided from all patients according to the Declaration of Helsinki.

The clinical characteristics of the patients in the retrospective study are shown in Table 2.

2.2 | MPN diagnosis and eligibility

Eligibility criteria were age ≥ 18 years and a diagnosis of *JAK2V617F* positive Philadelphia chromosome negative MPN according the World Health Organization criteria.⁵³ Patients from the DALIAH trial were all newly diagnosed or previously phlebotomized only, and all had evidence of active disease at enrolment. Active disease was defined by a requirement for phlebotomy, WBC $> 10 \times 10^9/L$ or

Characteristics	ET (n = 1)	PV (n = 4)	Post-PV MF (n = 1)	Total (n = 6)
Age (y)	68	66 (59-70)	75	68 (59-75)
Gender, male	0 (0)	4 (80)	1 (100)	5 (83)
History of major thrombohemorrhagic event	0 (0)	3 (75)	0 (0)	3 (50)
Prior cytoreductive therapy	1 (100)	2 (50)	1 (100)	4 (67)
Hydroxyurea	1 (100)	0 (0)	1 (100)	2 (33)
r-IFN α -2a	1 (100)	1 (100)	1 (100)	3 (50)
r-IFN α -2b	0 (0)	1 (100)	0 (0)	1 (17)
Time off cytoreductive therapy before first <i>JAK2V617F</i> measurement (months)	0.5	1.2 (0.6-1.8)	5.3	1.2 (0.5-5.3)
<i>JAK2V617F</i> allele (%)	6	6 (0.7-27)	93	8.5 (0.7-96)

TABLE 2 Retrospective study. Baseline demographics and clinical characteristics of *JAK2V617F* patients from the outpatient clinic at the time of first *JAK2V617F* measurement

platelets $> 400 \times 10^9/L$ in the absence of infection or inflammation, hypermetabolic symptoms ie weight loss $> 10\%$ within 6 months, night sweats, low-grade fever for more than 2 weeks without signs of infection, pruritus, splenomegaly with symptoms, or previous thrombosis.

Eligible patients from the outpatient clinic studied retrospectively off cytoreductive treatment have been described above.

2.3 | Intervention

DALIAH patients received monotherapy with either IFN α -2a or r-IFN α -2b subcutaneously once weekly at a starting dose of 45 and 35 μg , respectively. Dose escalation was performed in a stepwise manner at pre-defined time points in the absence of a complete hematological response (i.e., WBC $> 10 \times 10^9/L$ or platelets $> 400 \times 10^9/L$) after 4 and 12 months and in the absence of a partial or complete molecular response according to the 2009 European LeukaemiaNet (ELN) criteria⁵⁴ after 8 and 18 months. However, the IFN dose was de-escalated by the treating physician to the highest tolerable dose in the event of drug-related toxicity. Toxicity was graded according to the Common Terminology Criteria for Adverse Events (CTCAE) version 4.0 and IFN was discontinued in the event of grade 4 events or recurrent grade 3 events (See Supplementary Material E).

2.4 | Molecular diagnosis and *JAK2V617F*

The *JAK2V617F* allele burden was accessed by a highly sensitive quantitative real-time polymerase chain reaction (qPCR) on DNA from peripheral blood,⁵⁵ which has been assessed as the European Reference Assay.⁵⁶ In the DALIAH-trial, *JAK2V617F* measurements were performed every three

months the first year, once every six months the second year, and yearly thereafter until the end of the study. For patients followed in the outpatient clinic, the *JAK2V617F* allele burden was assessed according to the physician's decision. All patients with four or more *JAK2V617F* samples were eligible for data-driven analysis.

2.5 | *JAK2V617F* allele burden development in untreated patients

Due to the expanding nature of malignant cells, the *JAK2V617F* allele burden in untreated patients is expected to increase exponentially. Hence, it is reasonable to assume that an exponentially increasing function can be fitted to data and an exponential growth-rate for specific patients can be found.

To generalize from multiple patient-specific growth-rates, we calculated the mean of the growth-rates, resulting in an expression of the growth on a population level. The expression describes the expected growth of the *JAK2V617F* allele burden in a larger population across multiple orders of magnitude, even if the estimate is made on a small sample of the population. Since the *JAK2V617F* allele burden varies at diagnosis, we shifted data in time such that the individual patient-specific fits coalesced with the population-level growth-curve at the mean time of these observations. Data were then pooled into a single data-set, and the exponential growth was estimated, see Table S5. All growth rates were found with MATLAB R2018a, using the least square fitting method *fit* included in the *curve fit* toolbox.

Of the six patients available for this analysis, one was excluded since all measurements were $\geq 90\%$, and thus above the point at which the growth is expected to be exponential. Note that this patient is the single post-PV MF patient shown in Table 2. For two of the remaining patients, a low number of *JAK2V617F* measurements were available, due to which these

were excluded in the initial part of the analysis. This leaves three remaining patients, referred to as patient A, B, and C.

2.6 | *JAK2V617F* allele burden development during IFN monotherapy

To describe the *JAK2V617F* development in IFN treated patients, two simple descriptive models were fitted to the time series measurements. The first model is that of a monoexponential decay, i.e., of the form $Ae^{-\alpha t}$ (with A and α being positive constants and t the time from treatment onset), while the second model features a bi-exponential decay $Be^{-\beta t} - Ce^{-\gamma t}$ (With B , C , β and γ being positive constants and t the time from treatment onset) with the requirement that the slope at treatment onset is equal to the slope found for the monoexponential growth. This reduces the number of independent parameters from four to three. The bi-exponential model can be considered an extension of the mono-exponential model with the bi-exponential model describing a similar response but allowing for an initial *JAK2V617F* increase before the decay starts.

Since the bi-exponential model has three parameters, patients with three or less *JAK2V617F* measurements were excluded. This reduced the number of datasets available from 120 to 66. We identified how well the models fit data by the adjusted R^2 -value, as described in supplementary material A. Thus, fits with an adjusted R^2 -value below a threshold of 0.6 were excluded from further analysis. The analysis for each of the two models was done independently.

3 | RESULTS

3.1 | *JAK2V617F* allele burden development in untreated patients

Raw data used to estimate the *JAK2V617F* allele burden development in untreated patients are depicted in Figures S72-S76.

Three patients (A, B and C) received IFN treatment up to the date of the initial measurement.

After IFN discontinuation, there was an initial delayed response in the *JAK2V617F* allele burden of approximately 200 days. Only data after the initial delayed response were used to determine the growth-rates. Data are illustrated in Figure 1 as well as the least-square fits of mono-exponential growth to the data, with 95% prediction intervals.

An exponential growth-rate implies a constant period of doubling. The periods of doubling found for patients A, B, and C are shown in Table S5, along with confidence intervals.

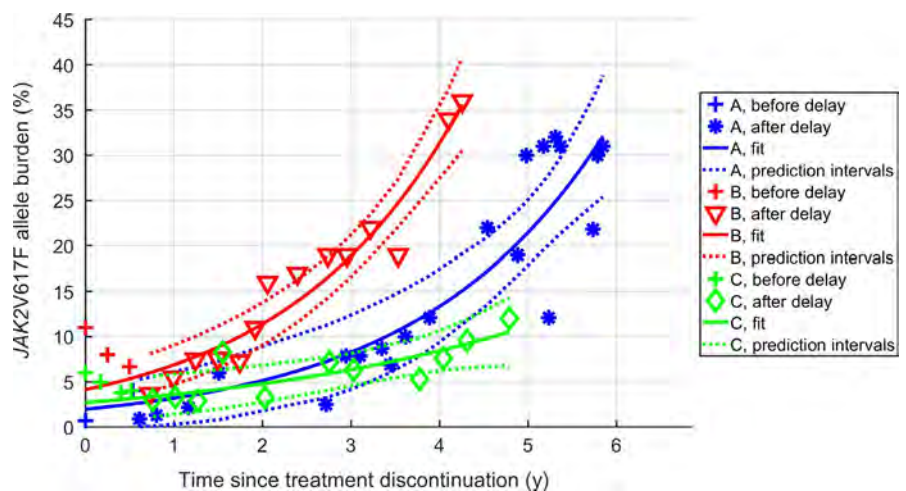
By pooling the data together, a new fit was made, yielding a general expression for the growth at population level. The resulting population level expression is shown in Figure 2 along with the pooled data and data for the two additional datasets which had only few *JAK2V617F* measurements. The additional datasets were timeshifted such that the mean of the *JAK2V617F* allele burden coalesced with the growth curve at the mean day of the dataset. While the two additional patients were not included in the fitting procedure, the data did not falsify the population level growth of the pooled data.

The period of doubling of the pooled data was found as 1.4 years (CI: 1.2 to 1.7 years). This implies that the allele burden grows from 0.01% to 1% in 9.3 years, while the growth from 1% to 33% takes 7.1 years. Therefore, detecting the *JAK2V617F* allele burden $\leq 1\%$ allows for a much longer time-window for detection and early therapeutic intervention before symptoms arise.

3.2 | *JAK2V617F* allele burden development during IFN monotherapy

All 66 eligible data-sets are depicted in the Figure S6 through S71.

FIGURE 1 *JAK2V617F* allele burden development in untreated patients. Serial measurements for patients A, B and C with least-square fits of exponential growth with 95% prediction intervals. Fits were based only on data after the initial delayed response



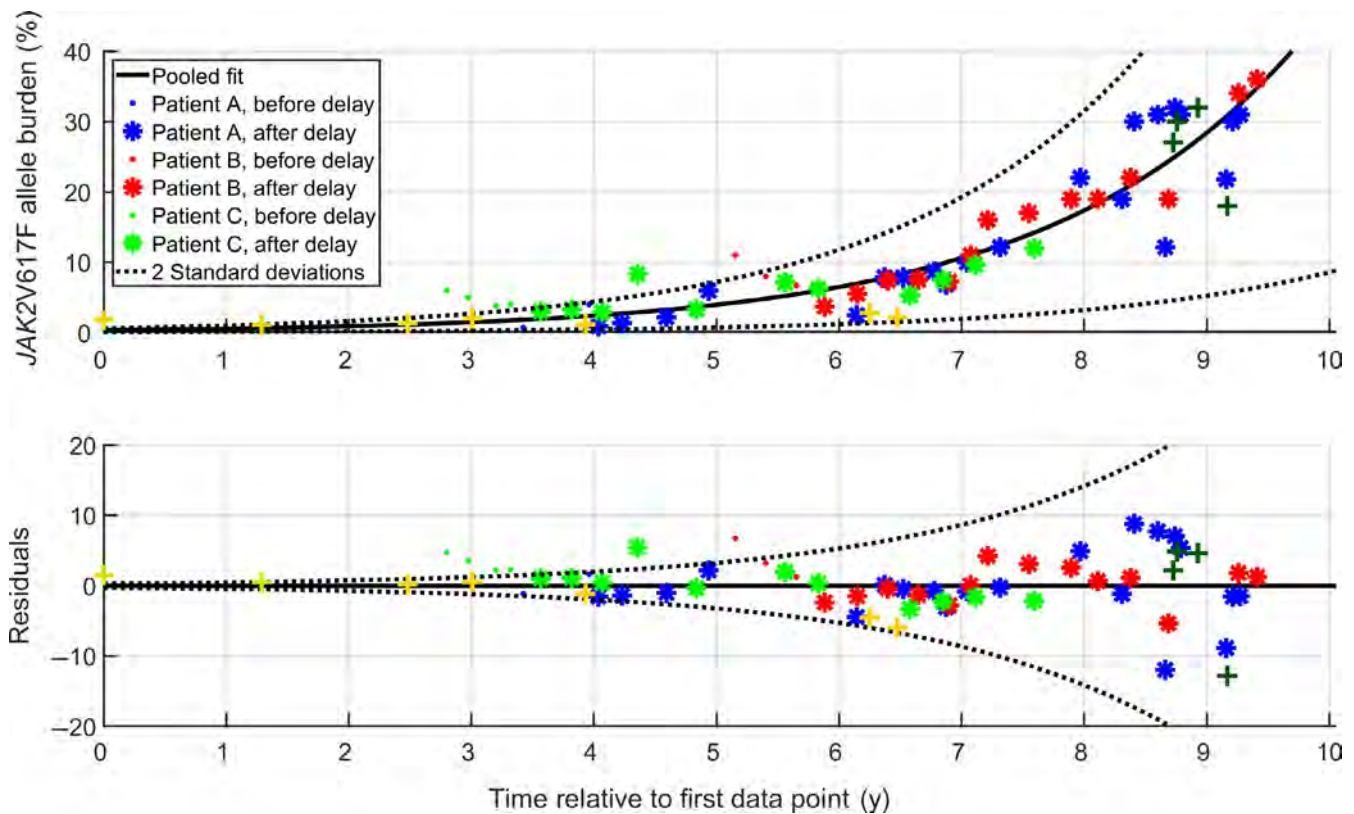


FIGURE 2 Exponential growth of the *JAK2V617F* allele burden. The top displays the exponential growth fit of the pooled data, while the bottom displays the relative residuals scaled with the size of allele burden. +-marks indicate the two patients with very few *JAK2V617F* measurements. The initial delayed response is included as dots. Each subject is depicted with a specific color. Two standard deviations around the mean of the scaled residuals are shown

Patient-specific parameters for the fits, the goodness of the fits, and which model was the better descriptor are shown in Supplementary Material A.

To generalize the *JAK2V617F* kinetics, a threshold for the goodness-of-fit was chosen and estimates for the population-level parameters were found, see Supplementary Material B.

Fits of 28 patients were deemed satisfactory for both response types (i.e., both mono- and bi-exponential). For 14 of these patients, the bi-exponential response was found to be the better fit for the patient data. Note that the goodness-of-fit measure chosen takes the complexity of the models into account, and as such the simpler monoexponential response was preferred when the models yielded almost identical results. Five additional patients had satisfactory fits for the bi-exponential response type but not for the monoexponential. Thus, the bi-exponential model was the best fit for 19 patients.

The datasets for the remaining 33 patients either featured responses not following any of the models or had no decay in the *JAK2V617F* allele burden and are hence considered nonresponders in the context of molecular response.

The monoexponential model using the population decay-rate is shown in Figure 3, along with patient-data for the patients for whom the goodness-of-fits were above the threshold.

The population decay rates found for the monoexponential model corresponded to a half-life of 575 days, or 1.6 years. (95% CI of the decay rates yields half-lives between 0.8 and 11.6 years).

For the monoexponential decay, the development was the same across all orders of magnitude, allowing for a single representative figure, Figure 3. Although the bi-exponential model features an initial growth depending on the starting level, it has a long-term behavior which is approximately monoexponential. This long-term behavior corresponds to a half-life of 1 year (CI: 0.2-4.3 years).

3.3 | Comparison of *JAK2V617F* allele burden development during early and late IFN monotherapy

In *silico* treatment schemes can be considered using the population level models and the growth rates found. Figure 4 displays the increase and decrease in *JAK2V617F* allele burden, with initiation of IFN treatment 7, 8 and 9 years after the allele burden reached 1%. The figure shows both the monoexponential response as well as the bi-exponential response at population level.

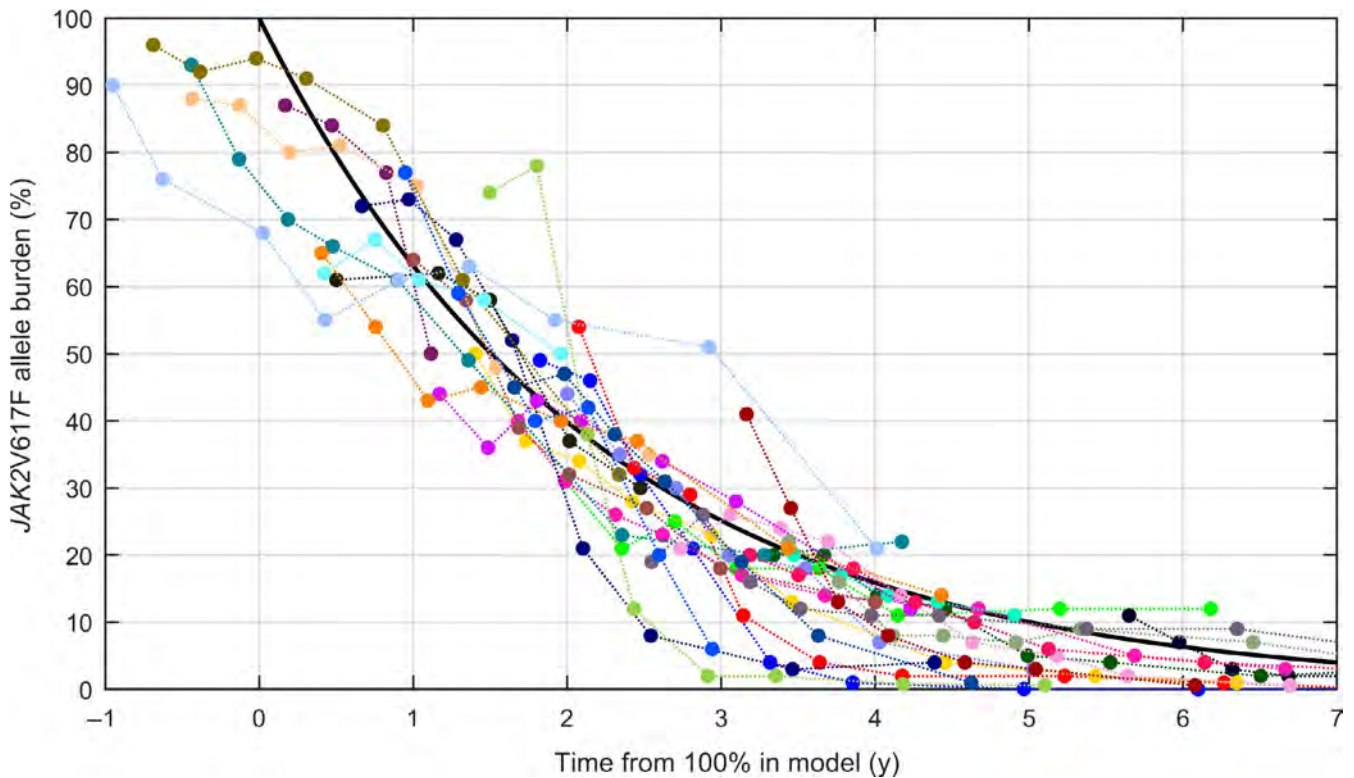
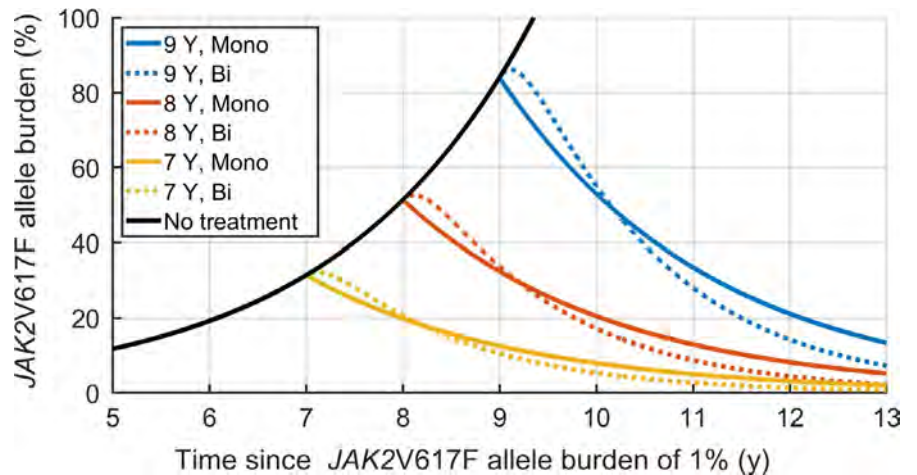


FIGURE 3 Population-level decay rate. The population-level decay rate of the mono-exponential model is shown in black, with data for the 29 patients with the best goodness-of-fits. Note that data were shifted in time such that the mean of the *JAK2V617F* allele burden coincides with the main curve at the mean day of measurement

FIGURE 4 Prediction of *JAK2V617F* development during IFN treatment. *JAK2V617F* development over time estimated by either the mono-exponential or bi-exponential response (full lines: Mono-exponential, dotted lines: bi-exponential), with simulated treatment starting at 7, 8 and 9 y after 1% was reached



The figure suggests that the initial 6 months of IFN treatment are associated with minor or no decrease in the *JAK2V617F* allele burden for the bi-exponential response. However, after a year, the *JAK2V617F* allele burden decreases faster than for the monoexponential response. As such, the efficacy of the treatment in decreasing the *JAK2V617F* allele burden may be difficult to determine within the first year.

From a specific baseline *JAK2V617F* allele burden, the population-level responses can be used to estimate the duration of treatment necessary to achieve a *JAK2V617F* allele

burden of 1%. In Figure 5 the duration of treatment necessary is illustrated, when treatment is initiated at a given *JAK2V617F* allele burden.

The monoexponential response features a longer treatment period necessary than the bi-exponential response, when the initial *JAK2V617F* allele burden is greater than a few percent. As such, even if a patient has an initial increase in *JAK2V617F* allele burden as is the case for the bi-exponential response, 1% will be reached faster than if the response was monoexponential.

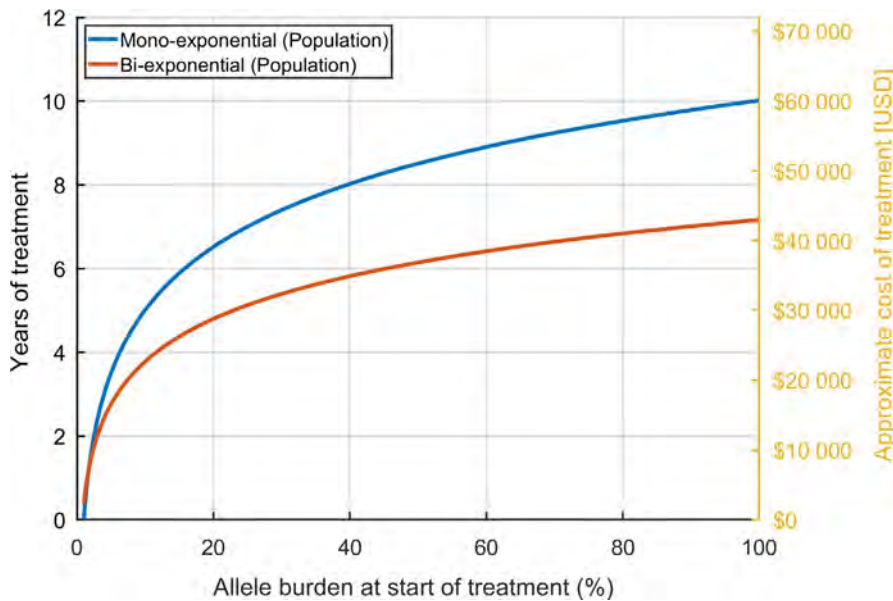


FIGURE 5 Estimated cost of IFN treatment. Years of treatment necessary to reach a *JAK2V617F* allele burden of 1%, if treatment is initiated at the allele burden shown on the first axis. The approximate monetary cost of IFN treatment (estimated price: \$500 USD/month) is also included

Figure 5 also includes a rough estimate of the total medical expenses to IFN treatment (approximately \$500 USD/month) based on the *JAK2V617F* allele burden at treatment onset. While relapse after treatment is still possible, the figure illustrates that the total cost of IFN treatment increases with the *JAK2V617F* allele burden at treatment onset due to the need for longer treatment duration to reach a specific *JAK2V617F* target value.

3.4 | Time span of the *JAK2V617F* allele burden development

The growth of the *JAK2V617F* allele burden from 0.01% to 1% was found to span almost a decade, while further growth to 33% required approximately 7 years. If patients are screened for the *JAK2V617F* mutation on a regular basis, eg once every 10 years, a detection limit of 1% might miss the disease onset, since the *JAK2V617F* allele burden would exceed 33% before the next screening. Conversely, a detection limit of 0.01% could be expected to identify an allele burden below 1% during the 9.3-year period, or it may grow to 1.4% 10 years after an allele burden of 0.01%. This also emphasizes the importance of methods to quantify the *JAK2V617F* allele burden down to low levels, in particular below 1%.

Although exponential growth may not be expected for low numbers of cells, extrapolating back to the time at which the initial mutation appeared (i.e., an allele burden corresponding to a single cell) yields a conservative estimate of the time span of the development before symptoms arise and MPN is diagnosed. The *JAK2V617F* allele burden for patients diagnosed with PV has previously been estimated as 33% (CI: 20-40).⁵⁷ We assume that the

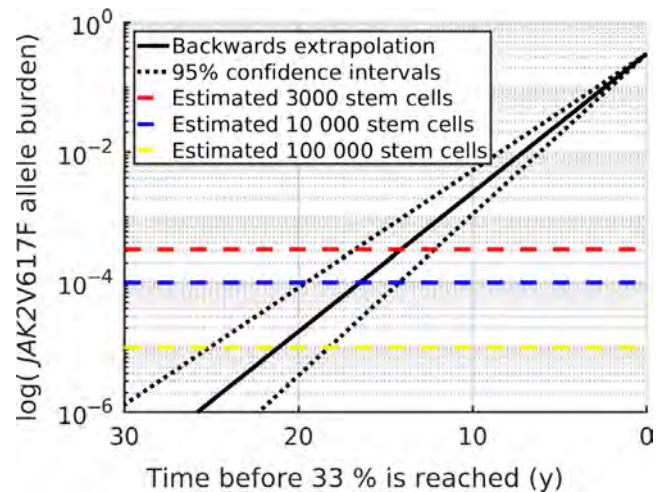


FIGURE 6 Backwards extrapolation to onset of initial mutation. The growth rate (and confidence intervals in dotted black) extrapolated back in time from 33%. The dashed lines mark the limits of $10^{-3.5}$, 10^{-4} and 10^{-5} as discussed in the text, in red, blue and yellow, respectively. Note the logarithmic y-axis

JAK2V617F allele burden in the peripheral blood and of the stem cells are similar. The total number of stem cells has been estimated to be between 11 200 and 22 400 cells,⁵⁸ which is of order 10^4 . As such, an estimate of the allele burden at initial mutation is 10^{-4} , ie one out of 10^4 . This implies a total time from initial mutation to allele burden of 33% of around 16.5 years (CI: 14.2-19.5 years). This estimate of the timespan of MPN development is in agreement with the literature.⁵⁹

Figure 6 shows the extrapolation from an allele burden of 33% backwards in time, with the growth-rate found. The estimate is highly dependent on the total number of stem cells. If another estimate of the number of stem cells is

used, the period before 33% is reached can be found from the graph, as well as the confidence intervals. Estimating a lower stem cell count of 3000⁶⁰ leads to an allele burden of $10^{-3.5}$ at initial mutation, and the time of development would be approximately 14 years. Similarly, estimating a stem cell count between 50 000 and 200 000 as in a most recent paper⁶¹ leads to an initial allele burden around 10^{-5} , and consequently a timespan of 21 years for the development of MPNs.

4 | DISCUSSION

In recent years, the interest of using IFN in the treatment of MPNs has increased due to studies reporting long-term treatment with IFN to be associated with MRD in a subset of patients as defined by sustained complete hematological remissions in concert with induction of low-burden *JAK2V617F* and normalization of the bone marrow.^{36,44,48} Even in the IFN era of 2019 where several safety and efficacy studies have enrolled > 1000 patients during the last 30 years, the MPN scientific community still recommends patients with low risk disease to be observed without any cytoreductive treatment. Using this “watch and wait” strategy translation of common knowledge on cancer biology to MPNs is neglected, implying progression of any cancer without treatment. Early treatment with IFN has been claimed to be a prerequisite for obtaining remarkable results to prohibit clonal evolution before subclones and additive mutations evolve.^{38,40,41,62-67}

The present study delivers novel information regarding the *JAK2V617F* kinetics during IFN-treatment based upon unique serial *JAK2V617F* measurements from the DALIAH trial. Through this description of the *JAK2V617F* kinetics, predictions about the development of disease for specific patients can be made. In untreated patients (i.e., without cytoreductive treatment), the *JAK2V617F* allele burden was demonstrated to grow exponentially with doubling time of 1.4 years (CI: 1.2 to 1.7 years). During IFN treatment, the *JAK2V617F* development followed either a monoexponential or a bi-exponential decay for a significant proportion of patients, with both models describing the development to a satisfactory extent for 28 patients. In a total of 33 patients, the bi-exponential response was found to be the better descriptor of the development when adjusting for model complexity.

The individual *JAK2V617F* developments were combined into two models of the development on a population level. The population-level model of the monoexponential decay showed a half-life of the *JAK2V617F* allele burden of 1.6 years (CI: 0.8 to 11.6 years), while the long-term behavior of the bi-exponential decay displayed a half-life of 1 year (CI: 0.2-4.3 years).

We emphasize that since these population-level models are based on a subset of patients who respond well to treatment, the models do not necessarily generalize to all patients. Determining the development for the poor responders remains an open problem as well as determining why there is a difference in the treatment response.

Analysis of the population-level responses suggests that treatment schemes should extend longer than one year, as the efficacy of IFN treatment on the *JAK2V617F* allele burden cannot be determined after just one year. By comparing early and late treatment modalities, our results suggest that treatment outcome will improve if IFN therapy is initiated early, or will in any case lead to early identification of patient response type. Additionally, some patients had a significantly slower response to treatment compared to other patients. For these slow-responders, our results show, that treatment should be initiated as early as possible, since a “watch and wait” strategy increases the time needed to obtain responses drastically for each day spent watching and waiting.

We and others have argued against the “watch and wait” strategy in low-risk patients.^{38,40,41,62-67} Our study emphasizes the urgent need to rethink this approach and set new standards for treatment of patients with MPNs, implying normalization of cell counts in all patients using IFN from the time of diagnosis. In addition to the rationales provided by the results in our present study, several others are supportive of the early-IFN-intervention concept. Thus, cancer biology in general dictates that any cancer steadily evolves over time with expansion of the malignant clone, increasing genomic instability, subclone formation and ultimately metastasis. Fortunately, MPNs are slowly growing neoplasms which have several transitional stages in the biological continuum from the earliest cancer stages (eg *JAK2V617F* and *CALR* mutations in the background population as clonal hematopoiesis of indeterminate potential (CHIP)) to ET, PV, and the advanced cancer stage with myelofibrosis, bone marrow failure, and huge splenomegaly before terminal leukemic transformation. During this MPN-biological continuum, the *JAK2V617F* mutation will steadily increase in those individuals who develop overt MPN in concert with an increase in the chronic inflammatory load that drives the malignant clone and likely fuels the development of additional mutations as well.⁶⁴⁻⁶⁷ Thus, in this context, it is tempting to suggest that the total number of mutated cells present at any given time may be the driver of additive mutations. Indeed, the sum of the *JAK2V617F* allele burden over a period of time may provide a measure for the risk of additive mutations as it correlates with the number of mutated cells in the given the period. As shown in Supplementary Material C, this measure—as assessed by the *JAK2V617F* allele burden—increases exponentially with the time spent without

treatment. Although speculative, this suggests that, after enough time has passed above a certain threshold, the potential risk of additive mutations may have the same exponential growth-rate (and thus the same period of doubling) as the growth of the *JAK2V617F* allele burden before treatment is initiated. As such, although the exact risk cannot be determined, postponing treatment by 1.4 years will double the risk of an additive mutation. Further data-driven mathematical studies on this potential association are needed, including results from next generation sequencing in IFN-treated *JAK2V617F* positive MPN-cohorts.

Treatment with IFN is associated with drop-out rates of 20%-30% and in some studies even up to 40% due to toxic side effects.³⁷⁻⁴³ It has been speculated whether intolerance to IFN is also dependent upon disease stage, implying more toxic side effects in the advanced myelofibrosis stage and less so in the early disease stages. If so, evidence for exponential growth with doubling time of 1.4 years further undermines the "watch and wait" strategy and adds to the rationales of early treatment with IFN.

Our results deliver important information about treatment duration with IFN to obtain deep molecular remissions and long-lasting sustained remissions after drug discontinuation. The mathematical models presented serve as a novel platform for predicting IFN response in individual patients. More advanced mechanism-based mathematical models are foreseen to allow for improved prediction and insight into IFN response.

Our study dictates that institution of IFN at the earliest time point possible may have important socio-economic implications as well. By minimizing the risk of complications (thrombosis, hemorrhages or cancer), a huge economic burden due to hospitalizations is likely markedly reduced. Importantly, costs concerning rehabilitation after these complications are reduced as well. Another important consequence of early treatment with IFN is the outlook to achieve MRD and at this time point the possibility of discontinuation of IFN for several years (up to 3-5 years) when the patient is feeling healthy with normal cell counts. Of note, our study also suggests that early treatment with IFN is cost-effective, implying a shorter treatment period with IFN if treatment is instituted at the earliest time point possible.

Although our data are supportive of early intervention with IFN it is important to underscore that our data do not deliver the clinical proof for this early intervention recommendation. This proof can only be delivered by the demonstration of reduction in clinically relevant end-points such as thrombotic events, rate of transformation to myelofibrosis and acute leukemia. Indeed, the demonstration of these hard end-points would require long-term follow up of large cohorts of patients treated with IFN and a well-designed control group. This study has never been reported and will

likely never be reported in these orphan diseases, where randomized studies are so difficult to conduct - in particular with follow-up times of decades rather than for instance 5 years, when taking into account that leukemic transformation in general is a late event, developing in the advanced myelofibrosis stage of MPNs. Importantly, the randomized Proud/Continuation-PV Phase III Trials showed RopegIFN (Besremi®) to be associated with a clear benefit over control (ie hydroxyurea) in achieving significant higher maintenance rates of complete hematological remission (CHR) over the course of treatment and in showing a significant lower risk of losing CHR. Since CHR can be considered as surrogate for risk of thrombosis, RopegIFN may be an optimal treatment modality for managing risk of thrombosis.⁷⁰

Our study has some limitations. Firstly, our estimate of the development of the *JAK2V617F* allele burden was based specifically on the data from three patients only (A, B, and C) and longitudinal *JAK2V617F* allele burden measurements in more patients might have substantiated and strengthened our findings of an exponentially growing pattern, which has not previously been described mathematically. Secondly, we did not include serial measurements of the *JAK2V617F* allele burden after discontinuation of hydroxyurea. Unfortunately, we have not such data in our cohort of patients. However, based upon current knowledge on the kinetics of the leukocyte and platelet counts after a few days off hydroxyurea treatment, displaying rapid increases in the cell counts to pretreatment levels, it is reasonable to assume that the *JAK2V617F* allele burden might similarly increase after hydroxyurea discontinuation. An increase in the *JAK2V617F* allele burden when treatment with hydroxyurea is terminated has been previously demonstrated.⁷¹

Third, although the findings in our study are supportive of early treatment with IFN, it does not deliver the definite proof, which would require a study, showing that early IFN-treatment from the time of diagnosis influences hard clinical end-points, such as risk of thrombosis and major bleeding, transformation to myelofibrosis and acute myeloid leukemia and ultimately survival. Hopefully, our DALIAH trial, from which our data in the present study have been retrieved, may provide such data within the next 10-20 years.

In conclusion, data-driven analysis is a novel tool for providing further evidence for the concept of early intervention with IFN in MPNs. Our observations also emphasize that starting treatment early allows for identification of patient responses. Understanding the kinetics of the *JAK2V617F* allele burden is highly valuable in guiding future clinical decisions about IFN-treatment of the individual patient. In this context, our findings substantiate and put in perspective the urgent need of personalized medicine with IFN in MPN-patients.

ACKNOWLEDGMENTS

The authors thank the patients and their families, as well as the research coordinators and site staff for their major effort. Our thanks are also extended to the clinician who helped identify eligible patients. Additionally the authors are grateful for the following grants which helped fund this study: “OUH Frie Forskningsmidler”, “OUH-Region Sjælland Fælles Forskningspulje”, “Fonden til Lægevidenskabens Fremme”, “Ellen og Aage Fausbølls Helsefond af 1975”, “Swedish Orphan”, “Den Forskningsfremmende Pulje for Kliniske Professorer ansat i Region Sjælland og ved Institut for Klinisk Medicin, Københavns Universitet”, “Region Sjællands Sundhedsvidenskabelige Forskningsfond (RSSF) 2018”, “Region Sjælland – Produktion, Forskning og Innovation (PFI)” and “Roskilde University Research Grant.”

CONFLICT OF INTEREST

HH has received a research grant from Novartis Oncology.

AUTHOR CONTRIBUTIONS

Rasmus K. Pedersen: Formal analysis (lead), project administration (supporting), methodology (supporting), software (lead), visualization, writing – original draft, and writing – review and editing. Morten Andersen: Formal analysis (supporting), methodology (supporting), software (supporting), supervision (supporting), and writing – review and editing. Trine A. Knudsen: Investigation (lead), and writing – review and editing. Zamra Sajid: Writing – review and editing. Johanne Gudmand-Hoeyer: Writing – review and editing. Marc J. B. Dam: Formal analysis (supporting), software (supporting), writing – review and editing. Vibe Skov: Investigation (supporting), methodology (supporting), writing – review and editing. Lasse Kjær: Investigation (supporting), methodology (supporting), writing – review and editing. Christina Ellervik: Writing – review and editing. Thomas S. Larsen: Investigation (supporting). Dennis Hansen: Data curation (lead), investigation (supporting). Niels Pallisgaard: Methodology (supporting). Hans C. Hasselbalch: Conceptualization (lead), funding acquisition (equal), methodology (supporting), investigation (supporting), supervision (supporting), validation (equal), and writing – review and editing. Johnny T. Ottesen: Conceptualization, funding acquisition (equal), methodology (lead), software (supporting), supervision (lead), validation (equal), and writing – review and editing.

ORCID

Rasmus K. Pedersen  <https://orcid.org/0000-0001-5946-8220>
 Morten Andersen  <https://orcid.org/0000-0001-7582-0685>
 Trine A. Knudsen  <https://orcid.org/0000-0001-9829-3099>
 Zamra Sajid  <https://orcid.org/0000-0002-9143-3092>
 Johanne Gudmand-Hoeyer  <https://orcid.org/0000-0002-4972-0653>

Marc J. B. Dam  <https://orcid.org/0000-0003-0096-9690>
 Vibe Skov  <https://orcid.org/0000-0003-0097-7826>
 Lasse Kjær  <https://orcid.org/0000-0001-6767-0226>
 Christina Ellervik  <https://orcid.org/0000-0002-3088-4375>
 Thomas S. Larsen  <https://orcid.org/0000-0002-8418-6708>
 Dennis Hansen  <https://orcid.org/0000-0002-4478-1297>
 Hans C. Hasselbalch  <https://orcid.org/0000-0003-3936-8032>
 Johnny T. Ottesen  <https://orcid.org/0000-0002-9786-0300>

DATA AVAILABILITY STATEMENT

The data that support the findings of this study are available on request from the corresponding author. The data are not publicly available due to privacy or ethical restrictions.

REFERENCES

- Campbell PJ, Green AR. The myeloproliferative disorders. *N Engl J Med.* 2006;355(23):2452-2466.
- Marchioli R, Finazzi G, Landolfi R, et al. Vascular and neoplastic risk in a large cohort of patients with polycythemia vera. *J Clin Oncol.* 2005;23(10):2224-2232.
- Björkholm M, Derolf ÅR, Hultcrantz M, et al. Treatment-related risk factors for transformation to acute myeloid leukemia and myelodysplastic syndromes in myeloproliferative neoplasms. *J Clin Oncol.* 2011;29(17):2410-2415.
- James C, Ugo V, Le Couédic J-P, et al. A unique clonal JAK2 mutation leading to constitutive signalling causes polycythaemia vera. *Nature.* 2005;434(7037):1144-1148.
- Kralovics R, Passamonti F, Buser AS, et al. A gain-of-function mutation of JAK2 in myeloproliferative disorders. *N Engl J Med.* 2005;352(17):1779-1790.
- Baxter EJ, Scott LM, Campbell PJ, et al. Acquired mutation of the tyrosine kinase JAK2 in human myeloproliferative disorders. *Lancet.* 2005;365(9464):1054-1061.
- Levine RL, Wadleigh M, Cools J, et al. Activating mutation in the tyrosine kinase JAK2 in polycythemia vera, essential thrombocythemia, and myeloid metaplasia with myelofibrosis. *Cancer Cell.* 2005;7(4):387-397.
- Larsen TS, Pallisgaard N, Møller MB, Hasselbalch HC. The JAK2 V617F allele burden in essential thrombocythemia, polycythemia vera and primary myelofibrosis - Impact on disease phenotype. *Eur J Haematol.* 2007;79(6):508-515.
- Klampfl T, Gisslinger H, Harutyunyan AS, et al. Somatic mutations of Calreticulin in myeloproliferative neoplasms. *N Engl J Med.* 2013;369(25):2379-2390.
- Nangalia J, Massie CE, Baxter EJ, et al. Somatic CALR mutations in myeloproliferative neoplasms with nonmutated JAK2. *N Engl J Med.* 2013;369(25):2391-2405.
- Cazzola M, Kralovics R. From Janus kinase 2 to calreticulin : the clinically relevant genomic landscape of myeloproliferative neoplasms. *Blood.* 2016;123(24):3714-3720.
- Lundberg P, Karow A, Nienhold R, et al. Clonal evolution and clinical correlates of somatic mutations in myeloproliferative neoplasms. *Blood.* 2014;123(14):2220-2228.
- Wolanskyj AP, Lasho TL, Schwager SM, et al. JAK2V617F mutation in essential thrombocythemia: clinical associations and

- long-term prognostic relevance. *Br J Haematol.* 2005;131(2):208-213.
14. Carobbio A, Finazzi G, Guerini V, et al. Leukocytosis is a risk factor for thrombosis in essential thrombocythemia: Interaction with treatment, standard risk factors, and Jak2 mutation status. *Blood.* 2007;109(6):2310-2313.
 15. Tefferi A, Strand JJ, Lasho TL, et al. Bone marrow JAK2V617F allele burden and clinical correlates in polycythemia vera. *Leukemia.* 2007;21(9):2074-2075.
 16. Vannucchi AM, Antonioli E, Guglielmelli P, et al. Clinical profile of homozygous JAK2 617V> F mutation in patients with polycythemia vera or essential thrombocythemia. *Blood.* 2007;110(3):840-846.
 17. Vannucchi AM, Antonioli E, Guglielmelli P, et al. Prospective identification of high-risk polycythemia vera patients based on JAK2V617F allele burden. *Leukemia.* 2007;21(9):1952-1959.
 18. Cheung B, Radia D, Pantelidis P, Yadegarfar G, Harrison C. The presence of the JAK2 V617F mutation is associated with a higher haemoglobin and increased risk of thrombosis in essential thrombocythemia. *Br J Haematol.* 2006;132(2):244-245.
 19. Tefferi A, Lasho TL, Schwager SM, et al. The clinical phenotype of wild-type, heterozygous, and homozygous JAK2V617F in polycythemia vera. *Cancer.* 2006;106(3):631-635.
 20. Passamonti F, Rumi E, Pietra D, et al. Relation between JAK2(V617F) mutation status, granulocyte activation, and constitutive mobilization of CD34+ cells into peripheral blood in myeloproliferative disorders. *Blood.* 2006;107(9):3676-3682.
 21. Arellano-Rodrigo E, Alvarez-Larrán A, Reverter JC, et al. Increased platelet and leukocyte activation as contributing mechanisms for thrombosis in essential thrombocythemia and correlation with the JAK2 mutational status. *Haematologica.* 2006;91(2):169-175.
 22. Bellucci S, Michiels JJ. The role of JAK2 V617F mutation, spontaneous erythropoiesis and megakaryocytopoiesis, hypersensitive platelets, activated leukocytes, and endothelial cells in the etiology of thrombotic manifestations in polycythemia vera and essential thrombocythemia. *Semin Thromb Hemost.* 2006;32(4):381-398.
 23. Falanga A, Marchetti M, Vignoli A, et al. V617F JAK-2 mutation in patients with essential thrombocythemia: relation to platelet, granulocyte, and plasma hemostatic and inflammatory molecules. *Exp Hematol.* 2007;35(5):702-711.
 24. Kittur J, Knudson RA, Lasho TL, et al. Clinical correlates of JAK2V617F allele burden in essential thrombocythemia. *Cancer.* 2007;109(11):2279-2284.
 25. Hsiao HH, Yang MY, Liu YC, et al. The association of JAK2V617F mutation and leukocytosis with thrombotic events in essential thrombocythemia. *Exp Hematol.* 2007;35(11):1704-1707.
 26. Barosi G, Rosti V, Bonetti E, et al. Evidence that prefibrotic myelofibrosis is aligned along a clinical and biological continuum featuring primary myelofibrosis. *PLoS ONE.* 2012;7(4):e35631.
 27. Kiladjian J-J. High molecular response rate of polycythemia vera patients treated with pegylated interferon -2a. *Blood.* 2006;108(6):2037-2040.
 28. Silver RT. Long-term effects of the treatment of polycythemia vera with recombinant interferon- α . *Cancer.* 2006;107(3):451-458.
 29. Kiladjian JJ, Giraudier S, Cassinat B. Interferon-alpha for the therapy of myeloproliferative neoplasms: targeting the malignant clone. *Leukemia.* 2016;30(4):776-781.
 30. Kjær L, Cordua S, Holmström MO, et al. Differential dynamics of CALR mutant allele burden in myeloproliferative neoplasms during interferon alfa treatment. *PLoS ONE.* 2016;11(10):e0165336.
 31. Masarova L, Yin CC, Cortes JE, et al. Histomorphological responses after therapy with pegylated interferon α -2a in patients with essential thrombocythemia (ET) and polycythemia vera (PV). *Exp Hematol Oncol.* 2017;6(1):1-13.
 32. Crisà E, Cerrano M, Beggiato E, et al. Can pegylated interferon improve the outcome of polycythemia vera patients? *J Hematol Oncol.* 2017;10(1). <https://doi.org/10.1186/s13045-017-0395-1>
 33. Foucar CE, Stein BL. Contemporary use of interferon therapy in the myeloproliferative neoplasms. *Curr Hematol Malig Rep.* 2017;12(5):406-414.
 34. Gowin K, Jain T, Kosiorek H, et al. Pegylated interferon alpha—2a is clinically effective and tolerable in myeloproliferative neoplasm patients treated off clinical trial. *Leuk Res.* 2017;54:73-77.
 35. Tashi T, Swierczek S, Kim SJ, et al. Pegylated interferon Alfa-2a and hydroxyurea in polycythemia vera and essential thrombocythemia: differential cellular and molecular responses. *Leukemia.* 2018;32(8):1830-1833.
 36. Larsen TS, Bjerrum OW, Pallisgaard N, et al. Sustained major molecular response on interferon alpha-2b in two patients with polycythemia vera. *Ann Hematol.* 2008;87(10):847-850.
 37. Hasselbalch HC, Larsen TS, Riley CH, Jensen MK, Kiladjian J. Interferon-alpha in the treatment of Philadelphia-negative chronic myeloproliferative neoplasms. Status and perspectives. *Curr Drug Targets.* 2011;12(3):392-419.
 38. Hasselbalch HC. A new era for IFN-alpha in the treatment of Philadelphia-negative chronic myeloproliferative neoplasms. *Expert Rev Hematol.* 2011;4(6):637-655.
 39. Samuelsson J, Hasselbalch H, Bruserud O, et al. A phase II trial of pegylated interferon α -2b therapy for polycythemia vera and essential thrombocythemia. *Cancer.* 2006;106(11):2397-2405.
 40. Silver RT, Hasselbalch HC, Kiladjian JJ. Interferon and the treatment of polycythemia vera, essential thrombocythemia and myelofibrosis. *Expert Rev Hematol.* 2013;6(1):49-58.
 41. Hasselbalch HC, Silver RT. Interferon in polycythemia vera and related neoplasms. Can it become the treatment of choice without a randomized trial? *Expert Rev Hematol.* 2015;8(4):439-445.
 42. Stauffer Larsen T, Iversen KF, Hansen E, et al. Long term molecular responses in a cohort of Danish patients with essential thrombocythemia, polycythemia vera and myelofibrosis treated with recombinant interferon alpha. *Leuk Res.* 2013;37(9):1041-1045.
 43. Stein BL, Tiu RV. Biological rationale and clinical use of interferon in the classical BCR-ABL-negative myeloproliferative neoplasms. *J Interf Cytokine Res.* 2013;33(4):145-153.
 44. Utke Rank C, Weis Bjerrum O, Larsen TS, et al. Minimal residual disease after long-term interferon-alpha2 treatment: A report on hematological, molecular and histomorphological response patterns in 10 patients with essential thrombocythemia and polycythemia vera. *Leuk. Lymphoma.* 2016;57(2):348-354.
 45. Masarova L, Patel KP, Newberry KJ, et al. Pegylated interferon alfa-2a in patients with essential thrombocythemia or polycythemia vera: a post-hoc, median 83 month follow-up of an open-label, phase 2 trial. *Lancet Haematol.* 2017;4(4):e165-e175.
 46. Kiladjian J, Cassinat B, Chevret S, et al. Pegylated Interferon-alfa-2a induces complete hematological and molecular responses with low toxicity in Polycythemia Vera. *Hematology.* 2008;112(8):3065-3073.
 47. Quintás-Cardama A, Kantarjian H, Manshouri T, et al. Pegylated interferon alfa-2a yields high rates of hematologic and molecular response in patients with advanced essential thrombocythemia and polycythemia vera. *J Clin Oncol.* 2009;27(32):5418-5424.

48. Larsen TS, Møller MB, de Stricker K, et al. Minimal residual disease and normalization of the bone marrow after long-term treatment with alpha-interferon2b in polycythemia vera. A report on molecular response patterns in seven patients in sustained complete hematological remission. *Hematology*. 2009;14(6):331-334.
49. Quintás-Cardama A, Abdel-Wahab O, Manshouri T, et al. Molecular analysis of patients with polycythemia vera or essential thrombocythemia receiving pegylated interferon α -2a. *Blood*. 2013;122(6):893-901.
50. Verger E, Cassinat B, Dosquet C, Giraudier S. Clinical and molecular response to interferon- α therapy in essential thrombocythemia patients with CALR mutations. *Blood*. 2015;126(24):2585-2592.
51. Gisslinger H, Zagrijtschuk O, Buxhofer-ausch V, et al. Ropeginterferon alfa-2b, a novel IFN α -2b, induces high response rates with low toxicity in patients with polycythemia vera. *Blood*. 2015;126(15):1762-1770.
52. Them NCC, Bagienski K, Berg T, et al. Molecular responses and chromosomal aberrations in patients with polycythemia vera treated with peg-proline-interferon alpha-2b. *Am J Hematol*. 2015;90(4):288-294.
53. Campo E, Swerdlow SH, Harris NL, Pileri S, Stein H, Jaffe ES. The 2008 WHO classification of lymphoid neoplasms and beyond: evolving concepts and practical applications. *Blood*. 2011;117(19):5019-5032.
54. Barosi G, Birgegard G, Finazzi G, et al. Response criteria for essential thrombocythemia and polycythemia vera: result of a European LeukemiaNet consensus conference. *Blood*. 2009;113(20):4829-4833.
55. Larsen TS, Christensen JH, Hasselbalch HC, Pallisgaard N. The JAK2 V617F mutation involves B- and T-lymphocyte lineages in a subgroup of patients with Philadelphia-chromosome negative chronic myeloproliferative disorders. *Br J Haematol*. 2007;136(5):745-751.
56. Jovanovic JV, Ivey A, Vannucchi AM, et al. Establishing optimal quantitative-polymerase chain reaction assays for routine diagnosis and tracking of minimal residual disease in JAK2-V617F-associated myeloproliferative neoplasms: A joint European LeukemiaNet/MPN&MPN-EuroNet (COST action BM0902) study. *Leukemia*. 2013;27(10):2032-2039.
57. Larsen TS, Pallisgaard N, Møller MB, Hasselbalch HC. The JAK2 V617F allele burden in essential thrombocythemia, polycythemia vera and primary myelofibrosis—impact on disease phenotype. *Eur J Haematol*. 2007;79(6):508-515.
58. Abkowitz JL, Catlin SN, McCallie MT, Gutter P. Evidence that the number of hematopoietic stem cells per animal is conserved in mammals. *Blood*. 2002;100(7):2665-2667.
59. Enblom A, Lindskog E, Hasselbalch H, et al. High rate of abnormal blood values and vascular complications before diagnosis of myeloproliferative neoplasms. *Eur J Intern Med*. 2015;26(5):344-347.
60. Laurenti E, Göttgens B. From haematopoietic stem cells to complex differentiation landscapes. *Nature*. 2018;553(7689):418-426.
61. Lee-Six H, Øbro NF, Shepherd MS, et al. Population dynamics of normal human blood inferred from somatic mutations. *Nature*. 2018;561(7724):473-478.
62. Bjørn ME, Hasselbalch HC. Minimal residual disease or cure in MPNs? Rationales and perspectives on combination therapy with interferon-alpha2 and ruxolitinib. *Expert Rev Hematol*. 2017;10(5):393-404.
63. Hasselbalch HC, Holmström MO. Perspectives on interferon-alpha in the treatment of polycythemia vera and related myeloproliferative neoplasms: minimal residual disease and cure? *Semin Immunopathol*. 2019;41(1):5-19.
64. Hasselbalch HC. Perspectives on chronic inflammation in essential thrombocythemia, polycythemia vera, and myelofibrosis: is chronic inflammation a trigger and driver of clonal evolution and development of accelerated atherosclerosis and second cancer? *Blood*. 2012;119(14):3219-3225.
65. Hasselbalch HC. The role of cytokines in the initiation and progression of myelofibrosis. *Cytokine Growth Factor Rev*. 2013;24(2):133-145.
66. Hasselbalch HC. Chronic inflammation as a promotor of mutagenesis in essential thrombocythemia, polycythemia vera and myelofibrosis. A human inflammation model for cancer development? *Leuk Res*. 2013;37(2):214-220.
67. Hasselbalch HC, Bjørn ME. MPNs as inflammatory diseases: the evidence, consequences, and perspectives. *Mediators Inflamm*. 2015;2015:1-16.
68. Fleischman AG. Inflammation as a driver of clonal evolution in myeloproliferative neoplasm. *Mediators Inflamm*. 2015;2015:1-6.
69. Čokić VP, Mitrović-Ajtić O, Beleslin-Čokić BB, et al. Proinflammatory cytokine IL-6 and JAK-STAT signaling pathway in myeloproliferative neoplasms. *Mediators Inflamm*. 2015;2015:1-13.
70. Gisslinger H, Klade C, Georgiev P, et al. Maintenance of Response in Long-Term Treatment with RopegInterferon Alfa-2b (Besremi®) vs. Hydroxyurea in Polycythemia Vera Patients (Proud/Continuation - PV Phase III Trials). Poster Presentation: 1457. EHA June 15, 2019.
71. Theocharides A, Passweg JR, Medinger M, et al. The allele burden of JAK2 mutations remains stable over several years in patients with myeloproliferative disorders. *Haematologica*. 2008;93(12):1890-1893.

SUPPORTING INFORMATION

Additional supporting information may be found online in the Supporting Information section.

How to cite this article: Pedersen RK, Andersen M, Knudsen TA, et al. Data-driven analysis of JAK2V617F kinetics during interferon-alpha2 treatment of patients with polycythemia vera and related neoplasms. *Cancer Med*. 2020;00:1–13. <https://doi.org/10.1002/cam4.2741>